

Systems pharmacology in the spotlight: trending technologies in network biology and drug discovery

Edited by

Raghuveera Kumar Goel, Kiven Erique Lukong and
Andrew Emili

Published in

Frontiers in Pharmacology



FRONTIERS EBOOK COPYRIGHT STATEMENT

The copyright in the text of individual articles in this ebook is the property of their respective authors or their respective institutions or funders. The copyright in graphics and images within each article may be subject to copyright of other parties. In both cases this is subject to a license granted to Frontiers.

The compilation of articles constituting this ebook is the property of Frontiers.

Each article within this ebook, and the ebook itself, are published under the most recent version of the Creative Commons CC-BY licence. The version current at the date of publication of this ebook is CC-BY 4.0. If the CC-BY licence is updated, the licence granted by Frontiers is automatically updated to the new version.

When exercising any right under the CC-BY licence, Frontiers must be attributed as the original publisher of the article or ebook, as applicable.

Authors have the responsibility of ensuring that any graphics or other materials which are the property of others may be included in the CC-BY licence, but this should be checked before relying on the CC-BY licence to reproduce those materials. Any copyright notices relating to those materials must be complied with.

Copyright and source acknowledgement notices may not be removed and must be displayed in any copy, derivative work or partial copy which includes the elements in question.

All copyright, and all rights therein, are protected by national and international copyright laws. The above represents a summary only. For further information please read Frontiers' Conditions for Website Use and Copyright Statement, and the applicable CC-BY licence.

ISSN 1664-8714
ISBN 978-2-8325-5820-1
DOI 10.3389/978-2-8325-5820-1

About Frontiers

Frontiers is more than just an open access publisher of scholarly articles: it is a pioneering approach to the world of academia, radically improving the way scholarly research is managed. The grand vision of Frontiers is a world where all people have an equal opportunity to seek, share and generate knowledge. Frontiers provides immediate and permanent online open access to all its publications, but this alone is not enough to realize our grand goals.

Frontiers journal series

The Frontiers journal series is a multi-tier and interdisciplinary set of open-access, online journals, promising a paradigm shift from the current review, selection and dissemination processes in academic publishing. All Frontiers journals are driven by researchers for researchers; therefore, they constitute a service to the scholarly community. At the same time, the *Frontiers journal series* operates on a revolutionary invention, the tiered publishing system, initially addressing specific communities of scholars, and gradually climbing up to broader public understanding, thus serving the interests of the lay society, too.

Dedication to quality

Each Frontiers article is a landmark of the highest quality, thanks to genuinely collaborative interactions between authors and review editors, who include some of the world's best academicians. Research must be certified by peers before entering a stream of knowledge that may eventually reach the public - and shape society; therefore, Frontiers only applies the most rigorous and unbiased reviews. Frontiers revolutionizes research publishing by freely delivering the most outstanding research, evaluated with no bias from both the academic and social point of view. By applying the most advanced information technologies, Frontiers is catapulting scholarly publishing into a new generation.

What are Frontiers Research Topics?

Frontiers Research Topics are very popular trademarks of the *Frontiers journals series*: they are collections of at least ten articles, all centered on a particular subject. With their unique mix of varied contributions from Original Research to Review Articles, Frontiers Research Topics unify the most influential researchers, the latest key findings and historical advances in a hot research area.

Find out more on how to host your own Frontiers Research Topic or contribute to one as an author by contacting the Frontiers editorial office: frontiersin.org/about/contact

Systems pharmacology in the spotlight: trending technologies in network biology and drug discovery

Topic editors

Raghuveera Kumar Goel — Boston University, United States

Kiven Erique Lukong — University of Saskatchewan, Canada

Andrew Emili — Oregon Health and Science University, United States

Citation

Goel, R. K., Lukong, K. E., Emili, A., eds. (2024). *Systems pharmacology in the spotlight: trending technologies in network biology and drug discovery*.

Lausanne: Frontiers Media SA. doi: 10.3389/978-2-8325-5820-1

Table of contents

- 04 **Editorial: Systems pharmacology in the spotlight: trending technologies in network biology and drug discovery**
Raghuveera Kumar Goel, Kiven Erique Lukong and Andrew Emili
- 07 **Network pharmacology, molecular docking, and experimental validation to explore the potential mechanism of Long Mu Qing Xin mixture for the treatment of attention deficit hyperactivity disorder**
Xuejun Li, Zhen Xiao, Wenyan Pu, Zhiyan Jiang, Shumin Wang and Yixing Zhang
- 29 **Integrated metabolomics and proteomics reveal biomarkers associated with hemodialysis in end-stage kidney disease**
Weiwei Lin, Fatemeh Mousavi, Benjamin C. Blum, Christian F. Heckendorf, Jarrod Moore, Noah Lampl, Mark McComb, Sergei Kotelnikov, Wenqing Yin, Nabil Rabhi, Matthew D. Layne, Dima Kozakov, Vipul C. Chitalia and Andrew Emili
- 44 **Pharmacological approaches to understanding protein kinase signaling networks**
Elloise H. Stephenson and Jonathan M. G. Higgins
- 64 **From desert flora to cancer therapy: systematic exploration of multi-pathway mechanisms using network pharmacology and molecular modeling approaches**
Adel Alblihy
- 82 **System biology approach to identify the novel biomarkers in glioblastoma multiforme tumors by using computational analysis**
Safar M. Alqahtani, Ali Altharawi, Alhumaidi Alabbas, Faisal Ahmad, Hassan Ayaz, Asia Nawaz, Sidra Rahman and Manal A. Alossaimi
- 101 **Growth hormone releasing peptide-6 (GHRP-6) prevents doxorubicin-induced myocardial and extra-myocardial damages by activating prosurvival mechanisms**
Jorge Berlanga-Acosta, Danay Cibrian, Juan Valiente-Mustelier, José Suárez-Alba, Ariana García-Ojalvo, Viviana Falcón-Cama, Baohong Jiang, Linlin Wang and Gerardo Guillén-Nieto
- 118 ***In Vitro* evaluation of the anti-pancreatic cancer activity of *epimedium* herb**
Yangfeng Chen, Han Xia and Xiaohong Zhong
- 133 **Potential mechanism of Luoshi Neiyi prescription in endometriosis based on serum pharmacochemistry and network pharmacology**
Lizheng Wu, Shuhong Lin, Yongjun Hu, Shangwen Jing, Bowen Sun, Xiaoxin Chen, Jinjin Jia, Cheng Zeng and Fangli Pei
- 154 **Mechanisms of action of *Sappan lignum* for prostate cancer treatment: network pharmacology, molecular docking and experimental validation**
Wenna Li, Honglin Jiang, Weina Zhang, Qiuyue Sun, Qiaoli Zhang, Jingnan Xu, Jinchang Huang and Yuxiang Wan



OPEN ACCESS

EDITED AND REVIEWED BY
Heike Wulff,
University of California, Davis, United States

*CORRESPONDENCE
Raghuveera Kumar Goel,
✉ goelr@ohsu.edu

RECEIVED 27 November 2024
ACCEPTED 28 November 2024
PUBLISHED 10 December 2024

CITATION
Goel RK, Lukong KE and Emili A (2024) Editorial:
Systems pharmacology in the spotlight:
trending technologies in network biology and
drug discovery.
Front. Pharmacol. 15:1535754.
doi: 10.3389/fphar.2024.1535754

COPYRIGHT
© 2024 Goel, Lukong and Emili. This is an open-
access article distributed under the terms of the
[Creative Commons Attribution License \(CC BY\)](https://creativecommons.org/licenses/by/4.0/).
The use, distribution or reproduction in other
forums is permitted, provided the original
author(s) and the copyright owner(s) are
credited and that the original publication in this
journal is cited, in accordance with accepted
academic practice. No use, distribution or
reproduction is permitted which does not
comply with these terms.

Editorial: Systems pharmacology in the spotlight: trending technologies in network biology and drug discovery

Raghuveera Kumar Goel^{1*}, Kiven Erique Lukong² and
Andrew Emili¹

¹Division of Oncological Sciences, Knight Cancer Institute, Oregon Health and Science University (OHSU), Portland, OR, United States, ²Department of Biochemistry, Microbiology and Immunology, College of Medicine, University of Saskatchewan, Saskatoon, SK, Canada

KEYWORDS

systems pharmacology, systems biology, protein-protein interaction (PPI), proteomics and bioinformatics, network biology, high throughput screen (HTS), drug, therapy

Editorial on the Research Topic

Systems pharmacology in the spotlight: trending technologies in network biology and drug discovery

Introduction

Systems pharmacology is an interdisciplinary field that combines pharmacological insights with systems biology to better understand the complex interactions between drugs, biological systems, and diseases. It moves beyond traditional pharmacology by integrating computational modeling, network analysis, and high-throughput data to predict drug effects at the systems level, including therapeutic benefits and potential side effects. By considering the dynamic interplay of molecular pathways, cellular responses, and organism-level physiology, systems pharmacology provides a holistic framework for drug discovery, personalized medicine, and the optimization of treatment strategies.

Recent advancements in systems pharmacology are deepening our understanding of complex disease mechanisms and have facilitated the development of targeted therapeutic interventions. Some of these engaging paradigms in early-stage discovery efforts involving kinase-inhibition for example, have been extensively reviewed by [Stephenson and Higgins](#). In this editorial, we spotlight the authors' contributions to our special Research Topic on systems pharmacology, emphasizing the importance of diverse methodologies. These include high-throughput screening, *in silico* modeling of drug-ligand docking with network-level interactions, and experimental validations (both *in vitro* and *in vivo*), all aimed at elucidating effects on cellular signaling networks within a therapeutic context.

High-throughput screening approaches

Anti-pancreatic cancer activity of epimedium herb

Chen et al. explore the Epimedium herb's therapeutic potential against pancreatic cancer. Through high-performance liquid chromatography, network pharmacology, and molecular docking, the authors identified active compounds like icariin and baohuoside I, targeting pathways such as Interleukin-4 and interleukin-13 signaling. *In vitro* assays demonstrated that Epimedium extracts significantly reduced Panc-1 cell viability, suggesting its promise as a multi-targeted therapeutic agent for pancreatic cancer.

Integrated metabolomics and proteomics in end-stage kidney disease

Lin et al. employed an integrative approach combining metabolomics and proteomics to identify biomarkers associated with hemodialysis in end-stage kidney disease (ESKD). Their analysis uncovered significant alterations in metabolic and protein profiles, providing insights into the physiological changes induced by hemodialysis. These findings have the potential to guide the development of targeted therapies and improve patient outcomes in ESKD management.

In silico analyses and experimental validation

Mechanisms of action of Sappan Lignum for prostate cancer treatment

Li et al. investigated the antitumor properties of Sappan Lignum, derived from *Caesalpinia sappan* L., against prostate cancer (PCa). The study identified 21 major active compounds within Sappan Lignum and their 32 highly probable target proteins mapped from 821 differentially expressed genes associated with PCa. Through network pharmacology and molecular docking, they pinpointed eight key targets, notably BCL-2 and CCNB1, with the p53 signaling pathway being central to the herb's antitumor effects. *In vitro* experiments demonstrated that 3-deoxysappanchalcone (3-DSC), a principal component, inhibited PCa cell proliferation, migration, and induced apoptosis, primarily by modulating the p53/p21/CDC2/CCNB1 pathway. These findings underscore Sappan lignum's promise as a multi-targeted therapeutic agent for PCa.

Luoshi Neiyi prescription in endometriosis: a network pharmacology approach

Wu et al.'s study explores the underlying mechanisms of action of Luoshi Neiyi prescription (LSNYP) for treating endometriosis,

utilizing serum pharmacology and network pharmacology approaches. By identifying active components and their targets, the research highlights LSNYP's regulation of hypoxia and inflammation-related pathways, notably the HIF1A/EZH2/ANTXR2 axis. Experimental validation demonstrated that LSNYP modulates key cellular proteins, suggesting its therapeutic potential in endometriosis management. This integrative approach provides a scientific basis for the therapeutic effects of LNP in endometriosis management.

Long Mu Qing Xin Mixture for ADHD: a multi-methodological study

Li et al. investigated the formulated medicine, Long Mu Qing Xin Mixture (LMQXM) for treating attention deficit hyperactivity disorder (ADHD). Network pharmacology and molecular docking approaches identified key components; beta-sitosterol, stigmasterol, rhynchophylline, baicalein, and formononetin, that interact with dopamine receptors DRD1 and DRD2. *In vivo* experiments confirmed that LMQXM modulates the dopamine and cAMP signaling pathways, suggesting its therapeutic potential for ADHD.

Systems biology approach to glioblastoma multiforme

This study (Alqahtani et al.) highlighted matrix metalloproteinase 9 (MMP9) as a critical molecular target in glioblastoma multiforme (GBM) pathophysiology. By prioritizing molecular compounds sourced from drug-ligand interaction databases and molecular docking, carmustine, lomustine, marimastat, and temozolomide demonstrated significant binding affinities to MMP9, suggesting their utility in modulating GBM's molecular network for enhanced therapeutic outcomes.

Desert flora in cancer therapy: network pharmacology and molecular modeling

Alblihy systematically explored the anticancer potential of phytochemical compounds derived from Arabian flora using network pharmacology and molecular modeling. The work highlighted multiple pathways through which these natural compounds exert their effects, including apoptosis, cell cycle arrest, and inhibition of metastasis. The study emphasizes the importance of integrating traditional knowledge with modern computational techniques to discover novel therapeutic agents in ovarian cancer.

GHRP-6 mitigates doxorubicin-induced cardiotoxicity

Berlanga-Acosta et al. explored the cardioprotective effects of Growth Hormone Releasing Peptide-6 (GHRP-6) against

doxorubicin (Dox)-induced cardiotoxicity. Through echocardiography, histopathology, and molecular analyses, the study found that GHRP-6 administration alongside Dox prevented myocardial fiber degradation and ventricular dilation, thereby preserving left ventricular systolic function. Mechanistically, GHRP-6 enhanced antioxidant defenses, upregulated the pro-survival gene Bcl-2, and maintained mitochondrial integrity in cardiomyocytes. These findings suggest that GHRP-6 activates pro-survival mechanisms, offering a potential therapeutic strategy to mitigate Dox-induced cardiac damage.

Collectively, these studies underscore four key tools of systems pharmacology for unraveling complex disease mechanisms and identifying potential therapeutic agents: high-throughput screening, biomolecular network modeling, simulated structural docking, and experimental validation. By integrating computational and experimental approaches, researchers can accelerate the discovery of novel treatments and deepen our understanding of disease pathology.

Looking forward; the age of generative artificial intelligence (AI)

The future of generative AI within systems pharmacology is poised to be transformative. Generative AI holds the potential to automate the design of therapeutic molecules and simulate their interactions across diverse biological systems, significantly reducing the time and cost required to move from concept to clinical trials. By modeling vast chemical spaces in predicting drug-target interactions and synergizing systems-level data such as multi-omics and dynamic network analyses, generative AI can enhance drug optimizations as well as evaluate safety and efficacy through iterative simulations on virtual patients. By democratizing drug discovery and fostering interdisciplinary collaboration, generative AI promises a more efficient and sustainable future for systems pharmacology.

Author contributions

RG: Conceptualization, Writing–original draft, Writing–review and editing. KL: Writing–review and editing. AE: Writing–review and editing.

Funding

The author(s) declare that financial support was received for the research, authorship, and/or publication of this article. RG acknowledges funding from the International Alliance for Cancer Early Detection (ACED) (Grant number: 24R0104).

Conflict of interest

The authors declare that the research was conducted in the absence of any commercial or financial relationships that could be construed as a potential conflict of interest.

The author(s) declared that they were an editorial board member of Frontiers, at the time of submission. This had no impact on the peer review process and the final decision.

Generative AI statement

The author(s) declare that no Generative AI was used in the creation of this manuscript.

Publisher's note

All claims expressed in this article are solely those of the authors and do not necessarily represent those of their affiliated organizations, or those of the publisher, the editors and the reviewers. Any product that may be evaluated in this article, or claim that may be made by its manufacturer, is not guaranteed or endorsed by the publisher.



OPEN ACCESS

EDITED BY

Raghuveera Kumar Goel,
Boston University, United States

REVIEWED BY

Oscar Vidal,
Universidad del Norte, Colombia
Adele Stewart,
Florida Atlantic University, United States

*CORRESPONDENCE

Zhen Xiao,
✉ xiaozhen@shutcm.edu.cn
Zhiyan Jiang,
✉ lhjzycm@163.com

SPECIALTY SECTION

This article was submitted to
Experimental Pharmacology and Drug
Discovery,
a section of the journal
Frontiers in Pharmacology

RECEIVED 15 January 2023

ACCEPTED 01 March 2023

PUBLISHED 17 March 2023

CITATION

Li X, Xiao Z, Pu W, Jiang Z, Wang S and
Zhang Y (2023), Network pharmacology,
molecular docking, and experimental
validation to explore the potential
mechanism of Long Mu Qing Xin mixture
for the treatment of attention deficit
hyperactivity disorder.
Front. Pharmacol. 14:1144907.
doi: 10.3389/fphar.2023.1144907

COPYRIGHT

© 2023 Li, Xiao, Pu, Jiang, Wang and
Zhang. This is an open-access article
distributed under the terms of the
[Creative Commons Attribution License](#)
(CC BY). The use, distribution or
reproduction in other forums is
permitted, provided the original author(s)
and the copyright owner(s) are credited
and that the original publication in this
journal is cited, in accordance with
accepted academic practice. No use,
distribution or reproduction is permitted
which does not comply with these terms.

Network pharmacology, molecular docking, and experimental validation to explore the potential mechanism of Long Mu Qing Xin mixture for the treatment of attention deficit hyperactivity disorder

Xuejun Li^{1,2}, Zhen Xiao^{1*}, Wenyan Pu^{1,2}, Zhiyan Jiang^{1*},
Shumin Wang^{1,2} and Yixing Zhang^{1,2}

¹Pediatrics, Longhua Hospital Affiliated to Shanghai University of Traditional Chinese Medicine, Shanghai, China, ²Longhua Clinical Medical College, Shanghai University of Traditional Chinese Medicine, Shanghai, China

Background: Long Mu Qing Xin Mixture (LMQXM) has shown potentially positive effects in alleviating attention deficit hyperactivity disorder (ADHD); however, the action mechanism is still not fully understood. This study aimed to predict the potential mechanism of LMQXM for ADHD using network pharmacology and molecular docking, which were then validated using animal experiments.

Methods: Network pharmacology and molecular docking techniques were used to predict the core targets and potential pathways of LMQXM for ADHD, and KEGG pathway enrichment analysis revealed the potential significance of dopamine (DA) and cyclic adenosine monophosphate (cAMP) signaling pathways. To verify the hypothesis, we conducted an animal experiment. In the animal experiment, the young spontaneously hypertensive rats (SHRs) were randomly divided into the model group (SHR), the methylphenidate hydrochloride group (MPH, 4.22 mg/kg), and 3 LMQXM groups (low-dose (LD) group, 5.28 ml/kg; medium-dose (MD) group, 10.56 ml/kg; and high-dose (HD) group, 21.12 ml/kg), and administered by gavage for 4 weeks; the WKY rats were set as the control group. The open field test and Morris water maze test were used to evaluate the behavioral performance of rats, high performance liquid chromatography mass spectrometry (LC-MS) was used to analyze DA levels in the prefrontal cortex (PFC) and striatum of rats, ELISA was used to detect cAMP concentrations in the PFC and striatum, and immunohistochemistry and qPCR were used to analyze positive cell expression and mRNA expression for indicators related to DA and cAMP pathways.

Results: The results showed that beta-sitosterol, stigmasterol, rhynchophylline, baicalein, and formononetin might be key components of LMQXM for ADHD and that these components bind well to the core targets, DA receptors (DRD1 and DRD2). Furthermore, LMQXM might act through the DA and cAMP signaling pathways. In the animal experiment, we found that MPH and LMQXM-MD controlled hyperactivity and improved learning and memory in SHRs, while

LMQXM-HD only controlled hyperactivity in SHR; meanwhile, MPH and LMQXM-MD upregulated DA and cAMP levels, mean optical density (MOD) of cAMP, and MOD and mRNA expression of DRD1 and PKA in the prefrontal cortex (PFC) and striatum of SHRs, while LMQXM-LD and LMQXM-HD upregulated DA and cAMP levels in the striatum, MOD of cAMP in the PFC, and mRNA expression of PKA in the PFC. However, we did not find a significant regulatory effect of LMQXM on DRD2.

Conclusion: To sum up, this study demonstrated that LMQXM may increase DA levels mainly by activating the cAMP/PKA signaling pathway through DRD1, thereby controlling the behavioral disorders of SHRs, which is most effective at moderate doses, and this may be a key mechanism for LMQXM in the treatment of ADHD.

KEYWORDS

attention deficit hyperactivity disorder, Long Mu Qing Xin Mixture, network pharmacology, molecular docking, dopamine, cAMP/PKA signaling pathway, spontaneously hypertensive rats

1 Introduction

Attention deficit hyperactivity disorder (ADHD) is a common, early-onset, persistent neurodevelopmental disorder in children (Banaschewski et al., 2017), with inattention, hyperactivity, and impulsivity as core symptoms, often accompanied by learning and memory deficits. The global prevalence of ADHD is about 5.29% (Posner et al., 2020), with boys having a higher incidence (Mahone and Denckla, 2017). In recent years, the prevalence rate of ADHD has been increasing (Carbray, 2018), and about 50% of patients have symptoms that persist into adulthood. In addition, these patients often face the risk of academic failure, accidental injury, criminal behavior, and even suicide (Faraone and Larsson, 2019), which brings a heavy psychological and economic burden to individuals, families, and society. Dopamine (DA) defects or dysregulated DA transmission is considered to be the core pathogenesis of ADHD (Drechsler et al., 2020); however, the specific pathogenesis has not yet been elucidated, and the prefrontal cortex (PFC) and striatum, as key regions for DA neurotransmission, have become a mainstream direction for studying attention and learning and memory deficits in ADHD (Sharma and Couture, 2013; Ruocco et al., 2014).

As methylphenidate (MPH) can increase the availability of extracellular DA in the synaptic gap by blocking dopamine transporter protein (DAT) (Faraone, 2018; Rostami Kandroodi et al., 2021), it has been used as a first-line drug for the treatment of ADHD. However, some scholars have suggested that children should be at least 6 years old when administered MPH because the long-term use of this drug could lead to addiction (Vergheze and Abdijadid, 2022). Furthermore, MPH has a risk of inducing abnormal behaviors such as anxiety, depression, sleep disorders, and even suicide (Ekhart et al., 2020). Considering these adverse factors, the main purpose of medical research is to explore safer and more effective treatment strategies based on ADHD neuropathological and physiological mechanisms.

Long Mu Qing Xin Mixture (LMQXM) is an empirical Chinese medicine formula for ADHD in children, consisting of radix astragal, radix angelicae sinensis, ramulus uncariae cum unciis, fructus jujubae, radix paeoniae alba, fructus schisandrae, radix scutellariae, cortex phellodendri, calcined dragon bone, calcined oyster shell, conch margaritifera usta, magnetitum, mix-fried licorice, light wheat, and caulis polygoni multiflori, which can tonify and replenish the heart

and spleen, nourish the heart and tranquilize the mind, and calm the liver and subdue yang. In a previous study, we used LMQXM to perform a small clinical randomized control study on 144 children with ADHD and found that LMQXM significantly improved abnormal behavior such as hyperactivity, inattention, impulsivity, and learning difficulties in patients, and the disease efficacy control rate was significantly better in the trial group than in the pediatric intelligence syrup control group (86.67% vs 50%, $p < 0.05$) (Chen and Xiao, 2016; Zhang and Jiang, 2016), which showed that LMQXM may be a potential new therapy to alleviate the symptoms of ADHD, but its targets of action and molecular mechanisms remain unclear. In addition, we also found that LMQXM improved learning and memory in ADHD model mice (Sun et al., 1991), so we hypothesized that LMQXM may exert therapeutic effects by acting on certain pathological processes in ADHD.

Network pharmacology can reflect the multi-component and multi-target characteristics of traditional Chinese medicine and has been widely used in traditional Chinese medicine research and advanced drug discovery (Xu et al., 2021). This study aimed to identify the key targets and pathways involved in LMQXM alleviating ADHD through network pharmacology and molecular docking and to conduct an animal experiment to verify the effect of LMQXM on behavioral performance in spontaneously hypertensive rats (SHRs). SHR is derived from an inbred strain of the Wistar-Kyoto (WKY) rat and exhibits similar etiological, pathological, biochemical, and symptomatological features to ADHD (Song et al., 2021). MPH increased attention and memory capacity and decreased impulsivity in SHRs (Leffa et al., 2019), and altered the expression of genes associated with impulse characteristics, such as nuclear receptor 4a2 (NR4A2), B-cell translocation gene 2 (Btg2), and Homer2 (Dela Peña et al., 2017), indicating that SHRs showed a positive response to neurostimulants and can better predict ADHD-related pathological mechanisms. SHR is considered a commonly used and well-studied animal model of ADHD because it exhibits behavioral disorders similar to ADHD in terms of hyperactivity, impulsivity, and learning disabilities, predicts molecular genetics and neuropathological mechanisms associated with ADHD, and responds to first-line ADHD therapeutic agents (Rahi and Kumar, 2021). Since ADHD is more common in boys than in girls, and male rats are superior to females in terms of surface validity (hyperactive/impulsive behavior), male SHRs are more suitable as an animal

model of ADHD (Bayless et al., 2015; Kozłowska et al., 2019). This study attempted to use male SHR as the ADHD animal model and WKY rats as the normal control to investigate the potential mechanisms of LMQXM for ADHD and explore the effects of LMQXM on behavioral performance and related factors in SHR. This is the first study of the behavioral effects of LMQXM on SHR and the potential molecular mechanisms for the treatment of ADHD, which will provide a research basis and new directions for experimental pharmacological studies in ADHD.

2 Materials and methods

2.1 Active ingredient screening and target prediction of LMQXM

Traditional Chinese Medicine Systems Pharmacology Database and Analysis Platform (TCMSP) (Zhang et al., 2019) (<https://tcmssp.com/tcmssp.php>) was used to screen LMQXM active ingredients and targets. ADME reference standards were as follows: oral bioavailability (OB) $\geq 30\%$, blood-brain barrier (BBB) permeability ≥ -0.3 , drug-like properties (DL) ≥ 0.18 (Yi et al., 2020). For ingredients not found in TCMSP, we used the ChemSrc database (<https://www.chemsrc.com/>) to query the CAS number of the compound, after which we used the PubChem database (Kim et al., 2021) (<https://pubchem.ncbi.nlm.nih.gov/>) to download the 2D molecular structure of the compound and uploaded them to SwissADME (<http://www.swissadme.ch/>), SwissTargetPrediction database (Daina et al., 2019) (<http://www.swisstargetprediction.ch>), and then based on standards of GI absorption (GIA) as “High”, BBB permeant as “YES”, DL had at least two meeting the criteria of “YES” and “*Homo sapiens*, Probability ≥ 0.12 ” to screen active ingredients and predict the corresponding targets (Han et al., 2020). Duplicate targets of the drugs were removed, and the final targets were imported into the Uniprot database (Yi et al., 2020) (<http://www.uniprot.org/>) for normalization.

2.2 Construction of Chinese medicine-active ingredient-target network

Cytoscape 3.7.2 (Otasek et al., 2019) was used to construct the Chinese medicine-active ingredient-target network to elucidate the relationship between Chinese medicine, active ingredients, and targets in LMQXM. Among them, “node” represented Chinese medicine, active ingredients, and targets, “edge” represented the inter-action relationship between each node of Chinese medicine, ingredients, and targets, and “degree” indicated the number of edges connected to them. The number of node degree values was positively correlated with the importance of nodes in the network.

2.3 Screening of the intersection targets of LMQXM and ADHD

DrugBank database (Wishart et al., 2006.) (<https://go.drugbank.com/>), GeneCards database (Rappaport et al., 2017) (<https://www.genecards.org/>), Therapeutic Target Database (TTD) (Wang et al., 2020a) (<http://db.idrblab.net/ttd/>), DisGeNET database (Piñero et al., 2020) (<https://www.disgenet.org/>) were used to screen ADHD-related targets, and the Uniprot database was used to normalize disease targets. LMQXM-related targets and ADHD-related targets were imported into Venny2.1.0 (<https://bioinfo.gp.cnb.csic.es/tools/venny/index.html>) to create Venn diagrams and screen intersection targets.

2.4 PPI network construction and core targets screening of LMQXM for ADHD

The intersection targets were uploaded to the STRING database (Szklarczyk et al., 2015) (<https://cn.string-db.org/>) to establish a protein-protein interaction (PPI) network for the treatment of ADHD with LMQXM. The “TSV” file of the PPI network was imported into Cytoscape 3.7.2 software for visualization processing. The Network Analyzer function was used to analyze the topological attributes of the PPI network and calculate the degree values, BC, and CC of each node. Targets above the median values of degree values, BC, and CC were selected as the core targets of LMQXM for ADHD (Li et al., 2022).

2.5 GO and KEGG pathway enrichment analysis

The core targets of LMQXM for ADHD were submitted to the Metascape platform (Zhou et al., 2019) for gene ontology (GO) and Kyoto encyclopedia of genes and genomes (KEGG) pathway enrichment analysis. GO enrichment analysis (Chen et al., 2017) is a bioinformatics program that covers biological processes, molecular functions, and cellular components. Biological processes involve the biological goals facilitated by genes or gene products; molecular functions are considered biochemical activities; cellular components refer to the parts of the cell where the gene product is active. KEGG (Chen et al., 2017) is a comprehensive knowledge base for functional interpretation and practical application of genomic information. Based on the species set as “*H. sapiens*”, $p < 0.01$, the core targets were subjected to GO and KEGG enrichment analysis. The results were visualized using the online platform for microbial information (<http://www.bioinformatics.com.cn/>).

2.6 Molecular docking

The core active ingredients were selected as ligands, and the 3D molecular structures (SDF format) of the compounds were downloaded from the PubChem database and converted to mol two format using OpenBabel 3.1.1. The core targets were used as the receptors, and the 3D structures (PDB format) of the targets were downloaded from the RCSB Protein Data Bank (PDB) database (Rose et al., 2020) (<https://www.rcsb.org/>). The selection of the target protein was based on the following principles (Yang et al., 2016): 1) human protein; 2) high resolution; 3) the original ligand

was preferred. PyMOL 2.4.1 (Mooers, 2020) was used to remove water molecules and original ligands from the core target protein. AutoDock 4.2.6 software (Goodsell et al., 2021) was used to hydrogenate the core target and convert it to pdbqt format, at the same time, the small molecule compound rotation bond was set and saved in pdbqt format. Molecular docking of core target proteins and small molecule compounds was performed using semi-flexible molecular docking, and the results were visualized with PyMOL software.

2.7 Animal experiment verification

The flow chart of the animal experimental study can be found in [Supplementary Figure S1](#).

2.7.1 Drug preparation

LMQXM (batch number: 2206001, HYZZ: Z05170218) was purchased from Longhua Hospital affiliated with the Shanghai University of Traditional Chinese Medicine. Preparation of medicinal solution was performed as follows: DLG, DML, ZZM, and CS were first decocted twice in distilled water of 5 times volume for 2 h each time, and then mixed with HQ, DG, GT, ZGC, DZ, FXM, BS, WWZ, YJT, HQIN, and HB. After being decocted two times, the filtrate was combined and concentrated into 4.17 g/ml crude herbal medicine by a rotary evaporator.

Methylphenidate hydrochloride sustained-release tablets (MPH, batch number: 1KE744) were provided by Xi'an Janssen Pharmaceutical Co, Ltd. A suspension was prepared with a concentration of 0.21 mg/ml with normal saline.

2.7.2 Component identification of LMQXM

One ml of LMQXM sample solution was diluted 2 times with 20% methanol, mixed well, and centrifuged at 12000 r/min for 5 min, after which the supernatant was extracted. The chemical composition of LMQXM was characterized by ultra-performance liquid chromatography-tandem quadrupole time-of-flight mass spectrometry (UPLC-Q-TOF-MS) in positive and negative ion modes. A total of 40 components were identified, including astragaloside, formononetin, baicalin, baicalein, rhynchophylline, isorhynchophylline, etc., which may be the material basis of LMQXM for the treatment of ADHD. The results of component identification and mass spectra are shown in [Supplementary Table S1](#), [Supplementary Figure S2](#).

2.7.3 Experimental animal

SPF grade 4-week-old male SHR (n = 30) and WKY rats (n = 6) were purchased from Beijing Weitong Lihua Experimental Animal Technology Co., Ltd (Beijing, China, SCXK (Jing) 2021-0006) and raised in the barrier environment of the Experimental Animal Center of Shanghai University of Traditional Chinese Medicine. All the animals were housed in an environment with a temperature of 23°C ± 2°C, relative humidity of 55% ± 5%, and a light/dark cycle of 12/12 h, and had free access to water and food. All rats received adaptive feeding for 1 week before drug administration. All animal studies (including the mice euthanasia procedure) were done in compliance with the regulations and guidelines of Shanghai University of Traditional Chinese Medicine institutional animal care and conducted according to the AAALAC and the IACUC guidelines (No. PZSHUTCM220711003).

2.7.4 Drug intervention

After 1 week of adaptive feeding, the rats will begin to receive treatment (5 weeks of age). The SHRs were divided into five groups according to the random number table: the model group (SHR), the methylphenidate hydrochloride group (MPH, 4.22 mg/kg), the LMQXM low dose group (LMQXM-LD, 5.28 ml/kg), the LMQXM medium dose group (LMQXM-MD, 10.56 ml/kg), and the LMQXM high dose group (LMQXM-HD, 21.12 ml/kg); WKY rats were used as a normal control group. The sample size of animals was determined by the resource equation method (Festing and Altman, 2002). The control and model groups were given normal saline by gavage, and the MPH and LMQXM groups were given corresponding drugs by gavage twice a day (8:00–9:00 a.m.; 14:00–15:00 p.m.) for 4 weeks, with a volume of 1 ml/100 g. Doses administered to rats were converted in parallel based on the body surface area of 9-year-old (26 kg body weight) children (0.991 m², Stevenson formula) and the body surface area of 4-week-old (60 g body mass) SHR pups (0.013947 m², Meeh-Rubner formula). Rats were weighed daily before gavage to determine the volume of the drug.

2.7.5 Behavioral tests

According to the previous behavioral testing methods, the open field test (OFT) was conducted at 0 and 4 weeks of treatment (at 5 and 9 weeks of age in rats) to evaluate the locomotor activity of rats, and the Morris Water Maze (MWM) test was performed after 3 weeks of treatment (at 8–9 weeks of age in rats) to evaluate the learning and memory abilities of the animals (Ding et al., 2017).

2.7.5.1 Open field test (OFT)

The experimental equipment consisted of a black open field test box (100 cm × 100 cm × 48 cm), a camera, and a computer. The rats were gently placed in the central area of the test box (50 cm × 50 cm area in the center of the test box), and a camera tracked the movement of each animal. Fiji Is Just ImageJ (Fiji) software was used to analyze the movement distance, speed, and time spent in the central area of the rats. The activity of each rat was observed for 5 min (Song et al., 2021; de Sousa Macedo et al., 2022). After the test, 75% alcohol was used to remove the odor.

2.7.5.2 Morris Water Maze (MWM) test

The MWM device consisted of a black round pool (150 cm in diameter and 50 cm in depth), a camera, and a computer tracking system (Ethovision XT). The pool was filled with water (23°C ± 2°C) and dyed with black ink to distinguish a rat inside the box more easily. The system software divided the water maze into four quadrants. The black round platform (12 cm in diameter) was located in the quadrant I and immersed about 1 cm below the water surface. White geometric figures of approximately 10 cm in size and differing shapes were set up on the inner wall of the pool above the horizontal plane as spatial references to help rats navigate spatially. The tests were conducted for 6 days. From day 1–5, rats were trained once a day and the time searching the escape platform was recorded; the maximum swim time was set to 60 s. If the mouse located the platform before 60 s had passed, it was immediately removed from the pool (this was recorded as escape latency). If the platform was not located after 60 s, the mouse was gently guided to the platform and allowed to re-orient to the distal visual cues for an additional 10 s before being removed from the pool. The sixth day was the probe trial, during which the platform was removed and the

TABLE 1 Antibody information.

Name	Item no.	Manufacturers	Genus	Dilution ratio
cAMP	A15653	abclonal	rab	1:200
PKA	ER1706-65	huabio	rab	1:200
DRD2	55084-1-AP	Proteintech	rab	1:500
DRD1	ET1703-45	huabio	rab	1:200

annulus visits and time spent in the target quadrant (s) within the 60 s were recorded by the Ethovision XT system.

2.7.6 Collection of prefrontal cortex and striatum samples

After the behavioral test, the rats were fasted for 12 h and anesthetized with Zoletil[®] (50 mg/kg). After decapitation of rats the PFC and striatum were quickly separated on the ice surface with a glass minute needle. The samples were quickly frozen in liquid nitrogen and stored at -80°C .

2.7.7 High performance liquid chromatography mass spectrometry (LC-MS)

UltiMate 3000 RS chromatograph and TSQ Quantum triple quadrupole mass spectrometer were used to analyze DA levels in the PFC and striatum. Chromatographic conditions were as follows: the chromatographic column was Welch Ultimate XB-C8 (150 mm \times 4.6 mm, 5 μm), the mobile phase consisted of pump A (0.1% formic acid aqueous solution) and pump B (0.1% formic acid acetonitrile), the gradient of the mobile phase was 0 min, 90% A-10% B; 2 min, 5%A-95%B; 4 min, 5%A-95%B; 4 min, 90%A-10%B; 5 min, and 90%A-10% B. The flow rate was 0.8 ml/min, the column temperature was 40°C , and the injection volume was 2 μL . Mass spectrometry conditions were as follows: an ion source, electrospray ionization source; scan mode, positive and negative ion switching scan; detection mode, selected reaction monitoring; electrospray voltage (Spray Voltage) (+) 4000 V capillary temperature (Source Temperature), 350°C ; atomization temperature (Vaporizer Temperature): 500°C ; collision gas, high-purity argon (purity $\geq 99.999\%$); sheath gas (Sheath Gas Pressure), nitrogen (purity $\geq 99.999\%$), 65Arb; auxiliary gas (Aux Gas Pressure), nitrogen (purity $\geq 99.999\%$), 20Arb; data acquisition time, 5min.

2.7.8 Enzyme-linked immunosorbent assay (ELISA)

The Rat ELISA kit (item number ER9351M) was purchased from BIOTHEC WELL (Shanghai, China), and cAMP concentration levels in the PFC and striatum were measured according to the protocol provided by the manufacturer.

2.7.9 Immunohistochemistry

Three rats were randomly selected from each group, and the PFC and striatum were fixed with 4% paraformaldehyde, then embedded in paraffin and cut into 3–4 μm thick sections. After antigen repair, samples were treated with 3% H_2O_2 (to block endogenous peroxidase activity) and serum/BSA, and then incubated with primary antibody (see Table 1 for corresponding antibody information) at 4°C overnight. Samples were then washed and incubated with a secondary antibody (HRP-labeled goat anti-rabbit

TABLE 2 qPCR primer sequences.

Gene name	—	Primer sequences
PKA (189 bp)	Upstream	CCGAACCTTGGACCTTGTGTGG
	Downstream	CGCACCTTCCCAGAGACGATT
DRD1 (125 bp)	Upstream	GTGCTCTACGGCGTCCATTC
	Downstream	CTACGCTAATCAGGATGAAGGCT
DRD2 (290 bp)	Upstream	AACCCTGACAGTCCTGCCAAA
	Downstream	CATGTGAAGGCGCTGTAGAGGA
Rat-GAPDH (138 bp)	Upstream	CTGGAGAAACCTGCCAAGTATG
	Downstream	GGTGAAGAATGGGAGTTGCT

IgG, 1:200 dilution, room temperature, 50 min) for 2 h at room temperature. Then DAB color development (positive expression is brownish yellow), hematoxylin re-staining of cell nuclei (3 min), and dehydration and sealing of the sections were performed. The sections were scanned under a microscope to observe the expression of dopamine D1 and D2 receptor (DRD1 and DRD2), cyclic adenosine monophosphate (cAMP), and protein kinase A (PKA). Image-Pro Plus 6.0 software was used to analyze related indicators' mean optical density value (MOD).

2.7.10 Fluorescent quantitative PCR analysis

The primer sequences are shown in Table 2. Total mRNA was extracted from the prefrontal and striatum using Trizol, and RNA concentration and purity were detected at 260 and 280 nm by ultramicro spectrophotometer (Piñero et al., 2020). RT first strand cDNA synthesis kit was used to reverse transcribe RNA to cDNA. The following conditions were applied: 25°C for 5 min, 42°C for 30 min, and 85°C for 5 s. PCR amplification conditions were: 95°C for the 30 s, 95°C for 15s, 60°C for 30 s, 40 cycles. Fluorescence quantitative PCR instrument (Bio-rad) output the experimental results, while $2^{-\Delta\Delta\text{Ct}}$ algorithm was used to analyze the relative expression of PFC and striatal PKA, DRD1, and DRD2 mRNA.

2.8 Statistical analysis

Data were analyzed using SPSS 25.0 software, and the measurement data were expressed as mean \pm standard deviation. One-way analysis of variance (ANOVA) was used for comparison between groups, and LSD and Dunet's method were used for multiple comparisons. A two-way ANOVA was used to analyze data sets involving treatments and time points. $p < 0.05$ indicated statistically significant differences. Graphs were plotted using GraphPad Prism 8.0 software.

3 Results

3.1 Active ingredient screening and target prediction of LMQXM

The number of active ingredients and targets of LMQXM were shown in Table 3. We eliminated duplicate compounds and

TABLE 3 The number of active ingredients and related targets of LMQXM.

Chinese medicine	Chinese name	Active ingredient	Target
Radix Astragail	Huangqi (HQ)	12	67
Radix Angelicae Sinensis	Danggui (DG)	2	50
Ramulus Uncariae cum Uncis	Gouteng (GT)	27	76
Fructus jujubae	Dazao (DZ)	18	84
Radix Paeoniae Alba	Baishao (BS)	3	36
Fructus Schisandrae	Wuweizi (WWZ)	8	16
Radix Scutellariae	Huangqin (HQIN)	27	116
Cortex Phellodendri	Huangbai (HB)	27	87
Calcined Os Draconis	Duan-Longgu (DLG)	32	107
Calcined Concha Ostreae	Duan-Muli (DML)	6	34
Conch Margartifera Usta	Zhenzhumu (ZZM)	18	20
Magnetitum	Cishi (CS)	8	48
Honey-fijed Licorice	Zhigancao (ZGC)	18	40
Tritici Levis	Fuxiaomai (FXM)	49	69
Caulis Polygoni Multiflori	Shouwuteng (SWT)	22	138

targets and filtered compounds without target information, resulting in 177 active ingredients and 355 corresponding targets. The information on related active ingredients was shown in [Supplementary Table S2](#). The shared ingredients of LMQXM such as mairin, beta-sitosterol, stigmasterol, rhynchophylline, hirsutine, berberine, fumarine, coptisine, and palmatine may be the key ingredients through which LMQXM exerts therapeutic effect ([Table 4](#)).

3.2 Construction of the Chinese medicine-active ingredient-target network

We imported the created “network” and “type” files into Cytoscape 3.7.2 to construct a Chinese medicine-active ingredient-target network ([Figure 1](#)). The results revealed that the network contained 547 nodes (15 Chinese medicine nodes, 177 ingredient nodes, and 355 target nodes) and 2,729 edges. The “Analyze Network” function was used to calculate the degree of each node in the network. The top ranked ingredients in degree were beta-sitosterol (B1, degree = 215), stigmasterol (B2, degree = 124), rhynchophylline (C2, degree = 113), fumarine (E2, degree = 46), wogonin (HQIN2, degree = 43), 7-O-methylisomucronulatol (HQ5, degree = 40), hirsutine (C3, degree = 39), baicalein (HQIN4, degree = 35), and formononetin (HQ8, degree = 35), which may be the core components of LMQXM, while PTGS2 (degree = 86), PTGS1 (degree = 76), SCN5A (degree = 73), AR (degree = 66), ADRA1B (degree = 54), ADRB2 (degree = 52), CHRM1 (degree = 51), KCNH2 (degree = 46), CHRM3 (degree = 46), and OPRM1 (degree = 42) may be the potential targets of LMQXM.

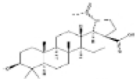
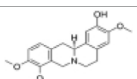
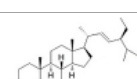
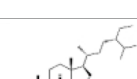
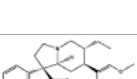
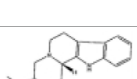

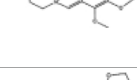
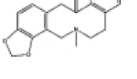
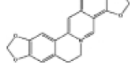
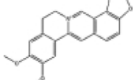
3.3 Intersection targets of LMQXM and ADHD

A total of 1543 targets relevant to ADHD were obtained from the disease databases, which included 179 targets from the DrugBank database, 873 targets from the GeneCards database (the median score >14.73 was set as the screening condition), 41 targets from TTD, and 967 targets from the DisGeNET database (Score >0.8). A Venn diagram was used to generate 121 intersection targets related to LMQXM and ADHD ([Figure 2](#)). These included SCN5A, CHRM3, CHRM1, SLC6A2, HTR3A, ADRB2, DRD1, DRD2, KCNH2, HTR2A, etc. These targets had higher degree values in the Chinese medicine-active ingredient-target network, and hence may be potential active targets of LMQXM for ADHD.

3.4 PPI network and core targets screening of LMQXM for ADHD

We uploaded the intersection targets to the STRING database and excluded the free node HRH2 and EBP. The PPI network was then generated with 119 nodes and 1019 edges with an average node degree value of 17 ([Figure 3A](#)). The PPI network “TSV” file was downloaded and imported into Cytoscape 3.7.2 to generate the core target visualization PPI network ([Figure 3B](#)). “Analyze Network” topology analysis indicated that the median degree was 15, the median of BC (Betweenness Centrality) was 0.0040, and the median of CC (Closeness Centrality) was 0.4683.46 target proteins with degree >15, BC > 0.0040, and CC > 0.4683 were screened out to generate the core targets for possible involvement of LMQXM in the treatment of ADHD ([Table 5](#)).

TABLE 4 Detailed information of shared active ingredients derived from LMQXM.

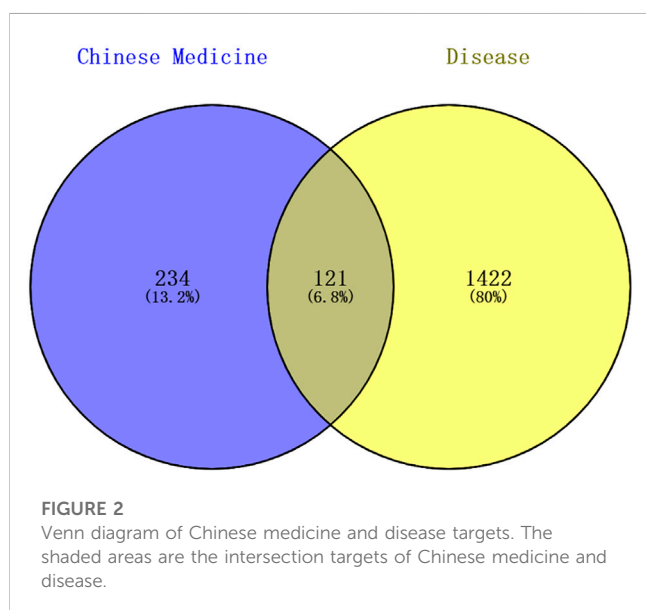
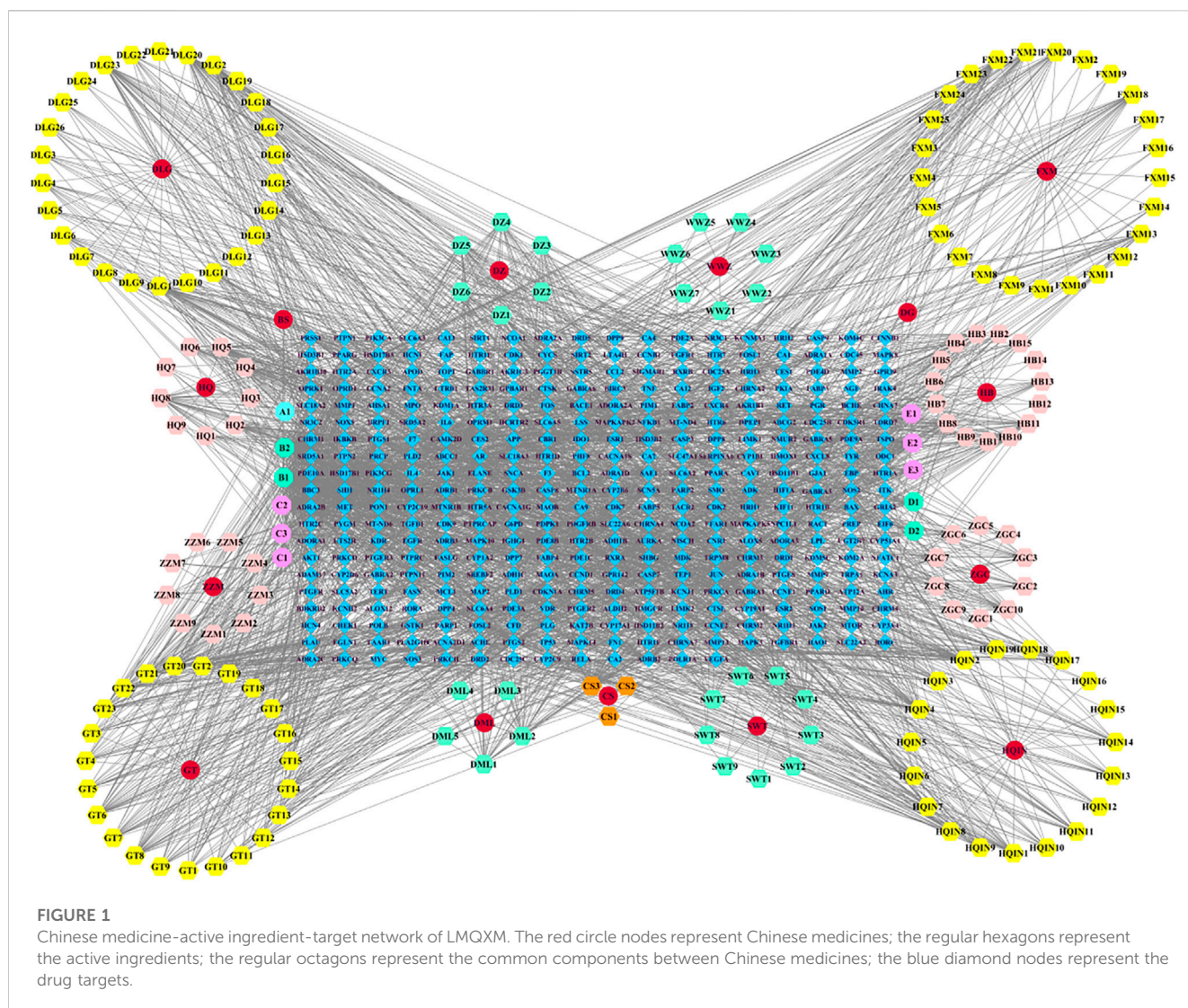
Mol ID/CAS	Number	Mol name	Mol structure	Mol formula	OB/GIA	BBB	DL	Related Chinese medicine
MOL000211	A1	Mairin		C ₃₀ H ₄₈ O ₃	55.38	0.22	0.78	HQ, DZ, BS
MOL000358	B1	Beta-sitosterol		C ₂₉ H ₅₀ O	36.91	0.99	0.75	DG, GT, DZ, BS, HQIN, HB
MOL000449	B2	Stigmasterol		C ₂₉ H ₄₈ O	43.83	1	0.76	DG, DZ, HQIN, HB
MOL000359	C1	Sitosterol		C ₂₉ H ₅₀ O	36.91	0.87	0.75	GT, BS, HQIN
MOL008469	C2	Rhynchophylline		C ₂₂ H ₂₈ N ₂ O ₄	41.82	0.38	0.57	GT, SWT
MOL008487	C3	Hirsutine		C ₂₂ H ₂₈ N ₂ O ₃	34.44	0.78	0.43	GT, SWT
MOL001454	E1	Berberine		C ₂₀ H ₁₈ NO ₄ ⁺	36.86	0.57	0.78	DZ, HB
MOL000787	E2	Fumarine		C ₂₀ H ₁₉ NO ₅	59.26	-0.13	0.83	DZ, HB
MOL001458	D2	Coptisine		C ₁₉ H ₁₄ NO ₄ ⁺	30.67	0.32	0.86	HQIN, HB
MOL002897	D1	Epiberberine		C ₂₀ H ₁₈ NO ₄ ⁺	43.09	0.4	0.78	HQIN, FXM
MOL000785	E3	Palmatine		C ₂₁ H ₂₂ NO ₄ ⁺	64.6	0.37	0.65	HB, SWT

3.5 Potential mechanism of LMQXM for ADHD

3.5.1 GO enrichment analysis

GO enrichment analysis was performed on 46 core targets using the Metascape platform. A total of 1102 items were obtained ($p < 0.01$) and included 922 items for biological process, 73 items for cell composition, and 107 items for molecular function. The top 20 most significant items were selected for visual analysis based on the LogP value (Figure 4A).

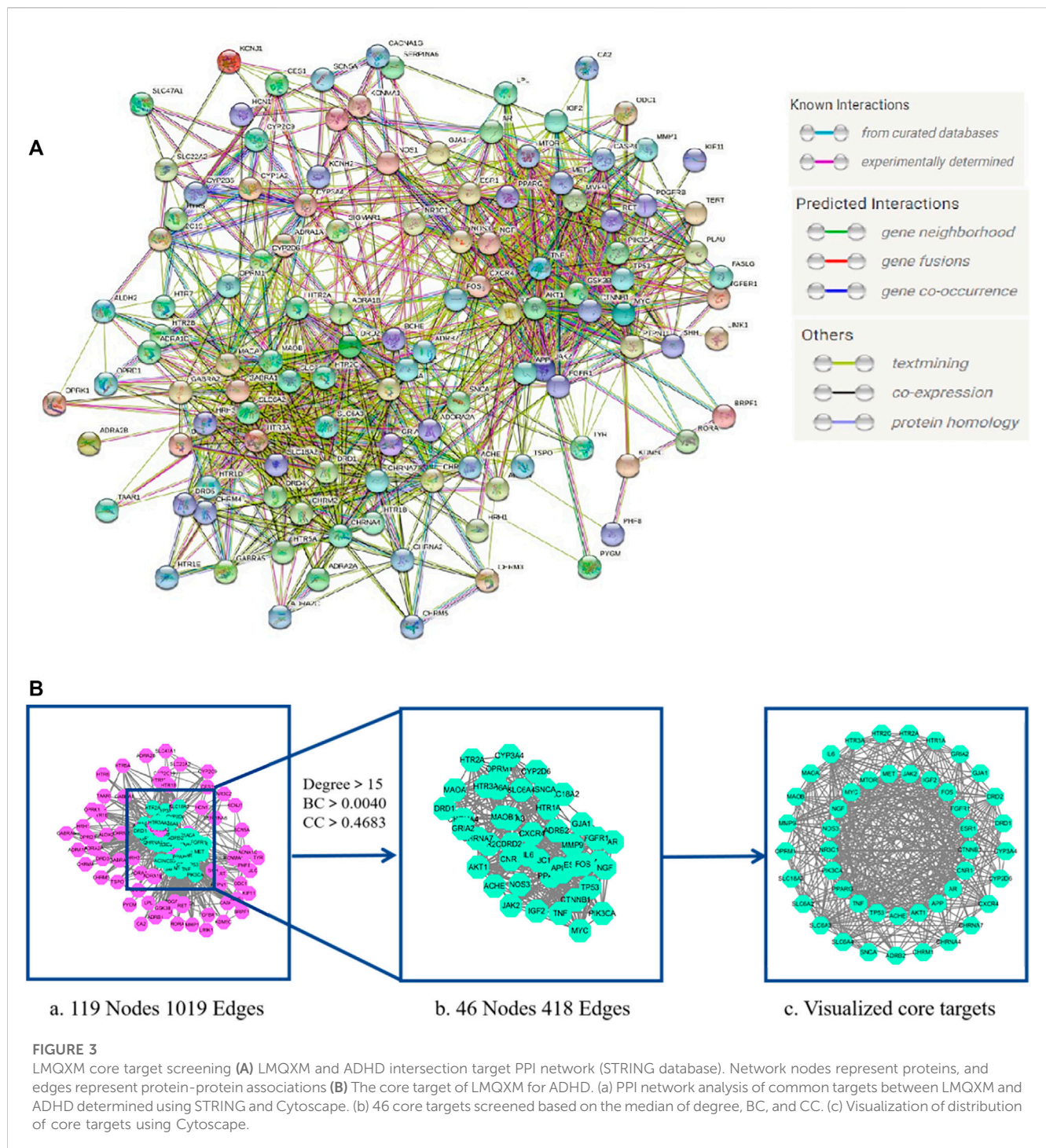
The results showed that the involved biological process was mainly cellular responses to nitrogen compounds, cellular response to organonitrogen compounds, synaptic signaling, chemical synaptic transmission, and anterograde trans-synaptic signaling. Cell composition was primarily related to the synaptic membrane, postsynapse, membrane raft, membrane microdomain, and postsynaptic membrane. Molecular function was mainly involved in neurotransmitter receptor activity, amine binding, serotonin binding, monoamine transmembrane transporter activity, and sodium: chloride



symporter activity. These findings suggested that the mechanism of action of LMQXM for the treatment of ADHD was the result of multiple synergistic effects of multiple molecular biological processes.

3.5.2 KEGG pathway enrichment analysis

To further explore the signaling pathways associated with LMQXM for ADHD, we used Metascape to identify signaling pathways enriched among the 46 core targets. A total of 134 signaling pathways were screened by KEGG pathway enrichment analysis, and some of the potential pathways related to ADHD are summarized in the (Supplementary Table S3). Based on LogP, we used the most significant top 30 pathways enriched by KEGG to generate a bubble map (Figure 4B). Based on the data and literature, enrichment of serotonergic synapse, neuroactive ligand-receptor interaction, calcium signaling pathway, dopaminergic synapse, cAMP signaling pathway, human cytomegalovirus infection, Alzheimer's disease, MAPK signaling pathway, and pathways of neurodegeneration may be how LMQXM acts on ADHD, among which dopaminergic synapses and cAMP signaling pathway are the perspective directions for the



current study of neurotransmitter transmission pathways regulating ADHD.

3.6 Molecular docking simulation

To further determine the regulatory effect of LMQXM active ingredients on target proteins, we screened beta-sitosterol,

stigmasterol, rhynchophylline, baicalein, formononetin, yohimbine, berberine, and palmatine active ingredients as ligands, and SLC6A4, IL-6, TNF, NGF, MAOA, MAOB, DRD1, DRD2 and HTR2A targets as receptors for molecular docking simulation based on the current status of ADHD research. Molecular docking results showed that the above 8 active ingredients could spontaneously bind to the nine targets in the natural state. The lower the binding energy, the more stable the conformation of the active ingredient binding to

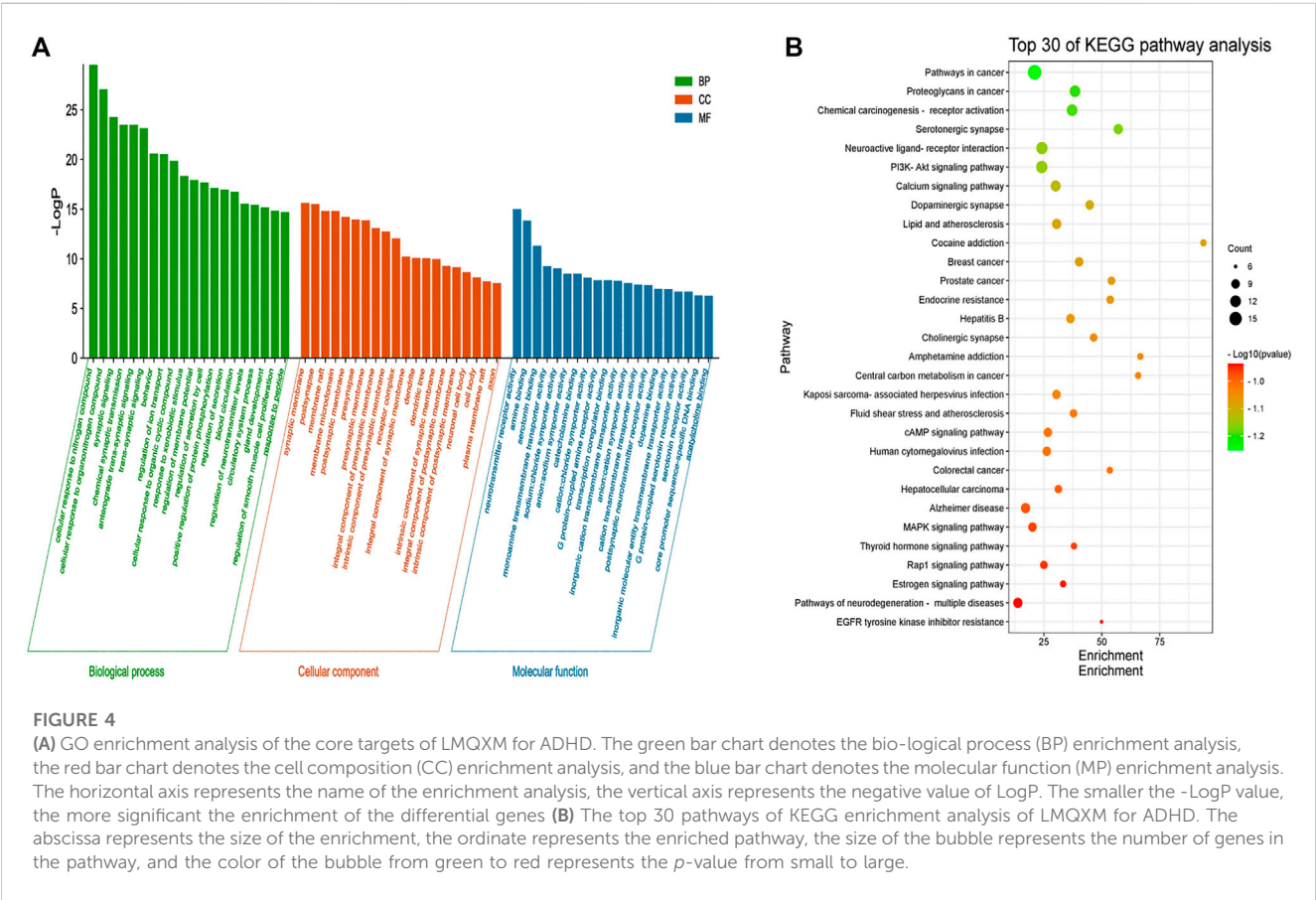
TABLE 5 The core targets of LMQXM for ADHD.

Number	Target	Description	BC	CC	Degree
1	SLC6A4	Sodium-dependent serotonin transporter	0.0750	0.6020	49
2	AKT1	RAC-alpha serine/threonine-protein kinase	0.0701	0.6146	47
3	SLC6A3	Sodium-dependent dopamine transporter	0.0633	0.5990	46
4	IL-6	Interleukin-6	0.0463	0.6020	44
5	CTNNB1	Catenin beta-1	0.0457	0.5784	41
6	FOS	Protein c-Fos	0.0506	0.5900	41
7	TP53	Cellular tumor antigen p53	0.0402	0.5413	40
8	TNF	Tumor necrosis factor	0.0165	0.5514	39
9	ESR1	Estrogen receptor	0.0270	0.5700	37
10	MYC	Myc proto-oncogene protein	0.0244	0.5488	36
11	SLC6A2	Sodium-dependent noradrenaline transporter	0.0457	0.5244	36
12	NGF	Beta-nerve growth factor	0.0149	0.5540	33
13	MAOA	Amine oxidase [flavin-containing] A	0.0141	0.5198	33
14	CHRNA4	Neuronal acetylcholine receptor subunit alpha-4	0.0206	0.5198	33
15	MAOB	Amine oxidase [flavin-containing] B	0.0151	0.5315	32
16	MTOR	Serine/threonine-protein kinase mTOR	0.0107	0.5086	30
17	CXCR4	C-X-C chemokine receptor type 4	0.0216	0.5413	30
18	DRD2	D 2) dopamine receptor	0.0254	0.5592	30
19	MMP9	Matrix metalloproteinase-9	0.0116	0.4979	29
20	HTR3A	5-hydroxytryptamine receptor 3A	0.0189	0.5364	29
21	NR3C1	Glucocorticoid receptor	0.0276	0.5592	28
22	CNR1	Cannabinoid receptor 1	0.0298	0.5438	28
23	MET	Hepatocyte growth factor receptor	0.0057	0.5021	27
24	CHRNA7	Neuronal acetylcholine receptor subunit alpha-7	0.0214	0.5244	27
25	HTR1A	5-hydroxytryptamine receptor 1A	0.0301	0.5514	27
26	HTR2A	5-hydroxytryptamine receptor 2A	0.0120	0.5438	26
27	PPARG	Peroxisome proliferator-activated receptor gamma	0.0046	0.5108	25
28	NOS3	Nitric oxide synthase	0.0147	0.5153	25
29	APP	Amyloid-beta precursor protein	0.0101	0.5315	25
30	CYP3A4	Cytochrome P450 3A4	0.0292	0.5268	24
31	SLC18A2	Synaptic vesicular amine transporter	0.0070	0.4777	24
32	ACHE	Acetylcholinesterase	0.0162	0.5291	24
33	PIK3CA	Phosphatidylinositol 4,5-bisphosphate 3-kinase catalytic subunit alpha isoform	0.0041	0.4701	22
34	HTR2C	5-hydroxytryptamine receptor 2C	0.0119	0.5130	22
35	DRD1	D (1A) dopamine receptor	0.0063	0.5021	21
36	FGFR1	Fibroblast growth factor receptor 1	0.0095	0.5021	21
37	IGF2	Insulin-like growth factor II	0.0060	0.4758	21
38	AR	Androgen receptor	0.0080	0.4876	21

(Continued on following page)

TABLE 5 (Continued) The core targets of LMQXM for ADHD.

Number	Target	Description	BC	CC	Degree
39	CYP2D6	Cytochrome P450 2D6	0.0165	0.5108	21
40	JAK2	Tyrosine-protein kinase JAK2	0.0082	0.5021	21
41	CHRM1	Muscarinic acetylcholine receptor M1	0.0154	0.4917	21
42	GRIA2	Glutamate receptor 2	0.0136	0.5175	20
43	ADRB2	Beta-2 adrenergic receptor	0.0109	0.5198	18
44	SNCA	Alpha-synuclein	0.0072	0.5064	18
45	OPRM1	Mu-type opioid receptor	0.0076	0.5021	16
46	GJA1	Gap junction alpha-1 protein	0.0138	0.4816	16



the target (Wei et al., 2020). Except for beta-sitosterol-MAOB and baicalein-NGF, the absolute value of the binding energy of all ligands and receptors were lower than 5 KJ/mol. The other active ingredients had high binding energy to targets, indicating that their docking results were good (Table 6). For example, beta-sitosterol was connected to the amino acid residues LYS-11 and ASP-10 of TNF through two hydrogen bonds (both with a bond length of 2.3 Å) to form a relatively stable conformation (binding energy = -20.13 kJ/mol, Figure 5A); rhynchophyllin stably bound to TRP-128 and LEU-66 amino acid residues of SLC6A4 by forming two hydrogen bonds (bond lengths are 2.4 Å and 2.0 Å, respectively) (binding

energy = -18.95 KJ/mol, Figure 5C); formononetin formed three hydrogen bonds with the amino acid residues ASP-330, ARG-360, and LYS-363 of MAOA (the bond lengths were 2.1 Å, 2.1 Å, and 2.5 Å, respectively), these resulted in a more stable docking (binding en-ergy = -14.90, Figure 5E). Palmatine also formed three hydrogen bonds with amino acid residues ASN-396 and SER-409 of DRD2 (bond lengths are 1.8 Å, 2.7 Å, and 2.1 Å, respectively) for stable binding (binding energy = -14.81, Figure 5H). Our findings further proved that the above 8 compounds could be the most critical core active ingredients of LMQXM for ADHD, with mechanisms of action involving multiple processes such as neuroinflammation and

TABLE 6 The binding energy of key active ingredients docked with target molecules.

Active ingredient	Target protein	PDB ID	Amino acid residue	Binding energy (KJ/mol)
Beta-sitosterol	SLC6A4	6VRH	TYR212, PHE213	−14.10
	IL6	1ALU	YLS-27	−14.48
	TNF	2AZ5	LYS-11, ASP-10	−20.13
	NGF	4EDW	—	−15.06
	MAOA	2Z5Y	ARG-369, LEU-364	−3.14
	MAOB	1S3E	GLN-216	−16.23
	DRD1	7JVP	LYS-339	−14.98
	DRD2	6CM4	—	−15.23
	HTR2A	7CW8	SER-115, TRP-200	−8.54
Stigmasterol	SLC6A4	6VRH	ARG-464	−16.90
	IL6	1ALU	LYS-27	−16.86
	TNF	2AZ5	TYR-151	−20.63
	NGF	4EDW	THR-205, SER-203	−16.40
	MAOA	2Z5Y	LYS-370	−12.84
	MAOB	1S3E	GLU-243	−20.00
	DRD1	7JVP	SER-145, THR-149	−13.72
	DRD2	6CM4	—	−24.02
	HTR2A	7CW8	HIS-70	−8.83
Rhynchophyllin	SLC6A4	6VRH	TRP-128, LEU-66	−18.95
	IL6	1ALU	ARG-30	−16.86
	TNF	2AZ5	LYS-65, PHE-144	−15.65
	NGF	4EDW	GLY-18	−13.47
	MAOA	2Z5Y	HIS-365	−8.28
	MAOB	1S3E	ARG-100	−13.56
	DRD1	7JVP	LYS-29	−10.96
	DRD2	6CM4	TRP-90	−12.22
	HTR2A	7CW8	LYS-195, LYS-191	−10.25
Baicalein	SLC6A4	6VRH	ASP-247, LEU-245, LEU-248	−12.01
	IL6	1ALU	ARG-182	−14.39
	TNF	2AZ5	GLN-47, ASP-45	−16.44
	NGF	4EDW	SER-115	−4.64
	MAOA	2Z5Y	—	−6.69
	MAOB	1S3E	LYS-81	−14.48
	DRD1	7JVP	ASP-310, GLU-89	−10.13
	DRD2	6CM4	VAL-49	−10.25
	HTR2A	7CW8	LYS-104	−10.33
Formononetin	SLC6A4	6VRH	LEU-248	−15.48
	IL6	1ALU	SRG-30, LYS-27, ARG-182	−17.03

(Continued on following page)

TABLE 6 (Continued) The binding energy of key active ingredients docked with target molecules.

Active ingredient	Target protein	PDB ID	Amino acid residue	Binding energy (KJ/mol)
	TNF	2AZ5	GLN-27, ASP-45, ASN-30	−17.32
	NGF	4EDW	VAL-121, ASP-208	−12.22
	MAOA	2Z5Y	ASP-330, ARG-360, LYS-363	−14.90
	MAOB	1S3E	SER-200	−14.52
	DRD1	7JVP	ASP-323	−10.92
	DRD2	6CM4	—	−10.67
	HTR2A	7CW8	ASN-354, GLU-355, ASP-356	−11.42
Yohimbine	SLC6A4	6VRH	TRY-46, ARG-117	−17.28
	IL6	1ALU	ARG-182, GLN-183	−18.87
	TNF	2AZ5	SER-147, ALA-145	−21.25
	NGF	4EDW	VAL-121, LYS-209	−15.98
	MAOA	2Z5Y	GLU-399	−19.66
	MAOB	1S3E	LYS-302	−20.33
	DRD1	7JVP	CYS-307	−15.02
	DRD2	6CM4	VAL-406, TYR-37	−15.15
	HTR2A	7CW8	LYS-104, ASN-384	−13.97
Berberine	SLC6A4	6VRH	GLN-194	−13.14
	IL6	1ALU	ARG-30, ARG-182	−13.68
	TNF	2AZ5	GLN-125	−15.52
	NGF	4EDW	LYS-13	−11.34
	MAOA	2Z5Y	VAL-244	−13.43
	MAOB	1S3E	ARG-38	−15.77
	DRD1	7JVP	LUE-11	−7.87
	DRD2	6CM4	THR-42	−11.63
	HTR2A	7CW8	LYS-1032	−12.51
Palmitate	SLC6A4	6VRH	ASN-211, ASN-217	−10.63
	IL6	1ALU	LYS-27	−13.26
	TNF	2AZ5	LYS-98	−17.24
	NGF	4EDW	SER-115	−5.06
	MAOA	2Z5Y	HIS-263	−8.12
	MAOB	1S3E	MET-280	−13.01
	DRD1	7JVP	SER-31, HIS-266	−9.96
	DRD2	6CM4	ASN-396, SER-409	−14.81
	HTR2A	7CW8	LYS-320, GLU-1004	−10.84

neurotransmitter dysregulation (Saedisomeolia et al., 2018). For the neurotransmitter dysregulation hypothesis, the cAMP signaling pathway, as a classical signaling pathway downstream of DA, plays an important role in regulating DA content in the brain through the activation of key targets DRD1 and DRD2 (Zhou et al., 2017). Part of the molecular docking model diagram is shown in Figure 5.

3.7 Animal experiments

3.7.1 Effect of LMQXM on weight of experimental rats

As shown in Table 7, LMQXM did not affect the weight gain of rats.

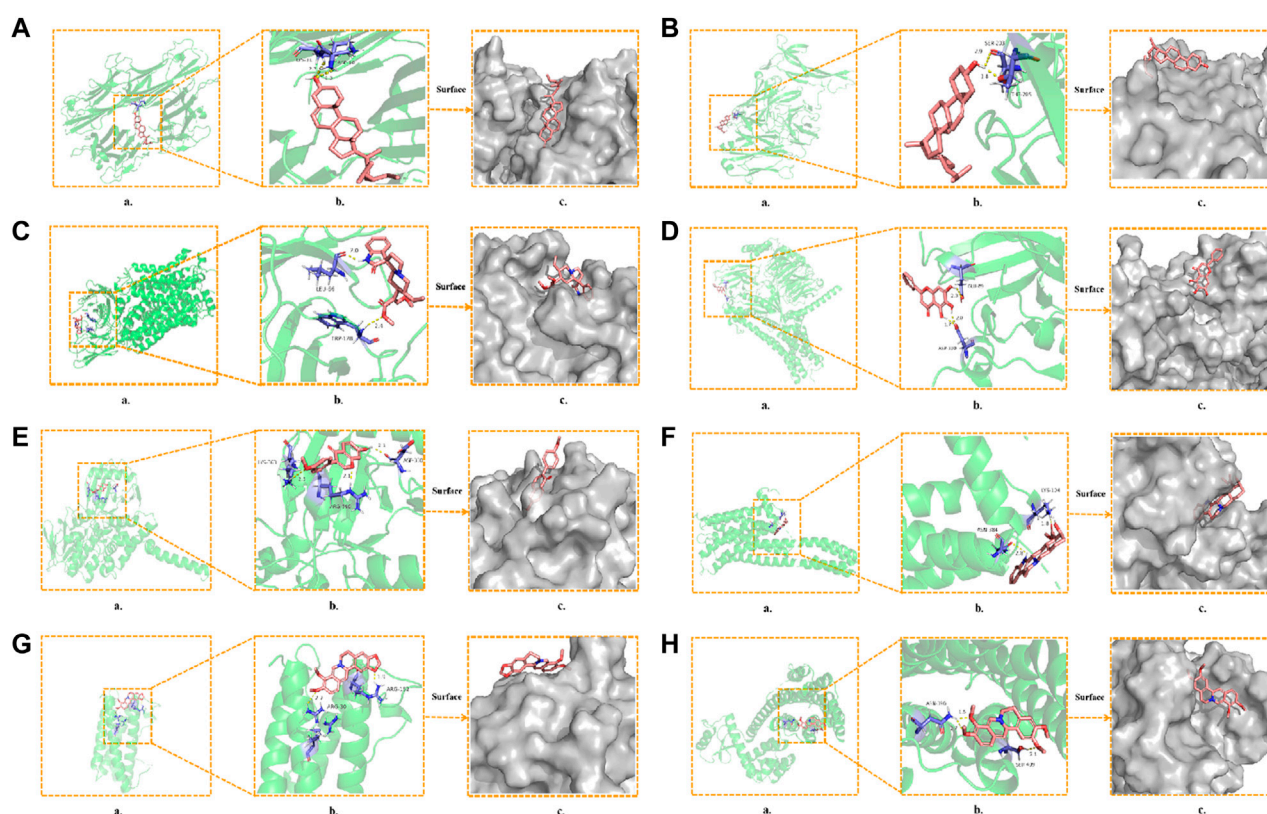


FIGURE 5

Molecular docking model diagram (A) Beta-sitosterol—TNF (B) Stigmasterol—NGF (C) Rhynchophyllin—SLC6A4 (D) Baicalein—DRD1 (E) Formononetin—MAOA (F) Yohim-bine—HTR2A (G) Berberine—IL6 (H) Palmatine—DRD2. (a) Molecular docking model, the red represents the 3D structure of the component ligand, the green represents the 3D structure of the target receptor, and the blue represents the amino acid residues (b) In the enlarged structure of the docking site, the yellow represents the hydrogen bond formed between the ligand and the amino acid residue, and the number represents the bond length (c) Combination diagram of the surface structure of the target receptor and the component ligand, the red represents the 3D structure of the ligand, and the gray represents the receptor surface structure.

TABLE 7 Changes in weight of rats in each group.

Group	0 week (g)	1 week (g)	2 weeks (g)	4 weeks (g)
WKY	90.28 ± 3.28	135.57 ± 3.90	189.98 ± 9.79	223.68 ± 11.30
SHR	93.65 ± 4.40	142.65 ± 5.42	191.92 ± 4.47	228.15 ± 3.47
MPH	87.38 ± 7.52	131.62 ± 5.97	180.38 ± 5.96	219.70 ± 8.19
LMQXM-LD	89.90 ± 4.39	136.08 ± 10.34	175.62 ± 12.00	224.22 ± 14.05
LMQXM-MD	85.65 ± 4.78	127.05 ± 7.92	185.68 ± 11.26	221.67 ± 13.05
LMQXM-HD	88.90 ± 5.27	136.22 ± 7.22	187.87 ± 8.92	230.37 ± 12.05

3.7.2 Effect of LMQXM on the rats' behavior based on OFT

The OFT was used to assess the effects of LMQXM on rats' locomotor activity, which was evaluated by the total moving distance, average speed, and the relative proportion of time spent in the center vs periphery. The data showed that before treatment, the SHR, MPH, LMQXM-LD, LMQXM-MD, and LMQXM-HD groups had significantly more total moving

distance and average speed compared with the WKY group ($p < 0.0001$, Figures 6A, B). There was no significant difference in the proportion of time spent in the center vs periphery at baseline levels in the WKY, SHR, MPH, LMQXM-LD, LMQXM-MD, and LMQXM-HD groups (Figure 6C).

After 4 weeks of drug intervention, SHRs still exhibited significantly higher total moving distance and average speed

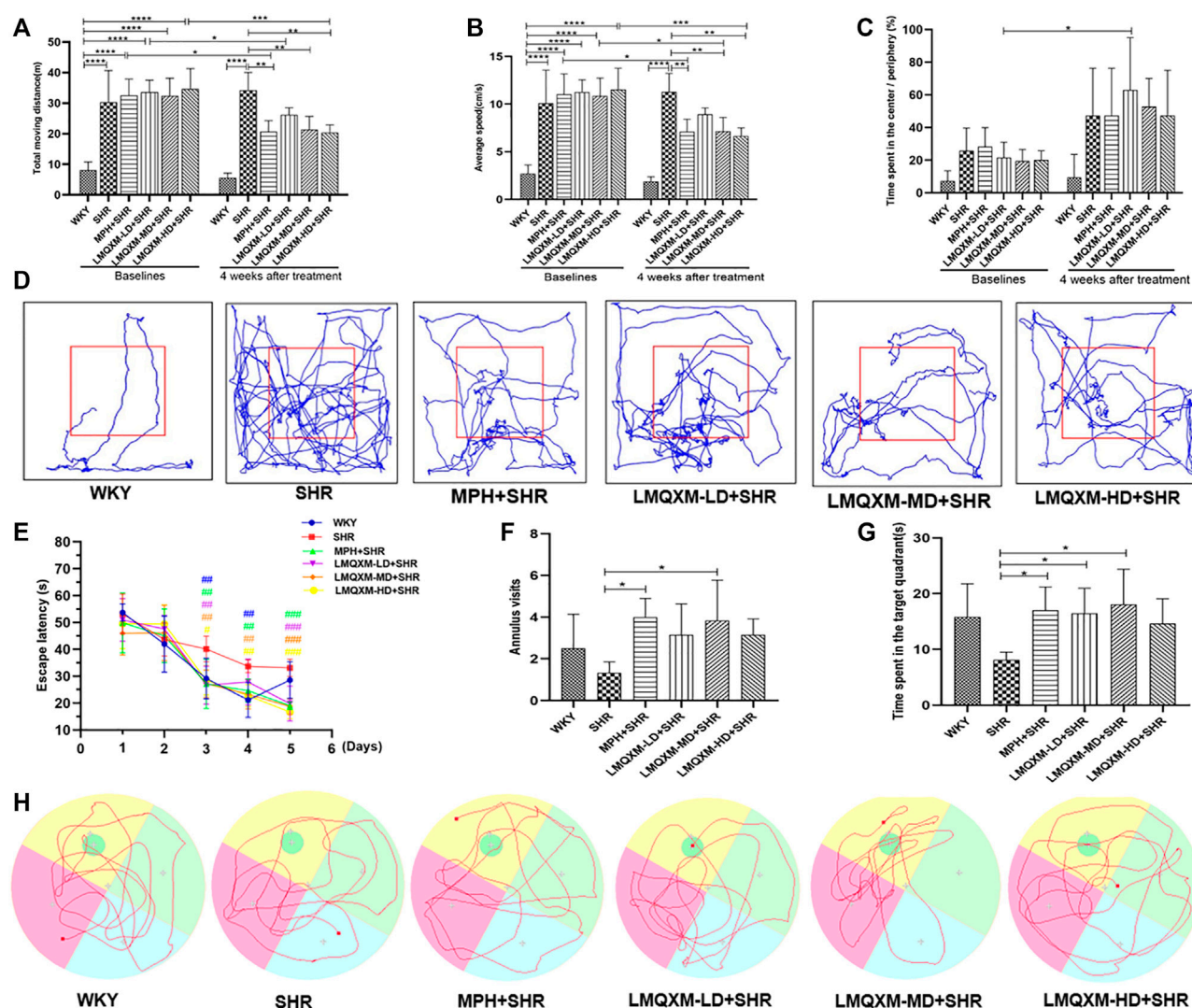


FIGURE 6

Behavioral performance of rats in each group in OFT and MWM tests (A) Moving distance in OFT (B) Average speed in OFT (C) Time spent in the center/Periphery in OFT (D) Representative trajectories of each group of rats in OFT (E) Escape latency in MWM test (F) Number of annulus visits in MWM test (G) Time spent in the target quadrant in MWM test (H) Representative trajectories of each group in MWM test. All data are presented as mean \pm SD, $n = 6$ for each group. * $p < 0.05$, ** $p < 0.01$, *** $p < 0.001$, **** $p < 0.0001$. # $p < 0.05$, ## $p < 0.01$, ### $p < 0.001$ vs SHR.

compared with WKY rats ($p < 0.0001$, Figures 6A,B), whereas total moving distance and average speed were significantly lower in the MPH, LMQXM-MD, and LMQXM-HD groups compared with the SHR group ($p < 0.01$, Figures 6A, B). Moreover, there was also a significant decrease in total moving distance and average speed in the MPH, LMQXM-MD, and LMQXM-HD groups compared with baseline levels after 4 weeks of treatment ($p < 0.05$, Figures 6A, B). After treatment, there was still no significant difference in the proportion of time spent in the center vs periphery in the WKY, SHR, MPH, LMQXM-LD, LMQXM-MD, and LMQXM-HD groups, while this ratio increased in the LMQXM-LD group after treatment compared with the baseline level ($p < 0.05$, Figure 6C). The representative movement paths of each group after administration are shown in Figure 6D.

3.7.3 Effect of LMQXM on the rats' behavior based on the MWM tests

From the third day, the escape latencies of the MPH, LMQXM-LD, LMQXM-MD, and LMQXM-HD groups were significantly shorter than those of the SHR group. WKY rats also had significantly lower escape latencies on days 3 and 4 than SHRs ($p < 0.01$, Figure 6E). In the probe trials, although the annulus visits appeared to increase in the four treatment groups compared with the SHR group, only the MPH and LMQXM-MD groups had significant differences vs the SHR group ($p < 0.05$, Figure 6F). In addition, the MPH, LMQXM-LD, and LMQXM-MD groups also spent more time in the target quadrant than the SHR group ($p < 0.05$, Figure 6G). However, there was no significant difference in the annulus visits and time spent in the target quadrant between WKY rats and SHRs in probe trials (Figures

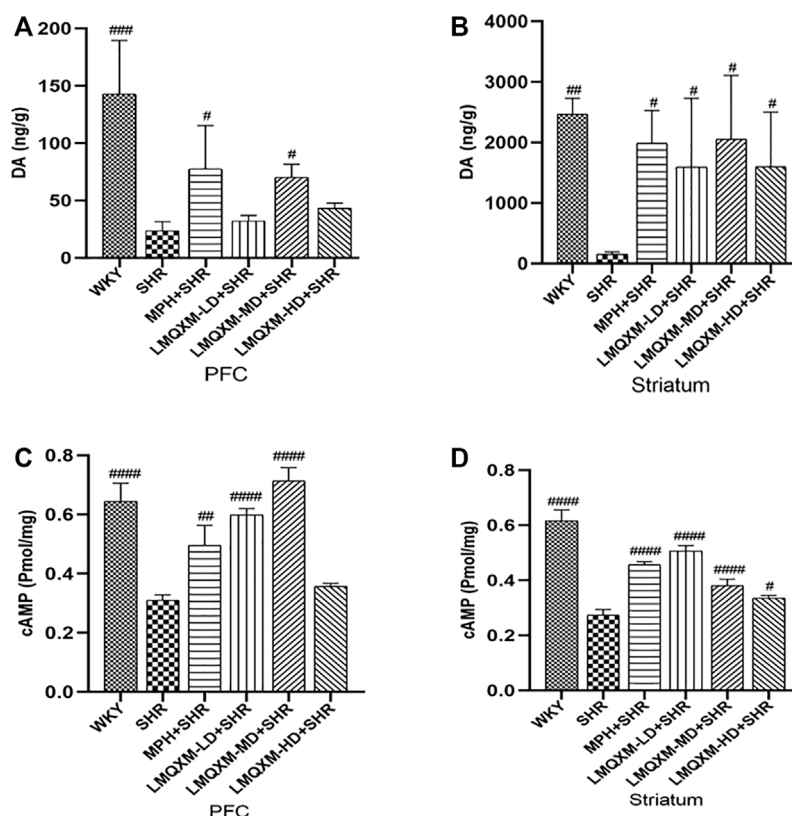


FIGURE 7

DA and cAMP levels in PFC and striatum for each group of rats (A). DA levels in PFC (B). DA levels in P striatum (C). cAMP levels in PFC (D). cAMP levels striatum. All data are presented as mean \pm SD, $n = 3$ for each group. * $p < 0.05$, ** $p < 0.01$, *** $p < 0.001$ vs SHR.

6F, G). The representative trajectories of each group are shown in Figure 6H.

3.7.4 Effect of LMQXM on DA and cAMP levels in PFC and striatum

DA is an important neurotransmitter in the brain that regulates movement, learning, and memory. cAMP is an important intracellular second messenger produced by DA GPCRs acting on adenylate cyclase (AC) to hydrolyze ATP. LC-MC and ELISA were used to detect DA and cAMP levels in brain tissue, respectively (Wang et al., 2019; Yu et al., 2022). The levels of DA and cAMP in the PFC and striatum were significantly lower in SHRs compared with WKY rats ($p < 0.01$, Figures 7A–D). After treatment, DA and cAMP levels in the PFC and striatum were significantly increased in the MPH and LMQXM-MD groups compared with the SHR group ($p < 0.05$, Figures 7A–D); meanwhile, LMQXM-HD upregulated DA and cAMP levels in the striatum of SHRs, while LMQXM-LD upregulated DA levels in the striatum and cAMP levels in the PFC of SHRs ($p < 0.05$, Figures 7B–D).

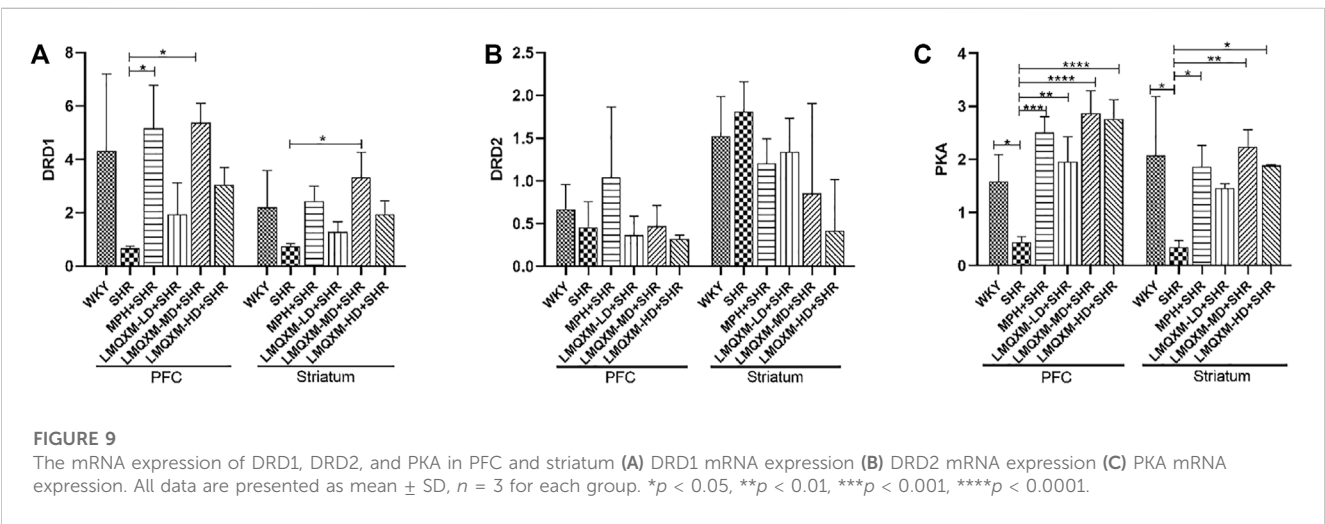
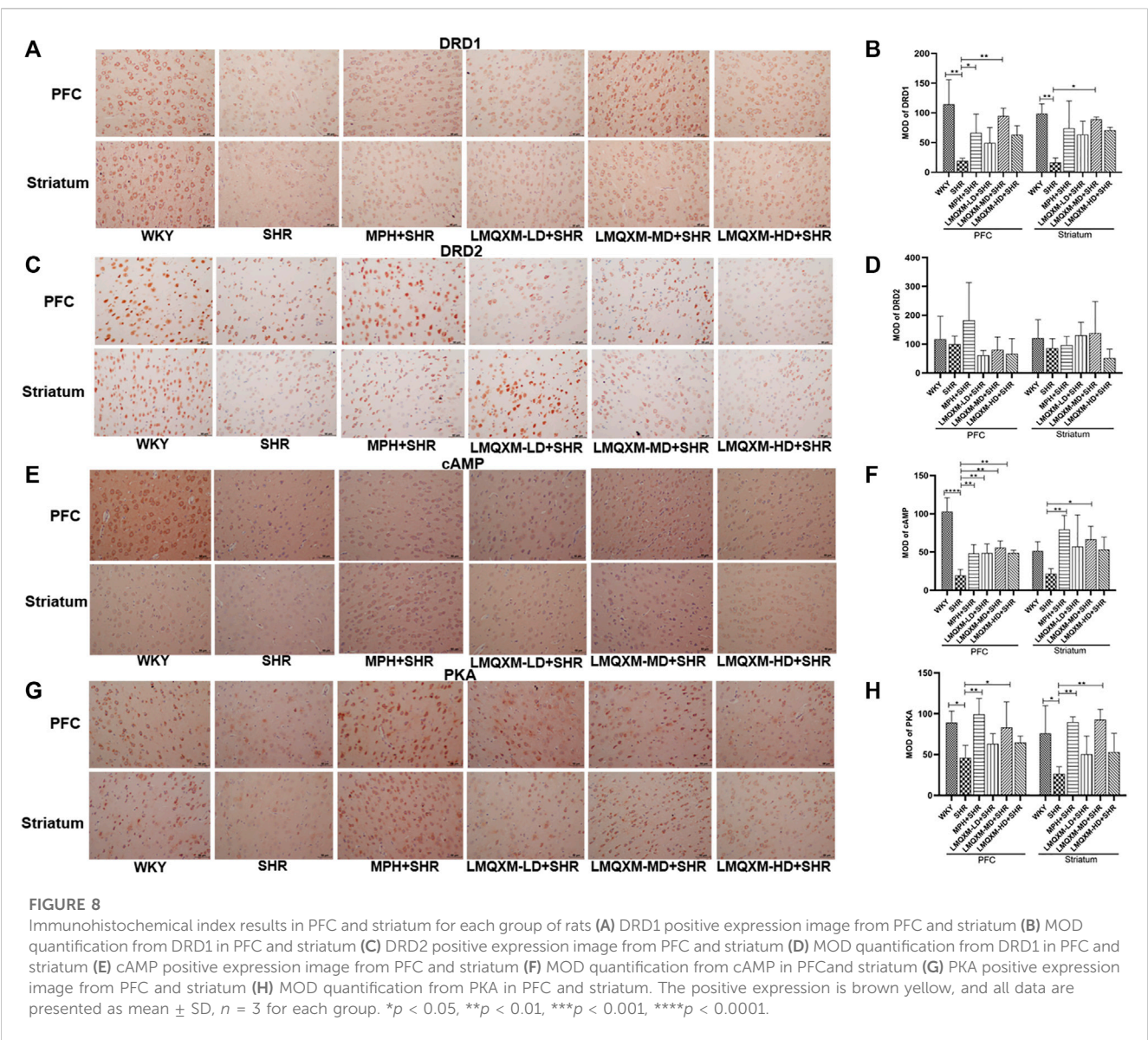
3.7.5 Effect of LMQXM on MOD of DRD1, DRD2, cAMP, and PKA in PFC and striatum

cAMP and PKA are DA downstream effectors that can have opposite effects on the cAMP/PKA signaling pathway when DA is coupled to DRD1 and DRD2, with an increase in cAMP most consistent with an increase in DRD1 activity or a decrease in DRD2 (Schmidt et al., 1998). They are also generally expressed in different

populations of striatal medium spiny neurons (direct vs indirect pathways) and cortical cells. To assess the effect of LMQXM in regulating the cAMP/PKA signaling pathway, immunohistochemistry was used to assess the MOD of DRD1, DRD2, cAMP, and PKA in the PFC and striatum. As shown in Figure 8, we observed lower expression of brownish-yellow positive cells for DRD1, cAMP, and PKA in the PFC and striatum of SHRs than in WKY rats (Figures 8A, B, E–H). MPH and LMQXM-MD administration significantly reversed the MOD of cAMP and PKA in the PFC and striatum of SHRs ($p < 0.05$, Figures 8E–H). Furthermore, MPH also upregulated the MOD of DRD1 in the PFC of SHRs, and LMQXM-MD upregulated the MOD of DRD1 in the PFC and striatum of SHRs ($p < 0.05$, Figures 8A, B). Interestingly, we also observed that LMQXM-LD and LMQXM-HD significantly upregulated the MOD of cAMP in the PFC of SHRs ($p < 0.01$, Figures 8E, F). However, we did not find significant differences in the expression of DRD2-positive cells in the PFC and striatum of SHRs and WKY rats, nor did MPH and LMQXM administration have significant effects on the MOD expression of DRD2 in the PFC and striatum of SHRs.

3.7.6 Effect of LMQXM on DRD1, DRD2, and PKA mRNA in PFC and striatum

To further evaluate the regulatory effect of LMQXM on the cAMP/PKA signaling pathway, qPCR was used to assess DRD1, DRD2, and PKA mRNA expression in the PFC and striatum. As



shown in Figure 9, there was a trend toward reduced DRD1 mRNA expression in the PFC and striatum in the SHR group compared with the WKY group, but there was no statistical difference (Figure 9A). DRD1 mRNA expression was significantly increased in the PFC of the MPH and LMQXM-MD groups compared with the SHR group, and DRD1 mRNA expression was also significantly increased in the striatum of the LMQXM-MD group ($p < 0.05$, Figure 9A). As for the expression of DRD2 mRNA, there was no significant difference between each group for either the PFC or striatum (Figure 9B). The expression of PKA mRNA in the PFC and striatum of SHRs was significantly lower than that of WKY rats ($p < 0.05$, Figure 9C). Compared with the SHR group, PKA mRNA expression in the PFC and striatum was significantly increased in the MPH, LMQXM-MD, and LMQXM-HD groups, whereas the expression of PKA mRNA was elevated in the LMQXM-LD group only in the PFC ($p < 0.05$ Figure 9C).

4 Discussion

Although MPH can effectively alleviate the symptoms of ADHD, it is often associated with certain adverse effects, including growth restriction, sleep disturbances, and cardiac effects (Espadas et al., 2018; Liang et al., 2018). In addition, its treatment compliance is suboptimal (Ishizuya et al., 2021), so it is necessary to find effective and suitable therapeutic regimens for pediatric use. In this study, we used network pharmacology and molecular docking to predict the potential mechanisms of LMQXM for the treatment of ADHD and performed animal experiments to validate the role of LMQXM on the behavioral performance of ADHD model rats and the mechanisms of the cAMP/PKA signaling pathway, which provide new insights and a basis for clinical treatment and pharmacological studies of ADHD.

The degree to which top ranking components in network pharmacology, such as beta-sitosterol, stigmasterol, rhynchophylline, hirsutine, baicalein, and formononetin, have been shown to have potential advantages for the treatment of neurological disorders, consistent with the composition identified by UPLC-Q-TOF-MS. Beta-sitosterol has neuroprotective, anxiolytic, sedative, immunomodulatory, and anti-inflammatory effects (Panayotis et al., 2021), which allowed it to reduce inhibitory stress in the PFC and dentate and contextual fear memory of mice (Zahiruddin et al., 2020) and increase the levels of brain-derived neurotrophic factor (BDNF) in the hippocampus, all of which are beneficial for improving cognitive, learning and memory functions (Alzoubi et al., 2017). According to recent research, stigmasterol has anxiolytic and anticonvulsant properties *via* the positive regulation of γ -aminobutyric acid receptors, and is thus considered a new candidate steroid drug for the treatment of neurological diseases (Karim et al., 2021). Animal experiments have shown that stigmasterol could increase swimming time in the target quadrant of vanadium-induced BALB/c mice in the MWM test, resulting in improved neurocognitive and motor function (Adebiyi et al., 2018). Rhynchophylline, the main indole alkaloid isolated from GT, can pass through the blood-brain barrier relatively quickly and effectively regulate calcium and potassium channels to exert a protective effect on the nervous system (Geetha and Ramachandran, 2021). Rhynchophylline has been shown to activate the cAMP signaling pathway and MAPK/NF- κ B signaling pathway to exert

neurotransmitter modulation, anti-inflammatory, antioxidant, sedative, anti-Alzheimer's disease, and anti-drug addiction effects (Geetha and Ramachandran, 2021; Qin et al., 2021). Furthermore, it can effectively rescue the spatial learning and memory deficits of rats in MWM tests and prevent and repair synaptic plasticity damage (Yang et al., 2018). Other ingredients such as berberine, hirsutine, and palmatine can also improve cognition and learning through neuroprotective effects (Sadeghnia et al., 2017; Wang et al., 2020b; Kushida et al., 2021). Baicalein has been shown to regulate motor ability and learning and memory function in ADHD model rats to improve the core symptoms of ADHD (Zhou et al., 2017).

PPI networks and topological property functions identified possible core targets for LMQXM treatment of ADHD, mainly involving the dopaminergic system (such as DRD1, DRD2, SLC6A3, MAOA, and MAOB), noradrenergic system (such as SLC6A2), and serotonergic system (such as SLC6A4, HTR1B, HTR1A, HTR2A, HTR3A, and HTR2C), whose mechanisms of action are closely related to the transmission of monoamine neurotransmitters, most of which have been classified as risk genes for ADHD (Lasky-Su et al., 2008; Banaschewski et al., 2010). The methylation status of SLC6A4 has been shown to be significantly associated with hyperactive and impulsive symptoms in ADHD (Park et al., 2015). DRD1 and DRD2 may contribute to the improvement of working memory and cognitive function in children with ADHD (Trampush et al., 2014). SLC6A3, the gene encoding DAT, is associated with the development of several psychiatric disorders, and deletion of this gene can cause mice to exhibit hyperactive and impulsive-like symptoms; therefore, DAT knockout mice are also frequently used as a classical animal model for studying ADHD (Salatino-Oliveira et al., 2018). Moreover, targets related to neuronal plasticity in ADHD (such as CHRNA4, CHRNA7, NGF, FOS, and MTOR) and targets related to neuroinflammation (such as IL-6, TNF, and MMP9) were also identified. The higher degree values of AKT1, TP53, ESR1, and MYC make them promising potential targets for LMQXM in the treatment of ADHD, but no studies have clearly shown their relevance to the pathogenesis of ADHD. AKT1 is involved in chronic neuroinflammation (Xiang et al., 2016), and TP53 has been shown to be associated with DA neuronal deformation (Kamath et al., 2022), so future studies should perhaps focus on their value in ADHD neuroinflammation and DA neuronal damage.

The most promising pathways for LMQXM treatment of ADHD, according to GO and KEGG pathway enrichment analysis, are serotonergic synapse, neuroactive ligand-receptor interaction, the PI3K-Akt signaling pathway, the calcium signaling pathway, dopaminergic synapse, the cAMP signaling pathway, Alzheimer disease, the MAPK signaling pathway, and so on. It is worth mentioning that dopaminergic synapses and the cAMP signaling pathway are the classical signaling pathways in ADHD, and they are also the current hot directions for studying neurotransmitter dysregulation in ADHD.

Dopamine deficiency or dysregulation of dopaminergic synaptic transmission mediates behavioral abnormalities or memory deficits in ADHD (Yan and Rein, 2022). cAMP is a DA downstream effector that mediates chemical or physiological responses produced by a variety of intracellular neurotransmitters (Zaccolo et al., 2021), and its expression is regulated by the opposite effects of DRD1 and DRD2. DRD1 activates adenylate cyclase (AC) by coupling to Gas and G α olf subtypes of the G protein α subunit, catalyzing ATP

hydrolysis to induce cAMP production (Rangel Barajas et al., 2015), which further acts on PKA regulatory subunits to promote phosphorylation of a range of substrates, thereby regulating the expression of neurotransmitters and neurotrophic factors in the brain (Jichao et al., 2017). DRD2 inhibits AC activity and negatively regulates cAMP production by coupling to G α i/o of the G protein α subunit (Thomas Broome et al., 2020). The cAMP/PKA signaling pathway may feedback affect the stabilization of DA content in brain tissue through the synergistic effect of DRD1 and DRD2. In the molecular docking, we found that the core components of LMQXM all bound well to DRD1 and DRD2. To investigate the effect of the cAMP/PKA signaling pathway on DA levels and behavioral disorders in ADHD model rats, we observed the possible mechanism of LMQXM action through animal experiments.

In this study, we used SHR as the animal model of ADHD. SHR presents symptoms similar to ADHD between 4 and 10 weeks of age, and is currently the most widely studied animal model of ADHD, whereas WKY rats are often used as natural controls (Rahi and Kumar, 2021). We found that LMQXM does not affect rats' weight gain, suggesting the drug's safety. OFT and MWM tests were used to assess the effects of LMQXM on the behavioral performance of experimental rats, including activity and learning and memory (Yuan et al., 2019). Consistent with previous studies, SHRs exhibited significantly increased total moving distance and average speed, which represent typical symptoms of hyperactivity. After treatment, the total moving distance and average speed were significantly lower in the MPH, LMQXM-MD, and LMQXM-HD groups vs the SHR group, indicating that MPH, medium and high doses of LMQXM effectively improved hyperactive behavior in SHRs. There was no significant difference between the WKY and SHR groups in the ratio of time spent in the center to time spent in the periphery, and no significant change after treatment, suggesting no difference in anxiety levels between the two. It has been suggested that WKY rats often show depressive and anxious behaviors in behavioral tests (Nam et al., 2014), but our results showed that WKY rats did not show significant anxiety compared to SHR rats. In the future, SD rats should be added as controls to compare the anxiety status of the three. The WKY, MPH, LMQXM-LD, LMQXM-MD, and LMQXM-HD groups showed significantly shorter escape latency from day 3 compared with the SHR group, indicating the learning and memory deficit in SHRs that could be reversed by MPH and LMQXM. In addition, the annulus visits and time spent in the target quadrant were significantly higher in the MPH and LMQXM-MD groups compared to the SHR group, suggesting that MPH and LMQXM-MD are more advantageous for improving learning and memory in SHRs. In conclusion, MPH and LMQXM-MD were most effective in reversing behavioral disorders in SHRs, while LMQXM-HD only improved hyperactivity performance, which provides a basis for LMQXM to improve the core symptoms of ADHD as well as dose reference.

The PFC receives projections from midbrain DA neurons, which in turn project to other DAergic regions such as the striatum, resulting in a complex neuromodulatory system that is critical for many motor, cognitive, and motivational processes (Chau et al., 2018; Adrover et al., 2020), which is a key region for studying behavioral cognitive disorders. The synthesis and release of DA in the PFC or striatum are regulated bidirectionally by the

cAMP/PKA signaling pathway (Nishi et al., 2008), a key pathway that mediates DA transmission and thus performs motor, learning, and memory functions (Nishi and Snyder, 2010). Studies have shown that the cAMP/PKA signaling pathway is closely related to the formation of DA defects in ADHD. The short chain portion of DRD2 activated by DA in the synaptic gap can inhibit the cAMP/PKA signaling pathway, which in turn feedbacks to suppress DA synthesis and reduce the rate of DA synthesis, ultimately leading to the DA-deficient state in the brain (Zhou et al., 2017). DAT-CI mice have hyperactive symptoms, and amphetamine enhances striatal DAergic neurotransmission and inhibits paradoxical movements in DAT-CI mice by a mechanism related to DRD1/cAMP/PKA/DARPP32 pathway activation (Napolitano et al., 2010). In addition, a significant DRD1/DRD2 imbalance was found in the brain tissue of SHRs, and the cAMP/PKA signaling pathway was in a downregulated state; tomoxetine (a non-neuroleptic stimulant for ADHD) or Jingning granules (an herbal prescription) rescued the DRD1/DRD2 imbalance by activating the cAMP/PKA signaling pathway, thereby improving behavioral and cognitive function in SHRs (Ding et al., 2022). In the present study, we measured the expression of DA, cAMP, DRD1, DRD2, and PKA in rat PFC and striatum. The DA levels in the PFC and striatum were significantly lower in SHRs compared with WKY rats, indicating that DA deficiency is the main mechanism of behavioral disorders in SHRs, which is consistent with previous reports in the literature. After treatment, the levels of DA in the PFC and striatum were significantly higher in the MPH and LMQXM-MD groups compared with the SHR group, indicating that MPH and LMQXM-MD rescued the behavioral disorder of SHRs by elevating the levels of DA in the PFC and striatum. In addition, LMQXM-LD and LMQXM-HD upregulated DA levels in the striatum of SHRs but had no significant effect on DA levels in the PFC, considering that this may be closely related to the relatively sparse distribution of DA neurons in the PFC, the low number of uptake sites, and the high DA turnover rate (Goto et al., 2007).

As previously described, the cAMP/PKA signaling pathway is subject to opposite regulation by DRD1 and DRD2, which in turn affects DA production in a feedback manner. In the present study, we found that SHRs had significantly lower cAMP levels and cAMP-positive cell expression in the PFC and striatum than WKY rats, suggesting that the SHRs' brain tissue cAMP pathway may be in a downregulated state, resulting in the DA-deficient state. Simultaneously, the expression of PKA and DRD1 brown yellow-stained particles, as well as PKA mRNA, was significantly downregulated in the PFC and striatum of SHRs, indicating that inactivation of DRD1 and the cAMP/PKA signaling pathway in SHRs resulted in behavioral manifestations similar to those of ADHD. MPH and LMQXM-MD increased the cAMP level and positive cell expression of SHRs in the PFC and striatum and upregulated the expression of PKA and DRD1 positive cells and mRNA in the PFC and striatum of SHRs, but had no significant effect on DRD2. In addition, LMQXM-LD and LMQXM-HD also upregulated striatal cAMP levels, cAMP-positive cell expression in the PFC, and PKA mRNA expression in the PFC of SHRs, indicating that LMQXM activates the cAMP/PKA signaling pathway mainly through activation of DRD1, which in turn elevates DA levels in the PFC and striatum, thereby alleviating SHRs' hyperactivity and learning and memory deficits, which is consistent with a model

in which SHRs exhibit a DRD1/AC/cAMP/PKA signaling defect that can be rescued with MPH or LMQXM without significant effects on D2-expressing cells.

Our study initially predicted the potential mechanism of LMQXM for the treatment of ADHD and verified through animal experiments that LMQXM mainly acts on DRD1 to regulate the cAMP/PKA signaling pathway to increase DA levels in the PFC and striatum to control the behavioral disorders of SHRs and is most effective at medium doses. Low and high doses were not as effective as medium doses, and we believed that this mixture has complex components, more targets, different affinity effects, and is affected by factors such as intestinal epithelial absorption rate and blood-brain barrier passage rate, thus producing different effects from medium doses.

Our study has some limitations: firstly, the sample size of the animal experiment was low due to the limitation of experimental funding, which may have some bias on the expression of the results; secondly, although WKY rats are often used as natural controls for SHRs, the addition of SD rats as a control would make the results more convincing; finally, the study did not conduct the DAT, the target of first-line drugs for the treatment of ADHD, to in-depth study was not conducted to compare with MPH to further reveal the mechanism of DA neurotransmission. In future studies, we will further expand the sample size, add SD rats as a control, further investigate the effect of LMQXM on the behavioral performance of SHRs and the effect of DAT, and focus on the possible role of DRD2. In addition, the role of ADHD neuroinflammation will also be a key direction for future research.

In conclusion, our study provided a preliminary explanation the centrality of DA deficiency in the pathogenesis of ADHD and that the specific binding of DA and DRD1 elevates DA levels in the PFC and striatum by activating the cAMP/PKA signaling pathway, which may be an effective way to improve the core symptoms of ADHD.

Data availability statement

The datasets presented in this study can be found in online repositories. The names of the repository/repositories and accession number(s) can be found in the article [Supplementary Material](#).

Ethics statement

The animal study was reviewed and approved by PZSHUTCM220711003.

References

- Adebiyi, O. E., Olopade, J. O., and Olayemi, F. O. (2018). Sodium metavanadate induced cognitive decline, behavioral impairments, oxidative stress and down regulation of myelin basic protein in mice hippocampus: Ameliorative roles of β -spinasterol, and stigmasterol. *Brain Behav.* 8 (7), e01014. doi:10.1002/brb3.1014
- Adrover, M. F., Shin, J. H., Quiroz, C., Ferré, S., Lemos, J. C., and Alvarez, V. A. (2020). Prefrontal cortex-driven dopamine signals in the striatum show unique spatial and pharmacological properties. *J. Neurosci.* 40 (39), 7510–7522. doi:10.1523/JNEUROSCI.1327-20.2020
- Alzoubi, K. H., Rawashdeh, N. Q., Khabour, O. F., El-Elmat, T., Albataineh, H., Al-Zghool, H. M., et al. (2017). Evaluation of the effect of moringa peregrina extract on

Author contributions

XL completed most of the experiments and wrote the manuscript; WP assisted with some of the experiments; SW and YZ supported several experiments; ZJ and ZX supervised the study and revised the manuscript. All authors contributed to the article and approved the submitted version.

Funding

This study was funded by the Shanghai “13th Five-Year Plan” Clinical Key Specialty TCM Pediatrics Project (shslczdk04102) and the Shanghai Three-Year Action Plan to Further Accelerate the Development of Chinese Medicine Inheritance and Innovation (2021-2023) Project (ZY (2021-2023)-0206-01).

Acknowledgments

The authors would like to thank all the reviewers who participated in the review and ZJ and ZX's strong support for ADHD research.

Conflict of interest

The authors declare that the research was conducted in the absence of any commercial or financial relationships that could be construed as a potential conflict of interest.

Publisher's note

All claims expressed in this article are solely those of the authors and do not necessarily represent those of their affiliated organizations, or those of the publisher, the editors and the reviewers. Any product that may be evaluated in this article, or claim that may be made by its manufacturer, is not guaranteed or endorsed by the publisher.

Supplementary material

The Supplementary Material for this article can be found online at: <https://www.frontiersin.org/articles/10.3389/fphar.2023.1144907/full#supplementary-material>

learning and memory: Role of oxidative stress. *J. Mol. Neurosci.* 63 (3-4), 355–363. doi:10.1007/s12031-017-0986-x

Banaschewski, T., Becker, K., Döpfner, M., Holtmann, M., Rösler, M., and Romanos, M. (2017). Attention-deficit/hyperactivity disorder. *Dtsch. Arztebl Int.* 114 (9), 149–159. doi:10.3238/arztebl.2017.0149

Banaschewski, T., Becker, K., Scherag, S., Franke, B., and Coghill, D. (2010). Molecular genetics of attention-deficit/hyperactivity disorder: An overview. *Eur. Child. Adolesc. Psychiatry* 19 (3), 237–257. doi:10.1007/s00787-010-0090-z

Bayless, D. W., Perez, M. C., and Daniel, J. M. (2015). Comparison of the validity of the use of the spontaneously hypertensive rat as a model of attention deficit

- hyperactivity disorder in males and females. *Behav. Brain Res.* 286, 85–92. doi:10.1016/j.bbr.2015.02.029
- Carbray, J. A. (2018). Attention-deficit/hyperactivity disorder in children and adolescents. *J. Psychosoc. Nurs. Ment. Health Serv.* 56 (12), 7–10. doi:10.3928/02793695-20181112-02
- Chau, B. K. H., Jarvis, H., Law, C. K., and Chong, T. T. (2018). Dopamine and reward: A view from the prefrontal cortex. *Behav. Pharmacol.* 29 (7), 569–583. doi:10.1097/FBP.0000000000000424
- Chen, L., Zhang, Y. H., Wang, S., Zhang, Y., Huang, T., and Cai, Y. D. (2017). Prediction and analysis of essential genes using the enrichments of gene ontology and KEGG pathways. *PLoS One* 12 (9), e0184129. doi:10.1371/journal.pone.0184129
- Chen, X. F., and Xiao, Z. (2016). Study on the clinical efficacy of Long Mu Qing Xin Mixture in the treatment of children with attention deficit hyperactivity disorder. *Chin. J. Basic Med. Tradit. Chin. Med.* 22 (10), 1366–1368+1381.
- Daina, A., Michielin, O., and Zoete, V. (2019). SwissTargetPrediction: Updated data and new features for efficient prediction of protein targets of small molecules. *Nucleic Acids Res.* 47 (W1), W357–W364. doi:10.1093/nar/gkz382
- de Sousa Macedo, L. L. B., Antunes, F. T. T., de Andrade Alvarenga, W., Batista, M. C. C., de Moura, M. S. B., Farias, M. N. L., et al. (2022). Curcumin for attention-deficit-hyperactivity disorder: A systematic review and preliminary behavioral investigation. *Naunyn Schmiedeberg. Arch. Pharmacol.* 395 (7), 803–813. doi:10.1007/s00210-022-02236-0
- Dela Peña, I., Dela Peña, I. J., de la Peña, J. B., Kim, H. J., Shin, C. Y., Han, D. H., et al. (2017). Methylphenidate and atomoxetine-responsive prefrontal cortical genetic overlaps in "impulsive" SHR/NCrl and wistar rats. *Behav. Genet.* 47 (5), 564–580. doi:10.1007/s10519-017-9861-3
- Ding, J., Ding, Y., Wu, J., Deng, J., Yu, Q., and Wang, J. (2022). Jing-ning granules" can alleviate attention deficit hyperactivity disorder in rats by modulating dopaminergic D2/D1-like receptor-mediated signaling pathways. *Evid. Based Complement. Altern. Med.* 2022, 9139841. doi:10.1155/2022/9139841
- Ding, K., Yang, J., Reynolds, G. P., Chen, B., Shao, J., Liu, R., et al. (2017). DAT1 methylation is associated with methylphenidate response on oppositional and hyperactive-impulsive symptoms in children and adolescents with ADHD. *World J. Biol. Psychiatry* 18 (4), 291–299. doi:10.1080/15622975.2016.1224928
- Drechsler, R., Brem, S., Brandeis, D., Grünblatt, E., Berger, G., and Walitzam, S. (2020). Adhd: Current concepts and treatments in children and adolescents. *Neuropediatrics* 51 (5), 315–335. doi:10.1055/s-0040-1701658
- Ekhart, C., Vries, T., and Hunsel, F. V. (2020). Psychiatric adverse drug reactions in the paediatric population. *Arch. Dis. Child.* 105 (8), 749–755. doi:10.1136/archdischild-2019-317933
- Espadas, M., Insa, I., Chamorro, M., and Alda-Diez, J. A. (2018). Side effects of methylphenidate in children and the young. *Rev. Neurol.* 66 (5), 157–162.
- Faraone, S. V., and Larsson, H. (2019). Genetics of attention deficit hyperactivity disorder. *Mol. Psychiatry* 24 (4), 562–575. doi:10.1038/s41380-018-0070-0
- Faraone, S. V. (2018). The pharmacology of amphetamine and methylphenidate: Relevance to the neurobiology of attention-deficit/hyperactivity disorder and other psychiatric comorbidities. *Neurosci. Biobehav. Rev.* 87, 255–270. doi:10.1016/j.neubiorev.2018.02.001
- Festing, M. F., and Altman, D. G. (2002). Guidelines for the design and statistical analysis of experiments using laboratory animals. *ILAR J.* 43 (4), 244–258. doi:10.1093/ilar.43.4.244
- Geetha, R. G., and Ramachandran, S. (2021). Recent advances in the anti-inflammatory activity of plant-derived alkaloid rhynchophylline in neurological and cardiovascular diseases. *Pharmaceutics* 13 (8), 1170. doi:10.3390/pharmaceutics13081170
- Goodsell, D. S., Sanner, M. F., Olson, A. J., and Forli, S. (2021). The AutoDock suite at 30. *Protein Sci.* 30 (1), 31–43. doi:10.1002/pro.3934
- Goto, Y., Otani, S., and Grace, A. A. (2007). The yin and yang of dopamine release: A new perspective. *Neuropharmacology* 53 (5), 583–587. doi:10.1016/j.neuropharm.2007.07.007
- Han, J., Wan, M., Ma, Z., Hu, C., and Yi, H. (2020). Prediction of targets of curculigoside A in osteoporosis and rheumatoid arthritis using network pharmacology and experimental verification. *Drug Des. Devel. Ther.* 14, 5235–5250. doi:10.2147/DDDT.S282112
- Ishizuya, A., Enomoto, M., Tachimori, H., Takahashi, H., Sugihara, G., Kitamura, S., et al. (2021). Risk factors for low adherence to methylphenidate treatment in pediatric patients with attention-deficit/hyperactivity disorder. *Sci. Rep.* 11 (1), 1707. doi:10.1038/s41598-021-81416-z
- Jichao, S., Xinmin, H., Xianguo, R., Dongqi, Y., Rongyi, Z., Shuang, L., et al. (2017). Saikosaponin A alleviates symptoms of attention deficit hyperactivity disorder through downregulation of DAT and enhancing BDNF expression in spontaneous hypertensive rats. *Evid. Based Complement. Altern. Med.* 2017, 2695903. doi:10.1155/2017/2695903
- Kamath, T., Abdulraouf, A., Burris, S. J., Langlieb, J., Gazestani, V., Nadaf, N. M., et al. (2022). Single-cell genomic profiling of human dopamine neurons identifies a population that selectively degenerates in Parkinson's disease. *Nat. Neurosci.* 25 (5), 588–595. doi:10.1038/s41593-022-01061-1
- Karim, N., Khan, I., Abdelhalim, A., Halim, S. A., Khan, A., and Al-Harrasi, A. (2021). Stigmasterol can be new steroidal drug for neurological disorders: Evidence of the GABAergic mechanism via receptor modulation. *Phytomedicine* 90, 153646. doi:10.1016/j.phymed.2021.153646
- Kim, S., Chen, J., Cheng, T., Gindulyte, A., He, J., He, S., et al. (2021). PubChem in 2021: New data content and improved web interfaces. *Nucleic Acids Res.* 49 (1), D1388–D1395. doi:10.1093/nar/gkaa971
- Kozłowska, A., Wojtacha, P., Równiak, M., Kolenkiewicz, M., Tsai, M. L., and Kozłowska, A. (2019). Differences in serum steroid hormones concentrations in Spontaneously Hypertensive Rats (SHR) - an animal model of Attention-Deficit/Hyperactivity Disorder (ADHD). *Physiol. Res.* 68 (1), 25–36. doi:10.33549/physiolres.933907
- Kushida, H., Matsumoto, T., and Ikarashi, Y. (2021). Properties, pharmacology, and pharmacokinetics of active indole and oxindole alkaloids in uncaria hook. *Front. Pharmacol.* 12, 688670. doi:10.3389/fphar.2021.688670
- Lasky-Su, J., Anney, R. J., Neale, B. M., Franke, B., Zhou, K., Maller, J. B., et al. (2008). Genome-wide association scan of the time to onset of attention deficit hyperactivity disorder. *Am. J. Med. Genet. B Neuropsychiatr. Genet.* 147 (8), 1355–1358. doi:10.1002/ajmg.b.30869
- Leffa, D. T., Panzenhagen, A. C., Salvi, A. A., Bau, C. H. D., Pires, G. N., Torres, I. L. S., et al. (2019). Systematic review and meta-analysis of the behavioral effects of methylphenidate in the spontaneously hypertensive rat model of attention-deficit/hyperactivity disorder. *Neurosci. Biobehav. Rev.* 100, 166–179. doi:10.1016/j.neubiorev.2019.02.019
- Li, X., Wei, S., Niu, S., Ma, X., Li, H., Jing, M., et al. (2022). Network pharmacology prediction and molecular docking-based strategy to explore the potential mechanism of Huanglian Jiedu Decoction against sepsis. *Comput. Biol. Med.* 144, 105389. doi:10.1016/j.combiomed.2022.105389
- Liang, E. F., Lim, S. Z., Tam, W. W., Ho, C. S., Zhang, M. W., McIntyre, R. S., et al. (2018). The effect of methylphenidate and atomoxetine on heart rate and systolic blood pressure in young people and adults with attention-deficit hyperactivity disorder (ADHD): Systematic review, meta-analysis, and meta-regression. *Int. J. Environ. Res. Public Health* 15 (8), 1789. doi:10.3390/ijerph15081789
- Mahone, E. M., and Denckla, M. B. (2017). Attention-deficit/hyperactivity disorder: A historical neuropsychological perspective. *J. Int. Neuropsychol. Soc.* 23 (9–10), 916–929. doi:10.1017/S1355617717000807
- Mooers, B. H. M. (2020). Shortcuts for faster image creation in PyMOL. *Protein Sci.* 29 (1), 268–276. doi:10.1002/pro.3781
- Nam, H., Clinton, S. M., Jackson, N. L., and Kerman, I. A. (2014). Learned helplessness and social avoidance in the Wistar-Kyoto rat. *Front. Behav. Neurosci.* 8, 109. doi:10.3389/fnbeh.2014.00109
- Napolitano, F., Bonito-Oliva, A., Federici, M., Carta, M., Errico, F., Magara, S., et al. (2010). Role of aberrant striatal dopamine D1 receptor/cAMP/protein kinase A/DARPP32 signaling in the paradoxical calming effect of amphetamine. *J. Neurosci.* 30 (33), 11043–11056. doi:10.1523/JNEUROSCI.1682-10.2010
- Nishi, A., Kuroiwa, M., Miller, D. B., O'Callaghan, J. P., Bateup, H. S., Shuto, T., et al. (2008). Distinct roles of PDE4 and PDE10A in the regulation of cAMP/PKA signaling in the striatum. *J. Neurosci.* 28 (42), 10460–10471. doi:10.1523/JNEUROSCI.2518-08.2008
- Nishi, A., and Snyder, G. L. (2010). Advanced research on dopamine signaling to develop drugs for the treatment of mental disorders: Biochemical and behavioral profiles of phosphodiesterase inhibition in dopaminergic neurotransmission. *J. Pharmacol. Sci.* 114 (1), 6–16. doi:10.1254/jphs.10r01fm
- Otasek, D., Morris, J. H., Bouças, J., Pico, A. R., and Demchak, B. (2019). Cytoscape automation: Empowering workflow-based network analysis. *Genome Biol.* 20 (1), 185. doi:10.1186/s13059-019-1758-4
- Panayotis, N., Freund, P. A., Marvaldi, L., Shalit, T., Brandis, A., Mehlman, T., et al. (2021). β -sitosterol reduces anxiety and synergizes with established anxiolytic drugs in mice. *Cell Rep. Med.* 2 (5), 100281. doi:10.1016/j.xcrm.2021.100281
- Park, S., Lee, J. M., Kim, J. W., Cho, D. Y., Yun, H. J., Han, D. H., et al. (2015). Associations between serotonin transporter gene (SLC6A4) methylation and clinical characteristics and cortical thickness in children with ADHD. *Psychol. Med.* 45 (14), 3009–3017. doi:10.1017/S003329171500094X
- Piñero, J., Ramírez-Anguaita, J. M., Saüch-Pitarch, J., Ronzano, F., Centeno, E., Sanz, F., et al. (2020). The DisGeNET knowledge platform for disease genomics: 2019 update. *Nucleic Acids Res.* 48 (D1), D845–D855. doi:10.1093/nar/gkz1021
- Posner, J., Polanczyk, G. V., and Sonuga-Barke, E. (2020). Attention-deficit hyperactivity disorder. *Lancet* 395 (10222), 450–462. doi:10.1016/S0140-6736(19)33004-1
- Qin, N., Lu, X., Liu, Y., Qiao, Y., Qu, W., Feng, F., et al. (2021). Recent research progress of uncaria spp. based on alkaloids: Phytochemistry, pharmacology and structural chemistry. *Eur. J. Med. Chem.* 210, 112960. doi:10.1016/j.ejmech.2020.112960
- Rahi, V., and Kumar, P. (2021). Animal models of attention-deficit hyperactivity disorder (ADHD). *Int. J. Dev. Neurosci.* 81 (2), 107–124. doi:10.1002/jdn.10089

- Rangel-Barajas, C., Coronel, I., and Florán, B. (2015). Dopamine receptors and neurodegeneration. *aging Dis.* 6 (5), 349–368. doi:10.14336/AD.2015.0330
- Rappaport, N., Fishilevich, S., Nudel, R., Twik, M., Belinky, F., Plaschkes, I., et al. (2017). Rational confederation of genes and diseases: NGS interpretation via GeneCards, MalaCards and VarElect. *Biomed. Eng. Online* 16 (1), 72. doi:10.1186/s12938-017-0359-2
- Rose, Y., Duarte, J. M., Lowe, R., Segura, J., Bi, C., Bhikadiya, C., et al. (2020). RCSB Protein Data Bank: Architectural advances towards integrated searching and efficient access to macromolecular structure data from the PDB Archive. *J. Mol. Biol.* 433 (11), 166704. doi:10.1016/j.jmb.2020.11.003
- Rostami Kandroodi, M., Cook, J. L., Swart, J. C., Froböse, M. I., Geurts, D. E. M., Vahabie, A. H., et al. (2021). Effects of methylphenidate on reinforcement learning depend on working memory capacity. *Psychopharmacol. Berl.* 238 (12), 3569–3584. doi:10.1007/s00213-021-05974-w
- Ruocco, L. A., Treno, C., Gironi Carnevale, U. A., Arra, C., Mattern, C., Huston, J. P., et al. (2014). Prepubertal intranasal dopamine treatment in an animal model of ADHD ameliorates deficient spatial attention, working memory, amino acid transmitters and synaptic markers in prefrontal cortex, ventral and dorsal striatum. *Amino Acids* 46 (9), 2105–2122. doi:10.1007/s00726-014-1753-8
- Sadeghnia, H. R., Taji, A. R., Forouzanfar, F., and Hosseinzadeh, H. (2017). Berberine attenuates convulsing behavior and extracellular glutamate and aspartate changes in 4-aminopyridine treated rats. *Iran. J. Basic Med. Sci.* 20 (5), 588–593. doi:10.22038/IJBMS.2017.8756
- Saedisomeolia, A., Samadi, M., Gholami, F., Seyedi, M., Effatpanah, M., Hashemi, R., et al. (2018). Vitamin D's molecular action mechanism in attention-deficit/hyperactivity disorder: A review of evidence. *CNS Neurol. Disord. Drug Targets* 17 (4), 280–290. doi:10.2174/1871527317666180501111627
- Salatino-Oliveira, A., Rohde, L. A., and Hutz, M. H. (2018). The dopamine transporter role in psychiatric phenotypes. *Am. J. Med. Genet. B Neuropsychiatr. Genet.* 177 (2), 211–231. doi:10.1002/ajmg.b.32578
- Schmidt, U., Pilgrim, C., and Beyer, C. (1998). Differentiative effects of dopamine on striatal neurons involve stimulation of the cAMP/PKA pathway. *Mol. Cell Neurosci.* 11 (1–2), 9–18. doi:10.1006/mcne.1998.0668
- Sharma, A., and Couture, J. (2013). A review of the pathophysiology, etiology, and treatment of attention-deficit hyperactivity disorder (ADHD). *Ann. Pharmacother.* 48 (2), 209–225. doi:10.1177/1060028013510699
- Song, Y., Yuan, H., Chen, T., Lu, M., Lei, S., and Han, X. (2021). An shen ding zhi ling alleviates symptoms of attention deficit hyperactivity disorder via anti-inflammatory effects in spontaneous hypertensive rats. *Front. Pharmacol.* 11, 617581. doi:10.3389/fphar.2020.617581
- Sun, Y. L., Wang, Y. R., Qu, X. H., Wang, J. H., Fang, J., and Zhang, L. (1991). Animal experimental observation of 'Yizhi syrup' in the treatment of children with ADHD. *J. Shanxi Univer Tradit. Chin. Med.* 4, 37–38.
- Szklarczyk, D., Franceschini, A., Wyder, S., Forslund, K., Heller, D., Huerta-Cepas, J., et al. (2015). STRING v10: Protein-protein interaction networks, integrated over the tree of life. *Nucleic Acids Res.* 43, D447–D452. doi:10.1093/nar/gku1003
- Thomas Broome, S., Louangaphay, K., Keay, K. A., Leggio, G. M., Musumeci, G., and Castorina, A. (2020). Dopamine: An immune transmitter. *Neural Regen. Res.* 15 (12), 2173–2185. doi:10.4103/1673-5374.284976
- Trampush, J. W., Jacobs, M. M., Hurd, Y. L., Newcorn, J. H., and Halperin, J. M. (2014). Moderator effects of working memory on the stability of ADHD symptoms by dopamine receptor gene polymorphisms during development. *Dev. Sci.* 17 (4), 584–595. doi:10.1111/desc.12131
- Verghese, C., and Abdijadid, S. (2022). *Methylphenidate*. Treasure Island, Florida, United States: StatPearls Publishing, 1–7.
- Wang, L. S., Zhang, M. D., Tao, X., Zhou, Y. F., Liu, X. M., Pan, R. L., et al. (2019). LC-MS/MS-based quantification of tryptophan metabolites and neurotransmitters in the serum and brain of mice. *J. Chromatogr. B Anal. Technol. Biomed. Life Sci.* 1112, 24–32. doi:10.1016/j.jchromb.2019.02.021
- Wang, Y., Yang, Y., Liu, M., Wei, Y., Liu, J., Pei, H., et al. (2020b). Rhizoma coptidis for alzheimer's disease and vascular dementia: A literature review. *Curr. Vasc. Pharmacol.* 18 (4), 358–368. doi:10.2174/157016117666190710151545
- Wang, Y., Zhang, S., Li, F., Zhou, Y., Zhang, Y., Wang, Z., et al. (2020a). Therapeutic target database 2020: Enriched resource for facilitating research and early development of targeted therapeutics. *Nucleic Acids Res.* 48 (1), D1031–D1041. doi:10.1093/nar/gkz981
- Wei, M., Li, H., Li, Q., Qiao, Y., Ma, Q., Xie, R., et al. (2020). Based on network pharmacology to explore the molecular targets and mechanisms of Gegen Qinlian Decoction for the treatment of ulcerative colitis. *Biomed. Res. Int.* 2020, 5217405. doi:10.1155/2020/5217405
- Wishart, D. S., Knox, C., Guo, A. C., Shrivastava, S., Hassanali, M., Stothard, P., et al. (2006). DrugBank: A comprehensive resource for *in silico* drug discovery and exploration. *Nucleic Acids Res.* 34, D668–D672. doi:10.1093/nar/gkj067
- Xiang, T., Yu, F., Fei, R., Qian, J., and Chen, W. (2016). CHRNA7 inhibits cell invasion and metastasis of LoVo human colorectal cancer cells through PI3K/Akt signaling. *Oncol. Rep.* 35 (2), 999–1005. doi:10.3892/or.2015.4462
- Xu, L., Zhang, J., Wang, Y., Zhang, Z., Wang, F., and Tang, X. (2021). Uncovering the mechanism of Ge-Gen-Qin-Lian decoction for treating ulcerative colitis based on network pharmacology and molecular docking verification. *Biosci. Rep.* 41 (2), BSR20203565. doi:10.1042/BSR20203565
- Yan, Z., and Rein, B. (2022). Mechanisms of synaptic transmission dysregulation in the prefrontal cortex: Pathophysiological implications. *Mol. Psychiatry* 27 (1), 445–465. doi:10.1038/s41380-021-01092-3
- Yang, X., Liu, H., Liu, J., Li, F., Li, X., Shi, L., et al. (2016). Rational selection of the 3D structure of biomacromolecules for molecular docking studies on the mechanism of endocrine disruptor action. *Chem. Res. Toxicol.* 29 (9), 1565–1570. doi:10.1021/acs.chemrestox.6b00245
- Yang, Y., Ji, W. G., Zhu, Z. R., Wu, Y. L., Zhang, Z. Y., and Qu, S. C. (2018). Rhynchophylline suppresses soluble Aβ1-42-induced impairment of spatial cognition function via inhibiting excessive activation of extrasynaptic NR2B-containing NMDA receptors. *Neuropharmacology* 135, 100–112. doi:10.1016/j.neuropharm.2018.03.007
- Yi, P., Zhang, Z., Huang, S., Huang, J., Peng, W., and Yang, J. (2020). Integrated meta-analysis, network pharmacology, and molecular docking to investigate the efficacy and potential pharmacological mechanism of Kai-Xin-San on Alzheimer's disease. *Pharm. Biol.* 58 (1), 932–943. doi:10.1080/13880209.2020.1817103
- Yu, L., Liu, S., Zhou, R., Sun, H., Su, X., Liu, Q., et al. (2022). Atorvastatin inhibits neuronal apoptosis via activating cAMP/PKA/p-CREB/BDNF pathway in hypoxic-ischemic neonatal rats. *FASEB J.* 36 (4), e22263. doi:10.1096/fj.202101654RR
- Yuan, H., Ni, X., Zheng, M., Han, X., Song, Y., and Yu, M. (2019). Effect of catalpol on behavior and neurodevelopment in an ADHD rat model. *Biomed. Pharmacother.* 118, 109033. doi:10.1016/j.biopha.2019.109033
- Zaccolo, M., Zerio, A., and Lobo, M. J. (2021). Subcellular organization of the cAMP signaling pathway. *Pharmacol. Rev.* 73 (1), 278–309. doi:10.1124/pharmrev.120.000086
- Zahiruddin, S., Basist, P., Parveen, A., Parveen, R., Khan, W., Gaurav, S., et al. (2020). Ashwagandha in brain disorders: A review of recent developments. *J. Ethnopharmacol.* 257, 112876. doi:10.1016/j.jep.2020.112876
- Zhang, C. Q., and Jiang, Z. Y. (2016). Clinical observation of Long Mu Qing Xin Mixture in the treatment of attention deficit hyperactivity disorder in children (heart and spleen deficiency and liver exuberance type). *J. Liaoning Univ. Tradit. Chin. Med.* 18 (11), 104–107. doi:10.13194/j.issn.1673-842x.2016.11.031
- Zhang, R., Zhu, X., Bai, H., and Ning, K. (2019). Network pharmacology databases for traditional Chinese Medicine: Review and assessment. *Front. Pharmacol.* 10, 123. doi:10.3389/fphar.2019.00123
- Zhou, R. Y., Han, X. M., Wang, J. J., Yuan, H. X., Sun, J. C., You, Y., et al. (2017). Effect of baicalin on behavioral characteristics of rats with attention deficit hyperactivity disorder. *Zhongguo Dang Dai Er Ke Za Zhi* 19 (8), 930–937. doi:10.7499/j.issn.1008-8830.2017.08.016
- Zhou, Y., Zhou, B., Pache, L., Chang, M., Khodabakhshi, A. H., Tanaseichuk, O., et al. (2019). Metascape provides a biologist-oriented resource for the analysis of systems-level datasets. *Nat. Commun.* 10 (1), 1523. doi:10.1038/s41467-019-09234-6



OPEN ACCESS

EDITED BY

Marcello Allegretti,
Dompé farmaceutici S.p.A., Italy

REVIEWED BY

Silvia Mihaila,
Utrecht University, Netherlands
Lidia De Filippis,
Dompé farmaceutici S.p.A., Italy

*CORRESPONDENCE

Andrew Emili,
✉ aemili@bu.edu

RECEIVED 20 June 2023

ACCEPTED 13 November 2023

PUBLISHED 27 November 2023

CITATION

Lin W, Mousavi F, Blum BC,
Heckendorf CF, Moore J, Lampl N,
McComb M, Kotelnikov S, Yin W, Rabhi N,
Layne MD, Kozakov D, Chitalia VC and
Emili A (2023), Integrated metabolomics
and proteomics reveal biomarkers
associated with hemodialysis in end-
stage kidney disease.
Front. Pharmacol. 14:1243505.
doi: 10.3389/fphar.2023.1243505

COPYRIGHT

© 2023 Lin, Mousavi, Blum, Heckendorf,
Moore, Lampl, McComb, Kotelnikov, Yin,
Rabhi, Layne, Kozakov, Chitalia and Emili.
This is an open-access article distributed
under the terms of the [Creative
Commons Attribution License \(CC BY\)](#).
The use, distribution or reproduction in
other forums is permitted, provided the
original author(s) and the copyright
owner(s) are credited and that the original
publication in this journal is cited, in
accordance with accepted academic
practice. No use, distribution or
reproduction is permitted which does not
comply with these terms.

Integrated metabolomics and proteomics reveal biomarkers associated with hemodialysis in end-stage kidney disease

Weiwei Lin^{1,2}, Fatemeh Mousavi¹, Benjamin C. Blum^{1,2},
Christian F. Heckendorf^{1,2}, Jarrod Moore^{1,2}, Noah Lampl^{1,2},
Mark McComb^{1,2}, Sergei Kotelnikov³, Wenqing Yin⁴, Nabil Rabhi²,
Matthew D. Layne², Dima Kozakov³, Vipul C. Chitalia^{4,5,6} and
Andrew Emili^{1,2,7*}

¹Center for Network Systems Biology, Boston University, Boston, MA, United States, ²Department of Biochemistry, Boston University School of Medicine, Boston, MA, United States, ³Department of Applied Mathematics and Statistics, Stony Brook University, Stony Brook, NY, United States, ⁴Renal Section, Department of Medicine, Boston University School of Medicine, Boston, MA, United States, ⁵Veterans Affairs Boston Healthcare System, Boston, MA, United States, ⁶Institute of Medical Engineering and Sciences, Massachusetts Institute of Technology, Cambridge, MA, United States, ⁷Department of Biology, Boston University, Boston, MA, United States

Background: We hypothesize that the poor survival outcomes of end-stage kidney disease (ESKD) patients undergoing hemodialysis are associated with a low filtering efficiency and selectivity. The current gold standard criteria using single or several markers show an inability to predict or disclose the treatment effect and disease progression accurately.

Methods: We performed an integrated mass spectrometry-based metabolomic and proteomic workflow capable of detecting and quantifying circulating small molecules and proteins in the serum of ESKD patients. Markers linked to cardiovascular disease (CVD) were validated on human induced pluripotent stem cell (iPSC)-derived cardiomyocytes.

Results: We identified dozens of elevated molecules in the serum of patients compared with healthy controls. Surprisingly, many metabolites, including lipids, remained at an elevated blood concentration despite dialysis. These molecules and their associated physical interaction networks are correlated with clinical complications in chronic kidney disease. This study confirmed two uremic toxins associated with CVD, a major risk for patients with ESKD.

Conclusion: The retained molecules and metabolite–protein interaction network address a knowledge gap of candidate uremic toxins associated with clinical complications in patients undergoing dialysis, providing mechanistic insights and potential drug discovery strategies for ESKD.

KEYWORDS

metabolomics, proteomics, nLC-MS/MS, ESKD, integrated omics

Introduction

End-stage kidney disease (ESKD) is a form of advanced chronic kidney disease (CKD) wherein the renal filtering capacity becomes insufficient to remove circulating metabolic waste and excess fluid from patient's blood. This results in the accumulation of uremic toxins, a life-threatening condition that necessitates kidney transplant or dialysis. Since kidney replacement is challenging, hemodialysis is widely applied to ESKD patients. During this procedure, blood is pumped through a dialyzer with a membrane designed to filter out toxins to restore fluid and electrolyte balance (Mohajerani et al., 2022). Although not a replacement for kidney function, dialysis remains a life-saving option for patients and the current standard-of-care therapy for patients with ESKD. However, the mortality remains high. Poor clinical outcomes are associated with an elevated risk of infection, anemia, and cardiovascular disease (CVD) (Virani et al., 2008). The mechanisms driving these outcomes are not fully understood, but they reflect the cumulative complexity of disease progression, the side effects of dialysis, and potential comorbidities (e.g., hypertension and diabetes) (Bello et al., 2017). Blood creatinine levels and urine output are commonly used as clinical markers of disease progression in CKD, but they show limited accuracy for predicting future complications in ESKD patients undergoing hemodialysis.

Liquid chromatography coupled to tandem mass spectrometry (LC/MS) enables sensitive, high-resolution, large-scale identification of circulating biomolecules (Dubin and Rhee, 2020). In principle, LC/MS-based proteomic and metabolomic profiles can provide complementary insights into the biochemical pathways altered during ESKD, revealing potential prognostic markers that could be used to improve clinical outcomes. Although a host of uremic toxins have been defined as cardiovascular risk factors, there is a dearth in studies comprehensively evaluating compounds that are preferentially retained at elevated levels in the plasma of patients undergoing hemodialysis. This knowledge gap compromises the mechanistic understanding and treatment of CVDs and other complications in patients with ESKD (Ravid et al., 2021). Although previous studies have documented a small set of candidate uremic toxins that are not effectively removed by hemodialysis, we hypothesized that the persistence of additional factors impacts clinical outcomes.

By combining robust nanoflow metabolomic and proteomic workflows, our study has gained a more comprehensive picture of the molecular changes and associated biochemical pathways and physical interaction networks that remain altered in ESKD disease. Our integrated analysis identified dozens of candidate uremic toxins, 21 of which were independently further confirmed as persistently elevated in patient plasma using reference standards. Additionally, we uncovered multiple factors with potential links to CVD, a major determinant of mortality among patients with ESKD (Himmelfarb et al., 2020).

Materials and methods

Chemical and materials

LC-MS grade solvents were obtained from Fisher Scientific. The solid-phase micro-extraction (SPME) blade unit and robotic

96 auto-sampler were purchased from Professional Analytical Systems Technology (Magdala, Germany) for metabolomic crude extracts' clean-up. Metabolite standards with purity greater than 95% were purchased from MetaSci (Canada). Doxycycline was purchased from Sigma. DMSO (Sigma) was used as a vehicle control.

Clinical samples

The ESKD serum samples were collected from patients at the Renal Section of the Department of Medicine at the Boston Medical Center. The protocols for patient recruitment and sample collection at Boston University Medical Campus were IRB-approved (H-26367) and supervised by Dr. Vipul Chitalia. Control serum (healthy cohort) was obtained from Research Blood Components, LLC (MA). All participants provided informed consent for the use of their blood for research purposes. Whole blood samples (~1 mL) from both the healthy cohort and ESKD patients (both before and after hemodialysis procedure) were collected and allowed to sit for 30 min at room temperature, and then centrifuged at 3,000 rpm at 4°C for 10 min. Serum (supernatant) was transferred to new tubes and quenched immediately at -80°C prior to metabolite extraction.

Human induced pluripotent stem cell-derived cardiomyocyte cell culture and cytotoxicity assay

Human induced pluripotent stem cell (hiPSC)-derived cardiomyocytes were generously provided by the Seidman Lab at Harvard Medical School. In brief, hiPSCs were cultured with mTESR1 media (STEMCELL Technologies) and differentiated into cardiomyocytes (day 0) via activation of the WNT pathway with 12 μ M CHIR 99021 (Tocris) in RPMI + GlutaMAX media supplemented with B27 minus insulin (RPMI and B27 minus, Thermo Fisher Scientific). After 48 h, the WNT pathway was inhibited via 5 μ M IWP-4 (Tocris). On day 9, the media was replaced with RPMI + GlutaMAX media supplemented with B27 plus insulin (Thermo Fisher Scientific). On days 11 and 13, the cardiomyocyte population was purified by metabolic selection via RPMI glucose-free media (Gibco) supplemented with 4 mM of DL-lactate (Millipore Sigma). On day 15, cardiomyocytes were placed in 50% FBS in PBS to deplete the protease, centrifuged, and the supernatant was aspirated. They were then placed in RPMI B27+ supplemented with 5 μ M Y-27632 (Tocris) and 2% fetal bovine serum (MilliporeSigma) for seeding.

Homocysteine, taurine, and positive control (doxorubicin) were dissolved into 1 mM stock solution using 0.5% DMSO and then serially diluted to a desired final concentration (100 μ M, 10 μ M, 1 μ M, 100 nM, and 10 nM) in media prior to cell treatment. The toxicity of vehicle (0.5% DMSO) alone was evaluated and found not to cause any noticeable toxicity on iPSC-derived cardiomyocytes. For the cytotoxicity assay, the cells were incubated with their respective metabolites for 24 h at 37°C and 5% CO₂ in five

replicates. Then, the cells were incubated with a 10 μ L cell proliferation reagent WST-1 (Sigma-Aldrich) for 4 h at 37°C and 5% CO₂. After shaking for 1 min, the samples were read on a microplate reader at 420 nm absorbance.

Metabolite extraction

Patient serum (50 μ L) was resuspended in a 4 vol. mixture of ice-cold methanol/acetonitrile/water (MeOH/ACN/H₂O, 40/40/20 v/v; Fisher) in chemically resistant microcentrifuge tubes (e.g., Eppendorf) and vortexed for 30 s. The mixture was incubated for 1 h at –20°C and centrifuged at 12,000 \times g and 4°C for 15 min to pellet the protein precipitate. The metabolite-containing supernatants were transferred to new tubes, dried under vacuum at 30°C, and kept at –80°C prior to LC-MS. For LC-MS analysis, extracts were thawed and resolubilized in 200 μ L of 2% methanol and subjected to SPME (see the following section) for sample clean-up. The protein precipitate was maintained at 4°C prior to tryptic digestion and proteomic analysis. Equal amounts of each sample were pooled as an internal quality control (QC).

Solid-phase micro-extraction

The metabolite mixtures were transferred to a 96-well plate for SPME processing. The coated blades were washed with EtOH/H₂O (70:30, v/v) for 30 min and preconditioned for 30 min in MeOH/H₂O (50:50, v/v). The samples were extracted by incubation with the blades for 1 h with shaking. The blades were briefly rinsed for ~20 s using water, and then, the bound metabolites were desorbed using ACN/H₂O (50:50, v/v) for 1 h. The solvent was evaporated to dryness using a vacuum concentrator at 30°C. For LC-MS analysis, metabolites were reconstituted in 20 μ L of 2% ACN. To prevent carryover particles, metabolites were centrifuged at 10,000 \times g at 4°C for 15 min, the supernatant was transferred to a new tube, and this step was repeated one more time prior to injection.

LC-MS analysis of metabolites

The analysis was performed on an Orbitrap Exploris 480 mass spectrometer (Thermo Fisher Scientific) interfaced to the EASY nanoLC1200 system (Thermo Fisher Scientific). The metabolites (including lipids) were loaded onto a C18 reverse-phase pre-column (75 μ m i. d. \times 2 cm, 3 μ m) and then separated by a capillary column (75 μ m i. d. \times 25 cm, 2 μ m, 100 Å, Thermo Fisher Scientific); the column oven was set to 40°C. The mobile phase A was 2% ACN, and the mobile phase B was 80% ACN. The nLC flow rate was 300 nL/min. The samples (3 μ L) were injected and separated over a 45-min gradient. The gradient consisted of 2%–60% mobile phase B for 20 min, was increased to 95% mobile phase B over 10 min, and maintained at 95% mobile phase B for 15 min. The MS instrument was operated in the automated switching ESI mode over a full mass scan range of *m/z* 67–1,000 at a resolution of 60,000. The AGC target was set to

300% (equal to 3×10^6 ions), and the maximum ion injection time was set to 25 ms. The source ionization parameters were optimized for a transfer temperature at 300°C, and a spray voltage was set to 2.1 kV and –1.8 kV for the positive and negative modes, respectively. MS2 scans were performed at 15,000 resolution with a maximum injection time of 64 ms using stepped normalized collision energies (NCEs) of 10, 20, and 40. Dynamic exclusion was enabled using a time window of 10 s.

Protein digestion

Five replicates were randomly selected from each condition for the pooled (multiplex) proteomic analysis. After pelleting, the protein precipitates from the organic solvent extraction were resuspended in 250 μ L of lysis buffer containing 6 M guanidine hydrochloride (GuHCl), protease inhibitors (Sigma), and phosphatase inhibitors (Roche). The samples were heated at 95°C for 10 min, cooled on ice for 10 min, and then briefly sonicated to shear the nucleic acids. The samples were diluted with 100 mM Tris (pH 8.5) to reduce the concentration of GuHCl to 0.75 M. After quantification with a BCA kit (Thermo Scientific), the proteins were digested overnight with sequence-grade trypsin (enzyme-to-protein ratio of 1:50) at 37°C, and formic acid was then added to obtain a final concentration of 1% in solution. The resulting peptides were desalted using a C18 Sep-Pak cartridge (Waters), according to the manufacturer's instructions.

TMT peptide labeling

Prior to tandem mass tag (TMT) labeling, peptide quantification was performed by the Pierce quantitative colorimetric assay (Thermo Scientific). According to the manufacturer's instructions, 100 μ g of peptide per sample was resuspended in 0.1 M triethylammonium bicarbonate (TEAB). Peptides (five channels per condition, healthy, and pre- and post-dialysis) were labeled with TMTpro (Thermo Scientific) for 1 h at room temperature. To quench the reaction, 5% hydroxylamine was added to each sample, and the resulting mixture was incubated at room temperature for 15 min. After labeling, equal amounts of each sample were combined in a new microtube and desalted using a C18 Sep-Pak cartridge (Waters).

High-pH reverse-phase peptide fractionation

Peptides (500 μ g) were fractionated offline on a Waters XBridge BEH C18 reverse-phase column (3.5 μ m, 4.6 \times 250 mm) using an Agilent 1100 HPLC system operated at a flow rate of 0.45 mL/min with two buffer lines: buffer A (consisting of 0.1% ammonium hydroxide–2% acetonitrile–water) and buffer B (consisting of 0.1% ammonium hydroxide–98% acetonitrile, pH 9). The peptides were separated by a gradient from 0% to 10% B in 5 min, followed by linear increases to 30% B in 23 min, to 60% B in 7 min, and then 100% in 8 min and maintained at 100% for 5 min. This separation yielded 48 collected fractions that were subsequently combined into

12 fractions and then evaporated to dryness in a vacuum concentrator. The peptides (2 µg) from each fraction were reconstituted in 0.1% formic acid and maintained at -80°C prior to analysis by nLC-MS/MS.

LC-MS analysis of peptides

An Orbitrap Exploris 480 mass spectrometer, interfaced with an EASY nanoLC1200 ultra-high pressure pump system, was used for peptide analysis. Peptides were loaded onto a C18 pre-column (75 µm i. d. \times 2 cm, 100 Å, Thermo Fisher Scientific) and then separated on a reverse-phase nano-spray column (75 µm i. d. \times 50 cm, 100 Å, Thermo Fisher Scientific) over a 150-min gradient. Mobile phase A consisted of 0.1% FA-2% ACN-water, and mobile phase B consisted of 0.1% FA-80% ACN-water. The gradient consisted of 6%–40% mobile phase B over 155 min, was increased to 95% mobile phase B over 4 min, and maintained at 95% mobile phase B for 3 min at a flow rate of 250 nL/min. The MS instrument was operated in a positive ion mode over a full mass scan range of m/z 350–1,400 at a resolution of 60,000 with a normalized AGC target of 300%. The source ion transfer tube temperature was set at 275°C , and a spray voltage was set to 2.5 kv. Data were acquired on a data-dependent mode with FAIMS running three compensation voltages at -50v , -57v , and -64v . MS2 scans were performed at 45,000 resolution with a normalized collision energy of 34. Dynamic exclusion was enabled using a time window of 60 s.

Metabolomic data processing

The raw chromatographic data files were converted to the mzML format and split into positive and negative ion mode files with msConvert (Adusumilli and Mallick, 2017) prior to analysis using MS-DIAL (V4.18) (Tsugawa et al., 2015). ‘Linear-weighted moving average’ was used for peak detection. The minimum peak height was set to 20,000. Afterward, spectral centroiding was performed by integrating the mass spectrum over the ± 0.01 and ± 0.025 Da ranges in MS1 and MS2, respectively. The spectra were searched using MS-DIAL (Tsugawa et al., 2015) against a metabolomic (MSMS-Public-Pos-VS15. msp) or lipidomic (LipidMsmsBinaryDB-VS68-FiehnO.lbm2) library with a matched mass tolerance of 0.025 and 0.05 Da for MS1 and MS2 ions, respectively. The QC samples were specified as reference files for sample alignment. The data matrixes were exported as tab-delimited text files. Features with high CV intensity (≥ 50), low fold change (≤ 5) in average sample intensity relative to negative controls, low signal/noise (≤ 3), and peak widths less than 6 scans were removed prior to subsequent downstream analysis. The accurate mass, retention time, and MS/MS spectra of metabolite standards were extracted and used to confirm the putative metabolites detected in ESKD, limiting by mass and retention time shift and validating by spectral similarity (matching score > 0.7).

We confirmed 21 altered candidate metabolites ($p < 0.05$, ≥ 1.5 -fold-change in ESKD *versus* control), by matching accurate mass, retention time, and/or MS2 spectrum with reference standards (MetaSci, Canada, see Table 2 for identifications). Compounds (purity $\geq 95\%$) that were dissolved in $\sim 50\%$ acetonitrile, methanol,

iso-propanol, or chloroform could be used for water-insoluble compounds. Pooled metabolite standards (~ 100 ng/mL) were separated using the same C18 pre-column and EASY-Spray column, and the same method was applied to acquire MS1 and MS/MS spectra. Metabolites were identified by accurate mass ($\leq 1\text{ppm}$ for the positive mode; $\leq 2\text{ppm}$ for the negative mode), retention time, and MS2 similarity (matching score ≥ 0.7).

Proteomic data analysis

MS2 spectra were processed and searched by MaxQuant (version 1.6.7) against the UniProt FASTA database (uniprot.org) downloaded on 2020-02-10 containing all canonical reviewed human protein sequences from Swiss-Prot. The search allowed for two missed trypsin cleavage sites, variable modifications of methionine oxidation, and N-terminal acetylation. The carbamidomethylation of cysteine residues was set as a fixed modification. Ion tolerances of 20 and 6 ppm were set for the first and second searches, respectively. Protein and peptide identifications were filtered at a 1% FDR threshold based on searching the target-decoy database strategy (Elias and Gygi, 2007). The candidate peptide identifications were filtered assuming a 1% FDR threshold based on searching the reverse sequence database. Quantification was performed using the TMT reporter on MS2. The reporter ion intensities were log-transferred and normalized based on quantiles. Protein–lipid 3D structure modeling was performed using an in-house template-based LigTBM protein–ligand docking protocol (Aleksenko et al., 2020). Bioinformatic analysis was performed in the R statistical computing environment (version 3.6.1).

Metabolite–protein network analysis

Enrichment analysis and disease-associated pathway analysis were performed against the set of metabolites elevated in ESKD using the web-based tool MetaboAnalyst 5.0 (Chong and Xia, 2020) to search the Small Molecule Pathway Database (SMPDB, <https://www.smpdb.ca/>). Metabolites resulting from the combination of category I and category II represented the significantly elevated compounds in ESKD compared with control, regardless of dialysis, while category II alone represented the persistent toxins; category III (down in ESKD) consisted of few metabolites. Analysis of these three groups of metabolites revealed both the changed metabolomic patterns of ESKD and, more notably, the (incomplete) effects of dialysis. We performed joint protein–metabolite network analysis based on significantly elevated metabolites (category I + category II annotations) and differential proteins ($\text{FC} > 1.5$, $p < 0.05$, including both up and downregulation) detected in patient serum samples. Metabolite and protein (enzyme/gene) associations were extracted from STITCH (Kuhn et al., 2008), a database including interaction networks of small molecules and proteins based on curated biochemical reactions from a similar chemical structure and similar molecular activities. The resulting association networks, consisting of physically associated metabolites and proteins and their direct neighbors, were visualized using Cytoscape 3.9.1.

TABLE 1 Patient characteristics.

Study/baseline participant	Patients with ESKD on HD	Control
	N = 10	N = 10
Age, year#	Mean: 64.4 ± 10.22	Mean: 50.2 ± 8.61
Male	5 (50%)	6 (60%)
BMI #	Mean: 31.63 ± 5.39	Mean: 25.72 ± 7.25
Ethnicity		
Hispanic	2	6
Non-Hispanic	8	4
Race		
Black population	8	4
White population	2	6
Asians	0	0
American Indians	0	0
Others	0	0
Smoke	6	0
Hypertension	10	0
Diabetes mellitus	8	0
Cardiovascular diseases		
Documented CAD	5	0
Angina	6	0
Coronary artery bypass	5	0
Congestive heart failure	5	0
Hypercholesterolemia	5	0
Peripheral vascular disease	2	0
Deep venous thrombosis	6	0
Pulmonary embolism	2	0
Blood pressure, mmHg		
Systolic#	Mean: 140.7 ± 22.31	Mean: 125 ± 14.69
Diastolic#	Mean: 79.2 ± 15.89	Mean: 74 ± 6.53
eGFR ml/min/sq mt body	Mean: 8.1 ± 7.89	Mean: >90

Results

Metabolomic and proteomic profiles differ during hemodialysis

Our unified workflow detects metabolite, lipid, and protein levels in serum samples collected from a matched cohort of ESKD patients ($n = 10$) before and after hemodialysis along with the healthy cohort ($n = 10$) (see Table 1 for patient characteristics). Renal function was estimated by the glomerular filtration rate (eGFR). ESKD patients (George and Gounden, 2019) had a significantly lower eGFR (mean = 8.1 ± 7.89 mL/min/sq mt body) than the age- and sex-matched cohort

(>90 mL/min/sq mt body) (Table 1). This cohort consisted primarily of African American and non-White Hispanic patients, with approximately half being male patients. All of the patients presented at least one comorbidity, including diabetes (80%), CVD (50%), peripheral artery disease (20%), and a remote history of deep vein thrombosis (60%) and pulmonary embolism (20%) (Table 1).

Serum samples were collected both pre- and post-dialysis (schematic representation in Figure 1A) and compared with serum from healthy controls matched for age, sex, and body mass index without diagnostic comorbidities (Table 1). The samples (three groups, $n = 30$ in total) were quenched by quick freezing and processed using a unified technical

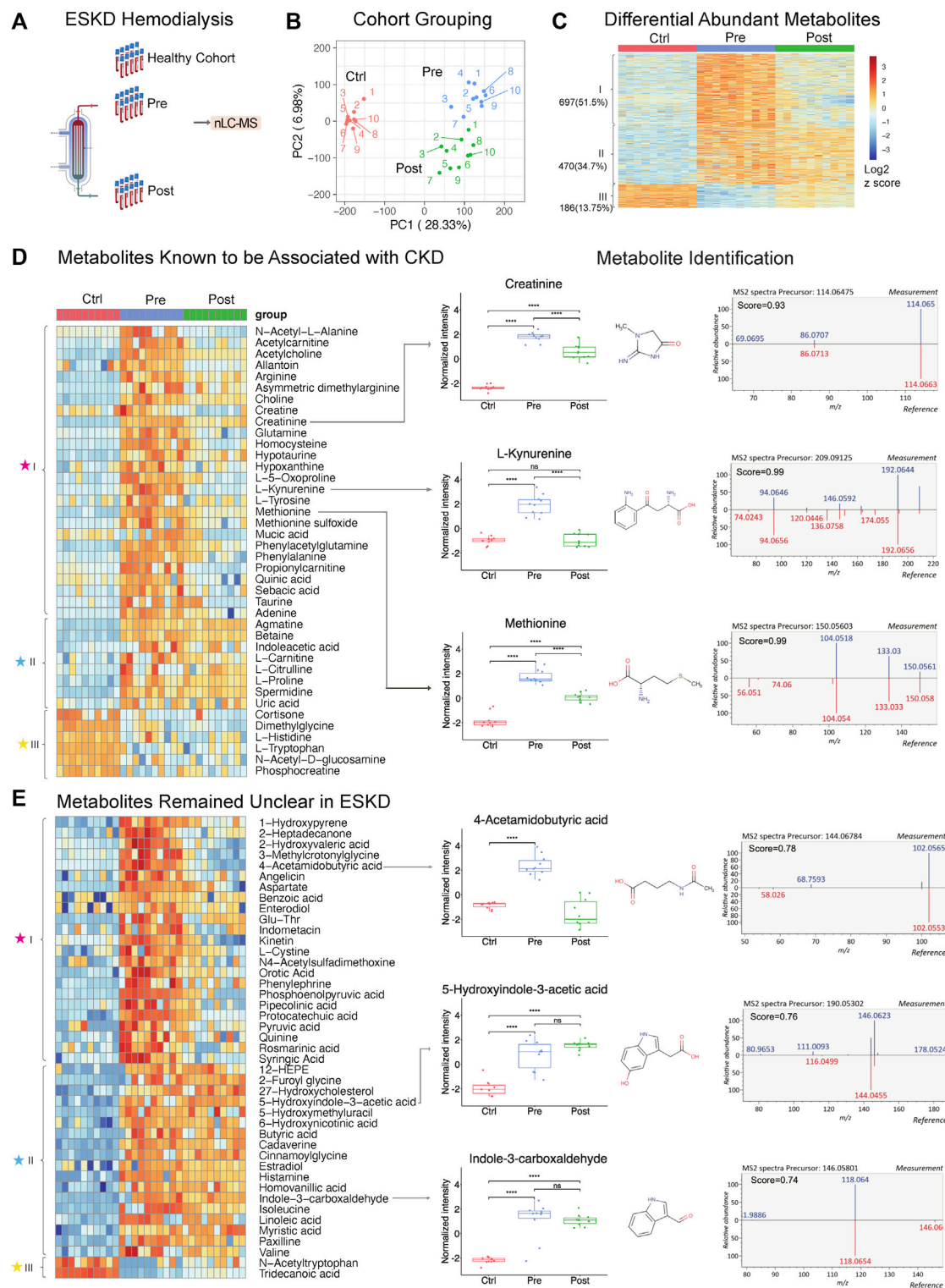


FIGURE 1

Untargeted metabolomic profiling of serum from patients with end-stage kidney disease. **(A)** ESKD clinical sample collection and processing. **(B)** PCA plot of LLE-SPME-nLC/MS sample profiles (healthy CTRL controls vs. pre- and post-dialysis ESKD cohorts). **(C)** Heatmap of differentially abundant metabolites ($p < 0.05$, >2 -fold change (FC), $FDR < 0.05$); metabolites are classified as class I (increased pre-dialysis, decreased post-dialysis), class II (increased pre-dialysis, but not significantly reduced post-dialysis), and class III (decreased in ESKD). **(D)** Heatmap of uremic solutes associated with CKD along with representative experimental data showing the circulating levels (relative intensity) and matched MS/MS fragmentation patterns obtained for creatine, L-kynurenine, and methionine (chemical structures from HMDB: <https://hmdb.ca/>). **(E)** Heatmap of metabolites significantly elevated (>5 -fold change, $p < 0.05$, $FDR < 0.05$) in ESKD along with representative data obtained for 4-acetamidobutyric acid, 5-hydroxyindole-3-acetic acid, and indole-3-carboxaldehyde.

workflow to acquire metabolomic and lipidomic (in the same LC/MS run) data and proteomic data from the same biospecimens. In brief, protein was precipitated using cold MeOH/ACN/H₂O (4/4/2, v/v), while soluble metabolites and lipids were collected from the supernatant by SPME, an in-house sample clean-up approach using resins optimized to selectively retain both polar and non-polar metabolites while removing matrix contaminants.

A total of 8,410 putative metabolites (both positive and negative modes) and 665 proteins (without depletion of albumin or other high-abundance blood proteins) were detected in serum (Supplementary Table S1; Supplementary Table S2). Strikingly, dozens of metabolites, lipids, and proteins that accumulated in the ESKD patient serum remained at high levels relative to healthy controls even right after hemodialysis.

Persistently elevated metabolites in ESKD patients undergoing hemodialysis

PCA plots revealed the distinct metabolomic profiles of each sample cohort (Figure 1B, C). Notably, 1,167 putative metabolites were significantly elevated ($p < 0.05$, FDR < 0.05, ≥ 2 -fold change; Supplementary Table S1) in the serum from patients with ESKD before dialysis (Pre, blue) relative to controls (Ctrl, red) (Figure 1C), while only 186 metabolites were decreased. These included 697 metabolites significantly decreased after dialysis and 470 of them showed no significant decrease after dialysis compared with pre-dialysis. Consistent with previous studies (Ravid and Chitalia, 2020), uremic solutes were enriched for products involved in amino acid, urea metabolism, and TCA pathways and other known markers of CKD (Supplementary Table S1). These included marked accumulation of creatinine (breakdown product of creatine normally cleared by the kidney (Zhang and Parikh, 2019)), asymmetric dimethylarginine (ADMA; an inhibitor of nitric oxide synthases linked to endothelial dysfunction), 4-hydroxyquinoline, acetylcarnitine, taurine, creatine, and homocysteine. (Figure 1D).

Strikingly, among all the significantly changed metabolites (1,167 increased and 186 decreased compounds, 1,353 in total) detected in ESKD as compared with the healthy cohort, only half (51.5%) of the elevated uremic compounds were quantitatively altered by hemodialysis (category 'I'; Figure 1C). Of the remainder, 34.7% serum metabolites remained significantly elevated in ESKD even post-dialysis (Post, green) relative to baseline levels (category 'II'), while 13.7% showed reduced levels compared with the healthy cohort (category 'III' in Figure 1C). The former included creatinine, whose levels in ESKD remained 7.5 times higher on average even post-dialysis than those in control (Figure 1D), as well as uric acid and 41 putative metabolites (FC > 5, $p < 0.05$; Supplementary Table S1) that remained unclear in previous CKD analyses (Liu et al., 2017; Ravid and Chitalia, 2020), such as cystine, 5-hydroxyindole-3-acetic acid (5-HIAA), 4-acetamidobutyric acid, indole-3-carboxaldehyde, 12-hydroxyicosatetraenoic acid (12-HEPE), cadaverine, and linoleic acid (Figure 1E).

Interestingly, while most of the metabolites maintained high circulating levels in patient's blood, we found that metabolites including tryptophan, dimethylglycine, phosphocreatine, and

acetyl-tryptophan were significantly lower in ESKD than those in the healthy cohort. Some of these metabolites might play important roles in progression of CKD. As reported in a previous study with the large cohort ($n = 1915$), a lower level of plasma tryptophan and high kynurenine-tryptophan ratios were associated with a high risk for ESKD progression. The tryptophan-kynurenine pathway alteration in ESKD showed a strong correlation with type 2 diabetes (Liu et al., 2023), which is one of the commonly observed complications in ESKD patients. This result was consistent with our finding, as shown in Figure 1D (increased kynurenine and decreased tryptophan), suggesting that shunting the tryptophan catabolism in kynurenine may slow the CKD progression.

Although metabolite identification remains challenging, a stringent match score cut-off (>0.7) was used to establish high-confident database (MSDIAL) search results (see Figures 1D, E for several spectra matching cases). We independently validated 21 of these candidate metabolite markers using reference standards (MetaSCI) using both MS/MS and retention time matching (Table 2).

Persistent elevation of lipids in ESKD patients undergoing hemodialysis

Our metabolic profiling also revealed numerous circulating lipids, showing differential accumulation in ESKD (Supplementary Table S1) from the same nLC-MS run. Consistent with previous studies (Reis et al., 2015; Chen et al., 2017), five main lipid classes were significantly elevated in the pre-dialysis samples (Figure 2A): glycerophospholipids (PC, PE, and PG), glycerolipids (TG, DG, and MG), sphingolipids (Cer, MIPC, SM, and SPB), sterol lipids (SE, ST, and BA), lysophospholipids (LPC, LPE, and LPG), and fatty acyls (FA). For example, LysoPC 16:0 was elevated significantly (FC = 8.9, $p < 0.01$) in pre-dialysis and maintained a high concentration even after dialysis compared with Ctrl (FC = 6.6, $p < 0.01$) (Figure 2B). The identity of LysoPC 16:0 was confirmed by MS2 spectral analysis and retention time matching using a reference standard (Figure 2B; Table 2). Although ceramides (Cer), steryl esters (SE), and glycerolipids (TG) were largely cleared by dialysis (Figure 2A), we also found that bile acids and lysophospholipids, such as lysophosphatidylethanolamine (LPE), lysophosphatidylcholine (LPC), and lysophosphatidylglycerol (LPG), were not efficiently removed, potentially contributing to the high incidence of CVD observed in ESKD.

Uremic toxins link to cardiovascular disease

To investigate the putative effect of persistent metabolites on cardiovascular disorders often observed in CKD, we performed a cytotoxicity assay with human iPSC-derived cardiomyocytes. Among the hundreds of elevated metabolites in ESKD compared with the healthy cohort, metabolites associated with methionine metabolism (e.g., methionine and homocysteine), glycine and serine metabolism, and taurine metabolism were identified. Homocysteine, a sulfur-containing amino acid derived from methionine metabolism, was previously reported to increase the risk of CVD using rodent cardiomyocytes isolated from mice or rats (Sipkens

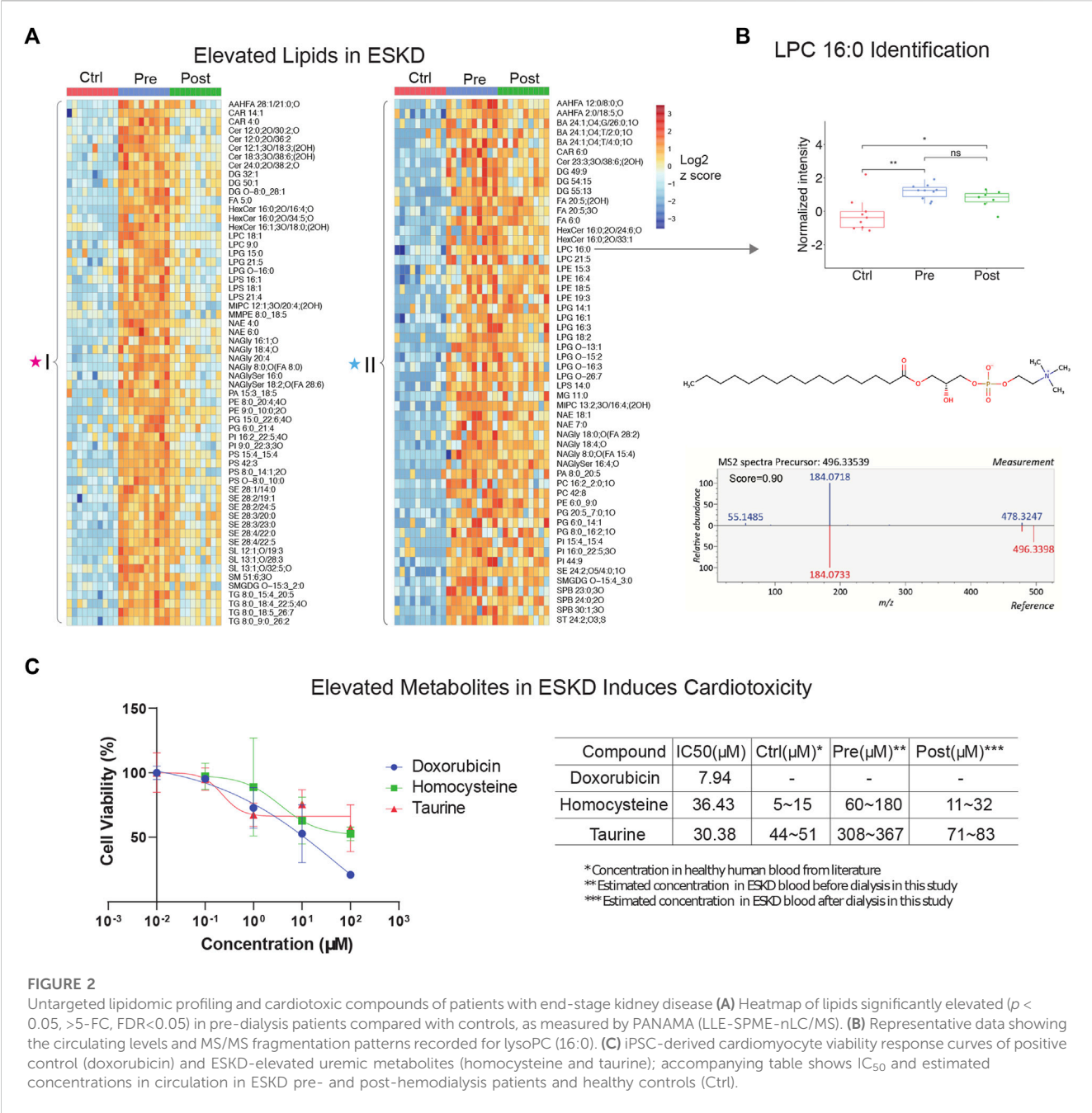
TABLE 2 Elevated metabolites identified in the serum from end-stage kidney disease patients confirmed by reference standards.

Metabolite name	Formula	m/z	Average Rt, min	Rt Δ,min	MS/MS matched	Adduct type	Accession
2,3-Dihydroxybenzoic acid	C ₇ H ₆ O ₄	153.01921	31.0	0.4	TRUE	[M-H] ⁻	HMDB0000397
4-Hydroxyquinoline	C ₉ H ₇ NO	146.05943	18.6	-0.8	TRUE	[M + H] ⁺	PUBCHEM CID69141
6-Methylcoumarin	C ₁₀ H ₈ O ₂	161.05898	24.9	-0.1	TRUE	[M + H] ⁺	HMDB0032394
Caffeine	C ₈ H ₁₀ N ₄ O ₂	195.08676	15.0	0.7	TRUE	[M + H] ⁺	HMDB0001847
Creatine anhydrous	C ₄ H ₉ N ₃ O ₂	132.07625	0.8	0.2	TRUE	[M + H] ⁺	HMDB0000064
Creatinine	C ₄ H ₇ N ₃ O	114.06605	0.4	0.5	TRUE	[M + H] ⁺	HMDB0000562
Famotidine	C ₈ H ₁₅ N ₇ O ₂ S ₃	338.05096	10.3	1.5	TRUE	[M + H] ⁺	HMDB0001919
L-Arginine	C ₆ H ₁₄ N ₄ O ₂	175.1183	0.2	2.0	TRUE	[M + H] ⁺	HMDB0000517
L-Glutamine	C ₅ H ₁₀ N ₂ O ₃	147.07596	1.3	-0.4	TRUE	[M + H] ⁺	HMDB0000641
L-Kynurenine	C ₁₀ H ₁₂ N ₂ O ₃	209.09135	11.5	-0.9	TRUE	[M + H] ⁺	HMDB0000684
L-Leucine	C ₆ H ₁₃ NO ₂	132.10136	4.5	-0.7	TRUE	[M + H] ⁺	HMDB0000687
L-Phenylalanine	C ₉ H ₁₁ NO ₂	166.08556	10.4	0.3	TRUE	[M + H] ⁺	HMDB0000159
L-Proline	C ₅ H ₉ NO ₂	116.07044	2.9	1.8	TRUE	[M + H] ⁺	HMDB0000162
L-Tryptophan	C ₁₁ H ₁₂ N ₂ O ₂	205.09622	12.3	0.2	TRUE	[M + H] ⁺	HMDB0000929
L-Tyrosine	C ₉ H ₁₁ NO ₃	182.08064	4.3	0.7	TRUE	[M + H] ⁺	HMDB0000158
LPC 16:0	C ₂₄ H ₅₀ NO ₇ P	496.3385	35.5	0.5	TRUE	[M + H] ⁺	HMDB0010382
Piperine	C ₁₇ H ₁₉ NO ₃	286.1423	31.3	-0.7	TRUE	[M + H] ⁺	HMDB0029377
Riboflavin	C ₁₇ H ₂₀ N ₄ O ₆	375.13385	15.5	0.1	TRUE	[M-H] ⁻	HMDB0000244
Taurine	C ₂ H ₇ NO ₃ S	124.00748	1.3	0.7	TRUE	[M-H] ⁻	HMDB0000251
Theobromine	C ₇ H ₈ N ₄ O ₂	181.07126	12.2	1.7	TRUE	[M + H] ⁺	HMDB0002825
Uracil	C ₄ H ₄ N ₂ O ₂	113.03434	7.5	-0.8	TRUE	[M + H] ⁺	HMDB0000300

et al., 2007; Wang et al., 2012), which are imperfect models of human pathophysiology. In contrast, we examined the toxicity of these compounds using human iPSC-derived cardiomyocytes. Although, other non-myocyte cells, including smooth muscle cells, endothelial cells, cardiofibroblasts, and epicardium, have been broadly used in cardiac condition evaluation (Funakoshi and Yoshida, 2021), iPSC-derived cardiomyocytes are a widely used model that has been used extensively for cardiotoxicity screenings (Fonoudi and Burridge, 2021). This model faithfully recapitulates characteristics unique to human pathobiology and provides a less heterogeneous source of cells, which we feel offers a better validation system for evaluating the potential clinical relevance of metabolites we found at persistently high levels in the human serum. Likewise, taurine, a sulfur amino acid-like compound similar to methionine and homocysteine, has been linked to cardiovascular disease during impaired kidney function (Bkaily et al., 2020). Although it is difficult to make a conclusion about the beneficial and possible toxic effects of taurine, particularly the effect on cardiovascular under ESKD, reaching a clear understanding requires further exploration.

Here, we evaluated two selected metabolites, homocysteine and taurine, to determine their relative cytotoxicity effect using DOX (a known cardiotoxin) as a positive control. It has been demonstrated

that iPSC-derived cardiomyocytes exposed to DOX show a decrease in cell viability, increased intracellular Ca²⁺, resulting in a decrease in spike amplitude, and an increase in the beat rate. These effects are correlated and are observed immediately after exposure and worsened with prolonged treatment (7–14 days) (Maillet et al., 2016). Notably, we observed homocysteine and taurine reduced cell viabilities (Figure 2C). In comparison with the IC₅₀ value of doxorubicin (7.94 μM), a compound with known cytotoxic effects on cardiomyocytes, the IC₅₀ values for homocysteine and taurine were 36.43 μM and 30.38 μM, respectively. In healthy human plasma, the concentration of homocysteine is typically 5–15 μM (Wang et al., 2019), whereas we estimate that the concentration of homocysteine in ESKD patients before dialysis is at least 12 times higher (60–180 μM, Figure 2C) than that in the control cohort using our precision LC-MS as relative quantification. The concentration was estimated using the relative intensities after normalization across control, and pre- and post-dialysis groups. The concentration of taurine was also seven times higher (estimated 308–367 μM) in the ESKD patient serum than that found in normal human plasma (Trautwein and Hayes, 1995) and remains 1.6 times higher even after hemodialysis. Significantly elevated blood concentrations of these compounds in patients potentially contribute to CVD and poor clinical outcomes. Unlike for DOX,



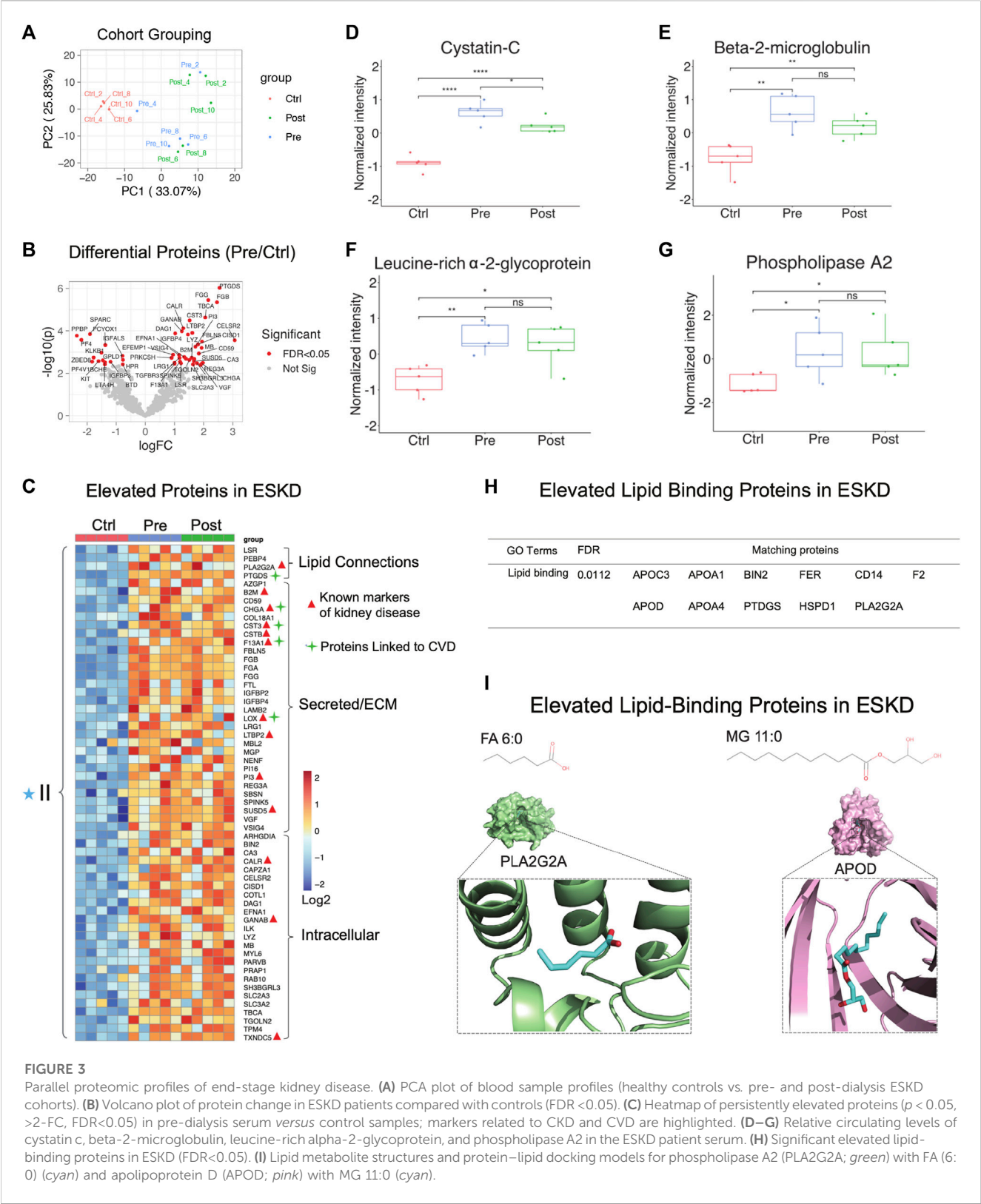
there was no significantly altered contraction observed for any of the concentrations of homocysteine and taurine tested. Hence, future studies are required to assess long-term functional consequences on heart cell function.

Parallel proteomic analysis reveals proteins elevated in ESKD

PCA showed that hemodialysis (using an Optiflux filter consisting of an inner diameter of ~200 microns) did not significantly alter circulating protein levels (Figure 3A, post vs. pre). As expected, among all 83 proteins which were significantly elevated ($p < 0.05$, ≥ 1.5 -fold-change) in ESKD patients relative to controls (Figure 3B, C), only

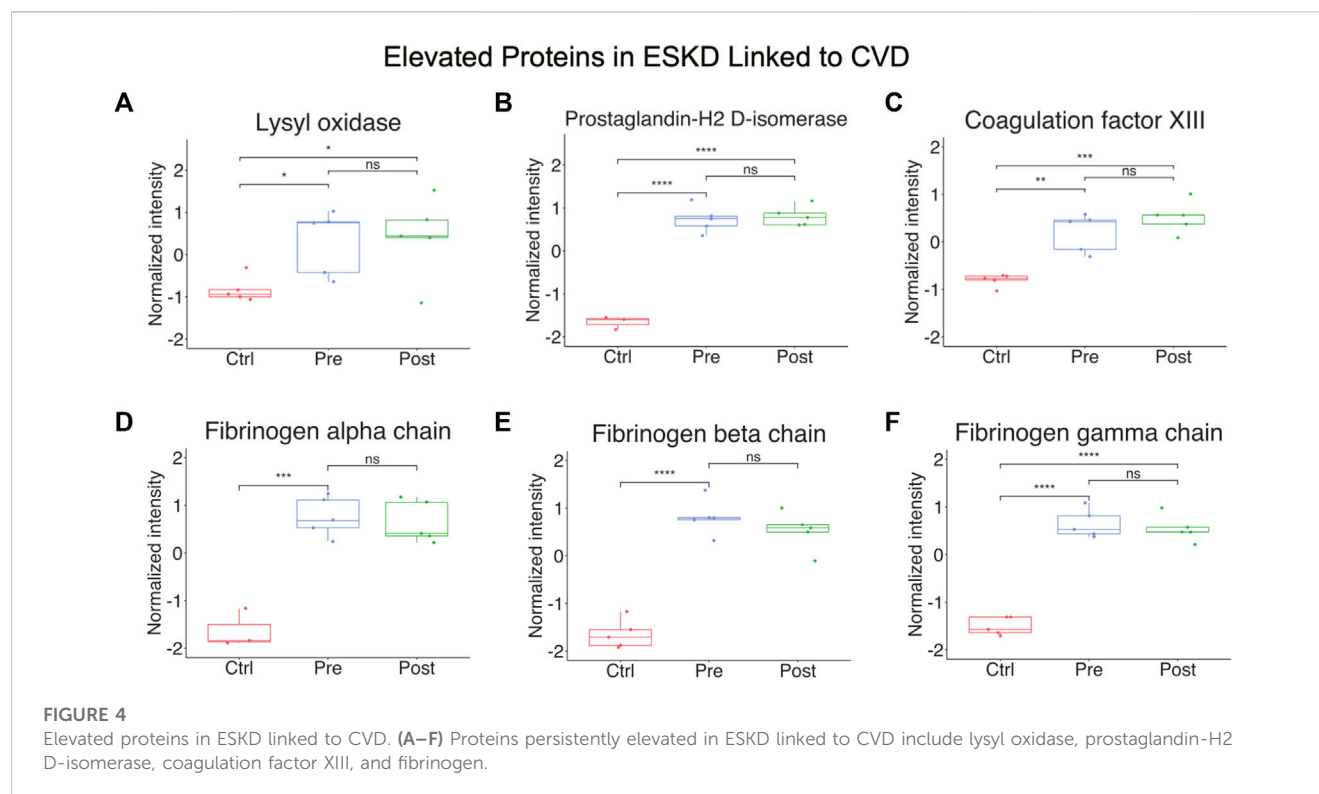
19 of them got slightly decreased after dialysis (1.2 fold-change in post vs. pre). In addition to known markers of renal dysfunction that accumulate when glomerular filtration is impaired (George and Gounden, 2019), such as PTGDS, LTBP2, F13A1, and the secreted factors cystatin C (CST3, Figure 3D) and beta-2 microglobulin (B2M) (Figure 3E), we also detected leucine-rich alpha-2-glycoprotein (LRG1) (Figure 3F), previously suggested (Glorieux et al., 2015) as an indicator of vascular damage and heart failure; TXNDC5, a mediator of cardiac fibrosis (Chen et al., 2021); and calreticulin (CALR, Figure 3C), a marker of renal fibrosis (Lu et al., 2020).

Consistent with the large-scale change in circulating lipids we detected, elevated levels in multiple lipid-binding proteins were observed, such as phospholipase A2 (PLA2G2A, Figure 3G), lipolysis-stimulated lipoprotein receptor (LSR),



phosphatidylethanolamine-binding protein 4 (PEBP4), prostaglandin-H2 D-isomerase (PTGDS), and apolipoprotein C3/D) (Figure 3H). Co-upregulated pairs include high-confidence associations (Aleksenko et al., 2020) between APOD and monoacylglycerol (MG, 11:0), and PLA2G2A with FA (6:0) (Figure 3I), reflecting a direct functional coupling between these proteins and their corresponding lipid ligands.

Other notable alterations in ESKD included upregulation of factors involved in cell adhesion, fibrosis, and blood coagulation (Figure 4A–F), and the downregulation of inhibitors



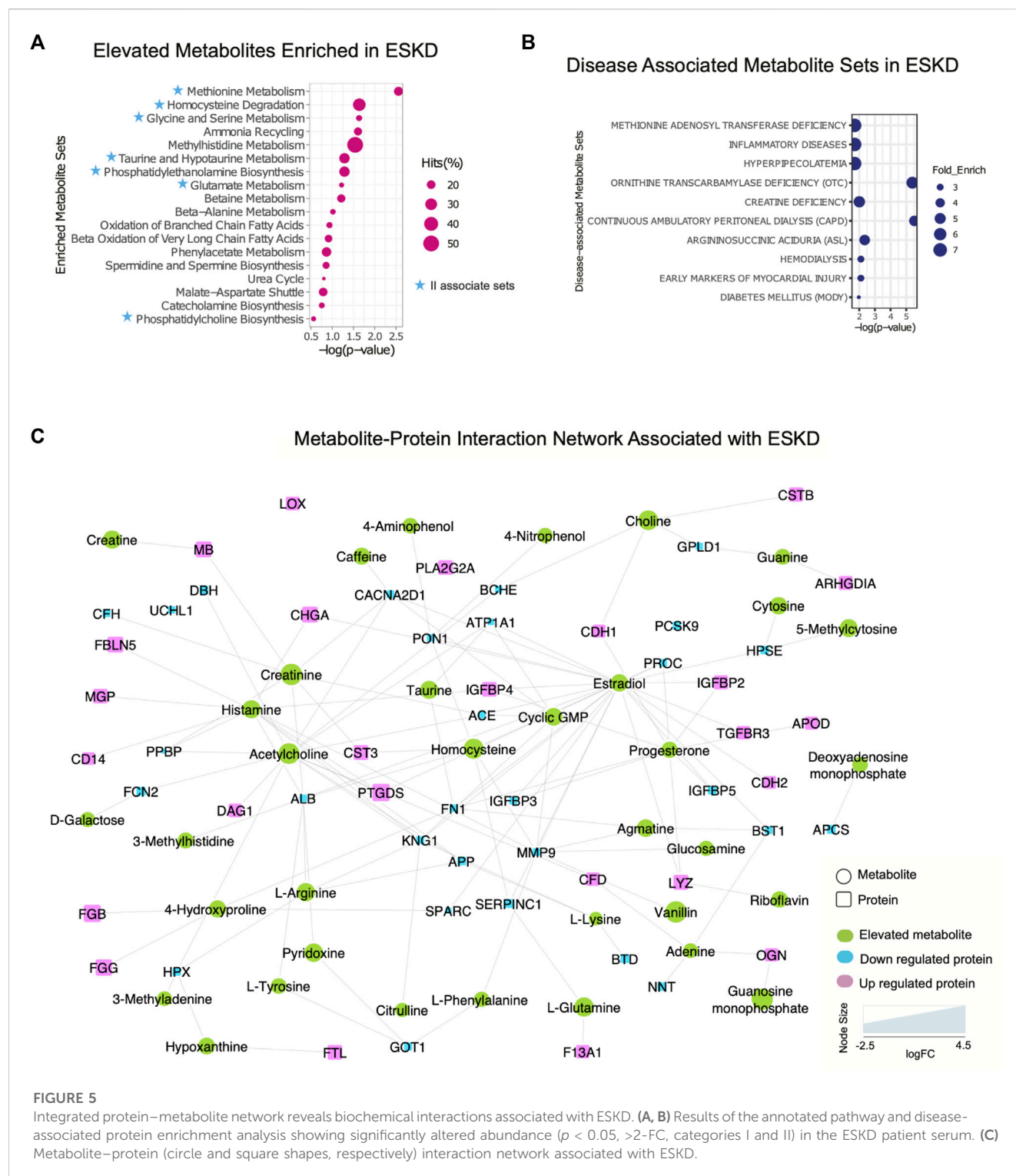
of inflammation. The former included integrin-linked protein kinase (ILK), implicated in cellular dysfunction, fibrosis, and inflammation in animal studies (Zhao et al., 2015), and lysyl oxidase (LOX, Figure 4A), an extracellular enzyme known to control fibrosis (Papadantonakis et al., 2012), while the latter included factors associated with atherothrombosis, such as PTGDS (platelet aggregation, Figure 4B), F13A1 (subunit of plasma coagulation factor XIII associated with arterial and venous thrombosis (Carreras-Torres et al., 2010)), and fibrinogen (Figure 4D–F), which is associated with recurrent DVT and pulmonary embolism (Bereczky et al., 2007)). These findings are particularly noteworthy, given that these clinical events had a high occurrence in our ESKD patient cohort (Table 1).

Dual workflow provides an integrated protein–metabolite network associated with ESKD

Metabolomic pathways play an important role in waste product breakdown and excretion in ESKD such that a better understanding of these pathways is essential to improve patient outcomes. To identify pathways and biological processes in which these metabolites played a role, we performed enrichment analysis using the Small Molecule Pathway Database (SMPDB). As shown in Figure 5A, elevated metabolites (categories I and II) associated with ESKD were involved in diverse metabolomic pathways, including ammonia recycling and urea cycle, and when the kidney failed to convert urea and ammonia into less toxic form (Weiner et al., 2015), along with methionine metabolism due to the poor renal clearance and degradation of homocysteine, a byproduct

of methionine, they were not efficiently removed by dialysis (Zhloba and Subbotina, 2022), as well as oxidation of fatty acids and amino acid metabolism (glycine, serine, methylhistidine and glutamate metabolism, etc.) (Figure 5A) (van de Poll et al., 2004). Additionally, compounds linked to taurine metabolism, phosphatidylethanolamine biosynthesis, betaine metabolism, phenylacetate metabolism, and phosphatidylcholine biosynthesis were found to be elevated in the blood of ESKD patients. Among these, metabolites related to ammonia recycling, urea cycle, methylhistidine metabolism, and phenylacetate metabolism were efficiently removed by dialysis ($FC > 2$, $p < 0.05$ of post/pre), whereas uremic compounds involved in methionine metabolism, homocysteine degradation, glycine and serine metabolism, taurine and hypotaurine metabolism, phosphatidylethanolamine biosynthesis, glutamate metabolism, and phosphatidylcholine biosynthesis remained elevated after hemodialysis (Figure 5A, blue star). Since persistent compounds are more likely to be associated with the poor outcomes, we tested some candidates' adverse effects *in vitro* and confirmed that homocysteine and taurine are cardiotoxic (Figure 2C).

We extended our investigation to explore the correlation of the elevated metabolites in the ESKD patient and clinical disease. Our disease enrichment analysis (Figure 5B) revealed metabolites (categories I and II) related to creatine deficiency and hemodialysis along with methionine adenosyl transferase, hyperpeicolatemia, and ornithine transcarbamylase deficiency, which depend on kidney clearance, and compounds linked to ESKD complications such as inflammation, diabetes (energy metabolism disturbance), and early markers on myocardial injury (presumably due to a larger blood volume that increases the heart workload in CKD) (Aoki and Ikari, 2017).



To explore the potential association between metabolites and proteins, we searched the STITCH database (Kuhn et al., 2008), which considers factors such as the chemical structure and molecular activities to establish physical or functional connections between small-molecule compounds and polypeptides. As shown in Figure 5C, creatinine, a key biomarker of CKD, showed direct physical interactions with the blood proteins

CST3, MB, serum albumin (ALB), angiotensin-converting enzyme (ACE), complement factor H (CFH), and voltage-dependent calcium channel subunit alpha-2/delta-1 (CACNA2D1), while homocysteine was connected to CST3, serum paraoxonase/arylesterase 1 (PON1), and antithrombin-III (SERPINC1) (Figure 5C). Both increased creatinine and cystatin C (CST3) are commonly measured to estimate the kidney function. Clinical studies have demonstrated

that a high creatinine–cystatin C ratio is correlated with better survival of CKD, which can reflect changes in muscle mass (Jung et al., 2021). For high creatinine levels, lowering blood cystatin C levels could be a strategy to potentially lower mortality. Conversely, the decrease in serum albumin (indirect indication of high urine ALB) associated with a decline renal function was apparent (Figure 5C), consistent with the albumin-to-creatinine ratio as a risk factor for diabetes-related outcomes (Gerstein et al., 2022). Importantly, the serum protein–metabolite interactions that annotated in our integrated analysis revealed a larger network encompassing other components associated with clinical complications of ESKD. For instance, meta-analysis revealed that serum paraoxonase 1 (PON1) activity is likely reduced in CKD (decreased level shown in Figure 5C), suggesting the antioxidant defense is impaired (Watanabe et al., 2023). The beneficial role of PON1 activity on reducing the cardiovascular event has been reported (Shih and Lusis, 2009). Intriguingly, the interaction of homocysteine and PON1 implies that changes in their levels exert a synergistic effect on clinical outcomes in ESKD patients.

Moreover, interactions/bindings of ALB with many other metabolites including creatinine, homocysteine, uric acid, arginine, pyridoxine, tyrosine, and 3-methylhistidine might relate to the low filtering efficiency for small molecules during dialysis (Figure 5C). A comprehensive protein network was annotated including the interactions of ESKD protein biomarkers (PTGDS, F13A1, and CSTB) with acetylcholine, histamine, choline, and lipid-binding proteins (PLA2G2A, PTGDS, APOD, and MG) with linoleic acid, isovaleric acid, atorvastatin, creatine, creatinine, and enzyme related to fibrinogen (LOX) with linoleic acid (Figure 5C). This global serum protein–metabolite interaction network enables exploration and visualization of functionally-related (through physical interactions) metabolites and proteins associated with ESKD and associated clinical outcomes.

Discussion

The identity of chronically dysregulated metabolites, lipids, and proteins in the blood of patients being treated for ESKD is not fully known (Slocum et al., 2012). To this end, we applied dual convergent metabolomics and proteomic workflows to characterize circulating biomolecules that remain elevated despite hemodialysis. This may reflect binding to blood proteins (e.g., albumin) that precludes clearance by filtration. Persistently elevated levels of uremic compounds have been implicated in serious clinical complications, including CVD (Ravid et al., 2021), as well as bone and mineral disruption, anemia, and infertility in patients with CKD (Zalunardo and Levin, 2006; Raggi and Kleerekoper, 2008; Dumanski and Ahmed, 2019), but the products that are differentially retained in CKD remain incompletely characterized.

Our cytotoxicity assay demonstrated that two of the identified uremic compounds, homocysteine and taurine, significantly reduced human iPSC-derived cardiomyocyte viability, which is a well-established model to determine cardiotoxicity (Satsuka and Kanda, 2020). Elevated homocysteine has previously been implicated in cardiac remodeling and coronary heart disease (Kar et al., 2019),

while taurine has been proposed to have a cardioprotective effect (Takatani et al., 2004). Although our taurine results are counterintuitive, prior studies documented its anti-apoptotic effect in the context of ischemia or heart disease. Although further investigation is required to determine their molecular targets in cardiac cells, our preliminary results are consistent with a putative role for these persistently elevated compounds in the observed cardiac phenotypes commonly observed in CKD.

High levels of primary bile acids have been reported to contribute to cardiac hypertrophy and heart failure (Desai et al., 2017), common risk factors for mortality associated with dialysis. The activation of PLA2 leads to the release of FA and elevation of the LPC level. Chronic elevation of these markers may be one reason for the accelerated atherosclerosis and CVD-related complications commonly observed in ESKD (Nusair et al., 2012). In CVDs, LPC induces macrophages to uptake oxidized low-density lipoproteins (ox-LDLs), leading to the formation of foam cells, and aggravates the development of atherosclerotic plaques (Aiyar et al., 2007; Reis et al., 2015), which is linked to the high incidence of CVD in dialysis patients. LPC's effects on endothelial cells and vascular smooth muscle cells play a vital role in the progression on CVDs (Liu et al., 2020). However, further studies are needed to investigate the effects of potential biomarkers, including LPC, PLA2, homocysteine, taurine, and other persistent metabolites we have identified in various disease models independently (e.g., endothelial cell and smooth muscle cells). It has been demonstrated that LPC, particularly 16:0, increases the release of inflammatory cytokines from endothelial cells (Morita et al., 2015). Additionally, LPC promotes the expression of adhesive molecules and enhances the adhesive effect of endothelial cells. Therefore, further evaluation of these effects of uremic toxins would shed light on the mechanism of the correlation between ESKD and heart failure in patients.

In summary, integration of untargeted metabolomics and proteomics enabled the exploration of multiple analyte types and their associated interactions starting from limiting amounts of biospecimens rich in interfering matrix components using widely available instrumentation to identify potentially clinically actionable prognostic markers of disease progression. Our integrated metabolite–protein network generates a comprehensive picture of the ‘disease interactome’ associated with ESKD patients despite them undergoing hemodialysis, providing mechanistic insights for better clinical management.

Data availability statement

The datasets presented in this study can be found in online repositories. The names of the repository/repositories and accession number(s) can be found in the article/Supplementary Material. Data for this project have been deposited to the MassIVE archive accession code MSV000091579 (doi:10.25345/C5CV4C23Z).

Ethics statement

The studies involving humans were approved by the Boston University Medical Campus and were IRB-approved (H-26367). The studies were conducted in accordance with the local legislation

and institutional requirements. The participants provided their written informed consent to participate in this study.

Author contributions

AE conceived and supervised the study. WL and FM developed and optimized the metabolite extraction protocol and the nLC-MS method and parameters. WL performed the data acquisition. WL, BB, and CH performed the data analyses. JM and NL contributed to the cardiotoxicity assay, MM provided technical support. SK, WY, NR, DK, ML, and VC contributed to the interpretation of the data. WL and AE co-wrote the manuscript. All authors contributed to the article and approved the submitted version.

Funding

This work was supported by operating funds to AE from the Canadian Institutes of Health Research (FDN-148399) and generous start-up funds from Boston University. This work was also supported by funds to VC from the National Heart Lung and Blood Institute (1R01HL166608).

Acknowledgments

The authors are grateful for the assistance and critical input provided by colleagues in Toronto and Boston. The authors thank

Juntuo Zhou from Peking University for the technical suggestion on metabolomics. The authors also thank Micheal A. McLellan for providing iPSC-cardiomyocytes cells and Thu Nguyen for helping with data interpretation.

Conflict of interest

The authors declare that the research was conducted in the absence of any commercial or financial relationships that could be construed as a potential conflict of interest.

Publisher's note

All claims expressed in this article are solely those of the authors and do not necessarily represent those of their affiliated organizations, or those of the publisher, the editors, and the reviewers. Any product that may be evaluated in this article, or claim that may be made by its manufacturer, is not guaranteed or endorsed by the publisher.

Supplementary material

The Supplementary Material for this article can be found online at: <https://www.frontiersin.org/articles/10.3389/fphar.2023.1243505/full#supplementary-material>

References

- Adusumilli, R., and Mallick, P. (2017). Data conversion with ProteoWizard msConvert. *Methods Mol. Biol.* 1550, 339–368. doi:10.1007/978-1-4939-6747-6_23
- Aiyar, N., Disa, J., Ao, Z., Ju, H., Nerurkar, S., Willette, R. N., et al. (2007). Lysophosphatidylcholine induces inflammatory activation of human coronary artery smooth muscle cells. *Mol. Cell Biochem.* 295 (1–2), 113–120. doi:10.1007/s11010-006-9280-x
- Alekseenko, A., Kotelnikov, S., Ignatov, M., Egbert, M., Kholodov, Y., Vajda, S., et al. (2020). ClusPro LigTBM: automated template-based small molecule docking. *J. Mol. Biol.* 432 (11), 3404–3410. doi:10.1016/j.jmb.2019.12.011
- Aoki, J., and Ikari, Y. (2017). Cardiovascular disease in patients with end-stage renal disease on hemodialysis. *Ann. Vasc. Dis.* 10 (4), 327–337. doi:10.3400/avd.ra.17-00051
- Bello, A. K., Alrukhai, M., Ashuntantang, G. E., Basnet, S., Rotter, R. C., Douthat, W. G., et al. (2017). Complications of chronic kidney disease: current state, knowledge gaps, and strategy for action. *Kidney Int. Suppl.* 7 (2), 122–129. doi:10.1016/j.kisu.2017.07.007
- Berczky, Z., Balogh, E., Katona, E., Pocsai, Z., Czuriga, I., Szeles, G., et al. (2007). Modulation of the risk of coronary sclerosis/myocardial infarction by the interaction between factor XIII subunit A Val34Leu polymorphism and fibrinogen concentration in the high risk Hungarian population. *Thromb. Res.* 120 (4), 567–573. doi:10.1016/j.thromres.2006.12.013
- Bkaily, G., Jazsar, A., Normand, A., Simon, Y., Al-Khoury, J., and Jacques, D. (2020). Taurine and cardiac disease: state of the art and perspectives. *Can. J. Physiol. Pharmacol.* 98 (2), 67–73. doi:10.1139/cjpp-2019-0313
- Carreras-Torres, R., Athanasiadis, G., Via, M., Trenchs, J., Gaya-Vidal, M., Santamaria, J., et al. (2010). Allele-allele interaction within the F13A1 gene: a risk factor for ischaemic heart disease in Spanish population. *Thromb. Res.* 126 (3), e241–e245. doi:10.1016/j.thromres.2010.04.021
- Chen, H., Chen, L., Liu, D., Chen, D. Q., Vaziri, N. D., Yu, X. Y., et al. (2017). Combined clinical phenotype and lipidomic analysis reveals the impact of chronic kidney disease on lipid metabolism. *J. Proteome Res.* 16 (4), 1566–1578. doi:10.1021/acs.jproteome.6b00956
- Chen, Y. T., Jhao, P. Y., Hung, C. T., Wu, Y. F., Lin, S. J., Chiang, W. C., et al. (2021). Endoplasmic reticulum protein TXNDC5 promotes renal fibrosis by enforcing TGF-beta signaling in kidney fibroblasts. *J. Clin. Invest.* 131 (5), e143645. doi:10.1172/JCI143645
- Chong, J., and Xia, J. (2020). Using MetaboAnalyst 4.0 for metabolomics data analysis, interpretation, and integration with other Omics data. *Methods Mol. Biol.* 2104, 337–360. doi:10.1007/978-1-0716-0239-3_17
- Desai, M. S., Mathur, B., Eblimit, Z., Vasquez, H., Taegtmeier, H., Karpen, S. J., et al. (2017). Bile acid excess induces cardiomyopathy and metabolic dysfunctions in the heart. *Hepatology* 65 (1), 189–201. doi:10.1002/hep.28890
- Dubin, R. F., and Rhee, E. P. (2020). Proteomics and metabolomics in kidney disease, including insights into etiology, treatment, and prevention. *Clin. J. Am. Soc. Nephrol.* 15 (3), 404–411. doi:10.2215/CJN.07420619
- Dumanski, S. M., and Ahmed, S. B. (2019). Fertility and reproductive care in chronic kidney disease. *J. Nephrol.* 32 (1), 39–50. doi:10.1007/s40620-018-00569-9
- Elias, J. E., and Gygi, S. P. (2007). Target-decoy search strategy for increased confidence in large-scale protein identifications by mass spectrometry. *Nat. Methods* 4 (3), 207–214. doi:10.1038/nmeth1019
- Fonoudi, H., and Burrige, P. W. (2021). Cellular model systems to study cardiovascular injury from chemotherapy. *J. Thromb. Thrombolysis* 51 (4), 890–896. doi:10.1007/s11239-020-02299-x
- Funakoshi, S., and Yoshida, Y. (2021). Recent progress of iPSC technology in cardiac diseases. *Arch. Toxicol.* 95 (12), 3633–3650. doi:10.1007/s00204-021-03172-3
- George, J. A., and Gounden, V. (2019). Novel glomerular filtration markers. *Adv. Clin. Chem.* 88, 91–119. doi:10.1016/bs.acc.2018.10.005
- Gerstein, H. C., Ramasundarathetig, C., Avezum, A., Basile, J., Conget, I., Cushman, W. C., et al. (2022). A novel kidney disease index reflecting both the albumin-to-creatinine ratio and estimated glomerular filtration rate, predicted cardiovascular and kidney outcomes in type 2 diabetes. *Cardiovasc. Diabetol.* 21 (1), 158. doi:10.1186/s12933-022-01594-6
- Glorieux, G., Mullen, W., Duranton, F., Filip, S., Gayraud, N., Husi, H., et al. (2015). New insights in molecular mechanisms involved in chronic kidney disease using high-resolution plasma proteome analysis. *Nephrol. Dial. Transplant.* 30 (11), 1842–1852. doi:10.1093/ndt/gfv254
- Himmelfarb, J., Vanholder, R., Mehrotra, R., and Tonelli, M. (2020). The current and future landscape of dialysis. *Nat. Rev. Nephrol.* 16 (10), 573–585. doi:10.1038/s41581-020-0315-4

- Jung, C. Y., Joo, Y. S., Kim, H. W., Han, S. H., Yoo, T. H., Kang, S. W., et al. (2021). Creatinine-cystatin C ratio and mortality in patients receiving intensive care and continuous kidney replacement therapy: a retrospective cohort study. *Am. J. Kidney Dis.* 77 (4), 509–516.e1. doi:10.1053/j.ajkd.2020.08.014
- Kar, S., Shahshahan, H. R., Kambis, T. N., Yadav, S. K., Li, Z., Lefer, D. J., et al. (2019). Hydrogen sulfide ameliorates homocysteine-induced cardiac remodeling and dysfunction. *Front. Physiol.* 10, 598. doi:10.3389/fphys.2019.00598
- Kuhn, M., von Mering, C., Campillos, M., Jensen, L. J., and Bork, P. (2008). STITCH: interaction networks of chemicals and proteins. *Nucleic Acids Res.* 36 (Database issue), D684–D688. doi:10.1093/nar/gkm795
- Liu, J. J., Ching, J., Wee, H. N., Liu, S., Gurung, R. L., Lee, J., et al. (2023). Plasma tryptophan-kynurenine pathway metabolites and risk for progression to end-stage kidney disease in patients with type 2 diabetes. *Diabetes Care*, dc231147. doi:10.2337/dc23-1147
- Liu, P., Zhu, W., Chen, C., Yan, B., Zhu, L., Chen, X., et al. (2020). The mechanisms of lysophosphatidylcholine in the development of diseases. *Life Sci.* 247, 117443. doi:10.1016/j.lfs.2020.117443
- Liu, S., Wang, L., Hu, C., Huang, X., Liu, H., Xuan, Q., et al. (2017). Plasma metabolomics profiling of maintenance hemodialysis based on capillary electrophoresis - time of flight mass spectrometry. *Sci. Rep.* 7 (1), 8150. doi:10.1038/s41598-017-08327-w
- Lu, A., Pallero, M. A., Owusu, B. Y., Borovjagin, A. V., Lei, W., Sanders, P. W., et al. (2020). Calreticulin is important for the development of renal fibrosis and dysfunction in diabetic nephropathy. *Matrix Biol. Plus* 8, 100034. doi:10.1016/j.mbplus.2020.100034
- Maillet, A., Tan, K., Chai, X., Sadananda, S. N., Mehta, A., Ooi, J., et al. (2016). Modeling doxorubicin-induced cardiotoxicity in human pluripotent stem cell derived-cardiomyocytes. *Sci. Rep.* 6, 25333. doi:10.1038/srep25333
- Mohajerani, F., Clark, W. R., Ronco, C., and Narsimhan, V. (2022). Mass transport in high-flux hemodialysis: application of engineering principles to clinical prescription. *Clin. J. Am. Soc. Nephrol.* 17 (5), 749–756. doi:10.2215/CJN.09410721
- Morita, M., Sekine, A., Urano, Y., Nishimura, T., Takabe, W., Arai, H., et al. (2015). Lysophosphatidylcholine promotes SREBP-2 activation via rapid cholesterol efflux and SREBP-2-independent cytokine release in human endothelial cells. *J. Biochem.* 158 (4), 331–338. doi:10.1093/jb/mvv044
- Nusair, M. B., Rajpurohit, N., and Alpert, M. A. (2012). Chronic inflammation and coronary atherosclerosis in patients with end-stage renal disease. *Cardiorenal Med.* 2 (2), 117–124. doi:10.1159/000337082
- Papadantonakis, N., Matsuura, S., and Ravid, K. (2012). Megakaryocyte pathology and bone marrow fibrosis: the lysyl oxidase connection. *Blood* 120 (9), 1774–1781. doi:10.1182/blood-2012-02-402594
- Raggi, P., and Kleerekoper, M. (2008). Contribution of bone and mineral abnormalities to cardiovascular disease in patients with chronic kidney disease. *Clin. J. Am. Soc. Nephrol.* 3 (3), 836–843. doi:10.2215/CJN.02910707
- Ravid, J. D., and Chitalia, V. C. (2020). Molecular mechanisms underlying the cardiovascular toxicity of specific uremic solutes. *Cells* 9 (9), 2024. doi:10.3390/cells9092024
- Ravid, J. D., Kamel, M. H., and Chitalia, V. C. (2021). Uraemic solutes as therapeutic targets in CKD-associated cardiovascular disease. *Nat. Rev. Nephrol.* 17 (6), 402–416. doi:10.1038/s41581-021-00408-4
- Reis, A., Rudnitskaya, A., Chariyavilaskul, P., Dhaun, N., Melville, V., Goddard, J., et al. (2015). Top-down lipidomics of low density lipoprotein reveal altered lipid profiles in advanced chronic kidney disease. *J. Lipid Res.* 56 (2), 413–422. doi:10.1194/jlr.M055624
- Satsuka, A., and Kanda, Y. (2020). Cardiotoxicity assessment of drugs using human iPSC cell-derived cardiomyocytes: toward proarrhythmic risk and cardio-oncology. *Curr. Pharm. Biotechnol.* 21 (9), 765–772. doi:10.2174/1389201020666190628143345
- Shih, D. M., and Lusis, A. J. (2009). The roles of PON1 and PON2 in cardiovascular disease and innate immunity. *Curr. Opin. Lipidol.* 20 (4), 288–292. doi:10.1097/MOL.0b013e32832ca1ee
- Sipkens, J. A., Krijnen, P. A., Meischl, C., Cillessen, S. A., Smulders, Y. M., Smith, D. E., et al. (2007). Homocysteine affects cardiomyocyte viability: concentration-dependent effects on reversible flip-flop, apoptosis and necrosis. *Apoptosis* 12 (8), 1407–1418. doi:10.1007/s10495-007-0077-5
- Slocum, J. L., Heung, M., and Pennathur, S. (2012). Marking renal injury: can we move beyond serum creatinine? *Transl. Res.* 159 (4), 277–289. doi:10.1016/j.trsl.2012.01.014
- Takatani, T., Takahashi, K., Uozumi, Y., Shikata, E., Yamamoto, Y., Ito, T., et al. (2004). Taurine inhibits apoptosis by preventing formation of the Apaf-1/caspase-9 apoptosome. *Am. J. Physiol. Cell Physiol.* 287 (4), C949–C953. doi:10.1152/ajpcell.00042.2004
- Trautwein, E. A., and Hayes, K. C. (1995). Plasma and whole blood taurine concentrations respond differently to taurine supplementation (humans) and depletion (cats). *Z. Ernährungswiss.* 34 (2), 137–142. doi:10.1007/BF01636947
- Tsugawa, H., Cajka, T., Kind, T., Ma, Y., Higgins, B., Ikeda, K., et al. (2015). MS-DIAL: data-independent MS/MS deconvolution for comprehensive metabolome analysis. *Nat. Methods* 12 (6), 523–526. doi:10.1038/nmeth.3393
- van de Poll, M. C., Soeters, P. B., Deutz, N. E., Fearon, K. C., and Dejong, C. H. (2004). Renal metabolism of amino acids: its role in interorgan amino acid exchange. *Am. J. Clin. Nutr.* 79 (2), 185–197. doi:10.1093/ajcn/79.2.185
- Virani, S. A., Khosla, A., and Levin, A. (2008). Chronic kidney disease, heart failure and anemia. *Can. J. Cardiol.* 24, 22B–4B–24B. doi:10.1016/s0828-282x(08)71026-2
- Wang, N., Chen, M., Gao, J., Ji, X., He, J., Zhang, J., et al. (2019). A series of BODIPY-based probes for the detection of cysteine and homocysteine in living cells. *Talanta* 195, 281–289. doi:10.1016/j.talanta.2018.11.066
- Wang, X., Cui, L., Joseph, J., Jiang, B., Pimental, D., Handy, D. E., et al. (2012). Homocysteine induces cardiomyocyte dysfunction and apoptosis through p38 MAPK-mediated increase in oxidant stress. *J. Mol. Cell Cardiol.* 52 (3), 753–760. doi:10.1016/j.jmcc.2011.12.009
- Watanabe, J., Kotani, K., and Gugliucci, A. (2023). Paraoxonase 1 and chronic kidney disease: a meta-analysis. *J. Clin. Med.* 12 (3), 1199. doi:10.3390/jcm12031199
- Weiner, I. D., Mitch, W. E., and Sands, J. M. (2015). Urea and ammonia metabolism and the control of renal nitrogen excretion. *Clin. J. Am. Soc. Nephrol.* 10 (8), 1444–1458. doi:10.2215/CJN.10311013
- Zalunardo, N., and Levin, A. (2006). Anemia and the heart in chronic kidney disease. *Semin. Nephrol.* 26 (4), 290–295. doi:10.1016/j.semnephrol.2006.05.005
- Zhang, W. R., and Parikh, C. R. (2019). Biomarkers of acute and chronic kidney disease. *Annu. Rev. Physiol.* 81, 309–333. doi:10.1146/annurev-physiol-020518-114605
- Zhao, Y. Y., Vaziri, N. D., and Lin, R. C. (2015). Lipidomics: new insight into kidney disease. *Adv. Clin. Chem.* 68, 153–175. doi:10.1016/bs.acc.2014.11.002
- Zhloba, A. A., and Subbotina, T. F. (2022). Methionine and total homocysteine in hypertensive patients with renal excretory dysfunction. *Klin. Lab. Diagn.* 67 (11), 625–632. doi:10.51620/0869-2084-2022-67-11-625-632



OPEN ACCESS

EDITED BY

Raghuveera Kumar Goel,
Boston University, United States

REVIEWED BY

Naga Praneeth Raja,
Oregon Health and Science University,
United States
Pedro Rodriguez Cutillas,
Queen Mary University of London,
United Kingdom

*CORRESPONDENCE

Jonathan M. G. Higgins,
✉ jonathan.higgins@ncl.ac.uk

RECEIVED 09 October 2023

ACCEPTED 27 November 2023

PUBLISHED 14 December 2023

CITATION

Stephenson EH and Higgins JMG (2023),
Pharmacological approaches to
understanding protein kinase
signaling networks.
Front. Pharmacol. 14:1310135.
doi: 10.3389/fphar.2023.1310135

COPYRIGHT

© 2023 Stephenson and Higgins. This is
an open-access article distributed under
the terms of the [Creative Commons
Attribution License \(CC BY\)](#). The use,
distribution or reproduction in other
forums is permitted, provided the original
author(s) and the copyright owner(s) are
credited and that the original publication
in this journal is cited, in accordance with
accepted academic practice. No use,
distribution or reproduction is permitted
which does not comply with these terms.

Pharmacological approaches to understanding protein kinase signaling networks

Elloise H. Stephenson and Jonathan M. G. Higgins*

Faculty of Medical Sciences, Biosciences Institute, Newcastle University, Newcastle upon Tyne, United Kingdom

Protein kinases play vital roles in controlling cell behavior, and an array of kinase inhibitors are used successfully for treatment of disease. Typical drug development pipelines involve biological studies to validate a protein kinase target, followed by the identification of small molecules that effectively inhibit this target in cells, animal models, and patients. However, it is clear that protein kinases operate within complex signaling networks. These networks increase the resilience of signaling pathways, which can render cells relatively insensitive to inhibition of a single kinase, and provide the potential for pathway rewiring, which can result in resistance to therapy. It is therefore vital to understand the properties of kinase signaling networks in health and disease so that we can design effective multi-targeted drugs or combinations of drugs. Here, we outline how pharmacological and chemo-genetic approaches can contribute to such knowledge, despite the known low selectivity of many kinase inhibitors. We discuss how detailed profiling of target engagement by kinase inhibitors can underpin these studies; how chemical probes can be used to uncover kinase-substrate relationships, and how these tools can be used to gain insight into the configuration and function of kinase signaling networks.

KEYWORDS

kinome, kinase, kinase inhibitor, cell signaling, chemo-genetics, phosphoproteomics, systems biology, drug development

1 Introduction

The clinical success of numerous protein kinase inhibitors has highlighted the importance of kinase signaling in disease (Cohen et al., 2021). It is clear that kinases function within complex signaling networks (Hopkins, 2008; Knight et al., 2010), and a better understanding of these networks will enable disease research and drug development. Pharmaceutical companies remain focused on well understood targets, and comprehensive characterization of kinase action within their networks in cells is needed to allow drug development to be pursued with a lower risk of failure (Oprea et al., 2018).

To fully understand kinase signaling in disease we must learn about the properties of the wider network in affected cells. For example, mutations or changes in expression level of one

Abbreviations: AML, Acute Myeloid Leukemia; BRET, Bioluminescence Resonance Energy Transfer; CETSA, Cellular Thermal Stability Assay; DSF, Differential Scanning Fluorimetry; EBDT, Expectancy of Being Downstream Target; KCGS, Kinase Chemogenomic Set; kiCCA, Kinobead Competition and Correlation Analysis; KiPIK, Kinase inhibitor Profiling to Identify Kinases; KiR, Kinome Regularization; KSEA, Kinase-Substrate Enrichment Analysis; KSR, Kinase-Substrate Relationship; MIBs, Multiplexed Immobilized Beads; PPI, Protein-Protein Interaction.

kinase are likely to invoke changes in the nature of other signaling pathways within the network that may contribute to the disease phenotype (Creixell et al., 2012). Indeed, it has been argued that increasing knowledge of signaling networks represents the most efficient approach to the development of new treatment options in cancer (Yaffe, 2013). Of course, an appreciation of how kinase signaling networks operate in normal cells will also be necessary to understand what changes in disease.

Importantly, drug efficacy is crucially dependent on the status of the pre-existing kinase networks in target cells. For instance, the growth of different tumors may be dependent on different components of signaling pathways, even in patients with apparently similar cancers (Mellinghoff et al., 2005). If the full potential of personalized medicine is to be fulfilled, we will need to characterize the status of signaling networks in individual patients and identify suitable diagnostic and prognostic disease biomarkers, as well as effective treatments (Knight et al., 2010; Graves et al., 2013; Cohen et al., 2021; Rocca and Kholodenko, 2021).

Many kinase inhibitors have been designed largely with a “one target—one drug” approach. However, signaling networks tend to be resilient and are often relatively unaffected by the inhibition of only one element (Hopkins, 2008; Knight et al., 2010). Indeed, the effectiveness of some drugs (e.g., sorafenib, cabozantinib) appears to rely on “off-target” activity of the agent in addition to the designed “on-target” activity (Wilhelm et al., 2006; 2004; Markowitz and Fancher, 2018). This reinforces the view that, in many cases, we may need to inhibit the activity of more than one type of kinase to obtain desired therapeutic effects. Therefore, another aim of systemic studies is to aid the identification of multiple sites for intervention in kinase networks to produce meaningful clinical responses.

Network pharmacology also aims to understand how cells respond to drug treatment. For example, during drug development, it is important to determine the on and off-target activity of kinase inhibitors in cells, and to understand the network-wide effects of drug action so that efficacy and potential side effects can be assessed. In some notable cases (e.g., imatinib), the identification of “off-target” activity of kinase inhibitors has led to drug repurposing and approval for use in additional conditions (Demetri et al., 2002).

Studies of networks should also help us understand how, particularly during cancer therapy, cells become resistant to kinase inhibitor drugs. Kinase mutations can directly prevent drug binding to the intended target but, more relevant here, signaling networks can also be rewired to evade drug action. For example, the activity of alternative kinases such as MET can circumvent the inhibition of EGFR by gefitinib (Engelman et al., 2007), and bypass pathways also occur upon inhibition of BRAF or CDK4/6 (Johannessen et al., 2010; Nazarian et al., 2010; Marusiak et al., 2014; Goel et al., 2022). We therefore need to be able to unravel the cellular signaling pathways that underlie drug resistance so that alternative therapies can be developed and made available to patients (Knight et al., 2010; Cohen et al., 2021; Rocca and Kholodenko, 2021). This highlights again an important wider point: kinase networks are plastic and context-dependent. The kinases that phosphorylate particular substrates may vary from cell type to cell type, or even in response to different stimuli. For example, either PKA or RSK1 can phosphorylate LKB1 Ser-431 depending on

the stimulus (Sapkota et al., 2001). This must be considered in the development of methods to map kinase networks.

A wide array of technologies has been employed with the aim of answering these questions. There are many examples of non-pharmacological approaches to understand kinase-substrate relationships (KSRs) and kinase network topologies, such as genetic manipulation of cells and *in silico* predictions. Nevertheless, as pharmaceuticals remain the primary means of intervention in disease, it makes sense to embed pharmacological methods in early stage discovery efforts (Moellering and Cravatt, 2012), and these methods also have some significant benefits. Here, we will focus on the major pharmacological technologies that have been employed to elucidate kinase signaling networks in health and disease, and their advantages and disadvantages compared to other approaches.

2 Selectivity versus efficacy: chemical probes versus kinase inhibitor drugs

Cell-permeable small molecule kinase inhibitors are key pharmacological tools for laboratory studies of cellular kinase networks, and for therapeutic intervention in kinase signaling pathways in patients. In other words, small molecule inhibitors can be used as chemical probes or as kinase inhibitor drugs (or both). It is important not to lose sight of the differences between these two types of application. A chemical probe is “a selective small-molecule modulator of a protein’s function that allows the user to ask mechanistic and phenotypic questions about its molecular target in biochemical, cell-based or animal studies” (Arrowsmith et al., 2015). Knowing the pattern of target engagement and specificity of action is vitally important for a chemical probe, since the underlying assumption is often that the function of only a single target protein is altered. Unknown off-target activity of chemical probes severely limits the quality of the biological interpretations that can be drawn from experimental results. In contrast, small molecule drugs may have undefined or incompletely defined modes of action. However, these may be tolerable as long as the agents have appropriate pharmaceutical properties that allow their safe and effective use in humans.

In principle, using kinase inhibitors as chemical probes has a number of advantages over non-pharmacological approaches. For example, methods like gene deletion, RNA interference (RNAi), or expression of mutated proteins require that cells can be efficiently transfected, and also involve long periods of days or weeks. This can allow time for compensatory changes in signaling networks to occur (Shogren-Knaak et al., 2001; Bodenmiller et al., 2010), and can preclude analysis of the distinct functions of a kinase at different stages within a biological process (e.g., the cell cycle) (Moffat et al., 2006). For example, a complete gene knockout prohibits simple analysis of a protein’s role at a late stage of a process if the deletion causes a defect in an earlier step. These methods also do not allow inhibition to be rapidly reversed, so it is hard to study the effect of kinase reactivation after an experimental manipulation. In addition, kinase proteins may have functions unrelated to their enzymatic activity, such as the formation of protein-protein interactions (PPIs). Methods such as RNAi, genetic knockout, or induced protein degradation, therefore may cause alterations in signaling

pathways that are not due to altered kinase activity (Weiss et al., 2007; Knight et al., 2010). In contrast, small molecule inhibitors typically act within minutes, they can be added to cells at different times during a cellular assay to test their effect on a particular stage without affecting a preceding one, and they can selectively target the enzymatic activity of the kinase. Inhibitors also can be applied to almost any cell type or cell extract, may allow essentially complete yet reversible inhibition, and can often be used in whole organism studies.

As with any experimental approach, chemical inhibitors also have potential disadvantages. There are over 500 kinases encoded by the human genome (Manning et al., 2002; Wilson et al., 2018), and one issue is the lack of effective inhibitors for many kinases, particularly the understudied proteins of the so-called “dark kinome.” Efforts such as the “Illuminating the Druggable Genome (IDG)” program and the Structural Genomics Consortium are working to fill these gaps and to identify useful inhibitors for all human kinases (Oprea et al., 2018; Wells et al., 2021).

The major pitfall of inhibitor approaches, however, can be summarized very simply: lack of selectivity. This is a huge concern for kinase inhibitors, most of which target the ATP binding site, a region that has some level of structural similarity in all members of the eukaryotic protein kinase family (Cohen, 2002). Seminal studies of a number of well-known “selective” inhibitors on a panel of kinases revealed an alarming degree of promiscuity (Davies et al., 2000; Bain et al., 2007; 2003). Unfortunately, there are numerous examples of publications reporting the application of chemical probes as “selective” inhibitors of target kinases, when there is strong evidence of off-target activity (Arrowsmith et al., 2015). While reasonable specificity of several kinase inhibitors (e.g., Lapatinib) has been confirmed, the ease with which the effects of inhibitors on large panels of kinases can now be tested has revealed that essentially no kinase inhibitor can be considered truly selective for a single kinase (Fedorov et al., 2007; Bamborough et al., 2008; Karaman et al., 2008; Anastassiadis et al., 2011; Davis et al., 2011; Metz et al., 2011; Gao et al., 2013; Elkins et al., 2016).

Does this non-selectivity mean that kinase inhibitors are not useful as tools to understand signaling networks? We believe there is still plenty of opportunity to effectively apply chemical probes in such studies, but that the design of these experiments must acknowledge the inherent limitations of kinase inhibitors. For example, the effects of an inhibitor of a particular kinase can be compared with the effects of additional “orthogonal” inhibitors with different off-target profiles (Davies et al., 2000; Bamborough et al., 2008). Alternatively, as discussed below, datasets can be analyzed in a way that explicitly accounts for the known off-target effects of the probes, or pharmacological methods can be combined with genetic manipulation in chemo-genetic approaches that aim for the “best of both worlds,” for example, where inhibitor selectivity is ensured by making specific mutations in the target kinase (Davies et al., 2000; Shogren-Knaak et al., 2001).

Regardless of these factors, a number of kinase inhibitors have been successful in the clinic for both cancer and non-malignant diseases (e.g., imatinib, gefitinib, tofacitinib and others), and there is an undeniable need to develop additional therapeutic agents that target kinase activity (Cohen et al., 2021). Consequently, it is vital that we develop methods to characterize the effects of such agents on cellular signaling networks. Indeed, the complexity, redundancy,

and flexibility of kinase signaling networks within cells are becoming increasingly obvious, and with this comes the realization that we may need to block multiple elements within a signaling network to develop effective treatment options. Polypharmacology refers to the idea that a single agent may be efficacious as a drug because it engages more than one target to cause the desired changes in cell function (Hopkins, 2008; Knight et al., 2010). In this case, the ability of a chemical entity to inhibit more than one kinase can be a benefit rather than a flaw. Clearly, we need “target deconvolution” approaches that can be used to understand how kinase inhibitor drugs are altering kinase signaling networks. In addition, to rationally design poly-pharmacological drugs or combinations of drugs, we must understand the larger signaling network so that we can identify potential combinations of kinases that can be simultaneously targeted for the treatment of specific diseases.

Here, we divide the process of understanding kinase networks using pharmacological approaches into three elements. First, detailed selectivity information on chemical probes must be obtained. Second, individual KSRs within the network must be identified and, third, these KSRs must be integrated (together with additional information) to understand network structure and behavior. We will discuss these three elements in turn.

3 Methods for profiling target engagement by kinase inhibitors

For pharmacological approaches to be useful to elucidate kinase networks, the direct targets of chemical probes need to be well-characterized. That is, the molecular entities in cells whose biological function is altered by direct binding to kinase inhibitors must be defined. Acknowledgement of the kinase inhibitor selectivity problem has led to the widespread commercial availability of kinase inhibitor profiling platforms and services. Using these, kinase inhibitors can be rapidly tested for selectivity. In some notable cases, knowledge of “off-target” activity of clinical agents has broadened their clinical utility. This is seen, for example, in the use of imatinib, first developed as an ABL inhibitor for chronic myelogenous leukemia, to target KIT and PDGFR in gastrointestinal stromal tumors (Demetri et al., 2002). The great majority of profiling methodologies test the activity of inhibitors on recombinant kinases *in vitro*. However, native kinases in their cellular environments have different properties that are likely to change their sensitivity to inhibitor action. Because of this, there have been increasing efforts to develop ways to assay inhibitor activity in cell extracts and living cells.

3.1 *In vitro* kinase inhibitor profiling to determine target engagement

There are many approaches to measure the activity of recombinant kinases that can be used for characterizing the effects of inhibitor compounds *in vitro*. Broadly speaking, such assays can be divided into those that measure the influence of inhibitor compounds on enzymatic activity, and those that measure the binding of small molecules to kinase proteins (either directly or in competition assays).

3.1.1 Kinase activity assays

Kinase activity assays are beneficial for characterization of chemical probes because they directly measure the property of the enzyme that is the target of inhibitors and of most kinase-directed drugs (*i.e.*, the ability to catalyze a substrate phosphorylation event). In addition, they can provide enzymological information that is valuable for compound optimization and utilization.

Perhaps the “gold standard” format remains the radioactive incorporation assay, typically using [γ - 32 P]ATP or [γ - 33 P]ATP. These assays are robust and sensitive, but do require the handling and disposal of radioactive material (Hastie et al., 2006). A number of providers offer inhibitor profiling assays covering hundreds of human protein kinases in this format, including MRC PPU Reagents and Services, Reaction Biology, and Eurofins. Studies that have profiled large panels of kinase inhibitors by radioactive ATP incorporation assays provide indispensable information for the selection of chemical probes and interpreting their cellular activities (Davies et al., 2000; Bain et al., 2007; 2003; Anastassiadis et al., 2011; Metz et al., 2011; Gao et al., 2013).

Alternative assay formats are available that measure phosphorylation using phospho-specific substrate antibodies, or by changes in substrate peptide charge and/or mass (e.g., mobility shift or IMAP assays from Nanosyn and Carna) or cleavability (e.g., Z-Lyte assays from ThermoFisher), or the generation of ADP (e.g., Adapta assays from ThermoFisher). Such assays are amenable to high throughput profiling, although the use of indirect detection in many of these technologies introduces additional potential for compound interference (e.g., fluorescent inhibitors may interfere with assays that use fluorescent substrates). Again, however, large inhibitor profiling efforts using these methods provide excellent sources of information about the selectivity of numerous inhibitors (Metz et al., 2011; Elkins et al., 2016).

It is worth remembering that essentially all of these profiling approaches use a single peptide substrate for each kinase. In reality, many kinases have multiple substrates and, because the kinetic properties of kinases may be affected by these substrates, it is possible that inhibitor profiles will be different for different kinase substrates (Sommese and Sivaramakrishnan, 2016). Perhaps more importantly, different kinase assay formats use different concentrations of ATP (typically either a fixed concentration such as 1 mM, or a concentration near the K_m of each kinase), which influences the inhibition observed for ATP-competitive inhibitors and therefore comparisons between kinases (Knight and Shokat, 2005).

3.1.2 Direct and indirect inhibitor binding assays

An alternative approach to characterizing inhibitor activity is to measure inhibitor binding to target kinases. In general, binding affinity of compounds that are known to be kinase inhibitors has been found to correlate well with ability to inhibit kinase activity (Sutherland et al., 2013; Elkins et al., 2016) but, of course, a small molecule may bind to a kinase without influencing its enzymatic activity. On the other hand, such assays can have the advantage of being able to determine substrate specificities of inhibitors for partially purified kinases as well as inactive kinases, which provides useful insights into kinase kinetics relevant to characterizing inhibitors (Wang and Ma, 2015).

Thermal stability shift assays provide one method to measure inhibitor binding with the advantage that no additional kinase or inhibitor-specific probes are required. In this approach, the change in stability of a kinase caused by inhibitor binding is measured as the kinase is denatured by heating. There are a number of ways to measure such protein unfolding, but differential scanning fluorimetry (DSF) has been used successfully for kinase inhibitor profiling *in vitro*, in which the increased binding of a hydrophobic dye to denaturing protein is measured (Figure 1A) (Fedorov et al., 2007; Echalié et al., 2014; Elkins et al., 2016). Notably, the method does not distinguish between compounds that bind to the active site *versus* other regions of the kinase.

Other approaches use competition assays to focus attention on the ATP binding sites of kinases. For example, KINOMEScan assays (from Eurofins/DiscoverX) monitor the capture of tagged recombinant kinases by beads carrying a suite of broad-spectrum kinase ATP-competitive inhibitors (Fabian et al., 2005). The binding affinities of added soluble kinase inhibitors that prevent the interaction of kinases with the immobilized ligands can then be inferred from the reduction in kinase capture by the beads (Figure 1B). KINOMEScan assays have been used to profile the activities of large panels of ATP competitive inhibitors on hundreds of kinases (Bamborough et al., 2008; Karaman et al., 2008; Davis et al., 2011; Jacoby et al., 2015). LanthaScreen Eu kinase binding assays (ThermoFisher) work on a similar principle, in which the displacement of fluorescent ATP-competitive inhibitors from tagged recombinant kinases is measured by time-resolved FRET (Figure 1C). Inhibitor competition can also be measured in complementation assays including split luciferase experiments (Jester et al., 2012). Such assays can provide information on both ATP-competitive and allosteric inhibitors that reduce binding at the ATP site. Notably, however, these competition binding assays cannot be used to profile inhibitors whose activity is driven by alternative mechanisms such as blocking protein substrate binding.

In summary, a number of well-validated profiling assay formats are available that allow the characterization of kinase inhibitors *in vitro*. These unambiguously provide information about the inhibition or binding of inhibitors to purified kinases. However, even the largest kinase panels currently include only about 400 of the approximately 530 wild type human protein kinases. Because the targets of inhibitors are difficult to predict based on the sequence-similarity of kinases (Bamborough et al., 2008; Anastassiadis et al., 2011), this leaves significant gaps in current *in vitro* profiling data. Furthermore, these assays typically use purified recombinant kinases that will not always replicate the properties of native kinases in cells, which may also be different in different cell types. Finally, these techniques tend to be largely “blind” to the possible effects of small molecules on non-kinase targets. Usually, what researchers really want to know is which targets are engaged and functionally altered *in vivo*.

3.2 Kinase inhibitor profiling to determine target engagement in cells and cell extracts

The need to understand target engagement *in vivo* has driven the development of methods to profile inhibitor activity in cell lysates and in living cells. A key problem for these approaches is how to

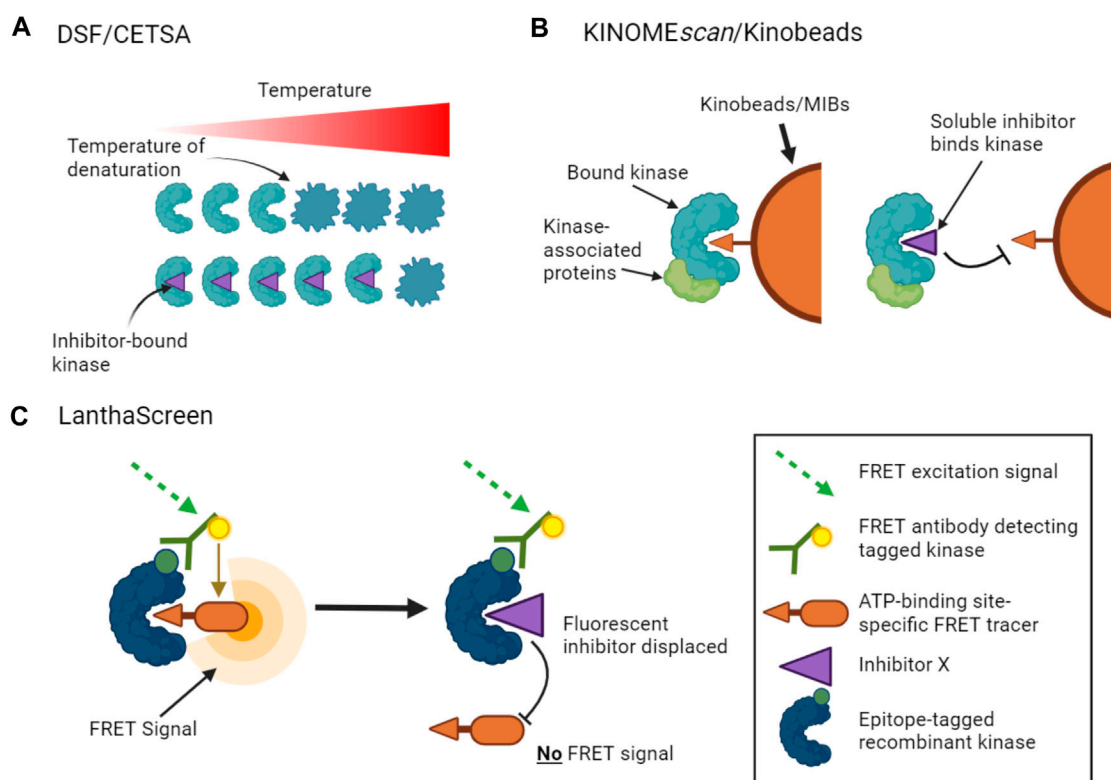


FIGURE 1

Binding assays to profile target engagement by kinase inhibitors *in vitro*. (A). DSF and CETSA assays infer inhibitor binding by detecting changes in the thermal stability of a kinase upon inhibitor binding. (B). Multiplex inhibitor beads (MIBs) such as Kinobeads display a suite of broad-spectrum kinase inhibitors that can bind recombinant kinases (KINOMEScan assays) or kinases in cell lysates. Addition of a soluble selective kinase inhibitor displaces only specific kinases from the beads, allowing these kinases to be identified as targets of the added inhibitor. A variant of the assay, kiCCA, measures the displacement of kinase-associated proteins to characterize protein complexes. (C). LanthaScreen binding assays measure target engagement by inhibitors from the reduction of FRET signal when a fluorescent ATP-competitive tracer is displaced from a tagged kinase bound to a fluorophore-labelled antibody.

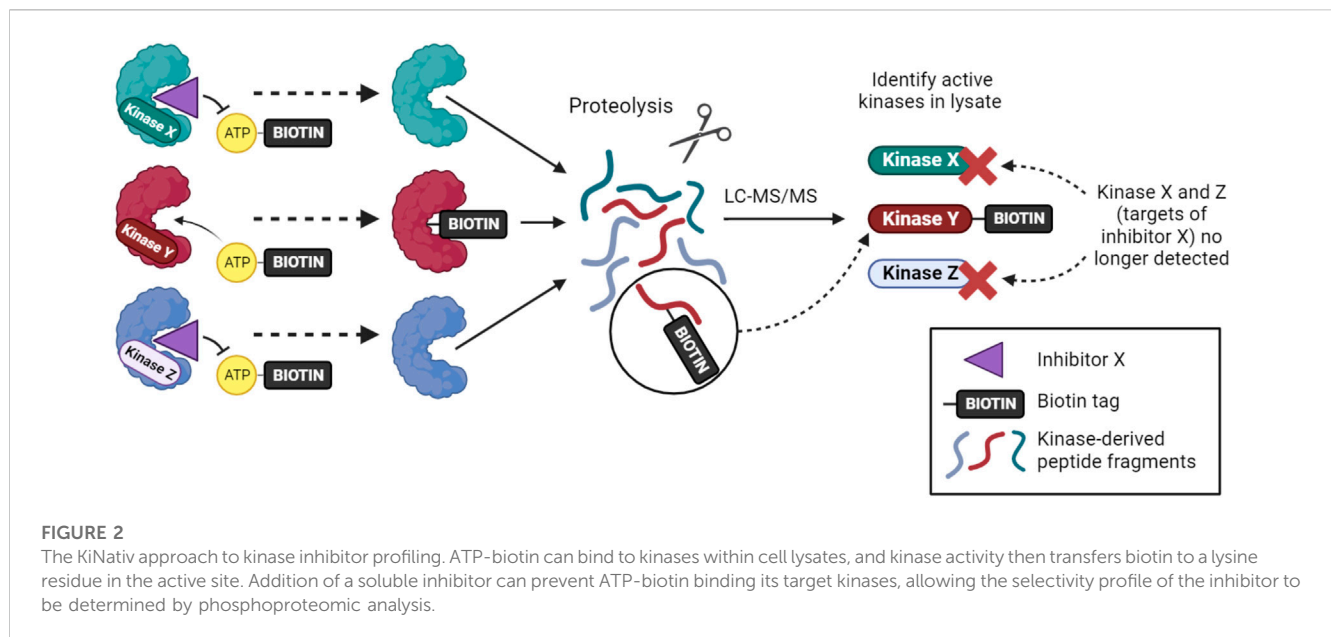
unequivocally identify specific kinases within a complex environment. This challenge has often been met by employing mass spectrometry to characterize kinase targets. Such “chemo-proteomic” approaches bring along their own possible disadvantages, such as a reduction in standardization and throughput compared to *in vitro* profiling, but their potential value cannot be questioned.

3.2.1 Affinity-based profiling

In principle, one way to identify the cellular targets of a chemical probe is to use the compound as an immobilized bait to fish for cellular proteins, and then to identify the captured proteins using mass spectrometry (Daub, 2005). This has the advantage that few assumptions are made about the nature of the proteins bound by the probe, and unexpected non-kinase targets of kinase inhibitors may be found. However, the compound must be derivatized to enable it to be immobilized, and this is likely to hinder binding to some cellular targets. In addition, the method is biased towards more abundant proteins in cells, and it is hard to quantify the affinity of binding interactions (Bantscheff et al., 2007). An adaptation of the method to allow quantification is to measure the ability of “free” (non-immobilized) compounds to compete for binding to the immobilized compound (Sharma et al., 2009). This approach,

however, still requires the bespoke synthesis of an immobilized probe for each new inhibitor.

A major step forward in this area was the realization that immobilized broad-spectrum kinase inhibitors could be used to simultaneously capture multiple kinases from cell lysates, as utilized in the *in vitro* KINOMEScan approach described above (Fabian et al., 2005; Bantscheff et al., 2007; Daub et al., 2008; Sharma et al., 2009). The ability of a free kinase inhibitor to compete for binding to the matrix can be measured by quantitative mass spectrometry, providing a reasonably standardized chemo-proteomic approach for profiling multiple unmodified inhibitors (Bantscheff et al., 2007; Sharma et al., 2009). A good example is known as the Kinobeads approach, in which a selection of broad-spectrum kinase ATP-competitive inhibitors are immobilized on beads (also known as multiplexed inhibitor beads, MIBs, see Figure 1B) (Bantscheff et al., 2007; Reinecke et al., 2019). Optimized Kinobead protocols can profile up to 350 kinases (Reinecke et al., 2019). This approach has several advantages: it does not require labeling of inhibitors or kinases, it can identify a subset of possible non-kinase targets of kinase inhibitors, and it can be applied to a wide variety of cell and tissue lysates from various species. For example, Klaeger et al. applied Kinobeads to evaluate the target spectrum of 243 clinically relevant kinase-targeted drugs in human cancer



cells (Klaeger et al., 2017), and to identify ferrochelatase as an off-target of a number of clinically relevant kinase inhibitors (Klaeger et al., 2016). Because proteins identified by this chemo-proteomic approach may bind directly or indirectly to Kinobeads (for example, as protein complexes), follow-up work is needed to distinguish direct from indirect drug targets.

Because ligands are immobilized on beads, Kinobead methods can only be used to capture kinases from cell lysates, and not from intact cells. In an alternative format of such assays, living cells are treated with inhibitors, followed by cell lysis and chemo-proteomic profiling. Assuming many kinase inhibitors have slow off-rates, this might allow the binding of inhibitors to kinases in their truly native state to be assessed. Indeed, differences between pre-lysis and post-lysis inhibition profiles have been observed, for example, for imatinib binding to KIT (Bantscheff et al., 2007). Nevertheless, the potential for confounding pre-lysis effects such as changes in kinase abundance, or post-lysis changes such as loss of cell compartmentalization, mean that these affinity-based approaches do not provide true intracellular profiling.

3.2.2 Activity-based profiling

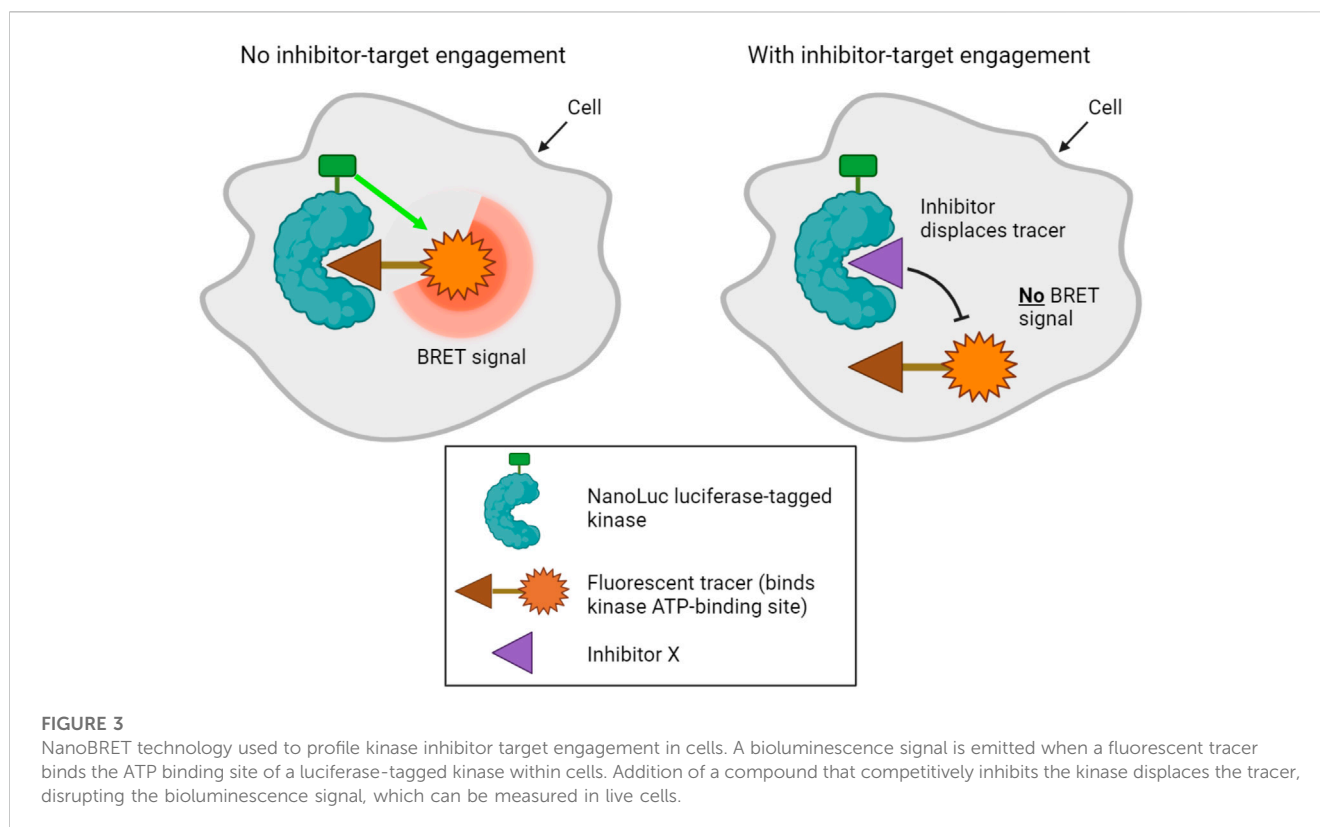
An alternative approach for inhibitor profiling in cell lysates is KiNativ. Overall, the method has similarities to Kinobeads, but it uses crosslinking to capture kinases rather than non-covalent affinity interactions. Specifically, when a biotinylated acyl-phosphate derivative of ADP or ATP binds to a kinase (or other ATP phosphohydrolase), the terminal acyl-phosphate is transferred covalently to one of the conserved lysine residues in the active site and the enzyme is thereby tagged with biotin (Figure 2). After limited proteolysis, biotin-containing peptides can be analyzed by targeted mass spectrometry to identify approximately 200 kinases from a single experiment (Patricelli et al., 2011; Patricelli et al., 2007). If capture is carried out in the presence of kinase inhibitors that reduce ATP binding, then KiNativ can be used to characterize inhibitor properties. The technique can thus be considered an activity-based profiling approach that probes the properties of

endogenous kinases, and it has been used successfully to profile a number of kinase inhibitors (Patricelli et al., 2011). Despite its name, however, KiNativ remains a cell lysate-based approach and so, arguably, kinases are not in their truly native cellular environment when analyzed.

More recently, cell permeable covalent sulfonyl fluoride ATP binding site probes have been designed (Zhao et al., 2017), and future development may allow broad activity-based kinase profiling in cells. However, not all kinases may be detectable using these methods, perhaps due to their low abundance or lack of suitably placed lysine residues, and the use of covalent binders prevents simple determination of true affinities.

3.2.3 Thermal shift assays in cells

In the quest to develop direct methods for monitoring the binding of drugs to their targets within cells, Martinez Molina et al. tested whether thermal shift assays (see Section 3.1.2; Figure 1A) could be carried out using cells (Molina et al., 2013). Indeed, they found that kinase inhibitors could protect target kinases within cells from denaturation. In this case, kinase unfolding was monitored (using antibodies) as a reduction in the amount of soluble kinase due to heat-induced aggregation and precipitation. The method was named the Cellular Thermal Shift Assay (CETSA). Savitski et al. (2014) combined the approach with mass spectrometry to detect inhibitor binding to over 7000 different proteins including 175 kinases, significantly enhancing the scope for identification of off-target binding compared to other methods. Although it does not yield straightforward K_d values, it is useful for comparing the binding of related inhibitors to particular targets. Also, because it is not a direct binding assay, the potential for indirect effects must be noted. For example, changes in post-translational modifications of downstream targets of inhibited kinases can influence their melting temperatures, potentially yielding “false positives.” Indeed, such effects appear more prominent in cellular *versus* lysate thermal profiling experiments (Shi et al., 2014). False negatives have also been reported (Savitski et al., 2014). Nevertheless, thermal proteome



profiling (TPP) has the clear advantage that it provides information on kinase and non-kinase target engagement within cells. In one example, ferrochelatase was identified as an off-target of the BRAF inhibitor vemurafenib responsible for kidney toxicity (Savitski et al., 2014; Bai et al., 2021).

3.2.4 NanoBRET

A final method designed to determine kinase target engagement in living cells is NanoBRET technology (Roberts et al., 2015; Vasta et al., 2018). This is a bioluminescence resonance energy transfer (BRET) technique that measures the affinity of inhibitors for cellular kinases by competitive displacement of a luminescent tracer from fused NanoLuc luciferase-kinase proteins (Figure 3). Currently, the method only assays one type of kinase per cell, and transfected cell lines that express each NanoLuc-tagged kinase of interest must be made. Furthermore, although NanoLuc is a relatively small protein with a number of advantageous features (Hall et al., 2012), fusion to NanoLuc has the potential to alter the properties of a kinase. Nevertheless, NanoBRET allows the analysis of inhibitor binding to kinases in genuinely living cells.

Vasta et al. (2018) showed that NanoBRET can be used to measure inhibitor selectivity within intact cells for 178 full-length kinases, and Wells et al. successfully profiled 46 cyclin-dependent kinase (CDK) inhibitors on a panel of CDK kinases (Wells et al., 2020). Comparing the results of a NanoBRET assay with other methods revealed important differences in cellular kinase occupancy compared to the results of *in vitro* assays, and suggested that NanoBRET results are more comparable to other cellular assays such as phospho-substrate ELISAs. Importantly for the further development and use of this technique, the activity of the

NanoLuc enzyme itself appears to be unaffected by the great majority of kinase inhibitors (Hall et al., 2012; Cartwright et al., 2022). Most current cellular NanoBRET assays make use of overexpressed kinases, but it is possible to use weak promoters or, in future, to tag kinases at their endogenous loci (Vasta et al., 2018; Yang et al., 2023). Efforts to rapidly expand the panel of NanoLuc-fused kinases (Yang et al., 2023) mean that this assay format seems likely to find increased use in the profiling of target engagement in living cells.

In summary, a number of methods have been developed that move researchers nearer to the ultimate goal of quantifying inhibition of kinase function in the native cell environment. Each of the methods has strengths and weaknesses, but NanoBRET technology arguably comes the closest to measuring kinase occupancy in true living cells. While many *in vitro* kinase activity and binding assays have been validated by cross-comparison between the different methods (Sutherland et al., 2013; Tang et al., 2014), broad validation of cell-based methods will need to wait for more widespread adoption of the approaches. It is also worth pointing out that a number of these techniques remain relatively poor at detecting off-target effects on non-kinase targets. Nevertheless, methods such as NanoBRET have great potential to increase our quantitative understanding of kinase inhibitor action *in vivo*.

3.3 *In silico* approaches

The availability of large datasets of kinase inhibitor profiles raises the prospect of using *in silico* techniques to predict the target

selectivity of kinase inhibitors (Tang, 2017). For example, machine-learning methods have been employed to predict *in vitro* kinase inhibitory activity for large compound libraries (Merget et al., 2017; Li et al., 2019). As experimental datasets grow, machine learning approaches improve, and these methods are extended to cellular inhibition profiling, their utility is likely to increase. Indeed, artificial intelligence is already a key tool in the drug discovery pipeline (Vamathevan et al., 2019).

4 Pharmacological approaches to define kinase-substrate relationships

A crucial part of understanding kinase networks is knowledge of individual kinase-substrate relationships (KSRs). Indeed, accurate definition of KSRs is crucial to correctly identify kinase pathways from phosphoproteomic data (Hernandez-Armenta et al., 2017). For this task, pharmacological approaches using well-characterized chemical probes are vital components of the kinase researcher's toolbox. Note that here we define a KSR as the relationship between a kinase and a downstream substrate it directly phosphorylates. Ideally, "substrate" refers to a single phosphosite within a target protein, but not all methods for identifying KSRs are phosphosite-specific.

4.1 Non-pharmacological approaches

There are numerous non-pharmacological ways to characterize KSRs (Johnson and Hunter, 2005). With a cellular assay for phosphorylation in hand (often using a phospho-specific antibody), approaches such as RNAi, genetic knockout and overexpression of kinases can all be used to investigate KSRs. These have limited off-target effects compared to small molecule inhibitors. However, because kinases operate in networks, these methods often identify pathways of kinases that are indirectly responsible for phosphorylation events (Bodenmiller et al., 2010), so other techniques are required to confirm direct phosphorylation events. Furthermore, as mentioned in Section 2, these approaches alter the amount of protein kinases in cells, rather than only preventing catalytic activity, and this may cause additional indirect effects (Weiss et al., 2007).

Biochemical methods such as *in vitro* kinase assays using panels of purified kinases or potential substrates can be used to identify possible KSRs (Ptacek et al., 2005; Newman et al., 2013), but such libraries are usually incomplete and expensive, and are unlikely to fully reflect the activity of kinases in their natural cellular context. Alternatively, in KESTREL and related approaches, purified kinases can be used to seek substrates in cell extracts that are then identified by mass spectrometry (Knebel et al., 2001; Huang et al., 2007; Müller et al., 2016), but these methods are biased towards identification of abundant cellular proteins. Classical techniques in which a specific kinase activity is tracked through biochemical enrichment steps are also possible, but these need large quantities of cells and multiple steps, as well as protein identification techniques to pinpoint candidate kinases (Rubin and Rosen, 1975; Kubota et al., 2009).

For many kinases, particularly serine/threonine kinases, optimal linear phosphorylation motifs have been determined using oriented

synthetic peptide libraries or phosphoproteomic analysis of cellular proteins phosphorylated *in vitro* (Songyang et al., 1994; Yaffe et al., 2001; Douglass et al., 2012; Kettenbach et al., 2012; Knight et al., 2012; Xue et al., 2012; Johnson et al., 2023). Specific phosphosites can be compared to these optimal motifs to infer KSRs *in silico*. However, such motifs are not known for all human kinases and are validated for far fewer. Also, natural kinase phosphosites diverge from optimal motifs, because it is likely that sub-optimal regulable phosphorylation is required in signaling networks, rather than phosphorylation at maximal efficiency. In addition, not all kinases may recognize linear motifs, and some kinases certainly make use of binding sites distant from phosphorylation sites to select their substrates (Miller and Turk, 2018). Finally, *in silico* approaches typically lack contextual information such as which kinases are expressed or activated in a specific cellular environment, or the presence of binding partners which may regulate kinase activity. Indeed, it is not necessarily the case that the kinase responsible for phosphorylation of a particular site is the same in different cell types, a point well-illustrated by the rewiring of kinase pathways that can occur in cancer (Knight et al., 2010; Cohen et al., 2021). It is therefore not surprising that false positives and negatives are frequent using such prediction techniques, even when attempts are made to combine them with contextual information such as co-expression or PPI data (Linding et al., 2007).

In sum, it is clear that genetic, biochemical and *in silico* approaches can all be employed to identify KSRs, though they each have limitations. In the rest of Section 4, we explore how the use of pharmacological tools provides an attractive category of complementary approaches.

4.2 From kinase to substrate: pharmacological approaches

A number of pharmacological approaches have been developed to determine the target substrates of a specific kinase, most notably phosphoproteomic analysis following inhibitor treatment, and use of chemo-genetic approaches involving modified kinase alleles.

4.2.1 Phosphoproteomics following inhibitor treatment

Inhibition of a particular kinase in cells will decrease the phosphorylation of its substrates. Therefore, kinase inhibitor treatment followed by phosphoproteomics has been used to infer KSRs for a number of kinases (Kettenbach et al., 2011; Knight et al., 2012). Even though kinase inhibitors are typically fast-acting, one of the major obstacles to the interpretation of such studies is the need to distinguish direct from indirect substrates. This arises because inhibition of a specific kinase may lead to a cascade of altered phosphorylation in a signaling network, as illustrated in Figure 4A. In many phosphoproteomics studies, identified phosphosites are subsequently compared with optimal sequence motifs defined for the kinase of interest to discriminate direct from indirect substrates. This, however, means that the method suffers from some of the same shortcomings as the *in silico* approaches mentioned in Section 4.1, including that not all *bona fide* substrates conform closely to these motifs. Another major concern is the underlying assumption that only one kinase is inhibited by the probe compound, when it is clear

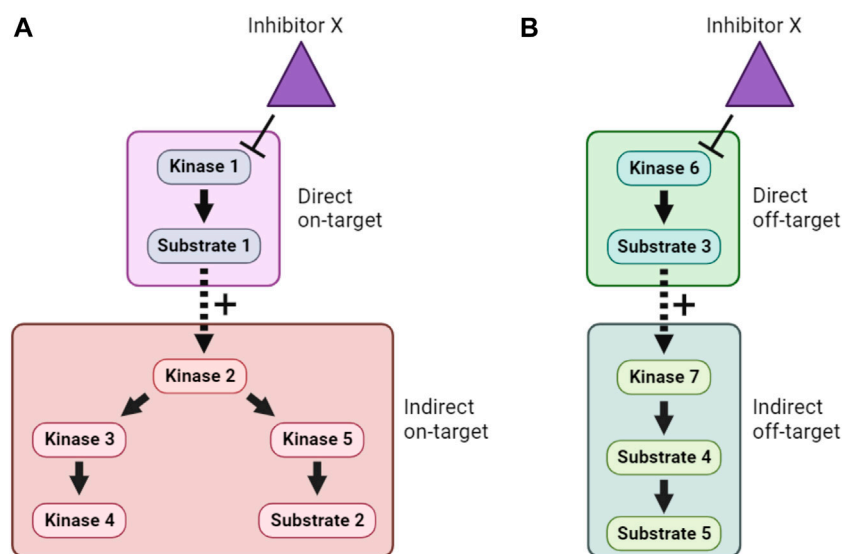


FIGURE 4

Direct, indirect and off-target effects of kinase inhibitors. **(A)**. In this example, Inhibitor X directly inhibits Kinase 1, and therefore lowers phosphorylation of Substrate 1. However, because Substrate 1 is a positive regulator of Kinase 2, this also causes indirect on-target effects on Kinase 2 and downstream signaling. **(B)**. In addition, if Inhibitor X has direct off-target effects on another kinase, Kinase 6, then both direct and indirect off-target effects on an unrelated cellular signaling pathway can occur. Distinguishing these effects is a major challenge when using inhibitor compounds to study the cellular function of target kinases.

that essentially all kinase inhibitors have additional targets (Figure 4B). Use of more than one distinct kinase inhibitor can mitigate these concerns to some extent, but caution and follow-up experimentation are required.

4.2.2 Chemo-genetic approaches

The combination of pharmacological and genetic approaches (“chemo-genetics”) can be used to alleviate concerns about inhibitor specificity (Figure 5). Shokat and co-workers developed an approach in which kinases of interest can be genetically modified to accept bulky ATP-competitive inhibitors that are not able to inhibit the activity of natural protein kinases (Bishop et al., 2001; 1998). By replacing the expression of a wild type kinase with a genetic variant containing a mutated residue in the ATP binding pocket, selective inhibition of only the mutant kinase in cells should be ensured (Figure 5E). Compared with traditional genetic knockouts, the approach still allows acute inhibition of kinase activity using small molecules, reducing the potential for compensatory changes in signaling pathways. These so-called analog-sensitive kinase alleles have undoubtedly been informative, though it remains a challenge to design and express the necessary mutated but active kinases in cells, making this a relatively low-throughput approach. There is also evidence that bulky inhibitor analogs such as 1NM-PP1 have off-target activity on some endogenous kinases such as PKA (Bain et al., 2007; Kanshin et al., 2017), though these off-targets are likely limited and they can be controlled for by examining the effect of the inhibitor analogs on wild type cells.

Analog-sensitive kinases have been used in combination with phosphoproteomics and motif analysis (as described in Section 4.2.1) to identify potential substrates of, for example, Polo

kinase-1 (Oppermann et al., 2012). More recently, a sophisticated methodology combining selective chemical inhibition of analog-sensitive kinases, quantitative phosphoproteomics, and machine learning has been reported (Kanshin et al., 2017). Here, the use of bulky inhibitors and modified kinases addressed the issue of inhibitor off-target effects, while a learning classifier aimed to address the common issue of incorrectly identifying phosphorylation events as direct targets of the kinase, when they may really be attributable to downstream effects. The authors used this strategy to identify direct substrates of Cdc28 and Snf1 in budding yeast (Kanshin et al., 2017).

Related chemo-genetic approaches also have potential. For example, kinases can be genetically modified to make them resistant to small molecule inhibition (Figure 5D). This approach is useful to validate that a specific kinase is involved in the phosphorylation of a substrate that is decreased by a particular kinase inhibitor (Davies et al., 2000). Kinases also can be engineered to accept bulky ATP analogs that cannot be utilized by wild type kinases (Figure 5F). In this way, substrates downstream of the kinase of interest can be specifically labeled, and this has been used to identify Cyclin-dependent kinase substrates in cell lysates, for example, (Shah et al., 1997; Allen et al., 2007; Blethrow et al., 2008; Chi et al., 2008; Michowski et al., 2020). However, these approaches require extensive validation that modified kinases are still capable of wild type kinase activity, and not all kinases are amenable to this form of modification. Auxin-Inducible Degradation (AID) is another chemo-genetic approach that might be exploited to acutely remove kinase activity from cells (Nishimura et al., 2009). For most of these methods, distinguishing indirect *versus* direct effects of inhibitors remains the major problem. Nevertheless, pharmacogenetic approaches offer an

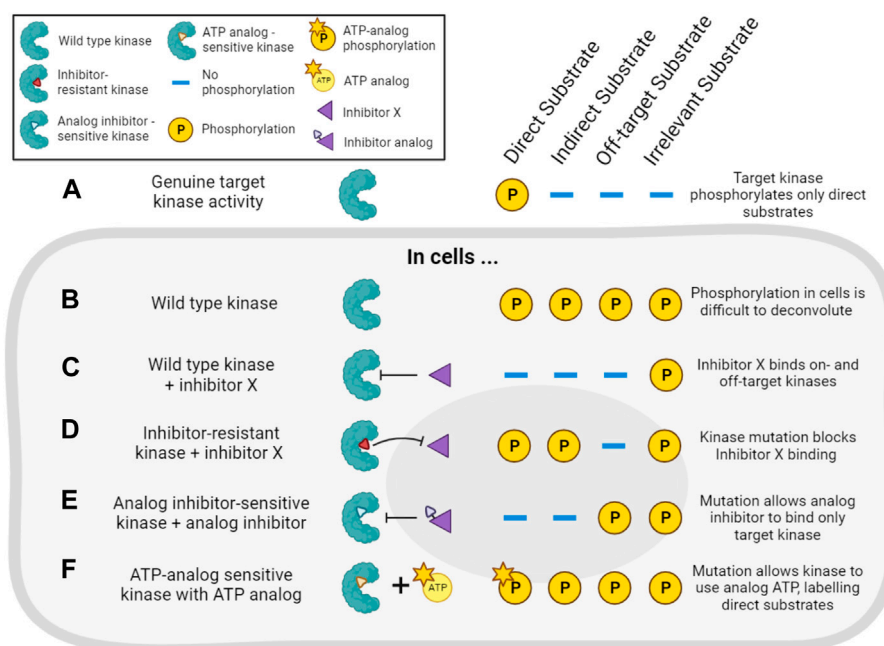


FIGURE 5

Chemo-genetic approaches for establishing kinase-substrate relationships (KSRs). (A). For the purposes of this figure, we consider a cellular “target kinase” that forms a KSR with a substrate that it directly phosphorylates in cells. By definition, this kinase does not phosphorylate indirect or other potential cellular substrates. (B). In cells, analysis of substrate phosphorylation (for example, by phosphoproteomics) will reveal phosphorylation of the direct substrate, as well as phosphorylation of many other proteins driven by other kinases. (C). Treatment of the cells with a typical incompletely selective kinase inhibitor of the target kinase (“inhibitor X”) will decrease the phosphorylation of direct and indirect downstream substrates, as well as substrates downstream of off-target kinases. (D). In cells expressing an inhibitor-resistant mutant of the target kinase, inhibitor X will no longer decrease phosphorylation of direct or indirect targets of the kinase, but off-target inhibition will still be observed. (E). In cells expressing an analog-sensitive version of the target kinase, treatment with an analog inhibitor will decrease phosphorylation of direct and indirect substrates of the kinase, but will spare the substrates of off-target kinases. (F). In cells expressing a mutated target kinase that can carry out phosphorylation using a bulky ATP-analog, only the direct substrates of the target kinase will be labeled with modified phosphate.

enticing alternative to genetic knockouts to study a kinase’s activity in live cells.

4.3 From substrate to kinase: pharmacological approaches

In addition to pharmacological approaches which aim to identify the substrate of a kinase, approaches have been developed that achieve the reverse, that is to identify the kinase responsible for a given phosphorylation event. These methods are particularly important for understanding the kinases involved in cellular phosphorylation events uncovered in large scale phosphoproteomic studies, for example,

4.3.1 Cross-linkable ATP analogs

In principle, kinases could be identified based on binding to their substrates, but such interactions are often transient and hard to capture. However, methods have been developed that use modified substrates and/or ATP analogs to covalently cross-link specific substrates to wild type kinases. In one approach, a modified substrate containing a reactive cysteine in place of the phosphorylation site is combined with a cross linkable ATP analog to enable activity-based crosslinking to kinases (Maly et al., 2004; Statsuk et al., 2008). In another, an ATP analog

containing a UV-activated reactive group allows crosslinking of kinases to a specific biotinylated substrate peptide (K-CLASP) or endogenous substrate (K-CLIP) (Dedigama-Arachchige and Pflum, 2016; Garre et al., 2018). Complexes containing crosslinked substrate and kinase can be purified by streptavidin pull-down or immunoprecipitation. Predicted KSRs can then be tested using western blots or, alternatively, unknown KSRs can be identified by proteomic analysis (Dedigama-Arachchige and Pflum, 2016; Beltman and Pflum, 2022). Not all kinases can utilize unnatural ATP analogs to phosphorylate substrates and another disadvantage is that, because the ATP analogs do not cross cell membranes, these techniques cannot be performed in cells. They can, however, be carried out using a variety of cell and tissue homogenates. These approaches may also not be effective at identifying kinase interactions for low abundance substrates, and K-CLASP and K-CLIP are prone to crosslinking interacting proteins in addition to the relevant kinase and substrate. On one hand, this lowers the specificity for kinase identification, but on the other hand provides additional information about the context of phosphorylation reactions (Dedigama-Arachchige and Pflum, 2016; Garre et al., 2018).

4.3.2 Kinome-wide inhibitor screens

One approach to identify the kinase responsible for a specific phosphorylation event is to genetically deplete or overexpress all

possible kinases and determine if the expected change in phosphorylation occurs (Friedman and Perrimon, 2006; Azorsa et al., 2010). As described above, these are relatively long-term experiments, and the nature of cellular signaling networks make indirect effects common. Methods that use kinase inhibitor libraries with the aim of mimicking one-agent-one-kinase genetic screens allow more acute inhibition of kinases and, with appropriate experimental design, can lower (but not eliminate) the potential for indirect effects. For such approaches to be broadly applicable, libraries with a high coverage of the kinome and the most selective inhibitors possible for each kinase must be assembled, and tools to facilitate design of such libraries have been developed (Drewry et al., 2017; Moret et al., 2019). An example of such an open source library is the kinase chemogenomic set (KCGS) assembled by the Structural Genomics Consortium (Elkins et al., 2016; Wells et al., 2021). KCGSv1.0 contains 187 potent kinase inhibitors that each have a narrow spectrum of activity when screened on a large panel of kinases *in vitro*. These inhibitors cover 215 human kinases using the consortium's potency and selectivity criteria. More recently this has been superseded by KCGSv2.0 which includes 295 kinase inhibitors with activity on 262 kinases. Nevertheless, few, if any, kinase inhibitors can be considered truly selective for one kinase.

An alternative conceptual approach is to accept that the majority of kinase inhibitors are not selective for a single kinase, and to develop kinase screening methods that exploit the known off-target effects of extensively profiled small molecule inhibitors. An example of this type of approach is Kinase inhibitor Profiling to Identify Kinases (KiPIK; Figure 6) (Watson et al., 2020). In this method, whole cell extracts are used as the source of all potentially relevant kinases to drive phosphorylation of an exogenous substrate of interest. Multiple such cell extract kinase reactions are carried out in parallel, each in the presence of a member of a panel of well-characterized kinase inhibitors. This yields an inhibition fingerprint that characterizes the cellular kinase mainly responsible for the observed phosphorylation. Then, to identify candidate kinases, this fingerprint is compared to the known inhibition fingerprints of all kinases in published profiling datasets (Fedorov et al., 2007; Anastassiadis et al., 2011; Davis et al., 2011; Gao et al., 2013; Elkins et al., 2016), which constitutes approximately 80% of human protein kinases. This step relies on the finding that inhibition profiles of kinase inhibitors in cell extracts are generally similar to those established *in vitro* (Bantscheff et al., 2007; Sharma et al., 2009; Patricelli et al., 2011). The technique has been validated using a number of known KSRs and successfully applied to identify cellular kinases for unassigned phosphosites such as a non-canonical Cdk1 site in the protein INCENP (Watson et al., 2020; Cartwright et al., 2022). KiPIK utilizes the rapid action of kinase inhibitors in cell extracts to focus on defined biological states. Indeed, there is evidence that the use of cell extracts can minimize the influence of upstream kinase signaling (Wang et al., 2011; Savitski et al., 2014; Watson et al., 2020), aiding the identification of direct KSRs, but indirect effects cannot be fully ruled out. KiPIK also rests on the assumption that kinase reactions in cell extracts preserve physiological kinase-phosphosite dependencies which may often, but not always, be true.

In summary, there are a number of pharmacological and chemogenetic approaches that provide potential advantages over genetic

methods for identifying direct KSRs, and advantages over predictive methods for revealing context-specific KSRs, as long as the limitations of kinase inhibitor selectivity are taken into account.

5 Pharmacological approaches for analyzing kinase signaling networks

So far, we have discussed approaches to characterize small molecule kinase inhibitors and to identify KSRs. Here, we outline how integrating this knowledge *in silico* (often with additional information) allows insight into the structure of kinase signaling on a network scale. We also discuss how experiments with well-characterized inhibitors can be used to probe signaling networks and to identify kinases that are involved in specific phenotypic responses. No matter how thoroughly a small molecule inhibitor has been characterized against its intended target and the wider kinome, we still need to understand the effects of inhibitors on specific cellular kinase networks, and to be able to predict which patients will respond to treatment. We describe ways in which these factors can be assessed in cell line and patient-specific ways.

5.1 Constructing kinase network models

Kinase pathway diagrams (see Figure 7A), which are essentially informal logic models, have long been a feature of cell signaling research. Early efforts to integrate information beyond single pathways focused on the use of KSRs to build networks of nodes (kinases and substrates) and edges (interactions between them; see Figure 7B). The KSRs used in these networks were determined by *in vitro* kinase assay screens (Ptacek et al., 2005; Newman et al., 2013) or predicted from optimal motif analysis, sometimes combined with additional information such as PPI or co-expression data (Linding et al., 2007; Song et al., 2012). Alternative kinase network models were also built using genetic or PPI data (Fiedler et al., 2009; Breitkreutz et al., 2010). Inevitably, the quality of such networks is limited by the quality of the experimentally-determined and predicted associations, and the scope of the datasets.

The rise of quantitative phosphoproteomics has allowed the status of kinase signaling to be monitored in unprecedented breadth and in specific cellular contexts. For example, a now classic report examined the spreading of phosphorylation through an EGF-induced signaling network over time in HeLa cells (Olsen et al., 2006). A limitation of phosphoproteomic studies is that they do not themselves delineate connections between kinases and their substrates, so approaches using known KSRs to predict the upstream kinases for phosphosites and to identify up or downregulated signaling pathways are crucial. In addition, the peptide under sampling inherent in current whole cell phosphoproteomic dataset acquisition influences the types of approaches that can be used for network building (Terfve et al., 2015). A number of algorithms have been developed, including those akin to gene set enrichment analysis (GSEA) (Drake et al., 2012; Weidner et al., 2014; Ochoa et al., 2016), parametric Z-tests (KSEA) (Casado et al., 2013; Wiredja et al., 2017), or heuristic machine learning (IKAP) (Mischnik et al., 2016). Benchmarking

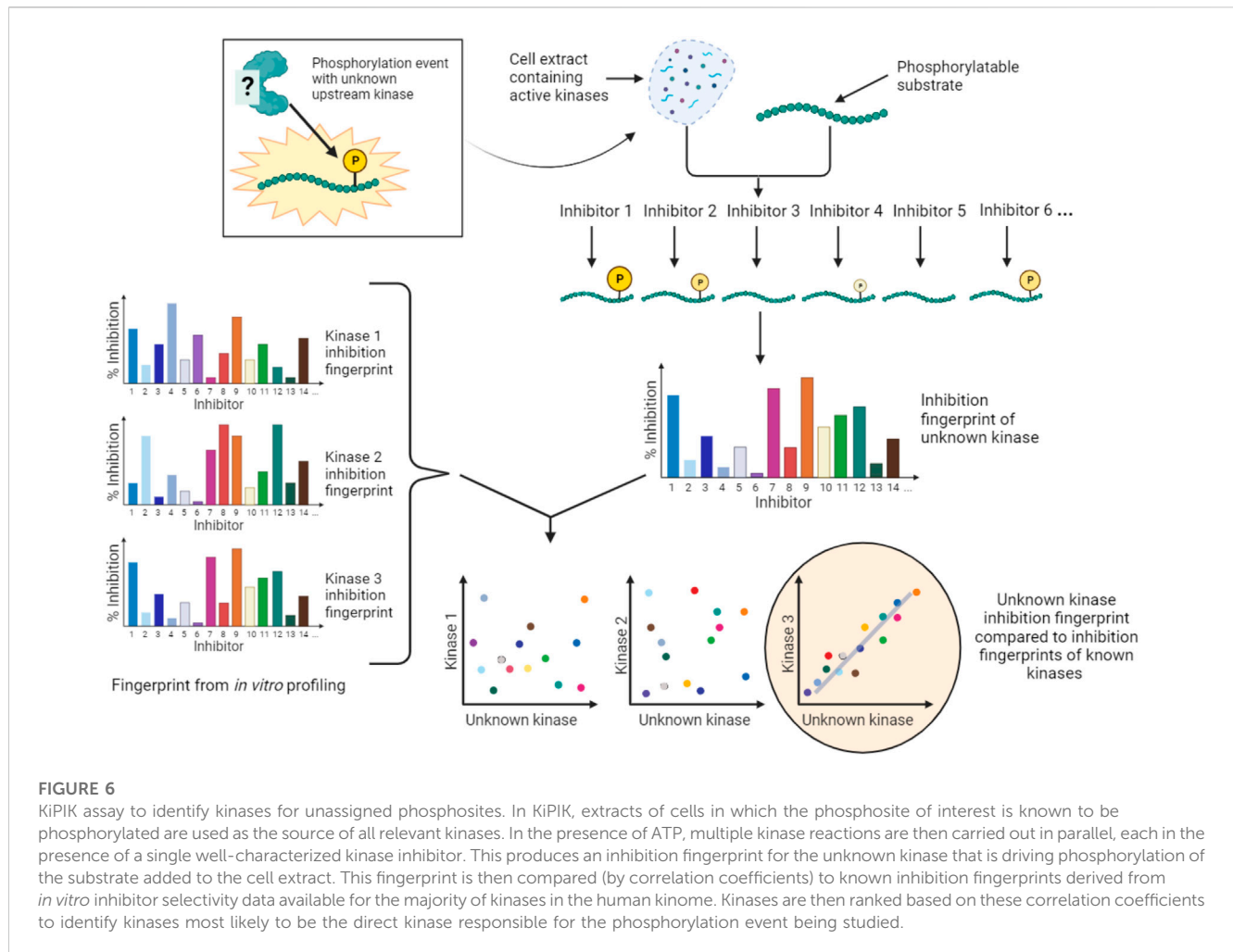


FIGURE 6

KiPIK assay to identify kinases for unassigned phosphosites. In KiPIK, extracts of cells in which the phosphosite of interest is known to be phosphorylated are used as the source of all relevant kinases. In the presence of ATP, multiple kinase reactions are then carried out in parallel, each in the presence of a single well-characterized kinase inhibitor. This produces an inhibition fingerprint for the unknown kinase that is driving phosphorylation of the substrate added to the cell extract. This fingerprint is then compared (by correlation coefficients) to known inhibition fingerprints derived from *in vitro* inhibitor selectivity data available for the majority of kinases in the human kinome. Kinases are then ranked based on these correlation coefficients to identify kinases most likely to be the direct kinase responsible for the phosphorylation event being studied.

these approaches against a high-quality set of curated KSRs provides confidence in a number of them, but confirms that the quality of the input KSRs used is paramount (Hernandez-Armenta et al., 2017). Alternatively, the combination of phosphoproteomic data with KSRs allows the construction of logic models that may provide greater mechanistic insight into network function (Vaga et al., 2014; Terfve et al., 2015; Schäfer et al., 2019). Machine learning approaches may also help distinguish direct and indirect substrates (Kanshin et al., 2017). Notably, though, assuming that KSRs are generic, and using KSRs determined in one environment in another, decreases the confidence with which context-specific network features can be uncovered.

As the field has developed, additional information beyond KSRs has been integrated into kinase network models, including PPIs, kinase interaction partners, phosphatases, co-regulation of phosphorylation, genetic mutation, expression data, and structural information (Breitkreutz et al., 2010; Reimand et al., 2013; Yang et al., 2015; Domanova et al., 2016; Drake et al., 2016; Rudolph et al., 2016; Yadav et al., 2017; Ayati et al., 2019; Buljan et al., 2020; Invergo et al., 2020; Bello et al., 2021a; Yılmaz et al., 2021). However, because kinase networks have a high level of plasticity and are partly context-specific, this cannot always be fully uncovered by combining experimental data obtained from different

cell lines or tissues. Here, pharmacological approaches to understanding kinase networks are likely to help answer a number of important questions.

5.2 Can we improve knowledge of networks using pharmacological methods?

When used appropriately, chemical probes can be used to increase our understanding of signaling network wiring. Many phosphoproteomic studies that aim to model kinase network changes upon kinase inhibitor treatment use KSR information to build network graphs or logic models (Terfve et al., 2015; Wilkes et al., 2015), or other interaction information (such as the STRING database) to produce networks (Bose et al., 2006; Pan et al., 2009; Stuart et al., 2015). Comparison of phosphoproteome changes in response to multiple different perturbations can increase the power of such analyses (Ochoa et al., 2016). Notably, these studies typically analyze data on the assumption that the inhibitors used are selective for particular kinases. As we have seen, this is rarely the case. Usefully, in some cases, two distinct inhibitors were used for each nominal target to provide additional confidence in the results (Terfve et al., 2015; Wilkes et al., 2015).

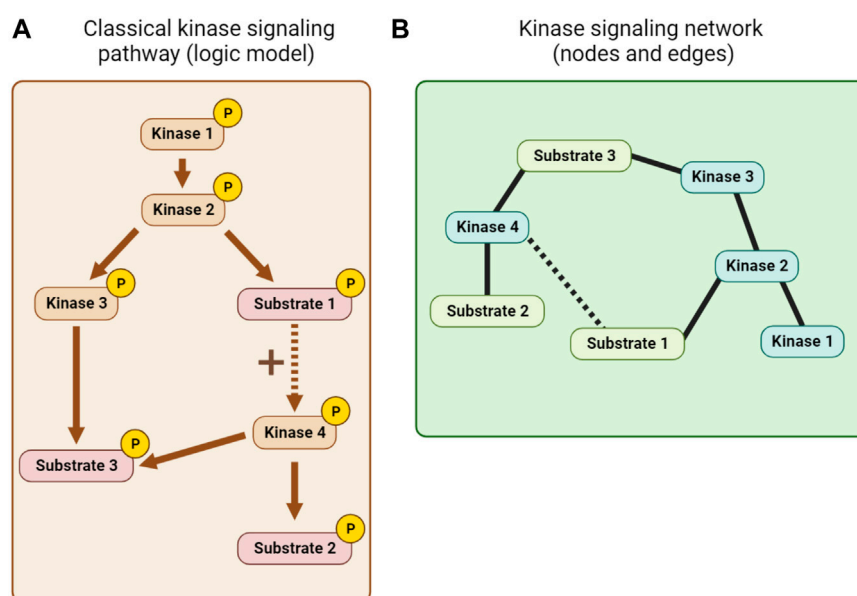


FIGURE 7

Kinase network visualization. (A) A classical kinase signaling pathway or logic model derived from KSR, PPI and other mechanistic information. (B) A node and edge kinase signaling network derived, for example, from KSR and PPI information.

More recently, an alternative approach was used in which broad selectivity information from the *in vitro* inhibition profiles of a panel of kinase inhibitors were used to identify kinase-phosphosite relationships from proteomics data. In these experiments, quantitative phosphoproteomics was utilized to monitor phosphorylation changes in cells treated with a panel of well-characterized kinase inhibitors. This approach is comparable to the KiPIK method (Section 4.3.2) in that it makes use of the incomplete specificity of kinase inhibitors rather than ignoring it. However, it differs from KiPIK because it uses intact cells, not cell extracts, and it does not seek to identify direct KSRs. Instead, it uses an “expectancy of being downstream target” (EBDT) algorithm to place phosphosites that might be directly or indirectly downstream of a particular kinase into groups of putative downstream targets (PDTs). This information can then be used to create context-specific network models in a way that does not depend on prior knowledge of KSRs or other information, and which can identify possible tumor vulnerabilities, for example, TTK in acute myeloid leukemia (AML) (Hijazi et al., 2020). This is a potentially powerful approach, though it depends on the assumption that kinase inhibitor specificity in living cells is similar to that *in vitro*.

The principle of using inhibitor selectivity profile information has been further exploited in another recent study which aimed to identify protein binding partners of specific kinases. In this work, the ability of a panel of kinase inhibitors to displace kinase-containing protein complexes from Kinobeads (see Figure 1B) was determined. Similar to KiPIK, by correlating the known inhibition fingerprints for kinases with displacement fingerprints of putative kinase-associated proteins determined by mass spectrometry, the “kiCCA” method was able to identify proteins associated with 238 different kinases. In this way, local context-specific kinase PPI networks can be examined (Golkowski et al., 2023).

5.3 Which kinases are good targets to bring about a specific change in cell phenotype?

In many cases, there may be a cellular phenotype that we wish to modulate with drugs for therapeutic benefit. This might be as conceptually simple as killing proliferating cancer cells, or more complicated, such as modulating the immunoregulatory functions of a particular cell type. In other situations, we may need to understand how kinases contribute to phenotypes we wish to avoid, such as drug-induced toxicity. In such systems, it is likely that multiple kinases influence the phenotypes in question, and we know that most drugs influence the activity of more than one kinase. Therefore, methods for “target deconvolution” are required that can tell us which kinases are actually involved in phenotypic changes so that we can understand the underlying signaling pathways and identify targets for drug development. Pharmacological approaches to address these questions have been developed that exploit kinase inhibitor selectivity data (see Section 3) in combination with the effects of inhibitors in phenotypic screens. These methods therefore have conceptual similarities to KiPIK, EBDT, and kiCCA (see Sections 4.3.2 and Section 5.2, and Figure 6).

In 2013, Tyner et al. (2013) published a study in which the ability of 66 kinase inhibitors to decrease leukemia cell proliferation was tested. To determine which kinases were responsible for the effect, they used a weighted scoring system based on the known kinome inhibition profiles of the 66 inhibitors to identify and rank the common kinase targets of effective inhibitors. Using this approach, they were able to successfully identify kinases driving proliferation in patients with oncogenic kinase mutations such as in FLT3 or ABL1. Ryall et al. (2015) described a similar Kinase Addiction Ranker (KAR) algorithm which appeared effective in identifying kinases responsible for the drug sensitivity of lung cancer cell lines.

In somewhat analogous methods, [Pemovska et al. \(2013\)](#) combined drug sensitivity data with kinase selectivity profiles to provide insight into particular kinases involved in AML, and [Sundberg et al. \(2014\)](#) ranked kinases that suppressed IL-10 production by dendritic cells. Another feature selection algorithm uses kinase inhibition profiles and the response of cells to drugs to infer kinase circuits involved in tumor proliferation ([Berlow et al., 2013](#)).

In an interesting variation on this theme, [Lamore et al. \(2017\)](#) wished to identify kinases responsible for the wide-spread problem of drug cardiotoxicity. First, they measured the effect of a panel of well-profiled kinase inhibitors on cardiomyocyte beating, providing a proxy fingerprint for cardiotoxicity. Then, they used a univariate correlation analysis to compare this fingerprint to the inhibition fingerprints of all kinases in the profiling dataset. This provided a ranked list of kinases that might be involved in the cardiotoxicity. In an alternative approach, they also narrowed down “sentinel kinases” with the highest predictive value using a classification tree based on recursive partitioning. Testing of drugs with known clinical cardiac warnings showed that, indeed, the majority inhibited these sentinel kinases (RPS6KB1, FAK, and STK35).

Other studies have used an alternative algorithm for deconvoluting kinases involved in cellular responses to kinase inhibitors: regression and variable selection. Kinome Regularization (KiR), uses elastic net regularization to whittle down the list of possible kinases to identify a minimal set with the most power to explain the inhibition of a phenotype. This approach was used to determine which kinases were involved in the inhibition of cell migration by a panel of well-characterized kinase inhibitors, and these were then validated by additional experiments including RNAi ([Gujral et al., 2014a; Gujral et al., 2014b; Rata et al., 2020](#)). KiR has also been used successfully to characterize kinases involved in prostate cancer cell proliferation, and in malaria parasite persistence in hepatocyte cultures ([Arang et al., 2017; Bello et al., 2021b](#)). Going a step further, the KiR algorithm can also be used successfully to predict polypharmacological inhibitors or combinations of inhibitors that will induce desired changes in cell behavior, even before the inhibitors have been tested in the phenotypic assay ([Gujral et al., 2014b; Bello et al., 2021b](#)). KiR has recently been expanded by integrating prior knowledge of PPIs to uncover kinase-focused cellular PPI networks ([Bello et al., 2021a](#)).

Machine learning approaches have also been applied to target deconvolution. Following a screen for neurite outgrowth using a kinase inhibitor library, a maximum relevance and support vector machine algorithm (MR-SVM) was used to exploit kinome profiling data to identify a small number of kinase groups that are most relevant in controlling axon growth. Significant hits could be validated by RNAi, and the results allowed the rational selection of compounds with complementary polypharmacology for further study ([Al-Ali et al., 2015](#)).

Notably, a major advantage of all these pharmacology-based deconvolution methods is that they provide context-specific information. Indeed, different kinases were identified as important in different cell lines or patient samples in a number of these studies ([Tyner et al., 2013; Gujral et al., 2014b; Ryall et al., 2015](#)). Because of this, these approaches could be applied to the study of other context-specific networks, such as cells that acquire resistance to cancer therapeutics. Further work is needed to fully

validate these methods, and to determine which prediction algorithms are most reliable, but the underpinning idea to make use of in-depth inhibitor selectivity data is a powerful one.

5.4 How is a kinase network influenced by a drug or chemical probe?

A common research question is how is the signaling network of a particular cell type or tissue influenced by a particular small molecule. For well-characterized chemical or chemo-genetic probes, answering this question can provide information on the direct and indirect targets of the kinase(s) of interest. For drugs, we can learn broadly about their mechanisms of action, including off target effects, similarities to the effects of other drugs, or how inhibitor resistance develops. Clearly, genomic and transcriptomic approaches such as monitoring gene expression changes in response to inhibitors ([Subramanian et al., 2017](#)), and the global phosphoproteomics methods discussed above (see [Section 5.1](#) and [Section 5.2](#)) have a vital role to play in such studies ([Bose et al., 2006; Pan et al., 2009; Stuart et al., 2015; Terfve et al., 2015; Wilkes et al., 2015; Zecha et al., 2023](#)). These approaches can, however, be augmented or complemented by additional methods that are particularly relevant for kinase networks ([Pierobon et al., 2015](#)).

For example, to reduce the complexity of phosphoproteome analysis and increase robustness, quantitative measurement of phosphorylation can be focused on a subset of key phosphosites, such as those known to be involved in major cancer signaling pathways. In AQUA, or in “kinase activity assay for kinome profiling” (KAYAK), suites of standard peptides facilitate quantification of phosphorylation by mass spectrometry ([Gerber et al., 2003; Kubota et al., 2009](#)), or targeted modes of mass spectrometry can be used ([Beck et al., 2017; Payne and Huang, 2017](#)). A number of antibody-based multiplex assays are available that can be used to quantify phosphorylation of specific phosphosites in cell extracts [e.g., MILLIPLEX (Merck) and scioPhospho (Sciomics)]. Such array techniques have been used, in combination with gene expression data, to analyze the consequences of sequential treatment of drugs including kinase inhibitors on the apoptosis of breast cancer cells ([Lee et al., 2012](#)). Alternatively, phosphorylation of substrate peptide microarrays such as PamChip can be used to profile kinase activities in lysates of cells or tissues during a variety of treatments ([Lemeer et al., 2007; Keersmaecker et al., 2008](#)). These assays include only a fraction of the possible cellular phosphorylation sites, and the particular kinases involved must be inferred based on previously known KSRs. Nevertheless, this system allows rapid comparison of multiple conditions, and works with small samples such as human BRAF-V600E melanoma biopsies ([Tahiri et al., 2013](#)).

Because the development of resistance to targeted kinase therapy is so common, approaches to discover the underlying causes are vital. The first mechanisms of resistance to BCR-ABL inhibitors were identified in imatinib-treated CML patients, revealing *BCR-ABL* gene amplification, or point mutations in the ABL kinase domain that prevented drug binding ([Gorre et al., 2001](#)). Potential resistance mechanisms can also be identified using

inhibitors *in vitro*. For example, isolation of cells that were resistant to killing by imatinib in cell culture uncovered ABL mutation-independent mechanisms, as well as *BCR-ABL* amplification (Mahon et al., 2000). Other studies combined directed mutagenesis of the ABL kinase domain with *in vitro* exposure to imatinib to identify additional kinase domain mutations that reduced inhibitor efficacy (Azam et al., 2003). More recent *in vitro* studies of kinase inhibitor resistance have identified non-genetic mechanisms of resistance such as epigenetic changes in gene expression, and have suggested that there is a wide diversity of such resistance mechanisms, even within genetically homogenous cell including clonal BRAF-V600E melanoma cells (Sharma et al., 2010; Goyal et al., 2023). The growing sophistication of *in vitro* cancer models and the use of animal tumor models is likely to further enhance the clinical relevance of similar studies of kinase inhibitor resistance in future.

5.5 Can kinase network features be used as biomarkers of drug efficacy?

Another clinically significant need is to predict patient-specific responses to kinase inhibitors so that appropriate personalized treatment regimens can be designed, both upon first diagnosis and if resistance to therapy subsequently develops. Currently, this often takes the form of specific biomarkers that indicate susceptibility to a particular drug, such as a mutation in the gene for a kinase. In other cases, “functional diagnostic” approaches might be used: for example, assays that test whether patient cells are susceptible to killing with a specific drug or combination of drugs. These functional approaches may uncover vulnerabilities that are not predicted by genetic analysis, and have been used to guide patient treatment, such as in refractory AML (Pemovska et al., 2013; Tyner et al., 2013; Crystal et al., 2014; Friedman et al., 2015; Robers et al., 2015).

Characterization of kinase network features provides another avenue to identify prospective biomarkers. Early studies that linked drug sensitivity to the genetic features of the NCI-60 panel of cell lines have matured and now include hundreds of compounds tested on almost 1000 cancer cell lines (Weinstein et al., 1997; Barretina et al., 2012; Garnett et al., 2012; Iorio et al., 2016). Such work has revealed associations between drug sensitivity and gene expression changes or mutations in kinase pathways, including during the development of drug resistance (Garnett et al., 2012; Pemovska et al., 2013). However, non-genetic changes are also important, and similar association studies can also be carried out using phosphoproteomics with the aim of identifying non-genetic features of kinase signaling that correlate with drug sensitivity (for example, in the EGFR signaling pathway (Guo et al., 2008)). Notably, suitable markers for drug sensitivity may not always be obvious components of the pathway presumed to be targeted by the inhibitors in question (Alcolea et al., 2012; Casado et al., 2013), illustrating the value of broad phosphoproteomic analysis.

In some cases, knowledge of multiple features of a phosphorylation network may provide improved prediction of patient responses compared with a single feature such as mutation of the gene encoding the perceived target kinase. For example, in a pre-clinical study of patient-derived AML cells,

Casado et al. (2018) found that a phosphoproteomic signature predicted the *ex vivo* response to the FLT3 kinase inhibitor midostaurin better than FLT3 mutational status. Importantly, kinases that contribute to such newly discovered signatures, or other regulators such as epigenetic modifiers, may also provide new targets for drug discovery (Casado et al., 2018; Pediconi et al., 2022). Drug sensitivity signatures may also be discovered using more targeted approaches such as PamChip (see section 5.4) (Elst et al., 2011) or using Kinobeads to enrich for kinases (Cooper et al., 2013; Golkowski et al., 2023; 2020).

Because of the expected complexity of predictive signatures, there have been numerous efforts to use machine-learning algorithms to integrate pharmacologic and ‘omic data to predict patient outcomes in response to kinase inhibitors and other drugs. Many of these approaches rely on genomic and gene expression information (Basu et al., 2013; Yang et al., 2013), but more recently the utility of (phospho) proteomic data has been explored. For example, drug ranking using machine learning (DRUML), developed by the Cutillas group, learns to rank cancer drug activity in patients based on a training dataset of drug sensitivity data for a panel of cell lines with corresponding proteomic, phosphoproteomic, and RNA-seq datasets (Gerdes et al., 2021).

6 Conclusion

As we have seen, chemical and chemo-genetic probes are undoubtedly useful for the discovery of KSRs and characterization of context-specific signaling networks. However, the target profiles of such probes first must be comprehensively characterized. Numerous techniques are now available to achieve this, but they still have some disadvantages. For example, kinase panels for *in vitro* profiling of inhibitors remain incomplete. So-called “dark kinases” are often absent, and coverage of mutant kinases that are involved in disease and drug resistance remains rather haphazard. Broadening these profiling panels is important both for understanding possible off-target effects, and for widening the net of target deconvolution approaches that rely on extensive inhibitor selectivity profiling of multiple kinases (such as KiR, EBDT, KiPIK and kiCCA).

Despite advances in profiling kinase inhibitor target engagement in living cells, such technologies remain relatively low throughput and are often complicated to perform. For *in vitro* assays, radiolabeled ATP assays are usually considered the “gold standard”, but the limited data obtained so far using cell and lysate inhibitor profiling makes it harder to define their limitations and to validate the results of methods such as CETSA and NanoBRET. Nonetheless, understanding target engagement in cells is the ultimate objective of most studies, so developments in this area are keenly anticipated.

Importantly, many profiling methods exclude possible non-kinase targets of inhibitors, or provide incomplete coverage. Such off-target interactions have the potential to dramatically alter the *in vivo* effects of drugs and chemical probes, and more attention to this aspect of inhibitor action would be welcome. Nevertheless, we have never been in a better position to comprehensively determine the target engagement profiles of kinase inhibitors, both *in vitro* and in cells.

It is clearly important to continue growing our understanding of individual kinase-substrate interactions. However, KSRs can be context specific; the kinase that phosphorylates a particular phosphosite may change depending on which upstream signaling pathway is activated, or from cell type to cell type (Sapkota et al., 2001; Zecha et al., 2023). Network models based on generic KSRs will not reflect these particularities. It is therefore imperative that we understand KSRs in the context of specific signaling networks. The ease with which chemical probes can be employed in different situations has significant advantages for such studies.

Developments in computational approaches are also likely to be key to unlocking the potential of pharmacological approaches to understand protein kinase signaling networks. Efforts to rationalize the inhibitor libraries used for phenotypic studies, either to create libraries of high selectivity for each target kinase (Moret et al., 2019; Wells et al., 2021) or suitable for deconvolution approaches (Gujral et al., 2014b; Rata et al., 2020; Watson et al., 2020; Golkowski et al., 2023), will help optimize the trade-off between library size and experimental practicality. Further work should help to determine which algorithms are most effective for identifying relevant kinases and pathways from inhibitor-induced perturbations in the phosphoproteome, for target deconvolution based on phenotypic screens, and for rational design of polypharmacological agents and drug combinations (Gujral et al., 2014b; Hernandez-Armenta et al., 2017; Tang, 2017; Rocca and Kholodenko, 2021). Finally, machine learning is poised to provide notable advances in determining features of kinase networks that predict drug efficacy for personalized medicine, as well as in these other areas.

In summary, in-depth knowledge of target engagement by chemical probes in cells, coupled with increasingly sophisticated data acquisition and analysis pipelines, suggest that pharmacological approaches to understanding context-specific kinase networks will continue to yield vital insights for the foreseeable future.

References

- Al-Ali, H., Lee, D. H., Danzi, M. C., Nassif, H., Gautam, P., Wennerberg, K., et al. (2015). Rational polypharmacology: systematically identifying and engaging multiple drug targets to promote axon growth. *ACS Chem. Biol.* 10, 1939–1951. doi:10.1021/acscchembio.5b00289
- Alcolea, M. P., Casado, P., Rodríguez-Prados, J. C., Vanhaesebroeck, B., and Cutillas, P. R. (2012). Phosphoproteomic analysis of leukemia cells under basal and drug-treated conditions identifies markers of kinase pathway activation and mechanisms of resistance. *Mol. Cell. Proteomics* 11, 453–466. doi:10.1074/mcp.M112.017483
- Allen, J. J., Li, M., Brinkworth, C. S., Paulson, J. L., Wang, D., Hübner, A., et al. (2007). A semisynthetic epitope for kinase substrates. *Nat. Methods* 4, 511–516. doi:10.1038/nmeth1048
- Anastassiadis, T., Deacon, S. W., Devarajan, K., Ma, H., and Peterson, J. R. (2011). Comprehensive assay of kinase catalytic activity reveals features of kinase inhibitor selectivity. *Nat. Biotechnol.* 29, 1039–1045. doi:10.1038/nbt.2017
- Arang, N., Kain, H. S., Glennon, E. K., Bello, T., Dudgeon, D. R., Walter, E. N. F., et al. (2017). Identifying host regulators and inhibitors of liver stage malaria infection using kinase activity profiles. *Nat. Commun.* 8, 1232. doi:10.1038/s41467-017-01345-2
- Arrowsmith, C. H., Audia, J. E., Austin, C., Baell, J., Bennett, J., Blagg, J., et al. (2015). The promise and peril of chemical probes. *Nat. Chem. Biol.* 11, 536–541. doi:10.1038/nchembio.1867
- Ayati, M., Wiredja, D., Schlatter, D., Maxwell, S., Li, M., Koyutürk, M., et al. (2019). CoPhosK: a method for comprehensive kinase substrate annotation using co-phosphorylation analysis. *PLoS Comput. Biol.* 15, e1006678. doi:10.1371/journal.pcbi.1006678
- Azam, M., Latek, R. R., and Daley, G. Q. (2003). Mechanisms of autoinhibition and STI-571/Imatinib resistance revealed by mutagenesis of BCR-ABL. *Cell* 112, 831–843. doi:10.1016/S0092-8674(03)00190-9
- Azorsa, D. O., Robeson, R. H., Frost, D., Hoovet, B. M., Brautigam, G. R., Dickey, C., et al. (2010). High-content siRNA screening of the kinome identifies kinases involved in Alzheimer's disease-related tau hyperphosphorylation. *BMC Genomics* 11, 25. doi:10.1186/1471-2164-11-25
- Bai, Y., Kim, J. Y., Bisunke, B., Jayne, L. A., Silvaroli, J. A., Balzer, M. S., et al. (2021). Kidney toxicity of the BRAF-kinase inhibitor vemurafenib is driven by off-target ferroxidase inhibition. *Kidney Int.* 100, 1214–1226. doi:10.1016/j.kint.2021.08.022
- Bain, J., Plater, L., Elliott, M., Shpiro, N., Hastie, C. J., McLauchlan, H., et al. (2007). The selectivity of protein kinase inhibitors: a further update. *Biochem. J.* 408, 297–315. doi:10.1042/BJ20070797
- Bain, J., McLauchlan, H., Elliott, M., and Cohen, P. (2003). The specificities of protein kinase inhibitors: an update. *Biochem. J.* 371, 199–204. doi:10.1042/BJ20021535
- Bamborough, P., Drewry, D., Harper, G., Smith, G. K., and Schneider, K. (2008). Assessment of chemical coverage of kinase space and its implications for kinase drug discovery. *J. Med. Chem.* 51, 7898–7914. doi:10.1021/jm8011036
- Bantscheff, M., Eberhard, D., Abraham, Y., Bastuck, S., Boesche, M., Hobson, S., et al. (2007). Quantitative chemical proteomics reveals mechanisms of action of clinical ABL kinase inhibitors. *Nat. Biotechnol.* 25, 1035–1044. doi:10.1038/nbt1328
- Barretina, J., Caponigro, G., Stransky, N., Venkatesan, K., Margolin, A. A., Kim, S., et al. (2012). The Cancer Cell Line Encyclopedia enables predictive modelling of anticancer drug sensitivity. *Nature* 483, 603–607. doi:10.1038/nature11003
- Basu, A., Bodycombe, N. E., Cheah, J. H., Price, E. V., Liu, K., Schaefer, G. I., et al. (2013). An interactive resource to identify cancer genetic and lineage dependencies targeted by small molecules. *Cell* 154, 1151–1161. doi:10.1016/j.cell.2013.08.003
- Beck, K., Camp, N., Bereman, M., Bollinger, J., Egerton, J., MacCoss, M., et al. (2017). "Development of selected reaction monitoring methods to systematically quantify kinase abundance and phosphorylation stoichiometry in human samples," in *Kinase signaling networks, methods in molecular biology*. Editors A.-C. Tan and P. H. Huang (New York, NY: Springer), 353–369. doi:10.1007/978-1-4939-7154-1_23

Author contributions

ES: Writing—original draft, Writing—review and editing. JH: Writing—original draft, Writing—review and editing.

Funding

The author(s) declare financial support was received for the research, authorship, and/or publication of this article. ES is supported by an MRC DiMeN DTP iCASE studentship (MR/R015902/1). Work in this area by JH has been supported by the Wellcome Trust (106951/Z/15/Z), an MRC Confidence in Concept award (MC_PC_18057), and funding from the Northern Accelerator.

Conflict of interest

ES holds an MRC DiMeN iCASE studentship between Newcastle University and Kinomica Ltd., United Kingdom. JH is a supervisor for the studentship above, and is an inventor on UK Patent 2583741 and international patent filing WO/2020/225535 which describes the KiPIK method.

Publisher's note

All claims expressed in this article are solely those of the authors and do not necessarily represent those of their affiliated organizations, or those of the publisher, the editors and the reviewers. Any product that may be evaluated in this article, or claim that may be made by its manufacturer, is not guaranteed or endorsed by the publisher.

- Bello, T., Chan, M., Golkowski, M., Xue, A. G., Khasnavis, N., Ceribelli, M., et al. (2021a). KiRNet: kinase-centered network propagation of pharmacological screen results. *Cell Rep. Methods* 1, 100007. doi:10.1016/j.crmeth.2021.100007
- Bello, T., Paindelli, C., Diaz-Gomez, L. A., Melchiorri, A., Mikos, A. G., Nelson, P. S., et al. (2021b). Computational modeling identifies multitargeted kinase inhibitors as effective therapies for metastatic, castration-resistant prostate cancer. *Proc. Natl. Acad. Sci. U. S. A.* 118, e2103623118. doi:10.1073/pnas.2103623118
- Beltman, R. J., and Pflum, M. K. H. (2022). Kinase-catalyzed crosslinking and immunoprecipitation (K-clip) to explore kinase-substrate pairs. *Curr. Protoc. 2*, e539. doi:10.1002/cpz1.539
- Berlow, N., Davis, L. E., Cantor, E. L., Séguin, B., Keller, C., and Pal, R. (2013). A new approach for prediction of tumor sensitivity to targeted drugs based on functional data. *BMC Bioinforma.* 14, 239. doi:10.1186/1471-2105-14-239
- Bishop, A. C., Buzko, O., and Shokat, K. M. (2001). Magic bullets for protein kinases. *Trends Cell Biol.* 11, 167–172. doi:10.1016/S0962-8924(01)01928-6
- Bishop, A. C., Shah, K., Liu, Y., Witucki, L., Kung, C., and Shokat, K. M. (1998). Design of allele-specific inhibitors to probe protein kinase signaling. *Curr. Biol.* 8, 257–266. doi:10.1016/S0960-9822(98)70198-8
- Blethrow, J. D., Glavy, J. S., Morgan, D. O., and Shokat, K. M. (2008). Covalent capture of kinase-specific phosphopeptides reveals Cdk1-cyclin B substrates. *Proc. Natl. Acad. Sci. U. S. A.* 105, 1442–1447. doi:10.1073/pnas.0708966105
- Bodenmiller, B., Wanka, S., Kraft, C., Urban, J., Campbell, D., Pedrioli, P. G., et al. (2010). Phosphoproteomic analysis reveals interconnected system-wide responses to perturbations of kinases and phosphatases in yeast. *Sci. Signal.* 3, rs4. doi:10.1126/scisignal.2001182
- Bose, R., Molina, H., Patterson, A. S., Bitok, J. K., Periaswamy, B., Baderh, J. S., et al. (2006). Phosphoproteomic analysis of Her2/neu signaling and inhibition. *Proc. Natl. Acad. Sci. U. S. A.* 103, 9773–9778. doi:10.1073/pnas.0603948103
- Breitkreutz, A., Choi, H., Sharom, J. R., Boucher, L., Neduva, V., Larsen, B., et al. (2010). A global protein kinase and phosphatase interaction network in yeast. *Science* 328, 1043–1046. doi:10.1126/science.1176495
- Buljan, M., Ciuffa, R., van Drogen, A., Vichalkovski, A., Mehnert, M., Rosenberger, G., et al. (2020). Kinase interaction network expands functional and disease roles of human kinases. *Mol. Cell* 79, 504–520. doi:10.1016/j.molcel.2020.07.001
- Cartwright, T. N., Meyer, S. K., and Higgins, J. M. G. (2022). Robustness of NanoBIT luciferase complementation technology in the presence of widely used kinase inhibitors. *SLAS Discov.* 27, 471–475. doi:10.1016/j.slasd.2022.09.004
- Casado, P., Rodriguez-Prados, J.-C., Cosulich, S. C., Guichard, S., Vanhaesebroeck, B., Joel, S., et al. (2013). Kinase-substrate enrichment analysis provides insights into the heterogeneity of signaling pathway activation in leukemia cells. *Sci. Signal.* 6, rs6. doi:10.1126/scisignal.2003573
- Casado, P., Wilkes, E. H., Miraki-Moud, F., Hadi, M. M., Rio-Machin, A., Rajeev, V., et al. (2018). Proteomic and genomic integration identifies kinase and differentiation determinants of kinase inhibitor sensitivity in leukemia cells. *Leukemia* 32, 1818–1822. doi:10.1038/s41375-018-0032-1
- Chi, Y., Welcker, M., Hizli, A. A., Posakony, J. J., Aebersold, R., and Clurman, B. E. (2008). Identification of CDK2 substrates in human cell lysates. *Genome Biol.* 9, R149. doi:10.1186/gb-2008-9-10-r149
- Cohen, P. (2002). Protein kinases - the major drug targets of the twenty-first century? *Nat. Rev. Drug Discov.* 1, 309–315. doi:10.1038/nrd773
- Cohen, P., Cross, D., and Jänne, P. A. (2021). Kinase drug discovery 20 years after imatinib: progress and future directions. *Nat. Rev. Drug Discov.* 20, 551–569. doi:10.1038/s41573-021-00195-4
- Cooper, M. J., Cox, N. J., Zimmerman, E. I., Dewar, B. J., Duncan, J. S., Whittle, M. C., et al. (2013). Application of multiplexed kinase inhibitor beads to study kinome adaptations in drug-resistant leukemia. *PLoS ONE* 8, e66755. doi:10.1371/journal.pone.0066755
- Creixell, P., Schoof, E. M., Erler, J. T., and Lindig, R. (2012). Navigating cancer network attractors for tumor-specific therapy. *Nat. Biotechnol.* 30, 842–848. doi:10.1038/nbt.2345
- Crystal, A. S., Shaw, A. T., Sequist, L. V., Friboulet, L., Niederst, M. J., Lockerman, E. L., et al. (2014). Patient-derived models of acquired resistance can identify effective drug combinations for cancer. *Science* 346, 1480–1486. doi:10.1126/science.1254721
- Daub, H. (2005). Characterisation of kinase-selective inhibitors by chemical proteomics. *Biochim. Biophys. Acta* 1754, 183–190. doi:10.1016/j.bbapap.2005.07.028
- Daub, H., Olsen, J. V., Bairlein, M., Gnad, F., Oppermann, F. S., Körner, R., et al. (2008). Kinase-selective enrichment enables quantitative phosphoproteomics of the kinome across the cell cycle. *Mol. Cell* 31, 438–448. doi:10.1016/j.molcel.2008.07.007
- Davies, S. P., Reddy, H., Caivano, M., and Cohen, P. (2000). Specificity and mechanism of action of some commonly used protein kinase inhibitors. *Biochem. J.* 351, 95–105. doi:10.1042/0264-6021:3510095
- Davis, M. I., Hunt, J. P., Herrgard, S., Ciceri, P., Wodicka, L. M., Pallares, G., et al. (2011). Comprehensive analysis of kinase inhibitor selectivity. *Nat. Biotechnol.* 29, 1046–1051. doi:10.1038/nbt.1990
- Dedigama-Arachchige, P. M., and Pflum, M. K. H. (2016). K-CLASP: a tool to identify phosphosite specific kinases and interacting proteins. *ACS Chem. Biol.* 11, 3251–3255. doi:10.1021/acscmbio.6b00289
- Demetri, G. D., von Mehren, M., Blanke, C. D., Van den Abbeele, A. D., Eisenberg, B., Roberts, P. J., et al. (2002). Efficacy and safety of imatinib mesylate in advanced gastrointestinal stromal tumors. *N. Engl. J. Med.* 347, 472–480. doi:10.1056/NEJMoa020461
- Domanova, W., Krycer, J., Chaudhuri, R., Yang, P., Vafae, F., Fazakerley, D., et al. (2016). Unraveling kinase activation dynamics using kinase-substrate relationships from temporal large-scale phosphoproteomics studies. *PLoS ONE* 11, e0157763. doi:10.1371/journal.pone.0157763
- Douglass, J., Gunaratne, R., Bradford, D., Saeed, F., Hoffert, J. D., Steinbach, P. J., et al. (2012). Identifying protein kinase target preferences using mass spectrometry. *Am. J. Physiol. - Cell Physiol.* 303, C715–C727. doi:10.1152/ajpcell.00166.2012
- Drake, J. M., Graham, N. A., Stoyanova, T., Sedghi, A., Goldstein, A. S., Cai, H., et al. (2012). Oncogene-specific activation of tyrosine kinase networks during prostate cancer progression. *Proc. Natl. Acad. Sci.* 109, 1643–1648. doi:10.1073/pnas.1120985109
- Drake, J. M., Paull, E. O., Graham, N. A., Lee, J. K., Smith, B. A., Titz, B., et al. (2016). Phosphoproteome integration reveals patient-specific networks in prostate cancer. *Cell* 166, 1041–1054. doi:10.1016/j.cell.2016.07.007
- Drewry, D. H., Wells, C. I., Andrews, D. M., Angell, R., Al-Ali, H., Axtman, A. D., et al. (2017). Progress towards a public chemogenomic set for protein kinases and a call for contributions. *PLoS ONE* 12, e0181585. doi:10.1371/journal.pone.0181585
- Echalier, A., Hole, A. J., Lolli, G., Endicott, J. A., and Noble, M. E. M. (2014). An inhibitor's-eye view of the atp-binding site of CDKs in different regulatory states. *ACS Chem. Biol.* 9, 1251–1256. doi:10.1021/cb500135f
- Elkins, J. M., Fedele, V., Szklarz, M., Azeze, K. R. A., Salah, E., Mikolajczyk, J., et al. (2016). Comprehensive characterization of the published kinase inhibitor set. *Nat. Biotechnol.* 34, 95–103. doi:10.1038/nbt.3374
- Elst, A. T., Diks, S. H., Kampen, K. R., Hoogerbrugge, P. M., Ruijtenbeek, R., Boender, P. J., et al. (2011). Identification of new possible targets for leukemia treatment by kinase activity profiling. *Leuk. Lymphoma* 52, 122–130. doi:10.3109/10428194.2010.535181
- Engelman, J. A., Zejnullahu, K., Mitsudomi, T., Song, Y., Hyland, C., Park, J. O., et al. (2007). MET amplification leads to gefitinib resistance in lung cancer by activating ERBB3 signaling. *Science* 316, 1039–1043. doi:10.1126/science.1141478
- Fabian, M. A., Biggs, W. H., Treiber, D. K., Atteridge, C. E., Azimioara, M. D., Benedetti, M. G., et al. (2005). A small molecule-kinase interaction map for clinical kinase inhibitors. *Nat. Biotechnol.* 23, 329–336. doi:10.1038/NBT1068
- Fedorov, O., Marsden, B., Pogacic, V., Rellos, P., Müller, S., Bullock, A. N., et al. (2007). A systematic interaction map of validated kinase inhibitors with Ser/Thr kinases. *Proc. Natl. Acad. Sci. U. S. A.* 104, 20523–20528. doi:10.1073/pnas.0708800104
- Fiedler, D., Braberg, H., Mehta, M., Chechik, G., Cagney, G., Mukherjee, P., et al. (2009). Functional organization of the *S. cerevisiae* phosphorylation network. *Cell* 136, 952–963. doi:10.1016/j.cell.2008.12.039
- Friedman, A., and Perrimon, N. (2006). A functional RNAi screen for regulators of receptor tyrosine kinase and ERK signalling. *Nature* 444, 230–234. doi:10.1038/NATURE05280
- Friedman, A. A., Letai, A., Fisher, D. E., and Flaherty, K. T. (2015). Precision medicine for cancer with next-generation functional diagnostics. *Nat. Rev. Cancer* 15, 747–756. doi:10.1038/nrc4015
- Gao, Y., Davies, S. P., Augustin, M., Woodward, A., Patel, U. A., Kovelman, R., et al. (2013). A broad activity screen in support of a chemogenomic map for kinase signalling research and drug discovery. *Biochem. J.* 451, 313–328. doi:10.1042/BJ20121418
- Garnett, M. J., Edelman, E. J., Heidorn, S. J., Greenman, C. D., Dastur, A., Lau, K. W., et al. (2012). Systematic identification of genomic markers of drug sensitivity in cancer cells. *Nature* 483, 570–575. doi:10.1038/nature11005
- Garre, S., Gamage, A. K., Faner, T. R., Dedigama-Arachchige, P., and Pflum, M. K. H. (2018). Identification of kinases and interactors of p53 using kinase-catalyzed cross-linking and immunoprecipitation. *J. Am. Chem. Soc.* 140, 16299–16310. doi:10.1021/jacs.8b10160
- Gerber, S. A., Rush, J., Stemman, O., Kirschner, M. W., and Gygi, S. P. (2003). Absolute quantification of proteins and phosphoproteins from cell lysates by tandem MS. *Proc. Natl. Acad. Sci. U. S. A.* 100, 6940–6945. doi:10.1073/pnas.0832254100
- Gerdes, H., Casado, P., Dokal, A., Hijazi, M., Akhtar, N., Osuntola, R., et al. (2021). Drug ranking using machine learning systematically predicts the efficacy of anti-cancer drugs. *Nat. Commun.* 12, 1850. doi:10.1038/s41467-021-22170-8
- Goel, S., Bergholz, J. S., and Zhao, J. J. (2022). Targeting CDK4 and CDK6 in cancer. *Nat. Rev. Cancer* 22, 356–372. doi:10.1038/s41568-022-00456-3
- Golkowski, M., Lau, H. T., Chan, M., Kenerson, H., Vidadala, V. N., Shoemaker, A., et al. (2020). Pharmacoproteomics identifies kinase pathways that drive the epithelial-mesenchymal transition and drug resistance in hepatocellular carcinoma. *Cell Syst.* 11, 196–207. doi:10.1016/j.cels.2020.07.006
- Golkowski, M., Lius, A., Sapre, T., Lau, H.-T., Moreno, T., Maly, D. J., et al. (2023). Multiplexed kinase interactome profiling quantifies cellular network activity and plasticity. *Mol. Cell* 83, 803–818.e8. doi:10.1016/j.molcel.2023.01.015

- Gorre, M. E., Mohammed, M., Ellwood, K., Hsu, N., Paquette, R., Rao, P. N., et al. (2001). Clinical resistance to STI-571 cancer therapy caused by BCR-ABL gene mutation or amplification. *Science* 293, 876–880. doi:10.1126/science.1062538
- Goyal, Y., Busch, G. T., Pillai, M., Li, J., Boe, R. H., Grody, E. I., et al. (2023). Diverse clonal fates emerge upon drug treatment of homogeneous cancer cells. *Nature* 620, 651–659. doi:10.1038/s41586-023-06342-8
- Graves, L. M., Duncan, J. S., Whittle, M. C., and Johnson, G. L. (2013). The dynamic nature of the kinome. *Biochem. J.* 450, 1–8. doi:10.1042/BJ20121456
- Gujral, T. S., Chan, M., Peshkin, L., Sorger, P. K., Kirschner, M. W., and Macbeath, G. (2014a). A noncanonical frizzled2 pathway regulates epithelial-mesenchymal transition and metastasis. *Cell* 159, 844–856. doi:10.1016/j.cell.2014.10.032
- Gujral, T. S., Peshkin, L., and Kirschner, M. W. (2014b). Exploiting polypharmacology for drug target deconvolution. *Proc. Natl. Acad. Sci. U. S. A.* 111, 5048–5053. doi:10.1073/pnas.1403080111
- Guo, A., Villén, J., Kornhauser, J., Lee, K. A., Stokes, M. P., Rikova, K., et al. (2008). Signaling networks assembled by oncogenic EGFR and c-Met. *Proc. Natl. Acad. Sci. U. S. A.* 105, 692–697. doi:10.1073/pnas.0707270105
- Hall, M. P., Unch, J., Binkowski, B. F., Valley, M. P., Butler, B. L., Wood, M. G., et al. (2012). Engineered luciferase reporter from a deep sea shrimp utilizing a novel imidazopyrazinone substrate. *ACS Chem. Biol.* 7, 1848–1857. doi:10.1021/cb3002478
- Hastie, C. J., McLauchlan, H. J., and Cohen, P. (2006). Assay of protein kinases using radiolabeled ATP: a protocol. *Nat. Protoc.* 1, 968–971. doi:10.1038/nprot.2006.149
- Hernandez-Armenta, C., Ochoa, D., Gonçalves, E., Saez-Rodriguez, J., and Beltrao, P. (2017). Benchmarking substrate-based kinase activity inference using phosphoproteomic data. *Bioinformatics* 33, 1845–1851. doi:10.1093/bioinformatics/btx082
- Hijazi, M., Smith, R., Rajeeve, V., Bessant, C., and Cutillas, P. R. (2020). Reconstructing kinase network topologies from phosphoproteomics data reveals cancer-associated rewiring. *Nat. Biotechnol.* 38, 493–502. doi:10.1038/s41587-019-0391-9
- Hopkins, A. L. (2008). Network pharmacology: the next paradigm in drug discovery. *Nat. Chem. Biol.* 4, 682–690. doi:10.1038/nchembio.118
- Huang, S. Y., Tsai, M. L., Chen, G. Y., Wu, C. J., and Chen, S. H. (2007). A systematic MS-based approach for identifying *in vitro* substrates of PKA and PKG in rat uteri. *J. Proteome Res.* 6, 2674–2684. doi:10.1021/pr070134c
- Invergo, B. M., Petrusson, B., Akhtar, N., Bradley, D., Giudice, G., Hijazi, M., et al. (2020). Prediction of signed protein kinase regulatory circuits. *Cell Syst.* 10, 384–396. doi:10.1016/j.cels.2020.04.005
- Iorio, F., Knijnenburg, T. A., Vis, D. J., Bignell, G. R., Menden, M. P., Schubert, M., et al. (2016). A landscape of pharmacogenomic interactions in cancer. *Cell* 166, 740–754. doi:10.1016/j.cell.2016.06.017
- Jacoby, E., Tresadern, G., Bembek, S., Wroblewski, B., Buyck, C., Neefs, J. M., et al. (2015). Extending kinome coverage by analysis of kinase inhibitor broad profiling data. *Drug Discov. Today* 20, 652–658. doi:10.1016/j.drudis.2015.01.002
- Jester, B. W., Gaj, A., Shomin, C. D., Cox, K. J., and Ghosh, I. (2012). Testing the promiscuity of commercial kinase inhibitors against the AGC kinase group using a split-luciferase screen. *J. Med. Chem.* 55, 1526–1537. doi:10.1021/jm201265f
- Johannessen, C. M., Boehm, J. S., Kim, S. Y., Thomas, S. R., Wardwell, L., Johnson, L. A., et al. (2010). COT drives resistance to RAF inhibition through MAP kinase pathway reactivation. *Nature* 468, 968–972. doi:10.1038/nature09627
- Johnson, J. L., Yaron, T. M., Huntsman, E. M., Kerelsky, A., Song, J., Regev, A., et al. (2023). An atlas of substrate specificities for the human serine/threonine kinome. *Nat* 613, 759–766. doi:10.1038/s41586-022-05575-3
- Johnson, S. A., and Hunter, T. (2005). Kinomics: methods for deciphering the kinome. *Nat. Methods* 2, 17–25. doi:10.1038/nmeth731
- Kanshin, E., Giguère, S., Jing, C., Tyers, M., and Thibault, P. (2017). Machine learning of global phosphoproteomic profiles enables discrimination of direct versus indirect kinase substrates. *Mol. Cell. Proteomics* 16, 786–798. doi:10.1074/mcp.M116.066233
- Karaman, M. W., Herrgard, S., Treiber, D. K., Gallant, P., Atteridge, C. E., Campbell, B. T., et al. (2008). A quantitative analysis of kinase inhibitor selectivity. *Nat. Biotechnol.* 26, 127–132. doi:10.1038/nbt1358
- Keersmaecker, K. D., Versele, M., Cools, J., Superti-Furga, G., and Hantschel, O. (2008). Intrinsic differences between the catalytic properties of the oncogenic NUP214-ABL1 and BCR-ABL1 fusion protein kinases. *Leukemia* 22, 2208–2216. doi:10.1038/leu.2008.242
- Kettenbach, A. N., Schweppe, D. K., Faherty, B. K., Pechenick, D., Pletnev, A. A., and Gerber, S. A. (2011). Quantitative phosphoproteomics identifies substrates and functional modules of Aurora and Polo-like kinase activities in mitotic cells. *Sci. Signal.* 4, rs5. doi:10.1126/scisignal.2001497
- Kettenbach, A. N., Wang, T., Faherty, B. K., Madden, D. R., Knapp, S., Bailey-Kellogg, C., et al. (2012). Rapid determination of multiple linear kinase substrate motifs by mass spectrometry. *Chem. Biol.* 19, 608–618. doi:10.1016/j.chembiol.2012.04.011
- Klaeger, S., Gohlke, B., Perrin, J., Gupta, V., Heinzlmeir, S., Helm, D., et al. (2016). Chemical proteomics reveals ferrochelatase as a common off-target of kinase inhibitors. *ACS Chem. Biol.* 11, 1245–1254. doi:10.1021/acschembio.5b01063
- Klaeger, S., Heinzlmeir, S., Wilhelm, M., Polzer, H., Vick, B., Koenig, P. A., et al. (2017). The target landscape of clinical kinase drugs. *Science* 358, eaan4368. doi:10.1126/science.aan4368
- Knebel, A., Morrice, N., and Cohen, P. (2001). A novel method to identify protein kinase substrates: eEF2 kinase is phosphorylated and inhibited by SAPK4/p38delta. *EMBO J.* 20, 4360–4369. doi:10.1093/emboj/20.16.4360
- Knight, J. D. R., Tian, R., Lee, R. E. C., Wang, F., Beauvais, A., Zou, H., et al. (2012). A novel whole-cell lysate kinase assay identifies substrates of the p38 MAPK in differentiating myoblasts. *Skelet. Muscle* 2, 5. doi:10.1186/2044-5040-2-5
- Knight, Z. A., Lin, H., and Shokat, K. M. (2010). Targeting the cancer kinome through polypharmacology. *Nat. Rev. Cancer* 10, 130–137. doi:10.1038/nrc2787
- Knight, Z. A., and Shokat, K. M. (2005). Features of selective kinase inhibitors. *Chem. Biol.* 12, 621–637. doi:10.1016/j.chembiol.2005.04.011
- Kubota, K., Anjum, R., Yu, Y., Kunz, R. C., Andersen, J. N., Kraus, M., et al. (2009). Sensitive multiplexed analysis of kinase activities and activity-based kinase identification. *Nat. Biotechnol.* 27, 933–940. doi:10.1038/nbt.1566
- Lamore, S. D., Ahlberg, E., Boyer, S., Lamb, M. L., Hortigon-Vinagre, M. P., Rodriguez, V., et al. (2017). Deconvoluting kinase inhibitor induced cardiotoxicity. *Toxicol. Sci.* 158, 213–226. doi:10.1093/toxsci/kfx082
- Lee, M. J., Ye, A. S., Gardino, A. K., Heijink, A. M., Sorger, P. K., MacBeath, G., et al. (2012). Sequential application of anticancer drugs enhances cell death by rewiring apoptotic signaling networks. *Cell* 149, 780–794. doi:10.1016/j.cell.2012.03.031
- Lemeer, S., Ruijtenbeek, R., Pinkse, M. W. H., Jopling, C., Heck, A. J. R., Hertog, J. den, et al. (2007). Endogenous phosphotyrosine signaling in zebrafish embryos. *Mol. Cell. Proteomics* 6, 2088–2099. doi:10.1074/mcp.M600482-MCP200
- Li, Z., Li, X., Liu, X., Fu, Z., Xiong, Z., Wu, X., et al. (2019). KinomeX: a web application for predicting kinome-wide polypharmacology effect of small molecules. *Bioinformatics* 35, 5354–5356. doi:10.1093/bioinformatics/btz519
- Linding, R., Jensen, L. J., Ostheimer, G. J., van Vugt, M. A. T. M., Jørgensen, C., Miron, I. M., et al. (2007). Systematic discovery of *in vivo* phosphorylation networks. *Cell* 129, 1415–1426. doi:10.1016/j.cell.2007.05.052
- Mahon, F. X., Deininger, M. W. N., Schultheis, B., Chabrol, J., Reiffers, J., Goldman, J. M., et al. (2000). Selection and characterization of BCR-ABL positive cell lines with differential sensitivity to the tyrosine kinase inhibitor STI571: diverse mechanisms of resistance. *Blood* 96, 1070–1079. doi:10.1182/blood.V96.3.1070
- Maly, D. J., Allen, J. A., and Shokat, K. M. (2004). A mechanism-based cross-linker for the identification of kinase-substrate pairs. *J. Am. Chem. Soc.* 126, 9160–9161. doi:10.1021/JA048659I
- Manning, G., Whyte, D. B., Martinez, R., Hunter, T., and Sudarsanam, S. (2002). The protein kinase complement of the human genome. *Science* 298, 1912–1934. doi:10.1126/science.1075762
- Markowitz, J. N., and Fancher, K. M. (2018). Cabozantinib: a multitargeted oral tyrosine kinase inhibitor. *Pharmacother. J. Hum. Pharmacol. Drug Ther.* 38, 357–369. doi:10.1002/phar.2076
- Marusiak, A. A., Edwards, Z. C., Hugo, W., Trotter, E. W., Girotti, M. R., Stephenson, N. L., et al. (2014). Mixed lineage kinases activate MEK independently of RAF to mediate resistance to RAF inhibitors. *Nat. Commun.* 5, 3901. doi:10.1038/ncomms4901
- Mellinghoff, I. K., Wang, M. Y., Vivanco, I., Haas-Kogan, D. A., Zhu, S., Dia, E. Q., et al. (2005). Molecular determinants of the response of glioblastomas to EGFR kinase inhibitors. *N. Engl. J. Med.* 353, 2012–2024. doi:10.1056/NEJMoa051918
- Merget, B., Turk, S., Eid, S., Rippmann, F., and Fulle, S. (2017). Profiling prediction of kinase inhibitors: toward the virtual assay. *J. Med. Chem.* 60, 474–485. doi:10.1021/acs.jmedchem.6b01611
- Metz, J. T., Johnson, E. F., Soni, N. B., Merta, P. J., Kifle, L., and Hajduk, P. J. (2011). Navigating the kinome. *Nat. Chem. Biol.* 7, 200–202. doi:10.1038/nchembio.530
- Michowski, W., Chick, J. M., Chu, C., Kolodziejczyk, A., Wang, Y., Suski, J. M., et al. (2020). Cdk1 controls global epigenetic landscape in embryonic stem cells. *Mol. Cell* 78, 459–476. doi:10.1016/j.molcel.2020.03.010
- Miller, C. J., and Turk, B. E. (2018). Homing in: mechanisms of substrate targeting by protein kinases. *Trends biochem. Sci.* 43, 380–394. doi:10.1016/j.tibs.2018.02.009
- Mischnick, M., Sacco, F., Cox, J., Schneider, H. C., Schäfer, M., Hendlich, M., et al. (2016). IKAP: a heuristic framework for inference of kinase activities from Phosphoproteomics data. *Bioinformatics* 32, 424–431. doi:10.1093/bioinformatics/btv699
- Moellering, R. E., and Cravatt, B. F. (2012). How chemoproteomics can enable drug discovery and development. *Chem. Biol.* 19, 11–22. doi:10.1016/j.chembiol.2012.01.001
- Moffat, J., Grueneberg, D. A., Yang, X., Kim, S. Y., Klopfner, A. M., Hinkle, G., et al. (2006). A lentiviral RNAi library for human and mouse genes applied to an arrayed viral high-content screen. *Cell* 124, 1283–1298. doi:10.1016/j.cell.2006.01.040
- Molina, D. M., Jafari, R., Ignatushchenko, M., Seki, T., Larsson, E. A., Dan, C., et al. (2013). Monitoring drug target engagement in cells and tissues using the cellular thermal shift assay. *Science* 341, 84–87. doi:10.1126/science.1233606
- Moret, N., Clark, N. A., Hafner, M., Wang, Y., Lounkine, E., Medvedovic, M., et al. (2019). Cheminformatics tools for analyzing and designing optimized small-molecule collections and libraries. *Cell Chem. Biol.* 26, 765–777. doi:10.1016/j.chembiol.2019.02.018

- Müller, A. C., Giambruno, R., Weißer, J., Májek, P., Hofer, A., Bigenzahn, J. W., et al. (2016). Identifying kinase substrates via a heavy ATP kinase assay and quantitative mass spectrometry. *Sci. Rep.* 6, 28107. doi:10.1038/srep28107
- Nazarian, R., Shi, H., Wang, Q., Kong, X., Koya, R. C., Lee, H., et al. (2010). Melanomas acquire resistance to B-RAF(V600E) inhibition by RTK or N-RAS upregulation. *Nature* 468, 973–977. doi:10.1038/nature09626
- Newman, R. H., Hu, J., Rho, H., Xie, Z., Woodard, C., Neiswinger, J., et al. (2013). Construction of human activity-based phosphorylation networks. *Mol. Syst. Biol.* 9, 655. doi:10.1038/msb.2013.12
- Nishimura, K., Fukagawa, T., Takisawa, H., Kakimoto, T., and Kanemaki, M. (2009). An auxin-based degenon system for the rapid depletion of proteins in nonplant cells. *Nat. Methods* 6, 917–922. doi:10.1038/nmeth.1401
- Ochoa, D., Jonikas, M., Lawrence, R. T., El Debs, B., Selkrig, J., Typas, A., et al. (2016). An atlas of human kinase regulation. *Mol. Syst. Biol.* 12, 888. doi:10.15252/msb.20167295
- Olsen, J. V., Blagoev, B., Gnäd, F., Macek, B., Kumar, C., Mortensen, P., et al. (2006). Global, *in vivo*, and site-specific phosphorylation dynamics in signaling networks. *Cell* 127, 635–648. doi:10.1016/j.cell.2006.09.026
- Oppermann, F. S., Grundner-Culemann, K., Kumar, C., Gruss, O. J., Jallepalli, P. V., and Daub, H. (2012). Combination of chemical genetics and phosphoproteomics for kinase signaling analysis enables confident identification of cellular downstream targets. *Mol. Cell. Proteomics* 11, 012351. doi:10.1074/mcp.O111.012351
- Oprea, T. I., Bologa, C. G., Brunak, S., Campbell, A., Gan, G. N., Gaulton, A., et al. (2018). Unexplored therapeutic opportunities in the human genome. *Nat. Rev. Drug Discov.* 17, 317–332. doi:10.1038/nrd.2018.14
- Pan, C., Olsen, J. V., Daub, H., and Mann, M. (2009). Global effects of kinase inhibitors on signaling networks revealed by quantitative phosphoproteomics. *Mol. Cell. Proteomics* MCP 8, 2796–2808. doi:10.1074/MCP.M900285-MCP200
- Patricelli, M. P., Nomanbhoy, T. K., Wu, J., Brown, H., Zhou, D., Zhang, J., et al. (2011). *In situ* kinase profiling reveals functionally relevant properties of native kinases. *Chem. Biol.* 18, 699–710. doi:10.1016/j.CHEMBIOL.2011.04.011
- Patricelli, M. P., Szardenings, A. K., Liyanage, M., Nomanbhoy, T. K., Wu, M., Weissig, H., et al. (2007). Functional interrogation of the kinome using nucleotide acyl phosphates. *Biochemistry* 46, 350–358. doi:10.1021/bi062142x
- Payne, L. S., and Huang, P. H. (2017). “Targeted analysis of phosphotyrosine signaling by multiple reaction monitoring mass spectrometry,” in *Kinase signaling networks, methods in molecular biology*. Editors A.-C. Tan and P. H. Huang (New York, NY: Springer), 263–281. doi:10.1007/978-1-4939-7154-1_17
- Pediconi, F., Casado, P., Hijazi, M., Gribben, J. G., Rouault-Pierre, K., and Cutillas, P. R. (2022). Targeting the lysine-specific demethylase 1 rewire kinase networks and primes leukemia cells for kinase inhibitor treatment. *Sci. Signal.* 15, eabl7989. doi:10.1126/scisignal.abl7989
- Pemovska, T., Kontro, M., Yadav, B., Edgren, H., Eldfors, S., Szajda, A., et al. (2013). Individualized systems monitoring strategy to tailor treatments for patients with chemorefractory acute myeloid leukemia. *Cancer Discov.* 3, 1416–1429. doi:10.1158/2159-8290.CD-13-0350
- Pierobon, M., Wulfkühle, J., Liotta, L., and Petricoin, E. (2015). Application of molecular technologies for phosphoproteomic analysis of clinical samples. *Oncogene* 34, 805–814. doi:10.1038/ncr.2014.16
- Ptacek, J., Devgan, G., Michaud, G., Zhu, H., Zhu, X., Fasolo, J., et al. (2005). Global analysis of protein phosphorylation in yeast. *Nature* 438, 679–684. doi:10.1038/nature04187
- Rata, S., Gruver, J. S., Trikoz, N., Lukyanov, A., Vultaggio, J., Ceribelli, M., et al. (2020). An optimal set of inhibitors for reverse engineering via kinase regularization. *bioRxiv*. Available at: <https://doi.org/10.1101/2020.09.26.312348>.
- Reimand, J., Wagih, O., and Bader, G. D. (2013). The mutational landscape of phosphorylation signaling in cancer. *Sci. Rep.* 3, 2651. doi:10.1038/srep02651
- Reinecke, M., Heinzlmeier, S., Wilhelm, M., Médard, G., Klaeger, S., and Kuster, B. (2019). “Kinobeads: a chemical proteomic approach for kinase inhibitor selectivity profiling and target discovery,” in *Target discovery and validation* (New York, United States: John Wiley & Sons, Ltd), 97–130. doi:10.1002/9783527818242.ch4
- Robers, M. B., Dart, M. L., Woodroffe, C. C., Zimprich, C. A., Kirkland, T. A., Machleidt, T., et al. (2015). Target engagement and drug residence time can be observed in living cells with BRET. *Nat. Commun.* 6, 10091. doi:10.1038/ncomms10091
- Rocca, A., and Kholodenko, B. N. (2021). Can systems biology advance clinical precision oncology? *Cancers* 13, 6312. doi:10.3390/cancers13246312
- Rubin, C. S., and Rosen, O. M. (1975). Protein phosphorylation. *Annu. Rev. Biochem.* 44, 831–887. doi:10.1146/annurev.bi.44.070175.004151
- Rudolph, J. D., de Grauw, M., van de Water, B., Geiger, T., and Sharan, R. (2016). Elucidation of signaling pathways from large-scale phosphoproteomic data using protein interaction networks. *Cell Syst.* 3, 585–593. doi:10.1016/j.cels.2016.11.005
- Ryall, K. A., Shin, J., Yoo, M., Hinz, T. K., Kim, J., Kang, J., et al. (2015). Identifying kinase dependency in cancer cells by integrating high-throughput drug screening and kinase inhibition data. *Bioinformatics* 31, 3799–3806. doi:10.1093/bioinformatics/btv427
- Sapkota, G. P., Kieloch, A., Lizzano, J. M., Lain, S., Arthur, J. S. C., Williams, M. R., et al. (2001). Phosphorylation of the protein kinase mutated in Peutz-Jeghers cancer syndrome, LKB1/STK11, at Ser431 by p90(RSK) is essential for LKB1 to suppress cell growth. *J. Biol. Chem.* 276, 19469–19482. doi:10.1074/jbc.M009953200
- Savitski, M. M., Reinhard, F. B. M., Franken, H., Werner, T., Savitski, M. F., Eberhard, D., et al. (2014). Tracking cancer drugs in living cells by thermal profiling of the proteome. *Science* 346, 1255784. doi:10.1126/science.1255784
- Schäfer, A., Gjerga, E., Welford, R. W., Renz, I., Lehembre, F., Groenen, P. M., et al. (2019). Elucidating essential kinases of endothelin signalling by logic modelling of phosphoproteomics data. *Mol. Syst. Biol.* 15, e8828. doi:10.15252/msb.20198828
- Shah, K., Liu, Y., Deirmengian, C., and Shokat, K. M. (1997). Engineering unnatural nucleotide specificity for Rous sarcoma virus tyrosine kinase to uniquely label its direct substrates. *Proc. Natl. Acad. Sci. U. S. A.* 94, 3565–3570. doi:10.1073/pnas.94.8.3565
- Sharma, K., Weber, C., Bairlein, M., Greff, Z., Kéri, G., Cox, J., et al. (2009). Proteomics strategy for quantitative protein interaction profiling in cell extracts. *Nat. Methods* 6, 741–744. doi:10.1038/nmeth.1373
- Sharma, S. V., Lee, D. Y., Li, B., Quinlan, M. P., Takahashi, F., Maheswaran, S., et al. (2010). A chromatin-mediated reversible drug-tolerant state in cancer cell subpopulations. *Cell* 141, 69–80. doi:10.1016/j.cell.2010.02.027
- Shi, H., Hugo, W., Kong, X., Hong, A., Koya, R. C., Moriceau, G., et al. (2014). Acquired resistance and clonal evolution in melanoma during BRAF inhibitor therapy. *Cancer Discov.* 4, 80–93. doi:10.1158/2159-8290.CD-13-0642
- Shogren-Knaak, M. A., Alaimo, P. J., and Shokat, K. M. (2001). Recent advances in chemical approaches to the study of biological systems. *Annu. Rev. Cell Dev. Biol.* 17, 405–433. doi:10.1146/annurev.cellbio.17.1.405
- Sommese, R. F., and Sivaramakrishnan, S. (2016). Substrate affinity differentially influences protein kinase C regulation and inhibitor potency. *J. Biol. Chem.* 291, 21963–21970. doi:10.1074/jbc.M116.737601
- Song, C., Ye, M., Liu, Z., Cheng, H., Jiang, X., Han, G., et al. (2012). Systematic analysis of protein phosphorylation networks from phosphoproteomic data. *Mol. Cell. Proteomics* 11, 1070–1083. doi:10.1074/mcp.M111.012625
- Songyang, Z., Blechner, S., Hoagland, N., Hoekstra, M. F., Piwnicka-Worms, H., and Cantley, L. C. (1994). Use of an oriented peptide library to determine the optimal substrates of protein kinases. *Curr. Biol.* 4, 973–982. doi:10.1016/S0960-9822(00)00221-9
- Statsuk, A. V., Maly, D. J., Seeliger, M. A., Fabian, M. A., Biggs, W. H., Lockhart, D. J., et al. (2008). Tuning a three-component reaction for trapping kinase substrate complexes. *J. Am. Chem. Soc.* 130, 17568–17574. doi:10.1021/ja807066f
- Stuart, S. A., Houel, S., Lee, T., Wang, N., Old, W. M., and Ahn, N. G. (2015). A phosphoproteomic comparison of B-RAFV600E and MKK1/2 inhibitors in melanoma cells. *Mol. Cell. Proteomics* 14, 1599–1615. doi:10.1074/mcp.M114.047233
- Subramanian, A., Narayan, R., Corsello, S. M., Peck, D. D., Natoli, T. E., Lu, X., et al. (2017). A next generation connectivity map: L1000 platform and the first 1,000,000 profiles. *Cell* 171, 1437–1452. doi:10.1016/j.cell.2017.10.049
- Sundberg, T. B., Choi, H. G., Song, J. H., Russell, C. N., Hussain, M. M., Graham, D. B., et al. (2014). Small-molecule screening identifies inhibition of salt-inducible kinases as a therapeutic strategy to enhance immunoregulatory functions of dendritic cells. *Proc. Natl. Acad. Sci. U. S. A.* 111, 12468–12473. doi:10.1073/pnas.1412308111
- Sutherland, J. J., Gao, C., Cahya, S., and Vieth, M. (2013). What general conclusions can we draw from kinase profiling data sets? *Biochim. Biophys. Acta* 1834, 1425–1433. doi:10.1016/j.bbapap.2012.12.023
- Tahiri, A., Roe, K., Ree, A. H., Wijn, R., Risberg, K., Busch, C., et al. (2013). Differential inhibition of ex-vivo tumor kinase activity by vemurafenib in BRAF(V600E) and BRAF wild-type metastatic malignant melanoma. *PLoS ONE* 8, e72692. doi:10.1371/journal.pone.0072692
- Tang, J. (2017). “Informatics approaches for predicting, understanding, and testing cancer drug combinations,” in *Kinase signaling networks, methods in molecular biology*. Editors A.-C. Tan and P. H. Huang (New York, NY: Springer), 485–506. doi:10.1007/978-1-4939-7154-1_30
- Tang, J., Szajda, A., Shakyawar, S., Xu, T., Hintsanen, P., Wennerberg, K., et al. (2014). Making sense of large-scale kinase inhibitor bioactivity data sets: a comparative and integrative analysis. *J. Chem. Inf. Model.* 54, 735–743. doi:10.1021/Ci400709D
- Terfve, C. D. A., Wilkes, E. H., Casado, P., Cutillas, P. R., and Saez-Rodriguez, J. (2015). Large-scale models of signal propagation in human cells derived from discovery phosphoproteomic data. *Nat. Commun.* 6, 8033. doi:10.1038/ncomms8033
- Tyner, J. W., Yang, W. F., Bankhead, A., Fan, G., Fletcher, L. B., Bryant, J., et al. (2013). Kinase pathway dependence in primary human leukemias determined by rapid inhibitor screening. *Cancer Res.* 73, 285–296. doi:10.1158/0008-5472.CAN-12-1906
- Vaga, S., Bernardo-Faura, M., Cokelaer, T., Maiolica, A., Barnes, C. A., Gillet, L. C., et al. (2014). Phosphoproteomic analyses reveal novel cross-modulation mechanisms between two signaling pathways in yeast. *Mol. Syst. Biol.* 10, 767. doi:10.15252/msb.20145112
- Vamathevan, J., Clark, D., Czodrowski, P., Dunham, I., Ferran, E., Lee, G., et al. (2019). Applications of machine learning in drug discovery and development. *Nat. Rev. Drug Discov.* 18, 463–477. doi:10.1038/s41573-019-0024-5

- Vasta, J. D., Corona, C. R., Wilkinson, J., Zimprich, C. A., Hartnett, J. R., Ingold, M. R., et al. (2018). Quantitative, wide-spectrum kinase profiling in live cells for assessing the effect of cellular ATP on target engagement. *Cell Chem. Biol.* 25, 206–214. doi:10.1016/j.chembiol.2017.10.010
- Wang, F., Ulyanova, N. P., Waal, M. S. V. D., Patnaik, D., Lens, S. M. A., and Higgins, J. M. G. (2011). A positive feedback loop involving haspin and aurora B promotes CPC accumulation at centromeres in mitosis. *Curr. Biol.* 21, 1061–1069. doi:10.1016/j.cub.2011.05.016
- Wang, Y., and Ma, H. (2015). Protein kinase profiling assays: a technology review. *Drug Discov. Today Technol., SI Profiling used Lead Optim.* Drug Discov. 18, 1–8. doi:10.1016/j.ddtec.2015.10.007
- Watson, N. A., Cartwright, T. N., Lawless, C., Cámara-Donoso, M., Sen, O., Sako, K., et al. (2020). Kinase inhibition profiles as a tool to identify kinases for specific phosphorylation sites. *Nat. Commun.* 11, 1684. doi:10.1038/s41467-020-15428-0
- Weidner, C., Fischer, C., and Sauer, S. (2014). PHOXTRACK—a tool for interpreting comprehensive datasets of post-translational modifications of proteins. *Bioinformatics* 30, 3410–3411. doi:10.1093/bioinformatics/btu572
- Weinstein, J. N., Myers, T. G., O'Connor, P. M., Friend, S. H., Fornace, A. J., Kohn, K. W., et al. (1997). An information-intensive approach to the molecular pharmacology of cancer. *Science* 275, 343–349. doi:10.1126/science.275.5298.343
- Weiss, W. A., Taylor, S. S., and Shokat, K. M. (2007). Recognizing and exploiting differences between RNAi and small-molecule inhibitors. *Nat. Chem. Biol.* 3, 739–744. doi:10.1038/nchembio1207-739
- Wells, C. I., Al-Ali, H., Andrews, D. M., Asquith, C. R. M., Axtman, A. D., Dikic, I., et al. (2021). The kinase chemogenomic set (KCGS): an open science resource for kinase vulnerability identification. *Int. J. Mol. Sci.* 22, 566. doi:10.3390/ijms22020566
- Wells, C. I., Vasta, J. D., Corona, C. R., Wilkinson, J., Zimprich, C. A., Ingold, M. R., et al. (2020). Quantifying CDK inhibitor selectivity in live cells. *Nat. Commun.* 11, 2743. doi:10.1038/s41467-020-16559-0
- Wilhelm, S., Carter, C., Lynch, M., Lowinger, T., Dumas, J., Smith, R. A., et al. (2006). Discovery and development of sorafenib: a multikinase inhibitor for treating cancer. *Nat. Rev. Drug Discov.* 5, 835–844. doi:10.1038/nrd2130
- Wilhelm, S. M., Carter, C., Tang, L., Wilkie, D., McNabola, A., Rong, H., et al. (2004). BAY 43-9006 exhibits broad spectrum oral antitumor activity and targets the RAF/MEK/ERK pathway and receptor tyrosine kinases involved in tumor progression and angiogenesis. *Cancer Res.* 64, 7099–7109. doi:10.1158/0008-5472.CAN-04-1443
- Wilkes, E. H., Terfve, C., Gribben, J. G., Saez-Rodriguez, J., and Cutillas, P. R. (2015). Empirical inference of circuitry and plasticity in a kinase signaling network. *Proc. Natl. Acad. Sci. U. S. A.* 112, 7719–7724. doi:10.1073/pnas.1423344112
- Wilson, L. J., Linley, A., Hammond, D. E., Hood, F. E., Coulson, J. M., MacEwan, D. J., et al. (2018). New perspectives, opportunities, and challenges in exploring the human protein kinome. *Cancer Res.* 78, 15–29. doi:10.1158/0008-5472.CAN-17-2291
- Wiredja, D. D., Koyutürk, M., and Chance, M. R. (2017). The KSEA App: a web-based tool for kinase activity inference from quantitative phosphoproteomics. *Bioinform. Oxf. Engl.* 33, 3489–3491. doi:10.1093/bioinformatics/btx415
- Xue, L., Wang, W. H., Iliuk, A., Hu, L., Galan, J. A., Yu, S., et al. (2012). Sensitive kinase assay linked with phosphoproteomics for identifying direct kinase substrates. *Proc. Natl. Acad. Sci. U. S. A.* 109, 5615–5620. doi:10.1073/pnas.1119418109
- Yadav, L., Tamene, F., Göös, H., van Drogen, A., Katainen, R., Aebersold, R., et al. (2017). Systematic analysis of human protein phosphatase interactions and dynamics. *Cell Syst.* 4, 430–444. doi:10.1016/j.cels.2017.02.011
- Yaffe, M. B. (2013). The scientific drunk and the lamppost: massive sequencing efforts in cancer discovery and treatment. *Sci. Signal.* 6, pe13. doi:10.1126/scisignal.2003684
- Yaffe, M. B., Lepar, G. G., Lai, J., Obata, T., Volinia, S., and Cantley, L. C. (2001). A motif-based profile scanning approach for genome-wide prediction of signaling pathways. *Nat. Biotechnol.* 19, 348–353. doi:10.1038/86737
- Yang, P., Zheng, X., Jayaswal, V., Hu, G., and Jothi, R. (2015). Knowledge-based analysis for detecting key signaling events from time-series phosphoproteomics data. *PLOS Comput. Biol.* 11, e1004403. doi:10.1371/journal.pcbi.1004403
- Yang, W., Soares, J., Greninger, P., Edelman, E. J., Lightfoot, H., Forbes, S., et al. (2013). Genomics of Drug Sensitivity in Cancer (GDSC): a resource for therapeutic biomarker discovery in cancer cells. *Nucleic Acids Res.* 41, D955–D961. doi:10.1093/nar/gks1111
- Yang, X., Smith, J. L., Beck, M. T., Wilkinson, J. M., Michaud, A., Vasta, J. D., et al. (2023). Development of cell permeable NanoBRET probes for the measurement of PLK1 target engagement in live cells. *Molecules* 28, 2950. doi:10.3390/molecules28072950
- Yilmaz, S., Ayati, M., Schlatter, D., Çiçek, A. E., Chance, M. R., and Koyutürk, M. (2021). Robust inference of kinase activity using functional networks. *Nat. Commun.* 12, 1177. doi:10.1038/s41467-021-21211-6
- Zecca, J., Bayer, F. P., Wiechmann, S., Woortman, J., Berner, N., Müller, J., et al. (2023). Decrypting drug actions and protein modifications by dose- and time-resolved proteomics. *Science* 380, 93–101. doi:10.1126/science.ade3925
- Zhao, Q., Ouyang, X., Wan, X., Gajiwala, K. S., Kath, J. C., Jones, L. H., et al. (2017). Broad-spectrum kinase profiling in live cells with lysine-targeted sulfonyl fluoride probes. *J. Am. Chem. Soc.* 139, 680–685. doi:10.1021/jacs.6b08536



OPEN ACCESS

EDITED BY

Raghuveera Kumar Goel,
Boston University, United States

REVIEWED BY

Chita Ranjan Sahoo,
Siksha O Anusandhan University, India
Ashish Shrivastava,
Indian Council of Medical Research (ICMR),
India

*CORRESPONDENCE

Adel Alblihy,
✉ Bliehia@kfsc.edu.sa

RECEIVED 27 November 2023

ACCEPTED 25 March 2024

PUBLISHED 11 April 2024

CITATION

Alblihy A (2024), From desert flora to cancer therapy: systematic exploration of multi-pathway mechanisms using network pharmacology and molecular modeling approaches.
Front. Pharmacol. 15:1345415.
doi: 10.3389/fphar.2024.1345415

COPYRIGHT

© 2024 Alblihy. This is an open-access article distributed under the terms of the [Creative Commons Attribution License \(CC BY\)](#). The use, distribution or reproduction in other forums is permitted, provided the original author(s) and the copyright owner(s) are credited and that the original publication in this journal is cited, in accordance with accepted academic practice. No use, distribution or reproduction is permitted which does not comply with these terms.

From desert flora to cancer therapy: systematic exploration of multi-pathway mechanisms using network pharmacology and molecular modeling approaches

Adel Alblihy^{1,2*}

¹Medical Center, King Fahad Security College (KFSC), Riyadh, Saudi Arabia, ²Department of Criminal Justice and Forensic Sciences, King Fahad Security Collage, Riyadh, Saudi Arabia

Ovarian cancer, often labeled a “silent killer,” remains one of the most compelling and challenging areas of cancer research. In 2019 alone, a staggering 222,240 new cases of ovarian cancer were reported, with nearly 14,170 lives tragically lost to this relentless disease. The absence of effective diagnostic methods, increased resistance to chemotherapy, and the heterogeneous nature of ovarian cancer collectively contribute to the unfavorable prognosis observed in the majority of cases. Thus, there is a pressing need to explore therapeutic interventions that offer superior efficacy and safety, thereby enhancing the survival prospects for ovarian cancer patients. Recognizing this potential, our research synergizes bioinformatics with a network pharmacology approach to investigate the underlying molecular interactions of Saudi Arabian flora (*Onopordum heteracanthum*, *Acacia ehrenbergiana*, *Osteospermum vaillantii*, *Cyperus rotundus*, *Carissa carandas*, *Carissa spinarum*, and *Camellia sinensis*) in ovarian cancer treatment. At first, phytoconstituents of indigenous flora and their associated gene targets, particularly those pertinent to ovarian cancer, were obtained from open-access databases. Later, the shared targets of plants and diseases were compared to identify common targets. A protein–protein interaction (PPI) network of predicted targets was then constructed for the identification of key genes having the highest degree of connectivity among networks. Following that, a compound–target protein–pathway network was constructed, which uncovered that, namely, hispidulin, stigmasterol, ascorbic acid, octopamine, cyperene, kaempferol, pungenin, citric acid, d-tartaric acid, beta-sitosterol, (–)-epicatechin gallate, and (+)-catechin demonstrably influence cell proliferation and growth by impacting the AKT1 and VEGFA proteins. Molecular docking, complemented by a 20-ns molecular dynamic (MD) simulation, was used, and the binding affinity of the compound was further validated. Molecular docking, complemented by a 20-ns MD simulation, confirmed the binding affinity of these compounds. Specifically, for AKT1, ascorbic acid showed a docking score of -11.1227 kcal/mol, interacting with residues Ser A:240, Leu A:239, Arg A:243, Arg C:2, and Glu A:341. For VEGFA, hispidulin exhibited a docking score of -17.3714 kcal/mol, interacting with Asn A:158, Val A:190, Gln B:160, Ser A:179, and Ser B:176. To sum up, both a theoretical and empirical framework were established by this

study, directing more comprehensive research and laying out a roadmap for the potential utilization of active compounds in the formulation of anti-cancer treatments.

KEYWORDS

Saudi Arabian flora, ovarian cancer, active constituents, multi-target drug discovery, molecular docking, MD simulation

1 Introduction

Ovarian cancer is a prevalent malignancy among females worldwide and is ranked eighth in terms of incidence (Kamilova and Valijonova, 2023). Ovarian cancer ranks as the seventh leading cause of cancer-linked mortalities, exerting a profound impact on socioeconomic and community health at a global level (Torre et al., 2017). Among gynecological malignancies, ovarian cancer exhibits the highest mortality rate in developed countries across the world (Raab et al., 2020). Additionally, ovarian cancer accounted for approximately 3% of all cancers occurring in women. Currently, the lifetime ovarian cancer risk is approximately 1 in 72 (Yang et al., 2017; Lisio et al., 2019). Studies have reported that the pathogenesis of ovarian cancer is affected by various endocrine factors such as pituitary gonadotropins, namely, luteinizing hormone and follicle-stimulating hormone, in addition to progesterone, androgens, insulin-like growth factor 1, and estrogens (Choi et al., 2007; Li et al., 2021). Moreover, the receptor expression of progesterone, estrogen, and androgen receptors has been proposed as a possible determinant for predicting the prognosis and chemosensitivity of ovarian cancer patients toward platinum agents (Li et al., 2021). Despite recent advancements in medical science, individuals affected by ovarian cancer continue to experience high morbidity rates, and currently available treatment options do not provide satisfactory outcomes. Consequently, higher death rates and the limited availability of effective treatment strategies have garnered significant attention from researchers worldwide. Given the grave statistics, with an estimated 314,000 new cases of ovarian cancer and 207,000 deaths annually worldwide, ovarian cancer stands as the most lethal gynecological malignancy (Sideris et al., 2024). Alarming, in Australia, the incidence of ovarian cancer cases and deaths is projected to increase by 42% and 55%, respectively, by the year 2040, underscoring an urgent need for effective therapeutic strategies. Therefore, researchers are increasingly concentrating on pharmacological interventions that incorporate natural agents. These agents present a promising avenue for ovarian cancer treatment, offering the potential to overcome limitations associated with current therapies, such as drug resistance and adverse side effects. Phytochemicals, with their diverse bioactive compounds, offer a rich repository for the identification of novel anticancer molecules with minimal side effects compared to conventional chemotherapy agents. The integration of bioinformatics tools further enhances this process by enabling the rapid and precise analysis of vast biochemical datasets, facilitating the identification of potential lead compounds (Sharma et al., 2022; Swain et al., 2023). These computational methods allow for the prediction of compound–target interactions, bioactivity, and the pharmacokinetic properties of phytochemicals, streamlining the drug development process. Notably, bioinformatics applications

in network pharmacology and molecular docking studies provide invaluable insights into the mechanistic pathways of cancer, helping pinpoint specific targets for therapeutic intervention (Noor et al., 2023). By leveraging the synergy between phytochemical potential and advanced bioinformatic techniques, researchers can significantly expedite the discovery and development of effective, targeted treatments for ovarian cancer, setting the stage for the establishment of novel lead molecules with optimized therapeutic profiles.

Although the Arabian Peninsula is known for its arid climate and limited biodiversity, the Kingdom of Saudi Arabia boasts a diverse range of flora, encompassing a variety of trees, herbs, and shrubs, including many edible and medicinal plants (Rahman et al., 2004). The extensive land area of Saudi Arabia comprises diverse geographical landscapes and climates, resulting in a wider range of plant distribution throughout the country (Aati et al., 2019). The indigenous uses and pharmacological activity of these plants in Saudi Arabia demonstrate the strong relationship between local remedies, diet, health, and traditional healing practices unique to their cultures. Previous studies provide shreds of evidence that indigenous plants in Saudi Arabia, including *Onopordum heteracanthum* (Gouda et al., 2014), *Acacia ehrenbergiana* (Makeen et al., 2020), *Osteospermum vaillantii* (Gouda et al., 2014), *Cyperus rotundus* (AlQathama et al., 2022), *Carissa carandas* (Alshehri, 2020), *Carissa spinarum* (AlQathama et al., 2022), and *Camellia sinensis* (Dou et al., 2021), have anti-cancer properties for ovarian cancer. Plants found in these regions have been used by local inhabitants for treating a wide range of ailments. However, the mechanism by which these plants exert their therapeutic effects remains poorly understood.

Recognizing the potential of active compounds, Hopkins (2007) introduced an innovative *in silico* approach known as “network pharmacology” that recognizes the potential of active compounds based on network perspectives. Network pharmacology has emerged as a valuable tool in the drug-designing process, aiding the resurgence of traditional knowledge (Noor et al., 2022a). This method serves as a standard for the preliminary identification of small molecules and the discovery of new treatment options, thereby enhancing our understanding of the disease pathophysiology (Batoool et al., 2022; Noor et al., 2023). As a result, network pharmacology had a profound impact on the revival of herbal medicines, leading to a major transformation in the process of pharmaceutical discovery. In summary, comprehending the intricate landscape of network pharmacology is crucial to successfully identifying candidate drugs (Noor et al., 2022b).

By merging network pharmacology with bioinformatics, an in-depth examination of the therapeutic effects of local Saudi plants on ovarian cancer was explored. This analysis was further validated using docking methodologies to predict binding affinities among

phytoconstituents and target proteins. Later, molecular dynamic (MD) simulations shed light on intricate conformational shifts and the potential interactions within molecular complexes. Notably, this research offered groundbreaking revelations about the therapeutic capacities of native flora in tackling ovarian cancer, serving as a beacon for subsequent explorations in the domain.

2 Materials and methods

2.1 Screening of the plant-derived compounds

Screening of plant-related small molecules is considered an initial step in understanding the multi-target effect of medicinal plants against diseases. In the current study, database and literature search were carried out for obtaining the main active constituents of plants. In the literature and databases, the search was confined to “*O. heteracanthum*,” “*A. ehrenbergiana*,” “*O. vaillantii*,” “*C. rotundus*,” “*C. carandas*,” “*C. spinarum*,” and “*C. sinensis*.” PubChem (<https://pubchem.ncbi.nlm.nih.gov/>) and Google Scholar were considered for the extensive literature survey, while the phytochemical databases, including KNApSACk (<http://www.knapsackfamily.com/KNApSACk/>) (Shinbo et al., 2006) and IMPPAT (<https://cb.imsc.res.in/imppat/home>) (Mohanraj et al., 2018), were searched for obtaining the active compounds of selected plants. After retrieval, the drug-like potential of active compounds was analyzed by predicting their oral bioavailability (OB) and drug-likeness (DL) values. In pharmacology, OB denotes the fraction of small molecules that successfully enter the systemic circulation after an oral dose, thereby enabling them to exert their desired pharmacological effects (Pathak and Raghuvanshi, 2015). A minimum OB of 30% is generally employed as a benchmark criterion for screening potential drug candidates since it indicates that a considerable portion of the oral usage of small molecules is capable of being absorbed and reaching systemic circulation. Conversely, small molecules with OB < 30% are likely to exhibit limited efficacy due to poor absorption. Thus, a higher OB value is positively correlated with drug effectiveness and is a key determinant of drug development and optimization. In a similar vein, DL analysis is employed to assess the potential of a molecule to serve as an oral drug by evaluating its bioavailability using qualitative measures (Jia et al., 2020). Following that, the DL and OB values of compounds were obtained using Molsoft (<https://molsoft.com/mprop/>) (James et al., 2015) and SwissADME software (<https://www.swissadme.ch/>) (Daina et al., 2017), and only those compounds having OB and DL values greater than 30% and 18% were considered the finalist compounds. Furthermore, the molecular weight and two-dimensional (2D) structure of predicted phytoconstituents were collected from PubChem (Kim et al., 2019) and Molinspiration (<https://molinspiration.com/>) (Molinspiration, 2011).

2.2 ADMET profiling

Although DL and OB are key elements in evaluating the drug-like potential of a compound, it is important to note that these parameters

do not serve as the sole determinants of a compound's effectiveness for further development. ADMET properties, which encompass absorption, distribution, metabolism, excretion, and toxicity, are equally important factors that must be evaluated to assess a compound's safety and efficacy (Rehman et al., 2022). The evaluation of ADMET properties is conducted during the initial phases of drug development, which substantially plays an essential role in predicting the potential safety, effectiveness, and pharmacokinetics of a drug. To this end, the SwissADME server (<https://www.swissadme.ch/>) (Daina et al., 2017) and the ProTox II tool (http://tox.charite.de/protox_II) (Banerjee et al., 2018) were used to assess the ADMET properties of small biologically active molecules. Small molecules demonstrating excellent absorption, favorable solubility properties, and low toxicity were selected for further analysis.

2.3 Prediction of known targets of active compounds

To determine the integrative efficacy of the compounds derived from local plants in Saudi Arabia, we used two different platforms, namely, STITCH (<http://stitch.embl.de/>) (Kuhn et al., 2007) and SwissTargetPrediction (Gfeller et al., 2014) databases, with a species limitation of “*Homo sapiens*.” Furthermore, the SMILES representation of the chosen ingredients was used as input for the SwissTargetPrediction (<https://www.swisstargetprediction.ch/>) platform. Specifically, only proteins with a probability > 0.7 were considered putative targets of Saudi plants. For the STITCH database, targets exhibiting a combined score >0.7 were considered the significant targets of particular compounds.

2.4 Identification of disease-related targets through microarray data analysis

Microarray data analysis is a technique used for the identification of genes that are differentially expressed among different conditions (Noor et al., 2021; Sufyan et al., 2021). This involves comparing the gene expression levels of samples from disease and control groups and calculating statistical measures to determine which genes are significantly differentially expressed. In this study, gene expression data were acquired from the NCBI-GEO database (<https://www.ncbi.nlm.nih.gov/>) (Barrett et al., 2005). The search term “Ovarian Cancer” was used to retrieve four microarray datasets, namely, GSE54388, GSE69428, GSE36668, and GSE40595. The selection of datasets was based on their inclusion of both affected and normal ovaries; the dataset must have >3 samples. After data selection, the gene expression data were processed through the limma package of R (Ritchie et al., 2015) for the screening of differentially expressed genes (DEGs) as disease-specific targets for ovarian cancer.

2.5 Construction of the compound–target network

Upon identifying putative targets associated with both ovarian cancer and local plants, a Venn diagram was created to determine

overlapping proteins. Subsequently, these identified genes were regarded as potential targets of indigenous Saudi Arabian plants, holding promise as potential biomarkers for intercepting the pathophysiological processes associated with ovarian cancer. Additionally, Cytoscape version 3.8 (<https://cytoscape.org/>) (Smoot et al., 2011) was used to construct an active ingredient–target network based on these overlapping genes. Within the compound–target network, the nodes indicated the small molecules along with their corresponding targets, while gray dotted lines depicted the possible interactions among these nodes. Finally, the NetworkAnalyzer plugin was used to evaluate the connectivity of targets exhibited by the chemical constituents among networks.

2.6 Gene Ontology and KEGG enrichment analyses

After identifying the common target, our study categorizes these targets based on their Gene Ontology (GO). GO covers three aspects of biology: cellular components (CCs), molecular functions (MFs), and biological processes (BPs). The BP term describes the protein's role in various biological activities, and the CC term signifies the precise intracellular localization of a protein. Concurrently, the MF records the specific molecular tasks and interactions in which the protein or gene is involved. To achieve this, the current study used the DAVID database (<https://david.ncicrf.gov/tools.jsp>) (Dennis et al., 2003) for GO and Kyoto Encyclopedia for Genes and Genomes (KEGG) pathway analyses. However, to filter-out those with significant relevance, a statistical cutoff of p -value < 0.05 was implemented.

2.7 Construction and analysis of the protein–protein interaction network

The common targets were then analyzed using the STRING database (<https://string-db.org/>) (von Mering et al., 2003) to produce a protein–protein interaction (PPI) network. PPIs exhibit high specificity, adaptability, and versatility and are, therefore, of considerable significance. PPI network common genes were then analyzed using Cytoscape version 3.8 (<https://cytoscape.org/>) (Smoot et al., 2011) to identify hub genes. Hub genes exhibit a high number of interactions with other proteins and are considered essential elements of the network as they contribute to its integrity and stability. Furthermore, central or 'hub' genes hold significance in a range of disease-linked pathways and biological processes, suggesting their pivotal role in diverse cellular functions. In the current study, we examined the topology of the PPI network to identify 'hub' genes. Metrics such as degree, closeness, and betweenness centrality can facilitate this process. Specifically, we employed the degree methods available in cytoHubba to discern these hub genes.

2.8 Compound–target–pathway network construction

The effects of Saudi Arabian flora on ovarian cancer were investigated by constructing compound–target and target

protein–pathway networks using Cytoscape version 3.8 (<https://cytoscape.org/>) (Smoot et al., 2011). By merging these networks, a final compound–target–pathway network was subsequently established. The networks comprise various nodes and edges, where nodes represent pathways, compounds, and targets relevant to the disease, while edges indicate the interactions among these nodes. The compound–target–pathway network offers valuable insights regarding the synergistic activity of phytoconstituents in ovarian cancer treatment.

2.9 Molecular docking analysis

Using advanced molecular docking methodologies, intricate interactions between small molecules and anticipated protein structures were analyzed. This rigorous analytical procedure illuminated potential pharmacological combinations, suggesting potential synergistic responses for precision therapeutics. Initially, the protein structures were obtained from the RCSB PDB database, which were then carefully prepared for docking. Missing atoms, residues, and side chains were addressed using the protein preparation tools within Chimera, ensuring a complete and accurate representation of the protein's conformation. Water molecules and non-essential ions were removed, and hydrogen atoms were added to the protein structures to reflect physiological pH conditions. After this refinement, the proteins were subjected to an energy minimization process using the steepest descent and conjugate gradient methods, terminating at an energy convergence threshold of 0.01 kcal/mol to attain stable conformations. Subsequent docking studies were conducted using AutoDock Vina 1.1.2 implemented within the PyRx 0.8 interface (<https://sourceforge.net/projects/pyrx/>) (Dallakyan and Olson, 2015). The SMILES strings for the phytoconstituents were sourced from the PubChem database and converted to 3D structures using Open Babel, which is integrated into the PyRx platform. A comprehensive energy minimization was configured for a total of 2000 steps to ensure the reliability of the ligand conformations prior to the docking simulations. Later, the active site residues of the target proteins were uncovered with the assistance of the CASTp tool (<http://sts.bioe.uic.edu/castp/index.html?2011>) (Dundas et al., 2006). PyRx 0.8 was employed for target docking, which facilitated the calculation of binding affinities between the small molecules and target proteins. In our study, docking scores were used as indicators of binding affinity between the identified phytochemicals and target proteins. A docking score of less than −5.00 kcal/mol was considered to indicate strong binding affinity, while a score of less than −7.00 kcal/mol was interpreted as signifying very strong binding affinity. These thresholds were based on established computational chemistry conventions and were used to prioritize compounds for further analysis. The docked complexes were then visualized employing Discovery Studio (<https://discover.3ds.com/discovery-studio-visualizer-download>) (Biovia, 2017), PyMOL (<https://pymol.org/2/>) (Seeliger and de Groot, 2010), and ChimeraX (<https://www.cgl.ucsf.edu/chimerax/>) (Pettersen et al., 2021) programs for a better understanding of the binding interactions.

TABLE 1 Pharmacological and molecular properties of phytochemicals.

Plant source	Phytochemical	Oral bioavailability> 0.30	Drug- likeness>0.18	Molecular weight (g/mol)	PubChem ID
<i>Onopordum heteracanthum</i>	Hispidulin	0.55	0.46	300.26	5281628
	Apigenin	0.55	0.39	270.24	5280443
	Luteolin	0.55	0.38	286.24	5280445
	Beta-sitosterol	0.55	0.78	414.7	222284
<i>Acacia ehrenbergiana</i>	Stigmasterol	0.55	0.62	412.7	5280794
	Ascorbic acid	0.56	0.74	176.12	54670067
<i>Osteospermum vaillantii</i>	Octopamine	0.55	0.54	153.18	4,581
	3,4-Dihydroxybenzoic acid	0.56	0.23	154.12	72
	Cyperene	0.55	0.18	204.35	12308843
	Rotundine A	0.55	0.37	231.33	10728239
	Rotundine B	0.55	0.75	233.35	21603505
<i>Cyperus rotundus</i>	Orientin	0.55	0.59	448.4	5281675
	Quercetin	0.55	0.52	302.23	5280343
	Kaempferol	0.55	0.5	286.24	5280863
	Pungenin	0.55	0.54	314.29	12314759
	Rotundine B	0.55	0.75	233.35	21603505
	Cyperene	0.55	0.18	204.35	12308843
<i>Carissa carandas</i>	Carissic acid	0.55	0.66	456.7	73242193
	Alpha1-sitosterol	0.55	0.47	426.7	9548595
	Citric acid	0.56	0.52	192.12	311
	d-Tartaric acid	0.56	0.59	150.09	439655
	Ascorbic acid	0.56	0.74	176.12	54670067
	Beta-ionone	0.55	0.33	192.3	638014
	Anethole	0.55	0.29	148.2	637563
	Ursolic acid	0.85	0.66	456.7	64945
	Beta-sitosterol	0.55	0.78	414.7	222284
<i>Carissa spinarum</i>	Carissic acid	0.85	0.66	456.7	73242193
	Kaempferol	0.55	0.5	286.24	5280863
	Quercetin	0.55	0.52	302.23	5280343
	Digitoxigenin	0.55	0.93	374.5	4369270
	Ursolic acid	0.85	0.66	456.7	64945
	Beta-sitosterol	0.55	0.78	414.7	222284
<i>Camellia sinensis</i>	(-)-Epicatechin gallate	0.55	0.93	442.4	107905
	(+)-Catechin	0.55	0.64	290.27	9,064
	Quercetin	0.55	0.52	302.23	5280343
	Kaempferol	0.55	0.5	286.24	5280863

2.10 Molecular dynamic (MD) simulation

All-atom molecular dynamics (MD) simulation is a computational approach that precisely represents each atom and bond within a system, facilitating an in-depth analysis of molecular dynamics (Sahoo et al., 2020). This method calculates the movements of every atom in a system, which are determined by the interactions amongst them, represented by interatomic potentials (Sahoo et al., 2022). In this research, to execute the MD simulations of the ultimate complexes, we implemented the OPLS-AA/L force field using GROMACS 2018 software. The three-dimensional configurations of the protein served as the initial structural inputs for the simulations. To enhance their quality and suitability for the simulations, additional optimization was performed using Dock Prep (Pettersen et al., 2004). The parameterization of the active ingredients was executed using the SwissParam webserver (Zoete et al., 2011). Subsequently, MD simulations were conducted for a duration of 20 nanoseconds (ns), following a methodology similar to previous studies (Alamri, 2020). Various general MD simulation parameters were assessed for each complex, including root mean square deviation (RMSD), radius of gyration (Rog), and root mean square fluctuation (RMSF) (Needle et al., 2015). These parameters provide important information about the stability, conformational changes, and flexibility of the complexes during the simulation period.

3 Results

3.1 Screening of active compounds

The screening of active compounds represents a critical initial step in the identification of promising phytoconstituents with potential therapeutic efficacy against ovarian cancer. After searching and filtering, four compounds, namely, hispidulin, apigenin, luteolin, and beta-sitosterol were obtained from *O. heteracanthum*; two compounds, namely, stigmasterol and ascorbic acid were obtained from *A. ehrenbergiana*; five compounds namely, octopamine, 3,4-dihydroxybenzoic acid, cyperene, rotundine A, and rotundine B were obtained from *O. vaillantii*; six compounds namely, orientin, quercetin, kaempferol, pungenin, rotundine B, and cyperene were obtained from *C. rotundus*; nine compounds namely, carissic acid, alpha1-sitosterol, citric acid, d-tartaric acid, ascorbic acid, beta-ionone, anethole, ursolic acid, and beta-sitosterol were obtained from *C. carandas*; six compounds, namely, carissic acid, kaempferol, quercetin, digitoxigenin, ursolic acid, and beta-sitosterol were obtained from *C. spinarum*; and four compounds, namely, (-)-epicatechin gallate, (+)-catechin, quercetin, and kaempferol were obtained from *C. sinensis*. These 36 compounds were considered potential phytoconstituents of local Saudi plants as they fulfill the criteria of molecular weight <500 g/mol, DL \geq 0.18, and OB \geq 0.30 (Table 1).

3.2 ADMET profiling

The chosen compounds were subjected to ADME analysis, and 12 compounds, namely, hispidulin, stigmasterol, ascorbic acid,

octopamine, cyperene, kaempferol, pungenin, citric acid, d-tartaric acid, beta-sitosterol, (-)-epicatechin gallate, and (+)-catechin, were identified as the main active constituents, with local good GI absorption and limited permeability of BBB, as presented in Table 2. Within the scope of ADMET analysis, hepatotoxicity refers to the capacity of compounds to inflict harm on the liver, potentially resulting in liver malfunction or complete failure. Notably, all selected compounds were found to have inactive hepatotoxicity in the current study. On the other hand, carcinogenicity characterizes the potential to induce cancer, while mutagenicity denotes its capacity to provoke DNA alterations that could lead to developmental anomalies, mutations in cancer, or many others. Compared to our results, the final active ingredients demonstrated themselves to be non-mutagenic and non-carcinogenic. In sum, these outcomes further support that the native plants of Saudi Arabia have drug-like potential that could be integral to preventing and treating diseases.

3.3 Known therapeutic targets acting on ovarian cancer

Analysis of microarray data offers crucial insights into the molecular processes associated with disease progression and assists in the identification of possible targets for therapeutic intervention. Four gene expression datasets, namely, GSE54388, GSE69428, GSE36668, and GSE40595, were obtained from the NCBI-GEO database. Subsequent processing for the detection of DEGs was carried out using the limma package (Table 3, Supplementary Material S4: Supplementary Tables S1–S3). Within the limma package, the LogFC >1.0 and p -value <0.05 criteria were set for the screening of DEGs. From the GSE54388 dataset, a total of 4,687 DEGs were obtained (2,457 upregulated and 2,230 downregulated), 2,084 DEGs (1,020 upregulated and 1,064 downregulated) from GSE69428, 6,924 DEGs (3,147 downregulated and 3,777 upregulated) from GSE36668, and 2,840 DEGs (1,423 upregulated and 1,417 downregulated) from the GSE40595 dataset (Figure 1, Supplementary Material S5). The identified DEGs were subsequently used as therapeutic targets for ovarian cancer.

3.4 Construction of the compound–target network

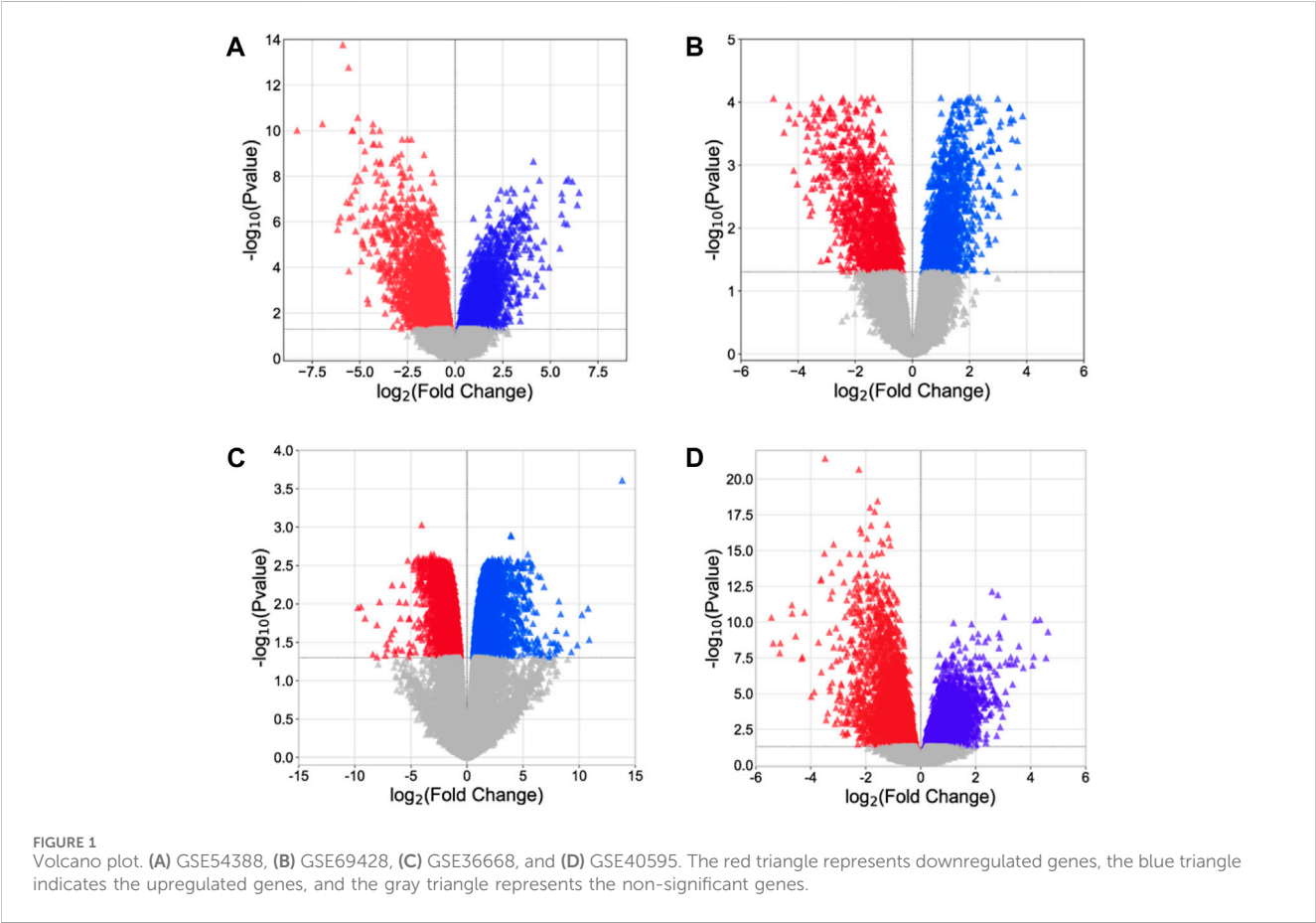
Following the prediction of disease-associated targets, a Venn tool was employed to uncover shared genes between plant-associated targets and disease-related targets. SwissTargetPrediction and STITCH databases yielded 469 potential targets of active compounds (Supplementary Material S1: Supplementary Table S1). Finally, 200 targets were found to be common among both plants and diseases (Supplementary Material S2: Supplementary Table S1). Compounds targeting these 200 genes were then imported into Cytoscape. This network suggests that these 200 identified targets could potentially work in synergy when these indigenous Saudi plants are used as an anticancer remedy.

TABLE 2 ADMET profiling of active compounds.

Plant source	Active compound	GI absorption	BBB permeant	P-gp substrate	CYP1A2 inhibitor	CYP2C19 inhibitor	CYP2C9 inhibitor	CYP2D6 inhibitor	CYP3A4 inhibitor	Log K_p (skin permeation)	Hepatotoxicity	Carcinogenicity	Mutagenicity	Cytotoxicity
<i>Onopordum heteracanthum</i>	Hispidulin	High	✗	✗	✓	✗	✗	✓	✓	-6.01 cm/s	✗	✗	✗	✗
	Beta-sitosterol	Low	✗	✗	✗	✗	✗	✗	✗	-2.20 cm/s	✗	✗	✗	✗
<i>Acacia ehrenbergiana</i>	Stigmasterol	Low	✗	✗	✗	✗	✓	✗	✗	-2.74 cm/s	✗	✗	✗	✗
	Ascorbic acid	High	✗	✗	✗	✗	✗	✗	✗	-8.54 cm/s	✗	✗	✗	✗
<i>Osteospermum vaillantii</i>	Octopamine	High	✗	✗	✗	✗	✗	✗	✗	-7.87 cm/s	✗	✗	✗	✗
	Cyperene	Low	✗	✗	✗	✓	✓	✗	✗	-4.48 cm/s	✗	✗	✗	✗
<i>Cyperus rotundus</i>	Kaempferol	High	✗	✗	✓	✗	✗	✗	✗	-6.70 cm/s	✗	✗	✗	✗
	Pungenin	Low	✗	✗	✗	✗	✗	✗	✗	-9.40 cm/s	✗	✗	✗	✗
	Cyperene	Low	✗	✗	✗	✓	✓	✗	✗	-4.48 cm/s	✗	✗	✗	✗
<i>Carissa carandas</i>	Citric acid	Low	✗	✗	✗	✗	✗	✗	✗	-8.69 cm/s	✗	✗	✗	✗
	d-Tartaric acid	Low	✗	✗	✗	✗	✗	✗	✗	-8.55 cm/s	✗	✗	✗	✗
	Ascorbic acid	High	✗	✗	✗	✗	✗	✗	✗	-8.54 cm/s	✗	✗	✗	✗
	Beta-sitosterol	Low	✗	✗	✗	✗	✗	✗	✗	-2.20 cm/s	✗	✗	✗	✗
<i>Carissa spinarum</i>	Kaempferol	High	✗	✗	✓	✗	✗	✗	✗	-6.70 cm/s	✗	✗	✗	✗
	Beta-sitosterol	Low	✗	✗	✗	✗	✗	✗	✗	-2.20 cm/s	✗	✗	✗	✗
<i>Camellia sinensis</i>	(-)-Epicatechin gallate	Low	✗	✗	✗	✗	✗	✗	✗	-7.91 cm/s	✗	✗	✗	✗
	(+)-Catechin	High	✗	✓	✗	✗	✗	✗	✗	-7.82 cm/s	✗	✗	✗	✗
	Kaempferol	High	✗	✗	✓	✗	✗	✗	✗	-6.70 cm/s	✗	✗	✗	✗

TABLE 3 Brief summary of GEO datasets used in the current study along with obtained DEGs.

GEO dataset	Total sample	Affected	Control	Upregulated gene	Downregulated gene	Total DEG
GSE54388	22	16	6	2,457	2,230	4,687
GSE69428	20	10	10	1,020	1,064	2084
GSE36668	8	4	4	3,147	3,777	6,924
GSE40595	77	63	14	1,423	1,417	2,840



3.5 GO and KEGG enrichment analyses

Analyses for GO and pathway enrichment of common 200 target genes were carried out employing the DAVID tool to discern their biological characteristics (Supplementary Material S3: Supplementary Tables S1–S4). A total of 388 BP, 57 CC, and 109 MF terms met the *p*-value criterion of <0.05. Analysis of the top GO terms suggested that the shared genes were primarily associated with the positive regulation of the MAPK, ERK1, and ERK2 cascade, positive regulation of vasoconstriction, intracellular signal transduction, regulation of cell proliferation, positive regulation of the apoptotic process, Hsp90 protein binding, estradiol 17-beta-dehydrogenase activity, estrogen response element binding, steroid binding, and steroid hormone receptor activity (Figure 2). A total of 103 KEGG pathways were identified, indicating that the intersecting targets were predominantly involved in the mechanisms

of growth hormone action, secretion, and synthesis, pathways in cancer, the estrogen signaling pathway, pI3K-Akt and ErbB signaling pathways, progesterone-mediated oocyte maturation, endometrial cancer, and many others (Figure 3).

3.6 Identification of hub genes

Constructing a PPI network is a fundamental step in network pharmacology, offering a structure to comprehend the intricate interactions between biological molecules and their impacts on disease pathways. Interactions among 200 common genes were predicted using the STRING database. This network comprised a total of 196 genes, forming 1,426 interactions with each other. One protein was found to interact with many proteins; therefore, the top 10 proteins with greater connectivity than other nodes were selected

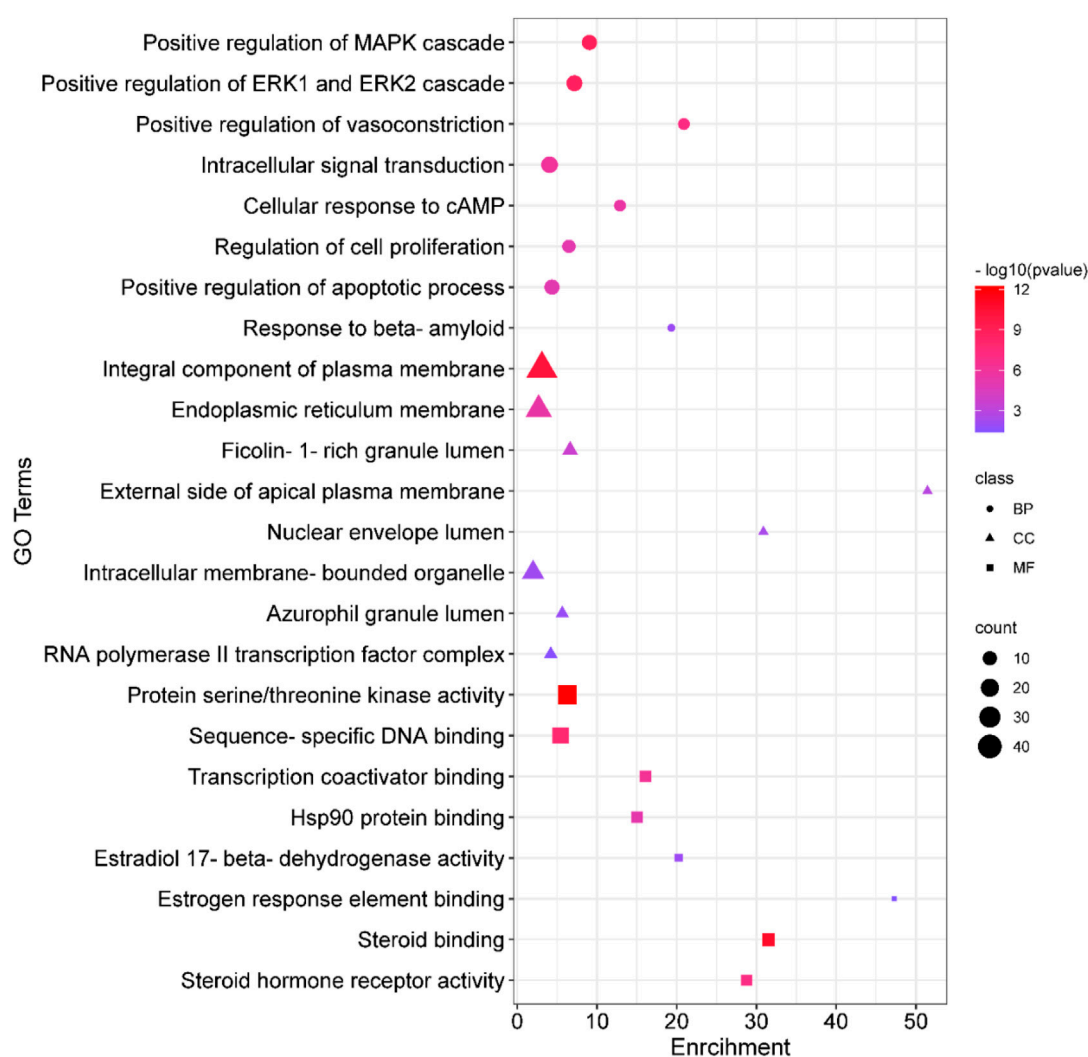


FIGURE 2
Gene Ontology (GO) enrichment analysis. In the plot, squares denote molecular functions, triangles depict cellular components, and circles signify biological processes. The size of each shape reflects the count, while the color indicates the p -value.

as hub genes. These genes are AKT1 (91), VEGFA (73), HSP90AA1 (63), JUN (63), HIF1A (60), PTGS2 (530), MAPK1 (53), PPARA (38), PIK3R1 (36), and AR (36) (Figure 4, Supplementary Material S6: Supplementary Table S1).

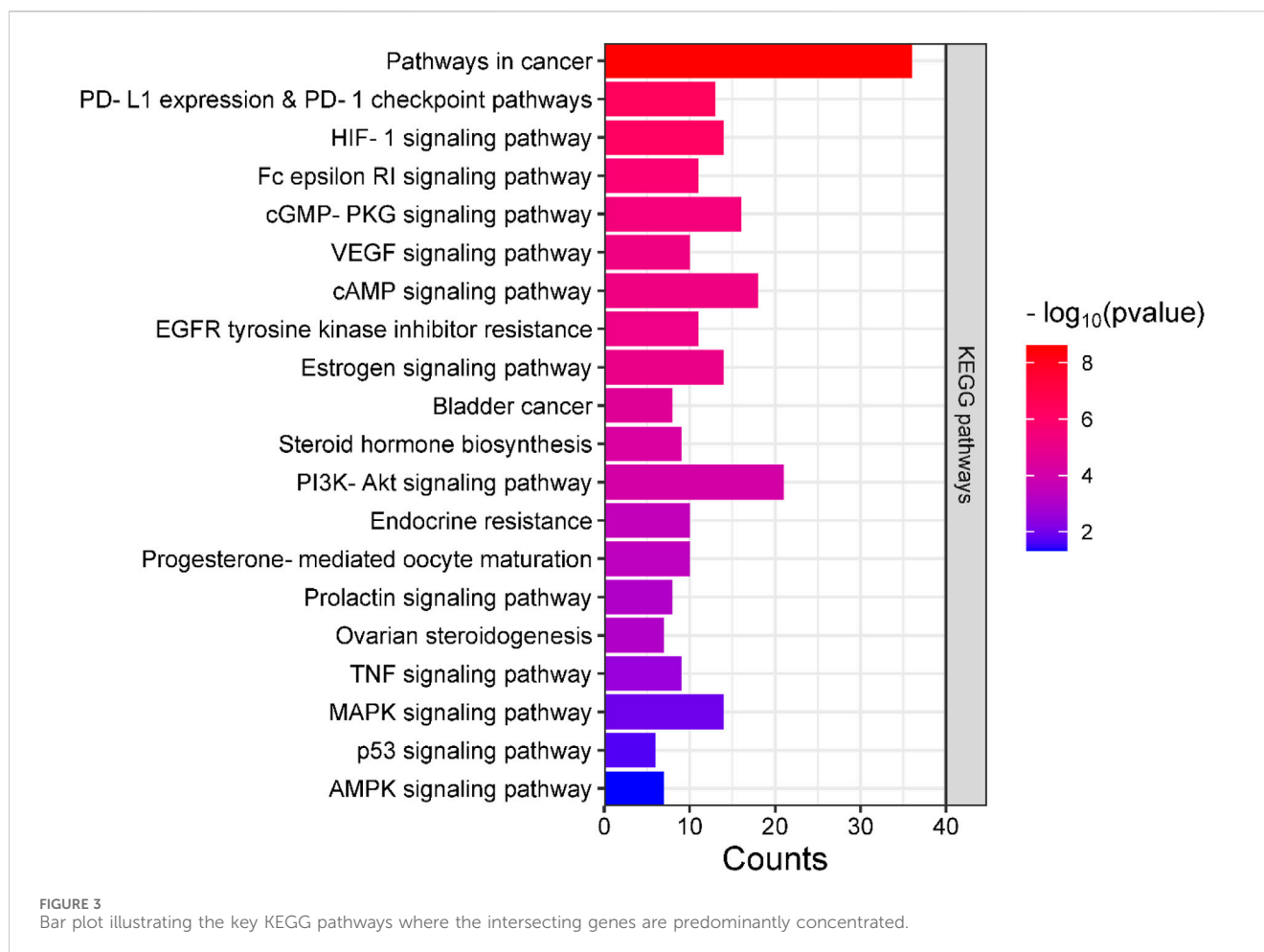
3.7 Compound–target protein–pathway network construction

For gaining a deep understanding of the underlying action mechanisms of indigenous plants in ovarian cancer, an integrated “active ingredient–target–pathway” network was constructed using the GO and KEGG pathway databases, and non-ovarian cancer-associated pathways were excluded from the analysis (Figure 5). Subsequently, a comprehensive analysis of the PPI network and active ingredient–target–pathway network was performed at the systematic level to identify top-ranked proteins, including AKT1 and VEGFA, which were further subjected to molecular docking analysis. AKT1 and VEGFA

were selected as most of the compounds targeted these genes, and these genes are mainly linked to ovarian cancer-related pathways, including the estrogen signaling pathway, progesterone-mediated oocyte maturation, the prolactin signaling pathway, Rap1 and ErbB signaling pathways, colorectal cancer, growth hormone action, secretion, and synthesis, and endometrial cancer.

3.8 Molecular docking analysis

After network analysis, two proteins, AKT1 and VEGFA, were chosen for docking analysis, as these proteins were found to be targeted by multiple compounds and also linked to disease-relevant pathways. All selected compounds were docked against AKT1 and VEGFA, allowing for the assessment of their binding affinity, interaction stability, and free energy within the target protein's active site. These proteins were docked with selected compounds; however, the top five compounds based on their binding affinity



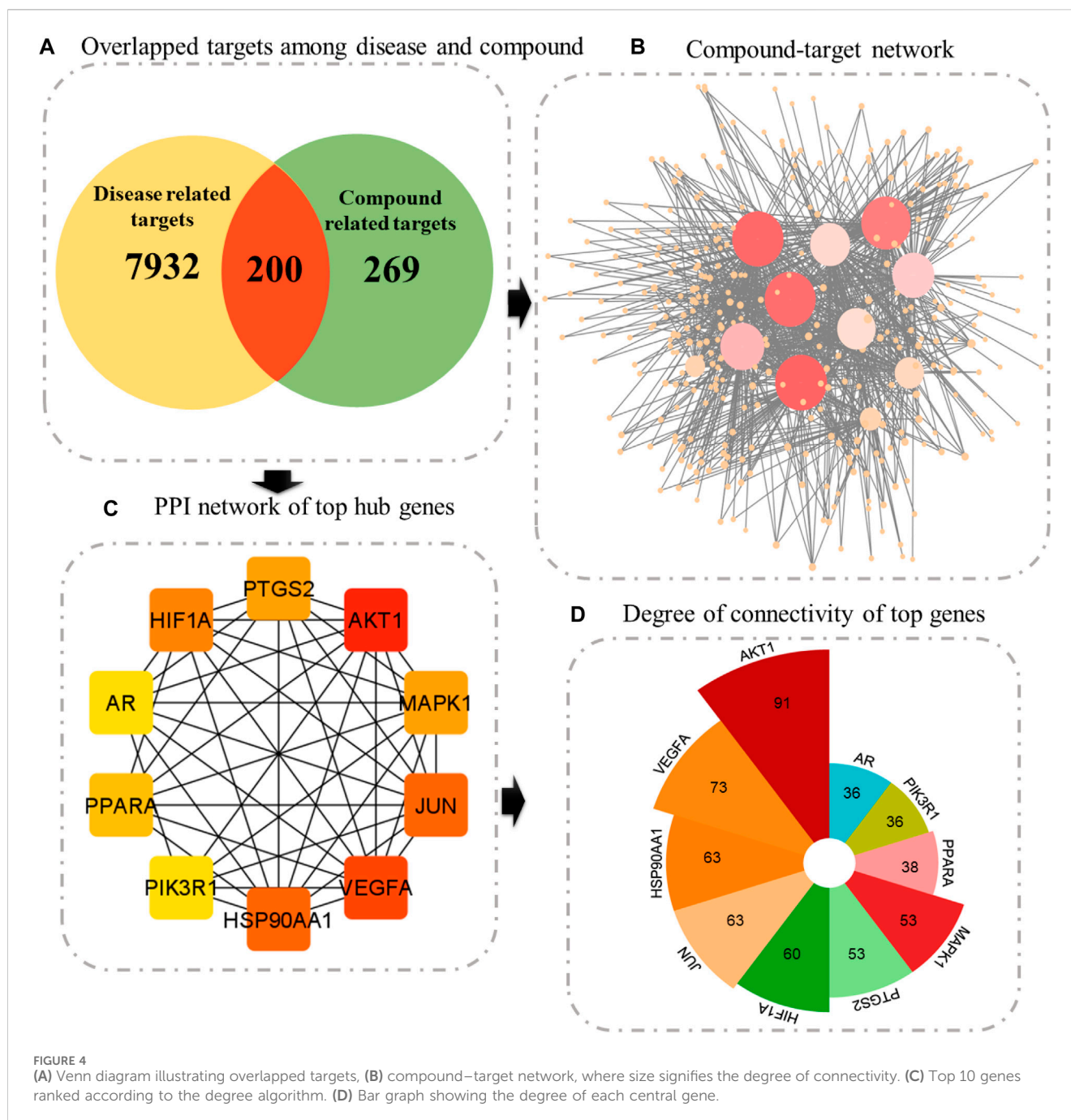
were selected. In the case of the AKT1 protein, the top five compounds with maximum binding affinities are ascorbic acid (−11.1227), citric acid (−10.2178), kaempferol (−11.4719), stigmasterol (−10.0388), and d-tartaric acid (−10.9147) (Figure 6). In the case of the AKT1–ascorbic acid complex, binding affinity contributed to H-bonds with the Ser A:240; Leu A:239; Arg A:243; Arg C:2; and Glu A:341 residues. In terms of citric acid, AKT1 formed H-bonds with Glu A:341 and Gly A:345; for kaempferol, AKT1 demonstrated H-bond interaction with Glu A:341; for stigmasterol, the H-bond interaction was found with Ser A:240 and Arg C:2; and d-tartaric acid showed H-bond interaction with Arg C:2; Glu A:341; Arg A:346; Gly C:1; and Leu A:239 residues (Table 4).

In the case of the VEGFA protein, (+)-catechin (−15.6498), citric acid (−14.7792), (−)-epicatechin gallate (−15.1182), hispidulin (−17.3714), and octopamine (−17.517) were found to have more binding affinity than other active ingredients (Figure 7). In the case of the VEGFA-(+)-catechin complex, binding affinity contributed to H-bonds with Asn B:158; Ser A:179; Ser A:176; Lys A:143; and Ser A:177; for citric acid, VEGFA has H-bond interactions with Ser A:177; Ser A:179; Leu A:178; Gln B:160; Ser B:176; Ser A:177; Ser A:179; Leu A:178; Gln B:160; and Ser B:176; for (−)-epicatechin gallate, VEGFA demonstrated H-bond interactions with Asn A:158; Thr B:180; Gln B:160; Lys A:143; and Asp A:144; for hispidulin, H-bond interactions were found with Asn A:158; Gln B:160; Ser A:179; and

Ser B:176; and octopamine showed H-bond interactions with Ser A:177; Ser A:179; Ser B:176; and Gln A:171 residues (Table 5).

3.9 MD simulation

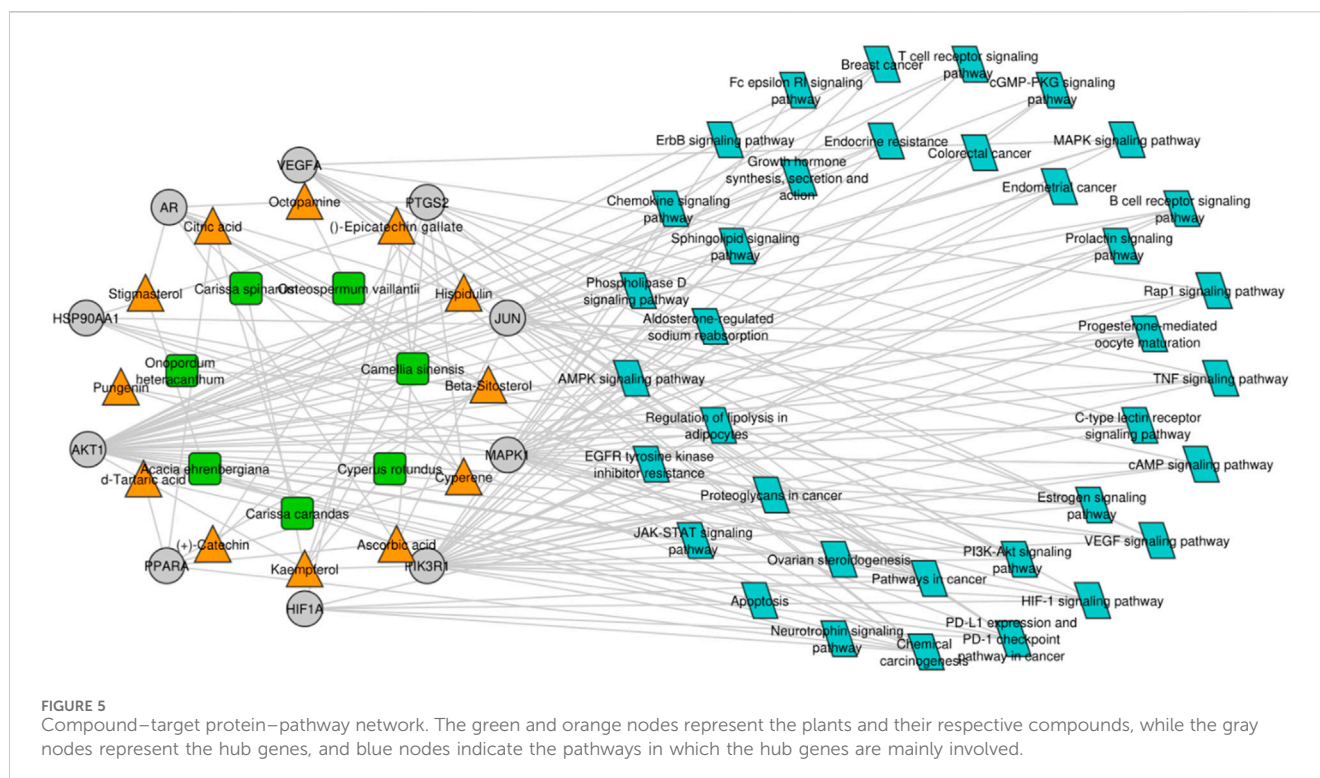
All-atom Molecular Dynamics (MD) simulations were conducted to analyze the relationship between the AKT1 and VEGFA proteins and to assess the stability of the active compounds. The simulation was run at 20 ns using GROMACS software. For each protein, the top two docked complexes based on their binding energies were chosen for MD simulation for evaluating their RMSD and RMSF values, which assist in analyzing conformational changes and interactions among small molecules and target proteins. RMSD offers an understanding of the extent of deviation that a set of atoms (complexes, compounds, and proteins) experience from their original reference structure. On the other hand, RMSF calculates the temporal progression of the average discrepancy for each residue from its initial position in the minimized structures. The RMSD analysis revealed that selected complexes stabilized within a 20-ns timeframe. The average RMSD of the backbone atoms of AKT1 with kaempferol and ascorbic acid–protein systems was found to be ~0.175 and ~0.23 Å, respectively (Figure 8A), while for VEGFA, the average RMSD for hispidulin and octopamine was found to be 0.45 and 0.5 Å,



respectively (Figure 9A). On the other hand, the RMSD of ligand atoms for AKT1 with ascorbic acid exhibits an average RMSD value of ~ 0.04 , with a sharp increase in RMSD (~ 0.12 Å) observed after 4–13 ns of simulation (Figure 8B), while for kaempferol, the RMSD falls within the range of ~ 0.08 to ~ 0.10 Å. In the case of the VEGFA protein, the average RMSD value for octopamine and hispidulin was ~ 0.14 and ~ 0.12 Å (Figure 9B). These findings suggest that octopamine was more stable at 20 ns in the case of the VEGFA protein, while for AKT1, kaempferol was found to be more stable. This was further substantiated by analyzing RMSF *versus* the residue number of AKT1, which showed that in comparison to AKT1–kaempferol, the AKT1–ascorbic acid complex exhibited greater fluctuations in backbone residues (Figure 8C). However,

in terms of the VEGFA complex, hispidulin indicated greater fluctuations in backbone residues than octopamine (Figure 9C).

The radius of gyration (R_g) serves as a crucial metric to evaluate changes in the compactness of a docked complex. For AKT1, ascorbic acid exhibited more pronounced fluctuations than kaempferol (Figure 8D). In the context of VEGFA, notably, the R_g values for VEGFA–hispidulin exhibited a narrower distribution, denoting a more consistent structural compactness relative to the VEGFA–octopamine complex, which displayed a broader range of R_g values, suggestive of increased flexibility and structural variability. This differential behavior in R_g implies that the binding of hispidulin may confer a greater degree of conformational restraint upon the VEGFA protein, potentially



influencing the stability and functional specificity of the ligand-protein interaction (Figure 9D). Furthermore, insights derived from the evaluation of Rg, RMSF, and RMSD metrics indicate that all complexes maintained consistent stability throughout the simulation period. Therefore, it could be concluded that these small molecules hold the potential to be used as an inhibitor for AKT1 and VEGFA; however, the finding needs further *in vivo* and *in vitro* validation.

4 Discussion

According to the National Cancer Registry in Saudi Arabia, ovarian cancer is the seventh most commonly diagnosed cancer among women, accounting for 3.3% of all cancers (Younes and Zayed, 2019). In 2020, the age-standardized incidence rate and mortality rate of ovarian cancer in Saudi Arabia were 3.8/100,000 women and 2.7/100,000 women, respectively. Additionally, 444 new cases were reported in 2020, constituting 1.6% of new cancer cases in Saudi Arabia, with 281 of those cases resulting in death (Aga et al., 2022). Unfortunately, effective treatment options for ovarian cancer are limited in the country. As a result, there is a critical need for the development of effective treatment options to fight against ovarian cancer. Research efforts aimed at identifying new therapeutic targets as well as improving existing treatments are highly recommended.

The utilization of natural products for the treatment of cancer is widely recognized and has garnered significant attention from researchers worldwide (Pangestuti and Kim, 2011). Saudi Arabia has a rich flora consisting of numerous plant species, some of which have been traditionally used in natural medicine (Aati et al., 2019). Many of these plants possess bioactive compounds that have shown

potential in cancer treatment. For example, *C. sinensis* is a rich source of polyphenols associated with numerous pharmacological properties such as anti-inflammatory, antimicrobial, and anti-aging (Rahmani et al., 2015; Naveed et al., 2018). With continued research, these and other Saudi Arabian plants may prove to be valuable sources of natural compounds for the development of new cancer therapies. Recent studies reported that local plant extracts from Saudi Arabia, including *O. heteracanthum* (Gouda et al., 2014), *A. ehrenbergiana* (Makeen et al., 2020), *O. vaillantii* (Gouda et al., 2014), *C. rotundus* (AlQathama et al., 2022), *C. carandas* (Alshehri, 2020), *C. spinarum* (AlQathama et al., 2022), and *C. sinensis* (Dou et al., 2021), exhibited remarkable and potent cytotoxic effects on the ovary cancer cell line. Nevertheless, the specific mechanisms of action underlying these medicinal plants remain unclear. The current study focused on identifying potential active compounds of these Saudi Arabian local plants as a new effective treatment option against ovarian cancer. Initially, the information related to the phytochemicals of *O. heteracanthum*, *A. ehrenbergiana*, *O. vaillantii*, *C. rotundus*, *C. carandas*, *C. spinarum*, and *C. sinensis* was retrieved from databases and reported in a literature survey. Later, the microarray data from the GSE54388, GSE69428, GSE36668, and GSE40595 datasets were obtained from GEO databases and screened for the identification of DEGs. The preprocessing of microarray data was performed through the limma package of R for the identification of DEGs. Later, the disease-related data were compared with plant-related data, which demonstrated 200 overlapped targets. These common targets were then considered for further network pharmacology. The functional annotation of these putative targets revealed that these genes are mainly involved in growth hormone action, secretion, and synthesis, pathways in cancer, the estrogen signaling pathway, p13K-Akt and ErbB signaling pathways,

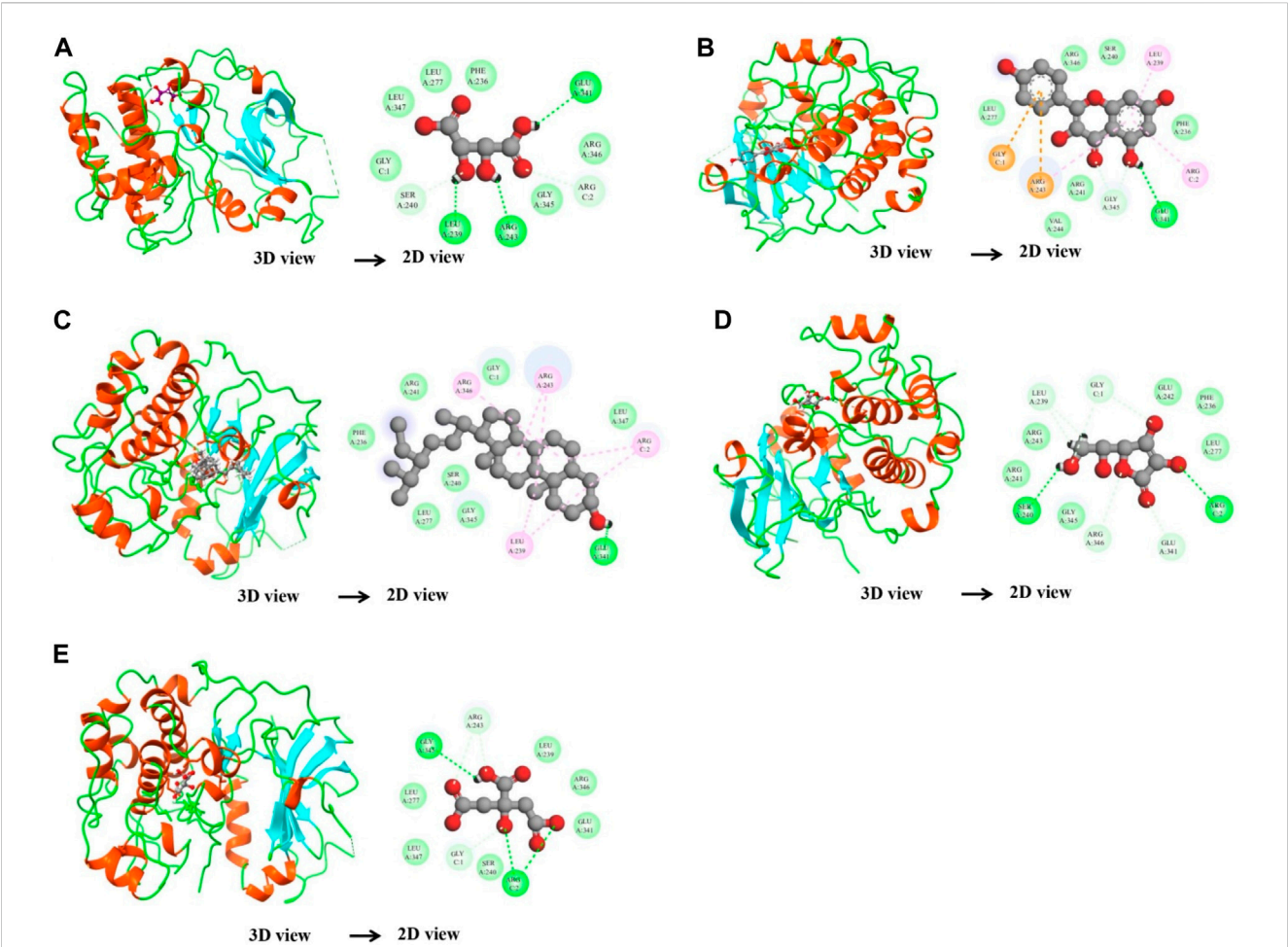


FIGURE 6 Binding interactions between the AKT1 protein and five different active compounds. Each panel (A–E) displays a 3D view of the protein–compound complex on the left and a corresponding 2D interaction diagram on the right. The compounds studied include ascorbic acid (A), citric acid (B), kaempferol (C), stigmasterol (D), and d-tartaric acid (E). These diagrams highlight the specific amino acid residues of the AKT1 protein involved in the interaction with each compound, providing insights into the molecular docking and potential binding efficacy.

TABLE 4 Binding affinity and RMSD value of AKT1 with top five compounds.

Protein	Compound	Docking score (kcal/mol)	RMSD (Å)	Interacting residues
AKT1_3QKK	Ascorbic acid	−11.1227	0.804941	Ser:240; Leu:239; Arg:243; Arg:2; Glu:341
	Citric acid	−10.2178	1.313716	Glu:341; Gly:345; Gly:1; Arg:2; Arg:243; Leu:239
	Kaempferol	−11.4719	0.877178	Arg:346; Arg:243; Arg:2; Leu:239; Glu:341
	Stigmasterol	−10.0388	1.137621	Ser:240; Arg:346; Arg:341; Arg:2; Gly:1; Leu:239
	d-Tartaric acid	−10.9147	0.994647	Arg:2; Glu:341; Arg:346; Gly:1; Leu:239

colorectal cancer, breast cancer, the Rap1 signaling pathway, progesterone-mediated oocyte maturation, endometrial cancer, and the prolactin signaling pathway.

In ovarian cancer, estrogen signaling can promote tumor growth and progression through several mechanisms. For instance, estrogen can promote the growth of ovarian cancer cells and enhance their resistance to chemotherapy (Choi et al., 2011). Additionally, estrogen signaling can promote the formation of new blood

vessels, which helps supply the tumor with nutrients and oxygen (Ribeiro and Freiman, 2014). Furthermore, estrogen signaling can interact with other pathways that are implicated in ovarian cancer, such as the PI3K/AKT/mTOR pathway (Langdon et al., 2020). This pathway assists in regulating cell growth, survival, and metabolism and is often dysregulated in ovarian cancer. Estrogen signaling can activate the PI3K/AKT/mTOR pathway, leading to further promotion of tumor growth and survival (Gil, 2014). Therefore,

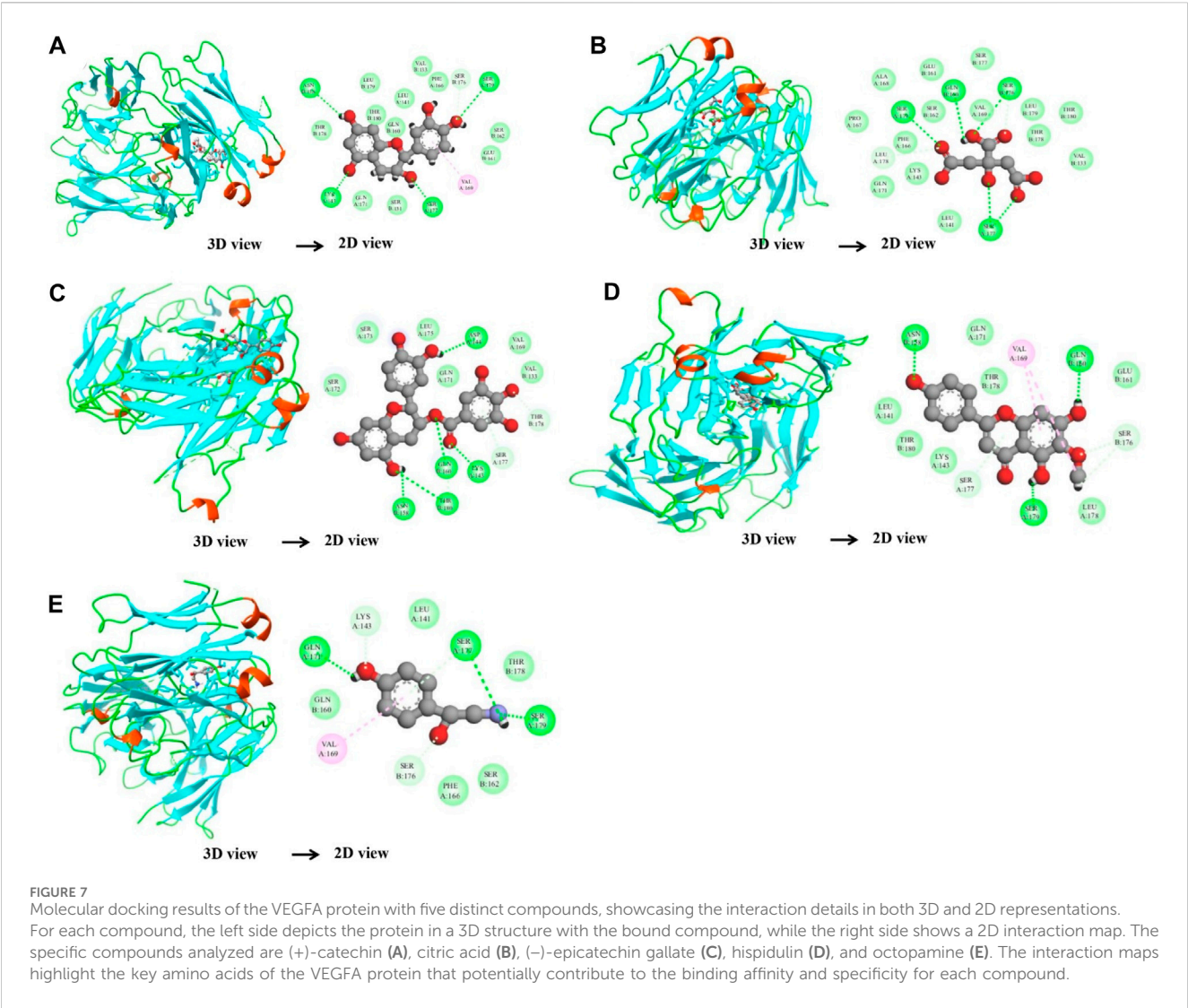


TABLE 5 Binding affinity and RMSD value of VEGFA with top five compounds.

Protein	Compound	Docking score (kcal/mol)	RMSD (Å)	Interacting residues
VEGFA_4ZFF	(+)-Catechin	-15.6498	1.208914	Asn:158; Ser:179; Ser:176; Lys:143; Ser:177; Val:169
	Citric acid	-14.7792	1.159474	Ser:177; Ser:179; Leu:178; Gln:160; Ser:176
	(-)-Epicatechin gallate	-15.1182	1.816931	Asn:158; Thr:180; Gln:160; Lys:143; Asp:144
	Hispidulin	-17.3714	0.916578	Asn:158; Val:190; Gln:160; Ser:179; Ser:176
	Octopamine	-17.517	1.156475	Ser:177; Ser:179; Ser:176; Gln:171

by directing efforts toward the genes active in PI3K-Akt pathways, the progression of ovarian cancer can be halted.

After functional annotation, AKT1 and VEGFA emerged as pivotal proteins due to their highest connectivity within the PPI network, compound-target network, and compound-target-disease network. Although molecular docking provides an estimation of compound suitability within the protein's active site, it solely provides information at the protein's active site. Hence, to analyze the compound-protein target system, the use of binding conformation data has become more prevalent, necessitating the application of MD simulations and their associated binding energy measurements. MD simulations facilitate in-depth exploration of the dynamic attributes of docked complexes as well as fluctuations in the energy scenario. These insights are crucial in determining the complex's stability and possible structural shifts in the protein initiated by ligand interaction. Overall, the assessment derived from molecular docking and MD simulations underscored a considerable binding affinity in the interactions involving active compounds and proteins.

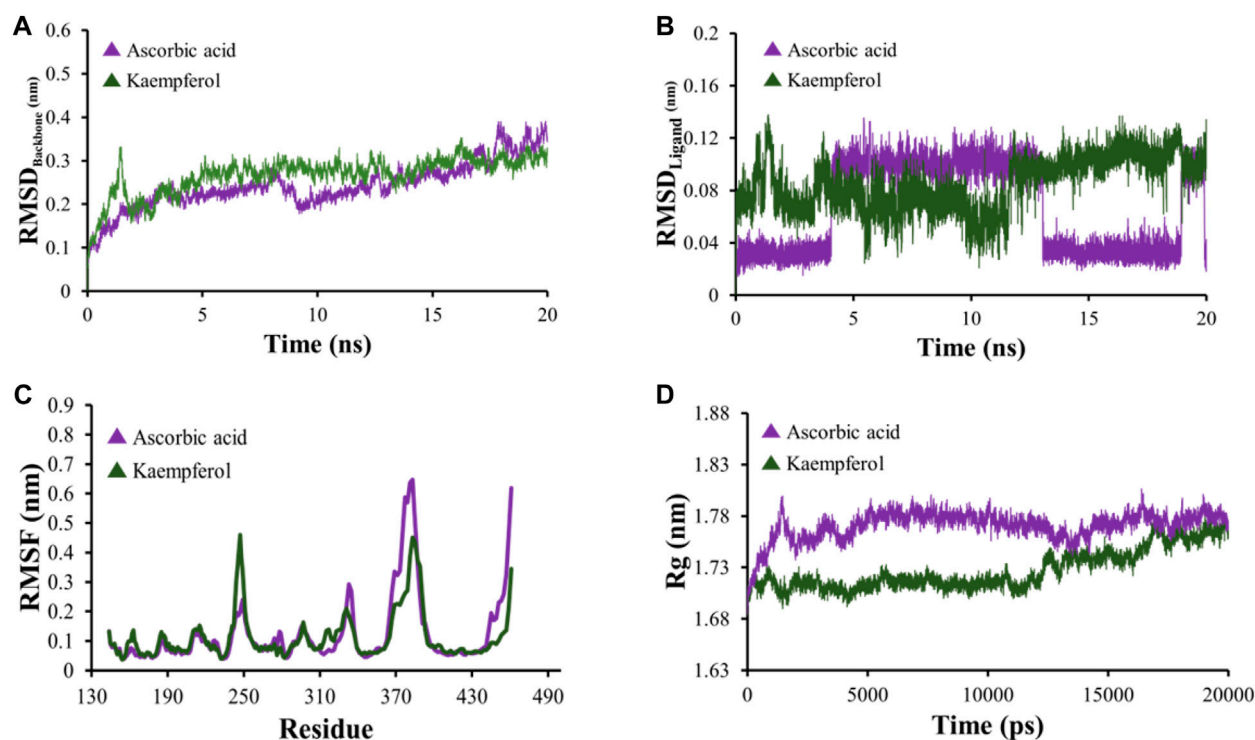


FIGURE 8

(A) RMSD analyses of backbone atoms (C, Ca, and N) within the AKT1–ligand complexes. (B) RMSD evaluations for ligand atoms in the AKT1–ligand systems. (C) RMSF measurements for backbone atoms in the AKT1–ligand setups. (D) Rg analysis pertaining to backbone atoms.

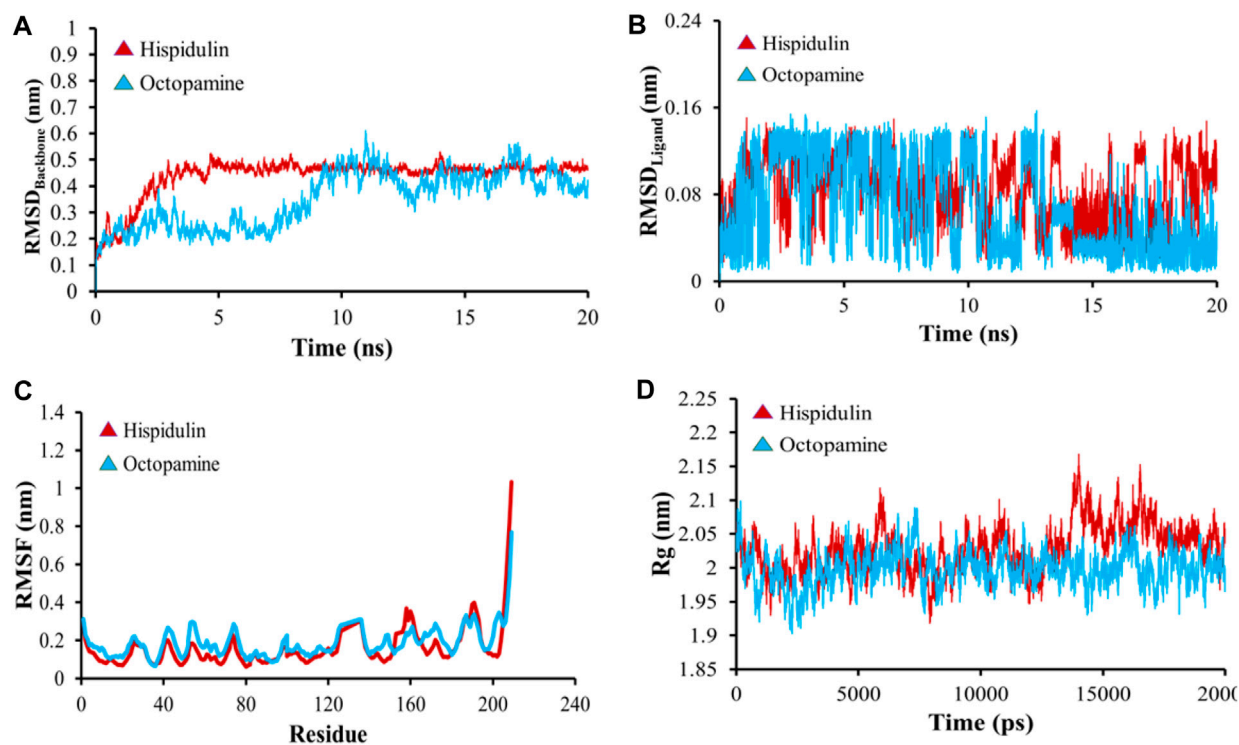


FIGURE 9

(A) RMSD analyses of backbone atoms (C, Ca, and N) within the VEGFA–ligand complexes. (B) RMSD evaluations for ligand atoms in the VEGFA–ligand systems. (C) RMSF measurements for backbone atoms in the VEGFA–ligand setups. (D) Rg analysis pertaining to backbone atoms.

Previous studies reported that AKT1 and VEGFA have key roles to play in the pathogenesis of ovarian cancer. AKT1 is a serine/threonine kinase that is frequently activated in ovarian cancer, and it is involved in promoting cell survival, proliferation, and migration (Tokunaga et al., 2008). When activated, AKT1 can stimulate the expression of VEGFA, which is a key pro-angiogenic factor that promotes the formation of new blood vessels (Hsieh et al., 2017; Zhu et al., 2018). In ovarian cancer, the upregulation of AKT1 and VEGFA is associated with proliferation, metastasis, and angiogenesis (Wang et al., 2019). Moreover, AKT1 and VEGFA can interact with each other, forming a positive feedback loop that further promotes ovarian cancer progression (Trinh et al., 2009). AKT1 activates the HIF-1 α regulator, which in turn can upregulate VEGFA expression (Mazure et al., 2003). VEGFA, in turn, activates the AKT1 pathway, creating a self-reinforcing loop that promotes tumor growth and angiogenesis. Thus, targeting the AKT1 and VEGFA signaling pathways is a promising approach for treating ovarian cancer. Inhibition of AKT1 and VEGFA signaling has been shown to reduce ovarian cancer cell proliferation, angiogenesis, and tumor growth in preclinical models. Furthermore, several clinical trials are currently needed to investigate the efficacy of AKT1 and VEGFA inhibitors in the treatment of ovarian cancer.

Recent advancements in the study of phytochemicals and their role in cancer therapy have underscored the potential of natural compounds as effective agents against ovarian cancer. For instance, Lu et al. (2023) highlighted the emerging role of plant-derived compounds in modulating key signaling pathways involved in cancer progression, including the PI3K-Akt and VEGFA pathways, which our research also identifies as critical targets. Furthermore, Song et al. (2015) reported the significant *in vivo* efficacy of kaempferol in reducing tumor growth and metastasis through the inhibition of cancer-related signaling pathways. These findings align with our computational predictions and molecular docking results, suggesting a promising avenue for future research to explore these compounds' clinical applications. Moreover, the integration of bioinformatics tools and network pharmacology in recent studies, as demonstrated by Batool et al. (Alshehri, 2020), has facilitated a deeper understanding of the complex interactions between natural compounds and cancer-related pathways, reinforcing the value of our approach in identifying novel therapeutic candidates. These contemporary findings not only validate our methodology but also indicate a growing consensus on the importance of targeting specific molecular pathways in ovarian cancer treatment, providing a robust framework for future experimental and clinical investigations.

To sum up, our investigation lays the groundwork for uncovering the multi-target effect of native Saudi Arabian plants as potential therapeutic agents for ovarian cancer. The combination of network pharmacology and bioinformatics methodologies aids in pinpointing essential interactions and molecular pathways contributing to ovarian cancer and supports the identification of prospective drug targets to combat this disease. Although we corroborated our findings using molecular docking and MD simulations, additional *in vitro* and *in vivo* studies are required to substantiate the efficacy of our results. Our study bears certain limitations, such as the requirement for further experimental validation of our findings, the need for a more comprehensive database of traditional medicinal plants and target genes to

enhance the precision of network pharmacology analysis results, and the incomplete understanding of the exact therapeutic mechanism employed by local plants in the treatment of ovarian cancer, even after merging the results from network pharmacology and molecular docking. Therefore, multidisciplinary integration is essential to fully grasp the operational mechanism of these local plants in relation to ovarian cancer.

5 Conclusion

The significant prevalence of ovarian cancer in Saudi Arabia underscores the urgent need for effective prevention, early detection, management strategies, and addressing its associated complications. In response, our study presents an innovative scientific framework that explores the complex multi-target interactions of active phytochemicals within native Saudi Arabian plants. By integrating bioinformatics with network pharmacology approaches, we have identified several potential compounds, including hispidulin, stigmaterol, ascorbic acid, octopamine, cyperene, kaempferol, pungenin, citric acid, d-tartaric acid, beta-sitosterol, (–)-epicatechin gallate, and (+)-catechin, that show promise in treating ovarian cancer. Our findings also highlight the therapeutic implications of targeting AKT1 and VEGFA pathways to mitigate cellular proliferation and growth, contributing valuable insights into the chemical constituents of indigenous Saudi plants and their synergistic mechanisms against ovarian cancer. Looking forward, our research paves the way for further in-depth studies to validate the efficacy and safety of these identified phytochemicals through clinical trials. Future work will also explore the optimization of these compounds for better bioavailability and specificity, along with investigating combination therapies to enhance their anti-cancer effects. Additionally, the development of more sophisticated bioinformatics tools and network pharmacology models will be crucial in unraveling the complexities of ovarian cancer pathogenesis and the multi-faceted roles of these compounds. Ultimately, our study lays the groundwork for novel therapeutic strategies that could significantly impact the prevention and treatment of ovarian cancer in Saudi Arabia and beyond.

Data availability statement

The original contributions presented in the study are included in the article/Supplementary Material; further inquiries can be directed to the corresponding author.

Author contributions

AA: writing—original draft.

Funding

The author(s) declare that no financial support was received for the research, authorship, and/or publication of this article.

Conflict of interest

The author declares that the research was conducted in the absence of any commercial or financial relationships that could be construed as a potential conflict of interest.

Publisher's note

All claims expressed in this article are solely those of the authors and do not necessarily represent those of their affiliated

organizations, or those of the publisher, the editors, and the reviewers. Any product that may be evaluated in this article, or claim that may be made by its manufacturer, is not guaranteed or endorsed by the publisher.

Supplementary material

The Supplementary Material for this article can be found online at: <https://www.frontiersin.org/articles/10.3389/fphar.2024.1345415/full#supplementary-material>

References

- Aati, H., El-Gamal, A., Shaheen, H., and Kayser, O. (2019). Traditional use of ethnomedicinal native plants in the Kingdom of Saudi Arabia. *J. Ethnobiol. ethnomedicine* 15, 2–9. doi:10.1186/s13002-018-0263-2
- Aga, S. S., Jaha, R., Khan, R., Junaydi, D., Hakami, A. Y., Khan, M. A., et al. (2022). Detailed demographics and the prevalence of comorbidities in ovarian cancer patients in Western Region of Saudi Arabia. *J. Nat. Sci. Med.* 5 (3), 254. doi:10.4103/jnsm.jnsm_158_21
- Alamri, M. A. (2020). Pharmacoinformatics and molecular dynamic simulation studies to identify potential small-molecule inhibitors of WNK-SPAK/OSR1 signaling that mimic the RFQV motifs of WNK kinases. *Arabian J. Chem.* 13 (4), 5107–5117. doi:10.1016/j.arabjc.2020.02.010
- AlQathama, A., Bader, A., Al-Rehaily, A., Gibbons, S., and Prieto, J. M. (2022). *In vitro* cytotoxic activities of selected Saudi medicinal plants against human malignant melanoma cells (A375) and the isolation of their active principles. *Eur. J. Integr. Med.* 49, 102083. doi:10.1016/j.eujim.2021.102083
- Alshehri, K. M. (2020). Anticancer plants naturally growing in Al-baha region, Saudi Arabia. *Int. J. Pharm. Res. Allied Sci.* 9 (4), 92–101.
- Banerjee, P., Eckert, A. O., Schrey, A. K., and Preissner, R. (2018). ProTox-II: a webserver for the prediction of toxicity of chemicals. *Nucleic Acids Res.* 46 (W1), W257–W63. doi:10.1093/nar/gky318
- Barrett, T., Suzek, T. O., Troup, D. B., Wilhite, S. E., Ngau, W.-C., Ledoux, P., et al. (2005). NCBI GEO: mining millions of expression profiles—database and tools. *Nucleic Acids Res.* 33 (Suppl. 1), D562–D566. doi:10.1093/nar/gki022
- Batool, S., Javed, M. R., Aslam, S., Noor, F., Javed, H. M. F., Seemab, R., et al. (2022). Network pharmacology and bioinformatics approach reveals the multi-target pharmacological mechanism of Fumaria indica in the treatment of liver cancer. *Pharmaceuticals* 15 (6), 654. doi:10.3390/ph15060654
- Biovia, D. S. (2017). BIOVIA discovery studio visualizer. *Softw.*
- Choi, J.-H., Lee, K.-T., and Leung, P. C. (2011). Estrogen receptor alpha pathway is involved in leptin-induced ovarian cancer cell growth. *Carcinogenesis* 32 (4), 589–596. doi:10.1093/carcin/bgq276
- Choi, J.-H., Wong, A. S., Huang, H.-F., and Leung, P. C. (2007). Gonadotropins and ovarian cancer. *Endocr. Rev.* 28 (4), 440–461. doi:10.1210/er.2006-0036
- Daina, A., Michielin, O., and Zoete, V. (2017). SwissADME: a free web tool to evaluate pharmacokinetics, drug-likeness and medicinal chemistry friendliness of small molecules. *Sci. Rep.* 7 (1), 42717. doi:10.1038/srep42717
- Dallakyan, S., and Olson, A. J. (2015). Small-molecule library screening by docking with PyRx. *Methods Mol. Biol.* 1263, 243–250. doi:10.1007/978-1-4939-2269-7_19
- Dennis, G., Jr., Sherman, B. T., Hosack, D. A., Yang, J., Gao, W., Lane, H. C., et al. (2003). DAVID: database for annotation, visualization, and integrated discovery. *Genome Biol.* 4 (5), R60. doi:10.1186/gb-2003-4-9-r60
- Dou, L., Zhang, X., Zangeneh, M. M., and Zhang, Y. (2021). Efficient biogenesis of Cu₂O nanoparticles using extract of Camellia sinensis leaf: evaluation of catalytic, cytotoxicity, antioxidant, and anti-human ovarian cancer properties. *Bioorg Chem.* 106, 104468. doi:10.1016/j.bioorg.2020.104468
- Dundas, J., Ouyang, Z., Tseng, J., Binkowski, A., Turpaz, Y., and Liang, J. (2006). CASTp: computed atlas of surface topography of proteins with structural and topographical mapping of functionally annotated residues. *Nucleic Acids Res.* 34 (Web Server issue), W116–W118. doi:10.1093/nar/gkl282
- Gfeller, D., Grosdidier, A., Wirth, M., Daina, A., Michielin, O., and Zoete, V. (2014). SwissTargetPrediction: a web server for target prediction of bioactive small molecules. *Nucleic acids Res.* 42 (W1), W32–W38. doi:10.1093/nar/gku293
- Gil, E. M. C. (2014). Targeting the PI3K/AKT/mTOR pathway in estrogen receptor-positive breast cancer. *Cancer Treat. Rev.* 40 (7), 862–871. doi:10.1016/j.ctrv.2014.03.004
- Gouda, Y. G., Abdallah, Q., Elbadawy, M. F., Basha, A. A., Alorabi, A. K., Altowerqe, A. S., et al. (2014). Cytotoxic and antimicrobial activities of some compositae plants growing in Taif area, Saudi Arabia. *Int. J. Pharm. Sci.* 3, 43–48.
- Hopkins, A. L. (2007). Network pharmacology. *Nat. Biotechnol.* 25 (10), 1110–1111. doi:10.1038/nbt1007-1110
- Hsieh, M.-J., Liu, H.-T., Wang, C.-N., Huang, H.-Y., Lin, Y., Ko, Y.-S., et al. (2017). Therapeutic potential of pro-angiogenic BPC157 is associated with VEGFR2 activation and up-regulation. *J. Mol. Med.* 95, 323–333. doi:10.1007/s00109-016-1488-y
- James, T., Hsieh, M.-L., Knipling, L., and Hinton, D. (2015). Determining the architecture of a protein–DNA complex by combining FeBABE cleavage analyses, 3-D printed structures, and the ICM Molsoft program. *DNA-Protein Interact. Princ. Protoc.* 1334, 29–40. doi:10.1007/978-1-4939-2877-4_3
- Jia, C.-Y., Li, J.-Y., Hao, G.-F., and Yang, G.-F. (2020). A drug-likeness toolbox facilitates ADMET study in drug discovery. *Drug Discov. today* 25 (1), 248–258. doi:10.1016/j.drudis.2019.10.014
- Kamilova, I. A., and Valijonova, S. A. (2023). Analysis of the role of the brca1 and brca 2 genes as a predictor of ovarian cancer. prevalence of ovarian cancer in the republic of uzbekistan. *World Bull. Public Health* 19, 142–144.
- Kim, S., Chen, J., Cheng, T., Gindulyte, A., He, J., He, S., et al. (2019). PubChem 2019 update: improved access to chemical data. *Nucleic acids Res.* 47 (D1), D1102–D19. doi:10.1093/nar/gky1033
- Kuhn, M., von Mering, C., Campillos, M., Jensen, L. J., and Bork, P. (2007). STITCH: interaction networks of chemicals and proteins. *Nucleic Acids Res.* 36 (Suppl. 1), D684–D688. doi:10.1093/nar/gkm795
- Langdon, S. P., Herrington, C. S., Hollis, R. L., and Gourley, C. (2020). Estrogen signaling and its potential as a target for therapy in ovarian cancer. *Cancers (Basel)* 12 (6), 1647. doi:10.3390/cancers12061647
- Li, H., Liu, Y., Wang, Y., Zhao, X., and Qi, X. (2021). Hormone therapy for ovarian cancer: emphasis on mechanisms and applications. *Oncol. Rep.* 46 (4), 1–27.
- Lisio, M.-A., Fu, L., Goyeneche, A., Gao, Z.-H., and Telleria, C. (2019). High-grade serous ovarian cancer: basic sciences, clinical and therapeutic standpoints. *Int. J. Mol. Sci.* 20 (4), 952. doi:10.3390/ijms20040952
- Lu, X., Friedrich, L. J., and Efferth, T. (2023). Natural products targeting tumour angiogenesis. *Br. J. Pharmacol.* doi:10.1111/bph.16232
- Makeen, H. A., Alhazmi, H. A., Khalid, A., Al Bratty, M., Syame, S. M., Abdalla, A. N., et al. (2020). Phytochemical, antimicrobial and cytotoxicity screening of ethanol extract of Acacia ehrenbergiana Hayne grown in Jazan Region of Saudi Arabia. *Trop. J. Pharm. Res.* 19 (2), 313–321. doi:10.4314/tjpr.v19i2.14
- Mazure, N., Brahimi-Horn, M., and Pouyssegur, J. (2003). Protein kinases and the hypoxia-inducible factor-1, two switches in angiogenesis. *Curr. Pharm. Des.* 9 (7), 531–541. doi:10.2174/1381612033391469
- Mohanraj, K., Karthikeyan, B. S., Vivek-Ananth, R., Chand, R. B., Aparna, S., Mangalapandi, P., et al. (2018). IMPPAT: a curated database of Indian Medicinal Plants, Phytochemistry and Therapeutics. *Sci. Rep.* 8 (1), 4329. doi:10.1038/s41598-018-22631-z
- Molinspiration, C. (2011). Calculation of molecular properties and bioactivity score. Available at: <http://www.molinspiration.com/cgi-bin/properties>.
- Naveed, M., BiBi, J., Kamboh, A. A., Suheryani, I., Kakar, I., Fazlani, S. A., et al. (2018). Pharmacological values and therapeutic properties of black tea (Camellia sinensis): a comprehensive overview. *Biomed. Pharmacother.* 100, 521–531. doi:10.1016/j.biopha.2018.02.048
- Needle, D., Lountos, G. T., and Waugh, D. S. (2015). Structures of the Middle East respiratory syndrome coronavirus 3C-like protease reveal insights into substrate specificity. *Acta Crystallogr. Sect. D. Biol. Crystallogr.* 71 (5), 1102–1111. doi:10.1107/S1399004715003521

- Noor, F., Asif, M., Ashfaq, U. A., Qasim, M., and Tahir ul Qamar, M. (2023). Machine learning for synergistic network pharmacology: a comprehensive overview. *Briefings Bioinforma.* 24, bbad120. doi:10.1093/bib/bbad120
- Noor, F., Rehman, A., Ashfaq, U. A., Saleem, M. H., Okla, M. K., Al-Hashimi, A., et al. (2022b). Integrating network pharmacology and molecular docking approaches to decipher the multi-target pharmacological mechanism of *Abrus precatorius* L. Acting on diabetes. *Pharmaceuticals* 15 (4), 414. doi:10.3390/ph15040414
- Noor, F., Saleem, M. H., Aslam, M. F., Ahmad, A., and Aslam, S. (2021). Construction of miRNA-mRNA network for the identification of key biological markers and their associated pathways in IgA nephropathy by employing the integrated bioinformatics analysis. *Saudi J. Biol. Sci.* 28 (9), 4938–4945. doi:10.1016/j.sjbs.2021.06.079
- Noor, F., Tahir ul Qamar, M., Ashfaq, U. A., Albutti, A., Alwashmi, A. S., and Aljasir, M. A. (2022a). Network pharmacology approach for medicinal plants: review and assessment. *Pharmaceuticals* 15 (5), 572. doi:10.3390/ph15050572
- Pangestuti, R., and Kim, S.-K. (2011). Biological activities and health benefit effects of natural pigments derived from marine algae. *J. Funct. Foods* 3 (4), 255–266. doi:10.1016/j.jff.2011.07.001
- Pathak, K., and Raghuvanshi, S. (2015). Oral bioavailability: issues and solutions via nanoformulations. *Clin. Pharmacokinet.* 54, 325–357. doi:10.1007/s40262-015-0242-x
- Pettersen, E. F., Goddard, T. D., Huang, C. C., Couch, G. S., Greenblatt, D. M., Meng, E. C., et al. (2004). UCSF Chimera—a visualization system for exploratory research and analysis. *J. Comput. Chem.* 25 (13), 1605–1612. doi:10.1002/jcc.20084
- Pettersen, E. F., Goddard, T. D., Huang, C. C., Meng, E. C., Couch, G. S., Croll, T. I., et al. (2021). UCSF ChimeraX: structure visualization for researchers, educators, and developers. *Protein Sci.* 30 (1), 70–82. doi:10.1002/pro.3943
- Raab, M., Kobayashi, N. F., Becker, S., Kurunci-Csacsko, E., Krämer, A., Strebhardt, K., et al. (2020). Boosting the apoptotic response of high-grade serous ovarian cancers with CCNE1 amplification to paclitaxel *in vitro* by targeting APC/C and the pro-survival protein MCL-1. *Int. J. Cancer* 146 (4), 1086–1098. doi:10.1002/ijc.32559
- Rahman, M. A., Mossa, J. S., Al-Said, M. S., and Al-Yahya, M. A. (2004). Medicinal plant diversity in the flora of Saudi Arabia 1: a report on seven plant families. *Fitoterapia* 75 (2), 149–161. doi:10.1016/j.fitote.2003.12.012
- Rahmani, A. H., Allemailem, K. S., Aly, S. M., and Khan, M. A. (2015). Implications of green tea and its constituents in the prevention of cancer via the modulation of cell signalling pathway. *BioMed Res. Int.* 2015, 925640. doi:10.1155/2015/925640
- Rehman, A., Ashfaq, U. A., Javed, M. R., Shahid, F., Noor, F., and Aslam, S. (2022). The Screening of phytochemicals against NS5 Polymerase to treat Zika Virus infection: integrated computational based approach. *Comb. Chem. High. Throughput Screen* 25 (4), 738–751. doi:10.2174/1386207324666210712091920
- Ribeiro, J. R., and Freiman, R. N. (2014). Estrogen signaling crosstalk: implications for endocrine resistance in ovarian cancer. *J. Steroid Biochem. Mol. Biol.* 143, 160–173. doi:10.1016/j.jsbmb.2014.02.010
- Ritchie, M. E., Phipson, B., Wu, D., Hu, Y., Law, C. W., Shi, W., et al. (2015). Limma powers differential expression analyses for RNA-sequencing and microarray studies. *Nucleic Acids Res.* 43 (7), e47. doi:10.1093/nar/gkv007
- Sahoo, C. R., Paidesetty, S. K., Dehury, B., and Padhy, R. N. (2020). Molecular dynamics and computational study of Mannich-based coumarin derivatives: potent tyrosine kinase inhibitor. *J. Biomol. Struct. Dyn.* 38 (18), 5419–5428. doi:10.1080/07391102.2019.1701554
- Sahoo, C. R., Paidesetty, S. K., Sarathbabu, S., Dehury, B., Senthil Kumar, N., and Padhy, R. N. (2022). Molecular dynamics simulation, synthesis and topoisomerase inhibitory actions of vanillin derivatives: a systematic computational structural integument. *J. Biomol. Struct. Dyn.* 40 (22), 11653–11663. doi:10.1080/07391102.2021.1961867
- Seeliger, D., and de Groot, B. L. (2010). Ligand docking and binding site analysis with PyMOL and Autodock/Vina. *J. Comput. Aided Mol. Des.* 24 (5), 417–422. doi:10.1007/s10822-010-9352-6
- Sharma, T., Mohapatra, S., Dash, R., Rath, B., and Sahoo, C. R. (2022). *Recent advances in CADD. Computer aided drug design (CADD): from ligand-based methods to structure-based approaches.* Elsevier, 231–281.
- Shinbo, Y., Nakamura, Y., Altaf-Ul-Amin, M., Asahi, H., Kurokawa, K., Arita, M., et al. (2006). KNApSack: a comprehensive species-metabolite relationship database. *Plant metabolomics* 165–181. doi:10.1007/3-540-29782-0_13
- Sideris, M., Menon, U., and Manchanda, R. (2024). Screening and prevention of ovarian cancer. *Med. J. Aust.* 220, 264–274. doi:10.5694/mja2.52227
- Smoot, M. E., Ono, K., Ruscheinski, J., Wang, P. L., and Ideker, T. (2011). Cytoscape 2.8: new features for data integration and network visualization. *Bioinformatics* 27 (3), 431–432. doi:10.1093/bioinformatics/btq675
- Song, H., Bao, J., Wei, Y., Chen, Y., Mao, X., Li, J., et al. (2015). Kaempferol inhibits gastric cancer tumor growth: an *in vitro* and *in vivo* study. *Oncol. Rep.* 33 (2), 868–874. doi:10.3892/or.2014.3662
- Sufyan, M., Ashfaq, U. A., Ahmad, S., Noor, F., Saleem, M. H., Aslam, M. F., et al. (2021). Identifying key genes and screening therapeutic agents associated with diabetes mellitus and HCV-related hepatocellular carcinoma by bioinformatics analysis. *Saudi J. Biol. Sci.* 28 (10), 5518–5525. doi:10.1016/j.sjbs.2021.07.068
- Swain, S., Bej, S., Mandhata, C. P., Bishoyi, A. K., Sahoo, C. R., and Padhy, R. N. (2023). Recent progress on phytochemistry and pharmacological activities of *Grewia asiatica* L. (Tiliaceae) and traditional uses. *South Afr. J. Bot.* 155, 274–287. doi:10.1016/j.sajb.2023.02.016
- Tokunaga, E., Oki, E., Egashira, A., Sadanaga, N., Morita, M., Kakeji, Y., et al. (2008). Deregulation of the Akt pathway in human cancer. *Curr. Cancer Drug Targets* 8 (1), 27–36. doi:10.2174/156800908783497140
- Torre, L. A., Islami, F., Siegel, R. L., Ward, E. M., and Jemal, A. (2017). Global cancer in women: burden and trends. *Cancer Epidemiol. Biomarkers Prev.* 26 (4), 444–457. doi:10.1158/1055-9965.EPI-16-0858
- Trinh, X., Tjalma, W., Vermeulen, P., Van den Eynden, G., Van der Auwera, I., Van Laere, S., et al. (2009). The VEGF pathway and the AKT/mTOR/p70S6K1 signalling pathway in human epithelial ovarian cancer. *Br. J. Cancer* 100 (6), 971–978. doi:10.1038/sj.bjc.6604921
- von Mering, C., Huynen, M., Jaeggi, D., Schmidt, S., Bork, P., and Snel, B. (2003). STRING: a database of predicted functional associations between proteins. *Nucleic Acids Res.* 31 (1), 258–261. doi:10.1093/nar/gkg034
- Wang, J., Yang, L., Liang, F., Chen, Y., and Yang, G. (2019). Integrin α_x stimulates cancer angiogenesis through PI3K/Akt signaling-mediated VEGFR2/VEGF-A overexpression in blood vessel endothelial cells. *J. Cell Biochem.* 120 (2), 1807–1818. doi:10.1002/jcb.27480
- Yang, W.-L., Lu, Z., and Bast, Jr R. C. (2017). The role of biomarkers in the management of epithelial ovarian cancer. *Expert Rev. Mol. Diagn.* 17 (6), 577–591. doi:10.1080/14737159.2017.1326820
- Younes, N., and Zayed, H. (2019). Genetic epidemiology of ovarian cancer in the 22 Arab countries: a systematic review. *Gene* 684, 154–164. doi:10.1016/j.gene.2018.10.044
- Zhu, G.-S., Tang, L.-Y., Lv, D.-L., and Jiang, M. (2018). Total flavones of *abelmoschus manihot* exhibits pro-angiogenic activity by activating the VEGF-A/VEGFR2-PI3K/Akt signaling axis. *Am. J. Chin. Med.* 46 (03), 567–583. doi:10.1142/S0192415X18500295
- Zoete, V., Cuendet, M. A., Grosdidier, A., and Michielin, O. (2011). SwissParam: a fast force field generation tool for small organic molecules. *J. Comput. Chem.* 32 (11), 2359–2368. doi:10.1002/jcc.21816



OPEN ACCESS

EDITED BY

Raghuveera Kumar Goel,
Boston University, United States

REVIEWED BY

Vishwambhar Bhandare,
Shivaji University, India
Prem Prakash Kushwaha,
Case Western Reserve University, United States

*CORRESPONDENCE

Safar M. Alqahtani,
✉ safar.alqahtani@psau.edu.sa
Faisal Ahmad,
✉ faisalahmad@abs.qau.edu.pk

RECEIVED 01 January 2024

ACCEPTED 22 April 2024

PUBLISHED 22 May 2024

CITATION

Alqahtani SM, Altharawi A, Alabbas A, Ahmad F,
Ayaz H, Nawaz A, Rahman S and Alossaimi MA
(2024), System biology approach to identify the
novel biomarkers in glioblastoma multiforme
tumors by using computational analysis.
Front. Pharmacol. 15:1364138.
doi: 10.3389/fphar.2024.1364138

COPYRIGHT

© 2024 Alqahtani, Altharawi, Alabbas, Ahmad,
Ayaz, Nawaz, Rahman and Alossaimi. This is an
open-access article distributed under the terms
of the [Creative Commons Attribution License](#)
(CC BY). The use, distribution or reproduction in
other forums is permitted, provided the original
author(s) and the copyright owner(s) are
credited and that the original publication in this
journal is cited, in accordance with accepted
academic practice. No use, distribution or
reproduction is permitted which does not
comply with these terms.

System biology approach to identify the novel biomarkers in glioblastoma multiforme tumors by using computational analysis

Safar M. Alqahtani^{1*}, Ali Altharawi¹, Alhumaidi Alabbas¹,
Faisal Ahmad^{2,3*}, Hassan Ayaz⁴, Asia Nawaz⁴, Sidra Rahman⁴ and
Manal A. Alossaimi¹

¹Department of Pharmaceutical Chemistry, College of Pharmacy, Prince Sattam Bin Abdulaziz University, Al Kharj, Saudi Arabia, ²Foundation University Medical College, Foundation University Islamabad, Islamabad, Pakistan, ³School of Biology Georgia Institute of Technology, Atlanta, GA, United States, ⁴Department of Biotechnology, Quaid-i-Azam University Islamabad, Islamabad, Pakistan

Introduction: The most common primary brain tumor in adults is glioblastoma multiforme (GBM), accounting for 45.2% of all cases. The characteristics of GBM, a highly aggressive brain tumor, include rapid cell division and a propensity for necrosis. Regrettably, the prognosis is extremely poor, with only 5.5% of patients surviving after diagnosis.

Methodology: To eradicate these kinds of complicated diseases, significant focus is placed on developing more effective drugs and pinpointing precise pharmacological targets. Finding appropriate biomarkers for drug discovery entails considering a variety of factors, including illness states, gene expression levels, and interactions between proteins. Using statistical techniques like p-values and false discovery rates, we identified differentially expressed genes (DEGs) as the first step in our research for identifying promising biomarkers in GBM. Of the 132 genes, 13 showed upregulation, and only 29 showed unique downregulation. No statistically significant changes in the expression of the remaining genes were observed.

Results: Matrix metalloproteinase 9 (MMP9) had the greatest degree in the hub biomarker gene identification, followed by (periostin (POSTN) at 11 and Hes family BHLH transcription factor 5 (HES5) at 9. The significance of the identification of each hub biomarker gene in the initiation and advancement of glioblastoma multiforme was brought to light by the survival analysis. Many of these genes participate in signaling networks and function in extracellular areas, as demonstrated by the enrichment analysis. We also identified the transcription factors and kinases that control proteins in the protein-protein interactions (PPIs) of the DEGs.

Discussion: We discovered drugs connected to every hub biomarker. It is an appealing therapeutic target for inhibiting MMP9 involved in GBM. Molecular docking investigations indicated that the chosen complexes (carmustine, lomustine, marimastat, and temozolomide) had high binding affinities of -6.3 , -7.4 , -7.7 , and -8.7 kcal/mol, respectively, the mean root-mean-square deviation (RMSD) value for the carmustine complex and marimastat complex was 4.2 Å and 4.9 Å, respectively, and the lomustine and temozolomide complex system showed an average RMSD of 1.2 Å and 1.6 Å, respectively. Additionally, high

stability in root-mean-square fluctuation (RMSF) analysis was observed with no structural conformational changes among the atomic molecules. Thus, these *in silico* investigations develop a new way for experimentalists to target lethal diseases in future.

KEYWORDS

biomarker, gene expression, glioblastoma, protein–protein interactions, molecular dynamic simulations

1 Introduction

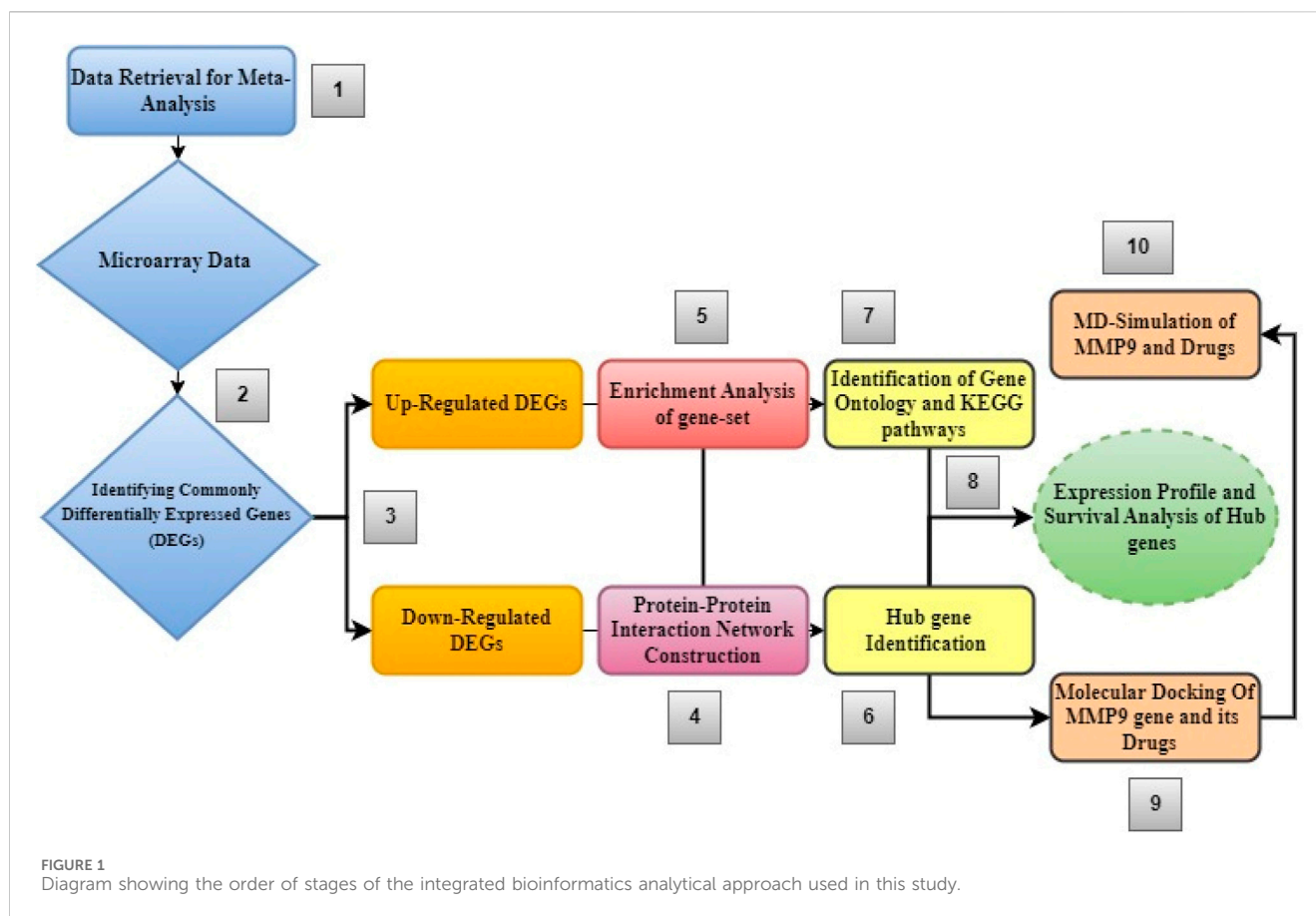
Glioblastoma multiforme (GBM) is a major form of primary brain tumor with a high incidence in the adult population, i.e., 45.2% of all the primary brain and central nervous system tumors. It has been categorized as a grade IV cancer by the WHO. GBM is highly malignant, mitotically active, and has a predisposition to necrosis with a poor prognosis. The survival rate of GBM patients is quite low as only 5.5% of patients survive after the diagnosis (Kanderi and Gupta, 2023a). GBM is associated with many genetic and epigenetic mutations. Genome-wide studies have revealed different risk factors that can increase the chances of GBM, including low susceptibility to allergy, defective immune system, genetic factor, and some single-nucleotide polymorphisms (SNPs) (Wrensch et al., 2009).

The survival rate for older people with GBM is unlike that for individuals aged from 20 to 39 years. This is mainly due to the suboptimal treatment therapy. Several different strategies are adopted for the treatment of GBM, including radiotherapy, chemotherapy (use of alkylating drugs such as temozolomide (TMZ) and antiangiogenic drugs such as bevacizumab), and surgical interventions. Some novel treatments and chemotherapy have proven to be promising in the prognosis of GBM. However, the overall survival rate and quality of life among GBM patients remain dismal (Kumari and Kumar, 2023). The design and incorporation of more potent drugs and the precise selection of treatment strategies including drug targets can possibly optimize the survival rate in GBM patients. Multi-omics data, including genomics, transcriptomics, and proteomics, can reveal important information that can be used for the optimization of prognosis and treatment methods. In this regard, utilizing *in silico* methods to anticipate structural consequences of mutations will prove highly valuable in gaining insights into the mechanisms behind drug resistance, allowing for a quantitative assessment of the resulting phenotypic resistance outcomes.

Network-based gene expression profiling is one of the recommended tools for discovering drug targets considering different aspects, including phases of disease, severity of disease indicated by the expression of certain genes, and protein–protein interactions (PPIs) (Su et al., 2018). System biology is a holistic approach that is adopted globally for the drug design and search of novel drug targets by incorporating all the linked components including genes, proteins, and enzymes rather than considering only a single component of this complicated and interconnected mesh (Noor et al., 2023b). It has been revealed that all these related genes and proteins interact and work coherently to construct a molecular network that plays a specific role in a pathological condition (Khan et al., 2020; Alamri and Tahir ul Qamar, 2024).

To find the potential biomarkers for GBM, an integrated approach was used that included the proteomic and transcriptomic modeling of molecular networks of microarray data (Noor et al., 2023a) that have not been established previously. We used gene expression data for defining the prospective gene/protein biomarkers that can be targeted for the treatment of glioblastoma multiforme utilizing the system biology approach based on microarray datasets. For the identification of differentially expressed genes (DEGs), the statistical method *p*-value and false discovery rate (FDR) were used, followed by survival and expression analyses and the construction of subnetwork modules. The obtained data for DEGs were evaluated for functional and structural roles via KEGG pathways and the interpretation of cellular components. Hub genes were identified, in which the matrix metalloproteinase 9 (MMP9) gene was selected as a biomarker gene.

The degradation of the extracellular matrix (ECM) is a crucial physiological process facilitated by matrix metalloproteinases (MMPs), which are zinc-dependent endopeptidases (Mondal et al., 2020). Research has shown that the ECM plays a significant role in the advancement of cancer (Dobra et al., 2023). Several ECM proteins, including fibronectin, thrombospondin-1, laminin, and osteopontin, influence the biological characteristics of tumors via their impact on cell migration and angiogenesis. The interaction between cancer cells and ECM components is crucial for both cell transformation and the development of cancer (Jabłońska-Trypuć et al., 2016). MMPs play several biological roles throughout all phases of cancer, ranging from the initial stages to the formation of metastases, in addition to their role in ECM degradation (Chambers and Matrisian, 1997; Mannello et al., 2005). Although MMPs are linked to the survival and dissemination of cancer cells, they are produced by cancer cells in minimal quantity. Cancer cells induce the production of MMPs in neighboring host cells by the secretion of interleukin, interferon, growth factors, and extracellular MMP inducers, hence exhibiting a paracrine mechanism (Dobra et al., 2023). Additionally, there were reports of increased levels of MMP9 in human brain tumors throughout the 1990s (Stetler-Stevenson, 1990). Rao et al. demonstrated a notable increase in the expression of MMP9 in highly malignant gliomas, which is shown to be associated with the course of the disease. This finding implies that MMP9 may play a role in facilitating the observed invasiveness (Rao et al., 1996). Molecular docking and molecular dynamic simulation of potential drugs for targeted genes provided valuable information that can provide the basis for further research to develop a better understanding of disease mechanisms and optimization of



therapeutic agents that can upscale the process of diagnosis and treatment of glioblastoma multiforme.

2 Materials and methods

Figure 1 shows the step-by-step process of an integrated system biology analytical technique used to find novel biomarkers and their associated pathways connected to glioblastoma multiforme tumors.

2.1 Retrieval dataset

The Gene Expression Omnibus (GEO) database of NCBI (<https://www.ncbi.nlm.nih.gov/geo/>), a freely accessible database that offers a full set of microarrays, high-throughput hybridization, chips, and other resources for research purposes, was used to collect the gene expression profile (GSE11100) of glioblastoma multiforme, which has a total of 22 samples, including from the healthy vs malignant regions of the human brain [2]. GSM280297, GSM280298, GSM280360, GSM280361, GSM280362, GSM280363, GSM280367, GSM280368, GSM280375, and GSM280376 were used as human brain healthy samples, and GSM279179, GSM279182, GSM279184, GSM279187, GSM280369, GSM280370, GSM280371, GSM280372, GSM280373, GSM280374, GSM280377, and GSM280378 were used as the human brain malignant samples. This information is based on the GPL570

Affymetrix Human Genome U133 Plus 2.0 Array (HG-U133_Plus_2). In this study, we used a variety of analytical techniques. We first investigated differential gene expression and then used principal component analysis (PCA) to organize data with related properties. To demonstrate the genes that showed differential expression visually, we also used heatmaps. Additionally, we created a system of PPIs that was especially targeted at the DEGs. We located sub-networks within this network and highlighted significant hub genes. We developed a network that shows how proteins and drugs interact. Finally, as the final step in our thorough research, we performed molecular docking and MD simulation tests.

2.2 Data preprocessing and identification of DEGs

Using the Network Analyst web server tool (<https://www.networkanalyst.ca/>), the dataset was evaluated for genes displaying differential expression. The focus of this assessment was to locate genes with statistically significant expression variations (Clough and Barrett, 2016). Rows representing specific gene entries and columns representing the various samples made up the dataset's structure. We used experimental data to determine the inclusion of 10 healthy samples and 12 malignant samples to achieve an equitable distribution. To provide uniformity and clarity throughout the dataset, all gene-probe IDs were also changed into Entrez IDs (Stacklies et al., 2007). We carried out a meta-

analysis of the microarray data using NetworkAnalyst, an integrated meta-analysis web application (Xia et al., 2015). Then, we normalized each dataset using a different technique, such as the log2 transformation, quantile normalization, and variance stabilization normalization (VSN). The normality of the data was then confirmed by inspecting principal component analysis (PCA) plots and box plots (Khan et al., 2020). Using a significance threshold of $p < 0.05$, we carried out differential expression analysis on each individual dataset. The Benjamini–Hochberg approach was used to determine an FDR cutoff of ≥ 2 , which we also used. In addition, a t -test using the Limma algorithm (LAT) was included in this analysis (Davis, 2007).

2.3 Analyzing the functional characteristics of gene sets

The initial ontology analysis of the DEGs was performed using the online bioinformatics program DAVID v6.8 (<https://david.ncifcrf.gov/>). This was done by tagging them with KEGG pathway information and Gene Ontology (GO) terminology, and annotations with a significance level of $p < 0.05$ were considered (Jiao et al., 2012). Both DEGs and hub genes were included in the modules that we uploaded. Next, we set up several characteristics, including mode-function, species (*Homo sapiens*), molecular function, cellular component, and ontology/pathway–biological process. Data from the Gene Ontology and KEGG databases were used as support for this analysis of functional roles and pathway enrichment (Ashburner et al., 2000; Hulsege et al., 2009). Utilizing the Benjamini–Hochberg approach, we performed an enrichment analysis utilizing the two-sided hypergeometric test. Using a kappa score of 0.96, the analysis was conducted, and the enrichment was calculated using a threshold value greater than 0.005.

2.4 Generating a PPI network

We created a PPI network including each DEG using the STRING database (<https://string-db.org/>) (Szklarczyk et al., 2015). The database currently comprises 67,592,464 human proteins and 20,052,394,041 documented interactions. The interactions were generated using Cytoscape_v3.10.1 and evaluated using a variety of essential variables. The protein interactions were first imported into Cytoscape version 3.10.1, and they were subsequently evaluated using the integrated tools (Chen Y.-C. et al., 2013). For the combined score to be deemed significant, it must be less than 0.75 (medium confidence score) (Oany et al., 2021). We searched for the direct interactions between each DEG and its first-level interactors. The network design was changed to only include the primary DEGs after a complete dataset with data on both DEGs was imported. Zero-order interactions were specifically chosen to enable exact PPI visualization while removing the crowded and complex network appearance commonly known as the hairball effect (Xia et al., 2014). The network can be analyzed and compared using several different topological variables. Even though Cytoscape is open-source, it has a “NetworkAnalyzer” capability that can be used to examine protein/gene networks. NetworkAnalyzer was used in this study to evaluate

significant characteristics such as clustering coefficient, power law-conforming node distribution, node degree distribution, network centralization, and density. These evaluations were carried out to separate the features of the three generated networks (Ma et al., 2011).

2.5 Selection of central hub proteins from the PPI network

In order to show and explore the generated PPI networks, Cytoscape version 3.10.1 (<https://cytoscape.org/>) was used (Shannon et al., 2003). The degree of nodes in the PPI network is determined by the number of edges to which they are connected. Hub genes are identified as nodes with high degree values (Ghafouri-Fard et al., 2023). We mapped the hub genes to examine their PPI details. Essentially, CytoHubba is a well-known integrated Cytoscape tool that analyzes the attributes and ranks the nodes correspondingly (Pan et al., 2023). It uses 11 approaches to examine the functionality of the network, including locating hub genes or network nodes. Therefore, we used CytoHubba to identify hub genes that would make viable novel therapeutic targets for glioblastoma multiforme tumor therapy.

2.6 Correlation between transcription factors and regulatory networks

The relationship between transcription variables and their related target genes was established using the X2K eXpression2Kinases (X2K) online application, which can be found at <http://www.maayanlab.net/X2K/>. This server received as input the whole set of DEGs, along with their individual gene symbols (Chen E. Y. et al., 2013). Established Fisher test p -values were used to determine the 10 most notable transcription factors (TFs) and kinases, as well as their enrichment scores. These results came from the TF and kinase module, which was built using information from the ChEA69 database to build the ChIP-X. A regulatory network was created, and Cytoscape was then used to view the “graphml” file (Brandes et al., 2001). It is ensured that the regulatory network has enough interconnected nodes throughout the network development process. If there is a gap in the pathway between kinases and TFs, the system automatically widens it to allow TFs to bind with enough intermediary proteins.

2.7 Hub gene survival and expression profile analysis

The Gene Expression Profiling Interactive Analysis (GEPIA2) (<http://gepia2.cancer-pku.cn/>) (Tang et al., 2017) is an extensive online platform that quickly and adaptably offers a variety of features based on information from The Cancer Genome Atlas (TCGA) and Genotype-Tissue Expression (GTEx). For genes that display differential expression in a particular cancer sample, GEPIA2 evaluates both the effect on survival and the analysis of expression patterns. The overall survival impact of hub genes in

GBM was assessed using the GEPIA2 single-gene analysis by calculating the log-rank p -value and the 95% confidence interval-based hazard ratio (HR) (Schröder et al., 2011). The hub genes, on the other hand, were chosen according to their relative levels of expression, with a log2FC cutoff value of less than 1 and a q -value cutoff of less than 0.01.

2.8 Construction of the protein and drug interaction network

The analysis focused on the top 10 hub genes to investigate gene–drug interactions. DrugBank version 5.1.10 (<https://go.drugbank.com/>), which was integrated with the NetworkAnalyzer program, provided information about the drugs and their corresponding targets. It has 16,222 medication entries in total, of which 2,751 are approved small-molecule pharmaceuticals, 1,604 are approved biologics (including proteins, peptides, vaccines, and allergens), and 134 are approved as nutraceuticals. More than 6,722 investigational medications are also now in the discovery stage. The data entry of each drug is detailed, offering a substantial quantity of information in its 200 or more data fields. This dataset includes information on a number of different topics, such as the chemical makeup and characteristics of the medicine and specifics regarding the target or targets (Wishart et al., 2018).

2.9 Molecular docking

Prior to docking, the 2D structures of all possible compounds as inhibitors against the target protein were sketched and minimized using MM2 Force-Field of ChemOffice 2012. Under the Tripos force field (TFF) of UCSF Chimera, a monomer of the target MMP9 protein (pdb id: 5th6) was assigned with Gasteiger charges and minimized for 1,500 steps, which may be divided into 750 of conjugate and 750 of the steepest descent. Molecular docking performed via PyRx 0.9 was used. Molecular docking is an *in silico* approach for determining the binding modes and affinities of two molecules. In the current work, Arg56-N, a charged amino acid, was employed as a binding site residue to dock a molecule with a protein-specific site. A total of four top ligands were docked in the MMP9 protein active site. PyRx 0.9 (Dallakyan and Olson, 2015) software was used to investigate the binding free energies of the docked complexes. For each molecule, 10 solutions were prepared and screened for the best docked pose with high binding affinity. Further investigation was performed to check the binding interactions among the inhibitor moieties and the atomic residues of the protein active site. This was inferred via Discovery Studio (Biovia, 2017), where hydrogen bonds and other active bonds were observed.

2.10 MD simulation analysis

First, docked complicated system preparatory simulation was carried out. For protein synthesis, AMBER16 (Case et al., 2016) force fields ff03.r1, GAFF (Sprenger et al., 2015), and ff14SB (Case et al., 2014) were utilized, and the system was solvated within a three-point

transferable intermolecular potential (TIP3P) (Brice and Dominy, 2013) water box of 8.0. Minimization was used to remove unfavorable conflicts. For minimization, a conjugate gradient with 1,000 steps and the steepest decent technique were used at a value of 8. Heating was carried out for 10-ps using the Langevin dynamics method for temperature control; at a constant temperature of 300 K, 100-ps equilibration is necessary before the manufacturing run begins. The total energy remains constant during equilibration, whereas kinetic and potential energies change. The docked complex was produced in 200-ns increments, followed by equilibration. Periodic boundary conditions were suggested in the simulation box using a canonical ensemble. To keep the temperature constant, the Berendsen coupling integration approach was applied (Berendsen et al., 1984). The AMBER16 PTRAJ (Process TRAJectory) (Roe and Cheatham, 2013) module was used to generate output files for result analysis. PTRAJ was used to calculate four attributes, and graphical representations were examined in xmgrace (Srivastava et al., 2021).

2.10.1 Binding free energies

The MM(PB/GB)SA approach, which was used in AMBER16, was used to calculate the binding free energy of the top five systems (Case et al., 2016; Srivastava et al., 2021). After extracting 1,000 frames from the simulation trajectories, the AMBER MMPBSA.py module was used for a comprehensive analysis. The MM(PB/GB)SA approach takes into account the difference between the complex free energy and the individual free energies of the ligand and receptor when computing binding free energy. To eliminate false positive results, avoid the limits of one method, and cross-validate the results, binding free energies were estimated using two alternative methods. An implicit solvent system is used by MM(PB/GB)SA to fill the space created by the ligand decoupling process. According to Woods et al. (2004), the water molecules that are inserted into the cavity that is created interact with the protein active site and greatly increase the total binding free energy.

3 Results

3.1 Assurance of quality and principal component analysis

The fundamental components of a biological system are genes and the products they produce, which interact randomly to form a complex network (Alamri and ul Qamar, 2023). Understanding immunology, the mechanisms of defense, signaling tasks, modes of transportation, and the onset of diseases more thoroughly can be accomplished by analyzing both genes and protein expression. Specifically, in situations where the variation is subject to fluctuations, the VSN, followed by the quantile normalization method, was used to standardize the expression data from microarray analysis. Box plots, density plots, and the data means are shown in Figure 2 both before and after the normalizing process. The figure illustrates how the normalization procedure produces constant means across all samples and successfully removes any noise that may have been present in the data. The PCA of the data revealed clear clusters. PCA was used to separate the controlled and mutant samples of the dataset into discrete clusters based on the levels of gene expression.

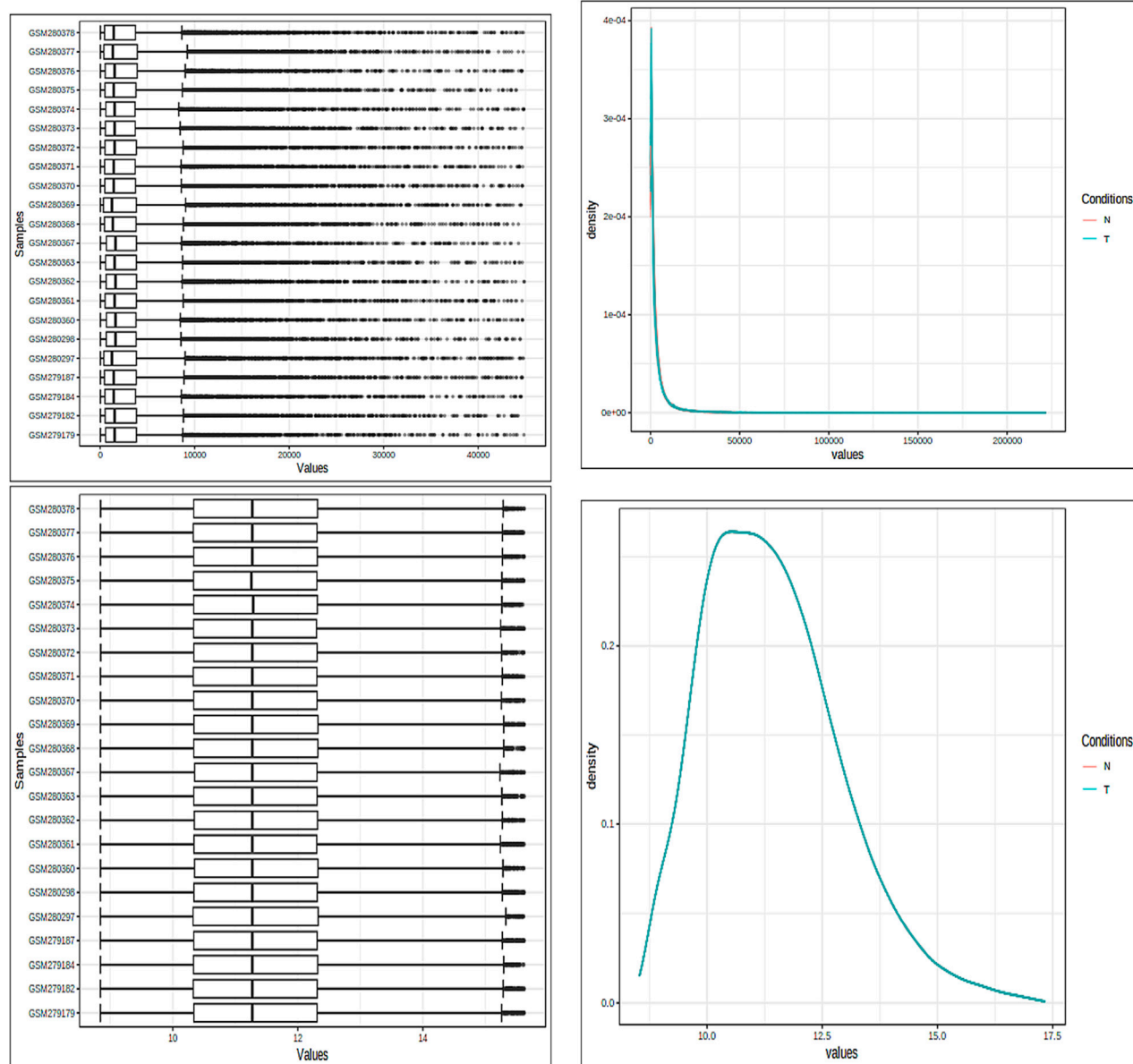


FIGURE 2
Both box plots and density plots are used to visualize the samples. These graphs are shown in the image both before and after the normalizing process. For mean correction and noise removal, variance stabilization normalization (VSN), followed by quantile normalization, was used.

3.2 Investigation of DEGs and network analysis of PPIs

Several statistical tests were run on the datasets for both the control and disease state, including Student's *t*-test, Benjamini–Hochberg technique, and Pearson's correlation test. A total of 132 DEGs were discovered Utilising these investigations (Table 1). A total of 13 of these DEGs showed upregulation, while only 29 showed downregulation individually, and the rest of genes were insignificant. Using the adjusted *p*-value, the final ranking of the DEGs was established (Table 2). The network of PPIs is very important for understanding the workings of cellular networking. To assess how serious the issue is, changes in the protein cellular network

in both healthy and diseased states are useful. In the present investigation, proteins and genes are represented by nodes, while interactions between these proteins and genes are represented by edges. We mapped these genes and created an interaction network for the identified DEGs. The mapped DEGs were shown graphically using Cytoscape. All interactions involving the DEGs were retrieved from the STRING database using a moderate confidence level of 0.40. The network created utilizing every DEG found is shown in Figure 3.

A created network consisted of 66 nodes linked by 105 edges. The network topological metrics showed that there were significant interactions within it, with an average node degree of 1.75 and an average local clustering coefficient of 0.304. Both a volcano plot and a heatmap are shown in Figure 4 to represent the DEGs.

TABLE 1 Top 10 DEGs in the protein–protein interaction network from the STRING database ranked by the degree method.

Rank	Gene name	Score	logFC	Adjusted p-value
1	Matrix Metallopeptidase 9 (MMP9)	14	1.4035	0.21842
2	Periostin (POSTN)	11	1.5999	0.25854
3	Hes Family BHLH Transcription Factor 5 (HES5)	9	−1.0343	0.18261
4	Achaete-Scute Family BHLH Transcription Factor 1 (ASCL1)	8	−1.0575	0.18658
4	Collagen Type V Alpha 2 Chain (COL5A2)	8	1.2027	0.21842
6	Fibroblast Growth Factor 1 (FGF1)	7	1.0553	0.17267
6	Collagen Type VI Alpha 2 Chain (COL6A2)	7	1.3605	0.20412
8	Syndecan 4 (SDC4)	6	1.2696	0.073206
8	Bone Morphogenetic Protein 2 (BMP2)	6	−1.0586	0.11314
8	Delta Like Canonical Notch Ligand 3 (DLL3)	6	−2.0239	0.028407

3.3 Analysis of the KEGG pathway and GO function enrichment

The top 10 results of the enrichment analysis for DEGs that are upregulated and downregulated in the context of GO analysis were determined using the DAVID database, including topics such as

cellular components, molecular functions, biological processes, and KEGG pathways, as described by GO. A highly significant criterion for the terms used in the analysis was the FDR. Our analysis of the GO cellular components (CCs) of the DEGs revealed a highly significant and distinctive distribution pattern for our proteins, including extracellular space, extracellular region, extracellular matrix, collagen trimer, cell surface, basement membrane, voltage-gated calcium channel complex, microtubule bundle, synapse, tertiary granule lumen, perinuclear region of the cytoplasm, GABAergic synapse, glutamatergic synapse, sarcoplasm, and voltage-gated sodium channel complex. We found 15 key functional categories for which our proteins actively participate in terms of molecular functioning (MF), such as extracellular matrix structural constituent, growth factor activity, heparin binding, carbohydrate binding, collagen binding, calcium ion binding, sequence-specific double-stranded DNA binding, identical protein binding, dehydroascorbic acid transporter activity, oxidoreductase activity, integrin binding, D-glucose transmembrane transporter activity, co-receptor binding, metalloendopeptidase inhibitor activity, and protein dimerization activity.

Furthermore, the significant KEGG pathways are primarily connected to cancer-related processes, and the reported pathways, which include ECM–receptor interaction, Notch signaling pathway, breast cancer, and endocrine resistance, are highly enriched.

The enhanced biological processes (BPs) identified in DEGs include extracellular matrix organization, cell adhesion, negative regulation of neuron differentiation, Notch signaling pathway, positive regulation of osteoblast differentiation, skeletal system development, negative regulation of cardiac muscle cell differentiation, regulation of neurogenesis, positive regulation of osteoblast proliferation, central nervous system myelination, cell–matrix adhesion, astrocyte differentiation, cell migration,

TABLE 2 Identification of proposed drugs against the hub proteins retrieved from the database.

S. no.	Protein	UniProt id	Drug name	DrugBank id	Groups
	Matrix Metallopeptidase 9 (MMP9)	P00390	Carmustine	DB00262	Approved
		Q9H169	Lomustine	DB01206	Approved
		P14780	Marimastat	DB00786	Investigational
		A0A6M3QJP3	Temozolomide	DB00853	Approved
	Periostin (POSTN)	P46721	Prednisolone	DB00860	Approved
		P35354	Salicylic acid	DB00936	Approved
	Hes Family BHLH Transcription Factor 5 (HES5)
	Achaete-Scute Family BHLH Transcription Factor 1 (ASCL1)
	Collagen Type V Alpha 2 Chain (COL5A2)	H6U5S3	Clofarabine	DB00631	Approved
	Fibroblast Growth Factor 1 (FGF1)	P05067	Flutemetamol F-18	DB09151	Approved
	Collagen Type VI Alpha 2 Chain (COL6A2)
	Syndecan 4 (SDC4)
	Bone Morphogenetic Protein 2 (BMP2)
	Delta Like Canonical Notch Ligand 3 (DLL3)

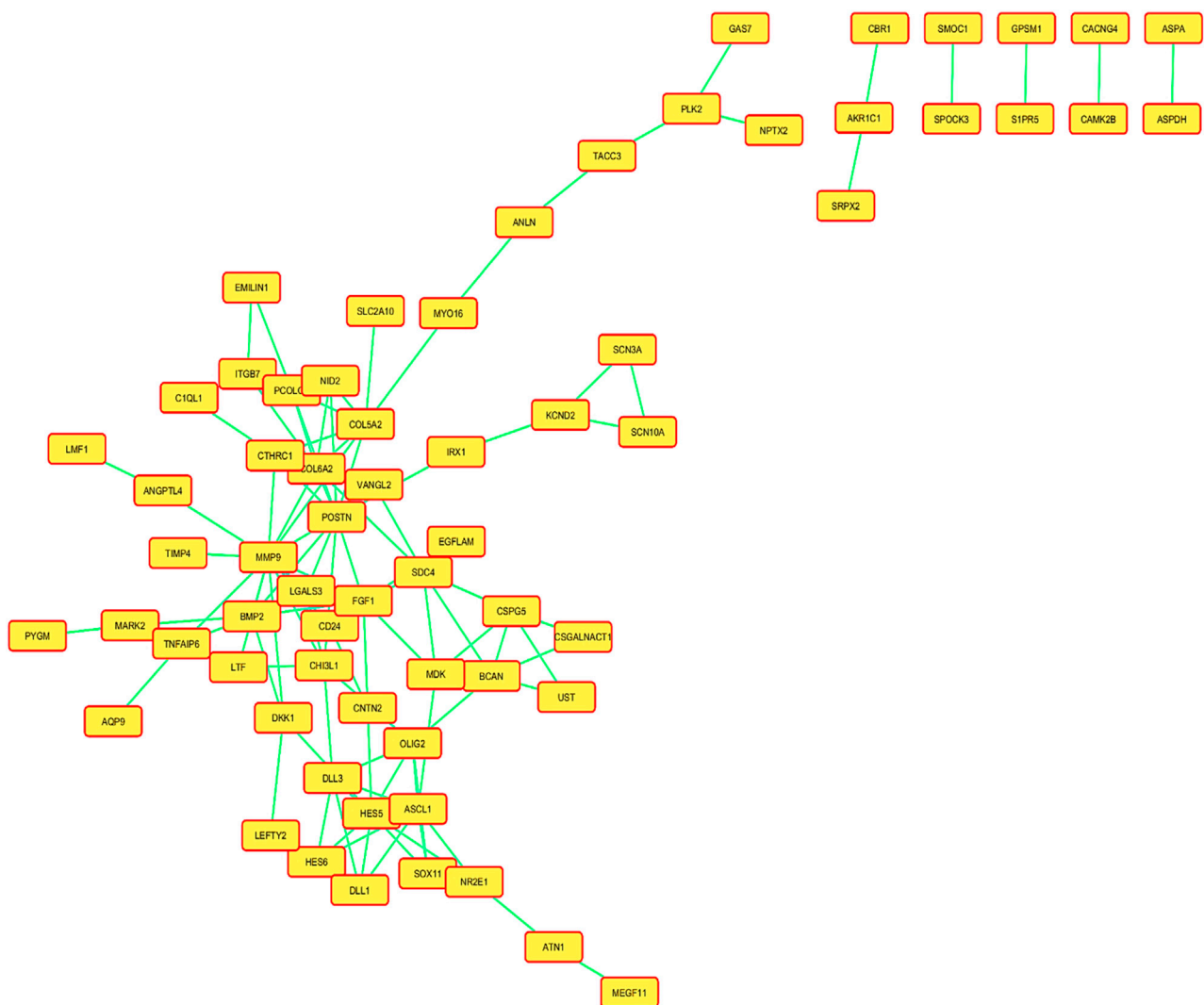


FIGURE 3
Network of the protein–protein interactions (PPIs) of all the mapped differentially expressed genes (DEGs), and a confidence level of 0.400 was used to build this network using information from the STRING database.

inner-ear receptor stereocilium organization, positive regulation of neural precursor cell proliferation, oligodendrocyte development, positive regulation of oligodendrocyte differentiation, positive regulation of sprouting angiogenesis, nervous system development, positive regulation of angiogenesis, positive regulation of the transforming growth factor beta receptor signaling pathway, and negative regulation of the canonical Wnt signaling pathway.

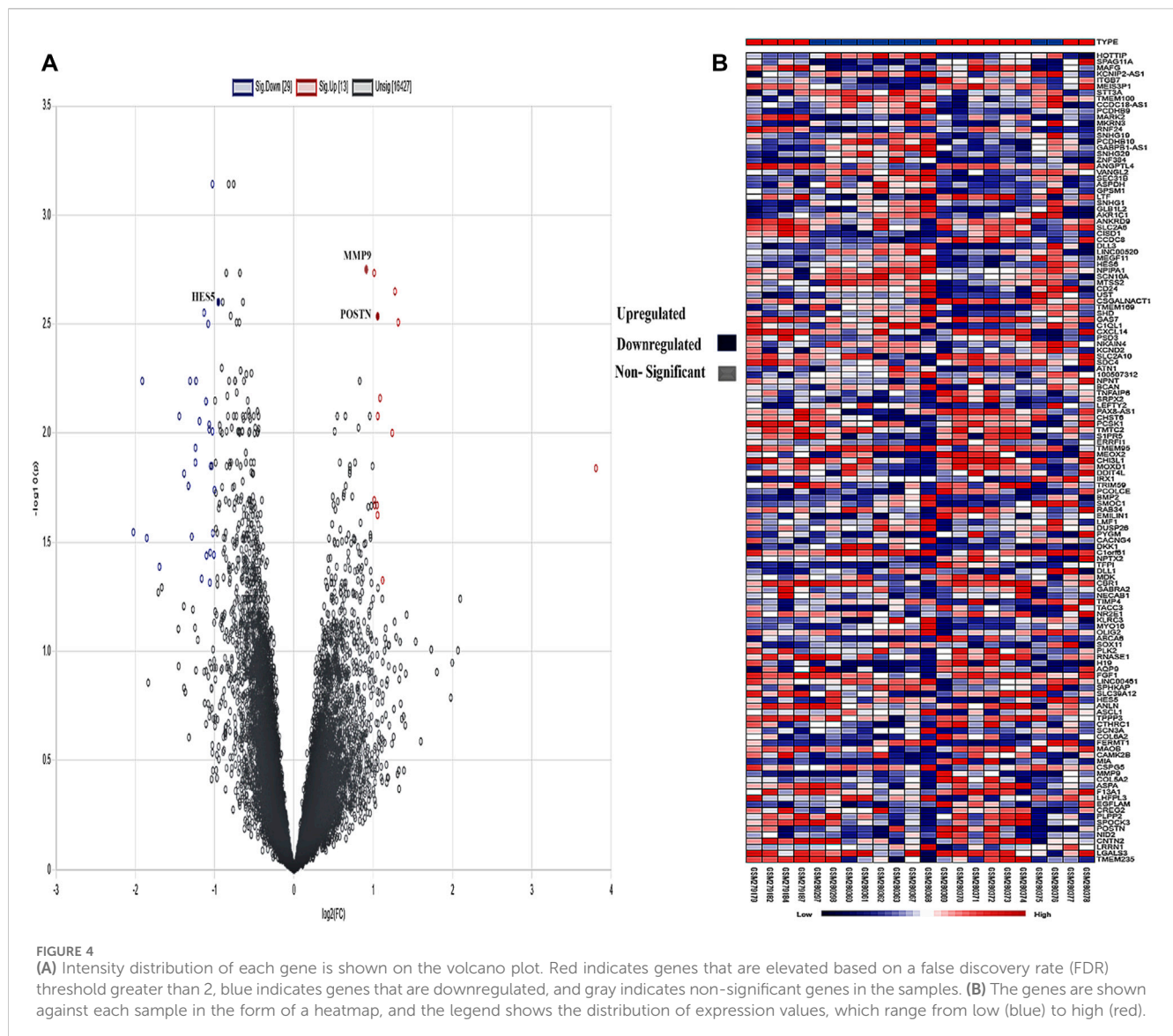
3.4 Hub gene identification

The interactions of hub genes with the red nodes determined and ranked the nodes according to their degree of significant connection. Nodes having a degree value > 10 were classified as hub nodes using CytoHubba, which calculated the node degrees (Table 1). *MMP9* had the highest degree, followed by 11 *POSTN* and Hes family BHLH transcription factor 5 (*HES5*) with a 9-degree score. Herein, achaete-

scute family BHLH transcription factor 1 (*ASCL1*), collagen type-V alpha 2 (*COL5A2*), fibroblast growth factor 1 (*FGF1*), collagen type-VI alpha 2 (*COL6A2*), syndecan 4 (*SDC4*), bone morphogenetic protein 2 (*BMP2*), and delta-like canonical notch ligand 3 (*DLL3*) were among the additional genes revealed to have lower degree values. The shortest path network of these hub gene interactions showing strong interactions based on the degree of score and color is given in Figure 5.

3.5 Transcription factor analysis

The most well-known TFs and protein kinases connected to DEGs were identified in this analysis based on their contributions to the development of regulatory network activities. TFs, kinases, and transient proteins involved in their development were connected to create a network that served as a regulatory complex. First, we used ChIP-seq experiments (ChEA) to identify integrated target genes for transcription factors, which were then used to predict the most



important TFs, which were then mapped onto PPI networks. **Figures 6A,B** depict the TFs predicted here and the PPI network. Based on the hypergeometric *p*-value, the main transcription factors in this case are SUZ12 polycomb repressive complex 2 subunit (*SUZ12*), enhancer of zeste 2 polycomb repressive complex 2 subunit (*EZH2*), tripartite motif containing 28 (*TRIM28*), SRY-box transcription factor 2 (*SOX2*), RE1 silencing transcription factor (*REST*), and (SMAD family member 4 (*SMAD4*). We also identified and subsequently added into the PPI network kinases that are most likely to behave as regulators for the extended PPI network, as shown in **Figures 6C,D**. The major kinases in these DEGs identified based on the hypergeometric *p*-value were cyclin-dependent kinase 1 (*CDK1*), casein kinase 2 alpha 1 (*CSNK2A1*), mitogen-activated protein kinase 14 (*MAPK14*), cyclin-dependent kinase 2 (*CDK2*), glycogen synthase kinase 3 beta (*GSK3B*), homeodomain interacting protein kinase 2 (*HIPK2*), mitogen-activated protein kinase 1 (*MAPK1*), mitogen-activated protein kinase 3 (*MAPK3*), AKT serine/threonine kinase 1 (*AKT1*), cyclin-dependent kinase 4 (*CDK4*), cyclin-dependent kinase 2 (*ERK2*), mitogen-activated

protein kinase 3 (*ERK1*), casein kinase 2 alpha 1 (*CK2ALPHA*), glycogen synthase kinase 3 beta (*GSK3BETA*), and component of inhibitor of nuclear factor kappa B kinase complex (*IKKALPHA*). All the TFs and kinases identified with their scores are given in **Supplementary Table S1**.

3.6 Identified hub gene survival and expression analysis

To analyze the overall impact on the survival of 10 important hub genes chosen from both the upregulated and downregulated DEGs, *GEPIA* survival evaluation was used. **Figure 7** shows the findings of the current study. *COL6A2* had a hazard ratio (HR) of 1.4 and was the only one of the 10 genes under investigation to show decreased overall survival in the group with increased expression. On the other hand, from the expression level of the hub genes, we identified that the nine hub genes *MMP9*, periostin (*POSTN*), *ASCL1*, *COL5A2*, *FGF1*, *COL6A2*, *SDC4*, *BMP2*, and *DLL3* were

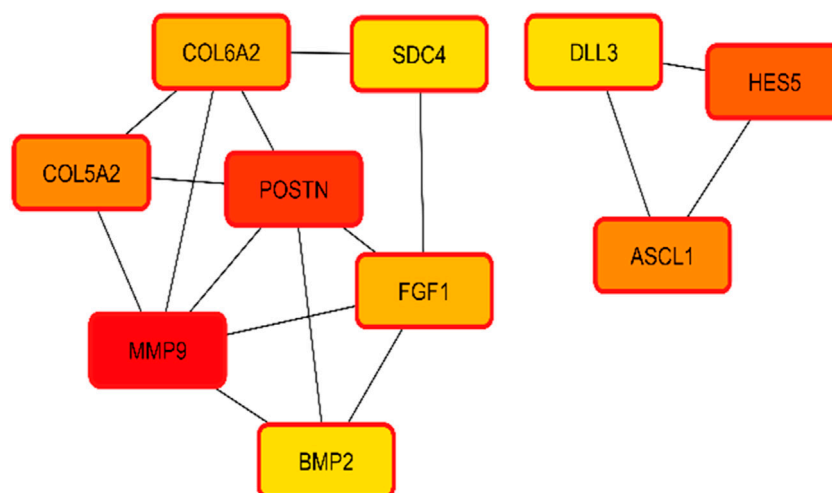


FIGURE 5
Hub gene identification and interactions based on the degree of color and score. Higher scores having strong interaction with other targets are shown in red, followed by orange and yellow.

downregulated in the normal cells, and only one hub gene, *HES5*, was upregulated in the tumor cells (Figure 8).

3.7 Protein–drug interactions

Following the identification of the top hub genes, the DrugBank database was searched for possible therapeutic candidates. In this study, we investigated each target and, using manual searches, identified the drugs related to them. The search panel included medication from a range of categories, including FDA-approved, investigational, and nutraceuticals. We manually searched for medications that interacted with each hub gene-recognized protein. In total, eight medications were found. Four drugs for MMP9, two for POSTN, and one each for COL5A2 and FGF1 were found, while no potential drugs were found for the rest of the targets. The identified drugs for all these targets are given in Table 2.

3.8 Molecular docking

We obtained the four best compounds from the database against the target hub gene. All the compounds were docked into the target protein active site, with the coordinates of the Arg56: N atom set as the center of binding. A radius of 10 Å was set around Arg56: N, and 10 iterations were generated for each docked compound. Docked scores were used to assess chemical binding affinity for protein activity. The docked score for the complexes carmustine, lomustine, marimastat, temozolomide, and solasodine (control drug) with the MMP9 protein is -6.3 , -7.4 , -7.7 , -8.7 , and -5.7 kcal/mol, respectively. Furthermore, major residues of the protein active site implicated in hydrogen bonding, such as Glu47, Arg56, Tyr179, Pro102, Phe107, Arg106, Pro180, Asp187, Phe59, Gl57, Pro54, and Val53, were involved in binding forces, as shown in Figure 9.

Some of the residues indicated possible hydrophobic interactions. The theoretical activity of a compound requires both hydrogen and hydrophobic contacts. Furthermore, numerous additional interactions were observed, which must be considered for the computational efficacy of the compound. Thus, it has been inferred that these chemical moieties are oriented in such a way that they bind along the channel of the active pocket. Thus, it prevents the total substrate access to the active site during the metabolic pathways and inhibits the final production of cancerous substances.

3.9 MD simulation

Protein conformational dynamics are the most essential aspect linked with their function. The functional information of a protein molecule is encoded in its structure. To comprehend the functional variability, an understanding of the structure is required (Karplus and Kuriyan, 2005). The current work used MD simulation to investigate the conformational aspect of protein–ligand interactions and assess the stability of the inhibitor complex system in a real-time environment. Data reduction analyses such as root-mean-square deviation (RMSD) and root-mean-square fluctuation (RMSF) were used to assess the conformational changes and stability index of secondary structure components of the simulated complexes. RMSD describes the backbone analysis Ca atom dynamics of the docked protein during a time scale of 100 ns, and fluctuation was observed at different time intervals among carmustine complex and marimastat complex systems, but a persisting graph of simulation stability was detected among the marimastat and temozolomide complex system. Figure 10 shows that the average RMSD value for the carmustine complex and marimastat complex system is 4.1 Å and 5.03 Å, respectively, whereas the average RMSD for the lomustine and temozolomide complex systems is 1.2 Å and 1.6 Å, respectively. To check the stability of the two carmustine complex and marimastat complex

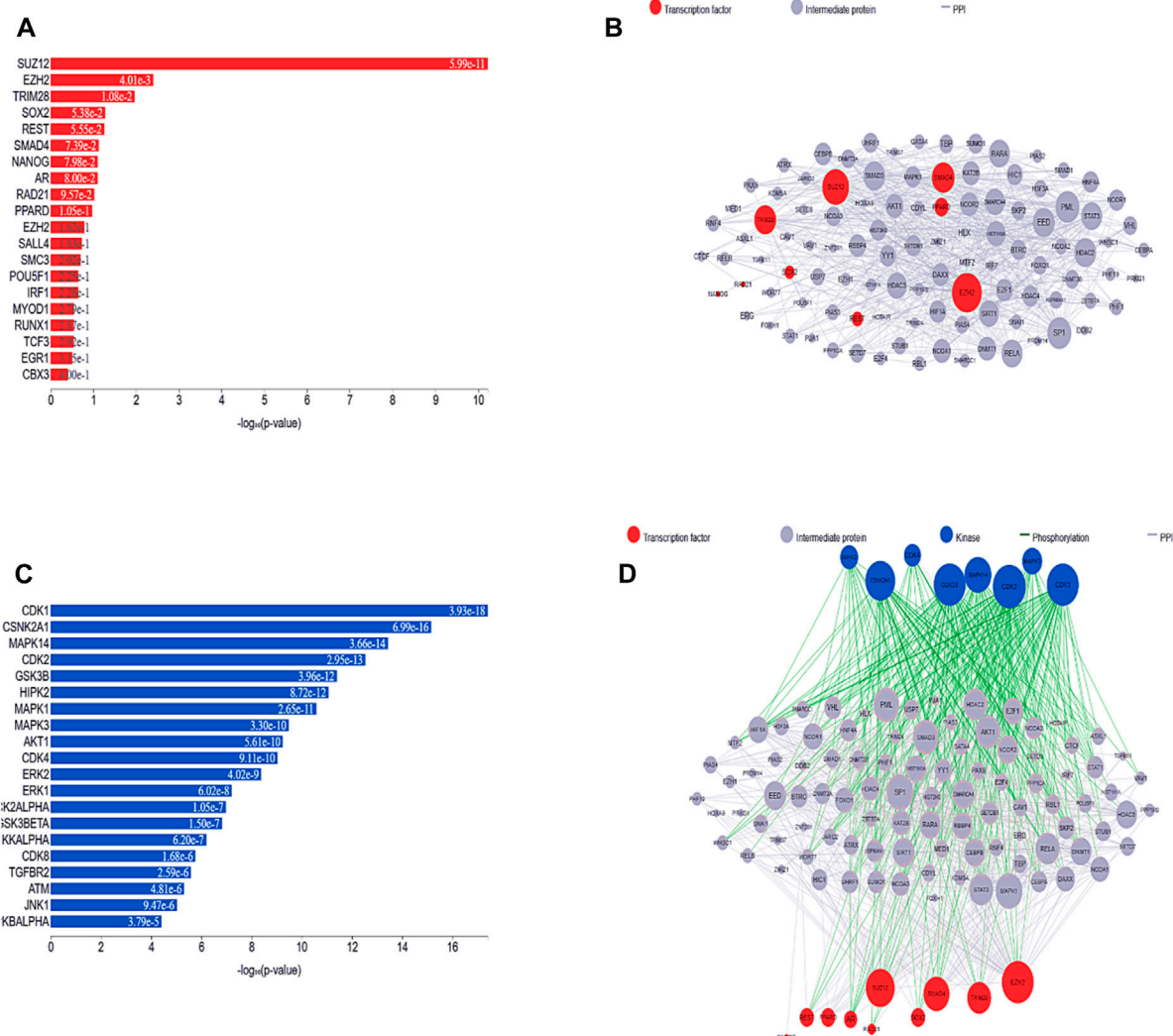


FIGURE 6

(A) Predicted transcription factors identified in the list of DEGs are shown in a bar chart. The height of each bar, which represents a transcription factor, reflects that factor score as determined by the hypergeometric p -value. (B) A subnetwork illustration is displayed, emphasizing interrelated transcription factors and the interacting proteins that go along with them. Pink nodes represent transcription factors, while gray nodes represent the proteins that connect them. The degree of connectedness between the nodes in this network determines how big they are. (C) Bar graph ranking the top predicted kinases. Hypergeometric p -values are used in the graph to display the scores of these kinases. (D) By investigating known protein-protein interactions between mutually overlapping differentially expressed genes (DEGs), one can gain insight into the involvement of transcription factors and kinases in the upstream pathway.

systems, simulation time intervals were extended for a further 100 ns. It was found that the system gains stability after 100 ns and remains equilibrated till 200-ns time intervals. Herein, the average RMSD recorded for both systems was 4.2 Å and 4.9 Å, respectively. It is possible that the natural flexibility of the N-terminal area is the cause of the oscillations shown in the simulation intervals. An overall structure may fluctuate because of the conformational changes introduced by the loop sections inside the N-terminal segment. These variations could be caused by the dynamic interactions the N-terminal residues with the surrounding solvent or other protein components. Furthermore, the RMSD for the protein target in Apo and complex states with the control inhibitor solasodine results in an average mean square value of 3.61 Å and 3.68 Å, respectively. Fluctuation was recorded in both

Apo and complex states with a time scale of 200 ns. This overall fluctuation was then observed in the residual system of the RMSF, where the N-terminal region of the protein target showed high conformational changes. The average RMSF recorded for the Apo state was 2.8 Å. Meanwhile, for the control complex, it was measured as 3.0 Å with a time scale of 200 ns, as shown in Figure 11. The binding poses during simulation time intervals were retrieved for all the complexes at the end of the simulation, where it was inferred that strong hydrogen bond linkages were observed with a time scale of 200 ns, as shown in Figure 12. Overall, the RMSD graph pattern supports any large domain alterations within the protein-ligand complex structural framework of carmustine complex and marimastat complex systems. Herein, the inhibitors remained inside the active site during the initial time frame but moved as

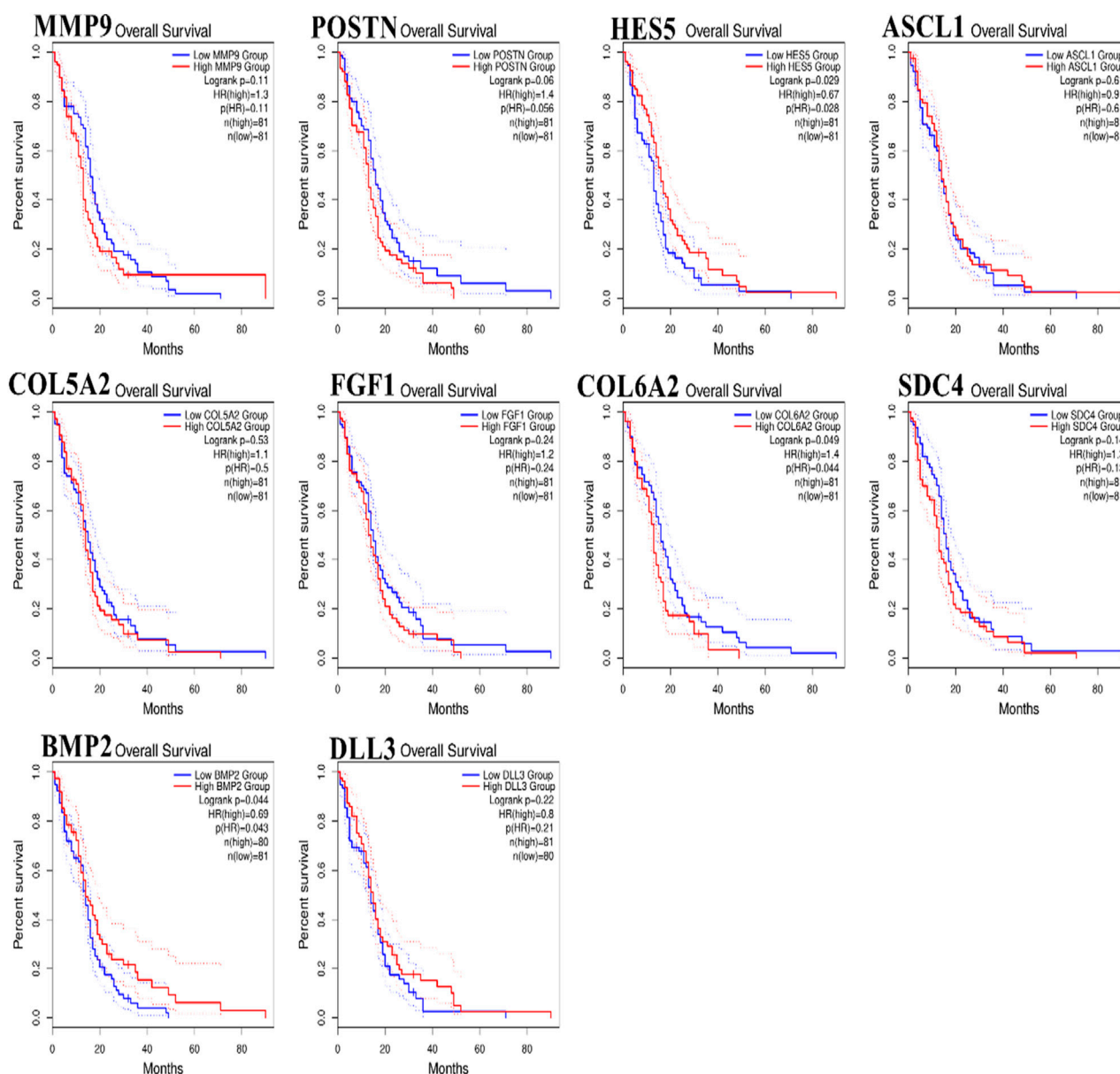


FIGURE 7
 Hub genes expressed in glioblastoma multiforme (GBM) patients were subject to Kaplan–Meier overall survival analysis. Using The Cancer Genome Atlas database as a base, curves were produced using Gene Expression Profiling Interactive Analysis ($p \leq 0.01$).

the time scale extended till the end of the simulation. On other hand, the ligands lomustine and temozolomide in the complex system were properly supplemented inside the binding site and did not destabilize the protein, as shown in Figure 10. Figure 13 shows RMSF values that detect the structure flexibility and volatility of Ca residues over time. A high pitch of fluctuation was recorded among the carmustine complex and marimastat complex systems. No such fluctuation was observed till 200-ns simulated time intervals, with a minor peak due to the loop region of the protein among lomustine and temozolomide in the complex system. Strong hydrogen bonds were monitored in the active zone of the MMP9 protein target. These residues include Asp187, Phe59, Gl57, and Pro54. The average RMSF of the carmustine complex and marimastat estimated from 200 ns was 1.4 Å and 1.7 Å, with a maximum peak of 4.1 Å and

6.3 Å, respectively, while substantial variations were noted at several residual points, and finally, at the conclusion of the graph for the other stable complex systems, a minor residual point was observed with an average RMSF of 1.0 Å and 0.7 Å, with no such displacement of atomic residues among the helix and sheet regions, which makes them highly stable systems. The binding pocket residues involved in RMSF include His188, Pro54, Asp187, Val53, Leu186, Gly185, Phe59, Phe62, Leu66, Ala143, Arg56, Arg51, Tyr50, Pro102, and Arg106. These residues may change as a result of ligands attaching to the active site. This implies that the flexibility or dynamics of these regions is higher. Active site residues may be involved in greater RMSF for a number of reasons; some of these residues have flexibility, whereas some are compact due to their carbon alpha background.

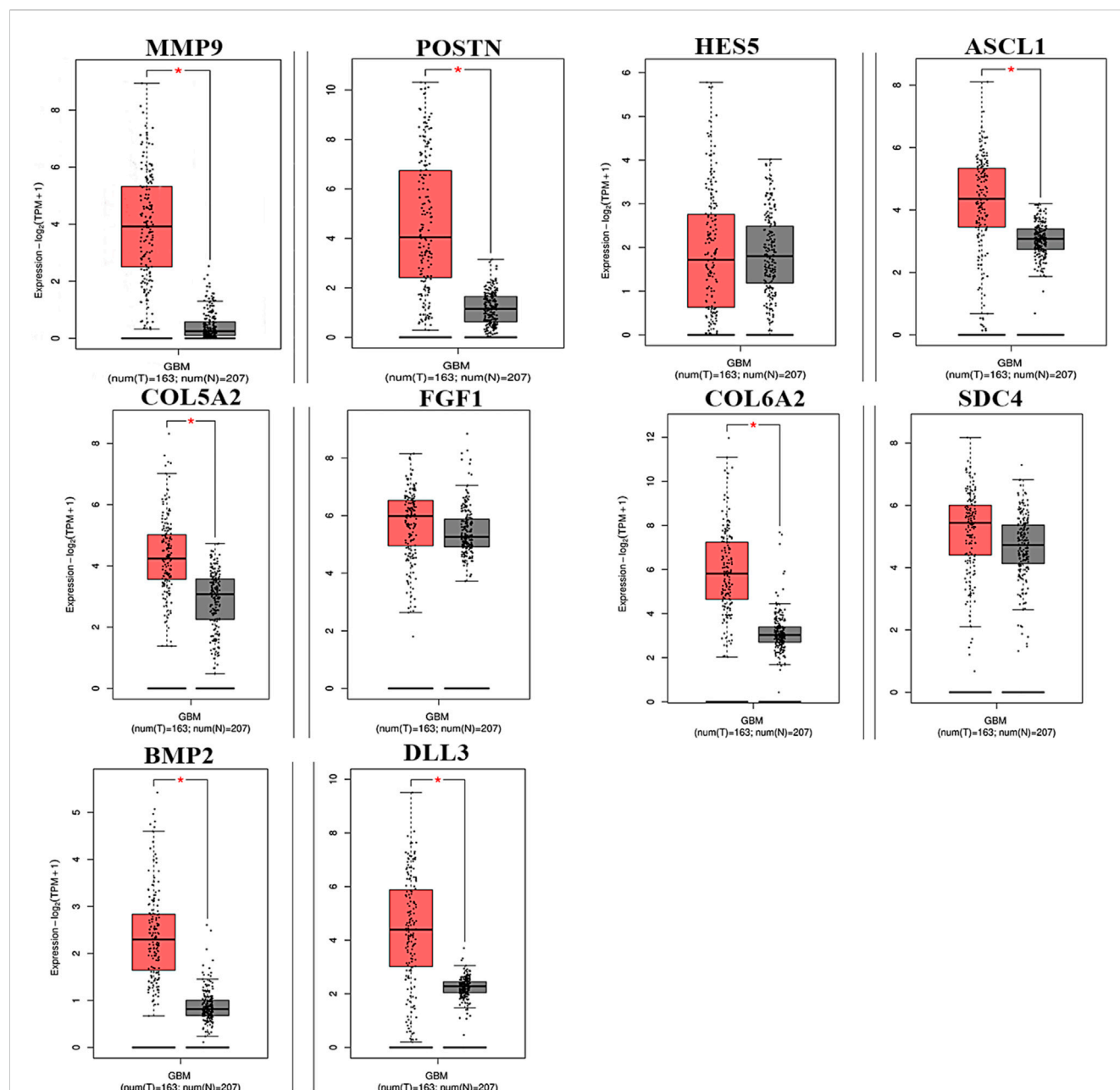


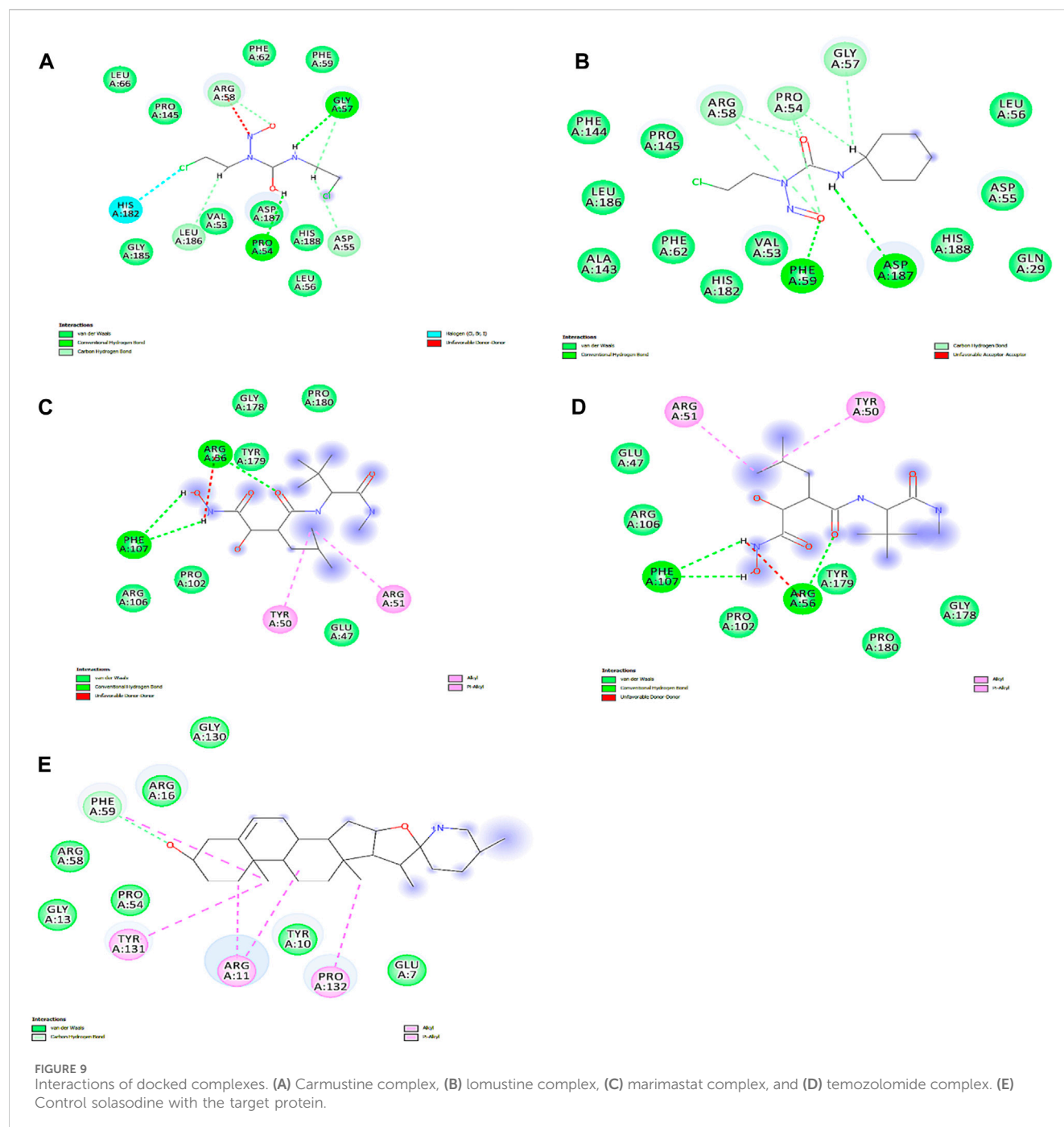
FIGURE 8

Hub genes expressed in GBM at different levels of relative expression. Relative gene expression levels for the tumor and normal samples are shown in red and black boxes, respectively. A total of 163 tumor samples and 207 normal samples from GEPIA are represented on the y-axis as the relative expression levels of genes in terms of log₂ (TPM +1) ($p \leq 0.01$) transcribing units per million (TPM).

3.9.1 Binding energy calculation

The binding free energies of all four ligands demonstrate their affinity for the protein active site. They are considered useful assessment criteria for leading chemical discovery and offer mechanistic insights into the binding ligands (Slynko et al., Citation 2016). Strong interactions between enzyme and inhibitor complexes were shown by the MM(PB/GB)SA technique of AMBER16, as shown in Table 3. The entropy computations were discarded because of a convergence issue. It was determined that in the instance of MM(PB/GB)SA, complex formation resulted in a highly favorable electrostatic contribution of -12.48 kcal/mol for

carmustine, -16.14 kcal/mol against lomustine, -10.97 kcal/mol for marimastat, -17.29 for temozolomide, and -13.35 kcal/mol for solasodine. Likewise, the dominating electrostatic energy contribution derived from MMPBSA was also identified. Furthermore, a highly beneficial contribution to inhibitor complexes comes from the van der Waal energy values of -25.10 kcal/mol (carmustine), -57.63 kcal/mol (lomustine), -30.98 kcal/mol (marimastat), and -51.17 kcal/mol (temozolomide), and the solasodine complex shows -34.54 from MMGBSA. Similarly, from MMPBSA, the following complexes had favorable van der Waal energies: the solvation energy with a binding



energy of 10.63 kcal/mol (carmustine), 9.03 kcal/mol (lomustine), 15.85 kcal/mol (marimastat), and 10.11 kcal/mol (temozolomide), whereas the control solasodine showed 11.23 kcal/mol after 200-ns time intervals. Finally, the total average binding energies regarding MMGB/PBSA were -24.95 kcal/mol for carmustine, -39.74 kcal/mol for lomustine, -31.07 kcal/mol for marimastat, -41.35 for temozolomide, and -28.55 kcal/mol for the control complex. These binding energies show that the simulated complexes lomustine and temozolomide had high binding affinities and remain stable during the whole time scale, which results in building a high ground for the experimentalist.

4 Discussion

Different digital methods are available for analyzing various kinds of genomic data, including the analysis of SNPs, genome-wide association studies (GWASs), and the analysis of gene expression using microarrays. These techniques are essential for gathering key knowledge about diseases, from diagnosis to treatment options (Akçay et al., 2018). All these methods, including genomics, proteomics, transcriptomics, metagenomics, epigenetics, and metabolomics, can be used to collect a variety of data from various phases. They frequently play a crucial role in the



mechanisms behind various diseases (Hu et al., 2019). The structural relationships between numerous proteins, which might differ between healthy and disease phenotypes, have a significant impact on various biological processes (Ni et al.,

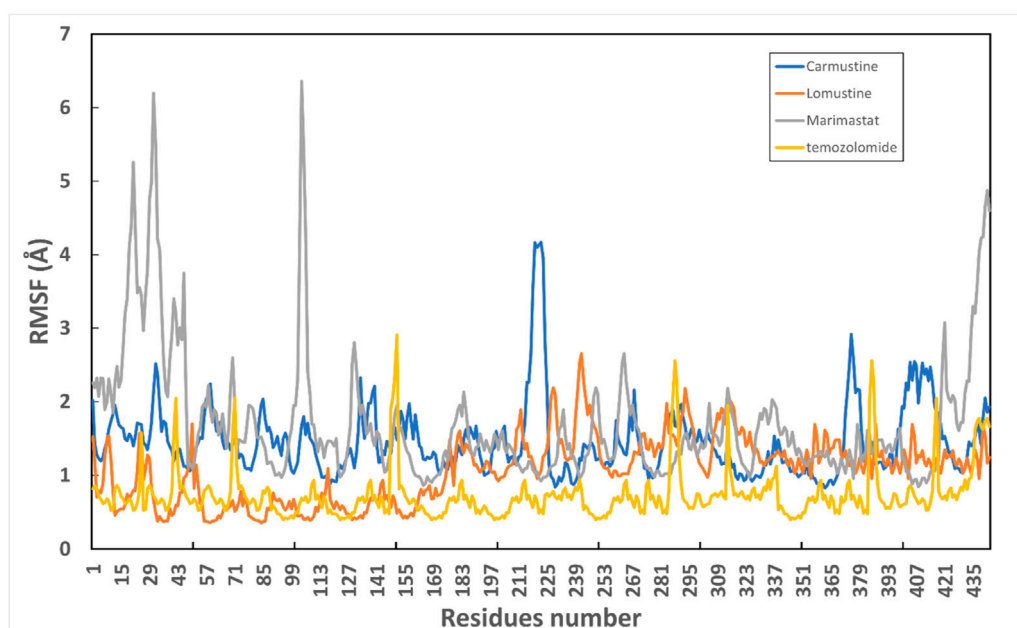


FIGURE 12

Binding pose of the interacting linkages at the end of simulation time intervals. Blue depicts hydrogen bonds inside the pocket residues along with other active residues throughout the simulation time intervals.

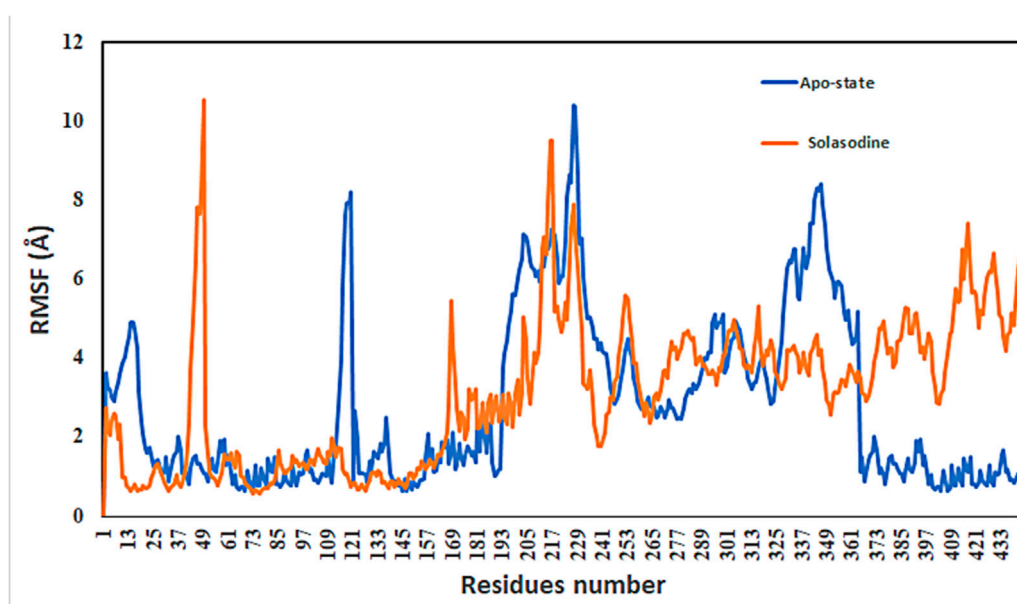


FIGURE 13

Graphical representation of RMSF of all four complex systems with the number of residues throughout simulation time intervals.

2009; Liu et al., 2018). Using microarray gene expression data analysis, one can identify targets for the creation of novel medications by identifying genes that are differentially expressed in the setting of a disease as opposed to the normal condition. The precision and robustness of detecting disease-linked biomarkers are improved by molecular network

interactions (Ma et al., 2016). Previous studies have demonstrated the value of such investigations in foretelling the core nodes and their key roles in a number of diseases (Nayariseri et al., 2013; Khan et al., 2018).

Compared to cases of GBM in advanced stages, the prognosis for early-stage cases is notably better. Through therapies including surgery,

TABLE 3 Binding free energies of all the compounds after 200-ns simulation time intervals.

Parameter	Carmustine	Lomustine	Marimastat	Temozolomide	Solasodine
MMGBSA					
van der Waals energy	−25.10	−57.63	−30.98	−51.17	−34.54
Electrostatic energy	−12.48	−16.14	−10.97	−17.29	−13.35
Total gas phase energy	−32.58	−48.77	−35.95	−55.46	−28.46
Total solvation energy	10.63	9.03	15.85	10.11	11.23
Net energy	−24.95	−39.74	−31.07	−41.35	−28.55
MMPBSA					
van der Waals energy	−25.10	−57.63	−30.98	−51.17	−34.54
Electrostatic energy	−12.48	−16.14	−10.97	−17.29	−13.35
Total gas phase energy	−32.58	−48.77	−35.95	−55.46	−28.46
Total solvation energy	10.17	9.30	15.97	10.37	10.21
Net energy	−24.41	−39.47	−31.98	−41.09	−29.53

chemotherapy, radiation therapy, or a combination of therapies, early-stage patients frequently experience significant cure rates. Patients with advanced-stage glioblastoma multiforme, however, experience extra challenges, mostly as a result of the tough nature of the disease and frequent inability to be cured (Henson, 2006).

In this study, we identified the DEGs in glioblastoma multiforme using microarray data. An enrichment evaluation identified 10 hub genes that may serve as targets for treatments. The top-ranking gene with the highest level was discovered to be MMP9. The role of MMP9 in glioblastoma multiforme has been explored by different studies, and the expression of MMP9 was reported to be significantly upregulated in highly malignant gliomas and correlates with the progression, suggesting a role for MMP9 in promoting the observed invasiveness (Rao et al., 1996). The development of GBM is demonstrated to be significantly influenced by POSTN (Park et al., 2016). HES5 was identified as a possible target for therapeutic intervention due to its involvement in a number of cancer-related processes, including increased cell proliferation (Wang et al., 2021). The other targets we identified are crucial for the development of GBM. The importance of these hub genes was highlighted by enrichment analysis, subnetwork building, and the inclusion of all hub genes within these subnetworks. The roles these genes play in various interrelated pathways were also clarified through the examination of KEGG pathways, molecular functions, cellular components, and biological processes. Determining the regulatory functions of transcription factors has been made possible by the identification of these factors and their roles within the enlarged network. The importance of ECM–receptor interaction and Notch signaling pathways in GBM has also been mentioned in earlier studies. Our KEGG pathways in this study include these specific pathways as well. Additionally, according to our research, GBM patients have considerable changes in immune-related pathways (Kanderi and Gupta, 2023b).

Furthermore, the drugs we discovered for these targets have given us a useful insight into how to potentially inhibit these targets and find brand-new FDA-approved medicines.

Furthermore, survival analysis extensively cleared the role of these hub genes in the progression of breast cancer. Because the compliance of patients to adjuvant treatment is different, this may influence the treatment result. This bioinformatics model suggested a catalog of candidate cellular proteins that could be the targets for breast cancer therapy. An advance computational strategy has been created to investigate the FDA-approved drug molecules screened against the MMP9 hub gene. While performing computer-aided drug design, the ligand structure has been refined against the therapeutic target. Furthermore, for validation of the docked complexes, MD simulation in the drug design process has far-reaching implications to study the dynamic behavior of receptor–ligand complexes. Molecular docking methods alone fail to address structural variability by limiting receptor flexibility and reducing the freedom of ligand-bound conformations. A simulation approach was used to examine the dynamic behavior of MMP9, which offered valuable insights into the structural basis of its potential as a drug.

5 Conclusion

In conclusion, our study not only provides important new understandings of putative biomarkers linked to patient prognoses for glioblastoma multiforme tumors but also emphasizes how critical it is to assess transcription factors and PPI networks as a solid framework. Identifying potential biomarkers and gaining a thorough grasp of the fundamental aspects affecting the prognosis of GBM patients are the main contributions of our research. All four of the compounds were confirmed as possible MMP9 inhibitors with high binding scores using the molecular docking approach. Furthermore, due to structural rearrangements in a physiochemical environment, MD simulations showed the extraordinary stability of receptor complexes including temozolomide and lomustine over a 200-ns time scale compared to Apo-state and with a control inhibitor system. Interestingly, small alterations to the side chain and loop

movement of these inhibitors showed very little effect on their stability. The potential of the chosen ligands as lead-like compounds was confirmed by the structural stability that was observed in the docked complexes after simulation. The binding energies finally calculated showed high binding affinities of the complexes throughout the time intervals. Using the strong insights obtained from this research, our study encourages researchers to investigate the creation of a modified and precisely targeted drug against GBM in light of these results. The continuous stability of the system throughout the simulations provides a solid basis for future research and development of successful glioblastoma multiforme therapies.

Data availability statement

The original contributions presented in the study are included in the article/[Supplementary Material](#); further inquiries can be directed to the corresponding authors.

Author contributions

SA: writing–original draft. AA: writing–original draft. AA: writing–original draft. FA: writing–review and editing. HA: writing–review and editing. AN: writing–review and editing. SR: writing–review and editing. MA: writing–review and editing.

Funding

The author(s) declare that financial support was received for the research, authorship, and/or publication of this article.

References

- Akcaay, I. M., Katrinli, S., Ozdil, K., Doganay, G. D., and Doganay, L. (2018). Host genetic factors affecting hepatitis B infection outcomes: insights from genome-wide association studies. *World J. Gastroenterol.* 24, 3347–3360. doi:10.3748/wjg.v24.i30.3347
- Alamri, M. A., and Tahir ul Qamar, M. (2024). Network pharmacology and molecular dynamic simulation integrated strategy for the screening of active components and mechanisms of phytochemicals from *Datura innoxia* on Alzheimer and cognitive decline. *J. Biomol. Struct. Dyn.*, 1–17. doi:10.1080/07391102.2024.2308756
- Alamri, M. A., and ul Qamar, M. T. (2023). Network pharmacology based virtual screening of Flavonoids from *Dodonaea angustifolia* and the molecular mechanism against inflammation. *Saudi Pharm. J.* 31, 101802. doi:10.1016/j.jsps.2023.101802
- Ashburner, M., Ball, C. A., Blake, J. A., Botstein, D., Butler, H., Cherry, J. M., et al. (2000). Gene ontology: tool for the unification of biology. The Gene Ontology Consortium. *Nat. Genet.* 25, 25–29. doi:10.1038/75556
- Biovia, D. S. (2017) *Discovery studio visualizer*. San Diego, CA, USA: Biovia.
- Brandes, U., Eiglsperger, M., Herman, I., Himsolt, M., and Marshall, M. S. (2001) *GraphML progress report ? Structural layer proposal*. Available at: <https://www.semanticscholar.org/paper/GraphML-Progress-Report-Structural-Layer-Proposal-Brandes-Eiglsperger/06429adb228b2241f2854819b6c9963120da6a48> (Accessed December 31, 2023).
- Brice, A. R., and Dominy, B. N. (2013). Examining electrostatic influences on base-flipping: a comparison of TIP3P and GB solvent models. *Commun. Comput. Phys.* 13, 223–237. doi:10.4208/cicp.210711.121011s
- Case, D. A., Babin, V., Berryman, J. T., Betz, R. M., Cai, Q., Cerutti, D. S., et al. (2014). The FF14SB force field. *Amber* 14, 29–31.
- Case, D. A., Betz, R. M., Cerutti, D. S., Cheatham, T., Darden, T., Duke, R. E., et al. (2016) *Amber 16*. San Francisco: University of California. doi:10.13140/rg.2.2.27958.70729
- Chambers, A. F., and Matrisian, L. M. (1997). Changing views of the role of matrix metalloproteinases in metastasis. *JNCI J. Natl. Cancer Inst.* 89, 1260–1270. doi:10.1093/jnci/89.17.1260
- Chen, E. Y., Tan, C. M., Kou, Y., Duan, Q., Wang, Z., Meirelles, G. V., et al. (2013a). Enrichr: interactive and collaborative HTML5 gene list enrichment analysis tool. *BMC Bioinforma.* 14, 128. doi:10.1186/1471-2105-14-128
- Chen, Y.-C., Hsiao, C.-C., Chen, K.-D., Hung, Y.-C., Wu, C.-Y., Lie, C.-H., et al. (2013b). Peripheral immune cell gene expression changes in advanced non-small cell lung cancer patients treated with first line combination chemotherapy. *PLoS One* 8, e57053. doi:10.1371/journal.pone.0057053
- Clough, E., and Barrett, T. (2016). The gene expression Omnibus database. *Methods Mol. Biol.* 1418, 93–110. doi:10.1007/978-1-4939-3578-9_5
- Dallakyan, S., and Olson, A. J. (2015). “Small-molecule library screening by docking with PyRx,” in *Chemical biology* (Berlin, Germany: Springer), 243–250.
- Davis, J. (2007). Bioinformatics and computational biology solutions using R and bioconductor. *J. Am. Stat. Assoc.* 102, 388–389. doi:10.1198/jasa.2007.s179
- Dobra, G., Gyukity-Sebestyén, E., Bukva, M., Harmati, M., Nagy, V., Szabó, Z., et al. (2023). MMP-9 as prognostic marker for brain tumours: a comparative study on serum-derived small extracellular vesicles. *Cancers* 15, 712. doi:10.3390/cancers15030712
- Ghafari-Fard, S., Safarzadeh, A., Taheri, M., and Jamali, E. (2023). Identification of diagnostic biomarkers via weighted correlation network analysis in colorectal cancer using a system biology approach. *Sci. Rep.* 13, 13637. doi:10.1038/s41598-023-40953-5
- Henson, J. W. (2006). Treatment of glioblastoma multiforme: a new standard. *Arch. Neurol.* 63, 337–341. doi:10.1001/archneur.63.3.337
- Hu, B., Chang, X., and Liu, X. (2019). Predicting functional modules of liver cancer based on differential network analysis. *Interdiscip. Sci.* 11, 636–644. doi:10.1007/s12539-018-0314-3

The authors acknowledge Prince Sattam bin Abdulaziz University for funding this research work through the project number PSAU/2023/03/27030.

Acknowledgments

The authors acknowledge Prince Sattam bin Abdulaziz University for funding this research work through the project number PSAU/2023/03/27030.

Conflict of interest

The authors declare that the research was conducted in the absence of any commercial or financial relationships that could be construed as a potential conflict of interest.

Publisher's note

All claims expressed in this article are solely those of the authors and do not necessarily represent those of their affiliated organizations, or those of the publisher, the editors, and the reviewers. Any product that may be evaluated in this article, or claim that may be made by its manufacturer, is not guaranteed or endorsed by the publisher.

Supplementary material

The Supplementary Material for this article can be found online at: <https://www.frontiersin.org/articles/10.3389/fphar.2024.1364138/full#supplementary-material>

- Hulsegge, I., Kommadath, A., and Smits, M. A. (2009). Globaltest and GOEAST: two different approaches for Gene Ontology analysis. *BMC Proc.* 3, S10. doi:10.1186/1753-6561-3-S4-S10
- Jabłońska-Trypuc, A., Matejczyk, M., and Rosochacki, S. (2016). Matrix metalloproteinases (MMPs), the main extracellular matrix (ECM) enzymes in collagen degradation, as a target for anticancer drugs. *J. Enzyme Inhib. Med. Chem.* 31, 177–183. doi:10.3109/14756366.2016.1161620
- Jiao, X., Sherman, B. T., Huang, D. W., Stephens, R., Baseler, M. W., Lane, H. C., et al. (2012). DAVID-WS: a stateful web service to facilitate gene/protein list analysis. *Bioinformatics* 28, 1805–1806. doi:10.1093/bioinformatics/bts251
- Kanderi, T., and Gupta, V. (2023a). Glioblastoma Multiforme. Available at: <https://www.ncbi.nlm.nih.gov/books/NBK558954> (Accessed December 31, 2023).
- Kanderi, T., and Gupta, V. (2023b). Glioblastoma multiforme. Available at: <http://www.ncbi.nlm.nih.gov/books/NBK558954/> (Accessed December 31, 2023).
- Khan, A., Ali, A., Junaid, M., Liu, C., Kaushik, A. C., Cho, W. C. S., et al. (2018). Identification of novel drug targets for diamond-blackfan anemia based on RPS19 gene mutation using protein-protein interaction network. *BMC Syst. Biol.* 12, 39. doi:10.1186/s12918-018-0563-0
- Khan, A., Rehman, Z., Hashmi, H. F., Khan, A. A., Junaid, M., Sayaf, A. M., et al. (2020). An integrated systems biology and network-based approaches to identify novel biomarkers in breast cancer cell lines using gene expression data. *Interdiscip. Sci.* 12, 155–168. doi:10.1007/s12539-020-00360-0
- Kumari, S., and Kumar, P. (2023). Design and computational analysis of an MMP9 inhibitor in hypoxia-induced glioblastoma multiforme. *ACS Omega* 8, 10565–10590. doi:10.1021/acsomega.3c00441
- Liu, S., Wang, X., Qin, W., Genchev, G. Z., and Lu, H. (2018). Transcription factors contribute to differential expression in cellular pathways in lung adenocarcinoma and lung squamous cell carcinoma. *Interdiscip. Sci.* 10, 836–847. doi:10.1007/s12539-018-0300-9
- Ma, L., Huang, Y., Zhu, W., Zhou, S., Zhou, J., Zeng, F., et al. (2011). An integrated analysis of miRNA and mRNA expressions in non-small cell lung cancers. *PLOS ONE* 6, e26502. doi:10.1371/journal.pone.0026502
- Ma, R., Wang, C., Wang, J., Wang, D., and Xu, J. (2016). miRNA-mRNA interaction network in non-small cell lung cancer. *Interdiscip. Sci.* 8, 209–219. doi:10.1007/s12539-015-0117-8
- Mannello, F., Tonti, G., and Papa, S. (2005). Matrix metalloproteinase inhibitors as anticancer therapeutics. *Curr. Cancer Drug Targets* 5, 285–298. doi:10.2174/1568009054064615
- Mondal, S., Adhikari, N., Banerjee, S., Amin, S. A., and Jha, T. (2020). Matrix metalloproteinase-9 (MMP-9) and its inhibitors in cancer: a minireview. *Eur. J. Med. Chem.* 194, 112260. doi:10.1016/j.ejmech.2020.112260
- Nayariseri, A., Yadav, M., and Wishard, R. (2013). Computational evaluation of new homologous down regulators of Translationally Controlled Tumor Protein (TCTP) targeted for tumor reversion. *Interdiscip. Sci.* 5, 274–279. doi:10.1007/s12539-013-0183-8
- Ni, Q.-S., Wang, Z.-Z., Li, G.-G., Wang, G.-Y., and Zhao, Y.-J. (2009). Effect of the quality of the interaction data on predicting protein function from protein-protein interactions. *Interdiscip. Sci. Comput. Life Sci.* 1, 40–45. doi:10.1007/s12539-008-0015-4
- Noor, F., Ashfaq, U. A., Bakar, A., Allemailem, K. S., Alharbi, B. F., Al-Megrin, W. A. I., et al. (2023a). Discovering common pathogenic processes between COVID-19 and HFRS by integrating RNA-seq differential expression analysis with machine learning. *Front. Microbiol.* 14, 1175844. doi:10.3389/fmicb.2023.1175844
- Noor, F., Asif, M., Ashfaq, U. A., Qasim, M., and Tahir ul Qamar, M. (2023b). Machine learning for synergistic network pharmacology: a comprehensive overview. *Briefings Bioinforma.* 24, bbad120. doi:10.1093/bib/bbad120
- Oany, A. R., Mia, M., Pervin, T., Alyami, S. A., and Moni, M. A. (2021). Integrative systems biology approaches to identify potential biomarkers and pathways of cervical cancer. *J. Pers. Med.* 11, 363. doi:10.3390/jpm11050363
- Pan, J., Liu, B., and Dai, Z. (2023). The role of a lung vascular endothelium enriched gene TMEM100. *Biomedicines* 11, 937. doi:10.3390/biomedicines11030937
- Park, S. Y., Piao, Y., Jeong, K. J., Dong, J., and de Groot, J. F. (2016). Periostin (POSTN) regulates tumor resistance to antiangiogenic therapy in glioma models. *Mol. Cancer Ther.* 15, 2187–2197. doi:10.1158/1535-7163.MCT-15-0427
- Rao, J. S., Yamamoto, M., Mohaman, S., Gokaslan, Z. L., Fuller, G. N., Stetler-Stevenson, W. G., et al. (1996). Expression and localization of 92 kDa type IV collagenase/gelatinase B (MMP-9) in human gliomas. *Clin. Exp. Metastasis* 14, 12–18. doi:10.1007/BF00157681
- Roe, D. R., and Cheatham, T. E. (2013). PTRAJ and CPTRAJ: software for processing and analysis of molecular dynamics trajectory data. *J. Chem. Theory Comput.* 9, 3084–3095. doi:10.1021/ct400341p
- Schröder, M. S., Culhane, A. C., Quackenbush, J., and Haibe-Kains, B. (2011). survcomp: an R/Bioconductor package for performance assessment and comparison of survival models. *Bioinformatics* 27, 3206–3208. doi:10.1093/bioinformatics/btr511
- Shannon, P., Markiel, A., Ozier, O., Baliga, N. S., Wang, J. T., Ramage, D., et al. (2003). Cytoscape: a software environment for integrated models of biomolecular interaction networks. *Genome Res.* 13, 2498–2504. doi:10.1101/gr.1239303
- Sprenger, K. G., Jaeger, V. W., and Pfäendtner, J. (2015). The general AMBER force field (GAFF) can accurately predict thermodynamic and transport properties of many ionic liquids. *J. Phys. Chem. B* 119, 5882–5895. doi:10.1021/acs.jpcc.5b00689
- Srivastava, M., Mittal, L., Kumari, A., and Asthana, S. (2021). Molecular dynamics simulations reveal the interaction fingerprint of remdesivir triphosphate pivotal in allosteric regulation of SARS-CoV-2 RdRp. *Front. Mol. Biosci.* 8, 639614. doi:10.3389/fmolb.2021.639614
- Stacklies, W., Redestig, H., Scholz, M., Walther, D., and Selbig, J. (2007). pcaMethods—a bioconductor package providing PCA methods for incomplete data. *Bioinformatics* 23, 1164–1167. doi:10.1093/bioinformatics/btm069
- Stetler-Stevenson, W. G. (1990). Type IV collagenases in tumor invasion and metastasis. *Cancer Metastasis Rev.* 9, 289–303. doi:10.1007/BF00049520
- Su, L., Meng, X., Ma, Q., Bai, T., and Liu, G. (2018). LPRP: a gene-gene interaction network construction algorithm and its application in breast cancer data analysis. *Interdiscip. Sci. Comput. Life Sci.* 10, 131–142. doi:10.1007/s12539-016-0185-4
- Szklarczyk, D., Franceschini, A., Wyder, S., Forslund, K., Heller, D., Huerta-Cepas, J., et al. (2015). STRING v10: protein-protein interaction networks, integrated over the tree of life. *Nucleic Acids Res.* 43, D447–D452. doi:10.1093/nar/gku1003
- Tang, Z., Li, C., Kang, B., Gao, G., Li, C., and Zhang, Z. (2017). GEPIA: a web server for cancer and normal gene expression profiling and interactive analyses. *Nucleic Acids Res.* 45, W98–W102. doi:10.1093/nar/gkx247
- Wang, Y., Sun, Q., Geng, R., Liu, H., Yuan, F., Xu, Y., et al. (2021). Notch intracellular domain regulates glioblastoma proliferation through the Notch1 signaling pathway. *Oncol. Lett.* 21, 303–307. doi:10.3892/ol.2021.12564
- Wishart, D. S., Feunang, Y. D., Guo, A. C., Lo, E. J., Marcu, A., Grant, J. R., et al. (2018). DrugBank 5.0: a major update to the DrugBank database for 2018. *Nucleic Acids Res.* 46, D1074–D1082. doi:10.1093/nar/gkx1037
- Woods, C. W., Bressler, A. M., LiPuma, J. J., Alexander, B. D., Clements, D. A., Weber, D. J., et al. (2004). Virulence associated with outbreak-related strains of burkholderia cepacia complex among a cohort of patients with bacteremia. *Clin. Infect. Dis.* 38, 1243–1250. doi:10.1086/383313
- Wrensch, M., Jenkins, R. B., Chang, J. S., Yeh, R.-F., Xiao, Y., Decker, P. A., et al. (2009). Variants in the CDKN2B and RTEL1 regions are associated with high-grade glioma susceptibility. *Nat. Genet.* 41, 905–908. doi:10.1038/ng.408
- Xia, J., Benner, M. J., and Hancock, R. E. W. (2014). NetworkAnalyst—integrative approaches for protein-protein interaction network analysis and visual exploration. *Nucleic Acids Res.* 42, W167–W174. doi:10.1093/nar/gku443
- Xia, J., Gill, E. E., and Hancock, R. E. W. (2015). NetworkAnalyst for statistical, visual and network-based meta-analysis of gene expression data. *Nat. Protoc.* 10, 823–844. doi:10.1038/nprot.2015.052



OPEN ACCESS

EDITED BY

Raghuveera Kumar Goel,
Boston University, United States

REVIEWED BY

Fatemeh Saheb Sharif-Askari,
University of Sharjah, United Arab Emirates
Liang Guo,
Bristol Myers Squibb, United States

*CORRESPONDENCE

Jorge Berlanga-Acosta,
✉ jorge.berlanga@cigb.edu.cu

RECEIVED 16 March 2024

ACCEPTED 06 May 2024

PUBLISHED 30 May 2024

CITATION

Berlanga-Acosta J, Cibrian D,
Valiente-Mustelier J, Suárez-Alba J,
García-Ojalvo A, Falcón-Cama V, Jiang B,
Wang L and Guillén-Nieto G (2024), Growth
hormone releasing peptide-6 (GHRP-6)
prevents doxorubicin-induced myocardial and
extra-myocardial damages by activating
prosurvival mechanisms.
Front. Pharmacol. 15:1402138.
doi: 10.3389/fphar.2024.1402138

COPYRIGHT

© 2024 Berlanga-Acosta, Cibrian, Valiente-
Mustelier, Suárez-Alba, García-Ojalvo, Falcón-
Cama, Jiang, Wang and Guillén-Nieto. This is an
open-access article distributed under the terms
of the [Creative Commons Attribution License](#)
(CC BY). The use, distribution or reproduction in
other forums is permitted, provided the original
author(s) and the copyright owner(s) are
credited and that the original publication in this
journal is cited, in accordance with accepted
academic practice. No use, distribution or
reproduction is permitted which does not
comply with these terms.

Growth hormone releasing peptide-6 (GHRP-6) prevents doxorubicin-induced myocardial and extra-myocardial damages by activating prosurvival mechanisms

Jorge Berlanga-Acosta ^{1*}, Danay Cibrian ¹,
Juan Valiente-Mustelier ², José Suárez-Alba ¹,
Ariana García-Ojalvo ¹, Viviana Falcón-Cama ¹,
Baohong Jiang ³, Linlin Wang ³ and
Gerardo Guillén-Nieto ¹

¹Center for Genetic Engineering and Biotechnology, Playa, Cuba, ²Institute of Cardiology and Cardiovascular Surgery, Havana, Cuba, ³Shanghai Institute of Materia Medica, Chinese Academy of Sciences, Shanghai, China

Introduction: Dilated cardiomyopathy (DCM) is a fatal myocardial condition with ventricular structural changes and functional deficits, leading to systolic dysfunction and heart failure (HF). DCM is a frequent complication in oncologic patients receiving Doxorubicin (Dox). Dox is a highly cardiotoxic drug, whereas its damaging spectrum affects most of the organs by multiple pathogenic cascades. Experimentally reproduced DCM/HF through Dox administrations has shed light on the pathogenic drivers of cardiotoxicity. Growth hormone (GH) releasing peptide 6 (GHRP-6) is a GH secretagogue with expanding and promising cardioprotective pharmacological properties. Here we examined whether GHRP-6 administration concomitant to Dox prevented the onset of DCM/HF and multiple organs damages in otherwise healthy rats.

Methods: Myocardial changes were sequentially evaluated by transthoracic echocardiography. Autopsy was conducted at the end of the administration period when ventricular dilation was established. Semiquantitative histopathologic study included heart and other internal organs samples. Myocardial tissue fragments were also addressed for electron microscopy study, and characterization of the transcriptional expression ratio between Bcl-2 and Bax. Serum samples were destined for REDOX system balance assessment.

Results and discussion: GHRP-6 administration in parallel to Dox prevented myocardial fibers consumption and ventricular dilation, accounting for an effective preservation of the LV systolic function. GHRP-6 also attenuated extracardiac toxicity preserving epithelial organs integrity, inhibiting interstitial fibrosis, and ultimately reducing morbidity and mortality. Mechanistically, GHRP-6 proved to sustain cellular antioxidant defense,

upregulate prosurvival gene Bcl-2, and preserve cardiomyocyte mitochondrial integrity. These evidences contribute to pave potential avenues for the clinical use of GHRP-6 in Dox-treated subjects.

KEYWORDS

doxorubicin, dilated cardiomyopathy, GHRP-6, heart failure, ventricular dilation

Introduction

Dilated cardiomyopathy (DCM) is a group of heterogeneous myocardial diseases, with structural and functional disorders defined by left ventricular (LV) or biventricular dilation, along with systolic dysfunction with abnormal left ventricle ejection fraction (LVEF) (Schultheiss et al., 2019). DCM pathophysiological changes include a decrease in stroke volume and cardiac output, impaired ventricular filling and an increase in end-diastolic pressure. Diastolic function is also impaired accounting for a reduction in myocardial relaxation, and consequently a poor ventricular filling (Riehle and Bauersachs, 2019; Schultheiss et al., 2019). This is a common and highly prevalent condition leading to heart failure (HF) (Hershberger et al., 2013). Despite the remarkable progress in HF control therapies over recent decades, DCM mortality rates are high, remaining as one of the leading causes of heart transplantation (Benjamin et al., 2018; Ferreira et al., 2023).

Genetic mutations are reported to account for 35% of DCM cases, whereas other lifetime acquired causes include viral myocarditis, toxins, endocrine-metabolic disturbances, and exposure to chemotherapy drugs in cancer-affected patients (Imanaka-Yoshida, 2020). Doxorubicin (Dox) is a chemotherapeutic anthracycline with proved efficacy against different cancer types but with remarkable cardiotoxicity. DCM and progressive HF are frequently-registered adversities in Dox-treated patients (Robert Li et al., 2023). Hence, different cardiovascular-damage drivers have been attributed to Dox, including myocardial cells DNA damage, interstitial inflammation, oxidative stress cytotoxicity, cardiomyocytes apoptosis, mitochondrial damages, and dysregulation of autophagy (Wang T-H. et al., 2023). Dox toxicity is not solely restricted to myocardial tissue; its cytotoxic effects impact a broad constellation of epithelial, mesenchymal, and nervous cells, affecting most organ systems (Alhowail et al., 2019; Prathumsap et al., 2020). Dox at different doses and treatment regimens has been for years a valuable tool for the experimental reproduction of DCM/HF, which has contributed to elucidate molecular pathogenic determinants of its underlying cardiotoxicity (Hullin et al., 2018; Lother et al., 2018; Zhu et al., 2019).

Growth hormone (GH) releasing peptide 6 (GHRP-6) (His-DTrp-Ala-Trp-DPhe-Lys-NH₂) is a small molecular weight peptide integrated into the GHRP family, which has progressively broadened its pharmacological spectrum from a GH-secretagogue to a promising cardioprotective agent (Berlanga-Acosta et al., 2017). This agent is a ghrelin analog that binds and activates the GH secretagogue receptor 1a (GHSR1a) (Xiao et al., 2020), whereas it also binds to the ectodomain of CD36 receptor (Demers et al., 2004).

GHRP-6 has proved to prevent and attenuate cardiac cell death and LV failure in a variety of experimental scenarios (Lucchesi, 2004;

Xu et al., 2005; Berlanga-Acosta et al., 2016; Berlanga-Acosta et al., 2017). Furthermore, we have also identified GHRP-6 anti-fibrotic properties which may contribute to mitigate the systemic complications of Dox administration (Berlanga-Acosta et al., 2012; Mendoza et al., 2016; Fernandez-Mayola et al., 2018). Beyond its ability to enhance the survival of a diversity of cells before an otherwise lethal stress, GHRP-6 and other mimetic ligands to the GHSR1a and CD36 receptors, play an agonistic effect on the GH/IGF-1 axis promoting a systemic anabolic response, and counterbalancing catabolism and sarcopenia (Giorgioni et al., 2022).

Here we describe that: (Schultheiss et al., 2019): GHRP-6 administration concomitant to Dox challenge prevented the onset of DCM/HF, (Riehle and Bauersachs, 2019), GHRP-6 significantly reduced animals' morbidity and mortality, attenuated epithelial damages in a multi-organs spectrum, and inhibited Dox-related parenchymal fibrotic induration, (Hershberger et al., 2013), GHRP-6 triggered multiple defense mechanisms, involving oxidative stress reduction and activation of detoxifying enzymes, enhancement of prosurvival gene expression, and cardiomyocytes mitochondrial structural preservation. To the best of our knowledge, this is the first demonstration on the GHRP-6 cardio and systemic protective and anti-fibrotic effects, in the scenario of Dox-related toxicity.

Materials and methods

Animals and ethics

Male Wistar rats with 200–250 g body weight and 9–10 weeks of age were used for the study. Rats were purchased from the National Center for Laboratory Animals Breeding (CENPALAB) and housed in a certified room of the animal facility at the Center for Genetic Engineering and Biotechnology (CIGB). Three animals per cage were allocated under controlled environmental conditions. Rats were allowed free access to food and water. Animals' manipulation, care, and investigational procedures were declared in the experimental protocols and approved by the Institutional Animal Care and Welfare Committee of CIGB. Orbital blood samples were obtained under ether anesthesia. Animals were terminated by anesthesia overdose (250 mg/kg sodium pentobarbital).

Reagents, treatments, and DCM induction

Medical grade, commercially injectable solution doxorubicin hydrochloride (Dox) was acquired from Lemery SA pharmaceutical company (Mexico) at a concentration of 2 mg/mL. DCM/HF pathological model was induced through the intraperitoneal administration of Dox at 2 mg/kg twice a week

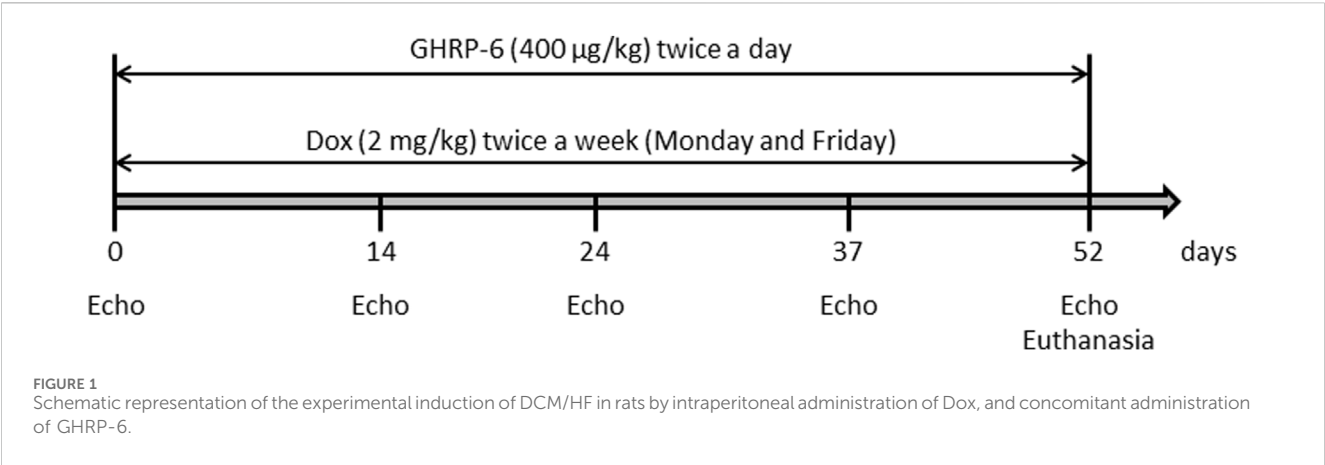


TABLE 1 Histological examination and damage scoring parameters.

Organ evaluated	Parameter evaluated	Evaluation procedure
Myocardial LV wall	% of damaged myofibrils. Damage criteria were: presence of granular basophilic material, loss of fibers, fiber thinning, tumefaction, fragmentation and reduction of eosin staining affinity	Ten random microscopic fields of longitudinal fibers (×20) were studied/ animal. The % of damaged fibers was determined, considering the total number of fibers evaluated in each field
Lungs	% of bronchi with mucosal necrosis	Ten random microscopic fields (×10) were studied per animal. The % of damaged bronchi was determined considering the total in each field
Kidneys	% of tubules with irreversible epithelial cells damages	Ten microscopic fields (×20) were studied per animal. The % of tubules irreversibly damaged was determined, out of the total in each field
Liver	Passive hepatic congestion	0- No congestion, 1- Mild congestion, 2- Evident congestion, 3- Severe congestion with a marked sinusoidal distortion

(Monday and Friday), for 52 days as described (Hayward and Hydock, 2007) (Figure 1). The hexapeptide GHRP-6 (His-d-Trp-Ala-Trp-d-Phe-Lys-NH2) was purchased from BCN Peptides (Barcelona, Spain). Fresh preparations were obtained by diluting the peptide in sterile normal saline solution to a final concentration of 400 µg/mL. Solutions were freshly prepared, conserved at 4°C and protected from light. GHRP-6 was intraperitoneally administered at a dose of 400 µg/kg.

Experimental protocols and study groups

The hypothesis for this study was that GHRP-6 concomitant administration to Dox treatment may attenuate myocardial structural and functional damages, and consequently, prevent the onset of DCM/HF. A total of 36 animals were used, distributed in three experimental groups with 12 rats each: (I)—A group of healthy not treated, sentinel animals was used to obtain echocardiographic and biochemical reference values at the end of the intoxication period. This is relevant considering that rats’ somatic maturation was still in progress during the study period (Cossio-Bolanos et al., 2013). (II)- Animals receiving GHRP-6 twice a day at a dose of 400 µg/kg concomitant to Dox. (III)- Animals receiving normal saline solution concomitant to Dox. Following to experimental groups formation and prior to Dox-administration regimen, all the rats were echocardiographically studied in order to obtain

baseline physiologic parameters. Subsequent serial echocardiographic evaluations were done during the Dox administration process on the following points: 14, 24, 37, and 52 days (Figure 1). For the later point, the rats had a Dox cumulative dose of 30 mg/kg and echocardiographic recordings indicated a clear LV deformity and functional failure, as described in previous studies (To et al., 2003). As mentioned, treatments with Dox and GHRP-6 were intraperitoneally administered until day 52 (see Figure 1 for experimental sequence).

Echocardiographic parameters

Prior to each echocardiography recording, animals were lightly sedated as recommended (Stein et al., 2007) with an intraperitoneal administration of ketamine (50 mg/kg) + xylazine (5 mg/kg), and placed in supine position in a stable horizontal plane. Once the animals were sedated and stabilized, transthoracic echocardiography recordings were carried out with a Sonos 5,500 equipment, coupled to a linear transducer of 11–15 MHz (Philips, United States). The M-mode structural parameters studied were: LV diastolic diameter (LVDd), LV systolic diameter (LVSD), inter-ventricular septum thickness in systole (IVSs), and LV posterior wall thickness in systole (LVWs). LVEF was considered the main functional parameter as previously indicated (Iwase et al., 2004).

TABLE 2 Primer sequences and amplification conditions.

Gen	Primers sequence	GenBank number	PCR Temp. (°C)	PCR product length (bp)
Bax	5'- TGA TTG CTG ACG TGG ACA CGG AC	236U23	68/94	321
	3'- TGA GCG AGG CGG TGA GGA CTC			
β-actin	5'-GGA GAT CGT GCG GGA CAT CAA GG	AY550069	68/94	482
	3'-GGC CGG ACT CGT CGT ACT CCT GC			
Bcl-2	5'- GCT ACC GTC GCG ACT TTG CAG AG	545U23	68/94	321
	3'- CAC TTG TGG CCC AGG TAT GCA CC			

TABLE 3 Body weight of the animals and relative organs weight index.

Groups	Body weight (g)	W.I. Heart	W.I. Lungs	W.I. Liver
Healthy sentinel	417.2 ± 27.2 (a)	0.28 ± 0.03 (b)	0.41 ± 0.07 (b)	3.54 ± 0.33 (c)
Saline	266.6 ± 32.5 (b)	0.51 ± 0.08 (a)	1.02 ± 0.28 (a)	6.79 ± 0.33 (a)
GHRP-6	295.5 ± 45.1 (b)	0.33 ± 0.05 (b)	0.62 ± 0.16 (b)	4.96 ± 0.51 (b)

The values are represented as the mean ± SD, per experimental group. The statistical analysis was made using an ANOVA, followed by the Newman-Keuls multiple comparison test. For each parameter, different letters (a, b or c) indicate statistically significant differences among the experimental groups, while equal letters indicate not significant differences, $p < 0.05$. W.I.: relative weight index.

Histopathologic evaluations

Animals were euthanized by anesthesia overdose at the end of the administration period. Alternatively, the rats that along the study evolved to a terminal irreversible clinical condition were sacrificed to ensure a proper autopsy and samples collection. Accordingly, these cases were included in the mortality record. Autopsy study was conducted following an internal protocol based on standard techniques (Scudamore et al., 2014). During the autopsies, gross pathological changes were described and recorded. Heart, lungs, and liver weights were used to calculate the relative organs weight indexes as described: Relative organ weight = [organ weight/body weight]×100 (Mossa et al., 2015). Representative fragments from apparently normal organs were also harvested. Hearts were sliced in four sagittal sections from apex to base as described (Li et al., 2019). Organs fragments and heart slices were 10% buffered formalin fixed and processed for paraffin embedding. Semi-thin sections (2–3 μm) were serially generated for subsequent hematoxylin/eosin staining. Semi-quantitative histological analyses of the heart, bronchial mucosa, kidneys, and liver passive congestion (Table 1) were conducted according to previous descriptions (Chen et al., 2016; Afsar et al., 2017). Histological images were obtained using an Olympus BX-53 light microscope (Olympus America Inc., United States) whereas the histological evaluations were independently and blindly performed by specialized researchers (JBA, DCV, JSA).

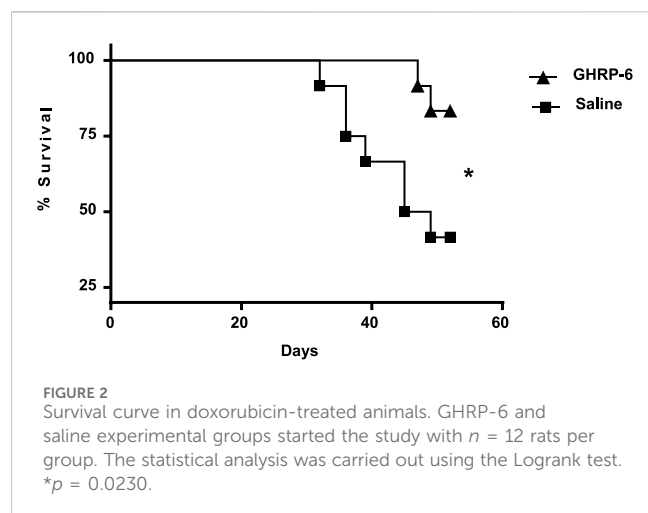
Electron microscopy study

Specimens were fixed in 3.2% glutaraldehyde and post-fixed in 1% osmium tetroxide, at 4°C and for 60 min, washed with PBS (0.1 M; pH 7.2) and dehydrated in increasing concentrations of ethanol at 4°C.

Inclusion was carried out as described (Glauert and Lewis, 1999). Ultrathin sections obtained with an ultramicrotome (NOVA, LKB, Germany), 400–500 Å thick; were placed on 400-hole copper-nickel grids, counterstained with saturated uranyl acetate and lead citrate, and subsequently examined with a JEOL JEM 2000 EX microscope (JEOL, Japan). A total of 20 photomicrographs at different magnifications of each sample collected were blindly analyzed by a qualified specialist (VFC). The presence of pathological changes in the ultrastructure of myofibrils, mitochondria, and intercellular junctions were qualitatively evaluated.

Serum biochemical analysis

Blood was collected from the retro-orbital plexus once the animals were anesthetized. Blood was centrifuged at 10,000 rpm for 15 min at 4°C to obtained serum. Serum samples were aliquoted and kept at –80°C for subsequent analysis. The concentration of total hydroperoxides (THP), malondialdehyde (MDA), and the activity of the enzymes superoxide dismutase (SOD) and catalase were determined using an UV/visible spectrophotometer Ultrospec 2000 (Pharmacia Biotech, United States). The quantification of THP and MDA contents was made using commercial kits Bioxytech H2O2-560 and Bioxytech LPO-586 (OXIS International Inc., United States), respectively, following the manufacturer’s instructions. Total SOD activity was evaluated by the classic method based on pyrogallol autoxidation as described (Rao et al., 2021). We consider 1 U of SOD as the amount of enzyme inhibiting 50% of pyrogallol autoxidation reaction at 25°C. Catalase activity was determined following the decomposition of the H2O2 at 240 nm in 10-s intervals for 1 min (Ajamieh et al., 2002). Alanine amino transferase (ALAT) serum levels were measured in an automatic analyzer (Hitachi 747, Germany), according to the manufacturer’s instructions.



Gene expression study

In order to evaluate the expression ratio between Bcl-2 and Bax as representative of pro-survival and apoptogenic gene, respectively; LV tissue fragments were collected from five rats of saline and GHRP-6 groups during the autopsy process. Fragments were stored in liquid nitrogen until processing. Total RNA purification was performed by treatment with Tri-Reagent (Sigma-Aldrich, United States), following the manufacturers' instructions. The quality and quantity of the purified RNA was estimated by determining the absorbance at 260 nm and 280 nm, together with the visualization by electrophoresis of the two ribosomal RNA bands. The contaminating genomic DNA was removed by digestion with the enzyme DNaseI (Epicentre Technologie, United States), free of RNase activity, following the manufacturers' instructions. An amount of 1 μ g of the RNA previously treated with DNaseI was used for the RT-PCR technique, using the commercial GeneAmp RNA PCR Core Kit (Applied Biosystems, United States), according to the manufacturers' specifications. The amplification of the genes of interest was carried out using the primers and temperatures specified below (Table 2). β -actin gene expression was used to normalize the expression of the target genes. The bands obtained were detected by applying 1/10 or 1/5 of the volume of the amplification reaction in a 1% agarose gel electrophoresis. The intensity of the bands was quantified using Kodak ID 3.6 software (Kodak, United States).

Statistical analyses

The statistical analyses were made with GraphPad Prism (California, United States), version 8.0.2. The Goodness of Fit tests to the normal distribution (Kolmogorov-Smirnov test) were made for all data, as well as the homogeneity of variances (Bartlett test). Given that in all cases the assumptions of normal distribution and homogeneity of variances were fulfilled, we carried out comparisons between pairs of groups using the Student's t -test. For multiple

comparisons, we used one-way or two-way analyses of variance (ANOVA) followed by the Newman Keuls, Sidak's or Dunnett's multiple comparisons tests. The results of survival were compared through the Logrank test. In all cases, the values of $p < 0.05$ were interpreted as indicative of statistically significant differences.

Results

Clinical evolution and mortality

Having completed 3 weeks of Dox administration, animals began to show a cachectic process evolving to clinical deterioration. Rats from both GHRP-6 and saline groups showed no differences in body weight loss along the Dox administration period (Table 3, $p = 0.1943$), which significantly differed to the body weights recorded for the healthy sentinel rats ($p < 0.0001$) on day 52.

Tendency to isolation, prostration, bristly hair, and dorsal hunched posture was observed in most of the animals exposed to Dox. Autopsies showed that GHRP-6 intervention significantly reduced the relative weights of the heart and lungs as compared to saline (all $p < 0.05$). No statistical difference was detected in the relative weights of the heart and lungs from the GHRP-6 intervention, and those of the healthy sentinel animals (Table 3). Most importantly, GHRP-6 intervention allowed for a significant survival percentage (84%) as compared to saline group (42%), (Figure 2).

GHRP-6 contributed to preserve ventricular morphology and physiology

The rats included in the study exhibited normal morphologic and functional baseline echocardiographic parameters. Average baseline LVEF recording was $92.78\% \pm 1.84\%$. The earliest myocardial morphological change in the saline group was detected on day 24th of the experiment, given by a significant increase ($p = 0.0279$) in the LV systolic diameter, (Figure 3A), and followed by a significantly larger LV diastolic diameter after 37 days of Dox administration ($p < 0.0001$) (Figure 3B). These impairments appeared concomitant to a significant thinning of the septum and the posterior wall in systole ($p < 0.05$) (Figures 3C, D) in relation to the baseline data. The myocardial structural deterioration translated in a significant reduction of the LVEF in the saline group when compared to its baseline values. Significant differences were also observed when the saline group LVEF was compared to the healthy sentinel and GHRP-6 groups. These alterations were progressively worse in correspondence with Dox cumulative dose. On day 52, saline group exhibited a decrease of about 30% in LVEF (Figure 3E). Concomitant GHRP-6 intervention prevented LV dilation regardless of the dose of Dox. Accordingly, no statistical differences in the diastolic and systolic diameters were detected in reference to its baseline data, and as compared to the healthy sentinel animals on day 52 (Figures 3A, B). Furthermore, GHRP-6 treated group also

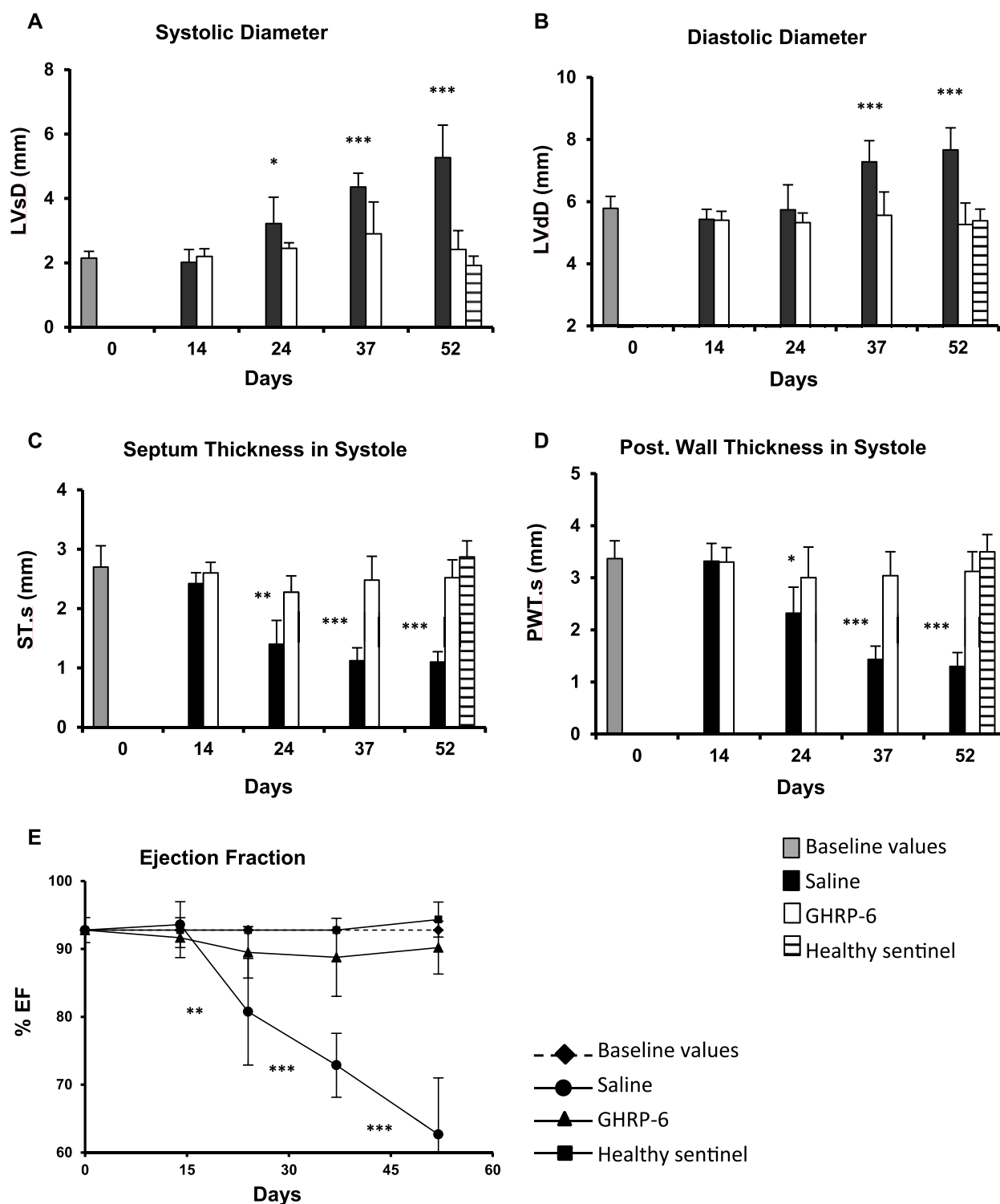


FIGURE 3 Echocardiographic characterization of morphologic and functional parameters in healthy and doxorubicin-treated animals. (A) Systolic diameter. (B) Diastolic diameter. (C) Septum thickness in systole. (D) Posterior wall thickness in systole. (E) LV ejection fraction. The data are represented as the mean \pm SD per experimental group. The baseline values correspond to pre-Dox administration phase. The statistical analyses were made using the unpaired Student's *t*-test. **p* < 0.05; ***p* < 0.01; ****p* < 0.001.

showed septal systolic thickness and posterior wall thickness values, similar to those measured in the healthy sentinel group (Figures 3C, D). Worth mentioning is that GHRP-6 group LVEF

figures, remained within the normal range during the entire evaluation period as compared to the healthy sentinel group recordings (Figure 3E, all *p* > 0.05).

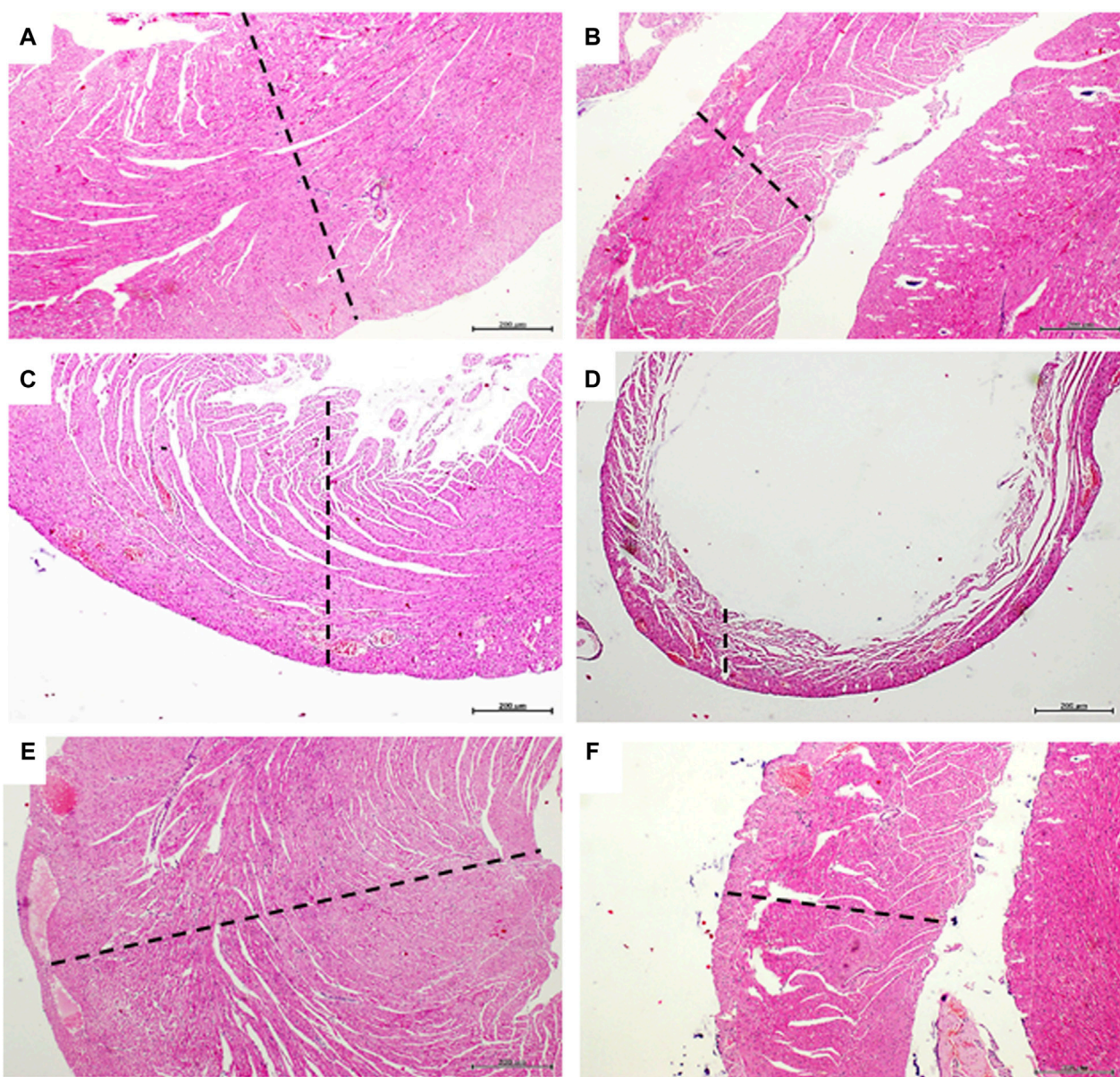


FIGURE 4

Myocardial histologic aspect of healthy and doxorubicin-treated rats. Microphotographs in the left column correspond to left ventricle. The right ventricle images are on the right column. **(A,B)** are representative images of left and right ventricle walls of animals from the healthy sentinel group where no evidence of pathologic changes were found. Tissue mass and fibers compactness are normal. **(C,D)** are images representing the major histopathologic damage brought about by Dox treatment in the saline group. It is evident the “loss-of-substance” by cardiomyocytes demise with evident wall thinning of both left and right ventricular walls. **(E,F)** are images representing the cardioprotective effect of GHRP-6. Myocardial cells demise and loss of ventricular tissue mass by Dox were evidently prevented by the concomitant intervention with the peptide. Dashed lines are introduced to facilitate the transmural view of ventricular walls. Autopsy collected samples and paraffin processing for semi-thin sections stained with H/E. For all, magnification is $\times 4$. Scale bar is 200 μm .

GHRP-6 intervention protected ventricular myofibrils from Dox toxicity

Figures 4A, B correspond to panoramic images of both ventricles free walls of rats from the healthy sentinel group, in which no histopathological damages were detected. As expected, Dox treatment produced a group of myocardial abnormalities on the saline-treated rats that encompassed: myofibrils thinning, wall slimming (Figures 4C, D), fibers undulation, fractures, and focal loss

of eosin staining affinity. GHRP-6 administration however, exerted a “sparing effect” on the ventricular myofibrils against Dox-induced damages. Myocardial histopathological damages attributable to Dox were minimal, whereas no microscopic differences were detected between GHRP-6 rats and the intact sentinel animals (Figures 4E, F). This microscopic cardioprotective effect was further supported by the quantitative morphometric analysis, attesting a significant reduction ($p < 0.00019$) in the percentage of damaged ventricular myofibrils (Saline: 91.0 ± 4.4 vs. GHRP-6: 42.2 ± 8.6).

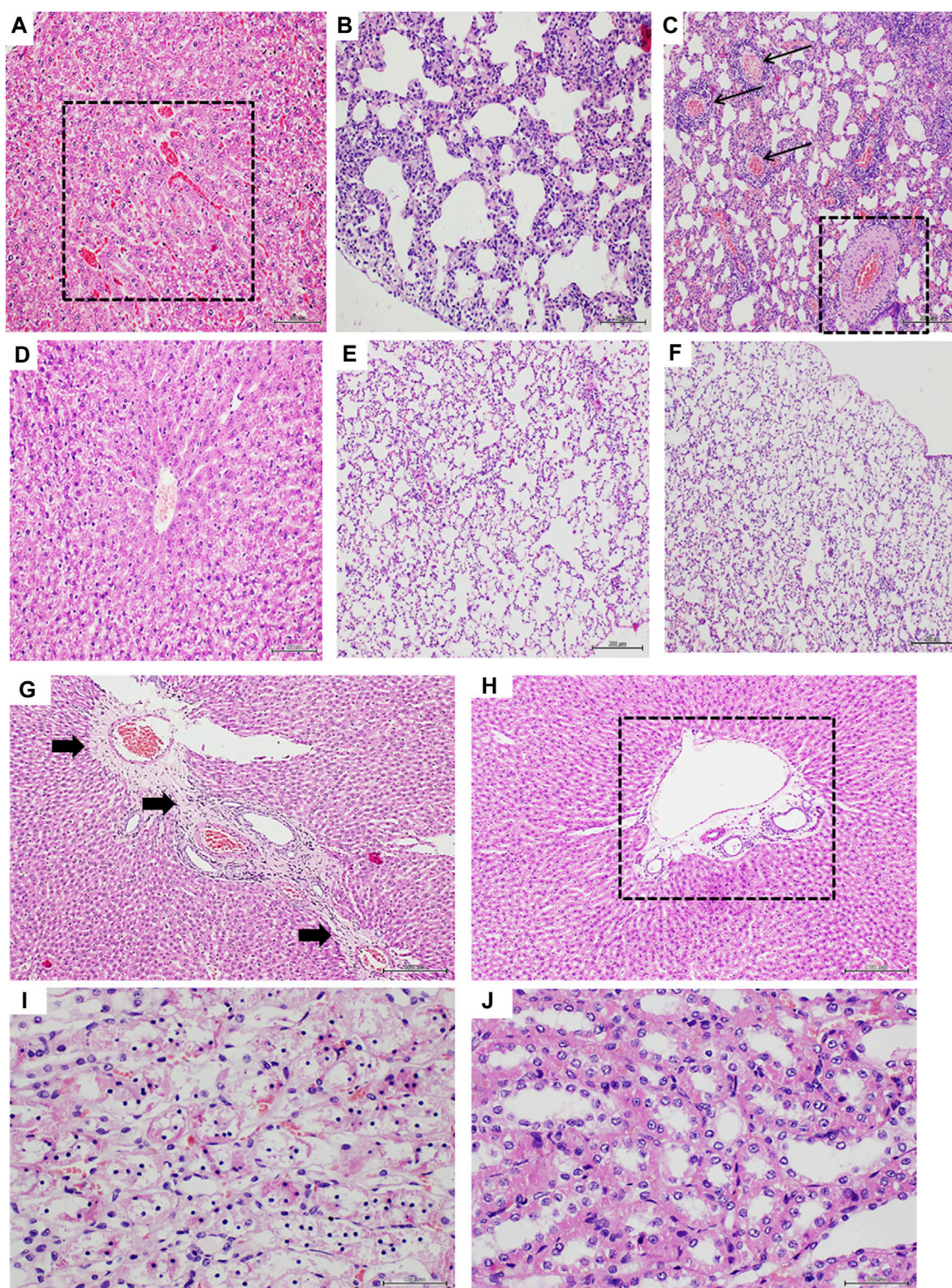


FIGURE 5

Histologic characterization of doxorubicin-induced extracardiac damages. (A–C) correspond to liver and lung parenchyma of saline group. (D–F) are representative of the effect of GHRP-6 treatment in these organs. (A) Liver section exhibiting passive congestion given by sinusoidal blood congestion (square). Magnification $\times 20$. (B) is representative of Dox-associated lung damage, expressed by a dramatic alveolar walls thickening and mixed hypercellularity, including round inflammatory cells. Magnification $\times 20$. (C) Shows the intense vessels congestion in lungs of control saline-treated rats. The arrows point to congested veins, and the square to a congested artery with a remarkable wall thickening. Note also the alveolar walls congestion and hypercellularity. Magnification $\times 10$. (D) Image representative of a liver with no venular/sinusoidal congestion in animals treated with GHRP-6. Magnification $\times 20$. (E) The image shows thin and normo-cellular alveolar walls with no collapse or reduction of the functional intra-alveolar space. Magnification $\times 20$. (F) Image of a normal lung parenchyma with no vascular congestion nor infiltration of inflammatory cells in animals receiving GHRP-6. Magnification $\times 10$. (G) is a representative image of the fibrotic process triggered by the Dox treatment in the liver of saline control group. Black arrows (Continued)

FIGURE 5 (Continued)

indicate the long trajectory of a thick fibrotic cord that crosses around veins. Magnification $\times 10$. (H) The image shows the effect of GHRP-6 in preventing liver perivascular fibrosis. The square remarks the presence of normal, no fibrotic matrix around a central vein. Magnification $\times 10$. (I) is a high magnification ($\times 40$) microphotograph of a kidney tubular system of control saline animals showing massive nuclear pyknosis and cytoplasmic ballooning, all irreversible lethal changes. (J) The image shows that GHRP-6 intervention exerted a nephro-protective effect, preventing degenerative and lethal nuclear and cytoplasmic damages. Magnification $\times 40$. All are semi-thin sections, H/E staining. Scale bar is 200 μm .

TABLE 4 Quantification of Dox-induced damages in extra-cardiac organs.

Variable	Saline	GHRP-6	<i>p</i>
Passive hepatic congestion (degree)	2.75 \pm 0.27	0.69 \pm 0.59	< 0.0001
Serum ALAT (U/L)	81.38 \pm 12.73	29.38 \pm 5.8	< 0.0001
Damaged renal tubules (%)	78.41 \pm 12.43	20.53 \pm 7.20	< 0.0001
Damaged bronchi (%)	70.95 \pm 14.82	42.98 \pm 11.50	0.0028

Data are expressed as mean \pm SD. Statistical analyses were performed using unpaired Student's *t*-test.

GHRP-6 also protected epithelial extra-cardiac organs

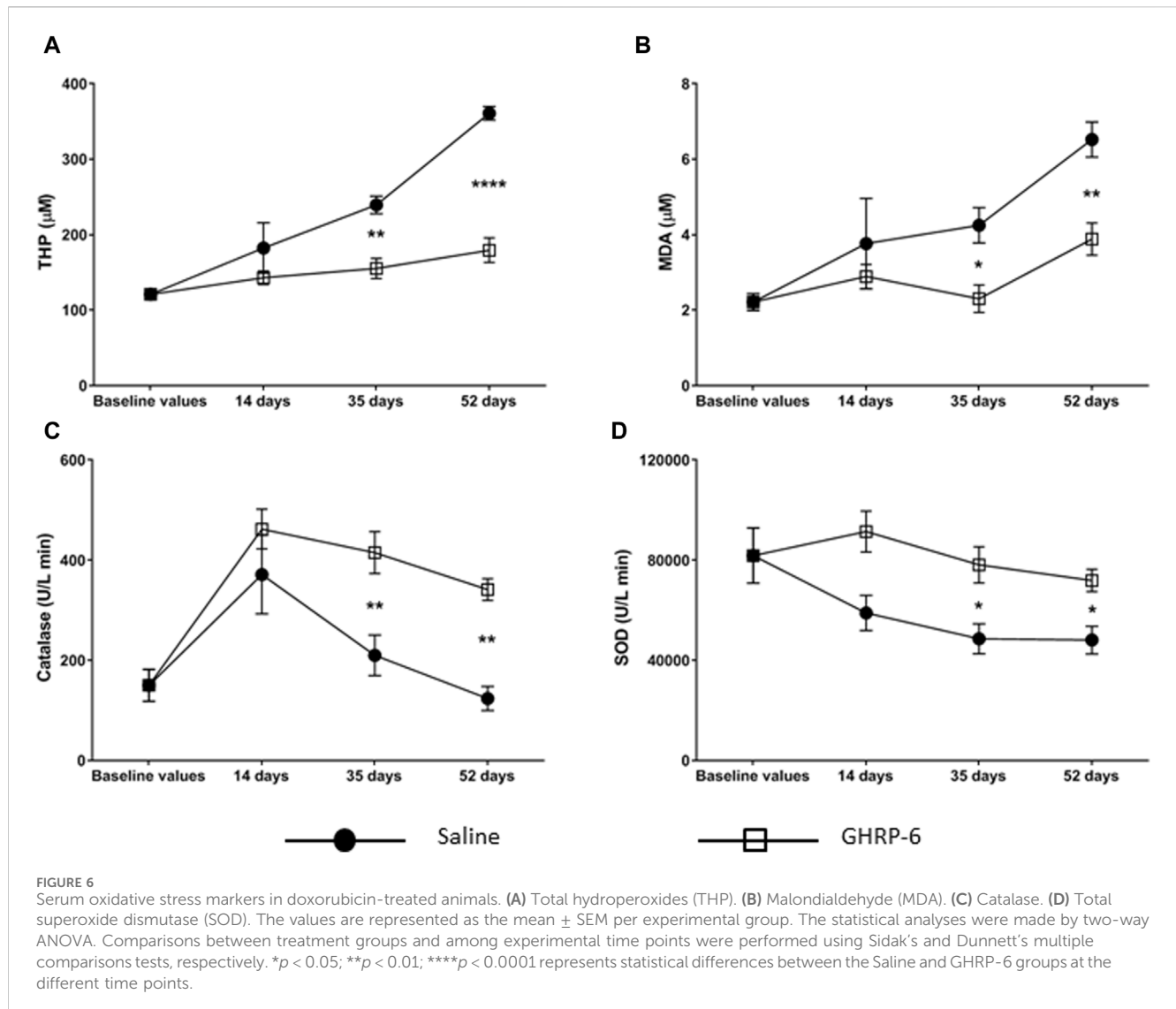
The histological examination of the lungs and liver parenchyma of animals receiving Dox and saline solution revealed pathognomonic changes of congestive heart failure (CHF). Passive liver congestion; as lungs alveolar septal thickening, edema, hypercellularity, and venous congestion were largely prevalent in the saline group (Figures 5A–C). All these pathological findings were partially or absolutely prevented by the intervention with GHRP-6 (Figures 5D–F). These histopathologic changes were substantiated by semiquantitative measurement scales as described in Table 1. Liver congestion in saline group was classified as evident-to-severe versus less than mild congestion for the GHRP-6 group (Table 4). In line with this, ALAT circulating levels were also significantly higher in the saline group than in rats receiving GHRP-6 (Table 4). In addition to focal necrosis, perivascular fibrotic induration (Figure 5G) was another hepatic change attributable to Dox cumulative toxicity and evidenced in the saline group. Interestingly, no evidences of pathologic fibrotic induration were ever detected in the liver of rats receiving GHRP-6 (Figure 5H). Small intestine, specially jejunum and ileum walls were also impacted by Dox administration. Intestinal damages included scattered foci of transmural necrosis in saline group which were consistently prevented by GHRP-6 administration (not shown). Kidneys were affected by Dox toxicity. Figure 5I illustrates tubular epithelial cells with cytoplasmic ballooning and nuclear pyknosis, which contrasts with the protective effect exerted by GHRP-6 treatment, in which most of the nuclei exhibit normal aspect (Figure 5J). The quantification of the tubular system damages in the saline group indicated the significant prevalence of lethal irreversible changes, as compared to the effect of GHRP-6. Similarly, the coagulative necrosis found in most microscopic fields of the bronchial epithelium in the saline group was broadly reduced by the GHRP-6 intervention (Table 4).

GHRP-6 intervention ameliorated oxidative stress cytotoxicity

The profile of the serum redox markers studied is shown in Figure 6. Dox administration provoked a progressive increase in the THP and MDA concentrations of the saline group ($p < 0.05$ in both cases) (Figures 6A, B). This increase was significantly higher than that produced in the GHRP-6 counterpart for both parameters on day 35 (THP: $p = 0.0010$; MDA: $p = 0.0442$) and day 52 ($p < 0.0001$ and $p = 0.0039$, respectively). Catalase levels showed a biphasic behavior (Figure 6C). During the first 14 days of Dox administration, the activity of this enzyme progressively increased in both saline ($p = 0.0052$) and GHRP-6 ($p < 0.0001$) groups with respect to baseline values. However, with increasing Dox cumulative levels, catalase activity became inhibited, which was far more pronounced in the saline rats than in those treated with GHRP-6 in both day 35 ($p = 0.0022$) and day 52 ($p = 0.0088$). Serum SOD activity became gradually depressed in correspondence with Dox administration time in saline group ($p < 0.05$ for days 35 and 52). Nevertheless, concomitant GHRP-6 intervention positively impacted in SOD enzyme activity preservation, as compared to baseline values ($p > 0.05$) and to saline group (Figure 6D, day 35: $p = 0.0462$; day 52: $p = 0.0363$).

GHRP-6 stimulated the expression of a survival gene

GHRP-6 concomitant intervention produced a significant increase in Bcl-2 myocardial expression with a simultaneous reduction of the pro-apoptotic Bax (for both $p < 0.001$), as compared to healthy sentinel rats, and definitely in relation to saline group. In the latter, Bax exhibited the largest expression level ($p < 0.001$). The maximal value of Bcl2/Bax ratio calculated for the GHRP-6 group significantly exceeded those estimated for the sentinel and the saline groups ($p < 0.05$) (Figure 7).



GHRP-6 treatment contributed to preserve cardiomyocytes organelles

Dox administration caused cardiomyocytes sarcolemmal vacuolization, myofibrils fragmentation, and mitochondrial damages that included membranes dilation, matrix ballooning, and cristae fragmentation and disappearance. Figure 8A shows the ultra-structural aspect of the myocardium of sentinel healthy animals. In contrast with this, Figure 8B is representative of the damages observed in the saline group, consistent on cardiomyocytes fragmentation and mitochondrial matrix damages. GHRP-6 intervention accounted for a noticeable sarcolemmal and mitochondrial structural preservation (Figure 8C).

Discussion

Dox has been known since late 1960s, and its use in the oncological armamentarium remains as a first-line drug for the treatment of a wide variety of cancers of epithelial and non-epithelial

origin. Nonetheless, its short and long-term cardiotoxic effects are of foremost clinical significance (Podyacheva and Toropova, 2022). Myriad of molecules have been historically investigated with the expectation to neutralize specific or multiple targets within the pleomorphic cardiomyocyte damaging cascade (Dulf et al., 2023). After all these efforts, dexrazoxane is the only currently approved treatment to prevent Dox-induced cardiotoxicity. In the meantime, cardioprotective prophylaxis strategies stand as an urgent requirement for cancer patients to prevent antineoplastic therapy disruption, and consequently reduce mortality (Wang et al., 2021).

The accumulated Dox dose of 30 mg/kg as an inducer of severe, progressive, and chronic cardiotoxicity was adopted from previous experiences (To et al., 2003). Since our pilot experiments, this dose proved to trigger an outspoken morbid state of DCM/CHF, characterized by echocardiographic signs of ventricular dilation, walls thinning, and LV mechanical failure. The heart failure involved an increase in both systolic and diastolic volumes, and the well-known distal complications as right side passive congestion with peritoneal, hepatic, and pulmonary expression. The fact that our echocardiographic, biochemical, and morphological findings are in

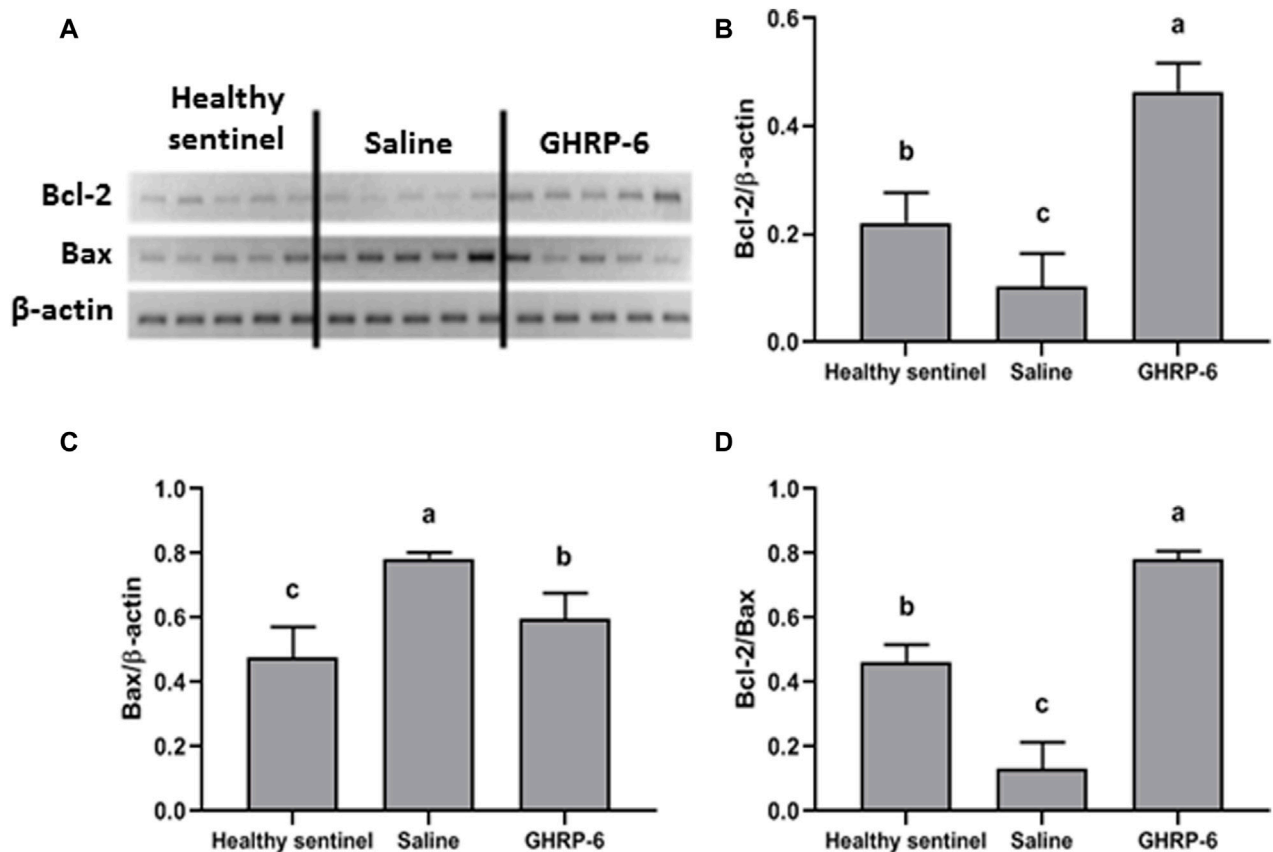


FIGURE 7
Influence of GHRP-6 in apoptosis regulatory gene in healthy and doxorubicin-treated groups. (A) Bands obtained by RT-PCR technique. Results normalized to β -actin gene expression are shown in the graphs: (B) Bcl-2; (C) Bax; (D) The Bcl-2/Bax ratio representing the balance between pro-survival and pro-apoptosis gene expression levels in favor to Bcl-2 expression. Bars indicate the mean \pm SD ($n = 5$) per group. For multiple statistical comparisons, a one-way ANOVA followed by the Newman Keuls multiple comparison test were used. Significant statistical differences among the three experimental groups ($p < 0.05$) are denoted by different letters (a,b,c).

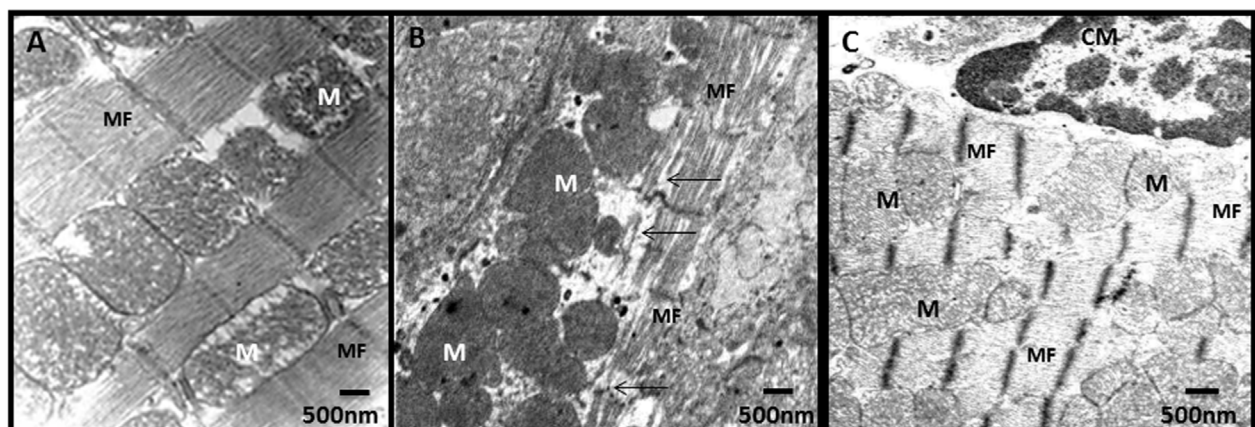


FIGURE 8
Myocardial ultrastructural characterization in samples of healthy and doxorubicin-treated rats. (A) Healthy sentinel control. The normal ultrastructure of the cardiac muscle is shown with myofibrils (MF) and mitochondria (M) within normal limits. (B) Saline. Loss of continuity of the myofibrils (arrows) and electron-dense mitochondria with loss of their cristae. (C) GHRP-6. Cardiomyocytes (CM), myofibrils, and mitochondria with cristae within normal limits. Bar: 500 nm.

line with previous descriptions of the experimental system (Shivakumar et al., 2012; Subburaman et al., 2014; Sandamali et al., 2019; Khedre et al., 2021), support and validate the practical usefulness of our model. Consequently, we examined on this scenario the hypothesis that GHRP-6 in concomitant administration to Dox, may prophylactically attenuate the myocardial and multiorgans changes associated to DCM/HF, and to the anthracycline intrinsic toxicity. The GHRP-6 dose used in this study had already evidenced cardioprotective effects by reducing infarct size over 70% in a porcine model of acute myocardial infarction (Berlanga et al., 2007). As described, GHRP-6 administration in parallel to Dox prevented cardiomyocytes fibrils consumption and ventricular cavities dilation, which accounted for an effective preservation of the LV systolic activity. This GHRP-6 mediated preservation of the systolic function, likely contributed to prevent extracardiac expressions of HF, as hepatic venous congestion and alveolar septal flooding. Comprehensively speaking, GHRP-6 concomitant administration to Dox attenuated cardiac and extracardiac toxicity, reducing animals' morbidity and mortality. This intervention however did not show to avert animals' cachexia. Preceding findings indicated that GHSR1a agonistic stimulation increases appetite and improves body weight gain (Yuan and Wang, 2020).

A previous study had already shown that GHRP-6 (100 µg/kg/day) administered during 4 weeks, prevented DCM in a completely different, non-toxic substrate, based in TO hamsters with an inborn deficiency in the myocardial δ -sarcoglycan (Iwase et al., 2004). In consonance with it, GHRP-2 (1 mg/kg), another synthetic GH secretagogue analog to GHRP-6, and ligand for GHS-R1a and CD36 (Titterton et al., 2009) also attenuated progressive LV remodeling and systolic dysfunction in the same TO hamster line (Kato et al., 2010).

Two relevant effects were displayed by GHRP-6 intervention in the realm of Dox-derived toxicity: (Schultheiss et al., 2019): the broad cytoprotective responses induced by the peptide in different internal epithelial organs, and (Riehle and Bauersachs, 2019) the anti-fibrotic response detected in both liver and kidney parenchyma. GHRP-6 intervention showed to rescue from coagulative necrosis a variety of epithelial cells as hepatocytes, kidneys tubular cells, bronchial epithelia, and the jejunum-ileum enterocytes. In relation to GHRP-6 extracardiac cytoprotective profile, the only precedent study we are aware of, revealed that a single prophylactic injection with GHRP-6 aborted the onset of Curling-like ulcers, and luminal bleeding in stressed conscious rats. Interestingly, GHRP-6 displayed a dual protective mechanism, one by directly activating survival signalers on the gastric epithelial cells, while simultaneously blunting the vagal efferent function, reducing the stress-stimulated gastric acid production (Guo et al., 2012). The anti-fibrotic effect, a previously described observation by our group appears to be driven by a transcriptional downregulation of TGF- β 1 and CTGF, and by counteracting the accumulation and formation of extracellular matrix ingredients and fibroblasts cytoskeleton organization proteins (Berlanga-Acosta et al., 2012; Fernandez-Mayola et al., 2018).

Altogether these data support the notion that these therapeutic bounties are driven by the agonistic stimulation of myocardial and extra-myocardial CD36 and/or GHSR1a receptors by activating

survival pathways, downregulating fibrogenic cytokines, and optimizing energetic homeostasis shunts that cooperate in cellular survival (Hosoda, 2022; Shu et al., 2022; Glatz et al., 2023). Whether these cytoprotective and anti-fibrotic effects are solely consequent to the stimulation of GHS-R1a has been debated (Yuan et al., 2021) and is beyond the scope of our study. However, this is a pharmacologically-relevant issue that deserves comment. A line of experimental evidences based on cardiac and non-cardiac cells in which GHS-R1a activation has been aborted through chemical antagonism and genetic silencing, incites to conclude that this receptor is irreplaceable for the activation of salvage kinases, as for the anti-fibrotic, anti-oxidant, anti-inflammatory, and proangiogenic effects upon its occupation by acylated ghrelin (Shati and El-Kott, 2019; Wang et al., 2020; Zhang and Xie, 2020; Shati and El-Kott, 2021; Wang et al., 2023). However, the early observation by Bladanzi and co-workers in which both ghrelin and des-acyl ghrelin inhibited apoptosis in H9c2 cardiomyocytes which do not express GHSR1a inaugurated the alternative line, sustaining that prosurvival pathways may be triggered and functionally activated through a GHSR-independent pathway (Baldanzi et al., 2002). More recent studies have demonstrated that des-acyl ghrelin exhibits cardioprotective activities and anti-fibrotic effects through a GHSR independent pathway (Pei et al., 2014; Liu et al., 2020). Accordingly, Delhanty and co-workers have indicated that unacylated ghrelin is a physiological component of the circulation (Delhanty et al., 2015), behaves like a separate hormone (Delhanty et al., 2012), and that it is likely endowed with its own receptor (Delhanty et al., 2013). Likewise, the potential contribution of CD36 on the light of our findings demands consideration. First, GHRP-6 binds CD36 while the recently generated azapeptide analogues retain high and selective binding affinity for CD36 (Proulx et al., 2020), second, CD36 plays a key role in providing the myocardium with its major energy substrate (Shu et al., 2022), third, agonistic binding of CD36 protected against myocardial damage and dysfunction by ischemia/reperfusion (Bessi et al., 2012), fourth, mice deficient for CD36 exhibit reduced tolerance to myocardial ischemia/reperfusion injury (Irie et al., 2003), whereas humans harboring inborn CD36 mutations, exhibit a variety of heart diseases including hypertrophic cardiomyopathy, dilated cardiomyopathy, or coronary heart disease (Tanaka et al., 2001), and fifth, alike GHSR-1a, CD36 is represented in a broad constellation of mammals tissues and organs (Zibara et al., 2002; Jacome-Sosa et al., 2021), including those that appeared protected by GHRP-6 in our experiment. Hence, further studies are warranted in order to selectively discern the role of each candidate receptor.

A thorough blueprint of the Dox-associated toxic mechanism is yet to be depicted (Pugazhendhi et al., 2018). However, it seems that mitochondrial damage/dysfunction with the ensued uncontrolled generation of reactive oxygen species (ROS), is as proximal trigger in the cascade of Dox-induced cardiomyocytes harms (Montalvo et al., 2020; Nordgren and Wallace, 2020; Kong et al., 2022). As described by others (Dulf et al., 2023; Shi et al., 2023), we observed that Dox administration was characterized by progressive increase of hydroperoxides and reactive aldehydes formation, along with a depletion of major neutralizing anti-oxidant enzymes. Concomitant GHRP-6 administration significantly counterbalanced these events, while keeping catalase and SOD

enzymes significantly active. This is not an unexpected finding since we had observed that GHRP-6 reduced myocardial injury in a porcine model of AMI, by the preservation of antioxidant defense systems and the ensuing decrease in ROS pool (Berlanga et al., 2007). Others also demonstrated that ghrelin, the unique endogenous ligand of GHSR-1a, prevented neuronal apoptosis in a model of hypoxia/ischemia by attenuating oxidative stress and enhancing other survival drivers as Sirt1, PGC-1 α , UCP2 (Huang et al., 2019). Mitochondria are identified as the major source of ROS and a main determinant of Dox-induced cardiac damages. Disruption of mitochondrial physiology contributes to alter metabolic and redox circuits in cardiac cells, ultimately culminating in increased apoptosis (Wallace et al., 2020). We therefore deem that the GHRP-6 effect on cardiac mitochondria structural preservation is noteworthy, and may have definitively contributed to reduce oxidative reactants spillover.

Since previous studies (Kagan et al., 2009) invoked Dox accumulation in cardiac mitochondria as primary trigger of apoptosis, we evaluated the expression ratio of Bcl-2/Bax genes. Interestingly, cardiac Bcl-2 expression associated to GHRP-6 administration exceeded the physiological expression level detected in the healthy sentinel group. Early pharmacological characterizations of GHSR1a ligands showed to inhibit cardiomyocyte apoptosis in a rat model of chronic heart failure (Xu et al., 2005). This GHRP-6 mediated antiapoptotic ability was further confirmed and extended through other *in vitro* and *in vivo* models (Paneda et al., 2003; Delgado-Rubin et al., 2009; Granado et al., 2011), which appeared mediated via the PI3 K/Akt/Bcl-2 salvage pathway (Yuan and Wang, 2020). Conclusively, Dox-associated myocardial cells demise may have been at least partially prevented by Bcl-2 upregulation, along with a concomitant decrease of Bax expression.

Although this work is limited for not having acquired cardiovascular/pulmonary hemodynamic constants, gasometry readings, or examined the integrity of the intestinal wall barrier function, for a more comprehensive evaluation of GHRP-6 cytoprotective spectrum; it provides the first evidences on the cardiac and extracardiac protective effect of a peptidyl GH secretagogue against an anti-neoplastic anthracycline. It also offers a foundational platform for subsequent cardio-and-cytoprotection studies within the cardio-oncology realm.

Although with an underlying controversial substrate; ghrelin, GHSR1a, and CD36 appear implicated in the multistep process of malignant transformation, and cancer cells progression and metastasis (Soleyman-Jahi et al., 2019; Guerrero-Rodriguez et al., 2022; Kotta et al., 2022). This may introduce regulatory constraints for the subsequent investigational development of these candidates. Nonetheless, oncology remains orphan of pharmacological tools that may act as “life-saving drugs” for empty niches as cancer-associated cachexia-anorexia syndrome, and chemotherapy-associated cardiotoxicity. Both processes may cause precocious mortality (Yeom and Yu, 2022; Dempke et al., 2023). Accordingly, we deem that GHRP-6 and/or other GHS “drugability” is justified, which will subsequently entail the clinical use of these candidates under the medical personalized analysis of risk-benefit balance.

Significance

Dilated cardiomyopathy (DCM) is a poor-prognosis condition characterized by ventricular dilation with evolving deterioration of the systolic function ultimately leading to heart failure (HF). Cancer patients treated with the chemotherapeutic anthracycline Doxorubicin (Dox) are frequently affected by the drug-related myocardial toxicity. This condition leads to chemotherapy scheme discontinuation and therefore to cancer progression. Despite continuous research efforts, DCM mortality rates are high, remaining as one of the leading causes of heart transplantation. This study confirms and extends that the classic growth hormone (GH) secretagogue GHRP-6, is endowed with potent cardio and cyto-protective abilities. In an experimental model of Dox-induced DCM, GHRP-6 concomitant administration prevented ventricular myofibrils consumption, dilation, and accordingly preserved within physiological limits left ventricle ejection fraction. Globally speaking, GHRP-6 reduced rats' morbidity and mortality in a significant manner as compared to saline control. Furthermore, GHRP-6 also exerted a broad cytoprotective effect by reducing the thresholds of parenchymal necrosis and apoptosis in most epithelial internal organs. The treatment proved to abort in this system the fibrotic induration in liver, kidneys, and lungs as a consequence of Dox-toxicity. From a mechanistic perspective, GHRP-6 attenuated the pro-oxidant arm and enhanced the anti-oxidant reserves before Dox-challenge, attenuated mitochondrial matrix-ultrastructural damages, and increased the expression of Bcl-2 as antiapoptotic gene. This is the first evidence on the cardiac and extracardiac protective effects of a peptidyl GH secretagogue against an anti-neoplastic anthracycline. GHRP-6 candidacy as cardioprotective drug is further supported by its broad safety and tolerability profile upon its parenteral administration.

Data availability statement

The original contributions presented in the study are included in the article/Supplementary material, further inquiries can be directed to the corresponding author.

Ethics statement

The animal study was approved by the Animal Welfare Committee Review Board—Animal facility and preclinical studies, Center for Genetic Engineering and Biotechnology, Havana, Cuba. Contact person: Dr Jorge Castro-Velazco, jorge.castro@cigb.edu.cu. The study was conducted in accordance with the local legislation and institutional requirements.

Author contributions

JB-A: Conceptualization, Data curation, Formal Analysis, Investigation, Methodology, Supervision, Writing—original draft, Writing—review and editing. DC-V: Conceptualization, Data curation, Formal Analysis, Investigation, Methodology,

Writing—original draft. JV-M: Conceptualization, Formal Analysis, Investigation, Methodology, Writing—review and editing. JS-A: Data curation, Investigation, Methodology, Writing—review and editing. AG-O: Conceptualization, Data curation, Formal Analysis, Investigation, Writing—original draft, Writing—review and editing. VF-C: Data curation, Investigation, Methodology, Writing—original draft. BJ: Data curation, Investigation, Writing—review and editing. LW: Data curation, Investigation, Writing—review and editing. GG-N: Funding acquisition, Project administration, Supervision, Writing—review and editing.

Funding

The author(s) declare financial support was received for the research, authorship, and/or publication of this article. Funds for this study corresponded to biomedical research area of the Center for Genetic Engineering and Biotechnology, account number IBM. 3051-280. Funds for this study were also provided by the “National Key R&D Program of China (2021YFE0111300)”. The authors

declare that the funders were not involved in the study design, collection, analysis, interpretation of data, the writing of this article, or the decision to submit it for publication.

Conflict of interest

The authors declare that the research was conducted in the absence of any commercial or financial relationships that could be construed as a potential conflict of interest.

Publisher's note

All claims expressed in this article are solely those of the authors and do not necessarily represent those of their affiliated organizations, or those of the publisher, the editors and the reviewers. Any product that may be evaluated in this article, or claim that may be made by its manufacturer, is not guaranteed or endorsed by the publisher.

References

- Afsar, T., Razak, S., Batoo, K. M., and Khan, A. (2017). Acacia hydasypica R. Parker prevents doxorubicin-induced cardiac injury by attenuation of oxidative stress and structural Cardiomyocyte alterations in rats. *BMC Complement. Altern. Med.* 17 (1), 554. doi:10.1186/s12906-017-2061-0
- Ajamieh, H., Merino, N., Candelario-Jalil, E., Menendez, S., Martinez-Sanchez, G., Re, L., et al. (2002). Similar protective effect of ischaemic and ozone oxidative preconditionings in liver ischaemia/reperfusion injury. *Pharmacol. Res.* 45 (4), 333–339. doi:10.1006/phrs.2002.0952
- Alhowail, A. H., Bloemer, J., Majrashi, M., Pinky, P. D., Bhattacharya, S., Yongli, Z., et al. (2019). Doxorubicin-induced neurotoxicity is associated with acute alterations in synaptic plasticity, apoptosis, and lipid peroxidation. *Toxicol. Mech. Methods* 29 (6), 457–466. doi:10.1080/15376516.2019.1600086
- Baldanzi, G., Filigheddu, N., Cutrupi, S., Catapano, F., Bonisconi, S., Fubini, A., et al. (2002). Ghrelin and des-acyl ghrelin inhibit cell death in cardiomyocytes and endothelial cells through ERK1/2 and PI 3-kinase/AKT. *J. Cell. Biol.* 159 (6), 1029–1037. doi:10.1083/jcb.200207165
- Benjamin, E. J., Virani, S. S., Callaway, C. W., Chamberlain, A. M., Chang, A. R., Cheng, S., et al. (2018). Heart disease and stroke statistics-2018 update: a report from the American heart association. *Circulation* 137 (12), e67–e492. doi:10.1161/CIR.0000000000000558
- Berlanga, J., Cibrian, D., Guevara, L., Dominguez, H., Alba, J. S., Seralena, A., et al. (2007). Growth-hormone-releasing peptide 6 (GHRP6) prevents oxidant cytotoxicity and reduces myocardial necrosis in a model of acute myocardial infarction. *Clin. Sci. (Lond.)* 112 (4), 241–250. doi:10.1042/CS20060103
- Berlanga-Acosta, J., Abreu-Cruz, A., Herrera, D. G. B., Mendoza-Mari, Y., Rodriguez-Ulloa, A., Garcia-Ojalvo, A., et al. (2017). Synthetic growth hormone-releasing peptides (GHRPs): a historical appraisal of the evidences supporting their cytoprotective effects. *Clin. Med. Insights Cardiol.* 11, 1179546817694558. doi:10.1177/1179546817694558
- Berlanga-Acosta, J., Guillen-Nieto, G., Lopez-Mola, E., and Herrera-Martinez, L. (2016). Growth hormone releasing peptide-6 (GHRP-6) and other related secretagogue synthetic peptides: a mine of medical potentialities for unmet medical needs. *Integr. Mol. Med.* 3 (2), 616–623. doi:10.15761/imm.1000213
- Berlanga-Acosta, J., Vázquez-Blomquist, D., Cibrián, D., Mendoza, Y., Ochagavía, M. E., Miranda, J., et al. (2012). Growth Hormone Releasing Peptide 6 (GHRP6) reduces liver fibrosis in CCl4 chronically intoxicated rats. *Biotechnol. Appl.* 29, 60–72.
- Bessi, V. L., Labbe, S. M., Huynh, D. N., Menard, L., Jossart, C., Febbraio, M., et al. (2012). EP 80317, a selective CD36 ligand, shows cardioprotective effects against post-ischaemic myocardial damage in mice. *Cardiovasc Res.* 96 (1), 99–108. doi:10.1093/cvr/cvs225
- Chen, X., Zhang, Y., Zhu, Z., Liu, H., Guo, H., Xiong, C., et al. (2016). Protective effect of berberine on doxorubicin-induced acute hepatorenal toxicity in rats. *Mol. Med. Rep.* 13 (5), 3953–3960. doi:10.3892/mmr.2016.5017
- Cossio-Bolanos, M., Gomez Campos, R., Vargas Vitoria, R., Hochmuller Fogaca, R. T., and de Arruda, M. (2013). Reference curves for assessing the physical growth of male Wistar rats. *Nutr. Hosp.* 28 (6), 2151–2156. doi:10.3305/nutrhosp.v28in06.6659
- Delgado-Rubin, A., Chowen, J. A., Argente, J., and Frago, L. M. (2009). Growth hormone-releasing peptide 6 protection of hypothalamic neurons from glutamate excitotoxicity is caspase independent and not mediated by insulin-like growth factor I. *Eur. J. Neurosci.* 29 (11), 2115–2124. doi:10.1111/j.1460-9568.2009.06770.x
- Delhanty, P. J., Huisman, M., Julien, M., Mouchain, K., Brune, P., Themmen, A. P., et al. (2015). The acylated (AG) to unacylated (UAG) ghrelin ratio in esterase inhibitor-treated blood is higher than previously described. *Clin. Endocrinol. (Oxf)* 82 (1), 142–146. doi:10.1111/cen.12489
- Delhanty, P. J., Neggers, S. J., and van der Lely, A. J. (2012). Mechanisms in endocrinology: ghrelin: the differences between acyl- and des-acyl ghrelin. *Eur. J. Endocrinol.* 167 (5), 601–608. doi:10.1530/EJE-12-0456
- Delhanty, P. J., Neggers, S. J., and van der Lely, A. J. (2013). Des-acyl ghrelin: a metabolically active peptide. *Endocr. Dev.* 25, 112–121. doi:10.1159/000346059
- Demers, A., McNicoll, N., Febbraio, M., Servant, M., Marleau, S., Silverstein, R., et al. (2004). Identification of the growth hormone-releasing peptide binding site in CD36: a photoaffinity cross-linking study. *Biochem. J.* 382 (Pt 2), 417–424. doi:10.1042/BJ20040036
- Dempke, W. C. M., Zielinski, R., Winkler, C., Silberman, S., Reuther, S., and Priebe, W. (2023). Anthracycline-induced cardiotoxicity - are we about to clear this hurdle? *Eur. J. Cancer* 185, 94–104. doi:10.1016/j.ejca.2023.02.019
- Dulf, P. L., Mocan, M., Coadă, C. A., Dulf, D. V., Moldovan, R., Baldea, I., et al. (2023). Doxorubicin-induced acute cardiotoxicity is associated with increased oxidative stress, autophagy, and inflammation in a murine model. *Naunyn-Schmiedeberg Arch. Pharmacol.* 396 (6), 1105–1115. doi:10.1007/s00210-023-02382-z
- Fernandez-Mayola, M., Betancourt, L., Molina-Kautzman, A., Palomares, S., Mendoza-Mari, Y., Ugarte-Moreno, D., et al. (2018). Growth hormone-releasing peptide 6 prevents cutaneous hypertrophic scarring: early mechanistic data from a proteome study. *Int. Wound J.* 15 (4), 538–546. doi:10.1111/iwj.12895
- Ferreira, A., Ferreira, V., Antunes, M. M., Lousinha, A., Pereira-da-Silva, T., Antunes, D., et al. (2023). Dilated cardiomyopathy: a comprehensive approach to diagnosis and risk stratification. *Biomedicines* 11 (3), 834. doi:10.3390/biomedicines11030834
- Giorgetti, G., Del Bello, F., Quaglia, W., Botticelli, L., Cifani, C., Micioni Di Bonaventura, E., et al. (2022). Advances in the development of nonpeptide small molecules targeting ghrelin receptor. *J. Med. Chem.* 65 (4), 3098–3118. doi:10.1021/acs.jmedchem.1c02191
- Glatz, J. F. C., Heather, L. C., and Luiken, J. (2023). CD36 as a gatekeeper of myocardial lipid metabolism and therapeutic target for metabolic disease. *Physiol. Rev.* 104, 727–764. doi:10.1152/physrev.00011.2023
- Glauert, A. M., and Lewis, P. R. (1999). *Biological specimen preparation for transmission electron microscopy*. Princeton: Princeton University Press.
- Granado, M., Garcia-Caceres, C., Tuda, M., Frago, L. M., Chowen, J. A., and Argente, J. (2011). Insulin and growth hormone-releasing peptide-6 (GHRP-6) have differential beneficial effects on cell turnover in the pituitary, hypothalamus and cerebellum of

- streptozotocin (STZ)-induced diabetic rats. *Mol. Cell. Endocrinol.* 337 (1–2), 101–113. doi:10.1016/j.mce.2011.02.002
- Guerrero-Rodriguez, S. L., Mata-Cruz, C., Perez-Tapia, S. M., and Velasco-Velazquez, M. A. (2022). Role of CD36 in cancer progression, stemness, and targeting. *Front. Cell. Dev. Biol.* 10, 1079076. doi:10.3389/fcell.2022.1079076
- Guo, S., Gao, Q., Jiao, Q., Hao, W., Gao, X., and Cao, J. M. (2012). Gastric mucosal damage in water immersion stress: mechanism and prevention with GHRP-6. *World J. Gastroenterol.* 18 (24), 3145–3155. doi:10.3748/wjg.v18.i24.3145
- Hayward, R., and Hydock, D. S. (2007). Doxorubicin cardiotoxicity in the rat: an *in vivo* characterization. *J. Am. Assoc. Lab. Anim. Sci.* 46 (4), 20–32.
- Hershberger, R. E., Hedges, D. J., and Morales, A. (2013). Dilated cardiomyopathy: the complexity of a diverse genetic architecture. *Nat. Rev. Cardiol.* 10 (9), 531–547. doi:10.1038/nrcardio.2013.105
- Hosoda, H. (2022). Effect of ghrelin on the cardiovascular system. *Biol. (Basel)*. 11 (8), 1190. doi:10.3390/biology11081190
- Huang, J., Liu, W., Doycheva, D. M., Gamdzky, M., Lu, W., Tang, J., et al. (2019). Ghrelin attenuates oxidative stress and neuronal apoptosis via GHSR-1a/AMPK/Sirt1/PGC-1 α /UCP2 pathway in a rat model of neonatal HIE. *Free Radic. Biol. Med.* 141, 322–337. doi:10.1016/j.freeradbiomed.2019.07.001
- Hullin, R., Metrich, M., Sarre, A., Basquin, D., Maillard, M., Regamey, J., et al. (2018). Diverging effects of enalapril or eplerenone in primary prevention against doxorubicin-induced cardiotoxicity. *Cardiovasc Res.* 114 (2), 272–281. doi:10.1093/cvr/cvx162
- Imanaka-Yoshida, K. (2020). Inflammation in myocardial disease: from myocarditis to dilated cardiomyopathy. *Pathol. Int.* 70 (1), 1–11. doi:10.1111/pin.12868
- Irie, H., Krukenkamp, I. B., Brinkmann, J. F., Gaudette, G. R., Saltman, A. E., Jou, W., et al. (2003). Myocardial recovery from ischemia is impaired in CD36-null mice and restored by myocyte CD36 expression or medium-chain fatty acids. *Proc. Natl. Acad. Sci. U. S. A.* 100 (11), 6819–6824. doi:10.1073/pnas.1132094100
- Iwase, M., Kanazawa, H., Kato, Y., Nishizawa, T., Somura, F., Ishiki, R., et al. (2004). Growth hormone-releasing peptide can improve left ventricular dysfunction and attenuate dilation in dilated cardiomyopathic hamsters. *Cardiovasc Res.* 61 (1), 30–38. doi:10.1016/j.cardiores.2003.10.012
- Jacome-Sosa, M., Miao, Z. F., Peche, V. S., Morris, E. F., Narendran, R., Pietka, K. M., et al. (2021). CD36 maintains the gastric mucosa and associates with gastric disease. *Commun. Biol.* 4 (1), 1247. doi:10.1038/s42003-021-02765-z
- Kagan, V. E., Bayir, H. A., Belikova, N. A., Kapralov, O., Tyurina, Y. Y., Tyurin, V. A., et al. (2009). Cytochrome c/cardiolin relations in mitochondria: a kiss of death. *Free Radic. Biol. Med.* 46 (11), 1439–1453. doi:10.1016/j.freeradbiomed.2009.03.004
- Kato, Y., Iwase, M., Ichihara, S., Kanazawa, H., Hashimoto, K., Noda, A., et al. (2010). Beneficial effects of growth hormone-releasing peptide on myocardial oxidative stress and left ventricular dysfunction in dilated cardiomyopathic hamsters. *Circ. J.* 74 (1), 163–170. doi:10.1253/circj.cj-09-0378
- Khedre, D., Osman, A., Moghazy, A., and Abdel, R. A. (2021). Propolis protective effects against doxorubicin-induced multi-organ toxicity via suppression of oxidative stress, inflammation, apoptosis, and histopathological alterations in female albino rats. *Biointerface Res. Appl. Chem.* 12, 1762–1777. doi:10.33263/BRIAC122.17621777
- Kong, C. Y., Guo, Z., Song, P., Zhang, X., Yuan, Y. P., Teng, T., et al. (2022). Underlying the mechanisms of doxorubicin-induced acute cardiotoxicity: oxidative stress and cell death. *Int. J. Biol. Sci.* 18 (2), 760–770. doi:10.7150/ijbs.65258
- Kotta, A. S., Kelling, A. S., Corleto, K. A., Sun, Y., and Giles, E. D. (2022). Ghrelin and cancer: examining the roles of the ghrelin Axis in tumor growth and progression. *Biomolecules* 12 (4), 483. doi:10.3390/biom12040483
- Li, Y., Wang, L., Dong, Z., Wang, S., Qi, L., Cho, K., et al. (2019). Cardioprotection of salvianolic acid B and ginsenoside Rg1 combination on subacute myocardial infarction and the underlying mechanism. *Phytomedicine* 57, 255–261. doi:10.1016/j.phymed.2018.12.040
- Liu, X., Guo, Y., Li, Z., and Gong, Y. (2020). The role of acylated ghrelin and unacylated ghrelin in the blood and hypothalamus and their interaction with nonalcoholic fatty liver disease. *Iran. J. Basic Med. Sci.* 23 (9), 1191–1196. doi:10.22038/ijbms.2020.45356.10555
- Lothar, A., Bergemann, S., Kowalski, J., Huck, M., Gilsbach, R., Bode, C., et al. (2018). Inhibition of the cardiac myocyte mineralocorticoid receptor ameliorates doxorubicin-induced cardiotoxicity. *Cardiovasc Res.* 114 (2), 282–290. doi:10.1093/cvr/cvx078
- Luchesi, P. A. (2004). Growth hormone-releasing peptides and the heart: secretagogues or cardioprotectors? *Cardiovasc Res.* 61 (1), 7–8. doi:10.1016/j.cardiores.2003.11.011
- Mendoza, M. Y., Fernandez, M. M., Aguilera Barreto, A., Garcia Ojalvo, A., Bermudez Alvarez, Y., Mir Benitez, A. J., et al. (2016). Growth hormone-releasing peptide 6 enhances the healing process and improves the esthetic outcome of the wounds. *Plast. Surg. Int.* 2016, 4361702. doi:10.1155/2016/4361702
- Montalvo, R. N., Doerr, V., Min, K., Szeto, H. H., and Smuder, A. J. (2020). Doxorubicin-induced oxidative stress differentially regulates proteolytic signaling in cardiac and skeletal muscle. *Am. J. Physiol. Regul. Integr. Comp. Physiol.* 318 (2), R227–R233–R33. doi:10.1152/ajpregu.00299.2019
- Mossa, A. H., Swelam, E. S., and Mohafrash, S. M. M. (2015). Sub-chronic exposure to fipronil induced oxidative stress, biochemical and histopathological changes in the liver and kidney of male albino rats. *Toxicol. Rep.* 2, 775–784. doi:10.1016/j.toxrep.2015.02.009
- Nordgren, K. K. S., and Wallace, K. B. (2020). Disruption of the keap1/nrf2-antioxidant response system after chronic doxorubicin exposure *in vivo*. *Cardiovasc Toxicol.* 20 (6), 557–570. doi:10.1007/s12012-020-09581-7
- Paneda, C., Arroba, A. I., Frago, L. M., Holm, A. M., Romer, J., Argente, J., et al. (2003). Growth hormone-releasing peptide-6 inhibits cerebellar cell death in aged rats. *Neuroreport* 14 (12), 1633–1635. doi:10.1097/00001756-200308260-00018
- Pei, X. M., Yung, B. Y., Yip, S. P., Ying, M., Benzie, I. F., and Siu, P. M. (2014). Desacyl ghrelin prevents doxorubicin-induced myocardial fibrosis and apoptosis via the GHSR-independent pathway. *Am. J. Physiol. Endocrinol. Metab.* 306 (3), E311–E323. doi:10.1152/ajpendo.00123.2013
- Podyacheva, E., and Toropova, Y. (2022). SIRT1 activation and its effect on intercalated disc proteins as a way to reduce doxorubicin cardiotoxicity. *Front. Pharmacol.* 13, 1035387. doi:10.3389/fphar.2022.1035387
- Prathumap, N., Shinlapawittayatorn, K., Chattipakorn, S. C., and Chattipakorn, N. (2020). Effects of doxorubicin on the heart: from molecular mechanisms to intervention strategies. *Eur. J. Pharmacol.* 866, 172818. doi:10.1016/j.ejphar.2019.172818
- Proulx, C., Zhang, J., Sabatino, D., Chemtob, S., Ong, H., and Lubell, W. D. (2020). Synthesis and biomedical potential of azapeptide modulators of the cluster of differentiation 36 receptor (CD36). *Biomedicines* 8 (8), 241. doi:10.3390/biomedicines8080241
- Pugazhendhi, A., Edison, T., Velmurugan, B. K., Jacob, J. A., and Karuppusamy, I. (2018). Toxicity of Doxorubicin (Dox) to different experimental organ systems. *Life Sci.* 200, 26–30. doi:10.1016/j.lfs.2018.03.023
- Rao, Y. L., Ganaraja, B., Marathe, A., Manjrekar, P. A., Joy, T., Ullal, S., et al. (2021). Comparison of malondialdehyde levels and superoxide dismutase activity in resveratrol and resveratrol/donepezil combination treatment groups in Alzheimer's disease induced rat model. *3 Biotech.* 11 (7), 329. doi:10.1007/s13205-021-02879-5
- Riehle, C., and Bauersachs, J. (2019). Small animal models of heart failure. *Cardiovasc Res.* 115 (13), 1838–1849. doi:10.1093/cvr/cvz161
- Robert Li, Y., Traore, K., and Zhu, H. (2023). Novel molecular mechanisms of doxorubicin cardiotoxicity: latest leading-edge advances and clinical implications. *Mol. Cell. Biochem.* doi:10.1007/s11010-023-04783-3
- Sandamali, J., Hewawasam, R., Jayatilaka, KAPW, and Mudduwa, L. (2019). Dose dependent cardiac effects of doxorubicin in Wistar rats: a biochemical and histopathological analysis. *Int. J. Pharm. Sci. Res.* 10, 2700. doi:10.13040/IJPSR.0975-8232.10(6).2700-10
- Schultheiss, H. P., Fairweather, D., Caforio, A. L. P., Escher, F., Hershberger, R. E., Lipshultz, S. E., et al. (2019). Dilated cardiomyopathy. *Nat. Rev. Dis. Prim.* 5 (1), 32. doi:10.1038/s41572-019-0084-1
- Scudamore, C. L., Busk, N., and Vowell, K. (2014). A simplified necropsy technique for mice: making the most of unscheduled deaths. *Lab. Anim.* 48 (4), 342–344. doi:10.1177/0023677214536555
- Shati, A. A., and El-Kott, A. F. (2019). Acylated ghrelin prevents doxorubicin-induced cardiac intrinsic cell death and fibrosis in rats by restoring IL-6/JAK2/STAT3 signaling pathway and inhibition of STAT1. *Naunyn Schmiedeberg. Arch. Pharmacol.* 392 (9), 1151–1168. doi:10.1007/s00210-019-01664-9
- Shati, A. A., and El-Kott, A. F. (2021). Acylated ghrelin protects against doxorubicin-induced nephropathy by activating silent information regulator 1. *Basic Clin. Pharmacol. Toxicol.* 128 (6), 805–821. doi:10.1111/bcpt.13569
- Shi, S., Chen, Y., Luo, Z., Nie, G., and Dai, Y. (2023). Role of oxidative stress and inflammation-related signaling pathways in doxorubicin-induced cardiomyopathy. *Cell. Commun. Signal* 21 (1), 61. doi:10.1186/s12964-023-01077-5
- Shivakumar, P., Rani, M. U., Reddy, A. G., and Anjaneyulu, Y. (2012). A study on the toxic effects of Doxorubicin on the histology of certain organs. *Toxicol. Int.* 19 (3), 241–244. doi:10.4103/0971-6580.103656
- Shu, H., Peng, Y., Hang, W., Nie, J., Zhou, N., and Wang, D. W. (2022). The role of CD36 in cardiovascular disease. *Cardiovasc Res.* 118 (1), 115–129. doi:10.1093/cvr/cvaa319
- Soleyman-Jahi, S., Sadeghi, F., Pastaki Khoshbin, A., Khani, L., Roosta, V., and Zendeheh, K. (2019). Attribution of ghrelin to cancer: attempts to unravel an apparent controversy. *Front. Oncol.* 9, 1014. doi:10.3389/fonc.2019.01014
- Stein, A. B., Tiwari, S., Thomas, P., Hunt, G., Levent, C., Stoddard, M. F., et al. (2007). Effects of anesthesia on echocardiographic assessment of left ventricular structure and function in rats. *Basic Res. Cardiol.* 102 (1), 28–41. doi:10.1007/s00395-006-0627-y
- Subburaman, S., Ganesan, K., and Ramachandran, M. (2014). Protective role of naringenin against doxorubicin-induced cardiotoxicity in a rat model: histopathology and mRNA expression profile studies. *J. Environ. Pathol. Toxicol. Oncol.* 33 (4), 363–376. doi:10.1615/jenviropatholtoxiconcol.2014010625
- Tanaka, T., Nakata, T., Oka, T., Ogawa, T., Okamoto, F., Kusaka, Y., et al. (2001). Defect in human myocardial long-chain fatty acid uptake is caused by FAT/CD36 mutations. *J. Lipid Res.* 42 (5), 751–759. doi:10.1016/s0022-2275(20)31637-0

- Titterton, J. S., Sukhanov, S., Higashi, Y., Vaughn, C., Bowers, C., and Delafontaine, P. (2009). Growth hormone-releasing peptide-2 suppresses vascular oxidative stress in ApoE^{-/-} mice but does not reduce atherosclerosis. *Endocrinology* 150 (12), 5478–5487. doi:10.1210/en.2009-0283
- To, H., Ohdo, S., Shin, M., Uchimaru, H., Yukawa, E., Higuchi, S., et al. (2003). Dosing time dependency of doxorubicin-induced cardiotoxicity and bone marrow toxicity in rats. *J. Pharm. Pharmacol.* 55 (6), 803–810. doi:10.1211/002235703765951410
- Wallace, K. B., Sardao, V. A., and Oliveira, P. J. (2020). Mitochondrial determinants of doxorubicin-induced cardiomyopathy. *Circ. Res.* 126 (7), 926–941. doi:10.1161/CIRCRESAHA.119.314681
- Wang, A. J., Zhang, J., Xiao, M., Wang, S., Wang, B. J., Guo, Y., et al. (2021). Molecular mechanisms of doxorubicin-induced cardiotoxicity: novel roles of sirtuin 1-mediated signaling pathways. *Cell. Mol. Life Sci.* 78 (7), 3105–3125. doi:10.1007/s00018-020-03729-y
- Wang, L., Chen, Q., and Pang, J. (2023b). The effects and mechanisms of ghrelin upon angiogenesis in human coronary artery endothelial cells under hypoxia. *Peptides* 160, 170921. doi:10.1016/j.peptides.2022.170921
- Wang, M., Qian, L., Li, J., Ming, H., Fang, L., Li, Y., et al. (2020). GHSR deficiency exacerbates cardiac fibrosis: role in macrophage inflammasome activation and myofibroblast differentiation. *Cardiovasc Res.* 116 (13), 2091–2102. doi:10.1093/cvr/cvz318
- Wang, T.-H., Ma, Y., Gao, S., Zhang, W.-W., Han, D., and Cao, F. (2023a). Recent advances in the mechanisms of cell death and dysfunction in doxorubicin cardiotoxicity. *RCM* 24 (11), 336. doi:10.31083/j.rcm2411336
- Xiao, X., Bi, M., Jiao, Q., Chen, X., Du, X., and Jiang, H. (2020). A new understanding of GHSR1a--independent of ghrelin activation. *Ageing Res. Rev.* 64, 101187. doi:10.1016/j.arr.2020.101187
- Xu, X. B., Pang, J. J., Cao, J. M., Ni, C., Xu, R. K., Peng, X. Z., et al. (2005). GH-releasing peptides improve cardiac dysfunction and cachexia and suppress stress-related hormones and cardiomyocyte apoptosis in rats with heart failure. *Am. J. Physiol. Heart Circ. Physiol.* 289 (4), H1643–H1651. doi:10.1152/ajpheart.01042.2004
- Yeom, E., and Yu, K. (2022). Understanding the molecular basis of anorexia and tissue wasting in cancer cachexia. *Exp. Mol. Med.* 54 (4), 426–432. doi:10.1038/s12276-022-00752-w
- Yuan, M. J., Li, W., and Zhong, P. (2021). Research progress of ghrelin on cardiovascular disease. *Biosci. Rep.* 41 (1). doi:10.1042/BSR20203387
- Yuan, M. J., and Wang, T. (2020). The new mechanism of Ghrelin/GHSR1a on autophagy regulation. *Peptides* 126, 170264. doi:10.1016/j.peptides.2020.170264
- Zhang, J., and Xie, T. (2020). Ghrelin inhibits cisplatin-induced MDA-MB-231 breast cancer cell apoptosis via PI3K/Akt/mTOR signaling. *Exp. Ther. Med.* 19 (3), 1633–1640. doi:10.3892/etm.2019.8398
- Zhu, W., Reuter, S., and Field, L. J. (2019). Targeted expression of cyclin D2 ameliorates late stage anthracycline cardiotoxicity. *Cardiovasc Res.* 115 (5), 960–965. doi:10.1093/cvr/cvy273
- Zibara, K., Malaud, E., and McGregor, J. L. (2002). CD36 mRNA and protein expression levels are significantly increased in the heart and testis of apoE deficient mice in comparison to wild type (C57bl/6). *J. Biomed. Biotechnol.* 2 (1), 14–21. doi:10.1155/S1110724302000335

Glossary

DCM	dilated cardiomyopathy
LV	left ventricle
LVEF	left ventricle ejection fraction
HF	heart failure
Dox	doxorubicin
DNA	deoxyribonucleic acid
GH	growth hormone
GHRP-6	GH releasing peptide 6
GHSR1a	GH secretagogue receptor 1a
CD36	cluster differentiation 36
IGF-1	insulin like growth factor type 1
CENPALAB	National Center for Laboratory Animals Breeding
CIGB	Center for Genetic Engineering and Biotechnology
LVDd	LV diastolic diameter
LVSd	LV systolic diameter
IVSs	inter-ventricular septum thickness in systole
LVWs	LV posterior wall thickness in systole
TEM	transmission electron microscopy
THP	total hydroperoxides
MDA	malondialdehyde
SOD	superoxide dismutase
ALAT	alanine amino transferase
Bcl-2	Abbreviation of B cell Lymphoma. The gene product family plays promotes cell survival
Bax	Also identified as bcl-2-like protein 4 with pro-apoptotic effect
RNA	Ribonucleic acid
RT-PCR	Reverse transcription-polymerase chain reaction
ANOVA	analysis of variance
CHF	congestive heart failure
TGF-β1	Transforming growth factor beta 1
CTGF	Connective tissue growth factor
Fas	Pro-apoptotic product
ROS	reactive oxygen species
AMI	Acute myocardial infarction
Sirt1	silent mating type information regulation 2 homolog. Regulator of metabolism, cell death, aging, oxidative stress defense, and inflammation
PGC-1α	peroxisome proliferator-activated receptor γ coactivator-1 α. Broad regulator of mitochondrial life cycle and function, metabolism and cell survival
UCP2	Uncoupling protein 2, involved in oxidative stress prevention
PI3 K	phosphatidylinositol 3-kinases. A family of proteins involved in cell growth, proliferation, differentiation, motility, and survival

Akt

Protein kinase B. It is involved in cell cycle progression, survival, protein synthesis, and cell growth



OPEN ACCESS

EDITED BY

Raghuveera Kumar Goel,
Boston University, United States

REVIEWED BY

Xiangxuan Zhao,
China Medical University, China
Amit Kumar Tripathi,
University of North Texas Health Science
Center, United States

*CORRESPONDENCE

Yangfeng Chen,
✉ chenylf@hunau.edu.cn
Xiaohong Zhong,
✉ xh-zhong@163.com

RECEIVED 21 February 2024

ACCEPTED 13 June 2024

PUBLISHED 01 July 2024

CITATION

Chen Y, Xia H and Zhong X (2024), *In Vitro*
evaluation of the anti-pancreatic cancer activity
of *epimedium* herb.
Front. Pharmacol. 15:1389221.
doi: 10.3389/fphar.2024.1389221

COPYRIGHT

© 2024 Chen, Xia and Zhong. This is an open-
access article distributed under the terms of the
[Creative Commons Attribution License \(CC BY\)](#).
The use, distribution or reproduction in other
forums is permitted, provided the original
author(s) and the copyright owner(s) are
credited and that the original publication in this
journal is cited, in accordance with accepted
academic practice. No use, distribution or
reproduction is permitted which does not
comply with these terms.

In Vitro evaluation of the anti-pancreatic cancer activity of *epimedium* herb

Yangfeng Chen^{1*}, Han Xia² and Xiaohong Zhong^{1*}

¹College of Horticulture, Hunan Agricultural University, Changsha, China, ²Changsha Central Hospital, Changsha, China

Introduction: Pancreatic cancer (PC) is a particularly aggressive malignancy with limited therapeutic options. The search for innovative treatments has focused on traditional Chinese medicine, specifically *epimedium*. This research investigates *epimedium*'s active ingredients, potential targets, and underlying mechanisms in treating PC.

Methods: High-performance liquid chromatography (HPLC) was used to quantify the active components of *epimedium* and HPLC-Q-TOF-MS was employed for qualitative identification. Potential targets of *epimedium*'s active ingredients were identified using the TCMSP, ETCM, CTD, and Swiss Target Prediction databases. Potential PC-related targets were sourced from DisGeNET, GeneCards, and OMIM databases. A Venn diagram was utilized to identify overlapping PC-related and *epimedium* targets. Core targets and pathways were elucidated through protein-protein interaction (PPI) network analysis, Gene Ontology (GO) assessments, and Reactome pathway enrichment analyses. Molecular docking techniques investigated interactions between active compounds and these targets. The expression and prognostic implications of target genes were evaluated using GEPIA2 and the Human Protein Atlas (HPA) databases. *In vitro* studies assessed the impact of *epimedium* extract (EPE) on Panc-1 cell viability, and Western blot analysis examined the expression levels of key targets.

Results: Network pharmacological indicate that *epimedium* contains active components such as baohuoside I, icariin, hyperoside, and epimedin B, which have potential therapeutic effects against PC. *In vitro* assays confirmed that EPE significantly reduced the viability of Panc-1 cells. Western blot analysis revealed a considerable decrease in the expression of key targets in EPE-treated cells, including AKT1, EGFR, p-EGFR, JUN, BCL2, IL6, and SRC. The R-HSA-1280215: Interleukin-4 and Interleukin-13 signaling pathways involving these genes were identified as potential therapeutic targets.

Discussion: *Epimedium* holds promise as a candidate for treating PC. The modulation of interleukin-4 and interleukin-13 signaling pathways could be a pivotal mechanism by which *epimedium* impedes tumor development. Further research is warranted to validate these findings and explore the clinical applicability of *epimedium* in PC treatment.

KEYWORDS

pancreatic cancer, *epimedium*, hyperoside, icariin, baohuoside I, interleukin-4, interleukin-13

Introduction

Pancreatic cancer (PC) is a highly aggressive malignancy that has been on the rise over the past decade, with its incidence increasing from 43,140 to 60,430 cases (Jemal et al., 2010; Siegel et al., 2021). As a result, it is now the third leading cause of cancer-related deaths in the United States, after lung and breast cancers (Grossberg et al., 2020). While established risk factors for PC include age, gender, race/ethnicity, family history of the disease, smoking habits, diabetes, and obesity (Yamaguchi et al., 2017), its prevalence is still increasing due to the aging global population (Goral, 2015; Jia et al., 2018; Klein, 2021). Despite this alarming trend, there is still hope for the development of new treatments and therapies to combat this deadly disease. PC is typically asymptomatic at onset and progresses rapidly with early metastasis, resulting in many patients being diagnosed too late for surgery and a high mortality rate (Song et al., 2020; Ye et al., 2021).

Surgery with negative margin resection under a microscope is challenging and only benefits a few patients (Kamisawa et al., 2016). Therefore, radiotherapy or chemotherapy is necessary for most patients. In recent years, targeted therapies and immunotherapies have emerged as novel treatments, offering more options for those with advanced disease. However, they can be associated with adverse effects such as rash, liver dysfunction, or diarrhea (Rudin et al., 2008; Suzumura et al., 2012), which can affect the patient's quality of life or lead to discontinuation of therapy. Furthermore, these costly drugs are effective only for certain patients, highlighting the need to find more effective yet less toxic new drugs.

Chinese herbal medicine has a long history of use in the treatment of critically ill patients. Traditional Chinese herbs have been used for centuries to treat various ailments and diseases, including cancer (Zhang et al., 2014; Zhang et al., 2016). However, it is essential to note that some whole herbs may also contain toxins and non-medicinal chemicals. Further research is needed to understand the mechanisms and pathways involved in cancer treatment. Investigating active substances with precise chemical structures separated from herbs may be beneficial. Many natural compounds, such as paclitaxel and vinblastine, have been found to possess anticancer activity, either directly or indirectly. Even at high concentrations, multiple natural chemicals can be effectively tolerated by patients (Jiang et al., 2016; Rejhová et al., 2018). Thus, novel natural substances offer great promise for developing effective yet less toxic anticancer drugs.

Epimedium, guided by Traditional Chinese Medicine (TCM) principles of reinforcing positive and eliminating negative energy, employed in cancer treatment for an extensive period (Liu et al., 2021; Zhao et al., 2022). The polysaccharide (EPS) derived from the *epimedium* plant has been demonstrated to enhance the secretion of immunomodulatory cytokines by peritoneal macrophages and T cells, thereby reducing tumor burden. Moreover, icariin, a derivative of *epimedium* known as a prenylflavonoid, has demonstrated antitumor effects on diverse human cell lines, including breast, prostate, endometrial cancer, renal cell carcinoma, and leukemia (Guo et al., 2011; Tong et al., 2011). Furthermore, Wang et al. (2019) discovered its capability to inhibit tumor cell growth by generating reactive oxygen species and inducing DNA damage.

In 2007, Hopkins and colleagues introduced the concept of “network pharmacology,” which involves investigating the effects of

drugs on disease networks. This approach established a “drug-target-disease” network, offering an innovative approach to drug development. This approach enabled researchers to understand better the complex interactions among drugs, targets, and diseases while identifying new drug targets and potential drug combinations. Through the aid of network pharmacology, researchers can now enhance their ability to predict the efficacy and safety of drugs and develop new drugs that are more effective and possess fewer side effects (Liu and Du, 2009). In recent times, network pharmacology has been successfully employed in numerous studies to investigate the mechanisms of TCM (Wu et al., 2020). To advance our understanding of the mechanisms and pathways involved in the therapeutic effects of *epimedium* on PC, we applied this approach to examine its impact on PC and confirm its regulatory associations with key signaling pathways.

Materials and methods

Cells and reagents

Epimedium was obtained from Hunan Zirantang Traditional Chinese Medicine Pieces Co., Ltd. (production batch number: 230401). Hyperoside, Epimedin A, epimedin B, epimedin C, icariin, and baohuoside I standards (Purity $\geq 98\%$) were purchased from Shanghai Yuanye Co., Ltd. (Shanghai, China). The human pancreatic cancer cell line PANC-1 was acquired from Procell Co., Ltd. (Wuhan, China). DEME medium (#C11995500CP), 10% fetal bovine serum (#FSP500), and penicillin-streptomycin were obtained from Gibco. The ELISA kit was purchased from BOSTER Technology Co., Ltd. (Wuhan, China). DMSO, CCK-8 kit, RIPA lysis buffer (#PC0020), and BCA protein assay kit (#PC0020) were purchased from Solarbio Technology Co., Ltd. (Beijing, China). The antibodies used are as follows: EGFR (#ab52894), p-EGFR (#ab40815), AKT1 (#ab81283), JUN (#ab32385), IL6 (#ab214429), SRC (#ab109381), BCL2 (#ab182858) and β -actin (#ab8227) were purchased from Abcam (Cambridge, United Kingdom) and Cell Signaling Technology (Boston, MA, United States).

Preparation of *epimedium* extract

Epimedium sagittatum (Sieb.etZucc.) Maxim., a Berberidaceae plant, was purchased from Hunan Zirantang Traditional Chinese Medicine Pieces Co., Ltd. (production batch number: 230401) and identified by Professor Xiaohong Zhong. *Epimedium* extract (EPE) preparation method involved taking 100 g of *epimedium*, adding 8 times 70% ethanol, soaking for 30 min, boiling for 1.5 h, centrifuging at 10,000 RPM for 30 min, and collecting the supernatant. This extraction process was repeated twice, and the supernatants were mixed and evaporated to obtain a powder and stored at -20°C for later use.

Chemical determination of extract contents

Flavonoids are regarded as the main active ingredient in *epimedium* (Yang et al., 2020; Zhao et al., 2018). Flavonoids were

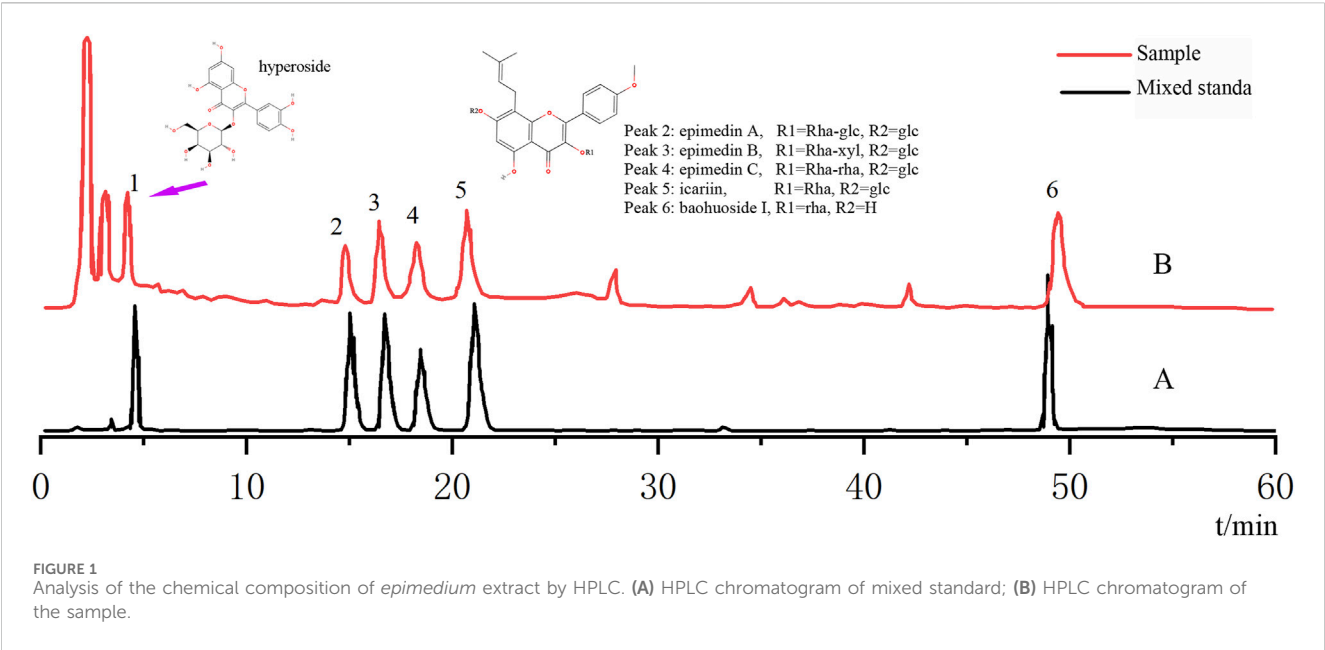


TABLE 1 Retention time (t_R), MS data, and UV spectra for identifying six compounds in *epimedium* extract by HPLC-Q-TOF-MS/MS.

Peak no.	R1	R2	t_R (min)	Identification	Formula for M	[M-H] ⁻		References
						Measured mass	Calcd mass	
1	---	---	4.67	Hyperoside	C ₂₁ H ₂₀ O ₁₂	463.0875	463.0882	Zhao et al. (2018)
2	Rha-glc	glc	14.38	Epimedin A	C ₃₉ H ₅₀ O ₂₀	837.2825	837.2823	Wang et al. (2010), Zhao et al. (2018)
3	Rha-xyl	glc	16.93	Epimedin B	C ₃₈ H ₄₈ O ₁₉	807.2714	807.2717	Wang et al. (2010), Zhao et al. (2018)
4	Rha-rha	glc	18.76	Epimedin C	C ₃₉ H ₅₀ O ₁₉	821.2866	821.2874	Wang et al. (2010)
5	Rha	glc	23.16	Icariin	C ₃₃ H ₄₀ O ₁₅	675.2291	675.2283	Wang et al. (2010), Zhao et al. (2018)
6	Rha	H	49.88	Baohuoside I	C ₂₇ H ₃₀ O ₁₀	513.1753	513.1766	Zhao et al. (2018)

detected and identified, and the contents were determined by liquid chromatography-ultraviolet/quadrupole-time-of-flight mass spectrometry (LC-Q-TOF-MS) (Wang et al., 2010; Zhao et al., 2018).

The preparation of the reference solution was carried out as follows: Accurately weigh an appropriate amount of each reference substance (hyperoside, epimedin A, epimedin B, epimedin C, icariin, baohuoside I) (5–10 mg) into a 50 mL volumetric flask, add 50% methanol to dissolve and dilute to the mark, filtered through a 0.45 μ m microporous membrane. Preparation of test solution: epimedium extract was accurately weighed and placed in a conical flask with a stopper. 70% ethanol (20 mL) was added, the weight was accurately measured, and the sample was sonicated for 10 min. The samples were then removed and left to cool down to room temperature, and the loss in weight was made up with 70% ethanol. After filtering through a 0.45 μ m microporous membrane, the filtrate was used as the test solution.

In brief, an ultra-performance liquid chromatograph, Agilent 1290, coupled with an Agilent 6495 tandem mass spectrometer (Agilent Technologies, Wilmington, DE, United States) was used. The chromatographic conditions were as follows: The chromatographic column was Hypersil BDS C18 (250 mm \times 4.6 mm, 5 μ m), column temperature was 25°C. The mobile phases of HPLC were composed of acetonitrile (A) and water (B). The linear gradient was adopted as follows: 24%–26% A at 0–20 min, 26%–30% A at 20–30 min, 30%–45% A at 30–45 min, 45%–60% A at 45–50 min, 60% to 24%A at 50–60 min. The flow rate was 1.0 mL/min with detection at 270 nm. The injection volume was 10.0 μ L. MS conditions: electrospray ion source (ESI), positive and negative ion modes, and scanning range of m/z 100–2,000; dry gas temperature 350°C, dry gas flow rate 10 L \cdot min⁻¹, spray voltage 30 psi, fragmentor voltage 135 V, cone voltage 65 V, ion spray voltage (IS) 3500 V (positive ion mode)/-4000 V (negative ion mode). For MS/

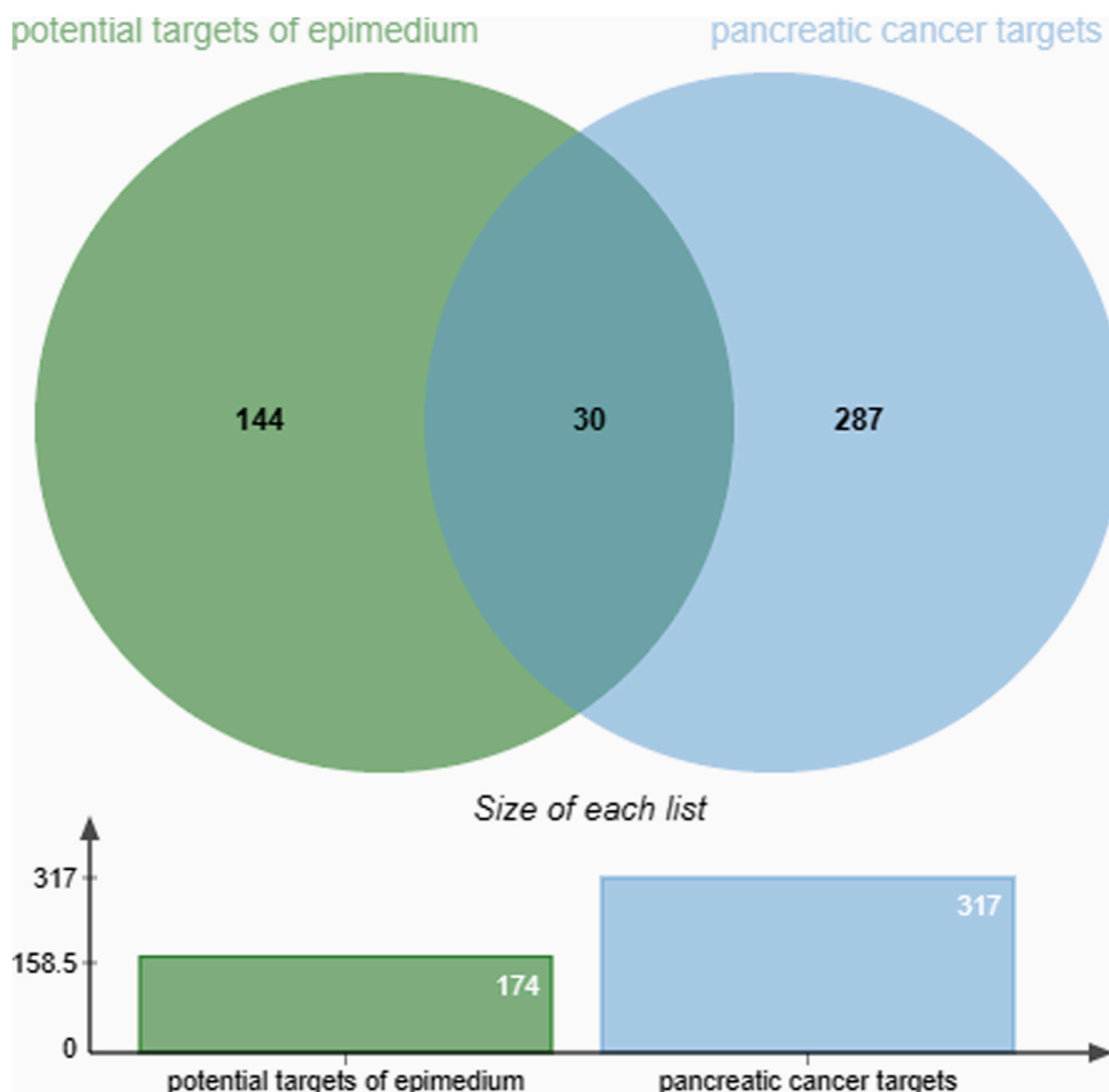


FIGURE 2

The intersection of the active ingredient and pancreatic cancer targets is represented in 30 overlapping targets.

MS analyses, auto-MS/MS was performed with a collision energy between 10 and 55 eV.

Screening of related targets

The potential targets of active ingredients of epimedium were screened from the following databases: Traditional Chinese Medicine Systems Pharmacology (TCMSP) database (<https://www.tcm-sp-e.com/>) (Ye et al., 2022) Encyclopedia of Traditional Chinese Medicine (ETCM, <http://www.tcmip.cn/ETCM2/front/#/>) (Xu et al., 2019), Swiss Target Prediction (<http://www.swisstargetprediction.ch/>), Comparative Toxicogenomics Database (CTD) (<https://ctdbase.org/>). Ultimately, the potential targets of *epimedium* were identified

by standardizing and removing duplicates using the Uniprot database (<https://www.uniprot.org/>).

Acquisition of potential anti-pancreatic cancer targets and their shared targets with *epimedium*

To identify genes associated with pancreatic cancer, we conducted a thorough search of the GeneCards, GeneCards, and OMIM databases, focusing on the "*Homo sapiens*" species and using the keywords "pancreatic cancer." As a result, we were able to pinpoint genes that have been previously reported to be linked with pancreatic cancer. Subsequently, we carefully eliminated any duplicate entries and false positives from the

TABLE 2 The overlapping targets of active ingredient targets and Pancreatic cancer targets.

Uniprot ID	Gene Symbol	Uniprot ID	Gene Symbol
O14746	TERT	P12931	SRC
O43521	BCL2L11	P15056	BRAF
P00533	EGFR	P15692	VEGFA
P01133	EGF	P17174	GOT1
P01137	TGFB1	P27361	MAPK3
P01375	TNF	P28482	MAPK1
P01584	IL1B	P31749	AKT1
P03372	ESR1	P37231	PPARG
P05231	IL6	P42345	MTOR
P05412	JUN	P60568	IL2
P07477	PRSS1	Q07812	BAX
P07900	HSP90AA1	Q13485	SMAD4
P10275	AR	Q14790	CASP8
P10415	BCL2	Q15465	SHH
P11388	TOP2A	Q16236	NFE2L2

gene list, cross-referencing it with previously identified potential targets of *epimedium*. Consequently, we successfully identified potential targets for combating pancreatic cancer using *epimedium*.

Protein-protein interaction construction

By inputting the potential anti-pancreatic cancer targets of *epimedium* into the STRING database (<https://cn.string-db.org/>), restricted to the “*H. sapiens*” species and filtered with a minimum interactome requirement score of >0.7 (Von Mering et al., 2005), we acquired protein-protein interaction relationships. Subsequently, we employed Cytoscape (version 3.7.1) to visually represent the PPI network. Moreover, we installed the CytoNCA package to conduct network topology analysis, aiming to identify crucial target genes associated with the mechanism of icariin. In order to identify highly interconnected subnetworks within the PPI network, we employed Cytoscape’s Molecular Complex Detection technique (MCODE) (Bader and Hogue, 2003).

Protein functional enrichment analysis

To gain a deeper understanding of the potential biological functions of *epimedium* in the treatment of pancreatic cancer, we carried out gene ontology (GO), biological processes (BPs), and Reactome pathway enrichment analyses using the DAVID Database (Sherman et al., 2022) and Reactome Database (Wright et al., 2022). The resulting data was organized according to their adjusted *p* values.

Ingredient-target-pathway network construction

An Ingredient-Target-Pathway (I-T-P) network was established in Cytoscape (version 3.7.1), encompassing overlapping genes, pathways, and selected active components. Nodes of diverse colors represented various clusters, while edges delineated node relationships.

Molecular docking verification of core active ingredients and core targets

Molecular docking was performed to validate the interaction between the core active ingredient and the core target identified in the PPI network. The three-dimensional structures of the core targets were obtained from the Protein Data Bank (PDB, www.rcsb.org), and the two-dimensional structures of the top five core compounds were acquired from PubChem in SDF format. PyMOL v2.4, an open-source molecular graphics tool, was used to remove solvent and organic components to prepare for molecular docking. Subsequently, AutoDock Tools (version 1.5.6) were employed for molecular docking, and the resulting data was analyzed and interpreted using PyMOL v2.4.

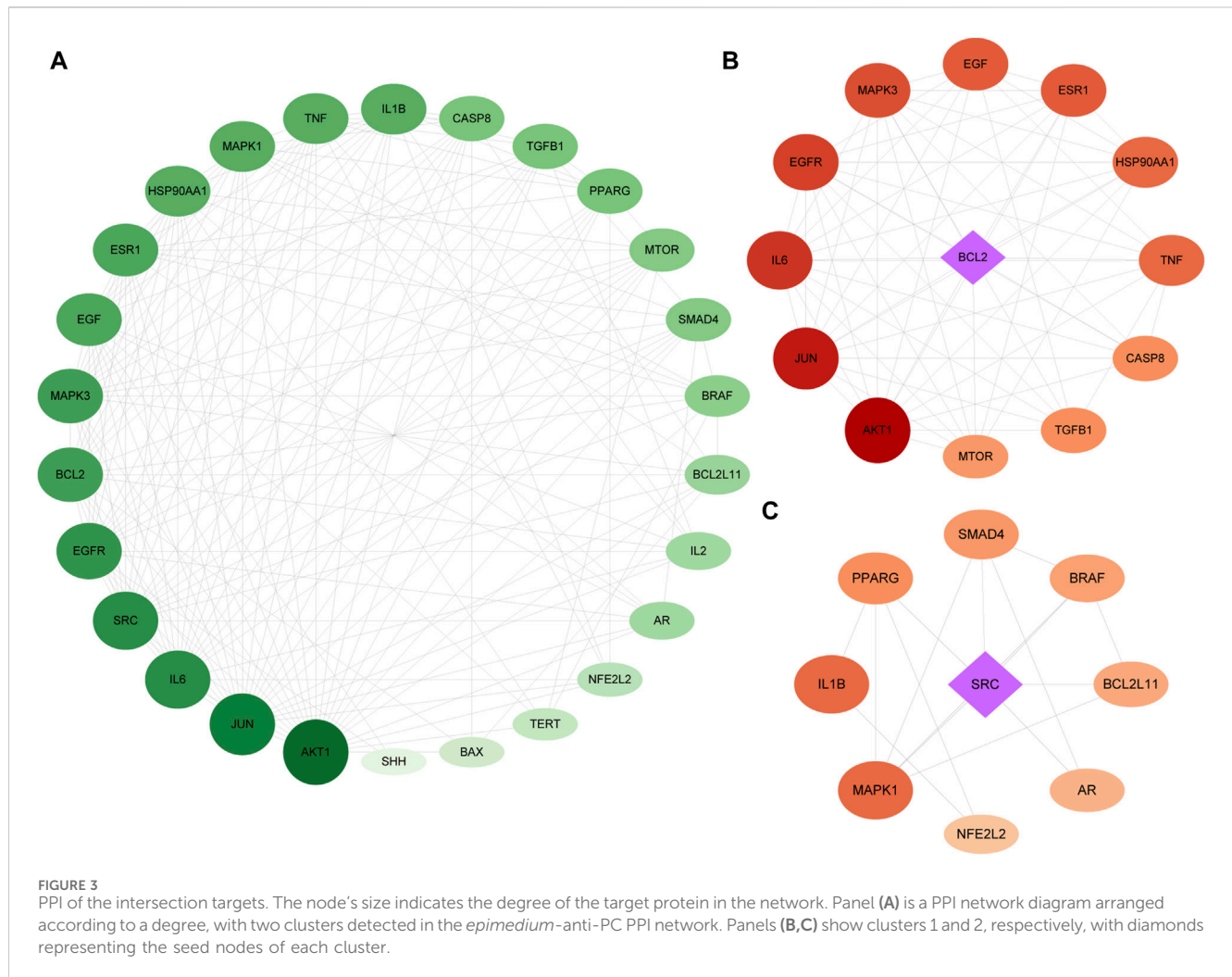
Validation of core targets in GEPIA2 and HPA database

The Gene Expression Profiling Interactive Analysis (GEPIA 2; <http://gepia2.cancer-pku.cn/>) web server is a publicly available database that analyzes gene expression in tumor and normal samples from TCGA and GTEx. We used GEPIA two to analyze the expression levels of core targets relevant to our research question in normal pancreatic and pancreatic adenocarcinoma (PAAD) tissues. Additionally, we investigated the overall survival data of these core targets using the Human Protein Atlas (HPA; <https://www.proteinatlas.org/>), an open-access database that employs various omics technologies. HPA provides comprehensive mappings of human protein expression patterns in cells, tissues, and organs through antibody-based imaging, mass spectrometry-based proteomics, and transcriptomics.

Experimental validation

Cell culture and viability assays

Cell culture and viability assays were performed as described previously (Shen et al., 2020). Briefly, Panc-1 cells were cultured in 10% fetal calf serum and 100 U/mol penicillin-streptomycin solution at 37°C, 5% CO₂, and 95% relative humidity. After the intervention, each cell was in the logarithmic growth phase. EPE was dissolved in DMSO at a concentration of 200 mg/mL and then diluted to different concentrations of EPE (0, 100, 200, 300, 400, 500, and 600 µg/mL) for pretreatment. The pretreatment time was 48 h. Cell viability was assessed using a Thermo Fisher microplate spectrophotometer with the CCK-8 assay, following the manufacturer’s instructions. The optical density (OD) of the



solution at 450 nm in each well was measured. All data were normalized to control wells without cells and expressed as mean \pm standard deviation (SD).

Western blot

Panc-1 cells were seeded in 6-well plates at a density of 3×10^5 cells per well. After incubating for 48 h, EPE (200 μ g/mL or 400 μ g/mL) was added and treated for 48 h. The cells were then collected, and total protein was extracted using radioimmunoprecipitation assay (RIPA) buffer, which contained phenylmethylsulfonyl fluoride (PMSF), aprotinin, and phosphatase inhibitors. The supernatant was collected after centrifugation ($14,000 \times g$, 4°C for 15 min), and the protein concentration was determined using a BCA protein assay kit (Genview, United States). 25 μ g of each protein sample was separated by SDS-PAGE and transferred to a polyvinylidene fluoride (PVDF) membrane (Millipore, Bedford, MA, United States). The membranes were then blocked with 5% bovine serum albumin (BSA) for 2 h at room temperature. Primary antibodies for AKT1, EGFR, p-EGFR, JUN, BCL2, IL6, and SRC were added and incubated overnight at 4°C . After three washes, an enzyme-labeled secondary antibody IgG (1:2000) was used to incubate for 2 h at room temperature under dark conditions. Finally, a secondary antibody (1:5000, ab clone) was added and incubated at room

temperature for 2 h. Finally, membranes were washed and developed by adding enhanced chemiluminescence (ECL) substrate (Thermo Fisher Scientific, Rockford, United States). Proteins were visualized using the intelligent gel imaging system iBright FL1000 (ThermoFisher, Rockford, United States).

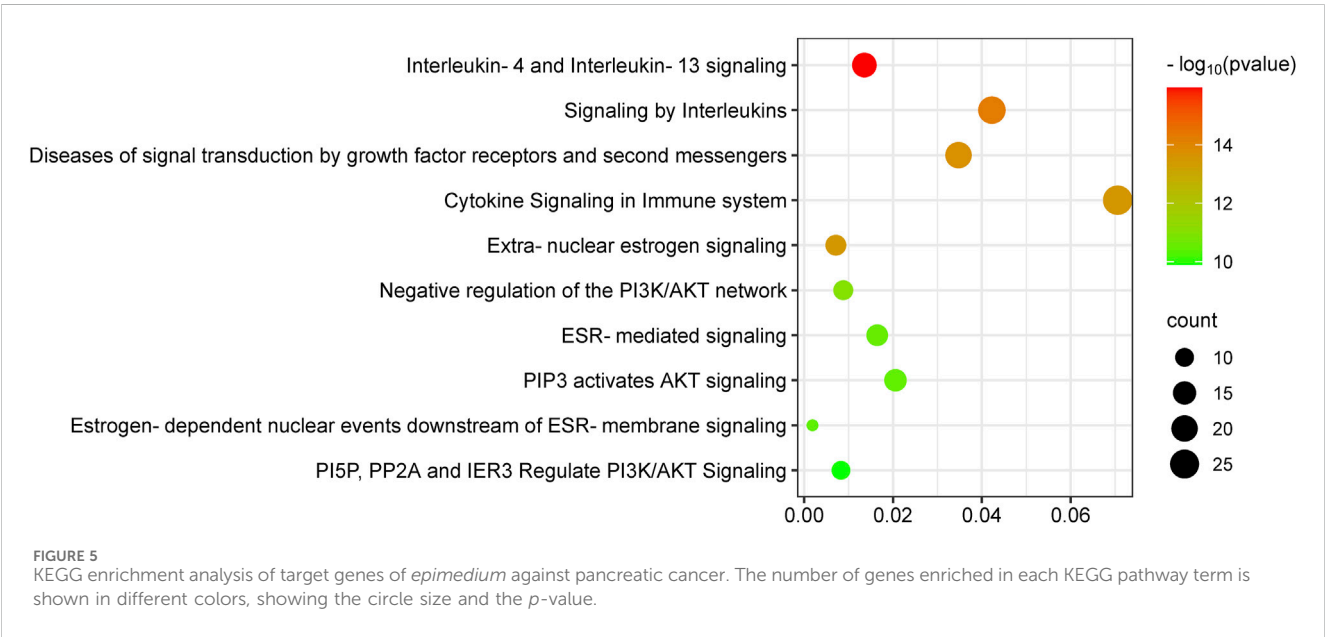
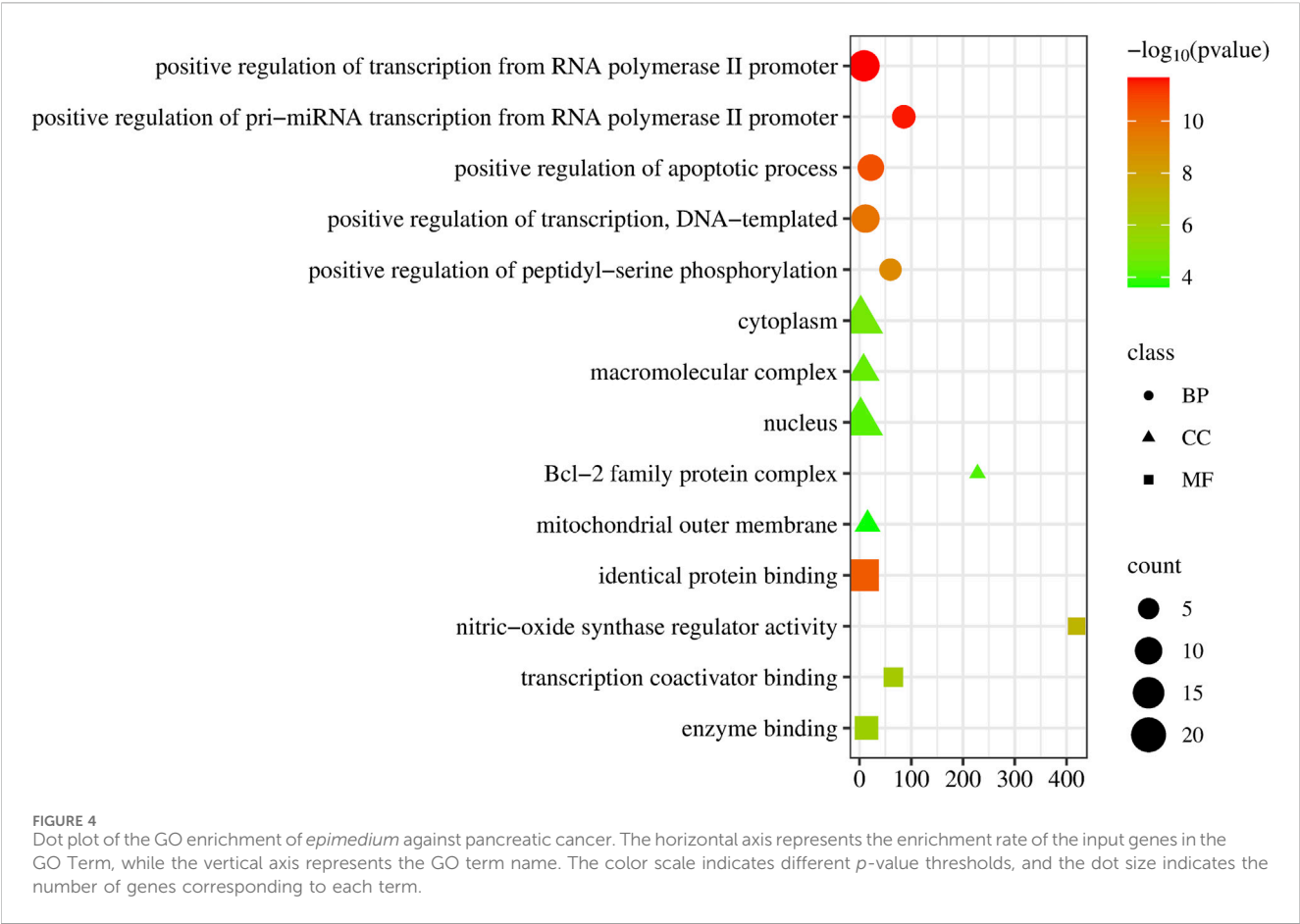
Statistical analyses

Statistical analysis was conducted on SPSS 22.0 (SPSS, Chicago, IL, United States), with a data-processing method of independent-sample *t*-test. Comparisons between groups were statistically analyzed, and $*p < 0.05$, $**p < 0.01$, $***p < 0.001$, $****p < 0.0001$ was considered to be statistically significant.

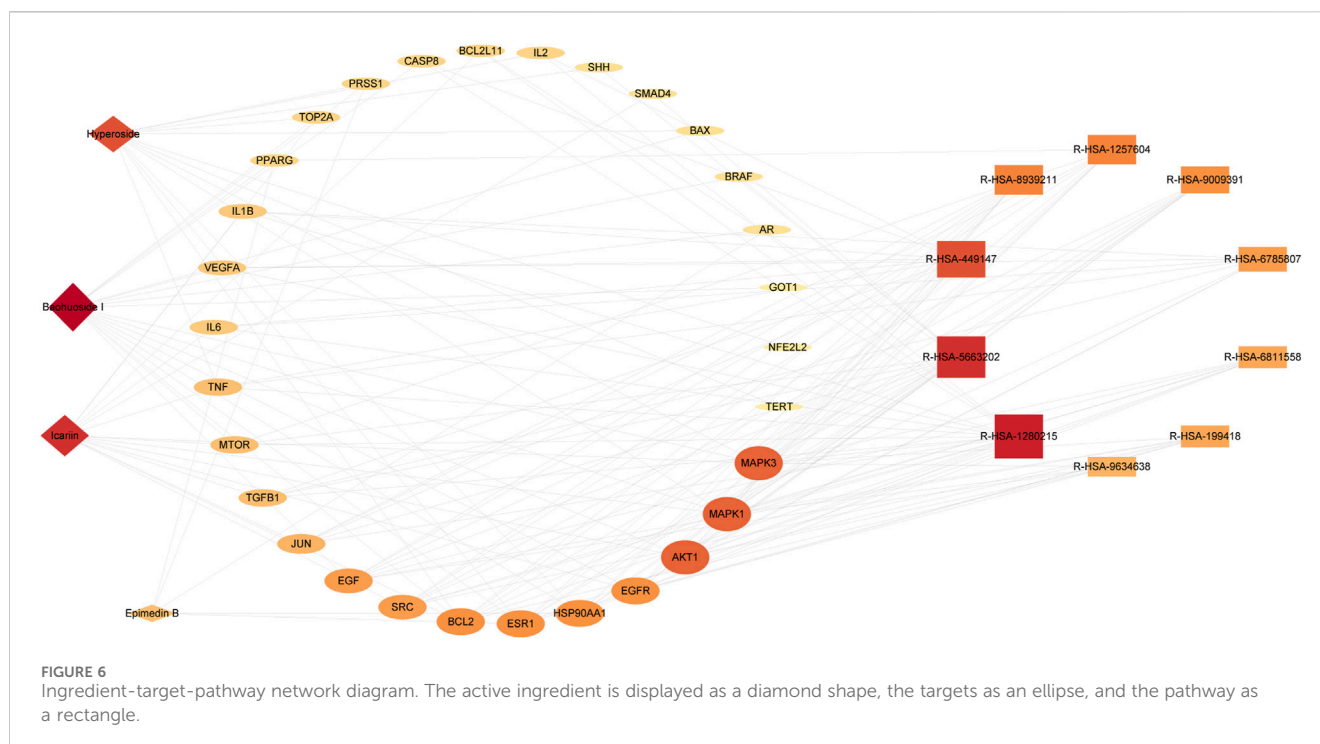
Results

Identification and content of active ingredients in *epimedium*

All the calibration curves showed a good linear regression relationship in the test range ($r > 0.999$). RSDs of precision, stability, and repeatability were all less than 3.0%. Therefore, the HPLC method was precise, accurate, and sensitive enough for simultaneous quantitative



analysis of the six flavonoids in *epimedium* extract. The HPLC analysis identified hyperoside, epimedin A, epimedin B, epimedin C, icariin, and baohuoside I as the primary compounds, with EPE at 200 $\mu\text{g/mL}$ containing 1.6 $\mu\text{g/mL}$ of hyperoside, 5.8 $\mu\text{g/mL}$ of icariin, 5.9 $\mu\text{g/mL}$ of epimedin A, 20.3 $\mu\text{g/mL}$ of epimedin B, and 3.4 $\mu\text{g/mL}$ of epimedin C, 4.8 $\mu\text{g/mL}$ of baohuoside I.



Based on the optimization of the elution program, we used high-performance HPLC-Q-TOF-MS/MS to perform a qualitative analysis of compounds in epimedium extract. By comparing the retention time (t_R) and characteristic fragment ions with reference compounds and literature data, a total of six compounds were identified. See Figure 1 and Table 1 for details.

Acquisition of potential targets of epimedium against PC

Based on TCMSP, ETCM, CTD database, and Swiss Target Prediction, a total of 174 potential targets were identified for the six active ingredients from *epimedium*, including hyperoside, epimedin A, epimedin B, and epimedin C, icariin, and baohuoside I (Supplementary Table S1).

The GeneCards, GeneCards, and OMIM databases revealed 316 targets associated with PC. Subsequently, a Venn diagram was utilized to identify 30 overlapping targets between the PC-related targets and the potential targets of *epimedium* (Figure 2; Table 2).

Construction of a protein-protein network

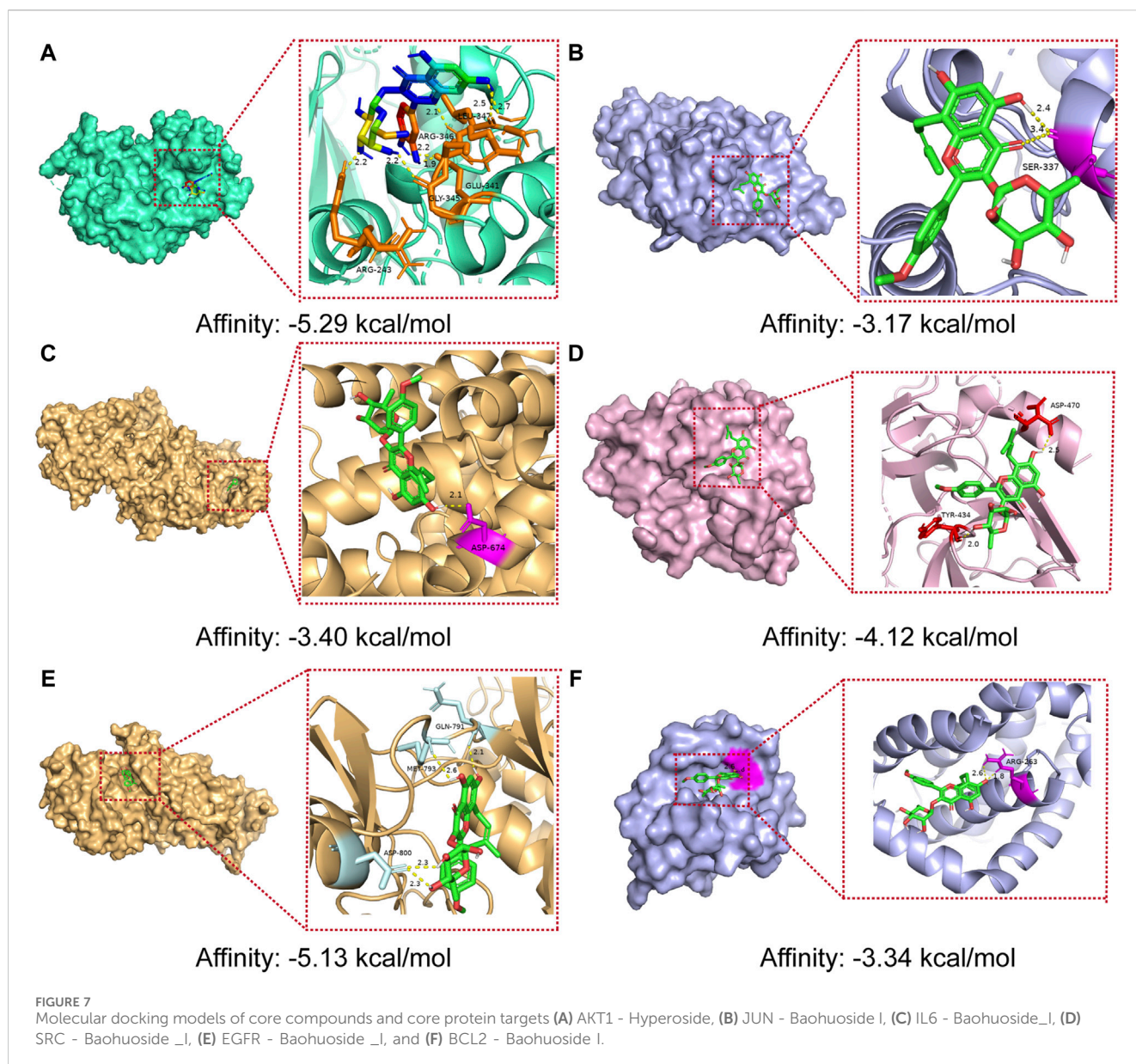
The genes related to the 30 overlapping targets were used to establish protein-protein interaction (PPI) relationships through the String database. The resultant PPI network was visualized using Cytoscape 3.7.1, revealing 26 protein nodes and 168 edges

representing their interactions. Nodes with a deeper shade of red indicated higher degree values, signifying a strong association between these targets and PC (Figure 3A).

We utilized MCODE analysis to identify three functionally related protein clusters based on topology within the PPI network. The cluster attributes are presented in Figures 3B, C. In PPI networks, clusters formed by interlinked nodes often represent protein complexes or pathways. Similarly, clusters in protein similarity networks typically indicate protein families, where the proteins within a cluster exhibit similar structures and functions.

GO enrichment and KEGG enrichment

Upon uploading the 30 overlapped targets to the DAVID database for GO enrichment analysis, we identified 129 biological processes (BP). The top five processes included positive regulation of transcription from RNA polymerase II promoter, positive regulation of pri-miRNA transcription from RNA polymerase II promoter, positive regulation of apoptotic process, positive regulation of transcription, DNA-templated, positive regulation of peptidyl-serine phosphorylation. Additionally, 32 cellular components (CC) were identified, with the top five being cytoplasm, macromolecular complex, nucleus, Bcl-2 family protein complex, and mitochondrial outer membrane. Moreover, 32 molecular functions (MF) were identified, with the top five being identical protein binding, nitric-oxide synthase regulator activity, nitric-oxide synthase regulator activity, transcription coactivator binding, and enzyme binding (Figure 4).



The Reactome pathway enrichment analysis identified 657 pathways, with the top 10 pathways visually represented in Figure 5. These pathways exhibit notable enrichment in processes associated with anti-PC effects, encompassing Interleukin-4 and Interleukin-13 signaling, Signaling by Interleukins, Diseases of signal transduction by growth factor receptors and second messengers, Cytokine Signaling in Immune system, and Extracellular estrogen signaling.

Ingredient-target-pathway network construction

The analysis of the Ingredients-Targets-Pathways network revealed 44 nodes and 152 edges, consisting of four active

constituents of *epimedium* (baohuoside I, icariin, hyperoside, epimedin B), 30 potential anti-PC targets, and 10 pathways (Figure 6). Our findings illustrated that baohuoside I had the highest level of connectivity with 18 targets, followed by icariin (15), hyperoside (13), and epimedin B (5), indicating their potential involvement in regulating pathways associated with PC.

Molecular docking verification of core active ingredients and core protein targets

The results of molecular docking studies have revealed the binding strength of the essential active constituents present in *epimedium* with their specific protein targets. After conducting I-T-P network screening, we identified baohuoside I, icariin, hyperoside, and epimedin B as the

TABLE 3 The binding energy values of core compounds of *epimedium* and core targets.

Target	Compounds	Binding affinity/(kcal/mol)
AKT1 (4GV1)	Baohuoside I	−4.61
	Icariin	−4.63
	Hyperoside	−5.29
	Epimedin B	−2.68
JUN (2P33)	Baohuoside I	−3.17
	Icariin	−1.79
	Hyperoside	−2.02
	Epimedin B	−1.45
IL6 (5SFK)	Baohuoside I	−3.40
	Icariin	−1.22
	Hyperoside	−1.84
	Epimedin B	−1.82
SRC (3SOS)	Baohuoside I	−4.12
	Icariin	−2.51
	Hyperoside	−2.78
	Epimedin B	−2.62
EGFR (3IKA)	Baohuoside I	−5.13
	Icariin	−2.84
	Hyperoside	−3.91
	Epimedin B	−1.25
BCL2 (6U64)	Baohuoside I	−3.34
	Icariin	−2.54
	Hyperoside	−2.18
	Epimedin B	−1.05

core compounds. The hub protein targets comprise the top five node degree proteins (AKT1, JUN, IL6, SRC, and EGFR) and two seed nodes in clusters (SRC and BCL2).

The binding affinities of the six core active ingredients to their respective target proteins were investigated. Baohuoside I displayed solid binding affinities, ranging from −3.17 kcal/mol to −5.13 kcal/mol, with JUN, IL6, SRC, EGFR, and BCL2, respectively, while icariin and hyperoside exhibited a high affinity of −4.63 and −5.29 kcal/mol with AKT1. The strong binding of the small-molecule active ingredients was attributed to various interactions (as shown in Figure 7; Table 3).

Validation of key targets in GEPIA2 and HPA database

The analysis using the GEPIA two database revealed that the expression of core targets (AKT1, IL6, and SRC) was higher in

PAAD samples compared to normal pancreas tissues ($p < 0.05$; Figure 8). Moreover, the examination of overall survival data from the HPA database indicated that high expression of EGFR and IL6 was correlated with a significantly poorer prognosis ($p < 0.05$; Figure 9).

In vitro experimental validation

To investigate the impact of EPE on pancreatic cancer cells, we employed Cell Counting Kit-8 (CCK-8) to assess the cell viability of Panc-1 cells following treatment with varying concentrations of EPE (Figure 10). Our findings revealed a noteworthy effect of EPE on the viability of Panc-1 cells in a dose-dependent manner with a half-maximal inhibitory concentration (IC₅₀) of 207.0 μg/mL.

The R-HSA-1280215: Interleu in-4 and Interleukin-13 signaling was the first pathway obtained in the KEGG pathway enrichment analysis, involving downstream proteins. To verify the effect of EPE on key targets, we utilized the Western blot method to measure the expression of AKT1, EGFR, p-EGFR, JUN, BCL2, IL6 and SRC proteins in Panc-1 cells. The results, shown in Figure 10B, indicate a significant decrease in the expression of AKT1, EGFR, p-EGFR, JUN, BCL2, IL6, and SRC in EPE-treated Panc-1 cells.

Discussion

PC exhibits a high mortality rate and is frequently diagnosed at advanced stages, posing significant challenges for effective treatment. Therefore, it is essential to develop novel therapeutics and drugs to improve the quality of life and extend the lifespan of affected individuals. The progression of PC involves intricate biological processes, such as metabolic disorders, local inflammation, and aberrant molecular pathways (Motoo et al., 2011; Ansari et al., 2019). As a result, single-drug therapies targeting a single pathway may not be sufficient to achieve optimal therapeutic efficacy (Li et al., 2019).

Studies have indicated that various components of TCM, including the Qingyi Huaji formula (Hua et al., 2014; Zhang et al., 2013) and Huang-Qin-Tang (Saif et al., 2014), can effectively boost the immune system and suppress the proliferation of PC cells. These components play a beneficial role in enhancing immunity against infectious diseases and mitigating factors that disrupt normal physiological functions (Li et al., 2015). Moreover, single-herb TCM or herbal formulas have demonstrated the ability to engage multiple targets and pathways of action.

In this study, network pharmacology was employed to investigate the mechanism of *epimedium*'s action against PC. By analyzing the PPI network, we identified six potential therapeutic core targets (AKT1, EGFR, JUN, BCL2, IL6, and SRC) that exhibited significant correlations with PC. Subsequently, we performed molecular docking calculations to evaluate the binding affinities of *epimedium*'s active ingredients to these proteins. The results revealed that baohuoside I, icariin, hyperoside, and epimedin B displayed high binding affinities to AKT1, EGFR, JUN, BCL2, IL6 and SRC, indicating their potential relevance in PC treatment.

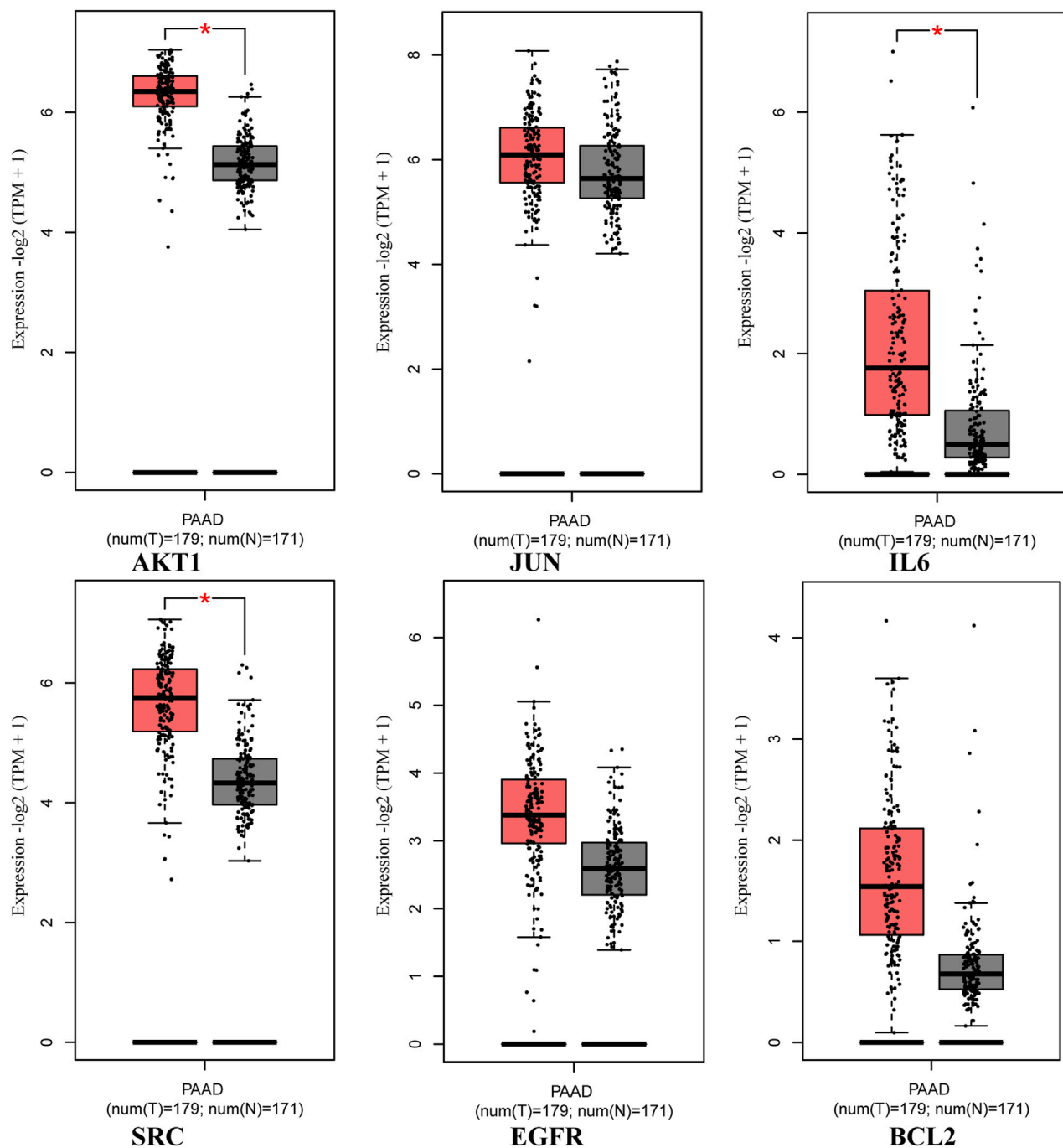
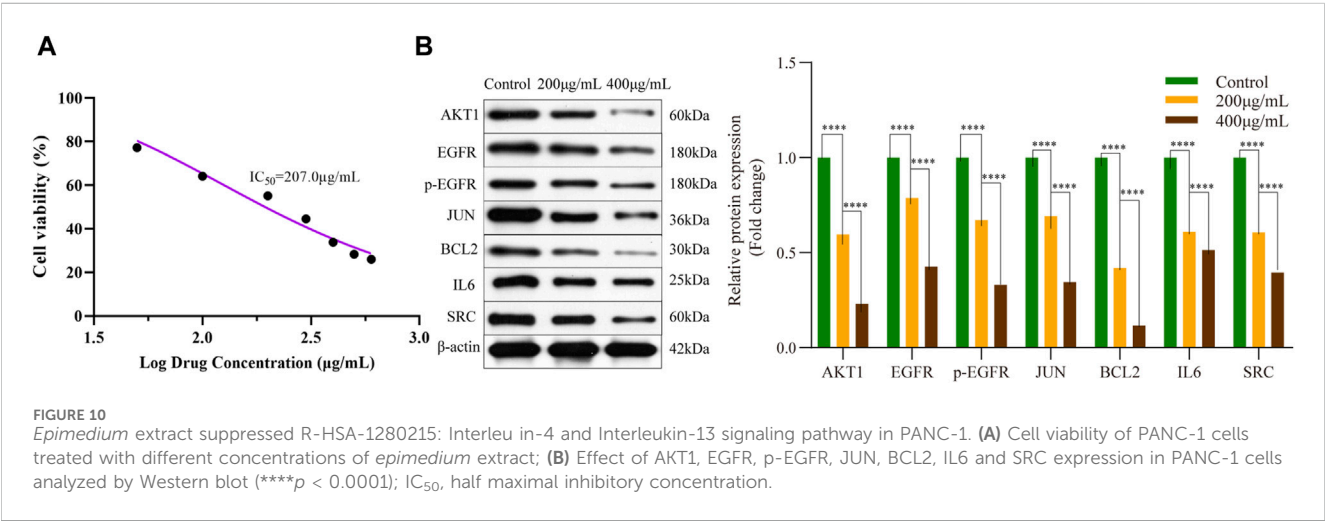
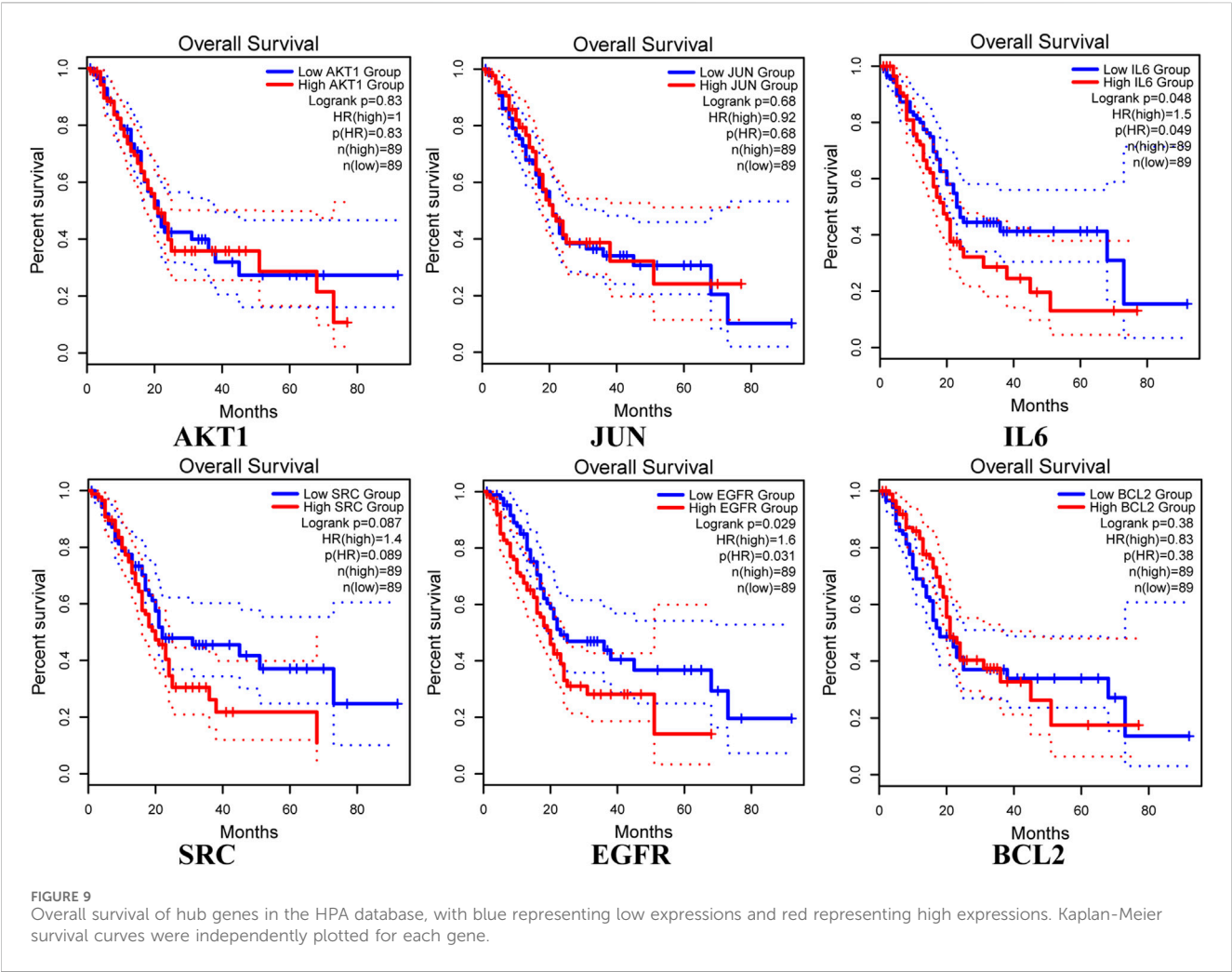


FIGURE 8
Expression of core targets in the GEPIA2 database. The red box plots represent the tumor, and the gray box plots represent normal. Match TCGA normal and GTEx data.

The validation of key targets using the GEPIA2 and HPA databases revealed significantly higher expressions of AKT1, IL6, and SRC in PAAD tissues compared to normal pancreatic tissues. Furthermore, high expressions of EGFR and IL6 were associated with significantly poorer survival rates.

In the development and progression of cancer, AKT1, JUN, IL6, SRC, EGFR and BCL2 plays a critical role. Akt1 (serine-threonine protein kinase) is a part of the PI3K-dependent

signaling pathway and is a key cell survival protein functionally involved in antiapoptosis in various cancers (Goswami et al., 2006). Epidermal growth factor receptor (EGFR) is a trans-membrane receptor tyrosine kinase. It plays a critical oncogenic role in cancer growth, survival, migration, and invasion (Jiang et al., 2017). The study demonstrated that epimedium extract inhibits the expression and phosphorylation of AKT1 and EGFR in the pancreatic cancer cell line PANC-1.



Similar findings have been previously documented. For instance, [Geng et al. \(2014\)](#) reported that icarisiide II inhibits the proliferation of transplantable tumors and the EGFR/mTOR signaling pathway, leading to reduced phosphorylation of EGFR and AKT1 proteins. In addition, [Ding et al. \(2018\)](#) indicated that Icarin enhances the sexual function of male mice by activating the PI3K/Akt/eNos/No signaling pathway. Furthermore, [Li et al. \(2020\)](#) demonstrated that icariin, via the

EGFR/PI3K/mTOR signaling pathways, decreases the expression and phosphorylation of EGFR and Akt proteins. Moreover, Sun et al. (2022) found that icariin interacts with the estrogen receptor on the cell membrane, resulting in elevated phosphorylation levels of Akt and Creb proteins and increased transcription of genes encoding steroidogenic enzymes and testosterone synthesis.

EGFR^{Y1068} phosphorylation can be characterized by its association with the recruitment of specific signaling proteins and its potential role as a predictive biomarker for treatment response in certain cancer patients (Sette et al., 2015; Wirth et al., 2023). EGFR^{Y1068} phosphorylation induces the recruitment of Grb2 and Gab1, leading to the activation of the AKT and STAT3/5 signaling pathways (Wirth et al., 2023). Prior research indicates that Icariin suppresses the epithelial-mesenchymal transition process induced by epidermal growth factor by downregulating the PI3K/Akt signaling pathway (Wang et al., 2021). Icariin can diminish the expression of ERα36 and hinder E2β-triggered Akt phosphorylation, showing heightened efficacy in suppressing TNBC cell proliferation and facilitating apoptosis when combined with the EGFR inhibitor Cetuximab (Yin et al., 2020). Additionally, it inhibits the activation of ERK1/2 and Akt induced by ionizing radiation (Hong et al., 2013), diminishes STAT3, and Akt in MDSCs, leading to the differentiation of MDSCs into dendritic cells and macrophages (Zhou et al., 2011). In our study, epimedium extract was found to inhibit EGFR^{Y1068} phosphorylation in the pancreatic cancer cell line, PANC-1. However, it should be noted that the epimedium extract used in this study consisted of various components, including hyperoside, epimedin A, epimedin B, epimedin C, icariin, and baohuoside I. Further investigation is required to discern the specific active ingredients and elucidate the underlying mechanisms responsible for the inhibitory effects of epimedium extract on EGFR^{Y1068} phosphorylation.

BCL2 is widely recognized as a multifunctional anti-apoptotic protein in various types of cancer. The overexpression of the BCL2 is linked to tumor initiation, progression, and resistance to current anticancer therapies (Das et al., 2020). Icariin has been shown to enhance its antioxidant and anti-apoptotic functions by inhibiting the phosphorylation of BCL2 (Zhang et al., 2016). Additionally, hyperoside relieved H₂O₂-induced oxidative stress and attenuated H₂O₂-induced apoptosis of granulosa cells, resulting in decreased expression of the BCL2 protein (Wang et al., 2019). Icariin and hyperoside are critical active components of epimedium extract in our study.

Conclusion

This study employed bioinformatics, network pharmacology, database verification, and *in vitro* validation to identify potential active compounds and pathways of *epimedium* in the treatment of PC. Through the regulation of genes such as AKT1, EGFR, JUN, BCL2, IL6 and SRC, *epimedium* was found to modulate the R-HSA-1280215: Interleu in-4 and Interleukin-13 signaling pathway. The findings suggest that further investigation of *epimedium* as a subsequent treatment for PC is warranted.

Data availability statement

The original contributions presented in the study are included in the article/Supplementary Material, further inquiries can be directed to the corresponding authors.

Ethics statement

Ethical approval was not required for the studies on humans in accordance with the local legislation and institutional requirements because only commercially available established cell lines were used. Ethical approval was not required for the studies on animals in accordance with the local legislation and institutional requirements because only commercially available established cell lines were used.

Author contributions

YC: Conceptualization, Formal Analysis, Investigation, Methodology, Validation, Writing–original draft, Writing–review and editing. HX: Investigation, Methodology, Visualization, Writing–review and editing. XZ: Conceptualization, Supervision, Validation, Writing–original draft, Writing–review and editing.

Funding

The author(s) declare that no financial support was received for the research, authorship, and/or publication of this article. This study was supported by the Science and Technology Innovation Program of Hunan Province (Grant no. 142203900999).

Conflict of interest

The authors declare that the research was conducted in the absence of any commercial or financial relationships that could be construed as a potential conflict of interest.

Publisher's note

All claims expressed in this article are solely those of the authors and do not necessarily represent those of their affiliated organizations, or those of the publisher, the editors and the reviewers. Any product that may be evaluated in this article, or claim that may be made by its manufacturer, is not guaranteed or endorsed by the publisher.

Supplementary material

The Supplementary Material for this article can be found online at: <https://www.frontiersin.org/articles/10.3389/fphar.2024.1389221/full#supplementary-material>

References

- Ansari, D., Ohlsson, H., Althini, C., Bauden, M., Zhou, Q., Hu, D., et al. (2019). The hippo signaling pathway in pancreatic cancer. *Anticancer Res.* 39 (7), 3317–3321. doi:10.21873/anticancer.13474
- Bader, G. D., and Hogue, C. W. V. (2003). An automated method for finding molecular complexes in large protein interaction networks. *BMC Bioinforma.* 4 (1), 2. doi:10.1186/1471-2105-4-2
- Das, J., Chakraborty, S., and Maiti, T. K. (2020). Mechanical stress-induced autophagic response: a cancer-enabling characteristic? *Semin. Cancer Biol.* 66, 101–109. doi:10.1016/j.semcancer.2019.05.017
- Ding, J., Tang, Y., Tang, Z., Zu, X., Qi, L., Zhang, X., et al. (2018). Icaritin improves the sexual function of male mice through the PI3K/AKT/eNOS/NO signalling pathway. *Andrologia* 50 (1), e12802. doi:10.1111/and.12802
- Geng, Y.-D., Yang, L., Zhang, C., and Kong, L.-Y. (2014). Blockade of epidermal growth factor receptor/mammalian target of rapamycin pathway by Icariside II results in reduced cell proliferation of osteosarcoma cells. *Food Chem. Toxicol.* 73, 7–16. doi:10.1016/j.fct.2014.08.002
- Goral, V. (2015). Pancreatic cancer: pathogenesis and diagnosis. *Asian Pac. J. Cancer Prev.* 16 (14), 5619–5624. doi:10.7314/apjcp.2015.16.14.5619
- Goswami, A., Ranganathan, P., and Rangnekar, V. M. (2006). The phosphoinositide 3-kinase/Akt1/Par-4 axis: a cancer-selective therapeutic target. *Cancer Res.* 66 (6), 2889–2892. doi:10.1158/0008-5472.Can-05-4458
- Grossberg, A. J., Chu, L. C., Deig, C. R., Fishman, E. K., Hwang, W. L., Maitra, A., et al. (2020). Multidisciplinary standards of care and recent progress in pancreatic ductal adenocarcinoma. *CA Cancer J. Clin.* 70 (5), 375–403. doi:10.3322/caac.21626
- Guo, Y., Zhang, X., Meng, J., and Wang, Z. Y. (2011). An anticancer agent icaritin induces sustained activation of the extracellular signal-regulated kinase (ERK) pathway and inhibits growth of breast cancer cells. *Eur. J. Pharmacol.* 658 (2–3), 114–122. doi:10.1016/j.ejphar.2011.02.005
- Hong, J., Zhang, Z., Lv, W., Zhang, M., Chen, C., Yang, S., et al. (2013). Icaritin synergistically enhances the radiosensitivity of 4T1 breast cancer cells. *PLoS One* 8 (8), e71347. doi:10.1371/journal.pone.0071347
- Hua, Y. Q., Chen, Z., Meng, Z. Q., Chen, H., Shen, J. G., Wang, K., et al. (2014). High expression of erythropoietin-producing hepatoma cell line-B2 (EphB2) predicts the efficiency of the Qingyihuaji formula treatment in pancreatic cancer CFPAC-1 cells through the EphrinB1-EphB2 pathway. *Oncol. Lett.* 8 (1), 17–24. doi:10.3892/ol.2014.2134
- Jemal, A., Siegel, R., Xu, J., and Ward, E. (2010). Cancer statistics, 2010. *CA Cancer J. Clin.* 60 (5), 277–300. doi:10.3322/caac.20073
- Jia, X., Du, P., Wu, K., Xu, Z., Fang, J., Xu, X., et al. (2018). Pancreatic cancer mortality in China: characteristics and prediction. *Pancreas* 47 (2), 233–237. doi:10.1097/mpa.0000000000000976
- Jiang, R., Tang, J., Chen, Y., Deng, L., Ji, J., Xie, Y., et al. (2017). The long noncoding RNA lnc-EGFR stimulates T-regulatory cells differentiation thus promoting hepatocellular carcinoma immune evasion. *Nat. Commun.* 8, 15129. doi:10.1038/ncomms15129
- Jiang, Y., Liu, L. S., Shen, L. P., Han, Z. F., Jian, H., Liu, J. X., et al. (2016). Traditional Chinese Medicine treatment as maintenance therapy in advanced non-small-cell lung cancer: a randomized controlled trial. *Complement. Ther. Med.* 24, 55–62. doi:10.1016/j.ctim.2015.12.006
- Kamisawa, T., Wood, L. D., Itoi, T., and Takaori, K. (2016). Pancreatic cancer. *Lancet* 388 (10039), 73–85. doi:10.1016/s0140-6736(16)00141-0
- Klein, A. P. (2021). Pancreatic cancer epidemiology: understanding the role of lifestyle and inherited risk factors. *Nat. Rev. Gastroenterol. Hepatol.* 18 (7), 493–502. doi:10.1038/s41575-021-00457-x
- Li, B., Gan, R., Yang, Q., Huang, J., Chen, P., Wan, L., et al. (2015). Chinese herbal medicines as an adjunctive therapy for unresectable pancreatic cancer: a systematic review and meta-analysis. *Evid. Based Complement. Altern. Med.* 2015, 350730. doi:10.1155/2015/350730
- Li, J., Ma, J., Tian, Y., Zhao, P., Liu, X., Dong, H., et al. (2020). Effective-component compatibility of Bufei Yishen formula II inhibits mucus hypersecretion of chronic obstructive pulmonary disease rats by regulating EGFR/PI3K/mTOR signaling. *J. Ethnopharmacol.* 257, 112796. doi:10.1016/j.jep.2020.112796
- Li, S., Xu, H. X., Wu, C. T., Wang, W. Q., Jin, W., Gao, H. L., et al. (2019). Angiogenesis in pancreatic cancer: current research status and clinical implications. *Angiogenesis* 22 (1), 15–36. doi:10.1007/s10456-018-9645-2
- Liu, A. L., and Du, G. H. (2009). Research progress of virtual screening aided drug discovery. *Acta Pharm. Sin.* 44 (6), 566–570. doi:10.3321/j.issn:0513-4870.2009.06.002
- Liu, X., Wang, S., Zheng, H., Liu, Q., Shen, T., Wang, X., et al. (2021). Epimedium koreanum C, a prenylated flavonoid isolated from Epimedium koreanum, induces non-apoptotic cell death with the characteristics of methuosis in lung cancer cells. *Am. J. Cancer Res.* 11 (7), 3496–3514.
- Motoo, Y., Shimasaki, T., Ishigaki, Y., Nakajima, H., Kawakami, K., and Minamoto, T. (2011). Metabolic disorder, inflammation, and deregulated molecular pathways converging in pancreatic cancer development: implications for new therapeutic strategies. *Cancers (Basel)* 3 (1), 446–460. doi:10.3390/cancers3010446
- Rejhová, A., Opattová, A., Čumová, A., Sliva, D., and Vodicka, P. (2018). Natural compounds and combination therapy in colorectal cancer treatment. *Eur. J. Med. Chem.* 144, 582–594. doi:10.1016/j.ejmech.2017.12.039
- Rudin, C. M., Liu, W., Desai, A., Karrison, T., Jiang, X., Janisch, L., et al. (2008). Pharmacogenomic and pharmacokinetic determinants of erlotinib toxicity. *J. Clin. Oncol.* 26 (7), 1119–1127. doi:10.1200/jco.2007.13.1128
- Saif, M. W., Li, J., Lamb, L., Kaley, K., Elligers, K., Jiang, Z., et al. (2014). First-in-human phase II trial of the botanical formulation PHY906 with capecitabine as second-line therapy in patients with advanced pancreatic cancer. *Cancer Chemother. Pharmacol.* 73 (2), 373–380. doi:10.1007/s00280-013-2359-7
- Sette, G., Salvati, V., Mottolese, M., Visca, P., Gallo, E., Fecchi, K., et al. (2015). Tyr1068-phosphorylated epidermal growth factor receptor (EGFR) predicts cancer stem cell targeting by erlotinib in preclinical models of wild-type EGFR lung cancer. *Cell Death Dis.* 6 (8), e1850. doi:10.1038/cddis.2015.217
- Shen, J., Li, L., Yang, T., Cohen, P. S., and Sun, G. (2020). Biphasic mathematical model of cell-drug interaction that separates target-specific and off-target inhibition and suggests potent targeted drug combinations for multi-driver colorectal cancer cells. *Cancers (Basel)* 12 (2), 436. doi:10.3390/cancers12020436
- Sherman, B. T., Hao, M., Qiu, J., Jiao, X., Baseler, M. W., Lane, H. C., et al. (2022). DAVID: a web server for functional enrichment analysis and functional annotation of gene lists (2021 update). *Nucleic Acids Res.* 50 (W1), W216–W221. doi:10.1093/nar/gkac194
- Siegel, R. L., Miller, K. D., Fuchs, H. E., and Jemal, A. (2021). Cancer statistics, 2021. *CA Cancer J. Clin.* 71 (1), 7–33. doi:10.3322/caac.21654
- Song, Z., Xiang, X., Li, J., Deng, J., Fang, Z., Zhang, L., et al. (2020). Ruscogenin induces ferroptosis in pancreatic cancer cells. *Oncol. Rep.* 43 (2), 516–524. doi:10.3892/or.2019.7425
- Sun, J., Xu, W., Zheng, S., Lv, C., Lin, J., Chen, S., et al. (2022). Icaritin promotes mouse Leydig cell testosterone synthesis via the Esr1/Src/Akt/Creb/Sf-1 pathway. *Toxicol. Appl. Pharmacol.* 441, 115969. doi:10.1016/j.taap.2022.115969
- Suzumura, T., Kimura, T., Kudoh, S., Umekawa, K., Nagata, M., Matsuura, K., et al. (2012). Reduced CYP2D6 function is associated with gefitinib-induced rash in patients with non-small cell lung cancer. *BMC Cancer* 12, 568. doi:10.1186/1471-2407-12-568
- Tong, J. S., Zhang, Q. H., Huang, X., Fu, X. Q., Qi, S. T., Wang, Y. P., et al. (2011). Icaritin causes sustained ERK1/2 activation and induces apoptosis in human endometrial cancer cells. *PLoS One* 6 (3), e16781. doi:10.1371/journal.pone.0016781
- Von Mering, C., Jensen, L. J., Snel, B., Hooper, S. D., Krupp, M., Foglierini, M., et al. (2005). STRING: known and predicted protein–protein associations, integrated and transferred across organisms. *Nucleic Acids Res.* 33 (Suppl. 1), D433–D437. doi:10.1093/nar/gki005
- Wang, M., Wan, Y., Liang, Z., Zhu, D., Huang, Y., Chen, M., et al. (2021). Effects of icaritin on EGF-induced breast cancer cell MCF-7 epithelial mesenchymal regulation process and its mechanism. *China J. Tradit. Chin. Med. Pharm.* 36 (5), 2545–2549.
- Wang, S., Wang, Q., Wang, H., Qin, C., Cui, X., Li, L., et al. (2019). Induction of ROS and DNA damage-dependent senescence by icaritin contributes to its antitumor activity in hepatocellular carcinoma cells. *Pharm. Biol.* 57 (1), 424–431. doi:10.1080/13880209.2019.1628073
- Wang, Y., Guo, Z., Jin, Y., Zhang, X., Wang, L., Xue, X., et al. (2010). Identification of prenyl flavonoid glycosides and phenolic acids in Epimedium koreanum Nakai by Q-TOF-MS combined with selective enrichment on “click oligo (ethylene glycol)” column. *J. Pharm. Biomed. Anal.* 51 (3), 606–616. doi:10.1016/j.jpba.2009.09.033
- Wirth, D., Özdemir, E., and Hristova, K. (2023). Quantification of ligand and mutation-induced bias in EGFR phosphorylation in direct response to ligand binding. *Nat. Commun.* 14 (1), 7579. doi:10.1038/s41467-023-42926-8
- Wright, A. J., Orlic-Milacic, M., Rothfels, K., Weiser, J., Trinh, Q. M., Jassal, B., et al. (2022). Evaluating the predictive accuracy of curated biological pathways in a public knowledgebase. *Database* 2022, baac009. doi:10.1093/database/baac009
- Wu, W., Zhang, Z., Li, F., Deng, Y., Lei, M., Long, H., et al. (2020). A network-based approach to explore the mechanisms of uncaria alkaloids in treating hypertension and alleviating alzheimer's disease. *Int. J. Mol. Sci.* 21 (5), 1766. doi:10.3390/ijms21051766
- Xu, H. Y., Zhang, Y. Q., Liu, Z. M., Chen, T., Lv, C. Y., Tang, S. H., et al. (2019). ETCM: an encyclopaedia of traditional Chinese medicine. *Nucleic Acids Res.* 47 (D1), D976–D982. doi:10.1093/nar/gky987
- Yamaguchi, K., Okusaka, T., Shimizu, K., Furuse, J., Ito, Y., Hanada, K., et al. (2017). Clinical practice guidelines for pancreatic cancer 2016 from the Japan pancreas society: a synopsis. *Pancreas* 46 (5), 595–604. doi:10.1097/mpa.0000000000000816
- Yang, X.-H., Li, L., Xue, Y.-B., Zhou, X.-X., and Tang, J.-H. (2020). Flavonoids from Epimedium pubescens: extraction and mechanism, antioxidant capacity and effects on CAT and GSH-Px of *Drosophila melanogaster*. *PeerJ* 8, e8361. doi:10.7717/peerj.8361

- Ye, X. W., Wang, H. L., Cheng, S. Q., Xia, L. J., Xu, X. F., and Li, X. R. (2022). Network pharmacology-based strategy to investigate the pharmacologic mechanisms of coptidis rhizoma for the treatment of alzheimer's disease. *Front. Aging Neurosci.* 14, 890046. doi:10.3389/fnagi.2022.890046
- Ye, Z., Zhuo, Q., Hu, Q., Xu, X., Mengqi, L., Zhang, Z., et al. (2021). FBW7-NRA41-SCD1 axis synchronously regulates apoptosis and ferroptosis in pancreatic cancer cells. *Redox Biol.* 38, 101807. doi:10.1016/j.redox.2020.101807
- Yin, L., Qi, X. W., Liu, X. Z., Yang, Z. Y., Cai, R. L., Cui, H. J., et al. (2020). Icaritin enhances the efficacy of cetuximab against triple-negative breast cancer cells. *Oncol. Lett.* 19 (6), 3950–3958. doi:10.3892/ol.2020.11496
- Zhang, J., Wang, P., Ouyang, H., Yin, J., Liu, A., Ma, C., et al. (2013). Targeting cancer-related inflammation: Chinese herbal medicine inhibits epithelial-to-mesenchymal transition in pancreatic cancer. *PLoS One* 8 (7), e70334. doi:10.1371/journal.pone.0070334
- Zhang, L., Wu, C., Zhang, Y., Liu, F., Wang, X., Zhao, M., et al. (2014). Comparison of efficacy and toxicity of traditional Chinese medicine (TCM) herbal mixture LQ and conventional chemotherapy on lung cancer metastasis and survival in mouse models. *PLoS One* 9 (10), e109814. doi:10.1371/journal.pone.0109814
- Zhang, Q. B., Meng, X. T., Jia, Q. A., Bu, Y., Ren, Z. G., Zhang, B. H., et al. (2016). Herbal compound songyou yin and moderate swimming suppress growth and metastasis of liver cancer by enhancing immune function. *Integr. Cancer Ther.* 15 (3), 368–375. doi:10.1177/1534735415622011
- Zhao, Y., Chen, S., Wang, Y., Lv, C., Wang, J., and Lu, J. (2018). Effect of drying processes on prenylflavonoid content and antioxidant activity of *Epimedium koreanum* Nakai. *J. Food Drug Anal.* 26 (2), 796–806. doi:10.1016/j.jfda.2017.05.011
- Zhao, Y.-D., Zhang, X., Yang, W.-Y., Zhang, R.-Q., Mu, L.-T., Han, L., et al. (2022). New anti-pulmonary fibrosis prenylflavonoid glycosides from *Epimedium koreanum*. *Chin. J. Nat. Med.* 20 (3), 221–228. doi:10.1016/S1875-5364(21)60116-4
- Zhou, J., Wu, J., Chen, X., Fortenbery, N., Eksioglu, E., Kodumudi, K. N., et al. (2011). Icaritin and its derivative, ICT, exert anti-inflammatory, anti-tumor effects, and modulate myeloid derived suppressive cells (MDSCs) functions. *Int. Immunopharmacol.* 11 (7), 890–898. doi:10.1016/j.intimp.2011.01.007



OPEN ACCESS

EDITED BY

Raghuveera Kumar Goel,
Boston University, United States

REVIEWED BY

Fei Fang,
Michigan State University, United States
Hao Wang,
Shenzhen University General Hospital, China

*CORRESPONDENCE

Cheng Zeng,
✉ drzcheng@gzucm.edu.cn
Fangli Pei,
✉ peifangli5369@gzucm.edu.cn

[†]These authors have contributed equally to
this work

RECEIVED 03 March 2024

ACCEPTED 09 July 2024

PUBLISHED 29 July 2024

CITATION

Wu L, Lin S, Hu Y, Jing S, Sun B, Chen X, Jia J,
Zeng C and Pei F (2024), Potential mechanism
of Luoshi Neiyi prescription in endometriosis
based on serum pharmacochimistry and
network pharmacology.
Front. Pharmacol. 15:1395160.
doi: 10.3389/fphar.2024.1395160

COPYRIGHT

© 2024 Wu, Lin, Hu, Jing, Sun, Chen, Jia, Zeng
and Pei. This is an open-access article
distributed under the terms of the [Creative
Commons Attribution License \(CC BY\)](#). The use,
distribution or reproduction in other forums is
permitted, provided the original author(s) and
the copyright owner(s) are credited and that the
original publication in this journal is cited, in
accordance with accepted academic practice.
No use, distribution or reproduction is
permitted which does not comply with these
terms.

Potential mechanism of Luoshi Neiyi prescription in endometriosis based on serum pharmacochimistry and network pharmacology

Lizheng Wu^{1†}, Shuhong Lin^{1†}, Yongjun Hu¹, Shangwen Jing¹,
Bowen Sun¹, Xiaoxin Chen¹, Jinjin Jia¹, Cheng Zeng^{2*} and
Fangli Pei^{2*}

¹Guangzhou University of Chinese Medicine, Guangzhou, Guangdong, China, ²Department of
Gynecology, The First Affiliated Hospital of Guangzhou University of Chinese Medicine, Guangzhou,
Guangdong, China

Introduction: Endometriosis (EMs) is characterized by ectopic growth of active endometrial tissue outside the uterus. The Luoshi Neiyi prescription (LSNYP) has been extensively used for treating EMs in China. However, data on the active chemical components of LSNYP are insufficient, and its pharmacological mechanism in EMs treatment remains unclear. This study aimed to explore the potential mechanism of LSNYP for EMs through network pharmacology based on the components absorbed into the blood.

Methods: Ultra-high performance liquid chromatography-quadrupole time-of-flight mass spectrometry was used to analyze blood components, and a series of network pharmacology strategies were utilized to predict targets of these components and EMs. Protein-protein interaction (PPI) network analysis, component-target-disease network construction, gene ontology (GO) functional enrichment analysis, and Kyoto Encyclopedia of Genes and Genomes (KEGG) pathway enrichment analysis were performed. Additionally, molecular docking, molecular dynamics simulations, and *in vitro* and *in vivo* experiments were conducted to validate the HIF1A/EZH2/ANTXR2 pathway associated with hypoxic pathology in EMs.

Results: Thirty-four absorbed components suitable for network pharmacology analysis were identified, and core targets, such as interleukin 6, EGFR, HIF1A, and EZH2, were founded. Enrichment results indicated that treatment of EMs with LSNYP may involve the regulation of hypoxia and inflammatory-related signaling pathways and response to oxidative stress and transcription factor activity. Experimental results demonstrated that LSNYP could decrease the expression of HIF1A, ANTXR2, YAP1, CD44, and β -catenin, and increased EZH2 expression in ectopic endometrial stromal cells and endometriotic tissues. Molecular docking

and molecular dynamics simulations manifested that there was stable combinatorial activity between core components and key targets of the HIF1A/EZH2/ANTXR2 pathway.

Conclusion: LSNYP may exert pharmacological effects on EMs via the HIF1A/EZH2/ANTXR2 pathway; hence, it is a natural herb-related therapy for EMs.

KEYWORDS

endometriosis, Luoshi Neiyi prescription, traditional Chinese medicine, HIF1A/EZH2/ANTXR2 pathway, network pharmacology, molecular docking, molecular dynamics simulation

1 Introduction

Endometriosis (EMs) is a chronic inflammatory disease characterized by the ectopic growth of active endometrial tissue (glands and stroma) beyond the confines of the uterus, affecting approximately 10% of females of childbearing age (Shafir et al., 2018). EMs is the primary etiological factor for dysmenorrhea, chronic pelvic pain, and infertility, imposing a substantial burden on patients' quality of life and social healthcare resources (Zubrzycka et al., 2021). In contemporary medical practice, therapeutic interventions, such as non-steroidal anti-inflammatory drugs, compound oral contraceptives, progesterone, gonadotropin-releasing hormone agonists, and surgical procedures are commonly employed to manage the condition. Traditional Chinese medicine (TCM) teaches that cyclic bleeding from the ectopic endothelium is indicative of stasis, and that the core pathogenesis of EMs is the stagnation of qi and blood. Consequently, the treatment approach often involves promoting qi and eliminating blood stasis to dissipate stagnation. The Luoshi Neiyi prescription (LSNYP), documented in Luo Yuankai's gynecology book, has been extensively used in the First Affiliated Hospital of Guangzhou University of Chinese Medicine and Guangzhou Women and Children's Medical Center for EMs treatment based on this fundamental principle (Ya-Nan et al., 2020; Kefei et al., 2022). LSNYP have demonstrated efficacy in suppressing endometriotic lesions, alleviating chronic pain, and reducing recurrence rates in clinical settings (Haiying et al., 2013; Ye et al., 2021). Furthermore, experimental studies have indicated that LSNYP induces atrophy of the ectopic endometrium and reduces cyst size (Liao et al., 2010; Guo, 2021). Nevertheless, data on the active chemical components of LSNYP are insufficient, and its pharmacological mechanism in EMs treatment remains unclear.

Network pharmacology is an interdisciplinary field rooted in systems biology, elucidating the mechanisms of drug action and investigating the interrelationships between drugs and diseases by constructing a comprehensive "component–target–pathway–disease" network (Wu et al., 2022). This approach is particularly relevant for understanding the intricate nature of TCM, which emphasizes a multi-component, multi-pathway, and multi-target approach for treatment (Luo et al., 2019). Research in serum pharmacochimistry suggests that drug components can only exert their intended effects in the body once they are absorbed into the bloodstream via the digestive tract and reach their target organs or targets (Ma et al., 2017). However, traditional network

pharmacology predominantly relies on databases to identify TCM components, thereby lacking assurance regarding the efficacy of the selected components. Hence, building on the prior identification of the chemical components of LSNYP *in vitro*, this study subsequently analyzed its prototype components entering the blood and explored the potential mechanism of action of LSNYP to provide a scientific basis for its actual utilization.

2 Materials and methods

2.1 Reagents

LSNYP (batch number: Yue Yao zhi Z20071247), with each bottle containing 250 mL, were produced by Guangzhou Kangyuan Pharmaceutical Co., Ltd. The production process was as follows: 14 types of Chinese medicines (Table 1) were mixed, and the mixture was firstly immersed in 2,500 mL of water for 30 min. The mixture was subsequently heated until boiling, decocted gently for 1.5 h, and filtered. The drug residue was boiled in 1,250 mL of water, decocted gently for 1 h, and filtered again. The two extracts were then mixed and concentrated to 250 mL, supplemented with 0.125 g of ethylp-hydroxybenzoate and 0.75 g of sodium benzoate, and stored in bottles.

Penicillin sodium for injection (North China Pharmaceutical Group Semisynth Co., Ltd., No. QM2201201) and danazol capsules (Jiangsu Lianhuan Pharmaceutical Co., Ltd., No. 20221201) were purchased from the Pharmacy of the First Affiliated Hospital of Guangzhou University of Chinese Medicine. Estradiol benzoate injection (batch number: 210301) was purchased from Shanghai Full Woo Biotechnology (Zhumadian) Company, and avertin (EasyCheck, 2104A) was purchased from Nanjing Aibei Biotechnology Co., Ltd. The following reagents, cell counting kit-8 (CCK-8; APEX BIO, K1018), fetal bovine serum (FBS; Gibco, 10099141C), 0.25% trypsin + phenol red (Gibco, 25200056), type I collagenase (Sigma, C0130), anti-HIF1A antibody (Affinity, BF8002), anti-EZH2 antibody (Proteintech, 21800-1-AP), anti-ANTXR2 antibody (Solarbio, K004586P), anti-YAP1 antibody (Proteintech, 66900-1-Ig), anti-CD44 antibody (Proteintech, 15675-1-AP), anti-beta catenin antibody (Proteintech, 51067-2-AP), and anti-GAPDH antibody (Goodhere biotech, AB-P-R 001) were purchased with the help of Guangzhou Huiwang Experimental Instrument Co., Ltd. Trizol (Ambion, 15596-026), HiScript® II Q Select RT SuperMix for qPCR (VAZYME, R233), SYBR Green Master Mix (VAZYME,

TABLE 1 Fourteen botanical drugs in 250 mL of LSNYP.

Chinese name	Name for publishing	Used parts	Amount (g)
Yimucao (YMC)	<i>Leonurus japonicus</i> Houtt. [Lamiaceae; Herba Leonuri]	Aboveground parts	33.5
Chuanxiong (CX)	<i>Conioselinum anthriscoides</i> “Chuanxiong” [umbelliferae; <i>Chuanxiong Rhizoma</i>]	Tuber	10.25
Taoren (TR)	<i>Prunus persica</i> (L.) Batsch [Rosaceae; <i>Persicae Semen</i>]	Seed	17
Danshen (DS)	<i>Salvia miltiorrhiza</i> Bunge [Lamiaceae; <i>Salviae Miltiorrhizae Radix Et Rhizoma</i>]	Root	17
Puhuang (PH)	<i>Typha angustifolia</i> L. [Typhaceae; <i>Typhae Pollen</i>]	Pollen	6.5
Yanhusuo (YHS)	<i>Corydalis yanhusuo</i> (Y.H.Chou & Chun C.Hsu) W.T.Wang ex Z.Y.Su & C.Y.Wu [Papaveraceae; <i>Corydalis Rhizoma</i>]	Tuber	17
Wuyao (WY)	<i>Lindera aggregata</i> (Sims) Kosterm. [Lauraceae; <i>Linderae Radix</i>]	Root	17
Haizao (HZ)	<i>Sargassum pallidum</i> (Turn.) C.Ag. [Sargassaceae; <i>Sargassum</i>]	Whole plant	33.5
Zhebeimu (ZBM)	<i>Fritillaria thunbergii</i> Miq. [Liliaceae; <i>Fritillariae Thunbergii Bulbus</i>]	Bulb	17
Wumei (WM)	<i>Prunus mume</i> (Siebold) Siebold & Zucc. [Rosaceae; <i>Mume Fructus</i>]	Fruit	11.25
Tubiechong (TBC)	<i>Eupolyphaga sinensis</i> Walker [Corydidae; <i>Eupolyphaga Steleophaga</i>]	Whole body	13.5
Shanzha (SZ)	<i>Crataegus pinnatifida</i> Bunge [Rosaceae; <i>Crataegi Fructus</i>]	Fruit	17
Wulingzhi (WLZ)	<i>Trogopterus xanthipes</i> Milne-Edwards [Talpidae; <i>Faeces Trogopterori</i>]	Dung	11.25
Muli (ML)	<i>Ostrea gigas</i> Thunberg [Ostreidae; <i>Ostreae Concha</i>]	Shell	28.25

TABLE 2 Primer sequences.

Gene	Primer	Sequence (5'-3')	Size
<i>Gapdh</i>	Forward	AGTCTACTGGCGTCTTCACC	225 bp
	Reverse	CCACGATGCCAAAGTTGTCA	
<i>Hlf1a</i>	Forward	GCGGCGAGAACGAGAAGAAAAATAG	129 bp
	Reverse	GAAGTGGCAACTGATGAGCAAG	
<i>Ezh2</i>	Forward	GCACACTGCAGAAAGATCCA	224 bp
	Reverse	AGGTAGCACGGACACTGCTT	
<i>Antxr2</i>	Forward	AACGGGATTGCAGCCATCATAGC	150 bp
	Reverse	CTCTTCTCTCTCTCTCTCTTTGG	
<i>Yap1</i>	Forward	AGCCGCCTGAGCCCAAGTC	105bp
	Reverse	GGGAGGCTGGAGACGAGTGAG	
<i>Cd44</i>	Forward	AAACACCACCCAAGAGGCAAGAAG	110 bp
	Reverse	TGACTCCGTACCAGGCATCTTCG	
<i>Ctnnb1</i>	Forward	TACCGCTGGGACCTACACAAC	137 bp
	Reverse	GCGTGGTGATGGCGTAGAACAG	

Q111-02), Taq Plus DNA Polymerase (TIANGEN, ET105-01), DL2000 DNA Marker (TIANGEN, MD114-02), TIANamp Genomic DNA Kit (TIANGEN, DP304), EpiTect Plus DNA Bisulfite Kit (QIAGEN, 59124), TransTaq DNA Polymerase High Fidelity (HiFi) (TransGen, AP131-02), and HIF1A downregulated lentiviral vector were obtained from Wuhan Bio-Tower Biotechnology Co., Ltd.

2.2 Animals

Seventy-two female specific pathogen-free Sprague–Dawley rats, aged approximately 10–12 weeks, were purchased from the Experimental Animal Center of Guangzhou University of Chinese Medicine (Certificate of Quality No: SCXK Yue 2018-0034) and fed at the Clean Experimental Animal Center of the First Affiliated Hospital of Guangzhou University of Chinese Medicine. The housing conditions were as follows: a temperature of 23°C ± 2°C, humidity of 40%–70%, a 12-h light-dark cycle, and free access to food and water. The experimental ethics were reviewed and approved by the First Affiliated Hospital of Guangzhou University of TCM Animal Ethical Review Standards (approval number: TCMF1-2021024).

2.3 Preparing *in vivo* serum sample of LSNYP

After 3 days of adaptive feeding, before the start of drug administration, twelve rats were fasted for 12 h. Rats were randomly divided into four groups: the control group and administration groups 1, 2, and 3, with three rats per group. As the dose of LSNYP administered to a 60 kg woman is 75 mL/d, according to the body surface area conversion method (Guanhua, 2014), a 200 g rat is equivalent to 0.018 times that of a 70 kg adult. Therefore, the equivalent dose for a rat is 0.78 mL/100 g, equivalent to 7.82 g/kg/d of the original dose. As the dosage of each drug in the prescription was small, considering the metabolic differences and the relatively low serum drug concentration after gavage with an equivalent drug dose in the preliminary experiment, the administration groups were orally administered a quadruple dose of LSNYP. This dosage was divided into two doses, one in the morning and one in the evening, for three

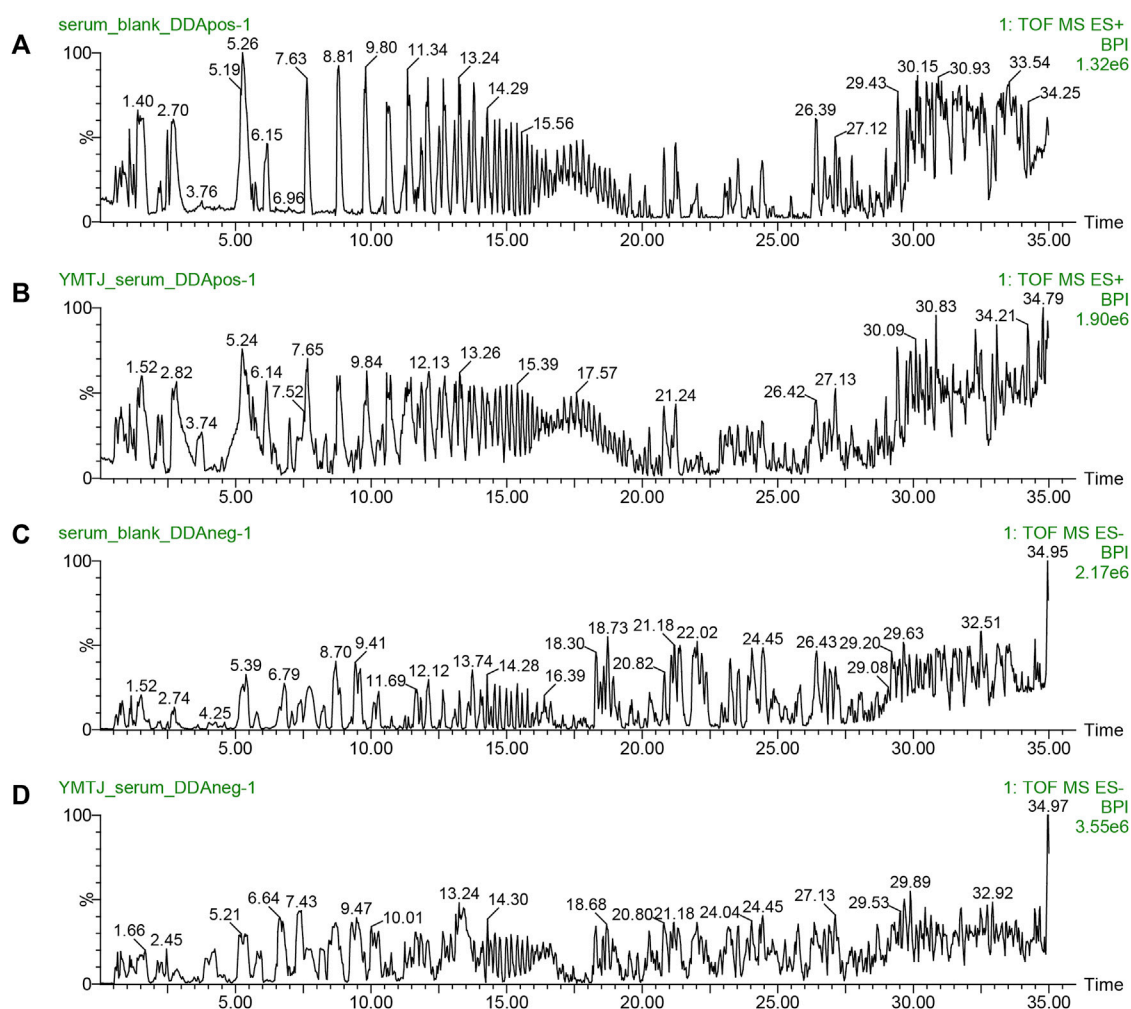


FIGURE 1
Ion flow diagrams of serum samples. The base peak intensity (BPI) chromatograms of in positive ion mode: (A) blank serum and (B) drug serum; BPI chromatograms in negative ion mode: (C) blank serum, (D) drug serum.

consecutive days. Rats in the control group were administered an equal volume of normal saline. To comprehensively analyze these components, blood samples were collected from the abdominal aortas of rats in the treatment groups at 0.5, 1.5, and 4 h (three rats each time) after the last gavage, and blood was collected from the control group at 1.5 h after saline administration. Blood samples were stored at 25°C for 2 h and then centrifuged at 3,000 rpm for 10 min to separate the serum. Finally, the sera of three rats in each group were mixed and preserved.

Equal volumes of serum from the three treatment groups were mixed, and methanol (chromatographic grade) was added at a 1:2 (serum: methanol) volume ratio. The mixture was vortexed for 5 min and then centrifuged at 13,000 rpm for 15 min at 4°C. The supernatant was dried in a centrifugal vacuum concentrator, and the residues were redissolved in 300 µL of methanol, vortexed for 5 min, and centrifuged at 13,000 rpm for 15 min. The supernatant was used for analysis. Serum samples from the control group were similarly processed.

An additional thirty rats were divided into control, LSYP, and positive drug (danazol) groups. The control and LSYP groups were

subjected to the same procedure, as described above. The rats in the positive drug group were administered danazol (8.4 g/kg/d), a synthetic androgen with anti-estrogenic effects, dissolved in an equal volume of normal saline. All rats were anesthetized 1 h after the last gavage, and blood samples were collected from the abdominal aorta. The samples were allowed to clot at 25°C and centrifuged at 3,000 rpm for 10 min. The serum was subsequently inactivated in a water bath at 56°C for 30 min. Following filtration and sterilization, using a 0.22 µm filter membrane, the serum was stored at -80°C for subsequent cell experiments.

2.4 Ultra-high performance liquid chromatography-quadrupole time-of-flight mass spectrometry (UPLC-Q/TOF-MS) analysis

Chromatographic separation was performed using a Waters ACQUITY UHPLC system (Waters Corporation, Massachusetts, United States) with a Waters ACQUITY UPLC HSS T3 column

TABLE 3 Potential active components of LSNYP.

Component name	QED	Component name	QED
Boldine	0.888	Dehydrocorydaline	0.661
Isoboldine	0.888	Vanillin	0.648
Stepholidine	0.888	p-Hydroxybenzoic acid	0.61
Rotundine	0.841	Macrophylloside A	0.598
Tetrahydropalmatine	0.841	1-(4-nonylphenoxy)-2-propanol	0.592
Lysergol	0.817	Cryptotanshinone	0.579
Norbracteoline	0.795	Isocryptotanshinone	0.579
Norisoboldine	0.795	Ethyl 4-methoxycinnamate	0.56
Senkyunolide F	0.78	Senkyunolide P	0.539
13-Methyl-dehydrocorydalmine	0.734	Hydroxylinderstrenolide	0.527
Moupinamide	0.716	Byzantionoside B	0.507
17 β -Hydroxy--2-oxa-5 α -androstan-3-one	0.698	Nikoenoside	0.485
Lindenenol	0.695	1,2-Dihexyloxybenzene	0.463
Shizukanolide A	0.694	Protocatechualdehyde	0.448
Deoxyschizandrin	0.676	Neocryptotanshinone	0.447
Palmatine	0.675	Tanshinoldehyde	0.396
n-Butylenephthalide	0.667	Dehydrocostuslactone	0.363

(100 mm \times 2.1 mm, 1.8 μ m). The mobile phase comprised acetonitrile (A) and water containing 0.1% formic acid (B) with a gradient elution of 4% A at 0–3 min, 4%–43% A at 3–26 min, 43%–70% A at 26–32 min, and 70%–100% A at 32–35 min. The flow rate was set at 0.35 mL/min, and the injection volume was 2 μ L.

A Waters Xevo G2 Q-T high-resolution mass spectrometer (MS) equipped with an electrospray ion source was used in this study. Data were collected in positive and negative ion modes, with capillary voltages set at 2.5 kV (+) and 2.5 kV (–), cone voltage at 40 V (–40 V), ion source temperature at 110°C, desolvation gas (N₂) temperature at 550°C, desolvation gas flow at 900 L/h, cone gas flow at 50 L/h, and scanning range from 50 to 1,300 m/z. Leucine enkephalin was used as the internal standard for real-time quality correction. Data were collected using a fast data-dependent acquisition method, and secondary ions corresponding to the top 10 primary mass spectra were gathered in each cycle. The collision energies for high and low molecular weights were 55 and 25 V, respectively.

By reviewing the pertinent literature and databases (Liu et al., 2022b), a summary of the chemical components of each botanical drug in LSNYP was compiled, including their Chinese and English names, molecular formulas, and structural formulas. A specialized database encompassing 517 components was established. The raw data were initially analyzed using UNIFI 1.8 software. The parameter settings were as follows: a peak intensity threshold was 200 counts for high energy and 1,000 counts for low energy in the 3D peak detection; component identity match tolerance set to five parts-per-million (ppm), and fragment match tolerance set to 20 ppm. The final results were confirmed through manual analysis.

2.5 Network pharmacology research methods

2.5.1 Screening the drug-likeness of absorbed components

Drug-likeness screening of compounds is a common method used to assess their absorption, distribution, metabolism, and excretion properties, often employing Lipinski's Rule of Five (Lipinski et al., 2012). In 2012, Bickerton et al. (2012) proposed a new drug-likeness descriptor called the Quantitative Estimate of Drug-Likeness (QED). Weight-based QED can be used to better evaluate the drug-likeness of compounds. The intersection of the previously mentioned absorbed prototype components and the chemical components with the Isomeric Simplified Molecular Input Line Entry System structure in the PubChem database was obtained, and ADMET lab2.0 (Guoli et al., 2021), an integrated online platform for accurate and comprehensive predictions of ADMET properties (<https://admetmesh.scbdd.com>), was used to screen the intersection components. To obtain the final potentially active components of LSNYP, the screening conditions were set to QED > 0.34.

2.5.2 Identification of components and EMs-Associated targets

The Swiss Target Prediction (Daina et al., 2019) (<http://swisstargetprediction.ch>) and Similarity Ensemble Approach (SEA, <https://sea.bkslab.org>) online platforms were used to forecast the component-related targets (Keiser et al., 2007). By employing “Endometriosis” as the search term, the top 25% of outcomes from the GeneCards database (Stelzer et al., 2016)

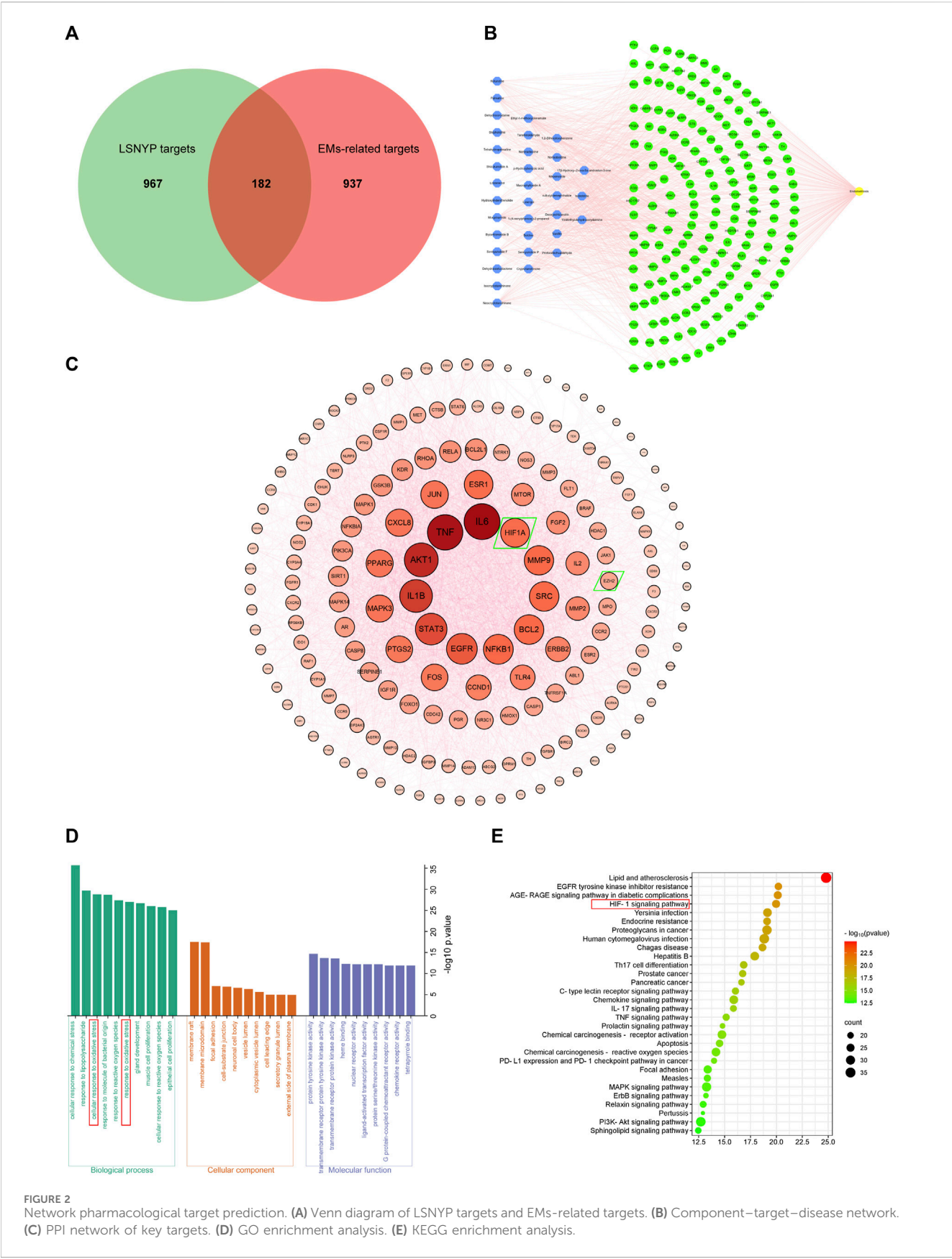


TABLE 4 Topological parameters of active component nodes (top10).

Component name	Degree	Betweenness centrality	Closeness centrality
Ethyl 4-methoxycinnamate	46	0.026342569	0.411992263
Moupinamide	46	0.026411848	0.413592233
Boldine	34	0.012370107	0.393715342
1,2-Dihexyloxybenzene	33	0.014842993	0.392265193
Neocryptotanshinone	33	0.011874793	0.392265193
1-(4-nonyl phenoxy)-2-propanol	32	0.013579075	0.387978142
Deoxyschizandrin	31	0.010996563	0.387978142
Isoboldine	30	0.009408465	0.389396709
Senkyunolide F	29	0.012241345	0.386569873
Palmatine	27	0.007814418	0.378330373

(<https://www.genecards.org>) and all outcomes from the Online Mendelian Inheritance (OMIM) database (McKusick, 2007) (<https://www.omim.org>) were chosen. After merging and deduplicating the results, they were used as the EMs-related targets. Finally, Origin8.0 software was used to identify the intersection of component-associated and EMs-associated targets, and a Venn diagram was constructed.

2.5.3 Construction of the component–target–disease and protein–protein interaction (PPI) networks

The active components, intersection targets, and disease data were imported into Cytoscape 3.5.1 software (Doncheva et al., 2018) to build the “component–target–disease” interaction network. The top 10 core components were identified based on the degree of each node. The STRING database (Szklarczyk et al., 2020) (<https://cn.string-db.org>) was utilized to retrieve the intersection targets and obtain the interaction relationship data between the targets. These data were then entered into Cytoscape, with the confidence level set at 0.4, to draw the PPI network and rank them according to their degree value.

2.5.4 Gene ontology (GO) functional enrichment and Kyoto Encyclopedia of genes and genomes (KEGG) pathway enrichment analyses

KEGG enrichment analysis of core targets was performed using R Studio software (Li et al., 2021), and GO analysis was obtained using the WeChat online platform (<http://www.bioinformatics.com.cn>). According to *p* values, the top 10 biological processes, cellular components, molecular functions, and the top 30 KEGG signaling pathways were selected for visualization in bar charts or bubble charts.

2.5.5 Molecular docking

The RCSB Protein Data Bank (Zardecki et al., 2021) (RCSB PDB, <https://www1.rcsb.org>) was used to acquire crystal structures of target proteins, and several filters were applied (Liu et al., 2022a), including 1) restriction of species origin to “Homosapiens,” 2) selection of high-resolution structures (resolution ≤ 2.5 Å), 3) preference for protein structures obtained through x-ray

single-crystal diffraction scanning, and 4) consideration of the protein’s structure (single-stranded, double-stranded, or other) based on the number of polymers present in the organism. Proligands, crystallization water, and irrelevant protein chains in the protein structure were removed using PyMOL 2.3.0 software (Rosignoli and Paiardini, 2022). The structures of the core components were retrieved from the PubChem database and imported into the Chem3D software (version 2020) to minimize and optimize energy. Subsequently, AutoDockTools 1.5.6 software (Liu Y. et al., 2022) was used to add hydrogen atoms to the optimized proteins and ligands, and the torsion bonds of the small-molecule ligands were also selected. The docking area was predicted according to the original active pocket of the protein using AutoDock Tools. AutoDock Vina 1.2.0 software (Eberhardt et al., 2021) was then used for docking and calculating the binding energy; the Lamarckian genetic algorithm and semi-flexible docking were chosen, default exhaustiveness was set to 8, and maximum output was set to 9. Finally, Discovery Studio 2020 and Pymol software were used to analyze and visualize the molecular docking results.

2.5.6 Molecular dynamics simulation

The Gromacs 2022.3 software (Van Der Spoel et al., 2005; Abraham et al., 2015; Eberhardt et al., 2021) was employed to conduct molecular dynamic simulations. Small molecules were preprocessed using AmberTools22 to incorporate a general AMBER force field. Gaussian 16 W was applied to hydrogenate small molecules and estimate the restrained electrostatic potential (Sasitha and John, 2021). The obtained potential data were integrated into the topology file of the molecular dynamics system. The procedures were performed under static conditions, the temperature was set to 300 K, and the atmospheric pressure was set to 1 bar. The Amber99sb-ildn with water molecules (Tip3p water model) was selected as the solvent. The simulated system achieved charge neutrality by introducing suitable quantities of Na⁺. The system employed the steepest descent method to minimize energy, followed by the 100,000 steps of isothermal isovolumic ensemble and isothermal isobaric ensemble equilibria. The coupling constant was set at 0.1 ps, and the duration was 100 ps. A free molecular dynamics simulation was

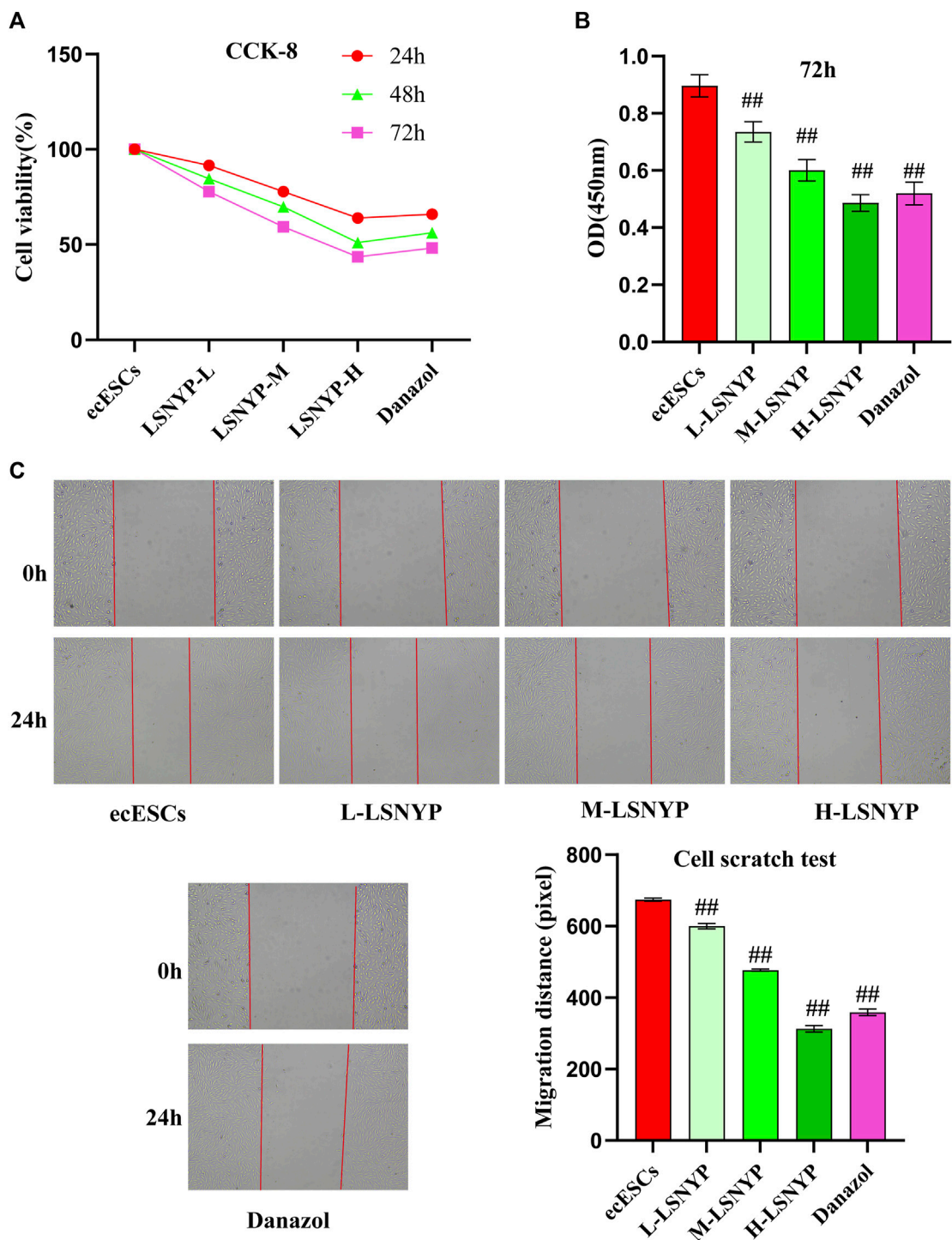


FIGURE 3 Effect of LSNYP on the proliferation and migration of ecESCs. (A) Effect of different intervention times on cell viability. (B) The impact of LSNYP on the viability of ecESCs 72 h after treatment. (C) Cell scratch experimental results. Compared with the ecESCs group, ## $P < 0.01$.

conducted, encompassing 5000,000 steps, the step length was set to 2 fs, and the total duration was 100 ns. Subsequently, the trajectory was analyzed, enabling the calculation of various parameters, such as root-mean-square variance (RMSD), and protein rotation radius of each amino acid trajectory, combined with free energy, free-energy topography, and other relevant data.

2.6 Cell experiments

2.6.1 Cell culture

Eutopic endometrial tissue and cyst walls of ovarian endometriotic cysts were collected from patients with EMs who received laparoscopy combined with hysteroscopy at our hospital.

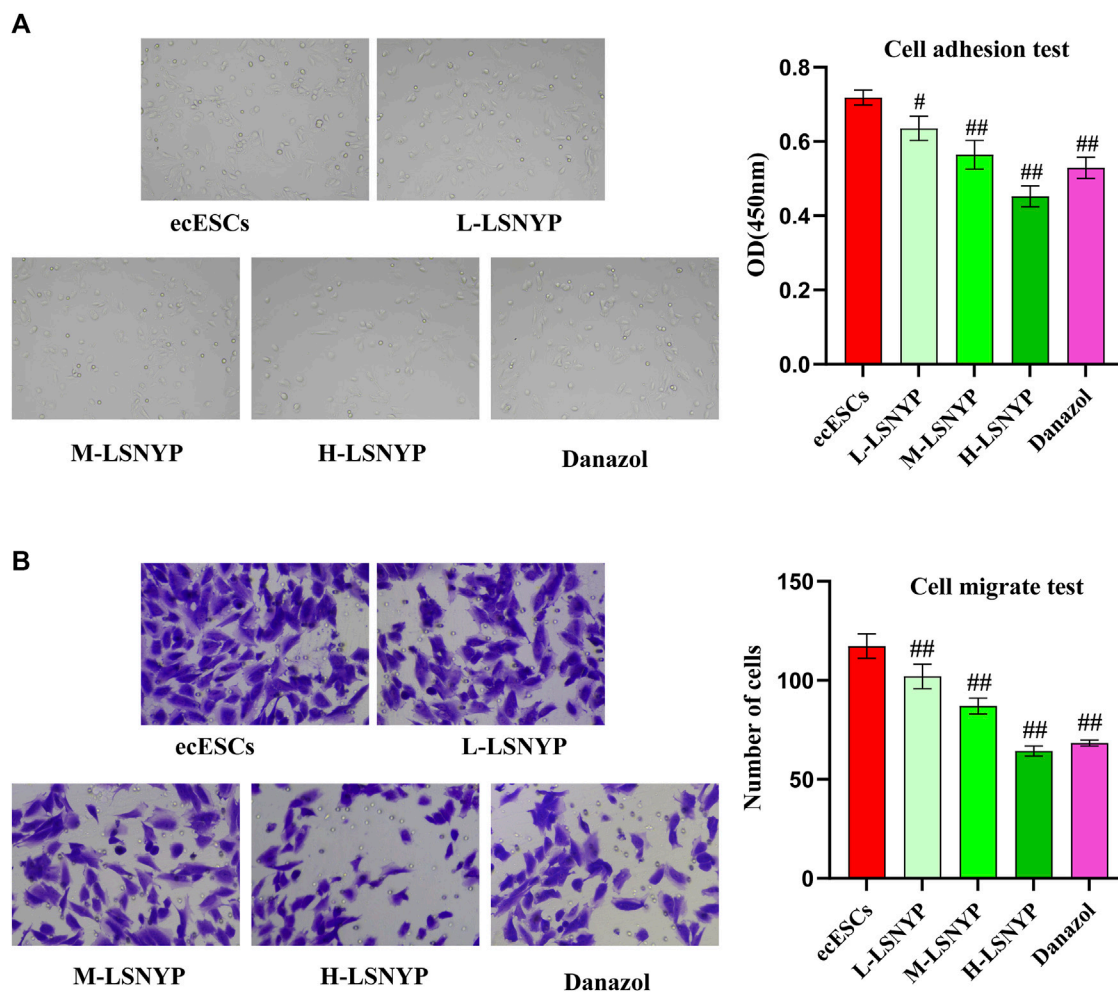


FIGURE 4
Effects of LSNYP on adhesion (A) and invasion (B) of ecESCs. Compared with the ecESCs group, [#] $P < 0.05$, ^{##} $P < 0.01$.

This protocol was approved by the Ethics Committee of The First Affiliated Hospital of Guangzhou University of Chinese Medicine (NO. K [2021] 053). Primary human endometrial stromal cells (ESCs) were obtained using an improved method (Zhou et al., 2019). The tissue was cleaned and then cut into fragments smaller than 1 cm³. The endometrial tissue was treated with an approximately equal volume of type I collagenase (1 g/mL) and digested at 37°C for 30 min. The capsule wall tissue was digested with approximately twice the volume of type I collagenase (1g/mL) for 60 min. The digestion was then terminated with twice the volume of Dulbecco's Modified Eagle Medium (DMEM)–F12 containing 10% FBS. The digestive fluid was first filtered through a 100-mesh sieve and then through a 400-mesh sieve. ESCs were contained in the filtrate. The filtrate was centrifuged at 1,000 rpm for 10 min, and the supernatant was discarded. The remaining supernatant was resuspended and precipitated using a complete medium. ESCs were seeded in a 6 cm diameter culture dish at a density of $1-2 \times 10^5$ cells/mL, and 3 mL of complete medium was added to each dish. The cells were then cultured in a cell incubator at 5% CO₂ and 37°C. The medium was changed 48 h after the primary cells were extracted and then once every 3–5 days, depending on the growth of

the cells. The cells were subcultured upon reaching a cell growth fusion of 80%–90%. Third-to fifth-generation ESCs were used for this experiment.

2.6.2 CCK-8 assay

Ectopic endometrial stromal cells (ecESCs) that were in the logarithmic growth phase and exhibited robust growth were seeded in 96-well plates at a density of 3×10^3 cells/well. Subsequently, the cells were incubated overnight at 37°C in a 5% CO₂ incubator. The cells were then divided into five groups: the ecESCs (10% blank serum), low LSNYP dose (10% LSNYP-containing serum: blank serum = 1:4), middle LSNYP dose (10% LSNYP-containing serum: blank serum = 3:2), high LSNYP dose (10% LSNYP-containing serum: blank serum = 1:0), and danazol (10% danazol-containing serum: blank serum = 1:0) groups. After the corresponding serum was added, the cells were cultured for 24, 48, and 72 h, and 10 μL of CCK8 was added to each well and incubated at 37°C for 1 h. The absorbance of each well was quantified using a microplate reader set to measure the optical density (OD) at a wavelength of 450 nm. Cell proliferation rate = (OD value of experimental group - OD value of blank well)/(OD value of model group - OD value of

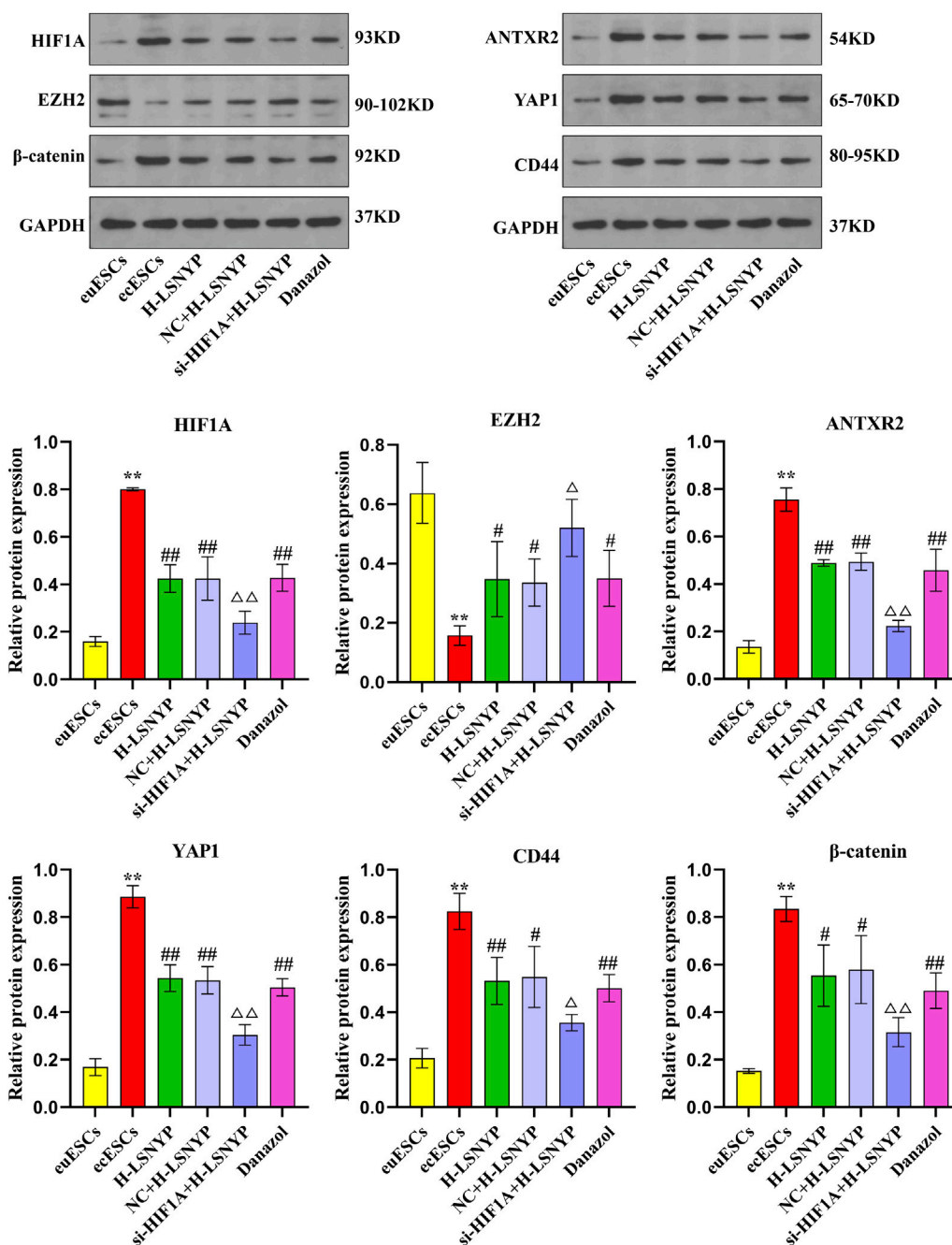


FIGURE 5

Effect of LSNYP on the HIF1A/EZH2/ANTXR2 pathway determined using western blotting. Compared with the euESCs group, ** $P < 0.01$; compared with the ecESCs group, # $P < 0.05$, ## $P < 0.01$; compared with the NC + H-LSNYP group, [△] $P < 0.05$, ^{△△} $P < 0.01$, $n = 3$.

blank well) $\times 100\%$. CCK-8 assay results showed that 72 h was the optimal time for the drug-containing serum to inhibit ecESC proliferation.

2.6.3 Cell adhesion assay

Cells were seeded in 6-well plates at a density of 5×10^5 cells/well and categorized as 1.6.2. Following a 72-h intervention with drug-containing serum, the cells were harvested using trypsin digestion, and the concentration was diluted to 6×10^4 cells/mL using the

DMEM/F12 medium. Subsequently, 50 μ L of Matrigel with a final concentration of 1 mg/mL was vertically added to the center of a 96-well plate and incubated at 37°C for 4–5 h until it solidified into a gelatinous state. The remaining medium was removed, and 100 μ L of each group's cell suspension was added. The cells were subsequently cultured in an incubator at 37°C and 5% CO₂ for 1 h. Finally, the non-adherent cells were washed off with DMEM/F12 medium, 10 μ L of CCK-8 was added to each well and cultured at 37°C for 3 h, and the OD was calculated.

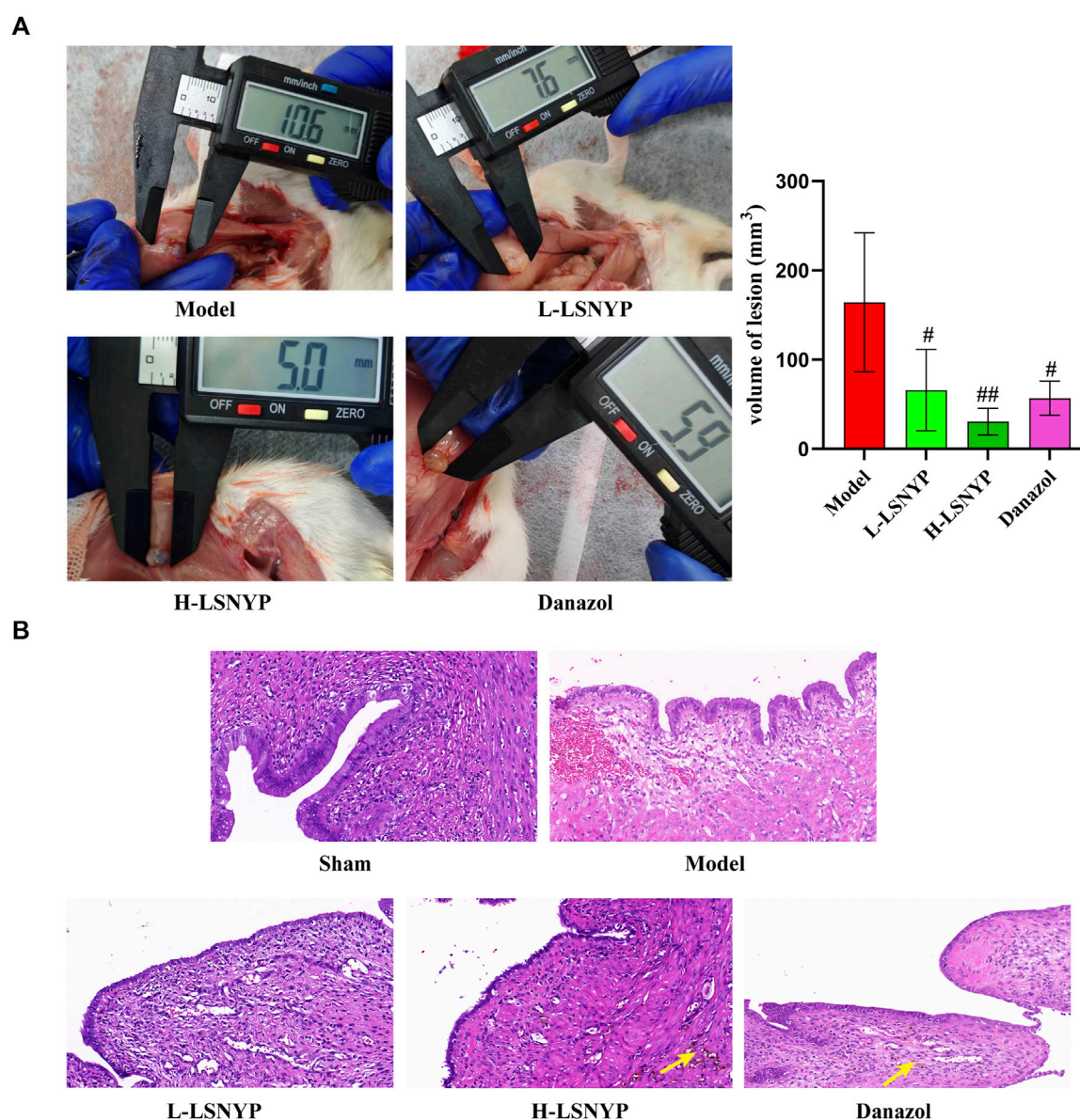


FIGURE 6
Effect of LSNYP on volume of lesion (A) and histopathology (B) in endometriotic tissues (x400). Compared with the model group, [#] $P < 0.05$, ^{##} $P < 0.01$, $n = 6$.

2.6.4 Transwell invasion assay

The cells were administered drug-containing serum for 72 h, and the cell concentration was adjusted to $3 \times 10^5/\text{mL}$ following digestion. Subsequently, 800 μL of DMEM/F12 medium containing 10% FBS was introduced into a 24-well plate and positioned within the transwell chamber. A 100 μL volume of Matrigel, with a final concentration of 0.5 mg/mL, was added vertically at the bottom of the upper chamber. Once the Matrigel had solidified into a gel, a 200 μL suspension of cells from each group was introduced into the upper chamber of the transwell and incubated at 37°C and 5% CO_2 environment. The transwell plate was removed, and the chamber was washed with phosphate-buffered saline (PBS). The cells were fixed with 70% ice-cold ethanol solution for 1 h, stained with 0.5% crystal violet staining solution, and incubated at 25°C for 20 min. After

rinsing with PBS, the non-migrating cells in the upper chamber were gently wiped off using cotton balls and then observed and captured under a microscope.

2.6.5 Cell scratch test

Using a marker pen, the back surface of a 6-hole plate was marked with evenly spaced lines at intervals ranging from 0.5–1 cm, ensuring that each hole was intersected by at least three lines (Wang and Li, 2021). The digested cells were seeded in 6-well plates at a density of 1×10^6 cells/well. Once the cell density exceeded 90%, a horizontal scratch was created perpendicular to the back of the plate. Next, the cells were washed thrice with PBS and treated with a serum-free medium, and images were captured at 0 h. Subsequently, they were cultured at 37°C in a 5% CO_2 incubator and photographed at 24 h.

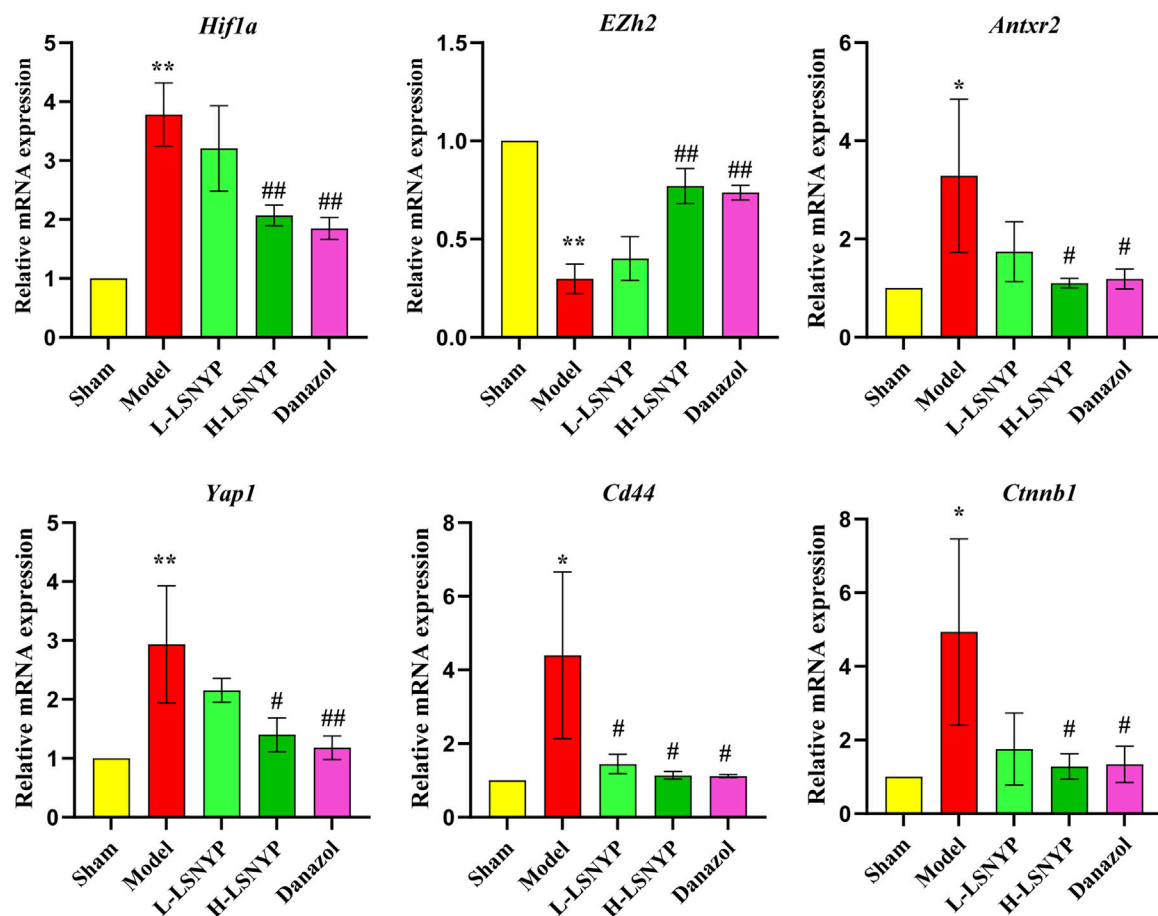


FIGURE 7
Effect of LSNYP on the expression of mRNA related to HIF1A/EZH2/ANTXR2 pathway in endometriotic tissues. Compared with the sham group, * $P < 0.05$, ** $P < 0.01$; compared with the model group, # $P < 0.05$, ## $P < 0.01$, $n = 3$.

2.6.6 Lentiviral transfection

Cells were inoculated into 6-well plates at a density of 5×10^4 cells/well. When the cell attachment rate was approximately 30%, the lentivirus rLV-shRNA containing HIF1A was introduced to establish a cell line with low expression of HIF1A. Subsequently, the cells were administered with drug serum and divided into six groups: the euESCs (10% blank serum), ecESCs (10% blank serum), high LSNYP dose (10% LSNYP-containing serum: blank serum = 1 : 0), si-NC (10% LSNYP-containing serum + si-NC), si-HIF1A (10% LSNYP-containing serum + si-HIF1A), and danazol (10% danazol-containing serum: blank serum = 1 : 0) groups. After the cells were cultured in the drug-containing serum for 72 h, the cell culture supernatant and cells were collected for experimentation.

2.6.7 Western blotting

Cells in each group were added with radioimmunoprecipitation assay lysate, placed on ice for 10 min, and centrifuged at 12,000 rpm for 5 min at 4°C. Protein concentration was determined using the bicinchoninic acid protein-concentration determination kit. Approximately 40 µg of protein was boiled in a boiling water bath for 10 min and then added to the sample hole with MAKER.

The proteins were separated by sodium dodecyl sulphate-polyacrylamide gel electrophoresis, and electrophoresis was conducted under a constant pressure of 80 V until the bromophenol blue indicator reached the junction of the concentrated and separation gel, after which the constant pressure was changed to 120 V until the bromophenol blue reached the bottom of the gel. This process took approximately 1.5 h. The isolated proteins were transferred onto a polyvinylidene fluoride membrane and blocked with 5% skim milk powder at 25°C for 2 h. The primary antibodies HIF-1A, EZH2, ANT XR2, YAP1, CD44, β-Catenin, and GAPDH, were diluted with Tris Buffered Saline with Tween 20 (TBST) at ratios of 1:1,000, 1:2,000, 1:1,000, 1:10,000, 1:3,000, 1:10,000, and 1:1,000, respectively. These antibodies were then added to the sample and allowed to react overnight at 4°C. The next day, these membranes were washed five times with TBST, and an HRP-labeled secondary antibody (1:10,000) was added. After another round of washing, the enhanced chemiluminescence reagent was applied for development. A gel imaging system was used for scanning exposure and filming. Finally, we used the Image-Pro Plus (IPP) software to calculate the gray value of the film (Mei et al., 2016).

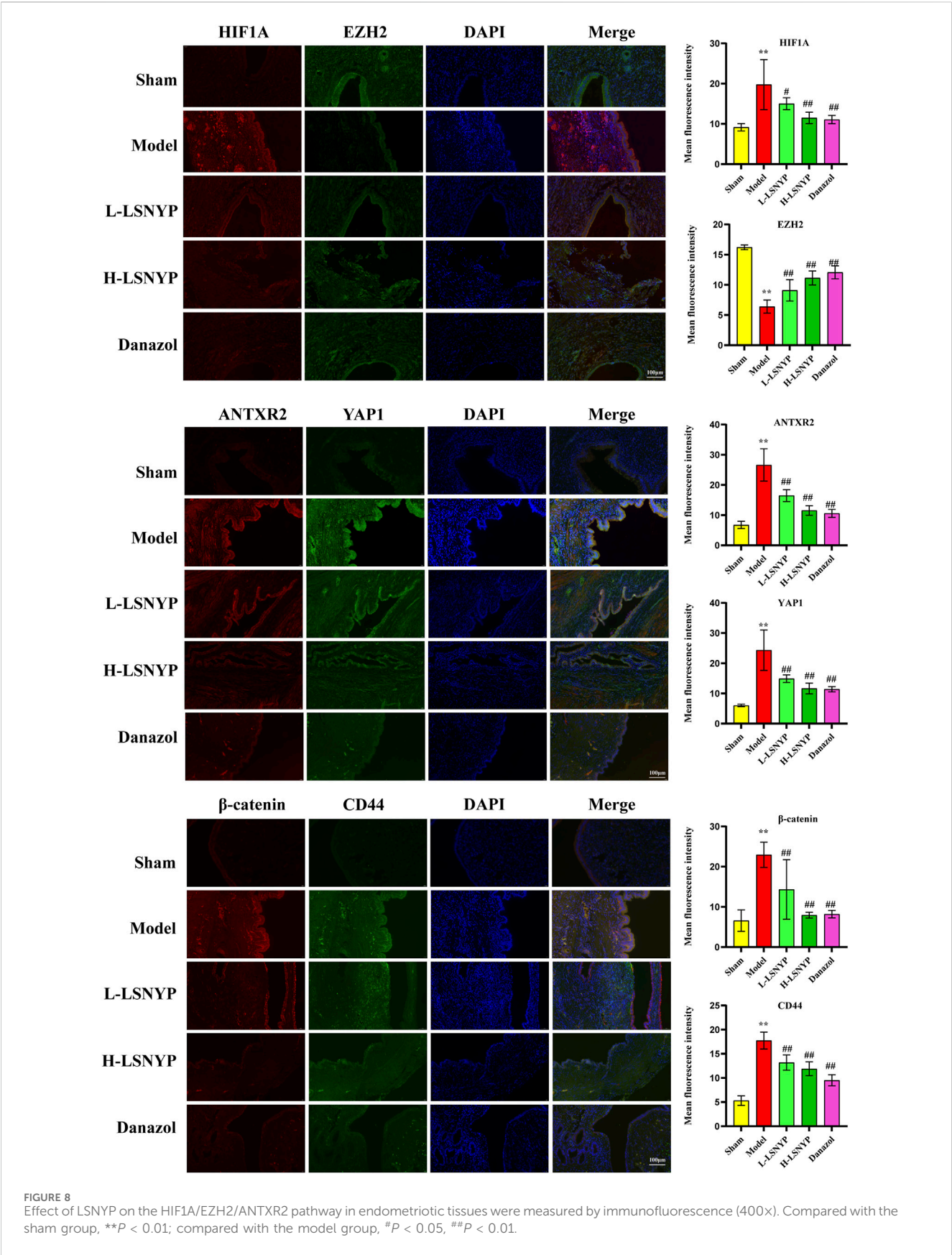


TABLE 5 The information of targets for molecular docking.

Target	PDB ID	Resolution	Structure	(X × Y × Z)/nm ³	Center (X, Y, Z)
HIF1A	1H2K	2.15 Å	single stranded	33.3 × 50.7 × 29.7	34.2, 19.9, 30.7
EZH2	4MI0	2.00 Å	single stranded	18.0 × 23.0 × 24.0	24.0, 27.5, 10.0
ANTXR2	1SHT	1.81 Å	single stranded	17.6 × 17.2 × 15.0	49.2, 66.4, −0.5
YAP1	4REX	1.60 Å	single stranded	20.0 × 22.0 × 30.0	7.0, 48.0, 55.0
CD44	1UUH	2.20 Å	single stranded	19.0 × 18.0 × 18.0	−4.5, 13.0, 19.0
β-Catenin	1JDH	1.90 Å	single stranded	21.0 × 18.0 × 18.0	12.5, 7.0, 15.0

2.7 Animal experiments

2.7.1 Experimental model of EMs and treatment

Twenty-four rats were randomly selected to establish the EMs model by autotransplantation in accordance with a previously described method (Oner et al., 2010). To synchronize their estrous cycles, the rats were intramuscularly injected with E2 benzoate (0.05 mg/kg/day) for 5 days prior to the operation. Subsequently, the rats were anesthetized and a 2 cm incision was made in the middle of the lower abdomen to expose the uterus. The left uterus was excised after ligation using 1# silk threads, and the surrounding adipose tissues were removed. The isolated uterus was cut open longitudinally and divided into two 5 mm × 5 mm pieces. Afterward, the samples were stitched to the right and left abdominal walls near the great vessels with 0/5 absorbable sutures. The endometrial surface of each implant faced the abdominal wall. After the surgery, the rats were treated with penicillin sodium by injection (160,000 units/kg/d) to prevent infection and E2 benzoate to promote the growth of the ectopic endometrium for 5 days. In addition, six rats were included in the sham-operated group, their abdomens were only opened and stitched, but their uteruses were not transplanted.

On the 29th postoperative day, the rats were divided into five groups: sham, model, low dose of LSNYP (L-LSNYP), high dose of LSNYP (H-LSNYP), and danazol. The L-LSNYP group were orally administered a double dose of LSNYP, and the H-LSNYP and danazol groups were subjected to the same procedure, as described in 2.3. The sham and model groups were administered an equal volume of normal saline. All rats were administered doses once per day for four consecutive weeks. Finally, the rats were euthanized, and their uterine tissues and endometriotic tissues were resected for pathological observations and other analyses.

2.7.2 Hematoxylin and eosin (H&E) staining

H&E staining was used for observing histopathology in endometriotic tissues. Tissues were fixed in a 4% paraformaldehyde solution and dehydrated with ethanol, then cleared with xylene and embedded in paraffin. Subsequently, the sections were cut from the paraffin blocks, then routinely dewaxed and hydrated. The hematoxylin was applied as a background staining. Hydrochloric acid and ethanol solution were used for color separation before counterstaining with eosin. Finally, the sections were rinsed, dehydrated, cleared, and mounted for microscopic observation.

2.7.3 Quantitative real-time PCR (qPCR)

Total RNA from the tissues was extracted using the Trizol reagent. The HiScript® II Q Select RT SuperMix was used to reverse transcribe the RNA into complementary DNA. The qPCR was performed with the SYBR Green Master Mix. PCR products were detected by fluorescence quantitative PCR equipment (Applied Biosystems, California, United States). The PCR program was performed as follows: pre-denaturation at 95°C for 10 min, denaturation at 95°C for 15 s, annealing at 60°C for 60 s and extension at 95°C for 15 s, for 40 cycles. The melting curve analysis of the amplification products was performed at 95°C for 15 s, at 60°C for 60 s, and at 95°C for 15 s again. *Gapdh* was used as an internal reference. Relative mRNA expression levels were calculated using the $2^{-\Delta\Delta Ct}$ method. The primers (Table 2) were obtained from Sangon Biotech (Shanghai) Co., Ltd.

2.7.4 Immunofluorescence analysis

After antigen retrieval was performed with 0.01 M sodium citrate buffer, the sections were treated with normal goat serum for 30 min to block nonspecific antibody binding and were incubated overnight at 4°C with primary antibodies against HIF1A (1:200), EZH2 (1:200), ANTXR2 (1:300), YAP1 (1:200), CD44 (1:200), and β-Catenin (1:300). On the next day, the sections were thoroughly washed with PBST three times for 3 min each, then the secondary antibody was added and incubated at 37°C for 1 h. Finally, the nuclei were counterstained with 4,6-diamino-2-phenyl indole (DAPI) for 5 min, and the slices were mounted with an anti-fluorescence quencher. Three fields were selected randomly from each section using a BX53 microscope (Olympus, Japan). The mean fluorescence intensity was analyzed with ImageJ software.

2.8 Statistical analysis

Data analysis was performed using SPSS version 27.0. Data are expressed as mean ± standard deviation (SD). One-way analysis of variance was used to compare multiple groups. $P < 0.05$ was considered statistically significant.

3 Results

3.1 Results of UPLC-Q-TOF/MS and drug-likeness screening

The ion flow diagrams of the serum samples in positive and negative ion modes are exhibited in Figure 1. Components present in

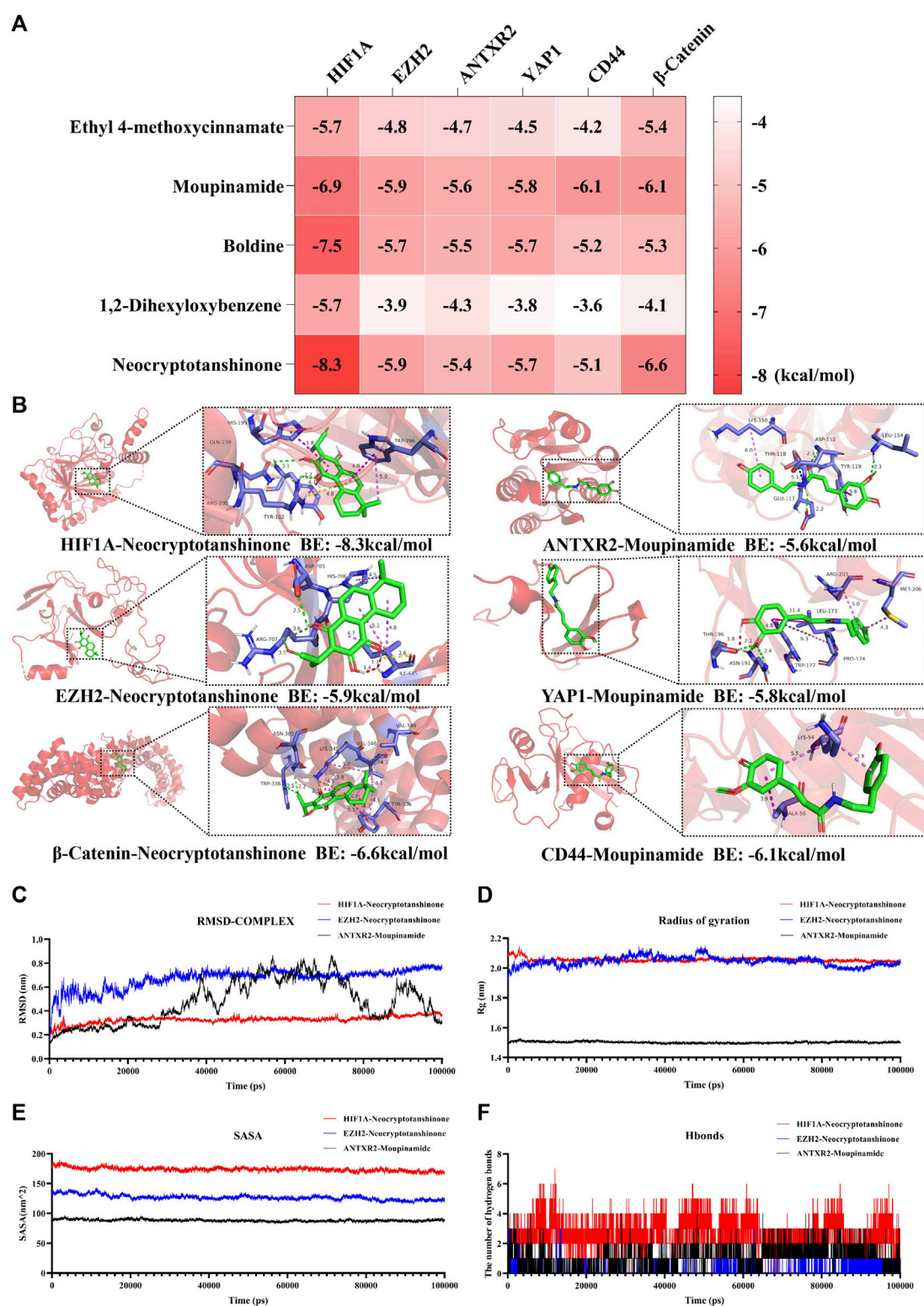


FIGURE 9 Molecular docking and molecular dynamics simulation results. (A) Heat map of molecular docking binding energy. (B) Molecular docking patterns with higher binding energy of compounds and pathway-associated targets. Analysis of RMSD (C), Rg (D), SASA (E), and hydrogen bonds (F) of HIF-1A-Neocryptotanshinone (red), EZH2-Neocryptotanshinone (blue), and ANTXR2-Moupinamide (black). BE is short for binding energy.

drug-containing serum samples and LSNYP, but absent in blank serum, were identified as prototype components. In our previously unpublished *in vitro* experiment with LSNYP samples, 185 components were detected under the same mass spectrum conditions (Supplementary Table S1). Through a new comparison, 45 prototype components (Supplementary Table S2) were confirmed to be absorbed in the blood, based on the retention time, primary MS data, and secondary MS data. These compounds underwent further screening using the PubChem database and ADMET lab2.0, and 34 compounds (Table 3) were identified as active compounds in LSNYP for subsequent analysis.

3.2 Network pharmacological target prediction

Based on SwissTargetPrediction and SEA databases, 1149 (Supplementary Table S3) potential targets were acquired after merging and eliminating duplicates. By incorporating the GeneCards (top 25%) and OMIM databases, 1119 (Supplementary Table S4) targets associated with EMs were obtained. A Venn diagram (Figure 2A) was constructed, and 182 (Supplementary Table S5) key targets of LSNYP in EMs treatment were identified. The component–target–disease network (Figure 2B) revealed that, on average, each compound was associated with 20 targets. Table 4 presents information on the top 10 compounds based on their degree value in the intersection network. A higher degree indicates a potentially greater number of associated targets (Liu et al., 2023a; Jiao et al., 2023). Notably, ethyl 4-methoxycinnamate, moupinamide, boldine, 1,2-dihexyloxybenzene, and neocryptotanshinone exhibited degrees ≥ 33 , indicating that they may be of great significance in the treatment of EMs. The PPI diagram (Figure 2C) showed that the core proteins included IL-6, EGFR, HIF1A, MMP9, and EZH2, which exhibit significant associations with hypoxia, adhesion, invasion, and angiogenesis. 2,425 biological process terms, such as cellular response to chemical stress, oxidative stress, and epithelial cell proliferation; 75 cellular component terms, including membrane raft, focal adhesion, and cell-substrate junction; and 154 molecular function categories focused on nuclear receptor and transcription factor activity, were identified for GO analysis. The top 10 terms were visually represented (Figure 2D). Additionally, KEGG analysis was performed, the top 30 pathways related to EMs were visualized (Figure 2E), including oxidative stress-related pathways, such as the HIF-1 signaling pathway, AGE–RAGE signaling pathway in diabetic complications; inflammation-related pathways, such as the TNF signaling and IL-17 signaling pathways; and cell proliferation-related pathways, such as the p13K–Akt signaling and MAPK signaling pathways.

The etiology of EMs remains incompletely understood; however, the widely-accepted theory of retrograde menstruation posits that shed-off endometrial tissues first lose blood supply and undergo hypoxic stress in the abdominal cavity. Within this microenvironment, upregulation of HIF1A serves as a key driver of endometriosis, activating multiple signaling pathways (Wu et al., 2019). The HIF1A/EZH2/ANTXR2 pathway involves deep epigenetic changes. HIF1A suppresses EZH2 expression and reduces H3K27 trimethylation, leading to abnormal

ANTXR2 expression in EMs, and activating proteins like YAP1, β -Catenin, CD44, COL5A2 and VEGFC (Lin et al., 2019). Additionally, YAP1 and β -Catenin, serving as crucial regulatory factors, increase downstream targets such as StAR, COX-2, IL-1 β , VEGF, MMP-9, and BCL2 (Liu et al., 2016; Song et al., 2016; Zhang et al., 2016; Lin et al., 2017), directly or indirectly promoting E2 and PGE synthesis and activating various pathways like EGFR, NF- κ B, and TNF α pathways in EMs (Banu et al., 2009; Lin et al., 2017). These help in the development of the complex gene regulatory networks and facilitate the development of EMs. Through GO and KEGG analysis, our study identified the response to oxidative stress and the HIF-1 signaling pathway. HIF1A, EZH2, and subsequent direct or indirect downstream targets like IL-1 β , COX-2, StAR, MMP-9, TNF, and BCL2 were identified as core targets. Because several key regulators and so many important downstream targets are involved in this pathway, we hypothesized that LSNYP may treat EMs by improving the hypoxic environment. Therefore, we chose the HIF1A/EZH2/ANTXR2 pathway for experimental verifications and molecular docking.

3.3 Cell experiments

3.3.1 Effect of LSNYP on the proliferation and migration of ecESCs

The inhibition rate of LSNYP on cellular activity increased with a prolonged intervention period (Figure 3A), and serum with varying drug concentrations had the potential to diminish cell viability after 24, 48, and 72 h of intervention. Nevertheless, the L-LSNYP, M-LSNYP, and H-LSNYP significantly differed only at 72 h when compared with the ecESCs group ($P < 0.01$; Figure 3B). The migration distance of cells was assessed after 72 h of serum intervention, and the results showed that the migration distance of cells in the LSNYP and danazol groups was significantly lower than that in the ecESCs group ($P < 0.01$; Figure 3C).

3.3.2 Effect of LSNYP on the adhesion and invasion of ecESCs

After 72 h of LSNYP treatment, ecESCs adhesion was observed. The results showed that the cell migration capability in the H-LSNYP and danazol groups was significantly diminished compared to that in the ecESCs group (Figure 4A) ($P < 0.01$). Additionally, invasive cells were detected, and the number of invasive cells in the LSNYP and danazol groups was significantly lower than that in the ecESCs group ($P < 0.01$; Figure 4B).

3.3.3 Effect of LSNYP on HIF1A/EZH2/ANTXR2 pathway in ecESCs

Based on the aforementioned series of experiments, H-LSNYP exhibited a superior inhibitory effect on cells following a 72-h intervention. Consequently, H-LSNYP were chosen as the optimal intervention condition for western blotting (Figure 5). Compared to the euESCs group, the ecESCs group demonstrated a significant increase in the expression levels of HIF1A, ANTXR2, YAP1, CD44, and β -catenin ($P < 0.01$), whereas the expression level of EZH2 was significantly reduced ($P < 0.01$). Following treatment with the H-LSNYP and danazol, the expression levels of HIF1A, ANTXR2, YAP1, CD44, and β -catenin were decreased ($P < 0.05$ or

$P < 0.01$), whereas the expression level of EZH2 was increased ($P < 0.05$). Compared to the NC + H-LSNYP group, the si-HIF1A + H-LSNYP group showed lower expression levels of HIF1A, ANT XR2, YAP1, CD44, and β -catenin ($P < 0.05$ or $P < 0.01$), with a higher expression level of EZH2 ($P < 0.05$).

3.4 Animal experimentations

3.4.1 Histopathological analysis

Macroscopic observation of endometriotic foci showed that there were cystic lesions containing clear fluid with vascularization visible on the surface and periphery. Partial lesions adhered to the intestines, but lysis was relatively easy. Than in the model group, smaller lesion volumes (Figure 6A) were observed in the LSNYP groups ($P < 0.05$ or $P < 0.01$). Endometriotic tissues (Figure 6B) in the sham group showed a monolayer of column-like epithelium with unaltered structures, even-sized, well-organized stromal cells, numerous glands, and few inflammatory cells. In comparison, the pathological results in the model group showed that epithelial cells were irregularly arranged, and some of them were structurally incomplete. There were increased, enlarged stromal cells and many inflammatory cells. The Danazol group exhibited thinner, more well-organized epithelial cells and fewer stromal cells and inflammatory cells after treatment. In addition, there were macrophages containing hemosiderin (represented by yellow arrows), which indicates that the phagocytic ability was good. The L-LSNYP group also showed a thinner columnar epithelium than the model and sham groups, but the improvements in inflammation and the increased number of macrophages were less than those in the Danazol group and the H-LSNYP group. The pharmacological effects in the H-LSNYP group were comparable to those in the Danazol group.

3.4.2 Effect of LSNYP on the expression of mRNA related to HIF1A/EZH2/ANTXR2 pathway in endometriotic tissues

The results of qPCR (Figure 7) showed that the expression of *Hif1a*, *Antxr2*, *Yap1*, *Cd44* and *Ctnnb1* mRNA increased significantly in the model group ($P < 0.05$ or $P < 0.01$), whereas *Ezh2* mRNA decreased significantly ($P < 0.01$). Compared with the model group, the expression of *Hif1a*, *Antxr2*, *Yap1*, *Cd44* and *Ctnnb1* mRNA decreased in the H-LSNYP group ($P < 0.05$ or $P < 0.01$), whereas the expression of *Ezh2* increased significantly after H-LSNYP intervention ($P < 0.05$).

3.4.3 Effect of LSNYP on the expression of proteins related to HIF1A/EZH2/ANTXR2 pathway in endometriotic tissues

The immunofluorescent staining results (Figure 8) showed that the model group demonstrated a significant increase in the expression levels of HIF1A, ANT XR2, YAP1, CD44, and β -catenin ($P < 0.01$) compared with the sham group, whereas the expression level of EZH2 was significantly reduced ($P < 0.01$). Following treatment with LSNYP and danazol, the expression levels of HIF1A, ANT XR2, YAP1, CD44, and β -catenin were decreased ($P < 0.05$ or $P < 0.01$), whereas the expression level of EZH2 was increased ($P < 0.01$).

3.5 Molecular docking and molecular dynamics simulation results

To further validate the relationship between LSNYP and the HIF1A/EZH2/ANTXR2 pathway, we conducted a molecular docking analysis between 34 components and the key proteins of the pathway. Information on the targets is listed in Table 5, and the docking binding energies are shown in Supplementary Table S6. Generally, small molecules can bind to proteins when the binding energy is less than -1.2 kcal/mol or -5 kJ/mol. Notably, all the binding energies were lower than -3.6 kcal/mol, suggesting that LSNYP has a high possibility of inhibiting the HIF1A/EZH2/ANTXR2 pathway in EMs.

Additionally, the binding energies between the top five core components and the key target were visualized (Figure 9A), and the molecular docking patterns with higher binding energies are also shown (Figure 9B) for better understanding (Jiao et al., 2023). Molecular dynamic simulations are a valuable tool for investigating the dynamics, stability, and structural intricacies of target–ligand complexes. Specifically, the stability of protein–ligand complexes, namely HIF1A-neocryptotanshinone, EZH2-neocryptotanshinone, and ANT XR2-moupinamide, was analyzed in this study. The conformational and structural stabilities of the complexes were assessed using RMSD analysis. The complexes of HIF-1A and neocryptotanshinone and EZH2 and neocryptotanshinone remained stable (Figure 9C), whereas the conformation of the complex ANT XR2-moupinamide showed a slightly larger fluctuation during the simulations, indicating that the small molecules found a position with less energy during the simulation. The radius of gyration (Rg) is an important indicator of the tightness of protein–ligand complexes. The results showed that the three-line segments were relatively stable (Figure 9D), and Rgs was less than 2.15 nm, suggesting that the complexes were stable. The solvent-accessible surface area, a surface area indicator of the protein (Figure 9E), slightly decreased, indicating that the protein gradually tightened. Notably, hydrogen bonds (H-bonds) can form between proteins and ligands (Figure 9F).

4 Discussion

EMs remains an incurable condition that necessitates prolonged management, imposing a substantial medical burden and profoundly affecting the physical and mental wellbeing of women (Wang et al., 2022). TCM teaches that EMs is classified under various categories, such as “Zhengjia” and “dysmenorrhea,” and clinical approaches targeting blood stasis in EMs treatment have demonstrated distinctive advantages. An increasing number of studies have proved the efficacy of TCM in alleviating pain, enhancing pregnancy rates, and improving the quality of life with fewer adverse effects (Feng et al., 2023). Consequently, it has emerged as a research hotspot and first-line solution for the long-term management of EMs in China (Ni et al., 2020). LSNYP was formulated by Professor Luo Yuankai, a distinguished specialist in gynecology, and its composition is based on the TCM theory of “Emperor–Minister–Assistant–Messenger.” Within this prescription, Yimucao enhances blood circulation, whereas Zhebeimu disperses phlegm and dissipates masses and is regarded as an emperor herb responsible for treating the main symptoms. Taoren, Danshen, Chuanxiong, Tubiechong, and Shanzha remove blood stasis and

promote blood regeneration, assisting the emperor herbs and acting as minister herbs. Puhuang, Wulingzhi, Wuyao, and Yanhusuo provide further assistance by promoting chi and pain relief; they are assistant herbs. Wumei, a messenger herb, removes the malignant flesh and counteracts the excessive promoting effects of other drugs. Combining these herbs resolves blood stasis and disperses masses, promoting qi circulation and relieving pain. However, the current state of research on LSNYP has not been sufficiently advanced. This study combined UPLC-Q/TOF-MS technology and network pharmacology methods to analyze the prototype components and mechanisms of action of LSNYP and provide a theoretical foundation for its utilization.

The intricate chemical composition of TCM prescriptions presents considerable obstacles in investigating the pharmacodynamic material basis. UPLC-Q/TOF-MS technology, known for its exceptional sensitivity, resolution, and accuracy, holds great potential for application in TCM (Liu et al., 2022b). By employing this technique along with drug-likeness screening conditions, we identified 34 absorbed components suitable for network pharmacology analysis. Notably, ethyl 4-methoxycinnamate reduced the levels of IL-1, TNF α , and VEGF and can be helpful for the treatment of inflammatory and angiogenesis-related diseases (Umar et al., 2014). Moupinamide is an alkaloid that plays an important role in reducing free radicals and relieving oxidative stress. Tetrahydropalmatine is often used for pain relief, and the combination of tetrahydropalmatine, ligustrazine, and ferulic acid inhibits the development of endometriotic tissue, decreases E2 levels, and enhances the phagocytic ability of peritoneal macrophages (Gao et al., 2019). Another study (Woo et al., 2019) found that dehydrocostus lactone, a sesquiterpene lactone compound, can reduce the production of PGE2 and neurotrophins and suppress the Akt and NF- κ B pathways in human endometriotic cells. Norisoboldine, a primary isoquinoline alkaloid found by Wuyao (Lv et al., 2018), can alleviate colitis in mice and enhance Treg polarization in a hypoxic microenvironment. Vanillin has anti-inflammatory, antibacterial, and antitumor properties. Liu et al. (2023c) found that vanillin decreased the weight and volume of endometriotic tissues through anti-inflammatory and anti-oxidant pathways in a mouse model. Although the parts do not represent the whole, these studies also suggest that LSNYP may treat EMs by regulating hypoxia, anti-inflammation, inhibition of cells, and blood vessel growth.

According to the PPI network analysis results, the core targets included IL-6, EGFR, HIF1A, MMP9, and EZH2. IL-6 is an important inflammatory factor in EMs, and an elevated level of IL-6 in women with EMs reduces the cytolytic activity of NK cells (Kang et al., 2014), activates macrophages, and amplifies angiogenesis (Ayaub et al., 2019; Song et al., 2020). EGFR, which is a tyrosine kinase receptor, can stimulate the formation of blood vessels. EGFR inhibitors can regress endometriotic lesions and reduce MMP-7 activities (Chatterjee et al., 2018). HIF1A, a transcription factor under hypoxic conditions, plays a vital role in the hypoxic mechanism of EMs (Wu et al., 2019), and downregulation of the HIF1A/VEGF pathway can be helpful in restraining the proliferation and invasion of eESCs (Qin et al., 2023). MMP9, which belongs to the MMP family, can degrade type IV collagen in both epithelial and stromal cells in the surgical tissues of EMs and overexpress MMP-9 (Wang et al., 2018). EZH2, a histone methyltransferase, can suppress the transcription of target genes by

catalyzing the trimethylation of lysine 27 on histone 3 (H3K27me3). Loss of EZH2 expression leads to increased downstream gene expression during the decidualization of human endometrial stromal cells (Grimaldi et al., 2011). According to previous reports, depleting EZH2 could upregulate angiotensin-converting enzyme II in human embryonic stem cells (Li et al., 2020) and ANTXR2 in euESCs (Lin et al., 2019). These targets suggested by the PPI network are associated with cell survival and the inflammatory response, which is also consistent with the GO enrichment results; that is, LSNYP can act on multiple functions of the predicted targets, such as response to oxidative stress, cell proliferation, focal adhesion, and transcription factor activity.

Based on the KEGG pathway analysis results, LSNYP may treat EMs by regulating hypoxia-, inflammation-, and cell proliferation-related signaling pathways, such as the HIF-1, AGE-RAGE in diabetic complications, TNF, and MAPK pathways. HIF1A is the active subunit of HIF-1, located in the cytoplasm, under hypoxic microenvironment. HIF1A is transported to the cell nucleus, where it combines with HIF1B to form the HIF (Wilson, 2018). Subsequently, HIF activates downstream genes. Studies have confirmed that HIF1A can regulate estrogen responsiveness, glycolytic metabolism, angiogenesis, cell proliferation, and inflammation in EMs (Zhan et al., 2016). AGE-RAGE binding is associated with oxidative stress and inflammation, and a previous study (Khan et al., 2018) showed that hypoxia induces AGE-RAGE-mediated cancer progression. Sharma et al. (2010) suggested that elevated levels of RAGE, EN-RAGE, and COX-2 are significant factors in the advancement of EMs. The most important angiogenic cytokine in the TNF pathway is TNF- α , which contributes to the generation of inflammatory factors (Sakamoto et al., 2003) and the adhesion of endometriotic stromal cells. A study indicated that resveratrol can act as a modulator of EMs and inhibit the release of IL-8 induced by TNF- α in ESCs (Khodarahmian et al., 2021). MAPKs, members of the serine/threonine kinase family, have been shown to play a crucial role in the pathogenesis of EMs by regulating processes such as invasion, proliferation, mitosis, angiogenesis, inflammation, and apoptosis (Yoshino et al., 2004; Leconte et al., 2015; Bora and Yaba, 2021; Giacomini et al., 2021).

Recent studies have found that EMs is a complex clinical syndrome of gene-gene and gene-microenvironment interactions, and the accumulation of HIF1A in hypoxic conditions is the key driving factor of EMs pathogenesis (Wu et al., 2019). To provide further evidence for the application of LSNYP, combined with the results of network pharmacology and current related research, we chose the HIF1A/EZH2/ANTXR2 pathway for experiments and molecular docking verification. HIF1A can inhibit EZH2, and abnormal methylation modifications result in an increase in downstream ANTXR2 expression in EMs (Lin et al., 2019). ANTXR2, also known as capillary morphogenesis gene 2 (CMG2), is involved in tumor angiogenesis (Ma et al., 2023), and activating ANTXR2 could promote the proliferation and vitality of ESCs (Liu et al., 2023b). YAP1, CD44, and β -catenin are the downstream proteins of ANTXR2. HIF1A expression is positively related to YAP1 in ectopic endometrial tissue. When suppressing the YAP1 function, key biological processes involved in EMs development, such as steroidogenesis, inflammation, and migration, are reduced (Lin et al., 2017). CD44 is a transmembrane glycoprotein, and increased CD44 splice variant expression in the eutopic endometrium makes it easier for shed endometrial cells to adhere to the abdominal cavity (Griffith et al., 2010; Knudtson et al., 2016). β -catenin is associated with the invasive

phenotype of eutopic endometrium. When the β -catenin gene was silenced with siRNA, the expression of its downstream target genes VEGF and MMP-9 was significantly inhibited (Liu et al., 2016). Therefore, inhibiting the HIF1A/EZH2/ANTXR2 pathway may help treat EMs. In these cell phenotype experiments, the results indicated that LSNYP suppressed the viability of eECSCs in a concentration- and time-dependent manner and that the adhesion, migration, and invasion abilities of eECSCs were reduced after 72 h of intervention with H-LSNYP, indicating that LSNYP can inhibit the growth of eECSCs. Western blotting results showed that LSNYP treatment reduced the expression levels of HIF1A, ANTXR2, YAP1, CD44, and β -catenin, and increased EZH2 expression in eECSCs. When the HIF1A knockdown vector was used to treat cells with LSNYP, the inhibitory effect of LSNYP on this pathway was more apparent. In the animal experiments, LSNYP ameliorated pathological injury and inflammatory responses, regulated the expression of genes and proteins related to HIF1A/EZH2/ANTXR2 pathway in endometriotic tissues. Additionally, the molecular docking and molecular dynamics simulation results showed that moupinamide and other core components are stably bound to the HIF1A, EZH2, ANTXR2, YAP1, CD44, or β -catenin. These findings suggest that this prescription may exert therapeutic effects by inhibiting the HIF1A/EZH2/ANTXR2 pathway in EMs.

This study has some limitations. First, identifying serum components and targets from self-built or existing databases may not be sufficiently comprehensive, and standard products should be added for quantitative analysis. Second, due to the limitation of time constraints and experimental funding, the sample size of the animal experiment was low, which may produce a bias in the expression of the results. Future studies expand the sample size and add other detection methods and indicators.

In summary, the mutual confirmation of serum pharmacochimistry, network pharmacology, and experiments enabled a preliminary exploration of the pharmacological mechanism of LSNYP in EMs, which may be related to the regulation of hypoxia and suppression of the HIF1A/EZH2/ANTXR2 pathway, providing theoretical evidence for the clinical application of LSNYP. The TCM formula, LSNYP, shows potential as an effective agent for preventing and treating EMs.

Data availability statement

The original contributions presented in the study are included in the article/**Supplementary Material**, further inquiries can be directed to the corresponding authors.

Ethics statement

The studies involving humans were approved by the Ethics Committee of The First Affiliated Hospital of Guangzhou University of Chinese Medicine (NO. K [2021] 053). The animal study was approved by the First Affiliated Hospital of Guangzhou University of TCM Animal Ethical Review Standards (approval number: TCMF1-2021024). The studies were conducted in accordance with the local legislation and institutional requirements.

Author contributions

LW: Methodology, Writing–original draft. SL: Writing–original draft. YH: Writing–review and editing. SJ: Writing–original draft, Methodology, Validation. BS: Writing–original draft, Methodology. XC: Resources, Writing–original draft. JJ: Writing–original draft, Methodology. CZ: Project administration, Supervision, Writing–review and editing. FP: Project administration, Supervision, Writing–review and editing.

Funding

The author(s) declare that financial support was received for the research, authorship, and/or publication of this article. This work was supported by the National Natural Science Foundation of China (No. 82074481, No. 82374500), the National Natural Science Foundation of China Youth Fund Grant (No. 82305288), the Research Project of Inheritance and Innovation of National Traditional Chinese Medicine (2022QN22, 2023ZD05), and the Young Talent Program of the First Affiliated Hospital of Guangzhou University of Chinese Medicine (No. ZYYY [2023]186).

Acknowledgments

The authors would like to thank all the reviewers who participated in the review and all staff of Lingnan Medical Research Center, Guangzhou University of Chinese Medicine for supporting this study.

Conflict of interest

The authors declare that the research was conducted in the absence of any commercial or financial relationships that could be construed as a potential conflict of interest.

Publisher's note

All claims expressed in this article are solely those of the authors and do not necessarily represent those of their affiliated organizations, or those of the publisher, the editors and the reviewers. Any product that may be evaluated in this article, or claim that may be made by its manufacturer, is not guaranteed or endorsed by the publisher.

Supplementary material

The Supplementary Material for this article can be found online at: <https://www.frontiersin.org/articles/10.3389/fphar.2024.1395160/full#supplementary-material>

References

- Abraham, M. J., Murtola, T., Schulz, R., Páll, S., Smith, J. C., Hess, B., et al. (2015). GROMACS: high performance molecular simulations through multi-level parallelism from laptops to supercomputers. *SoftwareX* 1–2, 19–25. doi:10.1016/j.softx.2015.06.001
- Ayoub, E. A., Tandon, K., Padwal, M., Imani, J., Patel, H., Dubey, A., et al. (2019). IL-6 mediates ER expansion during hyperpolarization of alternatively activated macrophages. *Immunol. Cell. Biol.* 97 (2), 203–217. doi:10.1111/imcb.12212
- Banu, S. K., Lee, J., Speights, V. O., Jr., Starzinski-Powitz, A., and Arosh, J. A. (2009). Selective inhibition of prostaglandin E2 receptors EP2 and EP4 induces apoptosis of human endometrial cells through suppression of ERK1/2, AKT, NFκappaB, and beta-catenin pathways and activation of intrinsic apoptotic mechanisms. *Mol. Endocrinol.* 23 (8), 1291–1305. doi:10.1210/me.2009-0017
- Bickerton, G. R., Paolini, G. V., Besnard, J., Muresan, S., and Hopkins, A. L. (2012). Quantifying the chemical beauty of drugs. *Nat. Chem.* 4, 90–98. doi:10.1038/nchem.1243
- Bora, G., and Yaba, A. (2021). The role of mitogen-activated protein kinase signaling pathway in endometriosis. *J. Obstet. Gynaecol. Res.* 47 (5), 1610–1623. doi:10.1111/jog.14710
- Chatterjee, K., Jana, S., DasMahapatra, P., and Swarnakar, S. (2018). EGFR-mediated matrix metalloproteinase-7 up-regulation promotes epithelial-mesenchymal transition via ERK1-AP1 axis during ovarian endometriosis progression. *Faseb J.* 32 (8), 4560–4572. doi:10.1096/fj.2017.01382RR
- Daina, A., Michielin, O., and Zoete, V. (2019). SwissTargetPrediction: updated data and new features for efficient prediction of protein targets of small molecules. *Nucleic Acids Res.* 47, W357–W364. doi:10.1093/nar/gkz382
- Doncheva, N. T., Morris, J. H., Gorodkin, J., and Jensen, L. J. (2018). Cytoscape StringApp: network analysis and visualization of proteomics data. *J. Proteome Res.* 18, 623–632. doi:10.1021/acs.jproteome.8b00702
- Eberhardt, J., Santos-Martins, D., Tillack, A. F., and Forli, S. (2021). AutoDock Vina 1.2.0: new docking methods, expanded force field, and Python bindings. *J. Chem. Inf. Model.* 61 (8), 3891–3898. doi:10.1021/acs.jcim.1c00203
- Feng, C., Zhao, D., Wang, X., and Xiao, M. J. T. M. H. M. (2023). Traditional Chinese medicine for the treatment of endometriosis: a comprehensive review of treatment mechanisms. *TMR Mod. Herb. Med.* 6 (2), 10. doi:10.53388/mhm20230010
- Gao, X., Wang, C., Chen, Z., Chen, Y., Santhanam, R. K., Xue, Z., et al. (2019). Effects of N-trans-feruloyltyramine isolated from laba garlic on antioxidant, cytotoxic activities and H(2)O(2)-induced oxidative damage in HepG2 and L02 cells. *Food Chem. Toxicol.* 130, 130–141. doi:10.1016/j.fct.2019.05.021
- Giacomini, E., Minetto, S., Li Piani, L., Pagliardini, L., Somigliana, E., and Viganò, P. (2021). Genetics and inflammation in endometriosis: improving knowledge for development of new pharmacological strategies. *Int. J. Mol. Sci.* 22 (16), 9033. doi:10.3390/ijms22169033
- Griffith, J. S., Liu, Y. G., Tekmal, R. R., Binkley, P. A., Holden, A. E., and Schenken, R. S. (2010). Menstrual endometrial cells from women with endometriosis demonstrate increased adherence to peritoneal cells and increased expression of CD44 splice variants. *Fertil. Steril.* 93 (6), 1745–1749. doi:10.1016/j.fertnstert.2008.12.012
- Grimaldi, G., Christian, M., Steel, J. H., Henriot, P., Poutanen, M., and Brosens, J. J. (2011). Down-regulation of the histone methyltransferase EZH2 contributes to the epigenetic programming of decidualizing human endometrial stromal cells. *Mol. Endocrinol.* 25 (11), 1892–1903. doi:10.1210/me.2011-1139
- Guanhua, D. (2014). *Experimental pharmacology*. Beijing: PEKING UNION MEDICAL COLLEGE PRESS.
- Guo, W. (2021). *Based on photoacoustic non-invasive imaging to study the Action mechanism of LuoShiNeiYi recipe on EndometriosisModel rats*. China: Guangzhou University of Chinese Medicine.
- Guoli, X., Zhenxing, W., Jiakai, Y., Li, F., Zhijiang, Y., Changyu, H., et al. (2021). ADMETlab 2.0: an integrated online platform for accurate and comprehensive predictions of ADMET properties. *Nucleic Acids Res.* 49, W5–W14. doi:10.1093/nar/gkab255
- Haiying, W., Yun, S., and Pengpeng, X. (2013). Effect of Luo's neiyi recipe on the concentration of ICAM-1 and IL-8 in the peritoneal fluid cytology among the infertility patients with endometriosis. *Chin. J. Birth Health & Hered.* 21 (03), 114–116. doi:10.13404/j.cnki.cjbhh.2013.03.003
- Jiao, Y., Shi, C., and Sun, Y. (2023). Unraveling the role of scutellaria baicalensis for the treatment of breast cancer using network pharmacology, molecular docking, and molecular dynamics simulation. *Int. J. Mol. Sci.* 24 (4), 3594. doi:10.3390/ijms24043594
- Kang, Y. J., Jeung, I. C., Park, A., Park, Y. J., Jung, H., Kim, T. D., et al. (2014). An increased level of IL-6 suppresses NK cell activity in peritoneal fluid of patients with endometriosis via regulation of SHP-2 expression. *Hum. Reprod.* 29 (10), 2176–2189. doi:10.1093/humrep/deu172
- Kefe, G., Gen, Z., Shuo, Y., Ruling, L., Sijin, L., Miaomiao, D., et al. (2022). A comparative study of Luo's Endometriosis Formula and combined oral contraceptives on the maintenance treatment of Stage IV ovarian endometriomas. *Guangdong Med. J.* 43 (11), 1386–1391. doi:10.13820/j.cnki.gdyx.20223007
- Keiser, M. J., Roth, B. L., Armbruster, B. N., Ernsterberger, P., Irwin, J. J., and Shoichet, B. K. (2007). Relating protein pharmacology by ligand chemistry. *Nat. Biotechnol.* 25 (2), 197–206. doi:10.1038/nbt1284
- Khan, M. I., Rath, S., Adhami, V. M., and Mukhtar, H. (2018). Hypoxia driven glycation: mechanisms and therapeutic opportunities. *Semin. Cancer Biol.* 49, 75–82. doi:10.1016/j.semcancer.2017.05.008
- Khodarahmian, M., Amidi, F., Moini, A., Kashani, L., Salahi, E., Danaii-Mehrabad, S., et al. (2021). A randomized exploratory trial to assess the effects of resveratrol on VEGF and TNF-α expression in endometriosis women. *J. Reprod. Immunol.* 143, 103248. doi:10.1016/j.jri.2020.103248
- Knudtson, J. F., Tekmal, R. R., Santos, M. T., Binkley, P. A., Krishnegowda, N., Valente, P., et al. (2016). Impaired development of early endometriotic lesions in CD44 knockout mice. *Reprod. Sci.* 23 (1), 87–91. doi:10.1177/1933719115594022
- Leconte, M., Santulli, P., Chouzenoux, S., Marcellin, L., Cerles, O., Chapron, C., et al. (2015). Inhibition of MAPK and VEGFR by sorafenib controls the progression of endometriosis. *Reprod. Sci.* 22 (9), 1171–1180. doi:10.1177/1933719115592708
- Li, W.-H., Han, J.-R., Ren, P.-P., Xie, Y., and Jiang, D.-Y. (2021). Exploration of the mechanism of Zisheng Shenqi decoction against gout arthritis using network pharmacology. *Comput. Biol. Chem.* 90, 107358. doi:10.1016/j.compbiolchem.2020.107358
- Li, Y., Li, H., and Zhou, L. (2020). EZH2-mediated H3K27me3 inhibits ACE2 expression. *Biochem. Biophys. Res. Commun.* 526 (4), 947–952. doi:10.1016/j.bbrc.2020.04.010
- Liao, H., Li, F., Huang, J., and Chen, Y. (2010). The influence of Luoshi Neiyi recipe on the endometrial morphology of endometriosis rat model. *Clin. Med. Eng.* 17 (6), 5–6. doi:10.3969/j.issn.1674-4659.2010.06.005
- Lin, S. C., Lee, H. C., Hou, P. C., Fu, J. L., Wu, M. H., and Tsai, S. J. (2017). Targeting hypoxia-mediated YAP1 nuclear translocation ameliorates pathogenesis of endometriosis without compromising maternal fertility. *J. Pathol.* 242 (4), 476–487. doi:10.1002/path.4922
- Lin, S. C., Lee, H. C., Hsu, C. T., Huang, Y. H., Li, W. N., Hsu, P. L., et al. (2019). Targeting anthrax toxin receptor 2 ameliorates endometriosis progression. *Theranostics* 9 (3), 620–632. doi:10.7150/thno.30655
- Lipinski, C. A., Lombardo, F., Dominy, B. W., and Feeney, P. J. (2012). Experimental and computational approaches to estimate solubility and permeability in drug discovery and development settings. *Adv. Drug Deliv. Rev.* 46, 3–26. doi:10.1016/s0169-409x(00)00129-0
- Liu, H., Mohammed, S. A. D., Lu, F., Chen, P., Wang, Y., and Liu, S. (2022a). Network pharmacology and molecular docking-based mechanism study to reveal antihypertensive effect of gedan jiangya decoction. *Biomed. Res. Int.* 2022, 3353464. doi:10.1155/2022/3353464
- Liu, H., Yang, L., Wan, C., Li, Z., Yan, G., Han, Y., et al. (2022b). Exploring potential mechanism of ciwujia tablets for insomnia by UPLC-Q-TOF-MS/MS, network pharmacology, and experimental validation. *Front. Pharmacol.* 13, 990996. doi:10.3389/fphar.2022.990996
- Liu, R., Liu, Y., Yu, L., Zheng, T., and Wang, G. (2016). Gene silencing of wnt/B-catenin signaling pathway by siRNA inhibits VEGF and MMP-9 expression in endometrial stromal cells in patients with endometriosis. *Acta Med. Univ. Sci. Technol. Huazhong* 45 (01), 6–11+26. doi:10.3870/j.issn.1672-0741.2016.01.002
- Liu, Y., Luo, D., and Xu, B. (2022c). The combination of molecular docking and network pharmacology reveals the molecular mechanism of Danggui Niantong decoction in treating gout. *Med. Baltim.* 101 (47), e31535. doi:10.1097/md.00000000000031535
- Liu, Y., Wang, S., Jin, G., Gao, K., Wang, S., Zhang, X., et al. (2023a). Network pharmacology-based study on the mechanism of ShenKang injection in diabetic kidney disease through Keap1/Nrf2/Ho-1 signaling pathway. *Phytomedicine* 118, 154915. doi:10.1016/j.phymed.2023.154915
- Liu, Y., Xie, C., Li, T., Lu, C., Fan, L., Zhang, Z., et al. (2023b). PCGEM1 promotes cell proliferation and migration in endometriosis by targeting miR-124-3p-mediated ANTXR2 expression. *BMC Womens Health* 23 (1), 104. doi:10.1186/s12905-023-02250-1
- Liu, Y. N., Kang, J. W., Zhang, Y., Song, S. S., Xu, Q. X., Zhang, H., et al. (2023c). Vanillin prevents the growth of endometriotic lesions through anti-inflammatory and antioxidant pathways in a mouse model. *Food Funct.* 14 (14), 6730–6744. doi:10.1039/d3fo00750b
- Luo, T.-t., Lu, Y., Yan, S.-k., Xiao, X., Rong, X.-l., and Guo, J. (2019). Network pharmacology in research of Chinese medicine formula: methodology, application and prospective. *Chin. J. Integr. Med.* 26, 72–80. doi:10.1007/s11655-019-3064-0
- Lv, Q., Wang, K., Qiao, S., Yang, L., Xin, Y., Dai, Y., et al. (2018). Norisoboldine, a natural AhR agonist, promotes Treg differentiation and attenuates colitis via targeting glycolysis and subsequent NAD(+)SIRT1/SUV39H1/H3K9me3 signaling pathway. *Cell. Death Dis.* 9 (3), 258. doi:10.1038/s41419-018-0297-3
- Ma, F.-X., Xue, P.-F., Wang, Y.-Y., Wang, Y.-N., and Xue, S.-Y. (2017). Research progress of serum pharmacokinetics of traditional Chinese medicine. *Zhongguo*

Zhong yao za zhi = Zhongguo zhongyao zazhi = China J. Chin. materia medica 42, 1265–1270. doi:10.19540/j.cnki.cjmm.20170224.010

Ma, L., Deng, D., Lan, C., Liu, S., Tang, H., Huang, X., et al. (2023). Mechanism of anthrax toxin receptor 2 expression regulated by miR-145-5p in pancreatic cancer. *J. Chongqing Med. Univ.* 48 (03), 261–268. doi:10.13406/j.cnki.cyx.003189

McKusick, V. A. (2007). Mendelian inheritance in man and its online version, OMIM. *Am. J. Hum. Genet.* 80, 588–604. doi:10.1086/514346

Mei, Y., Tang, Z., Li, Z., and Yang, X. (2016). Repeatability and reproducibility of quantitative corneal shape analysis after orthokeratology treatment using image-pro Plus software. *J. Ophthalmol.* 2016, 1732476. doi:10.1155/2016/1732476

Ni, X., Cheng, W., Sun, S., and Yu, C. (2020). Feasibility analysis of traditional Chinese medicine as the first line of conservative treatment for endometriosis. 35(01), 178–181. doi:10.19829/j.zgfybj.issn.1001-4411.2020.01.059

Oner, G., Ozelik, B., Ozgun, M. T., Serin, I. S., Ozturk, F., and Basbug, M. (2010). The effects of metformin and letrozole on endometriosis and comparison of the two treatment agents in a rat model. *Hum. Reprod.* 25 (4), 932–937. doi:10.1093/humrep/deq016

Qin, Q., Li, H., and Li, Z. (2023). miR-429 promotes proliferation, migration and invasion of ectopic endometrial stromal cells in endometriosis by regulating HIF-1 α /VEGF pathway. *Chin. J. Birth Health & Hered.* 31 (03), 580–585. doi:10.13404/j.cnki.cjbh.2023.03.015

Rosignoli, S., and Paiardini, A. (2022). DockingPie: a consensus docking plugin for PyMOL. *Bioinformatics* 38 (17), 4233–4234. doi:10.1093/bioinformatics/btac452

Sakamoto, Y., Harada, T., Horie, S., Iba, Y., Taniguchi, F., Yoshida, S., et al. (2003). Tumor necrosis factor- α -induced interleukin-8 (IL-8) expression in endometrial stromal cells, probably through nuclear factor- κ B activation: gonadotropin-releasing hormone agonist treatment reduced IL-8 expression. *J. Clin. Endocrinol. Metab.* 88 (2), 730–735. doi:10.1210/jc.2002-020666

Sasitha, T., and John, W. J. (2021). Design, docking, and DFT investigations of 2,6-bis(3,4-dihydroxyphenyl)-3-phenethylpiperidin-4-one. *Heliyon* 7, e06127. doi:10.1016/j.heliyon.2021.e06127

Shafir, A. L., Farland, L. V., Shah, D. K., Harris, H. R., Kvskoff, M., Zondervan, K., et al. (2018). Risk for and consequences of endometriosis: a critical epidemiologic review. *Best Pract. Res. Clin. Obstetrics Gynaecol.* 51, 1–15. doi:10.1016/j.bpobgyn.2018.06.001

Sharma, I., Dhawan, V., Saha, S. C., Rashmi, B., and Dhaliwal, L. K. (2010). Implication of the RAGE-EN-RAGE axis in endometriosis. *Int. J. Gynaecol. Obstet.* 110 (3), 199–202. doi:10.1016/j.ijgo.2010.03.037

Song, Y., Fu, J., Zhou, M., Xiao, L., Feng, X., Chen, H., et al. (2016). Activated hippo/yes-associated protein pathway promotes cell proliferation and anti-apoptosis in endometrial stromal cells of endometriosis. *J. Clin. Endocrinol. Metab.* 101 (4), 1552–1561. doi:10.1210/jc.2016-1120

Song, Y., Su, R. W., Joshi, N. R., Kim, T. H., Lessey, B. A., Jeong, J. W., et al. (2020). Interleukin-6 (IL-6) activates the NOTCH1 signaling pathway through E-proteins in endometrial lesions. *J. Clin. Endocrinol. Metab.* 105 (5), 1316–1326. doi:10.1210/clinem/dgaa096

Stelzer, G., Rosen, N., Plaschkes, I., Zimmerman, S., Twik, M., Fishilevich, S., et al. (2016). The GeneCards suite: from gene data mining to disease genome sequence analyses. *Curr. Protoc. Bioinforma.* 54, 1. doi:10.1002/cpbi.5

Szklarczyk, D., Gable, A. L., Nastou, K. C., Lyon, D., Kirsch, R., Pyysalo, S., et al. (2020). The STRING database in 2021: customizable protein–protein networks, and functional characterization of user-uploaded gene/measurement sets. *Nucleic Acids Res.* 49, D605–D612. doi:10.1093/nar/gkaa1074

Umar, M. I., Asmawi, M. Z., Sadikun, A., Majid, A. M., Al-Suede, F. S., Hassan, L. E., et al. (2014). Ethyl-p-methoxycinnamate isolated from *Kaempferia galanga* inhibits inflammation by suppressing interleukin-1, tumor necrosis factor- α , and angiogenesis by blocking endothelial functions. *Clin. (Sao Paulo)* 69 (2), 134–144. doi:10.6061/clinics/2014(02)10

Van Der Spoel, D., Lindahl, E., Hess, B., Groenhof, G., Mark, A. E., and Berendsen, H. J. C. (2005). GROMACS: fast, flexible, and free. *J. Comput. Chem.* 26, 1701–1718. doi:10.1002/jcc.20291

Wang, H. S., Tsai, C. L., Chang, P. Y., Chao, A., Wu, R. C., Chen, S. H., et al. (2018). Positive associations between upregulated levels of stress-induced phosphoprotein 1 and matrix metalloproteinase-9 in endometriosis/adenomyosis. *PLoS One* 13 (1), e0190573. doi:10.1371/journal.pone.0190573

Wang, P. H., Yang, S. T., Chang, W. H., Liu, C. H., Lee, F. K., and Lee, W. L. (2022). Endometriosis: Part I. Basic concept. *Taiwan J. Obstet. Gynecol.* 61 (6), 927–934. doi:10.1016/j.tjog.2022.08.002

Wang, X., and Li, T. (2021). Ropivacaine inhibits the proliferation and migration of colorectal cancer cells through ITGB1. *Bioengineered* 12 (1), 44–53. doi:10.1080/21655979.2020.1857120

Wilson, R. B. (2018). Hypoxia, cytokines and stromal recruitment: parallels between pathophysiology of encapsulating peritoneal sclerosis, endometriosis and peritoneal metastasis. *Pleura Perit.* 3 (1), 20180103. doi:10.1515/pp-2018-0103

Woo, J. H., Ahn, J. H., Jang, D. S., and Choi, J. H. (2019). Effect of dehydrocostus lactone isolated from the roots of *Aucklandia lappa* on the apoptosis of endometrial cells and the alternative activation of endometriosis-associated macrophages. *Am. J. Chin. Med.* 47 (6), 1289–1305. doi:10.1142/s0192415x19500666

Wu, M. H., Hsiao, K. Y., and Tsai, S. J. (2019). Hypoxia: the force of endometriosis. *J. Obstet. Gynaecol. Res.* 45 (3), 532–541. doi:10.1111/jog.13900

Wu, X., Zheng, X., Tang, H., Zhao, L., He, C., Zou, Y., et al. (2022). A network pharmacology approach to identify the mechanisms and molecular targets of curcumin against Alzheimer disease. *Med. Baltim.* 101 (34), e30194. doi:10.1097/md.00000000000030194

Ya-Nan, H., Yong, W., Fang-Li, P., Cong-Cong, Z., Yu-Yan, Z., and Cheng, Z. (2020). Retrospective study on postoperative recurrence and pregnancy rate of stage III-IV endometriosis infertility patients treated by Luoshi endometriosis formula combined with GnRH-a. *J. Guangzhou Univ. Traditional Chin. Med.* 37 (05), 850–855. doi:10.13359/j.cnki.gzxbtcm.2020.05.011

Ye, L., Kuang, Z., Wang, X., Pei, F., Su, R., and Zeng, C. (2021). Research progress of Luo's Neiyi Prescription for the treatment of endometriosis. *J. Guangzhou Univ. Tradit. Chin. Med.* 35 (5), 1067–1071. doi:10.13359/j.cnki.gzxbtcm.2021.05.037

Yoshino, O., Osuga, Y., Hirota, Y., Koga, K., Hirata, T., Harada, M., et al. (2004). Possible pathophysiological roles of mitogen-activated protein kinases (MAPKs) in endometriosis. *Am. J. Reprod. Immunol.* 52 (5), 306–311. doi:10.1111/j.1600-0897.2004.00231.x

Zardecki, C., Dutta, S., Goodsell, D. S., Lowe, R., Voigt, M., and Burley, S. K. (2021). PDB-101: educational resources supporting molecular explorations through biology and medicine. *Protein Sci.* 31, 129–140. doi:10.1002/pro.4200

Zhan, L., Wang, W., Zhang, Y., Song, E., Fan, Y., and Wei, B. (2016). Hypoxia-inducible factor-1 α : a promising therapeutic target in endometriosis. *Biochimie* 123, 130–137. doi:10.1016/j.biochi.2016.01.006

Zhang, L., Xiong, W., Xiong, Y., Liu, H., Li, N., Du, Y., et al. (2016). Intracellular wnt/beta-catenin signaling underlying 17 β -estradiol-induced matrix metalloproteinase 9 expression in human endometriosis. *Biol. Reprod.* 94 (3), 70. doi:10.1095/biolreprod.115.135574

Zhou, H., Zhang, Q., and Qi, C. (2019). Impact of a Chinese medicinal formula, xiao liu fang, on the “3A” ability of endometrial stromal cells in patients with endometriosis. *Mol. Ther. Oncolytics* 12, 1–8. doi:10.1016/j.omto.2018.11.001

Zubrzycka, A., Migdalska-Sek, M., Jędrzejczyk, S., and Brzeźniańska-Lasota, E. (2021). Circulating miRNAs related to epithelial-mesenchymal transitions (EMT) as the new molecular markers in endometriosis. *Curr. Issues Mol. Biol.* 43, 900–916. doi:10.3390/cimb43020064



OPEN ACCESS

EDITED BY

Raghuveera Kumar Goel,
Boston University, United States

REVIEWED BY

Muhammad Majid,
Guangdong Medical University, China
Kefeng Li,
Macao Polytechnic University, Macao SAR,
China

*CORRESPONDENCE

Jinchang Huang,
✉ zryhhuang@163.com
Yuxiang Wan,
✉ wanyuxiang@bucm.edu.cn

RECEIVED 26 March 2024

ACCEPTED 27 August 2024

PUBLISHED 10 September 2024

CITATION

Li W, Jiang H, Zhang W, Sun Q, Zhang Q, Xu J,
Huang J and Wan Y (2024) Mechanisms of
action of *Sappan lignum* for prostate cancer
treatment: network pharmacology, molecular
docking and experimental validation.
Front. Pharmacol. 15:1407525.
doi: 10.3389/fphar.2024.1407525

COPYRIGHT

© 2024 Li, Jiang, Zhang, Sun, Zhang, Xu, Huang
and Wan. This is an open-access article
distributed under the terms of the [Creative
Commons Attribution License \(CC BY\)](#). The use,
distribution or reproduction in other forums is
permitted, provided the original author(s) and
the copyright owner(s) are credited and that the
original publication in this journal is cited, in
accordance with accepted academic practice.
No use, distribution or reproduction is
permitted which does not comply with these
terms.

Mechanisms of action of *Sappan lignum* for prostate cancer treatment: network pharmacology, molecular docking and experimental validation

Wenna Li^{1,2}, Honglin Jiang¹, Weina Zhang¹, Qiuyue Sun¹,
Qiaoli Zhang^{1,2}, Jingnan Xu^{1,2}, Jinchang Huang^{1,2*} and
Yuxiang Wan^{1,2*}

¹The Third Affiliated Hospital, Beijing University of Chinese Medicine, Beijing, China, ²Institute of
Acupuncture and Moxibustion in Cancer Care, Beijing University of Chinese Medicine, Beijing, China

Background: Prostate cancer (PCa) is the most common non-cutaneous malignancy in men globally. *Sappan lignum*, which exists in the heartwood of *Caesalpinia sappan* L., has antitumor effects; however, its exact mechanism of action remains unclear. This study elucidated the underlying mechanisms of *Sappan lignum* in PCa through network pharmacology approaches and molecular docking techniques. Moreover, the therapeutic effects of *Sappan lignum* on PCa were verified through *in vitro* experiments.

Methods: The constituent ingredients of *Sappan lignum* were retrieved from the HERB database. Active plant-derived compounds of *Sappan lignum* were screened based on gastrointestinal absorption and gastric drug properties. Disease targets for PCa were screened using unpaired and paired case datasets from the Gene Expression Omnibus. Intersection targets were used for gene ontology and Kyoto encyclopedia of genes and genomes (KEGG) pathway enrichment analysis. Core targets were identified through topological analysis parameters and their clinical relevance was validated through The Cancer Genome Atlas database. The affinity between the phytochemicals of *Sappan lignum* and core proteins was verified using the molecular docking technique. Validation experiments confirmed the significant potential of *Sappan lignum* in treating PCa.

Results: Twenty-one plant-derived compounds of *Sappan lignum* and 821 differentially expressed genes associated with PCa were collected. Among 32 intersection targets, 8 were screened according to topological parameters. KEGG analysis indicated that the antitumor effects of *Sappan lignum* on PCa were primarily associated with the p53 pathway. The molecular docking technique demonstrated a strong affinity between 3-deoxysappanchalcone (3-DSC) and core proteins, particularly cyclin B1 (CCNB1). CCNB1 expression correlated with clinicopathological features in patients with PCa. Experimental results revealed that 3-DSC exhibited anti-proliferative, anti-migratory, and pro-apoptotic effects on 22RV1 and DU145 cells while also causing G2/M phase cell cycle arrest, potentially through modulating the p53/p21/CDC2/CCNB1 pathway.

Conclusion: This research highlights the promising therapeutic potential of *Sappan lignum* in treating PCa, with a particular focus on targeting the p53 pathway.

KEYWORDS

prostate cancer, *Sappan lignum*, network pharmacology, molecular docking, p53 signaling pathway, experimental validation *in vitro*

1 Introduction

Prostate cancer (PCa) is the most prevalent non-cutaneous malignancy and the primary cause of cancer-related deaths in men worldwide (Rizzo et al., 2022). However, delayed diagnosis often leads to higher mortality due to delayed diagnosis (Sekhoacha et al., 2022). PCa causes an estimated 307,000 fatalities and 1.1 million new cases annually (Xue et al., 2022). The rise in incidence is attributed to increased life expectancy and lifestyle changes. In Asia alone, more than 297,000 new cases of PCa are diagnosed each year, representing 23.3% of global cases, with over 118,000 deaths reported, accounting for approximately 33% of all PCa-related deaths (Zhu et al., 2020).

The primary treatment modalities for PCa include radical prostatectomy, endocrine therapy, chemotherapy, radiotherapy, and immunotherapy. Currently, aggressive PCa treatment options have adverse effects on urinary continence and erectile dysfunction (Sebesta and Anderson, 2017). In clinical practice, the majority of patients with advanced PCa develop metastatic castration-resistant PCa and subsequently become resistant to chemotherapy. The resistance poses a significant challenge in terms of management and significantly impacts patients' quality of life (Rezaeian et al., 2023). Therefore, it is crucial to promptly discover a safe and effective medicine for treating PCa.

Recent studies are exploring alternative therapeutic approaches, including investigating medicinal plants to develop novel anticancer medications. Plant-derived phytochemicals have demonstrated potential as anticancer agents for PCa treatment (Termini et al., 2020). These compounds inhibit various signal transduction pathways in tumor progression and metastasis, enhance anticancer drugs and radiation therapy tolerance, and exhibit multi-targeted antitumor effects (Afrin et al., 2020). Additionally, phytochemicals modulate the tumor microenvironment, inhibit angiogenesis, and have been found to have fewer adverse effects compared to conventional therapies (Kapinova et al., 2019).

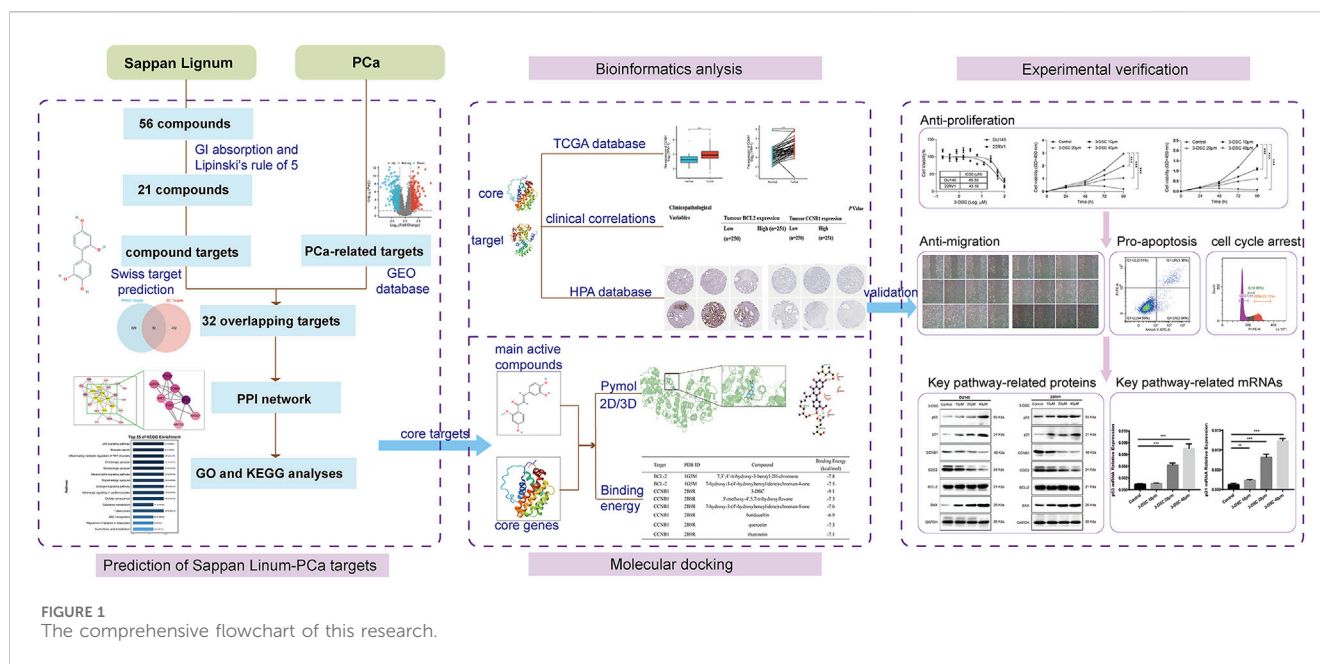
Active chemical compounds found in medicinal plants of the subfamily Caesalpinoideae have been reported to exhibit antiproliferative activity by regulating tumor cell apoptosis and oxidative stress (Kamal et al., 2022). *Sappan lignum*, the dry heartwood of *Caesalpinia sappan* L., is a natural medicinal plant within the subfamily Caesalpiniaceae extensively distributed in subtropical and tropical regions worldwide. Studies have reported that *Sappan lignum* possesses antioxidant, antibacterial, anti-inflammatory, vasodilatory, and immunomodulatory properties, as well as antitumor effects (Chen et al., 2021; Wang et al., 2023). Protosappanin B (PSB), a pivotal extract derived from *Sappan lignum*, has been demonstrated to effectively suppress the proliferation and migratory capabilities of colon cancer cells,

inducing apoptosis and suggesting its potential as a novel medication to treat tumor (Zheng et al., 2020).

Network pharmacology is a rapidly developing interdisciplinary field that combines biology, pharmacology, mathematics, and computer science to analyze the precise mechanism of drug action by constructing drug components-targets-pathways-diseases network. Network pharmacology utilizes bioinformatics and visualization techniques, including high-throughput screening and multiple network models, to analyze and forecast the mechanism of drug action (Feng et al., 2023). This approach has evolved into a comprehensive tool for investigating the potential active components of drugs and the mechanisms underlying disease prevention and control (Zhen et al., 2023). Recently, the research concepts within network pharmacology have advanced significantly (Zhao et al., 2023). The pharmacological effects and mechanisms of action of these compounds can be thoroughly understood through computational simulation, clinical data mining, and experimental investigations, thereby providing a novel approach to drug development (Khan and Lee, 2023).

Currently, studies have found that *Sappan lignum* has multi-targeted anti-inflammatory and antioxidant effects (Kang et al., 2021; Wang et al., 2023). However, no study has reported the potential mechanisms of *Sappan lignum* in PCa through network pharmacology or molecular docking techniques. Additionally, the anticancer effects of *Sappan lignum* on various PCa cells remain largely unexplored. *In vitro* studies have shown that the active ingredient of *Sappan lignum* inhibits the proliferation of PC3 PCa cells and suppresses cell cycle progression in a concentration-dependent manner (Lv et al., 2022). We believe that the possible signaling pathways and targets of *Sappan lignum* for PCa treatment can be examined through network pharmacology in a holistic, systematic, and comprehensive manner.

This investigation aimed to determine the active constituents of *Sappan lignum* with anti-PCa effects and construct a network for potential target modulation through network pharmacology. Based on data from the gene expression omnibus (GEO) dataset, we identified potential targets associated with PCa. We developed an "active chemical ingredient-disease target" network utilizing protein-protein interaction data. Subsequently, we screened the core targets and performed pathway enrichment analysis. Furthermore, we visualized the molecular docking interactions between the core components and PCa targets, selecting the core compounds with significant therapeutic effects. We used bioinformatic analysis to validate the target proteins of *Sappan lignum* for PCa treatment. *In vitro* cultures of PCa cells were treated with the active ingredient of *Sappan lignum* to provide a basis for developing new drugs targeting these core active compounds. The workflow is illustrated in Figure 1.



2 Materials and methods

2.1 Sappan lignum compounds screening and target fishing

HERB (<http://herb.ac.cn>) database (Fang et al., 2021) encompasses Traditional Chinese Medicine Integrated Database (TCMID), SymMap, Traditional Chinese Medicine Information Database (TCM-ID), and Traditional Chinese Medicine Systems Pharmacology (TCMSP) databases for an extensive collection of chemical constituents of *Sappan lignum*. All components' molecular formulas and smile information were standardized according to PubChem (<https://pubchem.ncbi.nlm.nih.gov/>) (Kim et al., 2021). The active ingredients and target proteins of *Sappan lignum* were obtained from the HERB database. Gastrointestinal (GI) absorption and Lipinski's rule of 5 for oral drug-likeness (Lipinski et al., 2001) provided by the SwissADME database (<http://www.swissadme.ch/>) (Hernandez et al., 2024) were utilized to select the active chemical compounds. The targets of the active constituents were subsequently predicted using SwissTargetPrediction (<http://www.swisstargetprediction.ch/>) (Zhang et al., 2021).

2.2 Retrieval of PCa-associated genes

The GSE46602 and GSE3325 datasets of PCa were retrieved from the GEO database (<http://www.ncbi.nlm.nih.gov/geo/>) (Clough et al., 2024) of the National Center for Biotechnology Information (NCBI). Before the analysis of differentially expressed genes (DEGs), data quality was assessed through principal component analysis (PCA) (Martins et al., 2019) to ensure that the GSE datasets were usable for differential analysis.

Screening criteria for DEGs in PCa and non-cancerous tissues were adjusted to $p < 0.05$ and $|\log FC| > 1$.

2.3 Targets gathering and network construction

The targets of *Sappan lignum* and PCa were compiled, deduplicated, and represented in a Venn diagram to illustrate the intersection of targets. After taking the intersection, we obtained 32 targets, the possible therapeutic targets of *Sappan lignum* in the context of PCa treatment. These targets were imported using the String platform (<https://www.stringdb.org/>) with the species "*Homo sapiens*." The obtained intersection targets were imported into Cytoscape software (version 3.9.1) to establish the intersection target library and visualize the protein-protein interaction (PPI) network. After screening by the median, eight key targets in the network were found based on the topological degree, closeness centrality, and betweenness centrality parameters, according to our previous research methods (Wan et al., 2019).

2.4 GO functional enrichment and KEGG pathway analysis

The biological information database KEGG Orthology-based Annotation System (KOBAS) (<http://www.bioinfo.org/kobas>) provides exhaustive and systematic functional annotation data for large-scale genes or proteins, primarily for functional and pathway enrichment analysis of differential genes (Wu et al., 2006). To analyze the enrichment of pathways in GO and the KEGG, we utilized the KOBAS platform. The filter criteria were $p < 0.05$. GO

annotations and KEGG pathways were visualized using R software (version 4.3.1).

2.5 Verification in the PCa cohort

For the two screened targets, differential expression between PCa and non-tumor was analyzed by the Wilcoxon test from the Cancer Genome Atlas (TCGA, <https://tcga-data.nci.nih.gov/tcga/>) database (Neuberger et al., 2023). Tumor samples in patients with PCa were retrieved from the TCGA database for correlation analysis of clinical data and pathological features. It included Tumor-Node-Metastasis (TNM) classification, residual tumor size, zonal tumor origin, histologic of “Gleason score” evaluation, and serum markers of PCa. We screened for underlying PCa-associated progression with the involvement of core proteins using a chi-square test. The Human Protein Atlas (HPA) database (<https://www.proteinatlas.org/>) is a comprehensive human gene and protein expression of information resources, integrating proteomics data from multiple tissues and cell types (Digre and Lindskog, 2021). We verified core protein expression to preserve the accuracy of results using the HPA database. Based on the analysis of clinical correlation data, we further observed the immunohistochemical expression of differential key targets in PCa and non-PCa tissues.

2.6 Molecular docking of candidate targets and active ingredients

We used the PubChem (<https://pubchem.ncbi.nlm.nih.gov/>) to import the structures of chemicals that docked to important proteins (Kim et al., 2022), including 7,3',4'-trihydroxy-3-benzyl-2H-chromene, 7-hydroxy-3-(4'-hydroxybenzylidene)-chroman-4-one, 3-DSC, 3'-methoxy-4',5,7-trihydroxyflavone, bonducellin, quercetin, and rhamnetin. We minimized the energy with Chem 3D and selected the mol2 format, and then downloaded B-cell lymphoma-2 (BCL-2) and cyclin B1 (CCNB1) protein crystal structures from the RCSB Protein Data Bank (PDB) database (<https://www.rcsb.org>, accessed on 6 January 2024) (Petros et al., 2001; Petri et al., 2007). We used Pymol software (version 1.5.6) to delete water molecules and small molecules, generated pdb format files of target receptor proteins, imported them into AutoDock Tools software for neutral hydrogenation, charge calculation, and generated pdbqt format files. The treated compounds were used as small molecule ligands, and the protein targets as receptors. We performed molecular docking through AutoDock Tool software (version 1.5.6) and used the Grid function to set the size and positional parameters of the active pockets. The central position of the Grid Box was determined based on the interaction between the small molecules and the targets (BCL-2: center_x = 3.664, y = -4.153, z = 2.012; CCNB1: center_x = -65.873, y = 41.523, z = -11.34). The size of the pockets was set according to the BCL-2 and CCNB1 ligand sizes, which were 40 × 40 × 40 and 60 × 60 × 60 in length, width and height, respectively. Molecular docking was executed utilizing Vina to ascertain the binding energies between the chemical components and the two target proteins. Flexible bonds of small molecule ligands were set to be rotatable, while the receptor proteins were set to semi-flexible docking (Trott and Olson, 2010).

The results were evaluated based on the binding energies and binding sites. As the binding energy decreased, the binding activity and affinity also decreased. The docking results were visualized by Pymol software (version 2.3.4).

2.7 Experimental verification

2.7.1 Cell culture and treatments

Our study obtained human PCa cell lines 22RV1 and DU145 from the Cell Resource Center, Institute of Basic Medical Sciences. 22RV1 and DU145 cells were cultured in RPMI 1640 and DMEM medium (Gibco Carlsbad) + 10% fetal bovine serum (FBS) + 1% penicillin-streptomycin and both were cultured at 37°C in a 5% CO₂ incubator (Cheng et al., 2021). Cells were passaged at a confluency of approximately 80% fusion, and the logarithmic growth phase was used to extract cells for experimental purposes after three passages. DU145 and 22RV1 cells were treated with 3-DSC for antitumor purposes, obtained from MedChemExpress.

2.7.2 CCK-8 assay

The cells were blown into single-cell suspensions and inoculated into 96-well plates with 100 µL per well. For cytotoxicity assays, the cell density was approximately 20%–25%. The culture was incubated for 24 h at 37°C in a 5% CO₂ incubator. Different concentrations of drug-containing media depended on the requirements of drug concentration. After 24 h of treatment, 100 µL medium containing 10% CCK-8 (CK04, Dojindo) was added into each well and incubated in the cell incubator for 1–2 h. The absorbance was measured at 450 nm.

For proliferation assay, cells were seeded at a 5%–7% density and placed in the 37°C in a 5% CO₂ incubator for 24 h. Experimental groups were treated with various doses of 3-DSC (10, 20, and 40 µM) for 24, 48, and 72 h, while the control group (0 µM) was treated with RPMI 1640 containing 10% FBS. Subsequently, CCK-8 reagent was added to cells, and the absorbance was measured.

2.7.3 Cell scratch test

Cells were put into six-well plates with 2 mL of medium in each well and cultured in an incubator for 24 h. Experimental and control groups were exposed to different concentrations of DSC and RPMI 1640. We used 200 µL tips to create a consistent width cell scratch in the center of the six-well plate after 24 h or 48 h and rinsed with PBS to remove cellular debris produced by scratching. Then a complete medium was added, and photographs were recorded as 0 h. By comparing the photographs at various time points, the migration and growth of cells near scratches could be observed.

2.7.4 Cell apoptosis detection

2 mL of single-cell suspension per well was inoculated onto a 6-well plate with a cell density of 20%. After treatment with 3-DSC or medium for 24 h, we collected 5 × 10⁴ cells, added Annexin V-FITC and propidium iodide (PI) to incubate at room temperature and dark for 20 min, then placed them in an ice bath and performed flow cytometry detection using CytoFLEX S flow cytometer (Beckman Coulter Life Sciences). PI emits red fluorescence, whereas Annexin V-FITC emits green fluorescence.

TABLE 1 Primer sequence information in this study.

Gene	Species	Primer sequence
p53	Human	F: 5'-GCTGCTCAGATAGCGATGGTCT-3'
	Human	R: 5'-CAACCTCAGGCGGCTCATAG-3'
p21	Human	F: 5'-ACCACTGGAGGGTGACTTC-3'
	Human	R: 5'-CGGCGTTTGAGTGGTAG-3'
CCNB1	Human	F: 5'-GCCTATTTTGGTTGATACTGCCTC-3'
	Human	R: 5'-CTCCATCTTCTGCATCCACATC-3'
CDC2	Human	F: 5'-AAACTACAGGTCAAGTGGTAGCC-3'
	Human	R: 5'-TCCTGCATAAGCACATCCTGA-3'
BCL-2	Human	F: 5'-ATCGCCCTGTGGATGACTGA-3'
	Human	R: 5'-GAGACAGCCAGGAGAAATCAAAC-3'
BAX	Human	F: 5'-TTTGTCTCAGGGTTTCATCCA-3'
	Human	R: 5'-TGCCACTCGGAAAAAGACCTC-3'

"F" represents "forward sequence;" "R" represents "reverse sequence."

2.7.5 Cell cycle distribution detection

Cells were digested into single-cell suspensions by trypsin, fixed with 70% ethanol at 4°C for 30 min, and precipitated by centrifugation. Excess RNA was removed by adding RNase A. Each tube of cell samples was added PI staining solution and incubated in a warm bath at 37°C temperature and light avoidance for 30 min. We utilized flow cytometry to analyze the distribution of the cell cycle by detecting red fluorescence at the excitation wavelength of 488 nm.

2.7.6 Western blotting analysis

We collected two types of cells, added RIPA lysis buffer (KeyGEN BioTECH) and centrifugated to obtain the whole cell protein extraction solution. The protein concentrations of cells were estimated using the BCA Protein Assay Kit (KeyGEN BioTECH). A protein sampling buffer was added for denaturation. We prepared 10% separation glue, and separated proteins were electro-transferred onto polyvinylidene fluoride (PVDF) membranes at constant current and low temperature. Ponceau stain was used to verify the membrane transfer efficiency. The blots were obstructed using a 5% solution of non-fat dry milk at 37°C on a shaking platform for 1 h. Then, we dilute d the primary antibody to the optimal concentration using 1×TBST, including anti-GAPDH (1:2500, ab9485, Abcam), anti-p53 (1:1000, ab32049, Abcam), anti-p21 (1:5000, ab109520, Abcam), anti-Cyclin B1 (1:50000, ab32053, Abcam), anti-CDK1 (1:10000, ab133327, Abcam, United Kingdom), anti-Bcl2(1:1000, ab182858, Abcam) and anti-Bcl2(1:10000, ab32503, Abcam). The membranes with the proteins were incubated at overnight 4°C, then the secondary antibody HRP-conjugated Affinipure Goat Anti-Rabbit IgG (1:2000, SA00001-2, Proteintech) was added and appropriate amounts of enhanced chemiluminescence (KGC4601-100, KeyGEN BioTECH) were dropwise added near the location of target proteins. Finally, protein bands were exposed by a gel imaging system and photographed for storage.

2.7.7 Quantitative real-time PCR (qRT-PCR)

Cellular total RNA was isolated utilizing TRIzol and chloroform (Sinopharm Chemical Reagent) precipitated by adding isopropanol and resuspended. Sequences of qPCR primers are listed in Table 1. cDNA synthesis was performed by GoScript™ Reverse Transcription System (Promega). AceQ qPCR SYBR Green Master Mix (Vazyme) was used for the amplification reaction system. The relative expression levels of BCL2 associated X protein (BAX), BCL-2, CCNB1, cell division cycle 2 (CDC2), p53, and p21 mRNA were measured by qRT-PCR.

2.7.8 Statistical analysis

Experimental data was expressed as mean ± standard deviation (SD). To determine differences between the treatment and control groups, the *t*-test or Mann-Whitney *U* test was utilized. *p*-value < 0.05 was deemed to indicate statistical significance. All of the statistical analyses listed above were conducted utilizing SPSS software (Version 20.0, IBM, Chicago, IL, United States).

3 Results

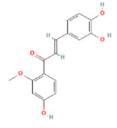
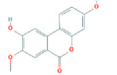
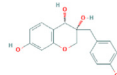
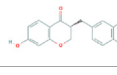
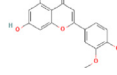
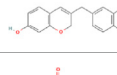
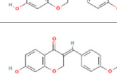
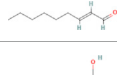
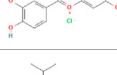
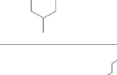
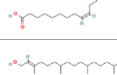
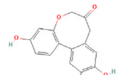
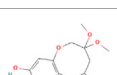
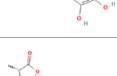
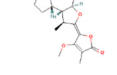
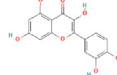
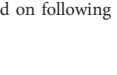
3.1 *Sappan lignum* compounds screening and target fishing

Of the 56 chemical ingredients of *Sappan lignum* obtained from the HERB database, 21 compounds were screened through SwissADME. Detailed information, GI absorption, and Lipinski's rule of 5 are given in Table 2. Lipinski's rule of 5, which evaluates oral drug-likeness in pharmacokinetic analysis, combines criteria from the Lipinski, Ghose, Veber, Egan, and Muegge rules. According to the screening criteria of "High" GI and 5 "yes" results of oral drug-likeness, 21 bioactive components of *Sappan lignum* were selected. Based on the chemical structure, 471 possible targets were predicted through target fishing on the Swiss target prediction platform. Cytoscape 3.9.2 was used to construct the component-targets network (Figure 2A). In total, 32 target classes were involved in related targets (Figure 2B). The top 10 target types were kinase (25.34%), enzyme (17.64%), G protein-coupled receptor (7.77%), protease (5.98%), nuclear receptor (5.83%), oxidoreductase (5.75%), lyase (4.56%), other cytosolic protein (3.51%), phosphatase (2.54%), and cytochrome P450 (2.32%) (Figure 2B).

3.2 Investigation of PCa-related targets

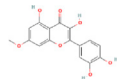
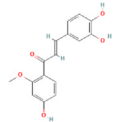
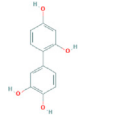
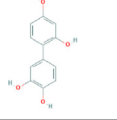
From the two PCa public datasets, GSE46602 and GSE3325, 15 non-cancer and 42 PCa samples were obtained. Quality-controlled box plot analysis exhibited that the median values of all samples were nearly identical (Figure 3A), indicating a high level of normalization and suitability for further differential gene analysis. Additionally, plot analysis (Figure 3B) exhibited a distinct separation between the normal prostate and PCa groups, suggesting a clear differentiation between the two sample sets. The parameters were modified to find 821 differentially expressed genes (*p* < 0.05 and |log FC| > 1). A total of 335 upregulated genes and 486 downregulated genes were identified in the study. These

TABLE 2 21 active compounds of *Sappan lignum* and their GI and Lipinski's rule of 5.

Compound name	PubChem CID	Molecular Formulas	GI	Lipinski's rule of 5	Structure
2'-methoxy-3,4,4'-trihydroxychalcone	5319493	C ₁₆ H ₁₄ O ₅	high	5 Yes	
3,9-dihydroxy-8-methoxydibenzo [b, d] pyran-6-one	102178085	C ₁₄ H ₁₀ O ₅	high	5 Yes	
3-deoxysappanchalcone	13846660	C ₁₆ H ₁₆ O ₅	high	5 Yes	
3-deoxysappanone b	91825567	C ₁₆ H ₁₄ O ₅	high	5 Yes	
3'-methoxy-4',5,7-trihydroxyflavone	5280666	C ₁₆ H ₁₂ O ₆	high	5 Yes	
7,3',4'-trihydroxy-3-benzyl-2H-chromene	71307370	C ₁₆ H ₁₄ O ₄	high	5 Yes	
7-hydroxy-3-(4'-hydroxybenzylidene)-chroman-4-one	91980449	C ₁₆ H ₁₂ O ₄	high	5 Yes	
bonducellin	14079439	C ₁₇ H ₁₄ O ₄	high	5 Yes	
(E)-2-nonenal	5283335	C ₉ H ₁₆ O	high	5 Yes	
gallic acid-3-O-(6'-O-galloyl)-glucoside	11972353	C ₂₀ H ₂₀ O ₁₄	high	5 Yes	
menthol	1254	C ₁₀ H ₂₀ O	high	5 Yes	
oleic acid	445639	C ₁₈ H ₃₄ O ₂	high	5 Yes	
phytol	5366244	C ₂₀ H ₄₀ O	high	5 Yes	
protosappanin a	128001	C ₁₅ H ₁₂ O ₅	high	5 Yes	
protosappanin a dimethyl acetal	11,347,693	C ₁₇ H ₁₈ O ₆	high	5 Yes	
protostemonine	25256772	C ₂₃ H ₃₁ NO ₆	high	5 Yes	
quercetin	5280343	C ₁₅ H ₁₀ O ₇	high	5 Yes	

(Continued on following page)

TABLE 2 (Continued) 21 active compounds of *Sappan lignum* and their GI and Lipinski's rule of 5.

Compound name	PubChem CID	Molecular Formulas	GI	Lipinski's rule of 5	Structure
rhamnetin	5281691	C ₁₆ H ₁₂ O ₇	high	5 Yes	
sappanchalcone	5319493	C ₁₆ H ₁₄ O ₅	high	5 Yes	
sappanin	5321124	C ₁₂ H ₁₀ O ₄	high	5 Yes	
Taraxerol	92097	C ₃₀ H ₅₀ O	high	5 Yes	

findings were visually represented in the volcano plot and hierarchical clustering heat map (Figures 3C,D).

3.3 Targets gathering and PPI network construction

We sorted out the relevant targets of *Sappan lignum* (432) and PCa (829) and removed duplicates. Venn established an intersection target library, and the resulting intersection targets were screened out (Figure 4A). The PPI was constructed from 32 intersection targets with 32 nodes and 50 edges (Figure 4B). According to the topological degree, closeness centrality and betweenness centrality parameters, eight core targets in the network were identified after screening by median: BCL-2 (Degree = 13), PTGS2 (Degree = 10), CCNB1 (Degree = 8), PGR (Degree = 8), AURKA (Degree = 7), MET (Degree = 6), NR3C1 (Degree = 5), ABCG2 (Degree = 4) (Figure 4C).

3.4 GO functional enrichment and KEGG pathway analysis

To determine the possible therapeutic targets of *Sappan lignum* concerning gene function and signaling pathways, 32 intersection targets of *Sappan lignum* against PCa were entered into the KOBAS platform for KEGG and GO function analysis. Enrichment items for molecular function (MF), biological process (BP), and cellular component (CC) were visualized (Figure 5A). According to the GO enrichment analysis, multiple genes collectively exerted biological effects. *Sappan lignum* primarily interfered with BP involving biological regulation, cellular process, single-organism process, CC comprising a cell, cell part, organelle, and MF, including binding, catalytic activity, and transducer activity in PCa.

According to these findings, the anti-PCa effects of *Sappan lignum* can be ascribed to cellular biological regulation.

We performed KEGG pathway analysis to screen the signaling pathways enriched in the 32 intersecting targets (Figure 5B). The top 10 pathways were tumor-associated p53 signaling pathway, PCa, inflammatory mediator regulation of TRP channels, cholinergic synapse, serotonergic synapse, neurotrophin signaling pathway, dopaminergic synapse, estrogenic synapse, adrenergic signaling in cardiomyocytes, and cellular senescence. The above pathways were primarily implicated in PCa disease, p53, cellular senescence, and neural signaling. Utilizing literature research and enrichment analysis, we focused on the p53 signaling pathway, which exhibited the most significant difference among the key targets of *Sappan lignum* for PCa treatment, with the associated proteins BCL-2 and CCNB1.

3.5 Verification in the PCa clinical cohort

Based on enrichment analysis, we focused on the critical links of *Sappan lignum* in treating PCa on the p53 signaling pathway, which exhibited the most significant differences. For the two potential targets associated with this pathway, we further verified the expression of CCNB1 and BCL-2 in the tissues of PCa patients through TCGA public clinical sample data. Significant expression differences of CCNB1 and BCL-2 were observed in 501 PCa tissue samples compared to 52 non-tumor tissue samples, with PCa tissues exhibiting significantly higher expression of CCNB1 and lower expression of BCL-2. Moreover, 53 paired samples of PCa and adjacent tissues further confirmed the above expression differences (Figures 6A,B). These findings were consistent with the expression trends in the GSE46602 and GSE3325 microarray datasets.

Immunohistochemical detection of key protein expression was studied in the HPA database (Figures 6C,D), which indicated that

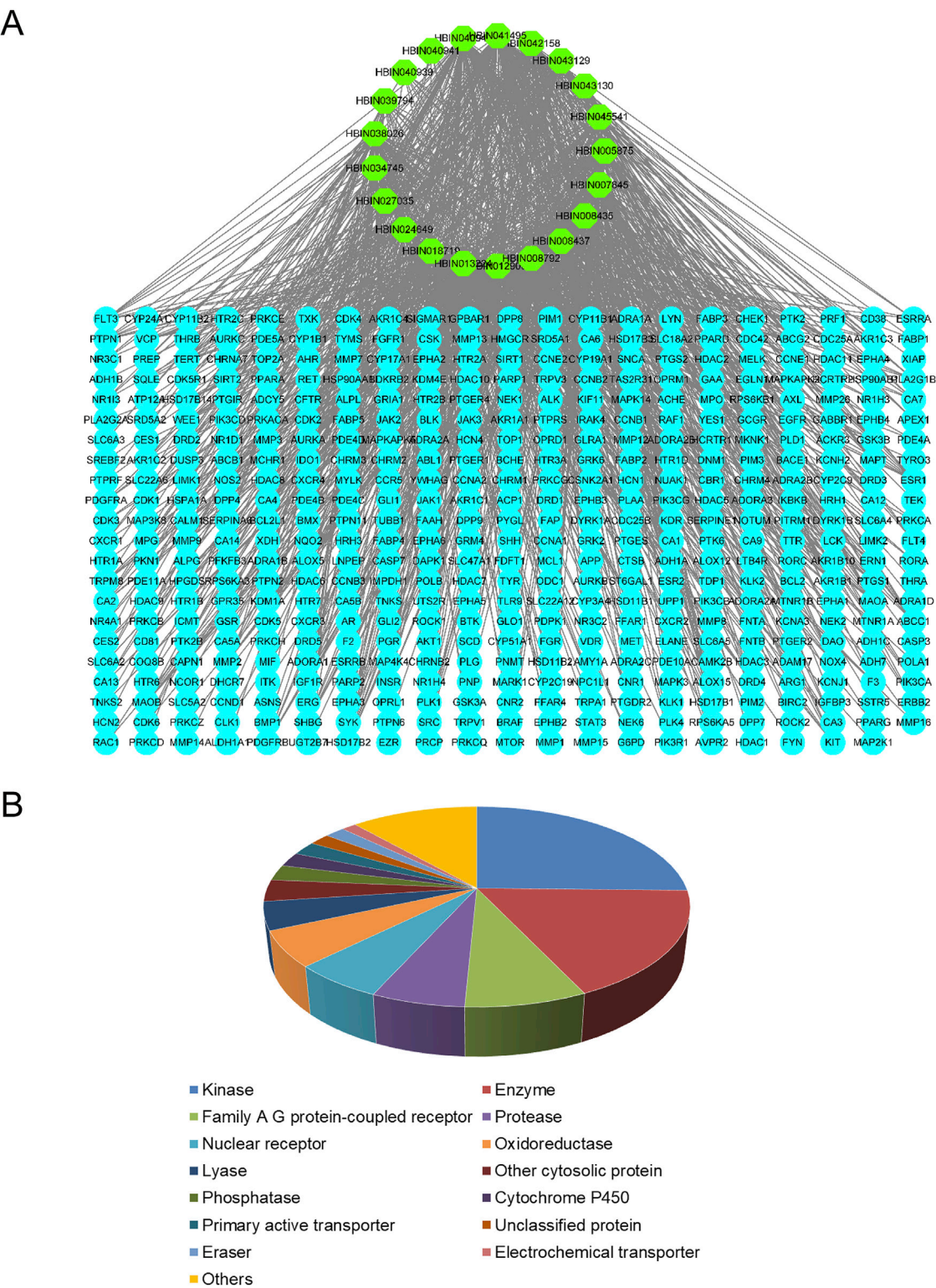


FIGURE 2
Active ingredient-targets of *Sappan lignum*. **(A)** Active ingredient-targets network. The green ellipse represents the 21 active components of *Sappan lignum*, and the blue ellipse signifies the corresponding target of the components. The edges represent the interaction between active compounds and targets **(B)** Key target types of active ingredients. Different colors represent different attribute classification targets of active ingredients, involving a total of 14 categories.

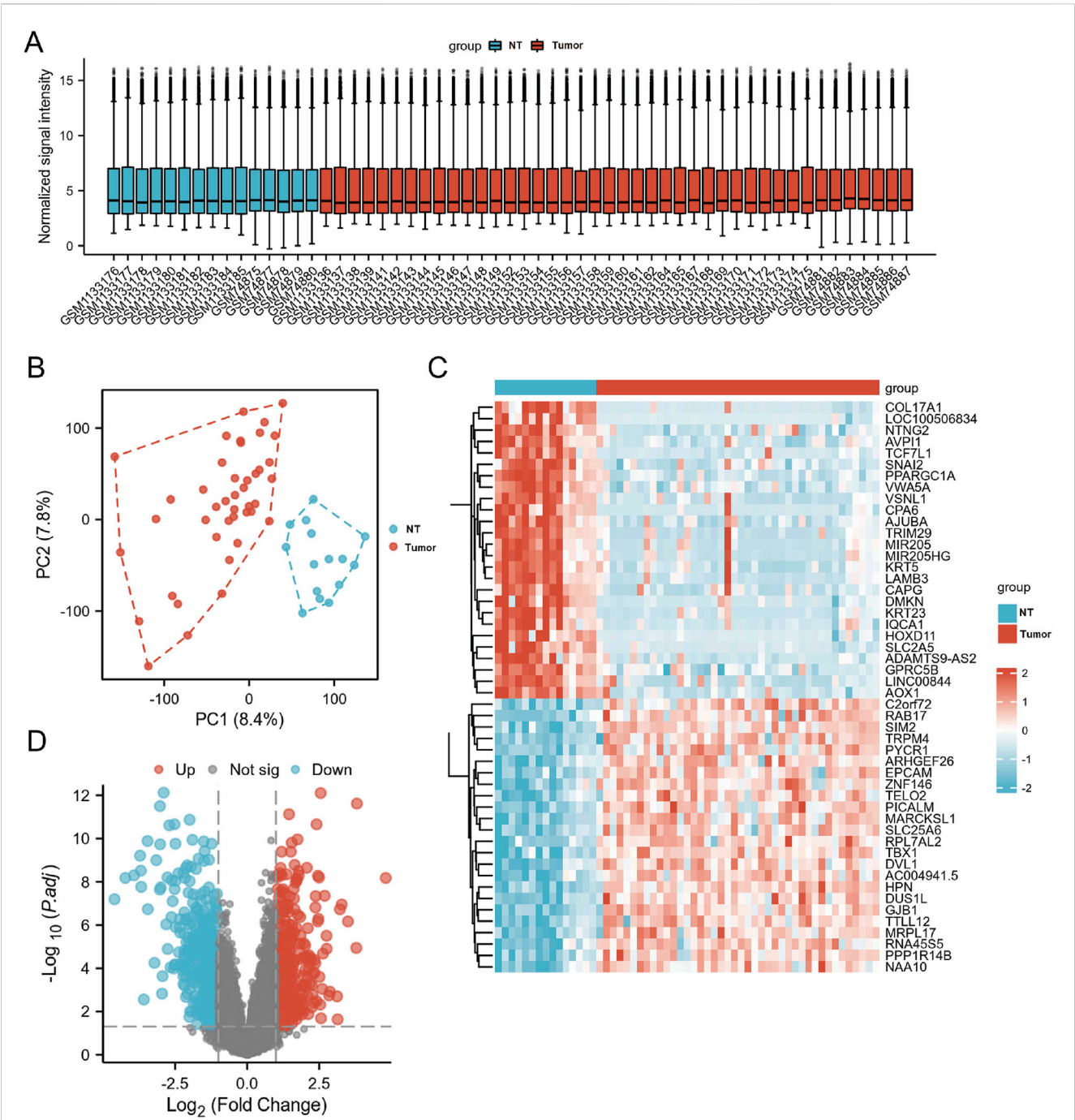


FIGURE 3 The DEGs in PCa and control samples were analyzed using data from GSE46602 and GSE3325. **(A)** Box plot of normalized analysis. The GSE46602 and GSE3325 data were combined for standardization analysis, with the number of sample datasets on the x-axis and the normalized signal intensity on the y-axis. **(B)** PCA of GSE46602 and GSE3325. The red dots represent tumor tissue, and the blue dots represent normal tissue. **(C)** Heatmaps of DEGs. Cluster analysis divided DEGs into two groups. The blue and red hues indicate downregulated and upregulated genes, respectively, and darker colors represent more marked differences in expression. **(D)** The volcano diagram of DEGs. Blue dots represent downregulated genes in PCa, grey dots represent genes with no significant difference, and red dots represent upregulated genes.

the expression of BCL-2 was significantly reduced in PCa tissues relative to non-tumorous tissues, while CCNB1 expression was significantly elevated. This is in accordance with the results of the TCGA clinical data.

The PCa clinical cohort was categorized into high and low expression based on the median CCNB1 and BCL-2 expression

levels. Correlation analysis of clinical features was then performed (Table 3). The results of our study exhibited a significant association between the expression of CCNB1 and age, residual tumor status, T stage, N stage, and Gleason score. Specifically, upregulation of CCNB1 expression was significantly higher in patients over 60 years, with R0 residual tumor status,

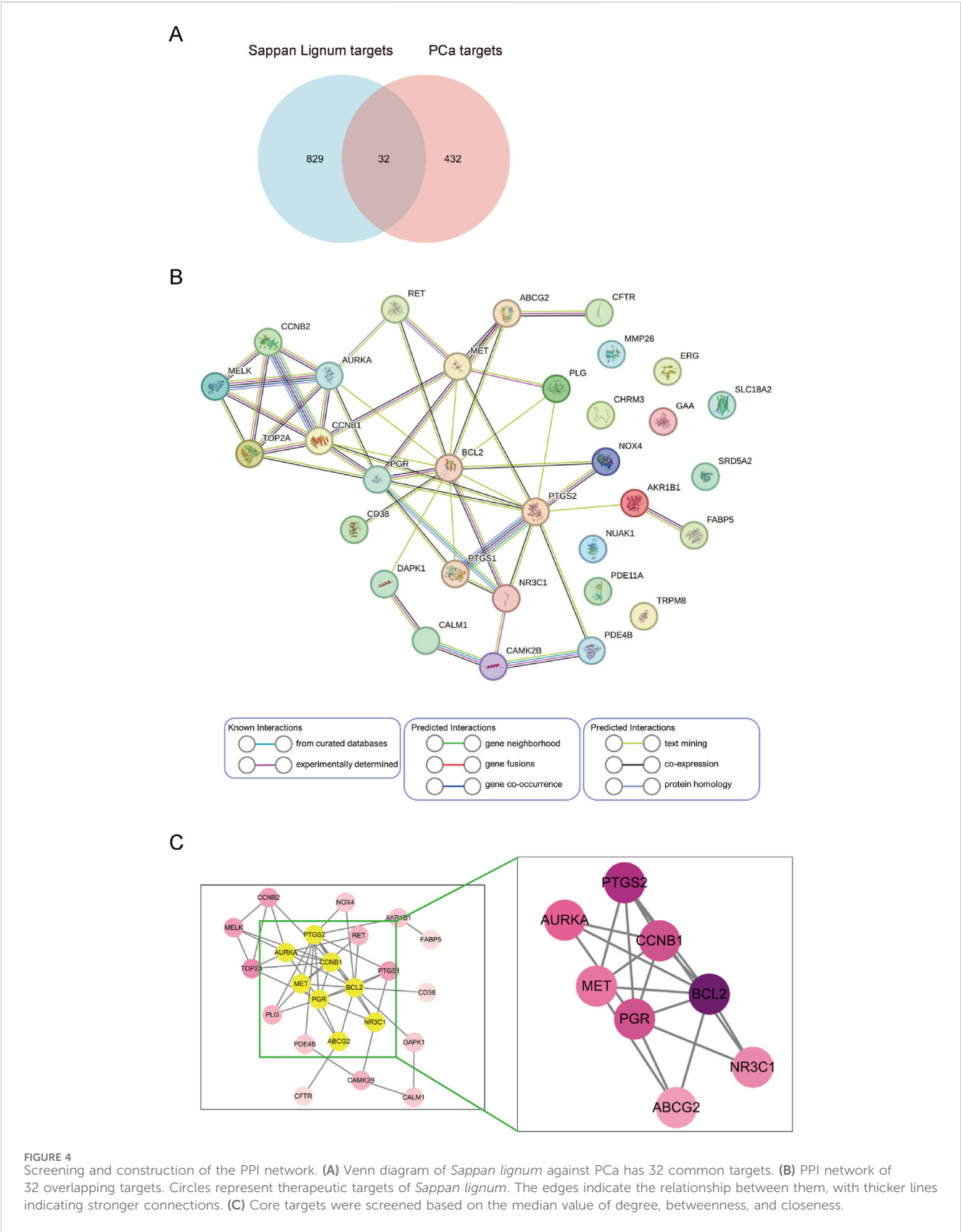


FIGURE 4 Screening and construction of the PPI network. **(A)** Venn diagram of *Sappan lignum* against PCa has 32 common targets. **(B)** PPI network of 32 overlapping targets. Circles represent therapeutic targets of *Sappan lignum*. The edges indicate the relationship between them, with thicker lines indicating stronger connections. **(C)** Core targets were screened based on the median value of degree, betweenness, and closeness.

T3 stage, N0 stage, and a Gleason score of 7. In conclusion, combined with the clinical cohort information and pathological data of TCGA and tissue and pathology results of the HPA database, we believed that the expression changes of BCL-2 and CCNB1 in the anti-PCA process of *Sappan lignum* may have improved stability.

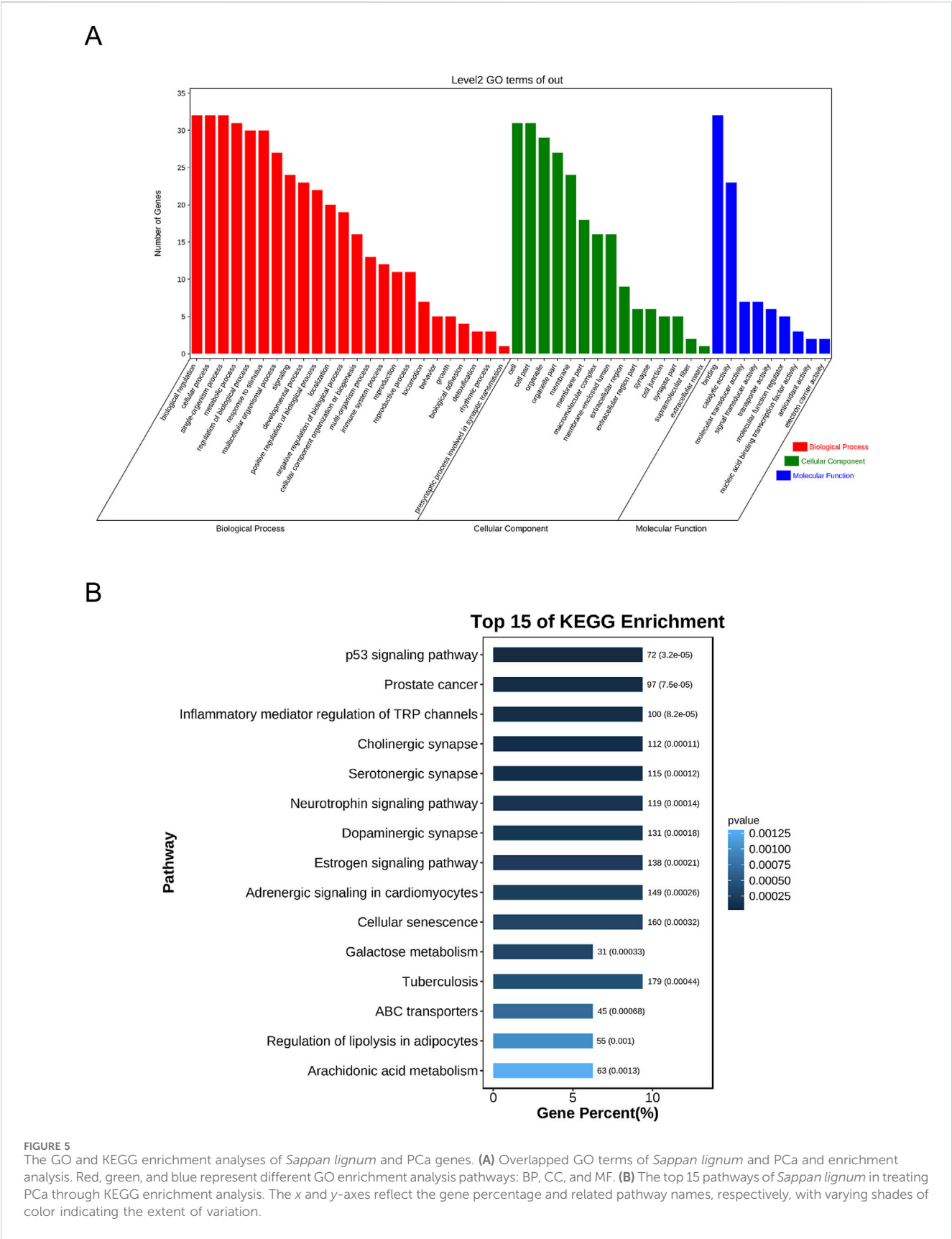


FIGURE 5 The GO and KEGG enrichment analyses of *Sappan lignum* and PCa genes. **(A)** Overlapped GO terms of *Sappan lignum* and PCa and enrichment analysis. Red, green, and blue represent different GO enrichment analysis pathways: BP, CC, and MF. **(B)** The top 15 pathways of *Sappan lignum* in treating PCa through KEGG enrichment analysis. The x and y-axes reflect the gene percentage and related pathway names, respectively, with varying shades of color indicating the extent of variation.

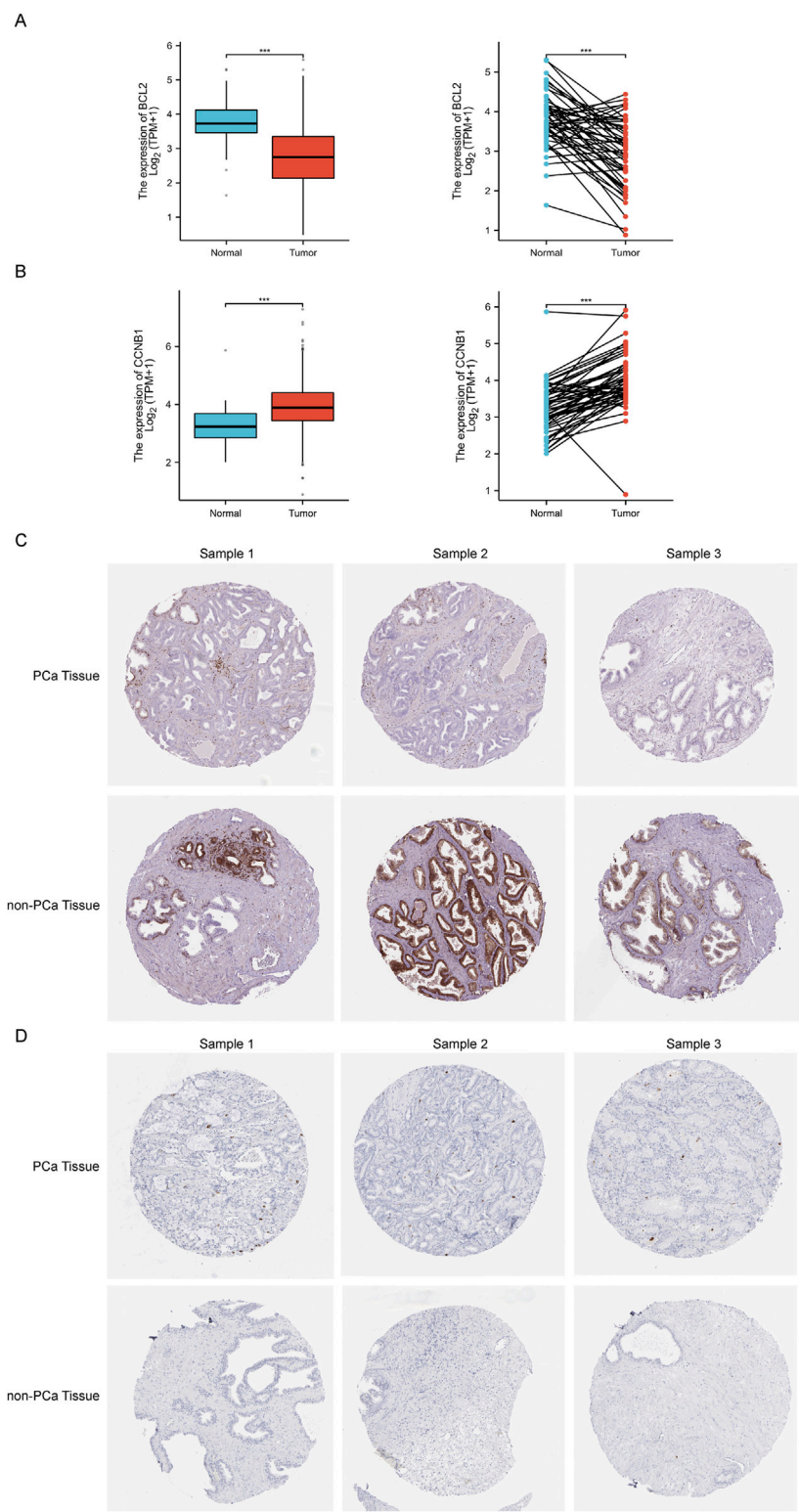


FIGURE 6
The relative expression levels of core targets BCL-2 and CCNB1 in TCGA and HPA databases. **(A, B)** The left and right figure illustrates the relative expression of BCL-2 and CCNB1 between independent and paired samples of PCa and non-tumor tissues severally. Red for tumor samples, blue for non-tumor samples. *** $p < 0.001$ compared with PCa group. **(C, D)** Representative immunohistochemical images of BCL-2 and CCNB1 in PCa and normal prostate tissue from the HPA database.

TABLE 3 Relationship between BCL2 and CCNB1 protein expression and clinical characteristic in patients with PCa.

Clinicopathological Variables	Tumour BCL2 expression		p-value	Tumour CCNB1 expression		p-value
	Low (n = 250)	High (n = 251)		Low (n = 250)	High (n = 251)	
Age, n (%)			0.625			0.005
>60	135 (26.9%)	141 (28.1%)		122 (24.4%)	154 (30.7%)	
≤60	115 (23.0%)	110 (22.0%)		128 (25.5%)	97 (19.4%)	
Residual tumor, n (%)			0.391			0.008
R0	156 (33.2%)	160 (34%)		173 (36.8%)	143 (30.4%)	
R1	73 (15.5%)	76 (16.2%)		61 (13%)	88 (18.7%)	
R2	4 (0.9%)	1 (0.2%)		1 (0.2%)	4 (0.9%)	
Zone of origin, n (%)			0.633			0.264
Central	2 (0.7%)	2 (0.7%)		2 (0.7%)	2 (0.7%)	
Multiple	68 (24.5%)	59 (21.3%)		50 (18.1%)	77 (27.8%)	
Peripheral	71 (25.6%)	67 (24.2%)		71 (25.6%)	67 (24.2%)	
Transition	6 (2.2%)	2 (0.7%)		4 (1.4%)	4 (1.4%)	
T stage, n (%)			0.165			<0.001
T2	104 (21.1%)	85 (17.2%)		117 (23.7%)	72 (14.6%)	
T3	139 (28.1%)	155 (31.4%)		127 (25.7%)	167 (33.8%)	
T4	4 (0.8%)	7 (1.4%)		3 (0.6%)	8 (1.6%)	
N stage, n (%)			0.305			0.010
N0	170 (39.7%)	178 (41.6%)		177 (41.4%)	171 (40%)	
N1	34 (7.9%)	46 (10.7%)		28 (6.5%)	52 (12.1%)	
M stage, n (%)			0.982			1.000
M0	232 (50.4%)	225 (48.9%)		227 (49.3%)	230 (50%)	
M1	1 (0.2%)	2 (0.4%)		1 (0.2%)	2 (0.4%)	
PSA (ng/mL), n (%)			0.749			0.050
<4	203 (45.7%)	214 (48.2%)		220 (49.5%)	197 (44.4%)	
≥4	14 (3.2%)	13 (2.9%)		9 (2%)	18 (4.1%)	
Gleason score,n (%)			0.130			<0.001
6	27 (5.4%)	19 (3.8%)		36 (7.2%)	10 (2%)	
7	124 (24.8%)	124 (24.8%)		137 (27.3%)	111 (22.2%)	
8	30 (6.0%)	35 (7.0%)		34 (6.8%)	31 (6.2%)	
9	68 (13.6%)	70 (14%)		42 (8.4%)	96 (19.2%)	
10	1 (0.2%)	3 (0.8%)		1 (0.2%)	3 (0.6%)	
OS event, n (%)			0.745			1.000
Alive	244 (48.7%)	247 (49.3%)		245 (48.9%)	246 (49.1%)	
Dead	6 (1.2%)	4 (0.8%)		5 (1%)	5 (1%)	
DSS event, n (%)			0.371			1.000
No	246 (49.3%)	248 (49.7%)		247 (49.5%)	247 (49.5%)	
Yes	4 (0.8%)	1 (0.2%)		3 (0.6%)	2 (0.4%)	
PFI event, n (%)			0.349			0.070

(Continued on following page)

TABLE 3 (Continued) Relationship between BCL2 and CCNB1 protein expression and clinical characteristic in patients with PCa.

Clinicopathological Variables	Tumour BCL2 expression		p-value	Tumour CCNB1 expression		p-value
	Low (n = 250)	High (n = 251)		Low (n = 250)	High (n = 251)	
No	199 (39.7%)	208 (41.5%)		211 (42.1%)	196 (39.1%)	
Yes	51 (10.2%)	43 (8.6%)		39 (7.8%)	55 (11%)	

TABLE 4 Binding energy of target protein docking.

Target	PDB ID	Compound	Binding energy (kcal/mol)
BCL-2	1G5M	7,3',4'-trihydroxy-3-benzyl-2H-chromene	−7.8
BCL-2	1G5M	7-hydroxy-3-(4'-hydroxybenzylidene)-chroman-4-one	−7.5
CCNB1	2B9R	3-DSC	−9.1
CCNB1	2B9R	3'-methoxy-4',5,7-trihydroxyflavone	−7.3
CCNB1	2B9R	7-hydroxy-3-(4'-hydroxybenzylidene)-chroman-4-one	−7.6
CCNB1	2B9R	bonducellin	−6.9
CCNB1	2B9R	quercetin	−7.3
CCNB1	2B9R	rhamnetin	−7.1

3.6 Molecular docking of candidate targets and related ingredients

Based on the identification of top target proteins in the PPI network and validation in the PCa cohort, our study focused on CCNB1 and BCL-2. We analyzed the interactions between key targets and their primary active constituents using molecular docking technology. Docking activity is indicated by a binding energy below 0 kcal/mol, and good docking activity is indicated by a binding energy below −6 kcal/mol. Our findings revealed that the binding energy between compound 3-DSC and CCNB1 was −9.1 kcal/mol, the lowest docking score among all 3-DSC active components and target proteins, suggesting that the binding conformation between them was the most stable. 3-DSC is the best candidate for *Sappan lignum* against PCa; the results are presented in Table 4. PyMOL and LigPlus were employed to analyze the specific docking patterns of active chemical components of *Sappan lignum* with key proteins in the p53 pathway, allowing for the visualization of multiple interactions. Representative images of the 3D and 2D binding conformations are illustrated in Figure 7. BCL-2 interacted with 7,3',4'-trihydroxy-3-benzyl-2H-chromene, and 7-hydroxy-3-(4'-hydroxybenzylidene)- chroman-4-one and formed a hydrogen bond, respectively. CCNB1 exhibited more hydrogen bonds with the active chemical constituents of *Sappan lignum* than BCL-2. These results indicated that CCNB1 is a crucial target protein in the p53 pathway for the relevant active components of *Sappan lignum*.

3.7 Experimental verification

3.7.1 3-DSC suppressed cell viability and proliferation of DU145 and 22RV1

To determine the cytotoxic impact of 3-DSC on 22RV1 and DU145 cells, the cells were exposed to varying concentrations of 3-

DSC for 24 h. At various concentrations, 3-DSC inhibited the proliferation of PCa cells (Figure 8A). The 24 h IC₅₀ of 3-DSC for 22RV1 and DU145 cells was 65.53 and 43.19 μM, respectively. The IC₅₀ value is an important reference for establishing the gradient concentrations in the subsequent experiments. Furthermore, it was observed that 3-DSC exerted a stronger inhibitory effect on 22RV1 cells than DU145 cells at equivalent concentrations.

To evaluate the effect of 3-DSC on the proliferation of two PCa cell lines over time, we performed a CCK-8 assay to determine cell proliferation following treatment with 3-DSC at varying doses (0, 10, 20, and 40 μM) for 24, 48, 72, and 96 h in 22RV1 and DU145 cells. The concentrations of 3-DSC were selected based on previously determined IC₅₀ values. The results (Figures 8B,C) indicated significant suppression of cell growth in the 3-DSC treatment groups compared to the control group at 24, 48, and 72 h, with statistical significance observed (*p* < 0.05). Additionally, as the treatment dosage was increased, the proliferative inhibition of PCa cells by 3-DSC became more pronounced.

3.7.2 3-DSC retrained migration of 22RV1 and DU145

Wound healing tests were used to examine PCa cell migration after the 3-DSC intervention. The findings revealed that different concentrations of 3-DSC effectively suppressed the migration ability of PCa cells after 24 and 48 h of treatment, with a stronger inhibitory effect observed at higher concentrations of 3-DSC (Figures 8D,E).

3.7.3 3-DSC promoted apoptosis of 22RV1 and DU145

To investigate the potential correlation between the suppressive effect of 3-DSC on proliferative viability and apoptosis, flow cytometry was utilized to determine apoptosis of

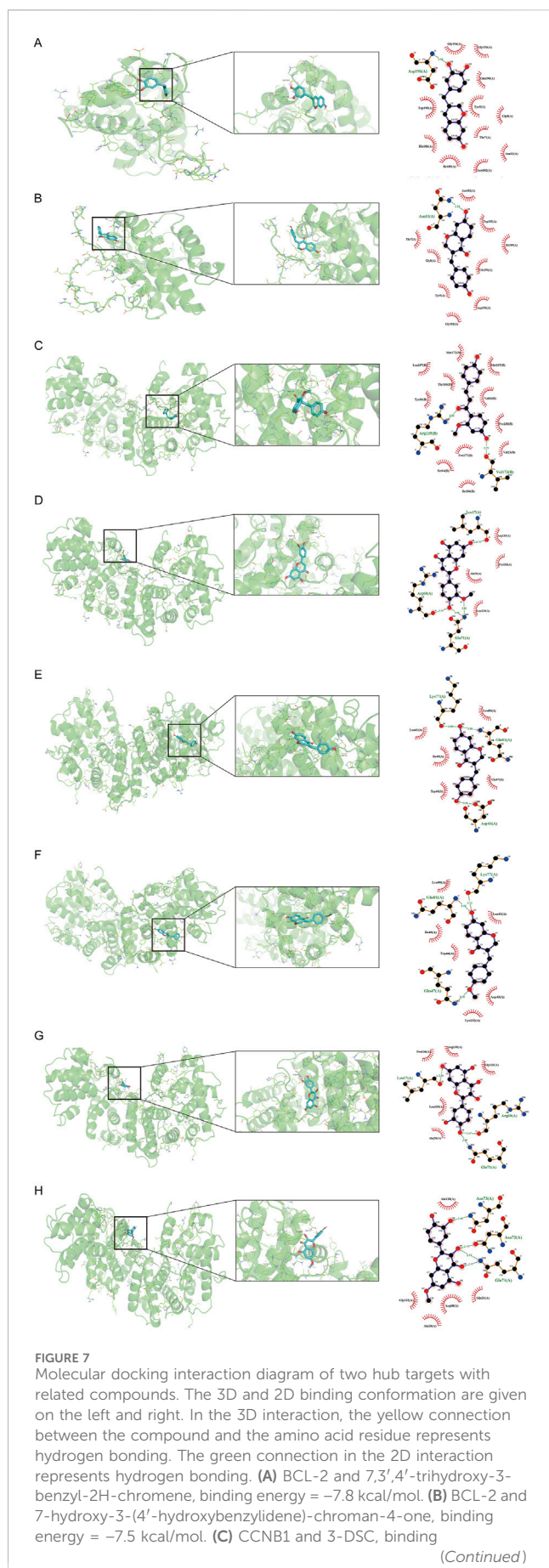


FIGURE 7 (Continued)

energy = -9.1 kcal/mol. (D) CCNB1 and 3'-methoxy-4',5,7-trihydroxyflavone, binding energy = -7.3 kcal/mol. (E) CCNB1 and 7-hydroxy-3-(4'-hydroxybenzylidene)-chroman-4-one, binding energy = -7.6 kcal/mol. (F) CCNB1 and bonducellin, binding energy = -6.9 kcal/mol. (G) CCNB1 and quercetin, binding energy = -7.3 kcal/mol. (H) CCNB1 and quercetin, binding energy = -7.1 kcal/mol.

DU145 and 22RV1 cells (Figure 9). The total number of apoptotic cells significantly increased in the three concentration groups of 3-DSC compared to the control group, indicating the ability of 3-DSC to induce apoptosis in PCa. Additionally, the effect of facilitating apoptosis became more significant as 3-DSC concentration increased.

3.7.4 3-DSC arrested DU145 and 22RV1 cells in the G2/M phase

Furthermore, we evaluated the impact of 3-DSC on the cell cycle of PCa cells using flow cytometry experiments (Figure 10). Treatment of DU145 cells with 3-DSC resulted in cell cycle arrest during the S and G2/M phases, whereas 22RV1 cells were arrested during the G2/M phase. In the 3-DSC-treated group, there was a decrease in the proportion of DU145 cells in the G0/G1 phase and an increase in the proportion of cells in the S and G2/M phases compared to the control group. Similarly, 22RV1 cells exhibited a reduction in the proportion of cells in the G0/G1 phase and increased the number of cells in the G2/M phase in the group treated with 3-DSC. We concluded that 3-DSC primarily caused the PCa cell cycle to block at the G2/M phase, thus inhibiting cell proliferation.

3.7.5 3-DSC regulated the expression of p53 pathway associated proteins

To further verify the role of 3-DSC in apoptosis promotion and proliferation suppression, cells were exposed to various doses of 3-DSC (10, 20, and 40 μ M) for 24 h. The expression of proteins relevant to the p53 pathway was then examined using Western blotting. The results revealed that 3-DSC decreased CCNB1 and CDC2 protein expression and promoted p53, p21, and BAX expression in DU145 and 22RV1 cells (Figures 11A, 12A). Furthermore, the relative expression of CCNB1 and CDC2 proteins was negatively correlated with the concentration of 3-DSC. Conversely, p53, p21, and BAX proteins positively correlated with the concentration of 3-DSC. Additionally, 3-DSC did not impact BCL-2 proteins in DU145 or 22RV1 cells. We concluded that 3-DSC enhanced BAX expression and restrained protein expression of CCNB1 and CDC2 in PCa cells through the p53/p21 pathway, thereby regulating the cell cycle.

3.7.6 3-DSC regulated the expression of p53 pathway associated mRNAs

We further validated p53 pathway-related mRNAs by qRT-PCR. The findings implicated that 3-DSC significantly reduced the levels of CCNB1 and CDC2 mRNAs and promoted p53, p21, and BAX mRNA expression in DU145 and 22RV1 cells. However, no effect was observed on BCL-2 mRNA. These findings are consistent with the alterations in protein expression observed (Figures 11B, 12B).

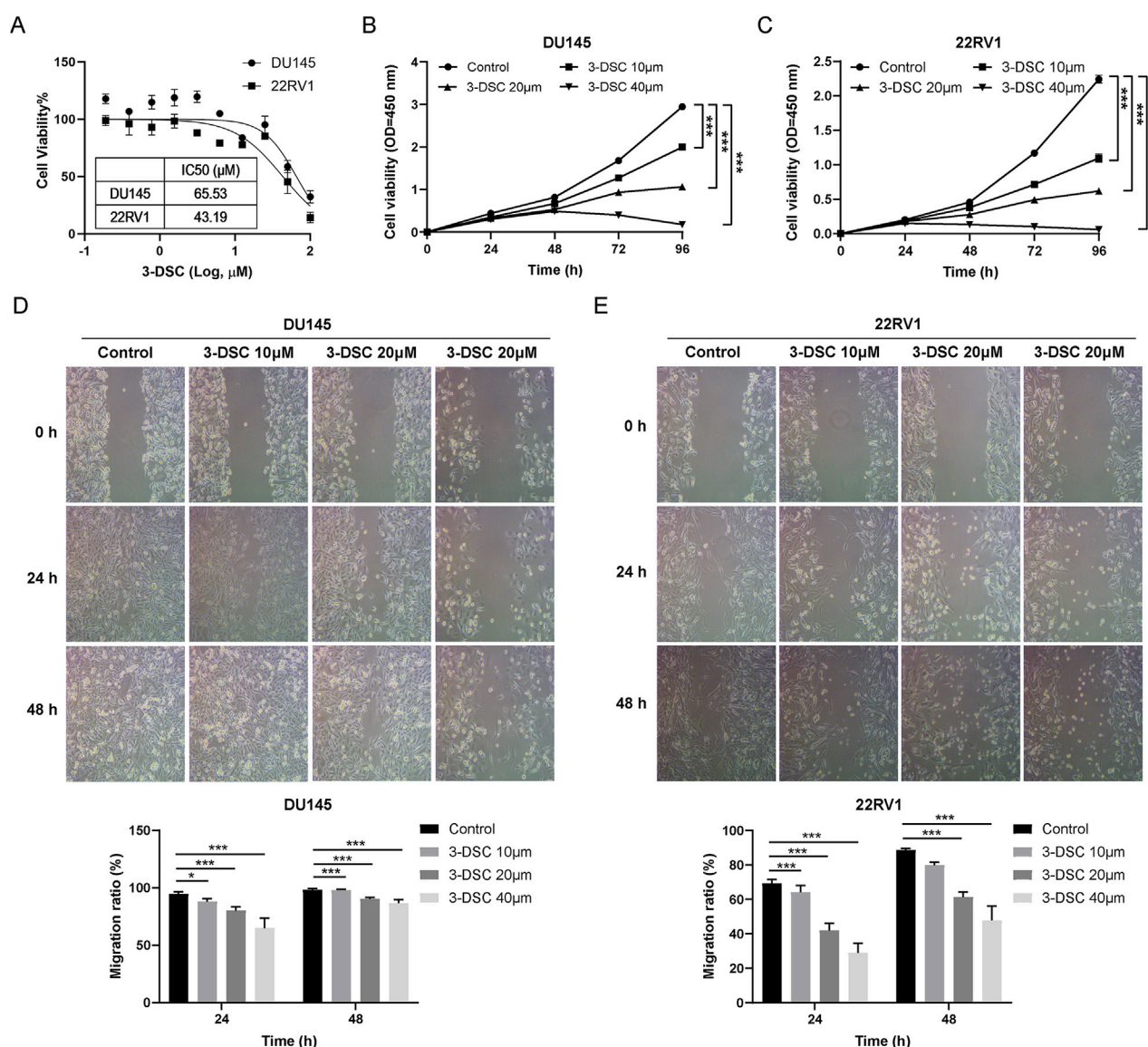


FIGURE 8
3-DSC restrained the proliferation and migration of 22RV1 and DU145. **(A)** Cell viability of 3-DSC concentration gradient treatment was determined after 24 h by CCK-8 assay. Proliferation of DU145 **(B)** and 22RV1 **(C)** 3-DSC-treated cells were 10 M, 20 M, and 40 M in concentration. Migration of DU145 **(D)** and 22RV1 **(E)** cells after 24 or 48 h 3-DSC treatment. Histograms demonstrate the cell migration ratio for different groups in PCa. Compared to the control group, * $p < 0.05$, *** $p < 0.001$.

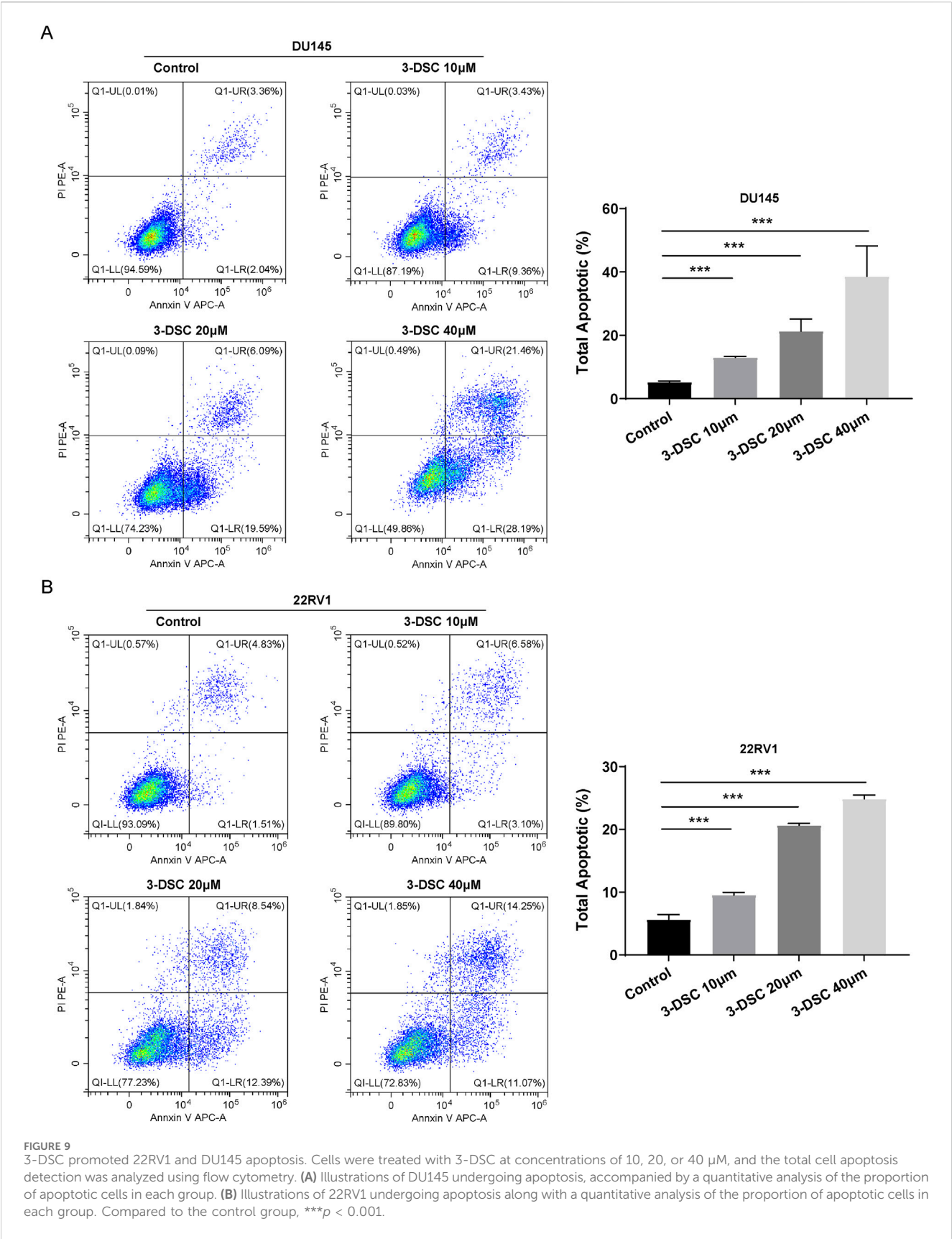
4 Discussion

PCa is the most prevalent non-skin malignancy in men worldwide, categorized into androgen-dependent and androgen-independent neoplasms. Patients often exhibit no obvious symptoms in the early stages of PCa, resulting in diagnosis at the advanced stages, where they are more susceptible to drug resistance and ultimately progress to fatal androgen-independent PCa. Therefore, novel therapeutic strategies for PCa that are less toxic and more effective are needed (Zhi et al., 2018).

Plants are the primary source of multiple chemotherapy drugs with potent antitumor properties (Ramzan et al., 2022). Combining plant-derived chemicals with conventional therapies exhibits promise in treating PCa (Mirzaei et al., 2022). Natural

compounds have been an important source in the exploration of novel drugs for tumors. Recently, herb and botanical drug extracts have emerged as promising clinical adjuvant treatments for PCa, demonstrating advantages in reducing toxic side effects, lowering tumor recurrence rates, and enhancing patient survival quality (Wang et al., 2018). However, the precise molecular mechanisms underlying these benefits remain unclear.

Sappan lignum, the heartwood of *Caesalpinia sappan* L, is predominantly distributed in Southeast Asia. The chemical composition of *Sappan lignum* is known to be complex (Yang et al., 2016). In this study, 21 active ingredients of *Sappan lignum* were screened based on Lipinski's rule of 5 and GI absorption. Compounds meeting Lipinski's rule of 5 for oral drug-likeness and GI absorption possessed improved



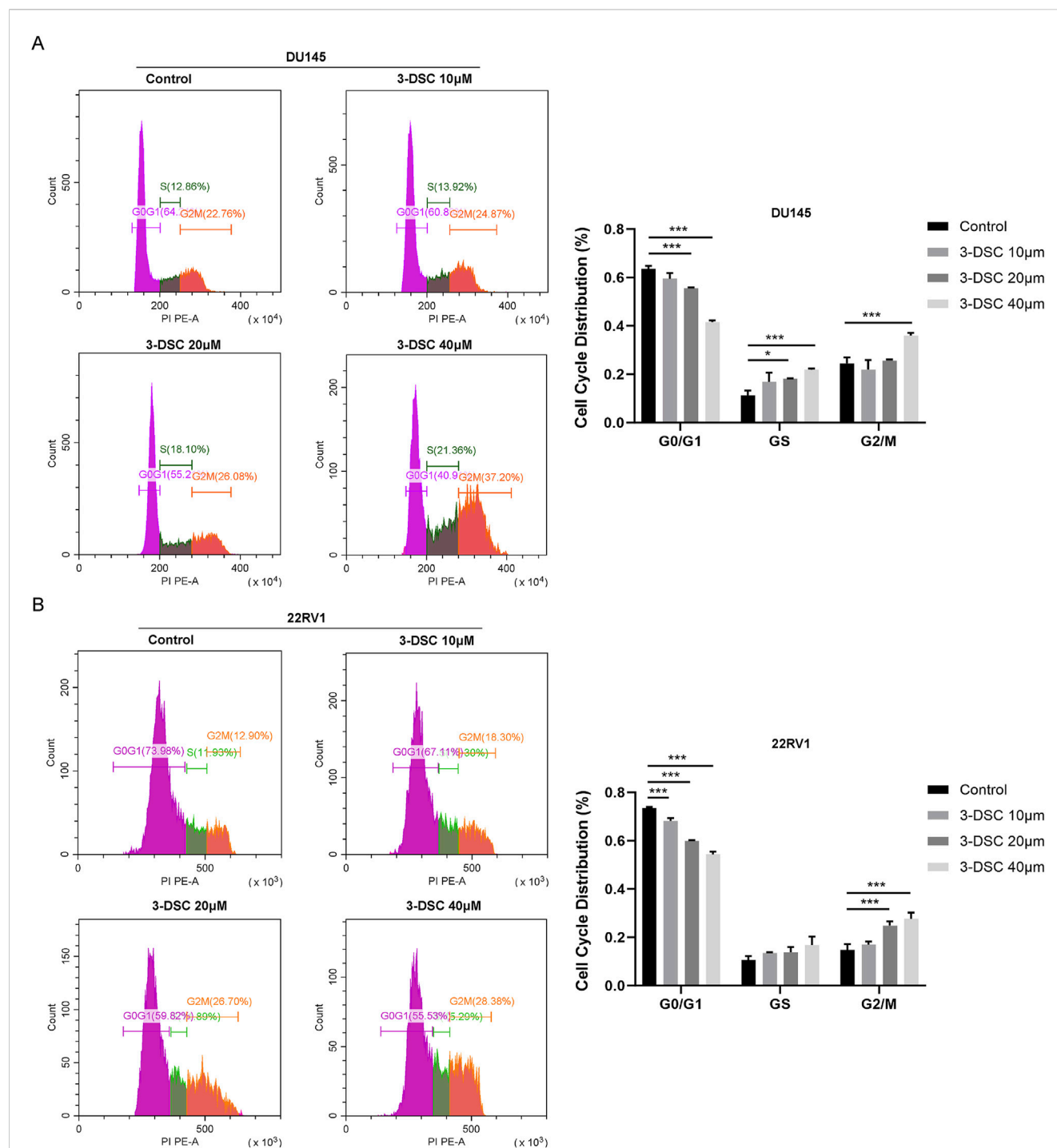


FIGURE 10

The treatment of 3-DSC resulted in S and G2/M phase cell cycle arrest in DU145 and G2/M phase cell cycle arrest in 22RV1. (A) Distribution of the typical cell cycle of DU145, with quantitative analysis of the proportions of cell cycle phases. (B) Distribution of the typical cell cycle of 22RV1, with quantitative analysis of the proportions of cell cycle phases. Compared to the control group, * $p < 0.05$, *** $p < 0.001$.

bioavailability and pharmacokinetic characteristics. However, if the compounds reach high concentrations, they can be efficiently absorbed and exert therapeutic effects (Ye et al., 2022). Therefore, it is necessary for us to conduct serum chemistry analysis on *Sappan lignum* in future research (Ye et al., 2023). The phytochemical compounds that complied with the requirements primarily consisted of flavonoids, alkaloids,

saponins, terpenoids, and additional components, including diphenyls, steroids, and fatty acids. Our investigation revealed that the target proteins for *Sappan lignum* primarily included kinase (25.34%) and enzyme (17.64%).

Sappan lignum has diverse biological actions, including anti-inflammatory, antitumor, immunosuppressive, and antioxidant properties (Jung et al., 2015; Yang et al., 2019). Extracts of

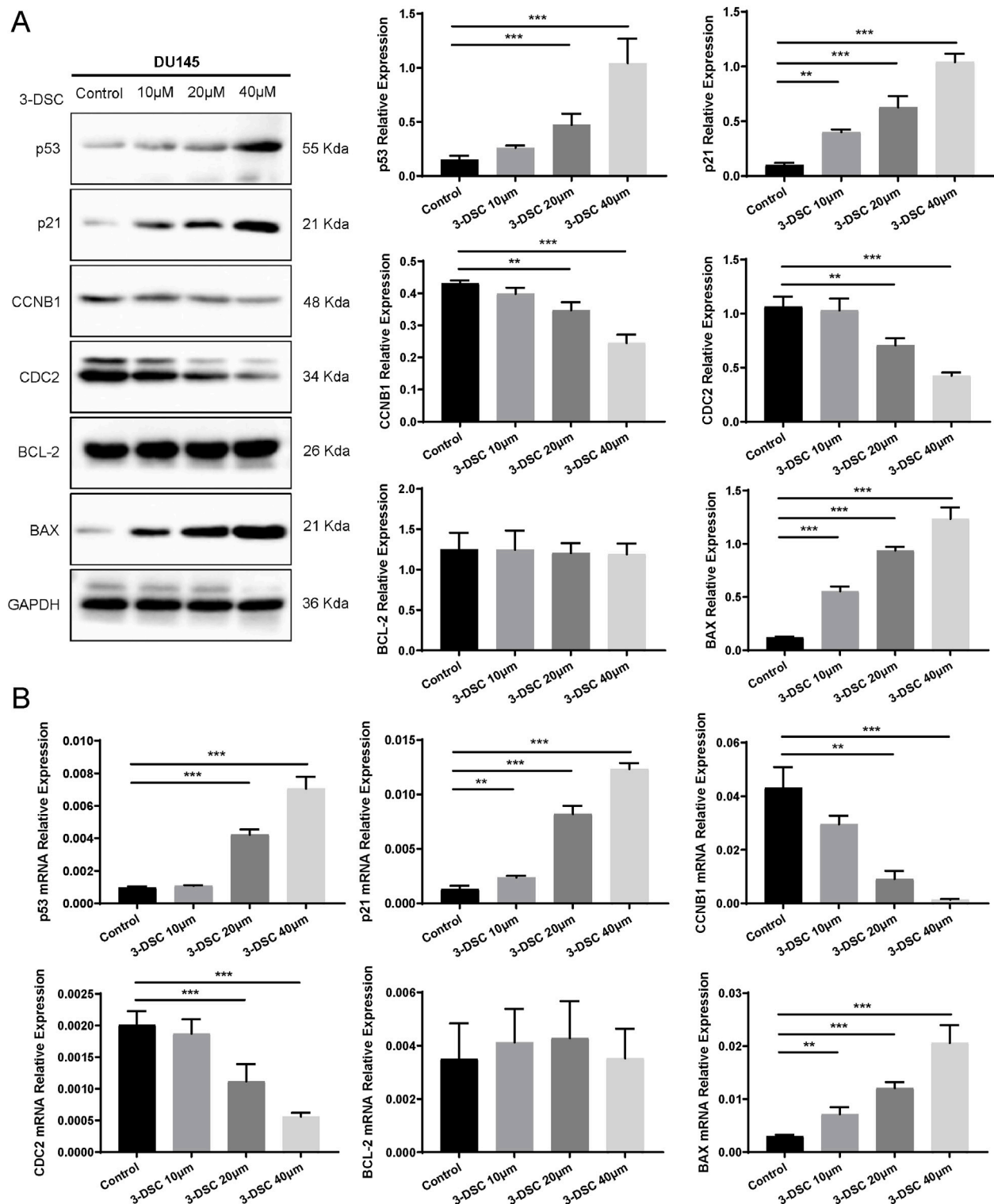


FIGURE 11
3-DSC downregulated CCNB1 and CDC2 and upregulated p53, p21, and BAX in DU145 cells. (A) Detection of p21, p53, BCL-2, BAX, CCNB1, and CDC2 protein expression levels of each group in DU145 cells via Western blotting. (B) Quantitative qRT-PCR of p21, p53, BCL-2, BAX, CCNB1, and CDC2 mRNA levels in DU145 cells. Compared with the control group, $**p < 0.01$, $***p < 0.001$.

Sappan lignum exhibit apparent inhibitory effects on various tumor cells and possess diverse applications. Recent studies have demonstrated that *Caesalpinia sappan* L. major extract increases

the generation of reactive oxygen species (ROS) and releases apoptosis-inducing factors in human colon cancer cells HCT116, suppressing proliferation and causing apoptosis (Seo et al., 2020).

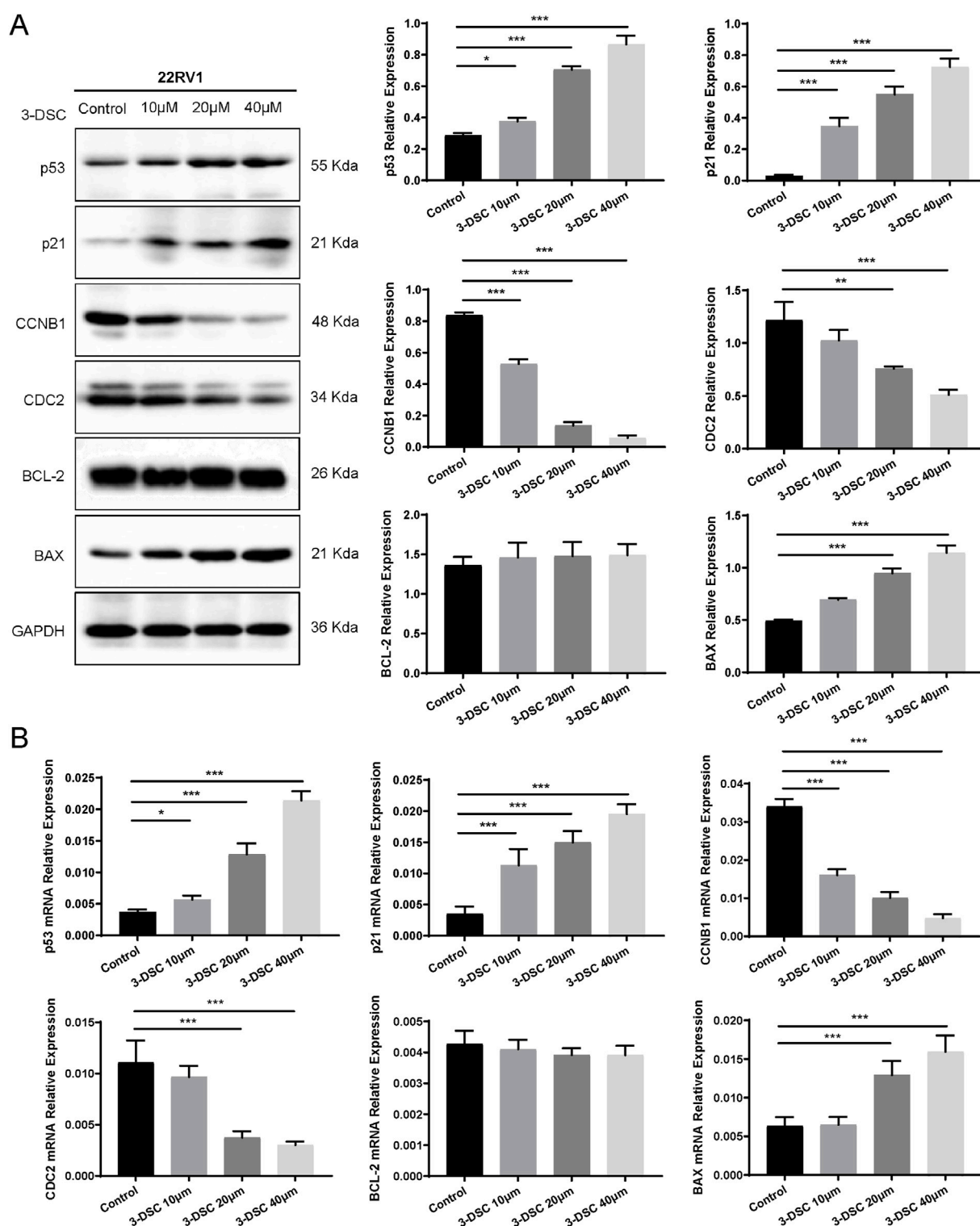


FIGURE 12

3-DSC downregulated CCNB1 and CDC2 and upregulated p53, p21, and BAX in 22RV1 cells. (A) Detection of p21, p53, BCL-2, BAX, CCNB1, and CDC2 protein expression levels of each group in 22RV1 cells via Western blotting. (B) Quantitative qRT-PCR of p21, p53, BCL-2, BAX, CCNB1, and CDC2 mRNA levels in 22RV1 cells. Compared with the control group, * $p < 0.05$, ** $p < 0.01$, *** $p < 0.001$.

The ethyl acetate extracts of *Sappan lignum* demonstrated the ability to induce cell cycle arrest at the G2/M phases and cell mitosis in lung, colon, and liver cancer cells *in vitro* while also inhibiting tumor

necrosis factor- α /nuclear factor kappa-B cellular signaling to exert antitumor effects (Zhang et al., 2014). Moreover, neck cancer cell viability was significantly reduced in response to the chloroform

extract of *Sappan lignum*. This antitumor effect is consistent with our findings and is ascribed to activating the apoptosis-related proteins p53 pathway, which induces apoptosis in tumor cells (Kim et al., 2005). 3-DSC is one of the main active ingredients of *Sappan lignum* with the molecular formula of $C_{16}H_{16}O_5$. The strongest binding affinity of 3-DSC to the primary targets of PCa was determined by molecular docking, indicating its potential as an active small molecule for treating PCa. 3-DSC has been confirmed to inhibit proinflammatory and anti-allergy activities. It promoted the arrest of the G2/M cell cycle, cell apoptosis, generation of ROS, and increased expression of cell cycle regulators (Kwak et al., 2021). Studies also have implied that 3-DSC increased mitochondria-related intrinsic apoptosis to restrain skin tumor cell growth (Fu et al., 2021). Besides, 3-DSC caused cell cycle arrest in colon and lung cancer cells by reducing the expression of CDC2, p27, and CCNB1 (Zhao et al., 2019; Lee et al., 2023).

Through intersecting the targets of *Sappan lignum* with 821 DEGs obtained from the public clinical datasets of PCa, eight core targets of *Sappan lignum* against PCa were retrieved, containing BCL-2, PTGS2, CCNB1, PGR, AURKA, MET, NR3C1, and ABCG2. The KEGG enrichment analysis indicated that tumor-associated p53 was the primary treatment pathway, including BCL-2 and CCNB1. p53 is an important tumor suppressor protein that regulates tumor cell cycle arrest, apoptosis, and DNA repair (Balakrishnan et al., 2006). p53 activation can increase the expression of its downstream effector molecules, p21 and BAX. p21 is a cell cycle inhibitor that prevents cell cycle progression by inhibiting the activity of the cyclin-cell division cycle gene complex (Jin et al., 2020). BAX is a pro-apoptotic protein that promotes apoptosis by interacting with the anti-apoptotic protein BCL-2 (Zhao et al., 2022).

In the *in vitro* part, we found that 3-DSC resulted in the proliferation and migration inhibition and apoptosis promotion of PCa cells, and the antiproliferative impact on PCa cells was enhanced with increasing concentrations of 3-DSC. Besides, we observed that 3-DSC promoted p53 expression in PCa cells, indicating that the p53 pathway was activated. p21, a downstream target gene of p53, was also significantly upregulated, which further decreased the expression of CCNB1-CDC2, leading to G2/M phase cell cycle arrest, thereby inhibiting tumor cell proliferation (Uzor et al., 2021; Chen et al., 2022). Dysregulation of CCNB1 and CDC2 is related to tumor cell cycle arrest, a process governed by the upstream protein p53 (Long et al., 2016). Additionally, this study showed that 3-DSC dramatically raised BAX levels in PCa cells, both in terms of protein and mRNA. The BCL-2/BAX ratio is crucial in the apoptosis regulation (Zhang et al., 2010). The results of KEGG pathway analysis and experimental data were consistent, indicating that 3-DSC exerted anti-proliferative and pro-apoptotic effects in PCa cells by through the p53/p21/CCNB1/CDC2 signaling pathway. These results highlighted the potential therapeutic benefits of *Sappan lignum* in PCa treatment.

This study selected human PCa cells DU145 and 22RV1. 22RV1 cells belong to androgen-independent PCa cell lines that are suppressed by reduced androgens (Duan et al., 2015), while DU145 cells are androgen-unresponsive and exhibit androgen-independent growth, indicating a poorer prognosis (Zhang et al., 2019). The 22RV1 and DU145 cell lines can validate the potential

therapeutic effects of drugs against prostate cancer and are valuable for modeling different types of PCa (Cheng et al., 2021). In the network pharmacology analysis, 32 targets of *Sappan lignum* against prostate cancer were identified, including SRD5A2, which is closely related to the androgen receptor (AR). In the PCa

Patients, the expression level of SRD5A2 is often elevated, leading to increased dihydrotestosterone (DHT) levels, thereby enhancing AR activity and affecting cell cycle and proliferation (Li et al., 2011). Combining the results of KEGG enrichment, we believe that *Sappan lignum* may regulate AR activity and function through SRD5A2, thereby co-regulating the cell cycle with the p53 pathway, ultimately inhibiting proliferation of androgen-independent PCa cell. Quercetin, another flavonoid of *Sappan lignum*, was able to inhibit AR protein expression in androgen-responsive prostate cancer cell lines, thereby suppressing the expression of prostate-specific, androgen-regulated tumor markers (Xing et al., 2001). This inhibition leads to reduced tumor proliferation through cell cycle regulation (Yang et al., 2015). The specific mechanisms of *Sappan lignum* need further *in vitro* experiments to verify AR-related gene regulation.

HPA and TCGA clinical data indicated elevated levels of CCNB1 in patients with PCa. Gene silencing of CCNB1 suppresses proliferation and promotes apoptosis by activating the p53 signaling pathway in tumor cells (Zhang et al., 2018). The expression level of CCNB1 varied among 501 PCa patients with different TMN stages and Gleason scores, with significantly higher upregulation observed in patients with T3 stage, N0 stage, and Gleason score of 7. Studies have reported that CCNB1 is a potential prognostic marker for recurrence following radical prostatectomy (Ersvør et al., 2020). These results confirmed that the inhibitory potential of 3-DSC for PCa provided a clinical advantage and suggested a potential new application of 3-DSC as an antitumor drug, with important implications for developing novel anticancer drugs.

There are some limitations in this study. Network pharmacology, bioinformatics, and *in vitro* experiments consistently verified and explored the main capacity of 3-DSC for proliferation suppression. However, in-depth investigation is required to comprehensively understand alternative plausible mechanisms of action. In subsequent investigations, a PCa xenograft mouse model

Should be employed to further examine the precise effects of 3-DSC, with an increased focus on *in vivo* studies. To further explore additional signaling pathways and targets influenced by *Sappan lignum*, multi-omics technologies can be utilized, having a clear understanding of its anti-cancer mechanism.

5 Conclusion

This study identified the active compound in *Sappan lignum* with anti-PCa properties. We found that the core compounds, specifically 3-DSC, could exert a therapeutic effect on PCa through the p53 pathway. *In vitro* experiments confirmed that 3-DSC exhibited significant antiproliferative, pro-apoptotic, and G2/M phase cell cycle arrest effects in 22RV1 and DU145 cell lines, potentially through modulating the p53/p21/CDC2/CCNB1 pathway. Additionally, clinical data analysis indicated

that CCNB1 is closely associated with the clinicopathological characteristics of PCa patients, further supporting the scientific basis for 3-DSC as a potential therapeutic agent. Our multi-level validation study provides crucial theoretical support and experimental basis for a new application of *Sappan lignum* as an antitumor drug.

Data availability statement

The original contributions presented in the study are included in the article/supplementary material, further inquiries can be directed to the corresponding authors.

Author contributions

WL: Writing-original draft, Methodology, Investigation, Formal Analysis, Data curation, Conceptualization. HJ: Writing-original draft, Investigation, Formal Analysis. WZ: Writing-original draft, Investigation. QS: Writing-original draft, Validation. QZ: Writing-original draft, Methodology. JX: Writing-original draft, Data curation. JH: Writing-review and editing, Supervision, Funding acquisition. YW: Writing-review and editing, Supervision, Funding acquisition, Conceptualization.

References

- Afrin, S., Giampieri, F., Gasparrini, M., Forbes-Hernández, T. Y., Cianciosi, D., Reboledo-Rodriguez, P., et al. (2020). Dietary phytochemicals in colorectal cancer prevention and treatment: a focus on the molecular mechanisms involved. *Biotechnol. Adv.* 38, 107322. doi:10.1016/j.biotechadv.2018.11.011
- Balakrishnan, K., Nimmanapalli, R., Ravandi, F., Keating, M. J., and Gandhi, V. (2006). Forodesine, an inhibitor of purine nucleoside phosphorylase, induces apoptosis in chronic lymphocytic leukemia cells. *Blood* 108 (7), 2392–2398. doi:10.1182/blood-2006-03-007468
- Chen, W. Y., Liang, G. Y., Zheng, Z. L., Wu, Y. S., Xu, F. F., Liu, B., et al. (2021). UPLC-ESI-Q-TOF/MS based metabolic profiling of protosappanin B in rat plasma, bile, feces, urine and intestinal bacteria samples. *Curr. Drug Metab.* 22 (6), 491–499. doi:10.2174/1389200222666210219123846
- Chen, X., Ma, J., Wang, X., Zi, T., Qian, D., Li, C., et al. (2022). CCNB1 and AURKA are critical genes for prostate cancer progression and castration-resistant prostate cancer resistant to vinblastine. *Front. Endocrinol. (Lausanne)* 13, 1106175. doi:10.3389/fendo.2022.1106175
- Cheng, H., Tang, S., Lian, X., Meng, H., Gu, X., Jiang, J., et al. (2021). The differential antitumor activity of 5-Aza-2'-deoxycytidine in prostate cancer DU145, 22RV1, and LNCaP cells. *J. Cancer* 12 (18), 5593–5604. doi:10.7150/jca.56709
- Clough, E., Barrett, T., Wilhite, S. E., Ledoux, P., Evangelista, C., Kim, I. F., et al. (2024). NCBI GEO: archive for gene expression and epigenomics data sets: 23-year update. *Nucleic. acids. Res.* 52 (D1), D138–d144. doi:10.1093/nar/gkad965
- Digre, A., and Lindskog, C. (2021). The Human Protein Atlas-Spatial localization of the human proteome in health and disease. *Protein Sci.* 30 (1), 218–233. doi:10.1002/pro.3987
- Duan, F., Li, Y., Chen, L., Zhou, X., Chen, J., Chen, H., et al. (2015). Sulfur inhibits the growth of androgen-independent prostate cancer *in vivo*. *Oncol. Lett.* 9 (1), 437–441. doi:10.3892/ol.2014.2700
- Ersvaer, E., Kildal, W., Vlatkovic, L., Cyll, K., Pradhan, M., Kleppe, A., et al. (2020). Prognostic value of mitotic checkpoint protein BUB3, cyclin B1, and pituitary tumor-transforming 1 expression in prostate cancer. *Mod. Pathol.* 33 (5), 905–915. doi:10.1038/s41379-019-0418-2
- Fang, S., Dong, L., Liu, L., Guo, J., Zhao, L., Zhang, J., et al. (2021). HERB: a high-throughput experiment- and reference-guided database of traditional Chinese medicine. *Nucleic. acids. Res.* 49 (D1), D1197–d1206. doi:10.1093/nar/gkaa1063
- Feng, X., Song, Z., Tao, A., Gong, P., Pei, W., and Zong, R. (2023). Prediction of active marker of seabuckthorn polysaccharides for prevention and treatment of cervical cancer and mechanism study. *Front. Nutr.* 10, 1136590. doi:10.3389/fnut.2023.1136590
- Fu, X., Zhao, R., Yoon, G., Shim, J. H., Choi, B. Y., Yin, F., et al. (2021). 3-Deoxysappanchalcone inhibits skin cancer proliferation by regulating T-lymphokine-activated killer cell-originated protein kinase *in vitro* and *in vivo*. *Front. Cell. Dev. Biol.* 9, 638174. doi:10.3389/fcell.2021.638174
- Hernandez, R. D., Genio, F. A. F., Casanova, J. R., Conato, M. T., and Paderes, M. C. (2024). Antiproliferative activities and SwissADME predictions of physicochemical properties of carbonyl group-modified rotenone analogues. *ChemistryOpen* 13 (1), e202300087. doi:10.1002/open.202300087
- Jin, J., Xu, H., Li, W., Xu, X., Liu, H., and Wei, F. (2020). LINC00346 acts as a competing endogenous RNA regulating development of hepatocellular carcinoma via modulating CDK1/CCNB1 Axis. *Front. Bioeng. Biotechnol.* 8, 54. doi:10.3389/fbioe.2020.00054
- Jung, E. G., Han, K. I., Hwang, S. G., Kwon, H. J., Patnaik, B. B., Kim, Y. H., et al. (2015). Brazilian isolated from *Caesalpinia sappan* L. inhibits rheumatoid arthritis activity in a type-II collagen induced arthritis mouse model. *BMC Complement. Altern. Med.* 15, 124. doi:10.1186/s12906-015-0648-x
- Kamal, Y., Khan, T., Haq, I., Zahra, S. S., Asim, M. H., Shahzadi, I., et al. (2022). Phytochemical and biological attributes of *Bauhinia variegata* L. (Caesalpinaceae). *Braz. J. Biol.* 82, e257990. doi:10.1590/1519-6984.257990
- Kang, X., Jin, D., Zhang, Y., Zhou, R., Zhang, Y., and Lian, F. (2021). Systematic elucidation of the mechanism of sappan lignum in the treatment of diabetic peripheral neuropathy based on network pharmacology. *Evid. Based Complement. Altern. Med.* 2021, 5528018. doi:10.1155/2021/5528018
- Kapinova, A., Kubatka, P., Liskova, A., Baranenko, D., Kruzliak, P., Matta, M., et al. (2019). Controlling metastatic cancer: the role of phytochemicals in cell signaling. *J. Cancer Res. Clin. Oncol.* 145 (5), 1087–1109. doi:10.1007/s00432-019-02892-5
- Khan, S. A., and Lee, T. K. W. (2023). Identifying potential pharmacological targets and molecular pathways of Meliae cortex for COVID-19 therapy. *Front. Immunol.* 14, 1128164. doi:10.3389/fimmu.2023.1128164
- Kim, E. C., Hwang, Y. S., Lee, H. J., Lee, S. K., Park, M. H., Jeon, B. H., et al. (2005). *Caesalpinia sappan* induces cell death by increasing the expression of p53 and p21WAF1/CIP1 in head and neck cancer cells. *Am. J. Chin. Med.* 33 (3), 405–414. doi:10.1142/s0192415x05003016
- Kim, S., Chen, J., Cheng, T., Gindulyte, A., He, J., He, S., et al. (2021). PubChem in 2021: new data content and improved web interfaces. *Nucleic. acids. Res.* 49 (D1), D1388–d1395. doi:10.1093/nar/gkaa971
- Kim, S., Cheng, T., He, S., Thiessen, P. A., Li, Q., Gindulyte, A., et al. (2022). PubChem protein, gene, pathway, and taxonomy data collections: bridging biology and chemistry

Funding

The author(s) declare that financial support was received for the research, authorship, and/or publication of this article. This research was funded by the Natural Science Foundation of China (Nos 82074545 and 82205292), Project of the China Association of Chinese Medicine (CACM-2022-QNRC2-B02), and Project of Beijing University of Chinese Medicine (2022-JYB-JBZR-042).

Conflict of interest

The authors declare that the research was conducted in the absence of any commercial or financial relationships that could be construed as a potential conflict of interest.

Publisher's note

All claims expressed in this article are solely those of the authors and do not necessarily represent those of their affiliated organizations, or those of the publisher, the editors and the reviewers. Any product that may be evaluated in this article, or claim that may be made by its manufacturer, is not guaranteed or endorsed by the publisher.

- through target-centric views of PubChem data. *J. Mol. Biol.* 434 (11), 167514. doi:10.1016/j.jmb.2022.167514
- Kwak, A. W., Lee, M. J., Lee, M. H., Yoon, G., Cho, S. S., Chae, J. I., et al. (2021). The 3-deoxysappanchalcone induces ROS-mediated apoptosis and cell cycle arrest via JNK/p38 MAPKs signaling pathway in human esophageal cancer cells. *Phytomedicine* 86, 153564. doi:10.1016/j.phymed.2021.153564
- Lee, J. Y., Lee, S. O., Kwak, A. W., Chae, S. B., Cho, S. S., Yoon, G., et al. (2023). 3-Deoxysappanchalcone inhibits cell growth of gefitinib-resistant lung cancer cells by simultaneous targeting of EGFR and MET kinases. *Biomol. Ther. Seoul.* 31 (4), 446–455. doi:10.4062/biomolther.2023.070
- Li, J., Ding, Z., Wang, Z., Lu, J. F., Maity, S. N., Navone, N. M., et al. (2011). Androgen regulation of 5 α -reductase isoenzymes in prostate cancer: implications for prostate cancer prevention. *PLoS ONE* 6 (12), e28840. doi:10.1371/journal.pone.0028840
- Lipinski, C. A., Lombardo, F., Dominy, B. W., and Feeney, P. J. (2001). Experimental and computational approaches to estimate solubility and permeability in drug discovery and development settings. *Adv. Drug. Deliv. Rev.* 46 (1–3), 3–26. doi:10.1016/s0169-409x(00)00129-0
- Long, J., Zhang, Z., Liu, Z., Xu, Y., and Ge, C. (2016). Identification of genes and pathways associated with pancreatic ductal adenocarcinoma by bioinformatics analyses. *Oncol. Lett.* 11 (2), 1391–1397. doi:10.3892/ol.2015.4042
- Lv, D., Lai, Q., Zhang, Q., Wang, J. H., Li, Y. C., Zeng, G. Z., et al. (2022). 3-Deoxysappanchalcone isolated from *Caesalpinia sinensis* shows anticancer effects on HeLa and PC3 cell lines: invasion, migration, cell cycle arrest, and signaling pathway. *Heliyon* 8 (10), e11013. doi:10.1016/j.heliyon.2022.e11013
- Martins, T. D., Annichino-Bizzacchi, J. M., Romano, A. V. C., and Filho, R. M. (2019). Principal component analysis on recurrent venous thromboembolism. *Clin. Appl. Thromb. Hemost.* 25, 1076029619895323. doi:10.1177/1076029619895323
- Mirzaei, S., Paskeh, M. D. A., Okina, E., Gholami, M. H., Hushmandi, K., Hashemi, M., et al. (2022). Molecular Landscape of LncRNAs in Prostate Cancer: a focus on pathways and therapeutic targets for intervention. *J. Exp. Clin. Cancer Res.* 41 (1), 214. doi:10.1186/s13046-022-02406-1
- Neuberger, M., Frey, L., Nitschke, K., Wessels, F., Westhoff, N., Waldbillig, F., et al. (2023). Integrin expression in localized prostate cancer: a TCGA and mscc cohort-based exploratory *in silico* analysis. *Anticancer Res.* 43 (1), 417–428. doi:10.21873/anticancer.16177
- Petri, E. T., Errico, A., Escobedo, L., Hunt, T., and Basavappa, R. (2007). The crystal structure of human cyclin B. *Cell. Cycle* 6 (11), 1342–1349. doi:10.4161/cc.6.11.4297
- Petros, A. M., Medek, A., Nettesheim, D. G., Kim, D. H., Yoon, H. S., Swift, K., et al. (2001). Solution structure of the antiapoptotic protein bcl-2. *Proc. Natl. Acad. Sci. U. S. A.* 98 (6), 3012–3017. doi:10.1073/pnas.041619798
- Ramzan, M., Karobari, M. I., Heboy, A., Mohamed, R. N., Mustafa, M., Basheer, S. N., et al. (2022). Synthesis of silver nanoparticles from extracts of wild ginger (zingiber zerumbet) with antibacterial activity against selective multidrug resistant oral bacteria. *Molecules* 27 (6), 2007. doi:10.3390/molecules27062007
- Rezaeian, A. H., Phan, L. M., Zhou, X., Wei, W., and Inuzuka, H. (2023). Pharmacological inhibition of the SKP2/p300 signaling axis restricts castration-resistant prostate cancer. *Neoplasia* 38, 100890. doi:10.1016/j.neo.2023.100890
- Rizzo, A., Santoni, M., Mollica, V., Fiorentino, M., Brandi, G., and Massari, F. (2022). Microbiota and prostate cancer. *Semin. Cancer Biol.* 86 (Pt 3), 1058–1065. doi:10.1016/j.semcancer.2021.09.007
- Sebesta, E. M., and Anderson, C. B. (2017). The surgical management of prostate cancer. *Semin. Oncol.* 44 (5), 347–357. doi:10.1053/j.seminoncol.2018.01.003
- Sekhoacha, M., Riet, K., Motloung, P., Gumenku, L., Adegoke, A., and Mashele, S. (2022). Prostate cancer review: genetics, diagnosis, treatment options, and alternative approaches. *Molecules* 27 (17), 5730. doi:10.3390/molecules27175730
- Seo, H. W., No, H., Cheon, H. J., and Kim, J. K. (2020). Sappanchalcone, a flavonoid isolated from *Caesalpinia sappan* L., induces caspase-dependent and AIF-dependent apoptosis in human colon cancer cells. *Chem. Biol. Interact.* 327, 109185. doi:10.1016/j.cbi.2020.109185
- Termini, D., Den Hartogh, D. J., Jaglanian, A., and Tsiani, E. (2020). Curcumin against prostate cancer: current evidence. *Biomolecules* 10 (11), 1536. doi:10.3390/biom10111536
- Trott, O., and Olson, A. J. (2010). AutoDock Vina: improving the speed and accuracy of docking with a new scoring function, efficient optimization, and multithreading. *J. Comput. Chem.* 31 (2), 455–461. doi:10.1002/jcc.21334
- Uzor, S., Porazinski, S. R., Li, L., Clark, B., Ajiro, M., Iida, K., et al. (2021). CDC2-like (CLK) protein kinase inhibition as a novel targeted therapeutic strategy in prostate cancer. *Sci. Rep.* 11 (1), 7963. doi:10.1038/s41598-021-86908-6
- Wan, Y., Xu, L., Liu, Z., Yang, M., Jiang, X., Zhang, Q., et al. (2019). Utilising network pharmacology to explore the underlying mechanism of Wumei Pill in treating pancreatic neoplasms. *BMC Complement. Altern. Med.* 19 (1), 158. doi:10.1186/s12906-019-2580-y
- Wang, X., Fang, G., and Pang, Y. (2018). Chinese medicines in the treatment of prostate cancer: from formulas to extracts and compounds. *Nutrients* 10 (3), 283. doi:10.3390/nu10030283
- Wang, Y. Z., Wang, Y. L., Che, H. J., Jia, Y. H., Wang, H. F., Zuo, L. F., et al. (2023). Sappanone A: a natural PDE4 inhibitor with dual anti-inflammatory and antioxidant activities from the heartwood of *Caesalpinia sappan* L. *J. Ethnopharmacol.* 304, 116020. doi:10.1016/j.jep.2022.116020
- Wu, J., Mao, X., Cai, T., Luo, J., and Wei, L. (2006). KOBAS server: a web-based platform for automated annotation and pathway identification. *Nucleic Acids Res.* 34 (Web Server issue), W720–W724. doi:10.1093/nar/gkl167
- Xing, N., Chen, Y., Mitchell, S. H., and Young, C. Y. (2001). Quercetin inhibits the expression and function of the androgen receptor in LNCaP prostate cancer cells. *Carcinogenesis* 22 (3), 409–414. doi:10.1093/carcin/22.3.409
- Xue, J., Chen, K., Hu, H., and Gopinath, S. C. B. (2022). Progress in gene therapy treatments for prostate cancer. *Biotechnol. Appl. Biochem.* 69 (3), 1166–1175. doi:10.1002/bab.2193
- Yang, F., Song, L., Wang, H., Wang, J., Xu, Z., and Xing, N. (2015). Quercetin in prostate cancer: chemotherapeutic and chemopreventive effects, mechanisms and clinical application potential (Review). *Oncol. Rep.* 33 (6), 2659–2668. doi:10.3892/or.2015.3886
- Yang, X., Ren, L., Zhang, S., Zhao, L., and Wang, J. (2016). Antitumor effects of purified protosappanin B extracted from *lignum sappan*. *Integr. Cancer Ther.* 15 (1), 87–95. doi:10.1177/1534735415588929
- Yang, X., Zhao, L., Zhang, T., Xi, J., Liu, S., Ren, L., et al. (2019). Protosappanin B promotes apoptosis and causes G(1) cell cycle arrest in human bladder cancer cells. *Sci. Rep.* 9 (1), 1048. doi:10.1038/s41598-018-37553-z
- Ye, B., Chen, P., Lin, C., Zhang, C., and Li, L. (2023). Study on the material basis and action mechanisms of *Sophora davidii* (Franch.) skeels flower extract in the treatment of non-small cell lung cancer. *J. Ethnopharmacol.* 317, 116815. doi:10.1016/j.jep.2023.116815
- Ye, X. W., Wang, H. L., Cheng, S. Q., Xia, L. J., Xu, X. F., and Li, X. R. (2022). Network pharmacology-based strategy to investigate the pharmacologic mechanisms of coptidis rhizoma for the treatment of alzheimer's disease. *Front. Aging Neurosci.* 14, 890046. doi:10.3389/fnagi.2022.890046
- Zhang, H., Zhang, X., Li, X., Meng, W. B., Bai, Z. T., Rui, S. Z., et al. (2018). Effect of CCNB1 silencing on cell cycle, senescence, and apoptosis through the p53 signaling pathway in pancreatic cancer. *J. Cell. Physiol.* 234 (1), 619–631. doi:10.1002/jcp.26816
- Zhang, L., Han, L., Wang, X., Wei, Y., Zheng, J., Zhao, L., et al. (2021). Exploring the mechanisms underlying the therapeutic effect of *Salvia miltiorrhiza* in diabetic nephropathy using network pharmacology and molecular docking. *Biosci. Rep.* 41 (6), BSR20203520. doi:10.1042/bsr20203520
- Zhang, Q., Liu, J. L., Qi, X. M., Qi, C. T., and Yu, Q. (2014). Inhibitory activities of *Lignum Sappan* extractives on growth and growth-related signaling of tumor cells. *Chin. J. Nat. Med.* 12 (8), 607–612. doi:10.1016/s1875-5364(14)60092-3
- Zhang, W., Ju, J., and Gronowicz, G. (2010). Odontoblast-targeted Bcl-2 overexpression impairs dentin formation. *J. Cell. Biochem.* 111 (2), 425–432. doi:10.1002/jcb.22722
- Zhang, X., Sun, Y., Wang, P., Yang, C., and Li, S. (2019). Reduced pim-1 expression increases chemotherapeutic drug sensitivity in human androgen-independent prostate cancer cells by inducing apoptosis. *Exp. Ther. Med.* 18 (4), 2731–2738. doi:10.3892/etm.2019.7862
- Zhao, J., Hu, W., Zhang, Z., Zhou, Z., Duan, J., Dong, Z., et al. (2022). Bee venom protects against pancreatic cancer via inducing cell cycle arrest and apoptosis with suppression of cell migration. *J. Gastrointest. Oncol.* 13 (2), 847–858. doi:10.21037/jgo-22-222
- Zhao, L., Zhang, H., Li, N., Chen, J., Xu, H., Wang, Y., et al. (2023). Network pharmacology, a promising approach to reveal the pharmacology mechanism of Chinese medicine formula. *J. Ethnopharmacol.* 309, 116306. doi:10.1016/j.jep.2023.116306
- Zhao, R., Huang, H., Choi, B. Y., Liu, X., Zhang, M., Zhou, S., et al. (2019). Cell growth inhibition by 3-deoxysappanchalcone is mediated by directly targeting the TOPK signaling pathway in colon cancer. *Phytomedicine* 61, 152813. doi:10.1016/j.phymed.2018.12.036
- Zhen, Z., Xue, D. J., Chen, Y. P., Li, J. H., Gao, Y., Shen, Y. B., et al. (2023). Decoding the underlying mechanisms of Di-Tan-Decoction in treating intracerebral hemorrhage based on network pharmacology. *BMC Complement. Med. Ther.* 23 (1), 44. doi:10.1186/s12906-022-03831-7
- Zheng, X. C., Shi, Z. S., Qiu, C. Z., Hong, Z. S., Wang, C. X., Zhuang, H. B., et al. (2020). Protosappanin B exerts anti-tumor effects on colon cancer cells via inhibiting GOLPH3 expression. *Integr. Cancer Ther.* 19, 1534735420972477. doi:10.1177/1534735420972477
- Zhi, Y., Wu, X., Shen, W., Wang, Y., Zhou, X., He, P., et al. (2018). Synthesis and pharmacological evaluation of novel epidermal growth factor receptor inhibitors against prostate tumor cells. *Oncol. Lett.* 16 (5), 6522–6530. doi:10.3892/ol.2018.9438
- Zhu, Y., Freedland, S. J., and Ye, D. (2020). Prostate cancer and prostatic diseases best of asia, 2019: challenges and opportunities. *Prostate Cancer Prostatic Dis.* 23 (2), 197–198. doi:10.1038/s41391-019-0193-7

Frontiers in Pharmacology

Explores the interactions between chemicals and living beings

The most cited journal in its field, which advances access to pharmacological discoveries to prevent and treat human disease.

Discover the latest Research Topics

[See more →](#)

Frontiers

Avenue du Tribunal-Fédéral 34
1005 Lausanne, Switzerland
frontiersin.org

Contact us

+41 (0)21 510 17 00
frontiersin.org/about/contact



Frontiers in Pharmacology

